Land Subsidence Analysis Using PAZ and Sentinel-1 Data on the Karstic Region of Konya Basin, Turkey

S. Abdikan [1*], C. Bayik[2], F. Calò[3], A. Pepe[3], M. Arikan[4], F. Balik Sanli[5]

1 Dept. of Geomatics Engineering, Hacettepe University, Beytepe/Ankara, Turkey - sayginabdikan@hacettepe.edu.tr
2 Dept. of Geomatics Engineering, Zonguldak Bulent Ecevit University, Zonguldak, Turkey - caglarbayik@beun.edu.tr
3 National Research Council (CNR) of Italy—Institute for the Electromagnetic Sensing of the Environment (IREA), Napoli, Italy - (calo.f, pepe.a)@irea.cnr.it
4 BeeSense, Consultancy and Engineering on Geo-information Technologies, Delft, Netherlands - m.arikan@beesense.nl
5. Dept. of Geomatic Engineering, Yildiz Technical University, Istanbul, Turkey - fbalik@yildiz.edu.tr

Session: Measuring and Monitoring of land subsidence / Earth Fissures & Sinkholes
Keywords: InSAR, karst, PAZ, Sentinel-1, subsidence

*Corresponding author

Introduction

Groundwater lowering due to excessive pumping, drought, and climate change; causes severe and long-term effects on the Earth's surface. Due to the increasing demand for food, dense agricultural activities have been carried out over the study area of Konya Closed Basin (Figure 1) (Calò et al., 2017). The underground water used for irrigation increased mainly due to overpumping from unregistered wells. The lithology of the study area is composed of clay, limestone, silt, sandstone, and its characteristics play an essential role in forming karstic depressions, often resulting in sinkholes (Ozdemir, 2015, Bayari et al., 2009). These human-induced and naturally developed phenomena affect the region and have threatened people heavily for the last thirty years. A previous study showed the spatial distribution of surface deformation using a small baseline Interferometric SAR (InSAR) approach on using Envisat data (2002-2010). The maximum observed subsidence rate was 15 mm/yr (Calò et al., 2015). A recent study carried out over the region using both Cosmo-SkyMed (2016-2017) and Sentinel-1 (2014-2018) found Line of Sight (LOS) deformation velocity ranging between -70 and 10 mm/yr in the area, while GNSS indicated 25 mm/yr (Orhan et al., 2021). Abdikan et al (2020) studied the performance of the PAZ satellite over the region and detected a 200 m sinkhole. The high-resolution PAZ based analysis pointed out the contribution of high-resolution X-band SAR for the extraction of small-scale sinkholes that may be harder to detect using Sentinel-1. Previously, the potential of PAZ for surface movement and scattering characterization was also explored over the Netherlands with co-polarized multi-temporal data (Chang & Stein, 2021). Abdikan et al. (2022) showed the contribution of the PAZ data over the study area using sequential interferograms with small-scale sinkhole shaped surface displacement.

The main contributions of this study are as follows:

- We produce a new map of subsidence rate due to groundwater levels declining in an agriculture dominated region.
- We evaluate the performance of PAZ data based on a Persistent Scatterer Interferometry (PSI) analysis over the karstic region.

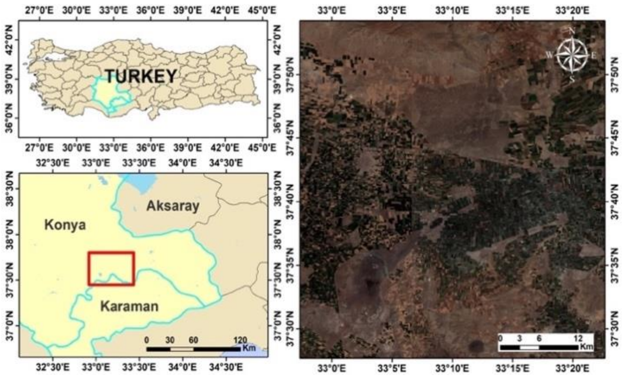

Figure 1 The study area

Methods and data

This study determines the surface deformation pattern using the Persistent Scatterer Interferometry (PSI) method. Freely available Sentinel-1A images from the European Space Agency (ESA) were used for this application. Image preprocessing was performed with the Open-Source Sentinel Application Platform (SNAP) software. For the following steps, the open-source StaMPS (Stanford Method for Persistent Scatterers) software was used (Hooper et al., 2010). With this software, processing steps such as PS selection, DEM error correction, and unwrapping of interferograms were carried out. Interferograms were generated in primary and secondary geometry. In total, 76 images of Sentinel-1A acquired along descending orbit are used and 75 interferograms are obtained between 2016 and 2021. One arc-second SRTM (30 m x 30 m) DEM was used to eliminate the topographic phase effect. For the PAZ analysis, 38 high resolution (1m) StripMap data (2019 Oct - 2021 Oct) were analyzed and 37 interferograms were generated. The stripmap mode PAZ data is also acquired in descending orbit and in VV polarization. All processing steps for Sentinel-1 are given in Figure 2. In the processing of PAZ data, interferograms are created using the software DORIS and the PSI is applied in the StaMPS (Figure 2). In the previous studies, the analysis indicates that the surface deformation is mainly developed along the vertical direction due to underground water depletion (Calò et al., 2017, Orhan et al., 2021). In this study, the results are extracted along the LOS direction.

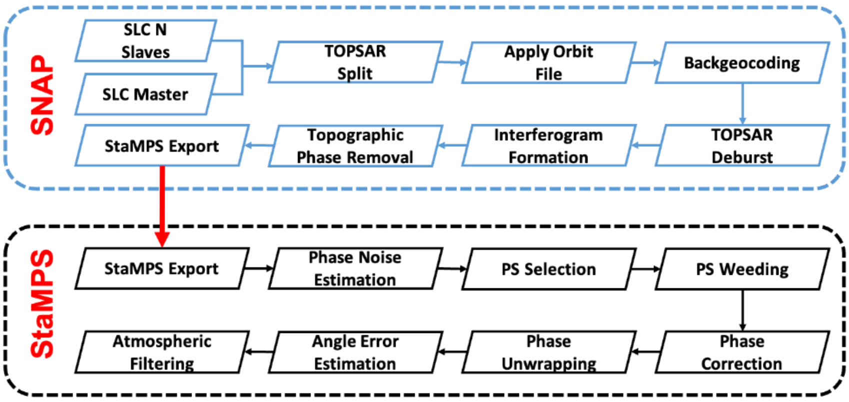

Figure 2 Flowchart of data processing for Sentinel-1 data

Results and discussions

The spatial distribution of surface deformation detected from the PSI analysis of Sentinel-1 data is shown in Figure 3. The maximum velocity of displacements reaches up to about -20 mm/yr (±1mm/yr) during the observed period (2016-2021). This points out that the deformation continues at an increasing rate. The subsidence pattern has similarities to the previous studies (Calò et al., 2017, Orhan et al., 2021). Furthermore, as we used the PSI approach in this study, we also extracted deformation over man-made structures; see the white boxes in Figure 3.

Moreover, the agriculture fields are highly decorrelated areas. However, we detected measurement points over the utility poles (i.e., electricity and telecommunication) developed within the agricultural fields, see linear infrastructural features visible in Figures 3b, 3c. In the eastern part of the region, we noticed the high density of points with high displacement rates located over the city of Karapinar (Figure 3d). Finally, an additional preliminary analysis is conducted using data acquired by the new generation X-band PAZ satellite mission. The maximum displacement obtained from PAZ results is about 20-25 mm/yr (±2 mm/yr) in the LOS direction (Figure 4). Even though the results of PAZ data provided denser point distribution than the results of Sentinel-1, it has also obtained an additional displacement pattern over bare lands that is not present in the Sentinel-1 analysis. The maximum displacement areas indicated by the red points in Figure 4a are could not determine in the long-term Sentinel-1 product. The agricultural activities and the change of plants over time have caused a decorrelation. As a common result, PS points could not be obtained with both satellite images in vegetated areas.

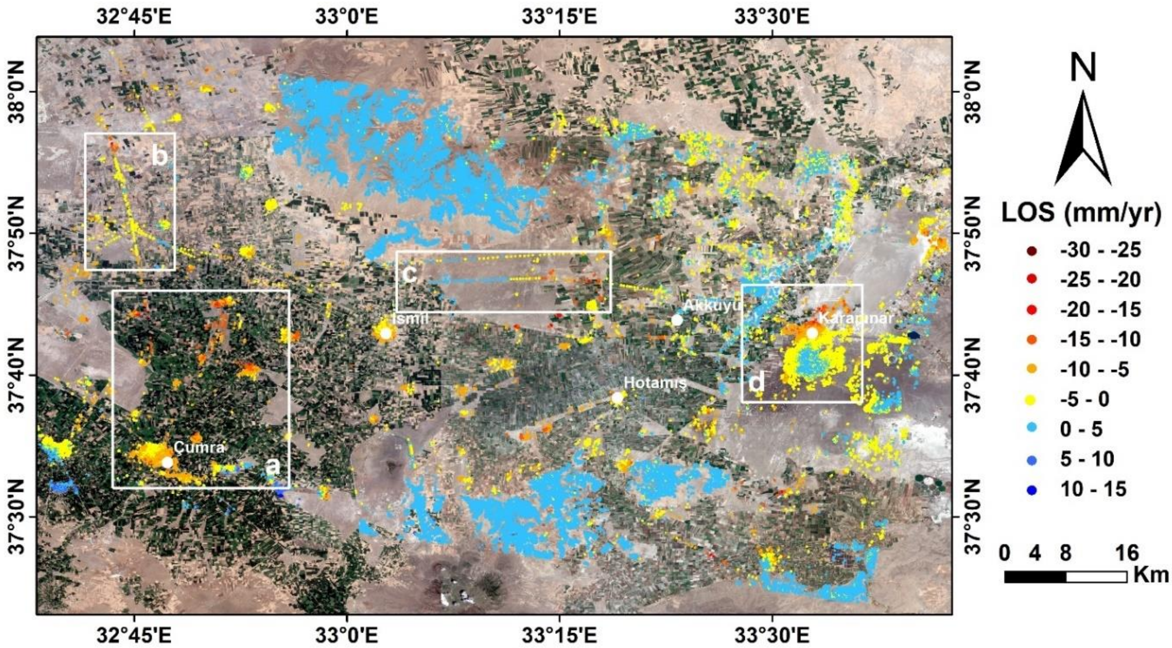

Figure 3 PSI results of Sentinel-1

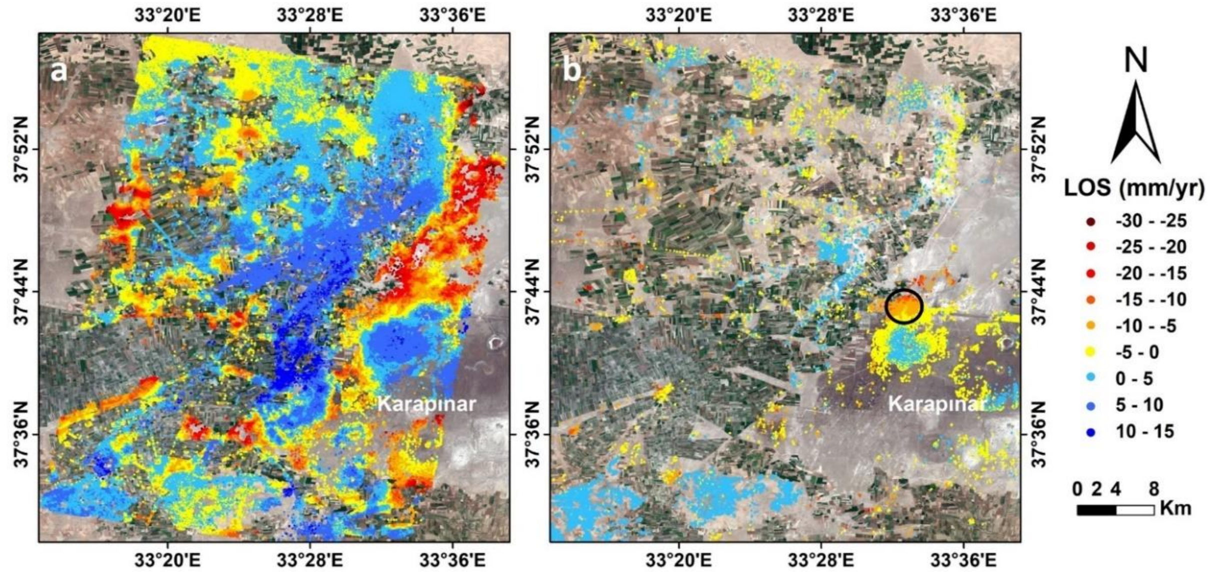

Figure 4 PAZ (a) and Sentinel-1 (b) descending LOS results of Karapınar (black circle) and its surroundings.

Conclusion

The study examines the current ground stability over the Konya Closed Basin study area located in central Turkey. Sentinel-1 has had a high impact on long-term monitoring with its large amount of archived data since 2014. On the other hand, the stripmap mode PAZ data cover a smaller area compared to Sentinel-1. The study showed that, along with the settlements (cities and villages), linear infrastructures were also determined. The PAZ results belong to a two-year analysis which obtained higher persistent scatterer points compared to Sentinel-1 analysis based on a five-year dataset. As further perspectives, since the region is dominated by agriculture, a small baseline approach will be applied to enhance the spatial distribution of surface displacement. We will also acquire and process ascending orbit Sentinel-1 dataset and extract both vertical and horizontal deformation for the first time over the study area. The results will be integrated with ground water level measurement data, and geospatial analysis will be performed to get deeper insights into the subsidence risk affecting the Konya region.

Acknowledgements

This study was financially supported by the Hacettepe University Scientific Research Projects Coordination Unit under Project No. FKB-2021-19389. The authors would like to thank Instituto Nacional de Técnica Aeroespacial (INTA) - PAZ Science Team for providing the PAZ data in the framework of the AO-001-031 project.

References

Abdikan, S., Bayik, C., Ustuner, M., Balik Sanli, F., 2020. Repeat-Pass Interferometric and Backscatter Analysis of X-Band Paz Satellite – First Results, *Int. Arch. Photogramm. Remote Sens. Spatial Inf. Sci., XLIII-B3-2020*, 253–258, https://doi.org/10.5194/isprs-archives-XLIII-B3-2020-253-2020

Abdikan, S., Bayik, C., Calò, F., Pepe, A., and Balik Sanli, F. 2022. Evaluation of DEM Derived by Repeat-Pass X-Band Stripmap Mode Paz Data, *Int. Arch. Photogramm. Remote Sens. Spatial Inf. Sci., XLIII-B3-2022,* 243–248, https://doi.org/10.5194/isprs-archives-XLIII-B3-2022-243-2022,

Bayari, C.S., Pekkan, E., Ozyurt, N.N., 2009. Obruks, as giant collapse dolines caused by hypogenic karstification in central Anatolia, Turkey: analysis of likely formation processes. *Hydrogeology Journal*, 17, pp. 327–345.

Calò, F., Notti, D., Galve, J. P., Abdikan, S., Görüm, T., Orhan, O., Makineci, H. B., Pepe, A., Yakar, M., Balik Şanli, F., 2018. A Multi-Source Data Approach for the Investigation of Land Subsidence in the Konya Basin, Turkey. *Int. Arch. Photogramm. Remote Sens. Spatial Inf. Sci.,* XLII-3/W4, 129–135, https://doi.org/10.5194/isprs-archives-XLII-3-W4-129-2018 .

Chang L. and Stein A., 2021. Exploring PAZ co-polarimetric SAR data for surface movement mapping and scattering characterization*. International Journal of Applied Earth Observation and Geoinformation,* 96, 102280

Hooper, A., Bekaert, D., Spaans, K., Arıkan, M., 2012. Recent advances in SAR interferometry time series analysis for measuring crustal deformation. *Tectonophysics* 514, 1-13.

Orhan, O., Oliver-Cabrera, T., Wdowinski, S., Yalvac, S., Yakar, M., 2021. Land Subsidence and Its Relations with Sinkhole Activity in Karapınar Region, Turkey: A Multi-Sensor InSAR Time Series Study. *Sensors,* 21, 774.

Ozdemir, A., 2015. Investigation of sinkholes spatial distribution using the weights of evidence method and GIS in the vicinity of Karapinar (Konya, Turkey). *Geomorphology*, 245, 40–50.

Back-analyse of a large-scale collapse of chalk mine (Château-Landon, France 1910)

M. Al Heib[1], N. Conil[1], P. Gombert[1]

1 Ineris (France)

marwan.alheib@ineris.fr

Abstract

The paper presents the feedback of a large collapse of an underground chalk mine in France (77). A 2D numerical model, using the distinct element method, was used. It considered the specific characterization of the site, presence of a slope, fault, hard layer, and water. The results of the numerical modelling highlighted the role of those elements, mainly the fault, where tension stresses favorite the sliding of a large mass over the underground mine.

Introduction

The subsidence phenomenon can occur several years after the end of the mining operation. Times to times an exceptional event, such as a large-scale collapse (massive collapse) of the underground mine, can happen and induce severe consequences (Al Heib et al., 2015). The subsidence hazard is generally related to natural, man-made, etc. factors. The large-scale mining collapse is one of these catastrophic events. The prediction of such an event is very difficult. In this paper, we present a historic large-scale collapse of a chalk mine. The objective is to discuss the role of the different factors (natural and man-made) at the origin of this catastrophic event.

Case study description

During the winter of 1910, the Seine and its tributaries overflowed causing a rise in the water table and the flooding of an active chalk mine, located at Château-Landon (Paris Basin, France, Figure 1). The collapse that occurred caused a large landslide, destroying both the nearby waterway and the hamlet and killed 7 persons (Watelet et al., 2016). The collapse occurred after few days of heavy and continuous raining. Gombert et al. (2013) studied the effect of the water which was considered the triggering factor. However, the analysis of the geology and topography of the mine shows (Figure 2): 1) the mine excavated with high extraction ratio, 2) a cliff zone with a slope equal to 24°, 3) the presence of a stiff limestone bed on the overburden and 4) the existing of a fault with a dip equal to 70°. The objective of the paper is to study numerically their effect and to compare the results to the in-situ observations.

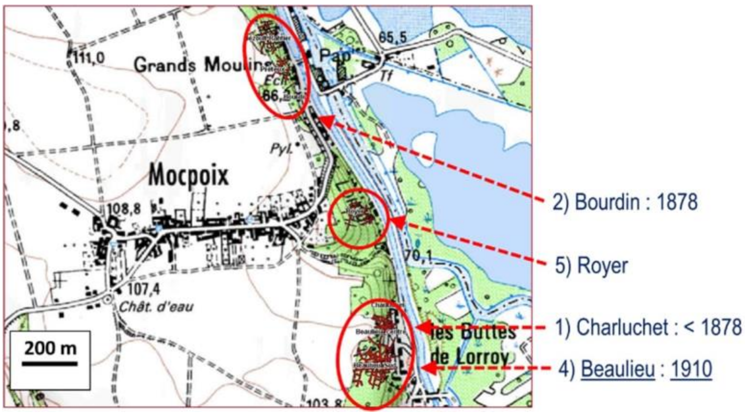

Figure 1   Localisation of the Château-Landon underground chalk mine (France), 1878, 1910: are the dates of the previous collapses

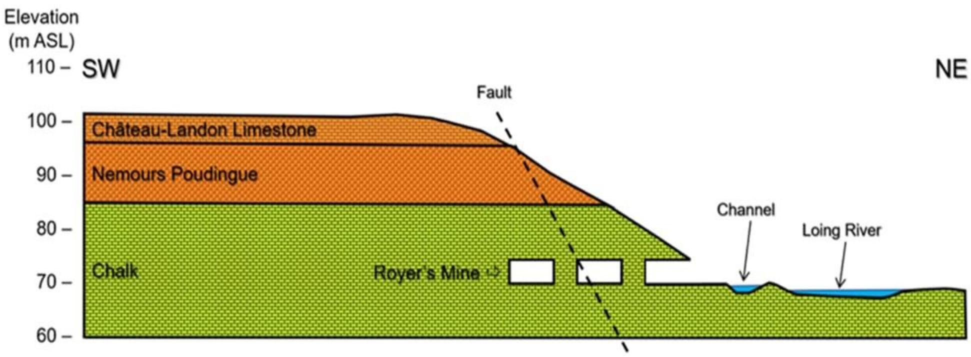

Figure 2   2D section illustrated the position of the chalk mine, the fault and the geology

Back analysis using 2D numerical modelling

Model description

To study the effect of the slope and fault, a 2D model of the mine collapsed in 1910 integrating a fault that cuts the cover and the various benches of the overburden as well as the cliff was produced (Figure 2). This model was based on observations and new data from the Royer mine, which reveal the presence of a fault-oriented North-South, with a slope of 70° relative to the horizontal. The mechanical characteristics of the chalk (Lafrance, 2016) result from laboratory characterization tests and the bibliography. Table 1 and 2 present the geomechanical characteristics of the different layers, joints, and fault (Figure 2).

Layer	Density	Young Modulus	Poisson ratio	Cohesion	Friction angle	Compression strength*	Tensile strength
Unit	kN/m^3	MPa		MPa	(°)	MPa	MPa
Unsaturated Chalk	20	500	0.22	1	30	3.5	0.2
Saturated chalk	20	100	0.23	0,35	30	0.9	0.2
Poudingue	22	2000	0.30		Elastic		
Limestone	25	4000	0.30				

Table 1   Geomechanical characteristics of the different rock layer

Joints/fault	Normal stiffness	Tangential stiffness	Cohesion	Friction angle	Tensional strength
Unit	MPa/m	MPa/m	MPa	(°)	MPa
Fault	298	205		30	
Degraded fault	298	205		10	
Horizontal joints	2500	1150	5	45	5

Table 2 Geomechanical characteristics of the joints (discontinuities) and fault

Five configurations were tested (Figure 3): • The first corresponds to a reference configuration (mine excavation without fault and slope); • The second corresponds to a configuration in the presence of a cliff but without fault; • The third corresponds to a configuration with a cliff cut by a fault at the front of the mine; • The fourth corresponds to configuration 3, but the fault cuts the mine in the middle; • The last configuration (configuration 5) is similar to configuration 3, but the fault is located at the border of the mine. The position of the fault was chosen to illustrate the role of the fault without necessarily corresponding to the exact configurations of the mine of Beaulieu (40 m) and Royer (60 m). A parametric study will be conducted to clarify the influence of the dip.

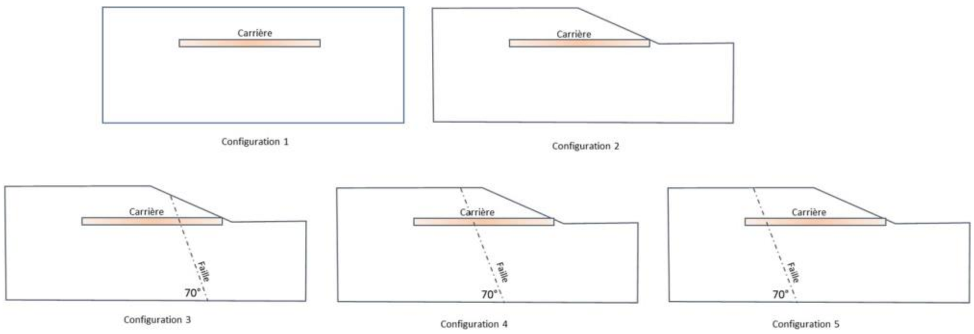

Figure 3 Different configurations for studying the effect of the slope and the fault

Results and conclusion

The stress, strain and displacement distributions are obtained thanks to the numerical modelling. The analysis herein is focused on the specific stress distribution related to two geometric and geologic aspects (slope and fault). The results highlighted the role of the reduction of the friction angle of the main fault and of the strength of the chalk layer (Figure 3).

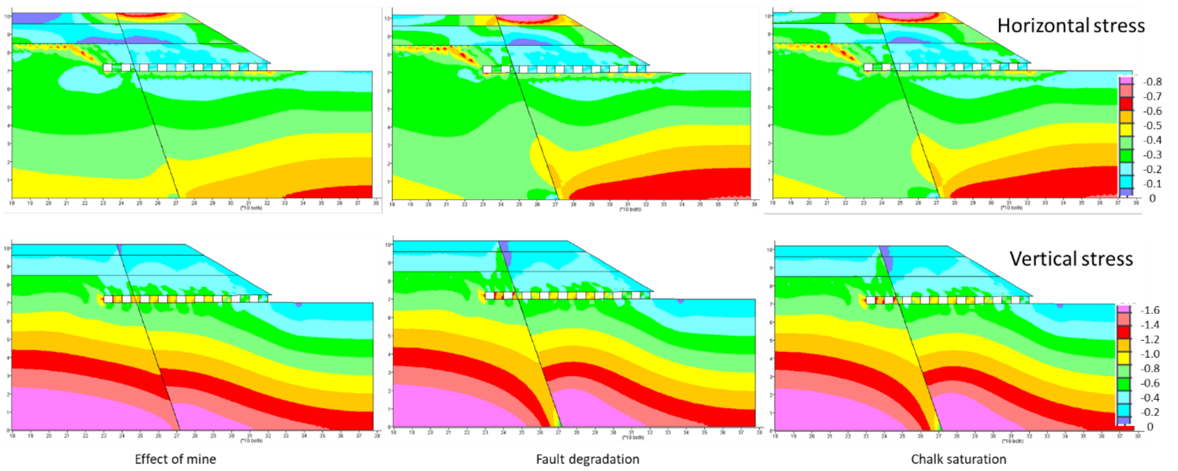

Figure 4 Numerical modelling results, stress distribution (horizontal and vertical) for the configuration (5) and for three scenarios: effect of mine excavation, plus effect of fault degradation and effect of chalk saturation

Figure 4 presents the results for the configuration 5 (effect of mine, fault degradation and chalk saturation). It is noted that horizontal tensile stresses (blue zones) developed in the steeper beds (limestone and puddingstone) are greater in the case where the chalk is saturated. The presence of the fault also changes the stress distribution: significantly lower tensile and compressive stresses are obtained the area behind the fault. The horizontal compressive stresses of the pillars are lower than in the case without cliffs or faults (red zones). On the other hand, the vertical stresses in the pillars located just behind the fault increase. In addition, the vertical stresses at the level of the fault plane are normal tensile or compressive stresses of low amplitude. The relaxation of the fault, or the decrease in the vertical stress, is maximum after the reduction of the friction angle of the fault to 10°. This configuration, which corresponds to a fault crossing the mine and located inside the massif, seems to be the most critical.

Figure 5 presents the suggested mechanism to explain the mine collapse and landslide. The water effect, due to a heavy raining and water table raising, is the main trigger factor. The increasing of the water content decreases the strength of the chalk and the fault.

However, that is not explained the role of the slope and the fault. In fact, the geological and topographic elements induce tensional stresses, the water saturation of the chalk and the presence of the fault increase the tensional stress and contribute to the landslide and the collapse of this old active mine. Based on in-situ observation and the analytical and numerical sensitive studies, one can make the following observation: the collapse is related to the presence of the slope, the fault and the stiff bed which together modify the induced stress. The combination of the geometrical (slope and fault) and the geomechanical modifications (reduction of the mechanical characterisation of the fault and the chalk layer) can explain the collapse.

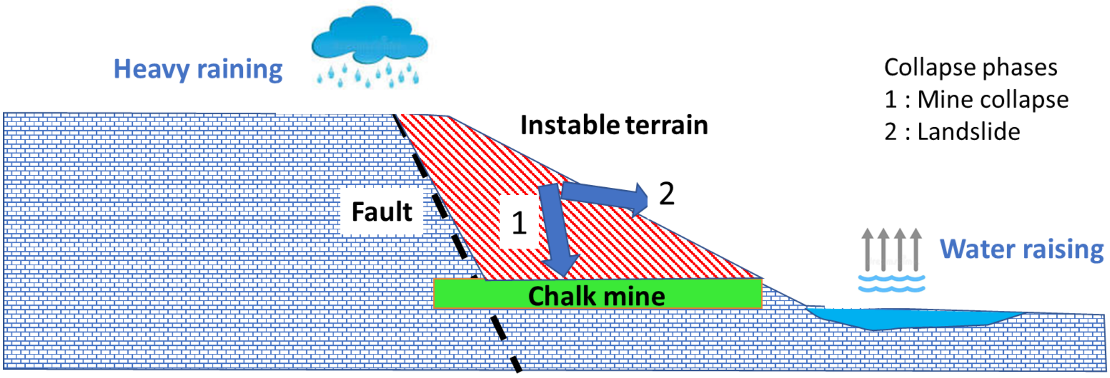

Figure 5 Suggested mechanism and phases to explain the historic collapse of the underground chalk mine

References

Al Heib, M., Duval, C., Theoleyre, F., Watelet, J-M., Gombert, P. (2015). Analysis of the historical collapse of an abandoned underground chalk mine in 1961 in Clamart (Paris, France). *Bulletin of Engineering Geology and the Environment* 74: 1001-1018. https://doi.org/10.1007/s10064-014-0677-6.

Gombert, P., Cherkaoui, A. (2013*). Role of water in the stability of abandoned and partially or temporarily flooded underground quarries and expected impact of climate change.* Tunnels and Underground Areas 240: 468-482.

Lafrance, N. (2016). Study of the effects of water on the phenomena of rupture and deformation affecting underground chalk quarries. *PhD thesis, University of Lorraine*.

Watelet, J-M., Kreziak, Ch., Al Heib, M. (2016). Analyse and questioning on 1910 collapse of Lorroy chalk underground quarry. *Journées Nationales de Géotechnique et de Géologie de l'Ingénieur – Nancy France.*

Land Subsidence Phenomena in Lowlands Occupied by Organic Soils. The Cases of the Densely Urbanized Coastal Cities of Messolonghi and Aitolikon (Greece)

N. Antoniadis[1], S. Alatza[2], C. Loupasakis[1], C. Kontoes[2]

1 School of Mining & Metallurgical Engineering, National Technical University of Athens, Athens, Greece
2 National Observatory of Athens, Institute for Astronomy and Astrophysics, Space Applications and Remote Sensing, BEYOND Center for EO Research and Satellite RS, Athens, Greece

antoniadis.nickolas@gmail.com

Abstract

The current study aims to focus on the surface deformation occurring in urban coastal areas founded on lowlands occupied by organic soils. The cities under investigation are Messolonghi and Aitolikon. Low-rate surface displacements have been reported along these sites, often resulting in building damages. The gradual subsidence of the sites combined with the climate change impact, resulted the last years to the occurrence of multiple floods. The rush of the sea water over the lowlands, has also been reported. The overexploitation of the underground water, the natural compaction of the under-consolidated clay soil layers, the consolidation due to the external loading of the constructions, the oxidation of the organic soils, the land use, the use of Synthetic Aperture Radar Interferometry (InSAR) and ground truth data were all examined collectively in order to comprehend this phenomenon. In the town of Messolonghi a variety of LOS deformation rates were recorded, with the maximum mean values in the eastern part (- 5mm/yr), whereas in Aitolikon the maximum values were in the range of - 4.5 mm/year. The displacements are mostly attributed to the building loads and natural compaction of the formations; however, it is evident that the increased precipitation rates and sea level rise, play a driving role in the occurrence of constant floods.

Introduction

The current study aims to focus on the surface deformation occurring in urban areas founded on lowlands occupied by organic soils. The cities under investigation are Messolonghi, a historical city of Greece, and Aitolikon, the so-called little Venice of Greece, which are located in Aitoloakarnania prefecture (Figure 1). In order to fully determine the phenomena occurring in these areas, results from the satellite data processing were examined together with the geological structure of the area as well as geotechnical study data gathered from a variety of sources.

Over the past few years, floodings and building damages have been reported in these rural areas. No previous research pertaining to the surface deformations and investigation of its causes, have been conducted to our knowledge. The study area is a densely populated environment, a fact that increases awareness towards this region and this phenomenon, as the risk and vulnerability from this geohazard are significant.

The gradual subsidence of the sites combined with the increasing mean annual precipitation rates, have resulted the last years to the occurrence of numerous floods. The rush of the sea water over the lowlands has also been reported. Both cities are densely populated and highly impacted by these displacements, which have resulted in numerous structural failures. These phenomena can be related with the exploitation of the underground water, the natural compaction of the under-consolidated clay soil layers, the consolidation due to the external loading of the constructions and the oxidation of the

organic soils. In the cities of Messolonghi and Aitolikon both uniform and differential settlements have been identified in many buildings, varying mainly in accordance to the foundation type.
The city of Messolonghi occupies a flat lowland and is founded on Quaternary formations consisting of fine grain sediments (clays, silts, and sands). On the other hand, Aitolikon was founded on an artificial island, constructed by earth fill materials deposited on top of 4 to 5 very small islands located in the center of the Aitolikon lagoon.

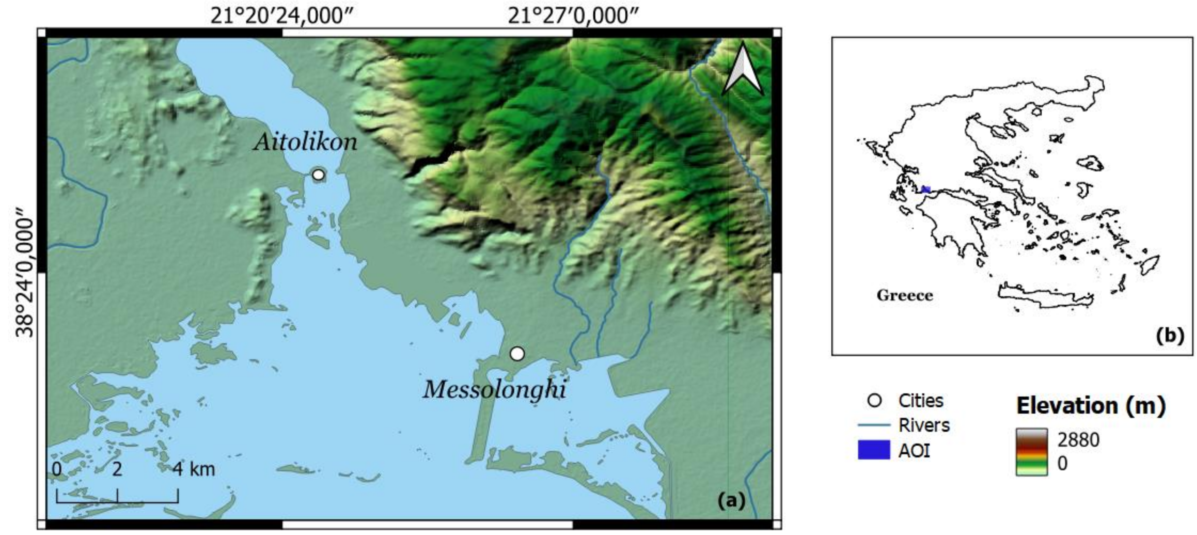

Figure 1. (a) The cities of Messolonghi and Aitolikon & (b) Location of study area

Methods

The investigation was divided into two phases:

Phase 1: Analysis of satellite data for a 7-year period (November 2015-February 2022)
The main tool for the analysis of the satellite data was the Stanford Method for Persistent Scatterers (StaMPS) (Hooper et al., 2007), enabling small-scale surface deformation monitoring over large time spans. Multi-temporal SAR (Synthetic Aperture Radar) interferometry is considered as a well-established method for monitoring ground displacements phenomena and is successfully applied in a variety of Earth deformation studies (Svigkas et al., 2020; Alatza et al., 2020[a], 2020[b]; Kontoes et al., 2021, 2022). 161 and 120 Sentinel-1A and 1B SLC images, from both descending and ascending satellite passes respectively, operated by the European Space Agency (ESA), were processed with the parallelized Persistent Scatterer Interferometry (P-PSI) processing chain (Papoutsis et al., 2020), developed in the Operational Unit BEYOND Center of EO Research and Satellite RS of the National Observatory of Athens (NOA). The estimated LOS (Line Of Sight) displacements provided insights on whether there is a considerable continuing hazard at the sites of interest. The timeseries exported during the investigation were also compared to the results presented from the European Ground Motion Service of Copernicus. The EGMS is the largest wide-area A-DInSAR service ever conceived. The EGMS aims to provide reliable information regarding natural and anthropogenic ground motion phenomena over Europe for the study of geohazards and human-induced deformation such as slow-moving landslides, subsidence due to groundwater exploitation or underground mining, volcanic unrests and many more (Costantini et al., 2021).

Phase 2: Analysis and statistical processing of all available geological and geotechnical data gathered from EAGME, Central Laboratory of Public Works and TCG archives. A total of 44 drilling profiles and over 100 oedometer tests were gathered for the city of Messolonghi. Moreover, field campaigns were carried out in these areas to record building damages.
The velocities of permanent scatterers combined geological, geotechnical, hydro-geological data, sea level rise and precipitation data validated the observed permanent scatterers negative velocities and enabled a more accurate interpretation of the phenomenon.

Results

As indicated in Figure 2 the deformation rates in Messolonghi vary. On the north part of the town the identified PS indicate relatively stable ground conditions, during the investigated time period, since the LOS values range from 0.3 – 1.3 mm/year. However, on other parts of the town the recorded deformations are higher. The east part of Messolonghi is an area with significant LOS deformations with a mean rate of −5mm/yr. The south and west parts of the town present a mean rate of -2.5mm/yr and -3mm/yr respectively. It is worth mentioning that the estimated subsidence rates increase towards the coastline.

Numerous buildings are affected by this subsidence phenomena, such as the buildings of Prefectural Administration of Aitoloakarnania, of the Port Authority and of the Public Finance Service of Messolonghi, as well as many residential buildings.

Drillings performed in the area indicate that the soil layers are extended horizontally along the site without any significant variations in thickness among which organic clay horizons with a thickness up to 5m, organic clayey silt to silt horizons, 5-10 m thick, and clayey sand to sand horizons with a thickness of 2-5m. The organic clay horizon contains a significant amount of plant residue and limestone fragments. According to laboratory tests that horizon is of low plasticity (I_p<14%) and can be described as soft to moderately stiff, with SPT values between 1 and 14. From the oedometer tests results it was discovered that the compression index values of those sediments are very high reaching up to 0.42. So, it is clear that the city is built on under consolidated formations subjected to subsidence due to natural compaction. Further investigations should be conducted for the identification of other co-acting mechanisms, such as ground water withdrawal or oxidation of organic soils.

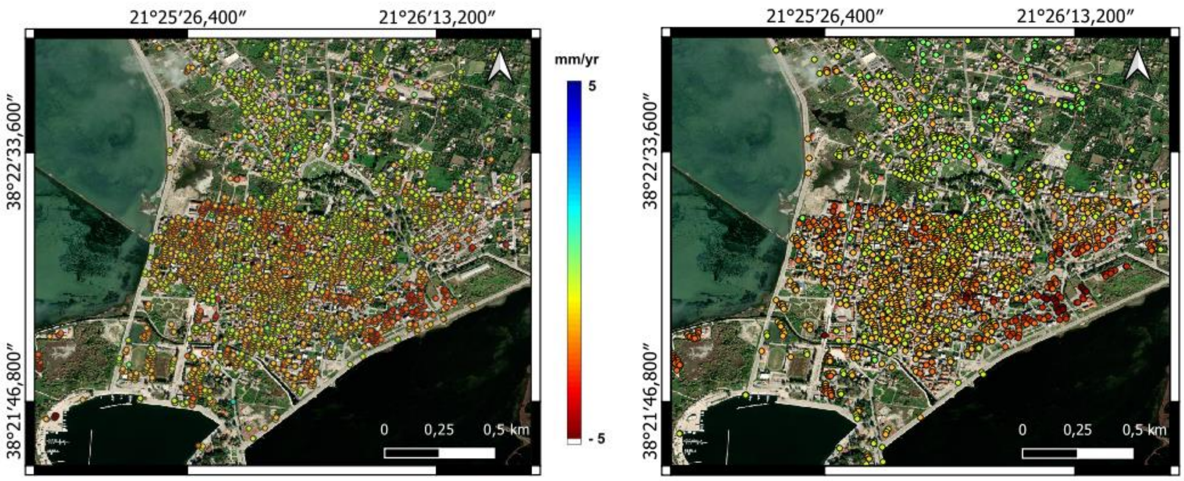

(a) (b)

Figure 2. (a) Spatial distribution of the Sentinel-1 LOS deformations in Messolonghi for the descending satellite pass (no. 80); (b) Spatial distribution of the Sentinel-1 LOS deformations in Messolonghi for the ascending satellite pass (no. 175).

In the city of Aitolikon maximum LOS deformation values reach a mean rate of −4 mm/yr. The highest deformations are observed in the south part of the Island, where Vaso Katraki Museum is located (mean values of 4.5 mm/year). In the north part of the town significant damages to buildings have been recorded. It is worth highlighting that in that area the houses' foundations were in the water before the addition of the 1969 filling.

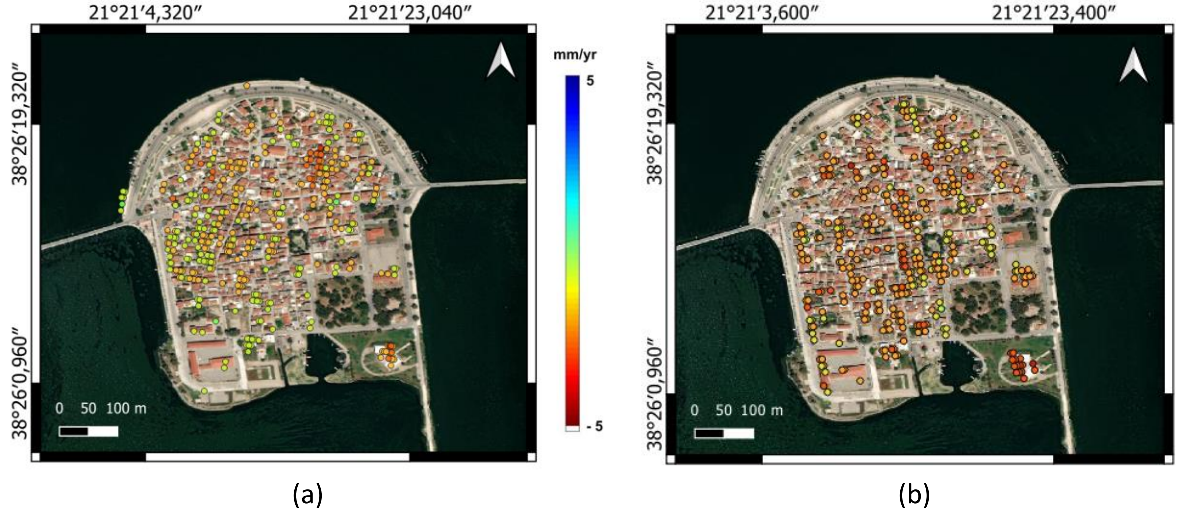

Figure 3. (a) Spatial distribution of the Sentinel-1 LOS deformations in Aitolikon for the descending satellite pass (no. 80); (b) Spatial distribution of the Sentinel-1 LOS deformations in Aitolikon for the ascending satellite pass (no. 175).

Conclusion

The 2015–2022 Sentinel 1 datasets, as well as the data provided by the European Ground Motion Service of Copernicus, were exploited to monitor the surface deformation in the areas of Messolonghi and Aitolikon. The analysis of SAR data proved that subsiding is still ongoing with a steady rate in both sites. During the study, PSI, geological and geotechnical data were evaluated. The deformation signals indicated subsidence in various areas of both cities. The geological and geotechnical data validated that the formations are rich in organic material and they are still under consolidated. These deformations are related to the natural compaction and probably to the oxidation of the alluvial deposits. The effect of the ground water fluctuation is still to be examined.

References

Alatza, S., Papoutsis, I., Paradissis, D., Kontoes, C., Papadopoulos, G.A., Raptakis, C. (2020) 'InSAR Time-Series Analysis for Monitoring Ground Displacement Trends in the Western Hellenic Arc: The Kythira Island, Greece', *Geosciences*, 10(8), p. 293. Available at: https://doi.org/10.3390/geosciences10080293

Alatza, S., Papoutsis, I., Paradissis, D., Kontoes, C. and Papadopoulos, G.A. (2020) 'Multi-Temporal InSAR Analysis for Monitoring Ground Deformation in Amorgos Island, Greece', *Sensors*, 20(2), p. 338. DOI: https://doi.org/10.3390/s20020338

Crosetto, M., Solari, L., Mróz, M., Balasis-Levinsen, J., Casagli, N., Frei, M., Oyen, A., Moldestad, D.A., Bateson, L., Guerrieri, L., Comerci, V., Andersen, H.S. (2020) 'The Evolution of Wide-Area DInSAR: From Regional and National Services to the European Ground Motion Service', *Remote Sensing*, 12(12), p. 2043. Available at: https://doi.org/10.3390/rs12122043

Hooper, A., Segall, P. and Zebker, H. (2007) 'Persistent scatterer interferometric synthetic aperture radar for crustal deformation analysis, with application to Volcán Alcedo, Galápagos', *Journal of Geophysical Research*, 112(B7), p. B07407. Available at: https://doi.org/10.1029/2006JB004763

Kontoes, C., Loupasakis, C., Papoutsis, I., Alatza, S., Poyiadji, E., Ganas, A., Psychogyiou, C., Kaskara, M., Antoniadi, S., Spanou, N. (2021) 'Landslide Susceptibility Mapping of Central and Western Greece, Combining NGI and WoE Methods, with Remote Sensing and Ground Truth Data', *Land*, 10(4), p. 402. Available at: https://doi.org/10.3390/land10040402

Kontoes, C., Alatza, S., Chousianitis, K., Svigkas, K., Loupasakis, C., Atzori, S., Apostolakis, A. (2022) 'Coseismic Surface Deformation, Fault Modeling, and Coulomb Stress Changes of the March 2021 Thessaly, Greece, Earthquake Sequence Based on InSAR and GPS Data', *Seismological Research Letters*, 93(5), pp. 2584–2598. Available at: https://doi.org/10.1785/0220210112

Papoutsis, I., Kontoes, C., Alatza, S., Apostolakis, A., Loupasakis, C. (2020) 'InSAR Greece with Parallelized Persistent Scatterer Interferometry: A National Ground Motion Service for Big Copernicus Sentinel-1 Data', *Remote Sensing*, 12(19), p. 3207. Available at: https://doi.org/10.3390/rs12193207

Svigkas, N., Loupasakis, C, Papoutsis, I., Kontoes, C., Alatza, S., Tzampoglou, P., Tolomei, C., Spachos, T. (2020) 'InSAR Campaign Reveals Ongoing Displacement Trends at High Impact Sites of Thessaloniki and Chalkidiki, Greece', *Remote Sensing*, 12(15), p. 2396. Available at: https://doi.org/10.3390/rs12152396

Evaluation and mitigation of soil subsidence in Mexico City

Gabriel Auvinet-Guichard[1] , Edgar Méndez-Sánchez[1], Moisés Juárez-Camarena[1].

1 Instituto de Ingeniería/UNAM, Mexico.

GAuvinetG@iingen.unam.mx

Abstract

The general subsidence of the lacustrine zone of Mexico Valley has serious implications for the conservation of the urban heritage and proper functioning of public utilities in the Mexican Capital. It is well known that subsidence is mainly a consequence of extraction of potable water from the deep aquifers located below the metropolitan area. This paper presents a brief state of the knowledge on this phenomenon and describes the actions undertaken to obtain a more accurate and updated information on its evolution. Possible strategies that could be considered to mitigate the consequences of subsidence and to control the phenomenon are also reviewed.

Introduction

The demographic development of Mexico City has created an accelerated demand for services, among which stands out supply of drinking water. One of the cheapest ways to respond to this demand has been the exploitation of the aquifer underneath the urban area by pumping water from deep wells. This activity has produced a regional subsidence phenomenon of the lake and alluvial-lacustrine areas of Mexico City. Due to the high cost of other alternatives, it is expected that extraction of water from the local aquifer will continue for many years. The regional subsidence in Mexico City affects the drainage system, transport infrastructure, foundations of buildings and generates serious risks to the population, since it induces other problems such as flooding of low areas and fissuring of the highly compressible soil. Therefore, although the regional subsidence is an ancient phenomenon, its study and analysis remain a priority nowadays.

Evaluation of regional subsidence

Based on the historical data and on the results of systematic levelling surveys performed in Mexico City during more than 100 years, it has been possible to reconstruct the history of the regional subsidence at some points of the downtown area of the City (Fig. 1). It has also been possible to define the original topographic configuration of the Valley of Mexico, prior to the start of water pumping from underground aquifers, on the basis of technical reports of geodesic and topographic surveys carried out in 1856.

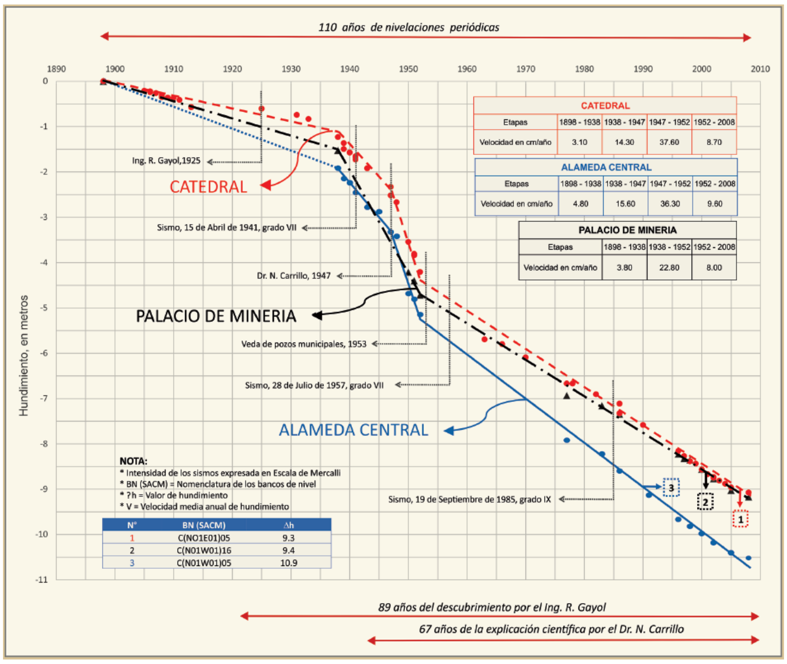

Figure 1 Evolution of regional subsidence at three sites of the Historic Center of Mexico City (Metropolitan Cathedral, Mining Palace and Alameda Central park) from 1898 to 2008. (horizontal scale: time in years; vertical scale: accumulated subsidence in meters)

A decision has been made to modernize the Monitoring System of piezometer readings and regional subsidence to suit the actual conditions of the urban zone covering the Valley of Mexico. For this purpose, in 2013, support was received to launch a system known as *"Sistema de Monitoreo de la Piezometría y de los Hundimientos del Valle de México por extracción de agua subterránea (*SIMOH*, Monitoring System of Piezometry and Subsidence of Mexico Valley due to water extraction",* Auvinet *et al.,* 2015) at the Laboratory of Geo-Informatics of *Instituto de Ingeniería (Institute of Engineering),* UNAM.

The SIMOH system generates databases and Geographic Information Systems containing historical and recent information on piezometric behaviour and on the subsidence of the Valley of Mexico. SIMOH was initially focused on the collection, retrieval and processing of information and on the diagnosis of the current status of the instrumentation, including an inventory of the existing benchmarks, piezometers and water wells.

To evaluate the spatial distribution of the regional subsidence covering the wide area occupied by the former lakes of the Valley of Mexico, a Geographic Information System was developed to store the huge collection of numerical data coming from the levelling surveys executed in a period of more than 100 years so as to expedite their processing and analysis.

Rates of subsidence in the Valley

The evaluation of the subsidence phenomenon implies basically the execution of periodic observations of the pore water pressure conditions existing in typical strata of the subsoil together with leveling of superficial benchmarks.

Figure 2 shows the spatial distribution of the subsidence rate for the 1999–2008 period in the lacustrine zone of the Valley of México (Auvinet et al., 2017). It can be noticed that the settlement rate is close to 40cm/year at some points. This map was plotted by combining topographical data supplied by several agencies and results of indirect measurements performed using the LIDAR and INSAR techniques. A geodetic network consisting of a number of GNSS stations is being implemented in Mexico Valley to improve the accuracy of indirect measurements. Mention should be made that at present the sites with the fastest rates are no longer located in the downtown area of the City but rather at several sites to the east and south of the Valley of Mexico. These sites correspond to the zones where the thickest clay deposits are found in the subsoil.

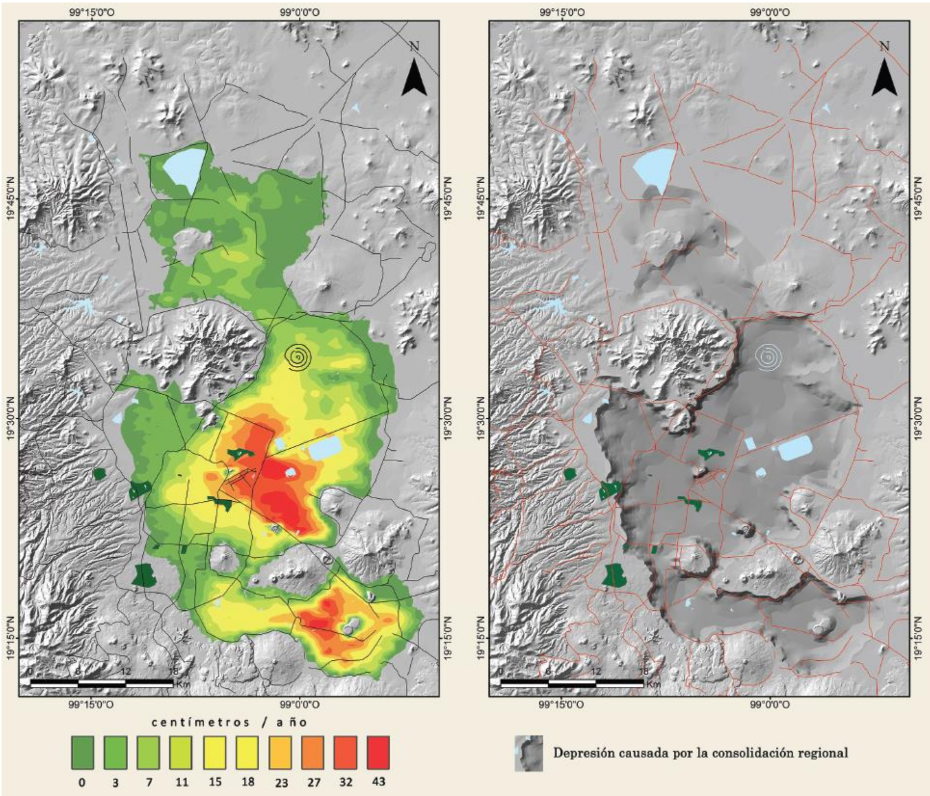

Figure 2 Mapping of rates of regional subsidence (in cm/year) and depression created by this phenomenon.

Perspectives for control of subsidence and mitigation of its effects

The control of subsidence demands the implementation of a policy for water supply different from the present one (Tortajada & Castelán, 2003). To be able to reduce local pumping it is possible to exploit external or deeper sources (Aguirre, 2014), although priority should be assigned to other actions such as the promotion of a more rational use of water and effective control of leaks in the potable water distribution network.

Strategies based in the concept of sustainability have been proposed to attain this objective (Calderhead et al., 2012; Reséndiz et al., 2016). It has also been suggested to adopt a pumping strategy such that, at no point of the subsoil, the overconsolidation pressure is exceeded (Larson et al., 2001; Reséndiz et al., 2016).

Locally, the possibility exists of a partial control of the subsidence effects. For this purpose, in several projects, the injection or extraction of water from the clays of the upper clay formation has been attempted (Pliego, 2008). It has also been proposed to resort to the injection of water into the pervious strata interbedded in the aquitard and, in particular, into the so called “first hard layer”. This possibility has been evaluated theoretically (García et al., 2012). The results obtained tend to demonstrate that with reasonable flow rates of water injected in the subsoil it would be possible to protect very important areas such as the Historic Center of Mexico City against the main effects of the regional subsidence. These conclusions should be, however, confirmed by the results of large scale trial injection tests.

Mitigation of the effects of subsidence demands on the other hand the development of increasingly refined methods of design of the civil works. Deep extensometers have been used to assess the contribution of different strata to the subsidence (Rángel, 2021). This information is required for a realistic evaluation of the effects of subsidence on deep foundations and underground structures, including negative skin friction.

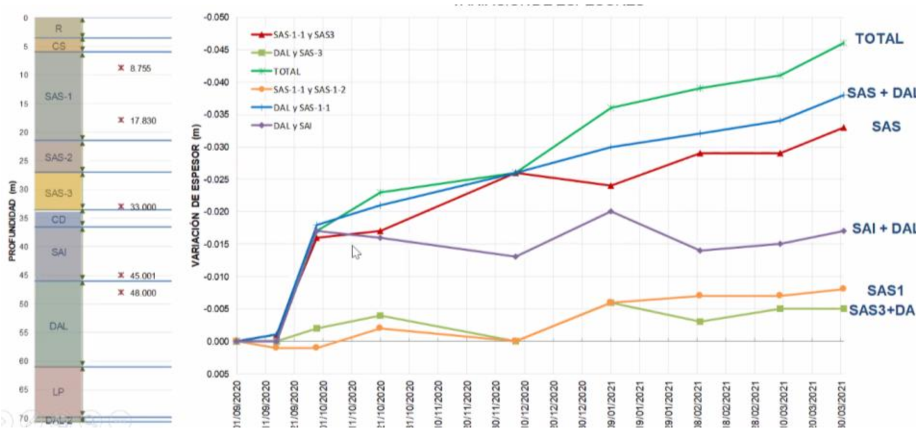

Figure 3   Contribution of different strata to the total subsidence.

Conclusion

The efforts undertaken by different groups and in particular by the Geo-Informatics Laboratory of the Engineering Institute, UNAM to achieve a satisfactory evaluation of the phenomenon of subsidence in Mexico City, and to deal with other geotechnical problems such as soil fissuring have given useful and promising results, but this is only the first stage of a huge job to be performed consistently in the future.

References

Auvinet, G., Méndez, E. y Juárez, M., 2015, Sistema de Monitoreo de la Piezometría y de los Hundimientos del Valle de México por extracción de Agua Subterránea (SIMOH), *Informe final de proyecto del Instituto de Ingeniería,* UNAM, Ciudad de México, México.

Auvinet, G., Méndez, E. and Juárez, M., 2017, "*The subsoil of Mexico City*, Vol. 3/El subsuelo de la Ciudad de México, Vol. 3", Instituto de Ingeniería, UNAM. ISBN Vol. 3 978-607-02-8198-3.

Calderhead, A.I., Martel, R., Garfias, J., Rivera, A. and Therrien, R., 2012, "Sustainable Management for Minimizing Land Subsidence of an Over-Pumped Volcanic Aquifer System", *Tools for Policy Design, Water Resources Management*, 26:1847–1864. DOI 10.1007/s11269-012-9990-7.

García, C., López Acosta N.P. y Auvinet, G., 2012, "*Análisis teórico para la inyección de agua en el subsuelo del valle de México*", Memoria, XXI Reunión Nacional de Mecánica de Suelos e Ingeniería Geotécnica, Sociedad Mexicana de Ingeniería Geotécnica, Cancún, Quintana Roo, México. Vol. 3: 1195-1204.

Larson, K. J., Basagaoglu, H., and Marino, M. A., 2001, "Prediction of optimal safe groundwater yield and land subsidence in the Los Banos-Kettleman City area, California, using a calibrated numerical simulation model", *Journal of Hydrology*, 242(1–2), pp. 79–102.

Pliego, L., 2008, "*Control de los efectos de la subsidencia regional mediante extracción e inyección de agua",* Proceedings, ISSMGE TC36 Workshop Geotechnical Engineering in Urban Areas Affected by Land Subsidence, pp. 117-130, Ciudad de México, México.

Rángel, J.L., 2021, "*Results of instrumentation, Barrio Letrán*", Personal communication.

Reséndiz, D., Auvinet G. y Méndez E., 2016, Subsidencia de la Ciudad de México: un proceso centenario insostenible, *Publicación en las Series del Instituto de Ingenie¬ría*, UNAM, Ciudad de México, México.

Tortajada, C. and Castelán, E., 2003, "Water Manage¬ment for a Megacity: Mexico City Metropolitan Area", *AMBIO,* 32(2):124-129. DOI: http://dx.doi.org/10.1579/0044-7447-32.2.124.

Land subsidence dynamics and inundation simulation in the Volta Delta: An application of InSAR and the Bathtub model

S.Y. Avornyo[1],* K.A. Addo[1], P. Teatini[2], P.S.J. Minderhoud[3] , E. Mahu[1], P. Jayson-Quashigah[4]

1 Department of Marine and Fisheries Sciences, University of Ghana, Accra, Ghana.
2 Department of Civil, Environmental and Architectural Eng., University of Padova, Italy.
3 Soil Geography and Landscape Group, Wageningen University, Wageningen, The Netherlands.
4 Institute for Environment and Sanitation Studies, University of Ghana, Accra, Ghana.

*Corresponding Author: syavornyo@st.ug.edu.gh

Abstract

Deltas are important coastal landforms that are home to diverse services. However, population growth and climate change along with their cascading impacts have had profound impacts on their topography and evolution. Consequently, many deltaic regions are subsiding and are incessantly plagued with hazards that are increasing in both magnitude and frequency. Coastal hazards such as flooding and erosion are already apparent in Ghana's Volta Delta. To provide a holistic understanding of the surge in inundation and erosion events in the Volta Delta, this study assessed altimetric changes in the Volta Delta to establish the subsidence regime and measure this against increasing rates of Sea Level Rise (SLR). Using Interferometric Synthetic Aperture Radar (InSAR) technique and Global Positioning System (GPS) surveys, interferograms of Sentinel-1 data from 2016 to 2020 indicated deformation rates ranging from -9.16 mm/yr to 1.77 mm/yr. The highest subsiding areas were within the floodplains of the dominant lagoons and along the Bight of Benin—areas heavily influenced by human activities. Albeit recording upliftment in fault-controlled areas, the Delta is considered a subsiding delta. The surface geology, which extensively (~70% areal coverage) constitutes compressible alluvial sand, silt and clay is posited to be a major natural driver of subsidence in the Delta. An inundation risk assessment using a simple Bathtub model and IPCC projections was investigated for both SLR and Relative SLR (rSLR) scenarios. Under the SLR scenarios, projections are that 25.29%, 26.29% and 29.68% of the Delta will be flooded by 2040, 2060 and 2100 respectively whereas 26.02% (2040), 27.09% (2060) and 30.78% (2100) of the Delta area will be flooded under the rSLR scenarios. Coupled with climate change, subsidence will increase the flood extents of the Delta by 19.79 km^2 and exacerbate the vulnerability of the Delta to other coastal hazards. To mitigate impacts, the study recommends the use of alternative and environmentally-friendly energy and water sources; a continuous and long-term monitoring framework for drivers of change; a hybrid approach and review of coastal management strategies; and the establishment of continuous GPS stations, tidal stations, and elevation benchmarks.

Introduction

Coastal areas are regions of essential value that provide a myriad of services. Consequently, little over half of the world's major urban communities are situated in coastal zones, and living within 100 km of these zones is forty percent of the global population (Nicholls et al., 2007). Chances are that these numbers may have surged based on global population growth rates of 0.9% as of 2021 (World Bank Group, 2022). However, coastal zones are increasingly having their makeup features, functioning, existence and services being threatened to points of complete collapse (Stouthamer & Asselen, 2015). Due to their settings, elevations and proximities to the sea, several human interventions and climate change amongst other natural occurrences, have been major factors impacting the sustainable usage of coastal zones, and their ecosystem services and landforms (Danladi et al., 2017). Additionally, coastal areas are being confronted with a far more immediate threat of sinking, thus subsidence which is exacerbating prevalent coastal hazards and devastating impacts of climate change (Brown & Nicholls, 2015; Johnston et al., 2021; Restrepo-Ángel et al., 2021). Globally, deltas—one of several coastal landforms—are not exempted. Population growth in deltaic regions coupled with infrastructure developments and rising sea levels have had a profound impact on their topography (Styvitski et al., 2009). Many deltaic regions around the globe are losing land and subsiding (Brown et al., 2018; Nienhuis and van de Wal, 2021).

The study, therefore, seeks to establish the subsidence regime in Ghana's Volta Delta using geodetic methods, to provide a holistic understanding of the frequent flooding and erosion events in the Delta. Additionally, it seeks to assess the future flood vulnerability of the Delta by simulating future Sea Level Rise (SLR) and Relative Sea Level Rise (rSLR) scenarios.

Methods

PSI Analysis using the SNAP to StaMPS Approach

The satellite data used are Sentinel-1 (S1) Single Look Complex (SLC) Synthetic Aperture Radar (SAR) images which are freely accessible on the Copernicus Science Hub online platform—356 SAR images in total. The InSAR technique employed for this study was the Persistent Scatterer Interferometry (PSI) technique based on the Permanent Scatterer algorithm by Ferretti et al., (2001) and following the workflow of Höser (2018) and Cian et al. (2019). The PSI analysis was done using the Sentinel Application Platform (SNAP) software, Version 8 and the Stanford Method for Persistent Scatterers (StaMPS)/Multi-Temporal InSAR open-source toolbox, Version 4.1b (Hooper et al., 2012). Global Positioning System (GPS) survey on some Ground Control Points (GCPs) was employed as a geodetic method to calibrate the results obtained from the InSAR processing technique (Teatini et al. 2012; Amato et al., 2020).

Simple Bathtub (Inundation) Model

Based on the assumption that the InSAR-derived deformation rates remained linear with no horizontal land motion, the bathtub model was used as a simple inundation model to predict coastal flooding and inundation extents (Leal-Alvesm et al., 2020; Alarcon et al., 2022) in the Volta delta at varying timescales for both SLR and rSLR scenarios. The IPCC (2021) categorized 2021 to 2040 as near-term; 2041 to 2060 as mid-term; and 2081 to 2100 as long-term, thus informing the selection of the years 2040, 2060 and 2100 as prediction timelines. The DEM used was the Multi-Error-Removed Improved-Terrain (MERIT) DEM developed by Yamazaki et al. (2017). Errors such as absolute bias, stripe noise, speckle noise, and tree height bias were removed from available spaceborne DEMs (Yamazaki et al., 2017). The global sea level rise projections were obtained from the IPCC Sixth Assessment Report (AR6), Working Group I (IPCC, 2021)—all projections are relative to the year, 1900. The Shared

Socioeconomic Pathways (SSP) scenario 5-8.5 (central, medium confidence) characterized by very high greenhouse gas emissions was selected.

Results

The number of persistent scatterers (PS) generated from the PSInSAR methodology was 119,477 in total with an areal PS density of 66.52 PS/km2—excluding the water-covered surfaces. Along the Sentinel-1 line of sight (LOS), the PS deformation velocities (Figure 1) ranged from uplifting rates of 1.77 mm/yr to subsiding rates of -9.16 mm/yr. The number of PSs with uplifting rates was 0.19% of the total PSs obtained whereas the subsiding PSs made up the remaining 99.81% of the total PS number.

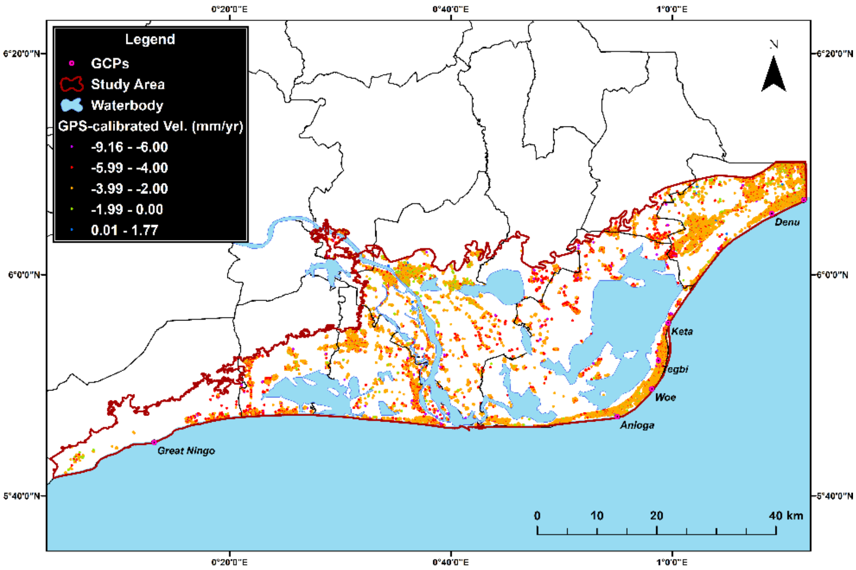

Figure 1 Map view of the line of sight (LOS) mean velocities of PSs in the Volta delta

Flood projections based on projected rSLR and SLR were done using the simple bathtub model to map out inundation-prone areas or hotspots within the Volta (Figure 2).

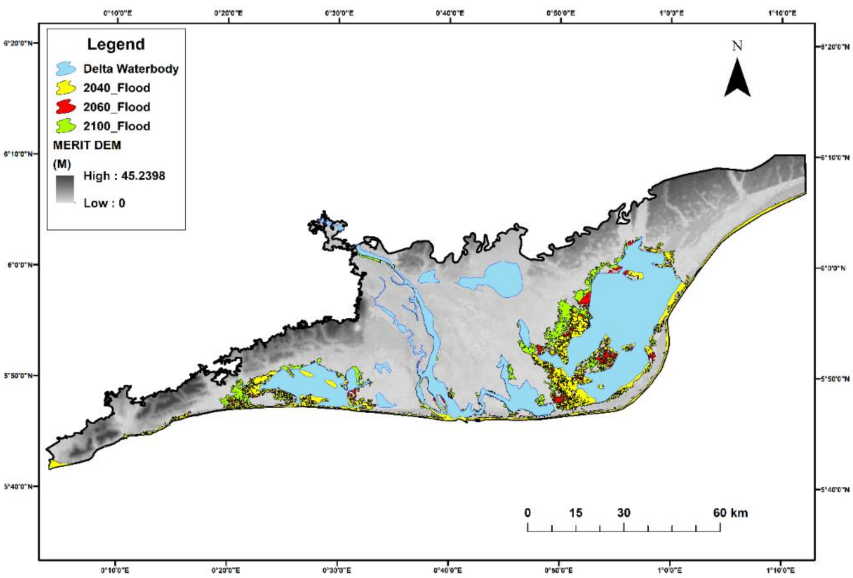

Figure 2 A map view of rSLR inundation projections in the Volta Delta using the bathtub model

The inundation risk assessment using a simple Bathtub model and IPCC projections was investigated for both SLR and rSLR scenarios. Under the SLR scenarios, projections are that 25.29%, 26.29% and 29.68% of the Delta will be flooded by 2040, 2060 and 2100 respectively whereas 26.02% (2040), 27.09% (2060) and 30.78% (2100) of the Delta area will be flooded under the rSLR scenarios (Figure 3A). The differences in the extent of areal flooding between rSLR and SLR show an inclining trend from 2040 to 2100 (Figure 3B).

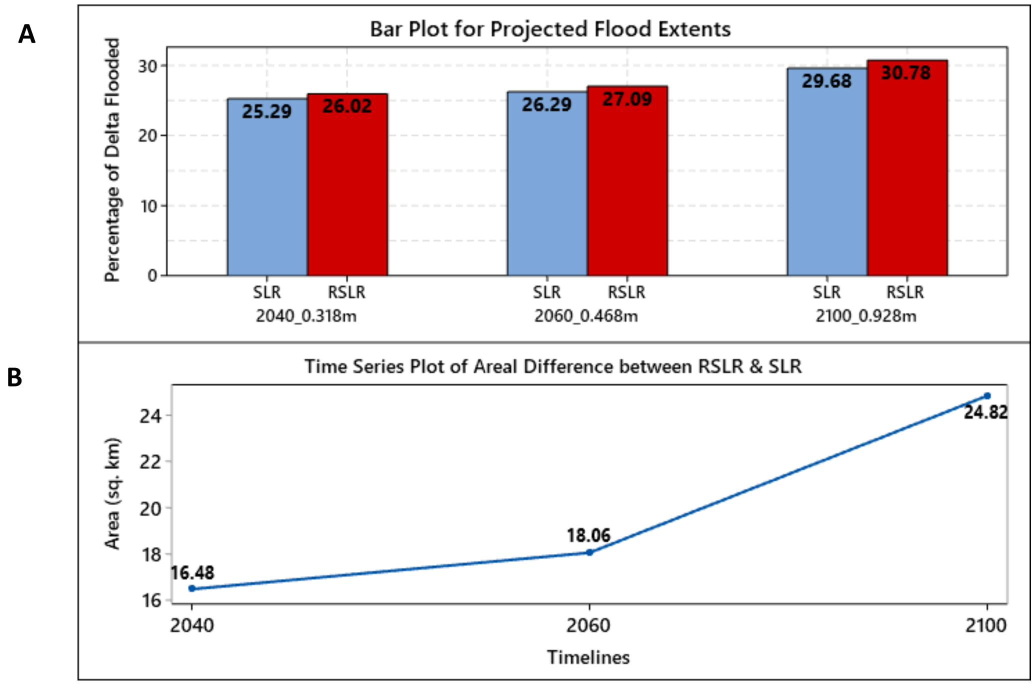

Figure 3 A graph showing projections of Delta flood extents and areal differences between SLR and rSLR scenarios

Conclusion

Based on the dominance of PSs (over two-thirds of total PSs) with subsiding rates, the Volta Delta is classified as a subsiding delta. Areas mostly located within the floodplains of the two dominant lagoons and lower Delta plain recorded subsiding velocities exceeding -8 mm/yr. The coastal stretch from Keta to Hlorve has been identified as one of the most subsiding areas and is already a hotspot for periodic floods and erosion. Subsidence in coastal hotspots will increase the depth and coverage extent of the floods. The inundation projections in this study for both SLR and rSLR scenarios suggest a substantial surge in Delta inundation along with more devastating impacts even in the near term (2040). The projection timelines show an inclining trend in areal inundation for both SLR and rSLR with a minimum of 29.68% of the Delta area being inundated by the end of the century. Averagely, subsidence (rSLR) will increase the flood extents of the Delta by 19.79 km^2 when compared to SLR scenarios. These findings, therefore, accentuate the need to implement measures to stall the impending threats subsidence poses to the sustainable use of the Volta Delta.

References

Alarcon, V. J., Linhoss, A. C., Kelble, C. R., Mickle, P. F., Sanchez-Banda, G. F., Mardonez-Meza, F. E., ... & Ashby, S. L. (2022). Coastal inundation under concurrent mean and extreme sea-level rise in Coral Gables, Florida, USA. *Natural Hazards*, 111(3):2933-2962, https://doi.org/10.1007/s11069-021-05163-0

Amato, V., Aucelli, P. P. C., Corrado, G., Di Paola, G., Matano, F., Pappone, G., & Schiattarella, M. (2020). Comparing geological and Persistent Scatterer Interferometry data of the Sele River coastal plain, southern Italy:

Implications for recent subsidence trends. *Geomorphology*, 351, 106953. https://doi.org/10.1016/j.geomorph.2019.106953

Brown, S., & Nicholls, R. J. (2015). Subsidence and human influences in mega deltas: The case of the Ganges–Brahmaputra–Meghna. *Science of the Total Environment*, 527–528, 362–374. https://doi.org/10.1016/j.scitotenv.2015.04.124

Brown, S., Nicholls, R. J., Lázár, A. N., Hornby, D. D., Hill, C., Hazra, S., … Tompkins, E. L. (2018). What are the implications of sea-level rise for a 1.5, 2 and 3 °C rise in global mean temperatures in the Ganges-Brahmaputra-Meghna and other vulnerable deltas? *Regional Environmental Change*, 1–14. https://doi.org/10.1007/s10113-018-1311-0

Cian, F., Blasco, J. M. D., & Carrera, L. (2019). Sentinel-1 for monitoring land subsidence of coastal cities in Africa using PSInSAR: A methodology based on the integration of SNAP and staMPS. *Geosciences (Switzerland*), 9(3). https://doi.org/10.3390/geosciences9030124

Danladi, I. B., Kore, B. M., & Gül, M. (2017). Vulnerability of the Nigerian coast: An insight into sea level rise owing to climate change and anthropogenic activities. *Journal of African Earth Sciences*, 134, 493–503. https://doi.org/10.1016/j.jafrearsci.2017.07.019

Ferretti, A., Prati, C., Rocca, F., Inf, D.E., 2001. Permanent scatterers in SAR interferometry. IEEE *Transactions on Geoscience and Remote Sensing* 39 (1), 8–20.

Hooper A; Bekaert D; Spaans K; Arikan M (2012), Recent advances in SAR interferometry time series analysis for measuring crustal deformation, *Tectonophysics*, 514-517, pp.1-13. doi:10.1016/j.tecto.2011.10.013

Höser, T. (2018). Analysing the Capabilities and Limitations of InSAR using Sentinel-1 data for Landslide Detection and Monitoring. *University of Bonn*. https://doi.org/10.13140/RG.2.2.35085.59362

IPCC, 2021: Summary for Policymakers. In: *Climate Change 2021: The Physical Science Basis. Contribution of Working Group I to the Sixth Assessment Report of the Intergovernmental Panel on Climate Change* [Masson-Delmotte, V., P. Zhai, A. Pirani, S.L. Connors, C. Péan, S. Berger, N. Caud, Y. Chen, L. Goldfarb, M.I. Gomis, M. Huang, K. Leitzell, E. Lonnoy, J.B.R. Matthews, T.K. Maycock, T. Waterfield, O. Yelekçi, R. Yu, and B. Zhou (eds.)]. Cambridge University Press, Cambridge, United Kingdom and New York, NY, USA, pp. 3−32, doi:10.1017/9781009157896.001.

Johnston, J., Cassalho, F., Miesse, T., & Ferreira, C. M. (2021). Projecting the effects of land subsidence and sea level rise on storm surge flooding in Coastal North Carolina. *Scientific Reports*, 11(1), 1–13. https://doi.org/10.1038/s41598-021-01096-7

Leal-Alves, D. C., Weschenfelder, J., da Guia Albuquerque, M., de Almeida Espinoza, J. M., Ferreira-Cravo, M., & de Almeida, L. P. M. (2020). Digital elevation model generation using UAV-SfM photogrammetry techniques to map sea-level rise scenarios at Cassino Beach, Brazil. *SN Applied Sciences,* 2(12), 1-19.

Nicholls, R.J., Wong, P.P., Burkett, V., Codignotto, J., Hay, J., McLean, R., Ragoonaden, S.; Woodroffe, C. D.; Abuodha, P. A. O.; Arblaster, J.; Brown, B.; Forbes, D.; Hall, J.; Kovats, S.; Lowe, J.; McInnes, K.; Moser, S.; Rupp-Armstrong, S.; Saito, Y., 2007. Coastal systems and low-lying areas. In: Parry, M.L., Canziani, O.F., Palutikof, J.P., van der Linden, J.P., Hanson, C.E. (Eds.), # Climate Change 2007: Impacts, Adaptation and Vulnerability: Contribution of Working Group II to the Fourth Assessment Report of the Intergovernmental Panel on Climate Change. *Cambridge University Press*, Cambridge, UK, pp. 315–356. http://ro.uow.edu.au/scipapers/164

Nienhuis, J. H., & van de Wal, R. S. W. (2021). Projections of Global Delta Land Loss From Sea-Level Rise in the 21st Century. *Geophysical Research Letters*, 48(14), 1–9. https://doi.org/10.1029/2021GL093368

Restrepo-Ángel, J. D., Mora-Páez, H., Díaz, F., Govorcin, M., Wdowinski, S., Giraldo-Londoño, L., … Duque-Trujillo, J. F. (2021). Coastal subsidence increases vulnerability to sea level rise over twenty-first century in Cartagena, Caribbean Colombia. *Scientific Reports*, 11(1), 1–13. https://doi.org/10.1038/s41598-021-98428-4

Stouthamer, E., & Asselen, S. V. A. N. (2015). *DRIVERS OF DELTA SUBSIDENCE*. In IAHR World Congress (pp. 1–2). https://doi.org/10.1038/ngeo629.2

Syvitski, J. P. M., Kettner, A. J., Overeem, I., Hutton, E. W. H., Hannon, M. T., Brakenridge, G. R., … Nicholls, R. J. (2009). Sinking deltas due to human activities. *Nature Geoscience*, (September), 1–6. https://doi.org/10.1038/ngeo629

Teatini, P., Tosi, L., Strozzi, T., Carbognin, L., Cecconi, G., Rosselli, R., & Libardo, S. (2012). Resolving land subsidence within the Venice Lagoon by persistent scatterer SAR interferometry. *Physics and Chemistry of the Earth*, 40–41, 72–79. https://doi.org/10.1016/j.pce.2010.01.002

World Bank Group. (2022). Population growth (annual %). Retrieved from https://data.worldbank.org/indicator/SP.POP.GROW (Accessed on 26th July, 2022).

Yamazaki, D., Ikeshima, D., Tawatari, R., Yamaguchi, T., O'Loughlin, F., Neal, J. C., … Bates, P. D. (2017). A high-accuracy map of global terrain elevations. *Geophysical Research Letters*, 44(11), 5844–5853. https://doi.org/10.1002/2017GL072874

Poro-mechanical modelling of an in-situ loading experiment in a natural marsh in the Venice Lagoon

S. Baldan[1], M. Ferronato[1], A. Franceschini[1], C. Zoccarato[1], V. Girardi[1], P.S.J. Minderhoud[1,2], L. Tosi[3], M. Cosma[3], C. Da Lio[3], A. Bergamasco[4], and P. Teatini[1]

1 Department of Civil, Environmental and Architectural Engineering, University of Padova, Padova, Italy
2 Soil Geography and Landscape Group, Wageningen University, Wageningen, The Netherlands
3 Institute of Geosciences and Earth Resources, National Research Council, Padova, Italy
4 Institute of Marine Sciences, National Research Council, Venice, Italy

selena.baldan@phd.unipd.it

Session: Modelling and Matching of land subsidence – Coastal areas

Introduction

The survival of salt marshes is strictly connected to their elevation above mean sea level (MSL). The ability to keep up with sea-level rise is primarily controlled by the speed of sea-level rise, the amount of accumulated organic/inorganic sediments, and how fast the land is subsiding. Recent studies have shown that, in the absence of anthropogenic stressors, the elevation variation of a marshland surface is regulated by sediment deposition over the marsh surface, hydrological regime, erosion, and loss of vertical elevation due to natural compaction (Allen et al, 1999). The latter process, known as autocompaction, is caused by compaction of sediments under their own weight and can be significant in relatively young Holocene deposits (Zoccarato et al., 2018; Xotta et al., 2022). The hydro-geomechanical characterization of these young shallow deposits is not always straightforward. Gathering undisturbed samples for laboratory testing has many limitations because of the high porosity and compressibility of these loose sediments (Brain et al., 2015), and their high heterogeneity (Cola & Simonini, 2002), which makes small lab samples not representative for in-situ conditions and geomechanical behavior.

A campaign of novel in-situ loading tests was carried out in the Venice Lagoon (Italy) salt marshes from 2019 to 2022 (Zoccarato et al., 2022). In this work we describe the results of the first (out of four) loading test executed at the Lazzaretto Nuovo salt marsh and its model interpretation (Fig. 1). The experiment was set up to measure the salt marsh hydrological and geomechanical subsurface dynamics in undisturbed field conditions. The test replicates the standard oedometric test at the field scale, with loading conditions of a few kPa (i.e., the typical values driving autocompaction of shallow soils) and accounting for the vertical, in-situ heterogeneity of the marsh landform. The experiment consisted of several loading and unloading cycles with different duration and load, which was obtained by filling up to eight 500-l plastic tanks with seawater, for a maximum load of ~40 kN applied to a surface area of ~4 m2. A monitoring system tracks the marsh response to the applied loads using pressure and displacement transducers established at different depths and locations below the tanks. The collected measurements are interpreted using the 3-D coupled flow-deformation model by Ferronato et al. (2010), properly updated to account for the non-elastic constitutive relationship. The model was calibrated to provide reliable compressibility and hydraulic conductivity estimates for each monitored depth interval.

Methods

A coupled 3D poro-mechanical model solving the Biot (1941) equations was applied to reproduce the experimental loading test performed at the Lazzaretto Nuovo salt marsh. Specifically, we employed a three-field mixed (MFE) simulator, where the unknowns are the nodal displacements, Darcy's velocity through the element faces, and the elemental fluid pore pressure (Ferronato et al., 2010).

A hypo-plastic (or hypo-elastic) model is adopted to characterize the nonlinear constitutive relationship between the sediment compressibility and the vertical effective intergranular stress. The soil becomes stiffer as the vertical effective stress increases. The outcomes of the field experiment were used to calibrate the constitutive relationship describing the marsh mechanical behaviour. The initial parameters were estimated from the results of lab oedometric tests carried out on a few samples cored at the location of the experimental site.

The finite-element computational grid is more refined within the loading area and in the shallowest two m depth to obtain a more accurate solution in the part of the domain subjected to the largest stress changes. The subsurface build-up of the model was schematized to represent the lithological sequence resulting from sedimentary core analysis carried out at the site. A first 20-cm thick peat layer with the presence of halophyte roots overlies a silty soil. The presence of wooden pallets that support the tanks generating the load were also simulated. This rigid surface element ensures a uniform load distribution on the marsh surface. The wooden pallets and the deepest layers (below 6 m depth from the marsh platform) have been simulated using a linear elastic constitutive law with a prescribed constant stiffness E. The two superficial layers were simulated using a nonlinear soil compressibility vs effective stress constitutive law, whose coefficients together with the hydraulic conductivity, were calibrated. In addition, the role played by the mechanical hysteresis was accounted for during the unloading phase. The simulated domain is a portion of the lagoon subsurface with horizontal dimension 20 × 15 m and thickness 10 m, cantered at the applied load. The domain was discretized with 8-node hexahedral elements, totalling 217'392 nodes, 212'440 elements, and 642'216 faces where land displacements, groundwater pressure and velocity, respectively, were computed.

Results and discussions

Table 1 provides the hydro-geomechanical parameters obtained from the model calibration.

Parameters	Pallet	Superficial layer	Intermediate layer	Deep layer
Young modulus E (MPa)	10^4	-	-	10.0
Poisson coefficient ν (-)	0.2	0.2	0.2	0.2
Vertical permeability k_z (m/s)	5.0×10^{-7}	5.0×10^{-7}	5.0×10^{-6}	5.0×10^{-7}
Porosity	0.4	0.4	0.4	0.4
a (MPa^{-1})	-	230.0	572.0	-
b (-)	-	-7.5	-29.0	-
c (MPa)	-	0.2	4.0	-
Recompression ration r (-)	-	3.0	2.0	-
Surface void ratio (-)		1.8	0.8	

Table 1 Hydro-geomechanical parameters calibrated using vertical displacement and overpressure records from the field test conducted on the Lazzaretto Nuovo marsh. The coefficients a, b and c refer to a constitutive law of type $M = a\sigma_z^2 + b\sigma_z + c$ where M is the edometric module (MPa) and σ_z the effective intergranular stress (MPa).

The model results in terms of vertical displacements and overpressure during the main loading and unloading cycle are compared with field measurements at the sensor positions, i.e., at the surface (C0), at 0.1 m depth (C10, M10, E10) and 0.5 m depth (C50) (Fig. 1).

The comparison between the simulated and measured displacements in the field show that:

- the displacement dynamics over time is generally well captured by the model;
- the numerical model adequately reproduces the displacements measured below the artificial load. The maximum displacement during the loading phase amounts to 7 mm;

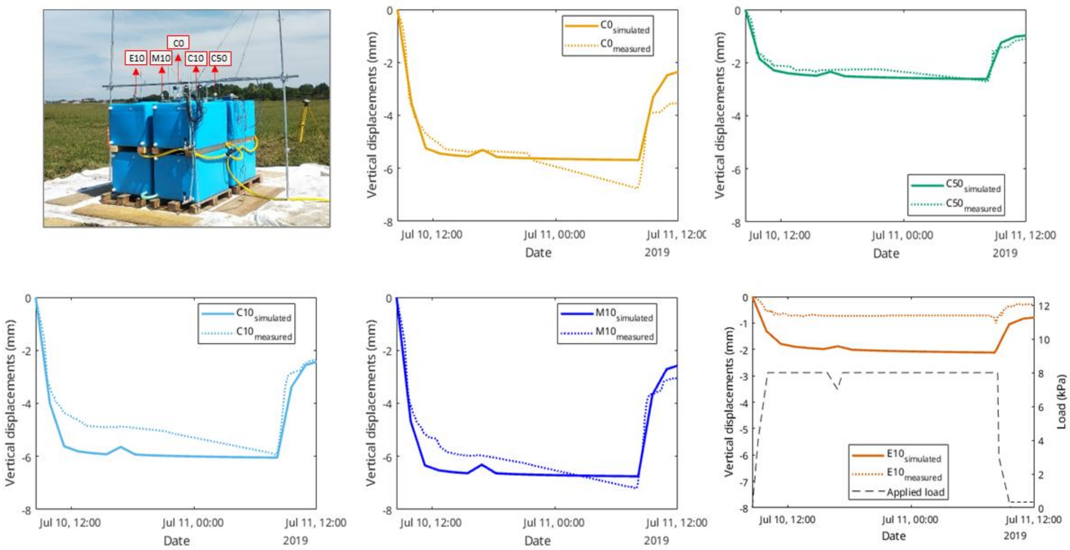

Figure 1 Vertical displacements vs time as measured by the sensors installed below the loading area and simulated with the mixed finite element numerical model. The comparison refers to a loading and subsequent unloading phase of about 8 kPa carried out during about one day. The top-left panel shows a photo of the loading experiment indicating the different sensors at the Lazzaretto Nuovo salt marsh.

- the displacements recorded by the external sensor E10 (1 mm) are overestimated by the model (2 mm);
- the unloading phase is properly simulated with a hysteresis factor of 3 for the superficial sediments and 2 for the underlying layer;
- the measured displacements show a linear deformation over time when the load is kept constant and the overpressure generated by the load itself dissipated (Fig.2). Clearly, creep (i.e., secondary, viscous deformation) characterizes this phase. However, the adopted constitutive law does not account for secondary deformation.

Fig. 2a shows a comparison of the pressure recorded by the piezometer in the most superficial layer (0.2 m depth) and the respective value provided by the model, which has been appropriately shifted to consider the depth of the measuring point. The tide significantly impacts the recorded trends and make the comparison with the model not straightforward. The main peak of the interstitial water pressure recorded by the sensor (about 0.30 m H2O) is caused by the tidal peak. The effect of the 8 kPa load and subsequent unloading may be quantified in 0.04-0.05 m. The two subpanels in Figure 2a show that the model outcome satisfactorily matches the over-pressure and under-pressure evolution over time and the maximum and minimum values. Fig. 2b shows the modelled overpressure for a vertical section across the loading area subsurface at three distinct moments, i.e., at beginning and the end of the loading phase and after the unloading.

Conclusions

In-situ loading tests and their numerical interpretation represent a powerful tool to understand the importance of natural soil compaction in controlling the capability of soil marshes to keep peace with sea-level rise. The reproduction of the experiment results through a fully-coupled geomechanical simulator has allowed the estimation of the hydrological and geomechanical properties of the superficial layers of salt marshes in the Venice Lagoon, at a scale much more representative than that of traditional laboratory tests. The calibrated constitutive law allows to satisfactorily capture the recorded movements throughout both loading and unloading stages, although it cannot reproduce the creep behavior. This effect will be the object of future work together with the analyses of datasets collected from other loading tests recently conducted in the Venice Lagoon. They will provide a first clear picture of the hydro-geomechanical variability of shallow soils in this unique depositional environment. The outcome highlights the importance to properly account for the role of the "subsurface system" when studying processes occurring on the marsh surface like sediment accretion. The geomechanical features that will derive from field experiment modelling will improve long-term biomorpho-geomechanical models of tidal marsh evolution.

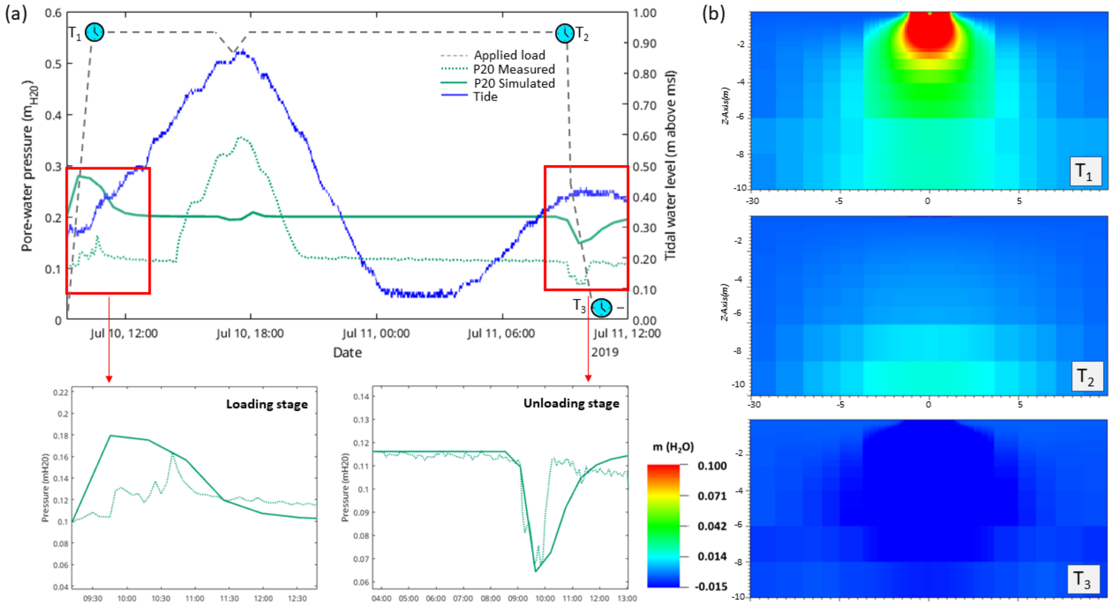

Figure 2 a) Comparison between measured and modelled overpressure (green). The two zoom windows (below) facilitate the comparison of measured and modelled overpressure during the loading and unloading stages. The tidal fluctuation and the behavior of the load applied on the marsh surface are provided. b) Overpressure on a vertical section through the load center as obtained with the calibrated model. The comparison refers to different temporal instants: (T1) 1.5 hours from the start of the load application, (T2) 24 hours after the load application, and (T3) at the end of the load removal.

References

Allen, J. R. L.: *Geological impact on coastal wetland landscapes: some general effects of sediment autocompaction in the Holocene of northwest Europe*. Holocene 9, 1–12, 1999.

Biot, M. A.: A general theory of three-dimensional consolidation. *J. Appl. Phys*., 12(2), 155–164, 1941.

Brain, M. J., Kemp, A. C., Horton, B. P., Culver, S. J., Parnell, A. C., and Cahill, N.: Quantifying the contribution of sediment compaction to late Holocene salt-marsh sea-level reconstruction, North-Carolina, USA, *Quaternary Res.,* 83, 1151, doi:10.1016/j.yqres.2014.08.003, 2015.

Cola, S. and Simonini, P.: Mechanical behavior of silty soils of the Venice lagoon as a function of their grading characteristics*, Can. Geotech. J.*, 39, 879–893, 2002.

Ferronato, M., Castelletto, N., and Gambolati, G.: A fully 3-D mixed finite element model of Biot consolidation. *J. Comp. Phys.* 229, 4813–4830, 2010.

Xotta, R., Zoccarato, C., Minderhoud, P. S. J., & Teatini, P.: Modeling the role of compaction in the three-dimensional evolution of depositional environments. *J. Geophys. Res. - Earth Surface*, 127, e2022JF006590, doi:10.1029/2022JF006590, 2022.

Zoccarato, C., Minderhoud, P. S. J., & Teatini, P.: The role of sedimentation and natural compaction in a prograding delta: insights from the mega Mekong delta, Vietnam. *Scientific Reports*, 8(11437), doi:10.1038/s41598-018-29734-7, 2018.

Zoccarato, C., Minderhoud, P.S.J., Zorzan, P., Tosi, L., Bergamasco, A., Girardi, V., Simonini, P., Cavallina, C., Cosma, M., Da Lio, C., Donnici, S., and Teatini, P.: In-situ loading experiments reveal how the subsurface affects coastal marsh survival. *Comm. Earth & Environment* 3, 264, doi:10.1038/s43247-022-00600-9, 2022.

Cultural heritage and subsidence: the emblematic case study of Santa Croce in Ravenna (Italy)

I. Bertolini[1], G. Gottardi[1], M. Marchi[1], A. Ugolini[2]

1 DICAM Department, Alma Mater Studiorum, Università di Bologna, viale del Risorgimento, 2, 40136, Bologna, Italy
2 Architecture Department, Alma Mater Studiorum, Università di Bologna, viale del Risorgimento, 2, 40136, Bologna, Italy

michela.marchi@unibo.it

Abstract

The paper deals with subsidence and flooding risks associated to the Archaeological Site of Santa Croce, encompassing a 5th century church together with the remains of a Roman domus and its mosaics, located in the centre of the historic town of Ravenna (Italy). A geotechnical field campaign and the installation of a new piezometer monitoring system were carried out in 2022, under the framework of H2020 SHELTER project, to investigate the critical issues generated by water drainage in the site, requested by the significant natural and anthropic land subsidence phenomenon that has affected the site since its origins. The case study is presented herein, together with a brief description of the ongoing investigation activities and a few preliminary results.

The church and the archeological area of Santa Croce in Ravenna

The ancient city of Ravenna, located in the Northern Italy ~10 km from the Adriatic Sea and ~60 km from the Po River Delta, is worldwide known for its magnificent and well-preserved Byzantine architectures. Over the past centuries, the city has been affected by a phenomenon of intense subsidence, both natural and anthropogenic; at present, the cumulated settlement of most ancient monuments has brought their ground level well below the current water table, causing permanent flooding in the crypt of monumental churches, such as S. Francesco's Basilica, and in the basement of old buildings. The archaeological area of Santa Croce is located in the historic centre of Ravenna, close to San Vitale Basilica and Galla Placidia Mausoleum, in the buffer zone of the UNESCO world heritage site of the Early Christian monuments of Ravenna (see Figure 1A). The peculiarities of the Santa Croce area include an archaeological excavation, carried out during the second half of the 20th century and left open in order to make the unique archaeological stratification permanently visible from the public street (see Figures 1B and 1C). Being the bottom of the excavation over 3 m below the current ground level and more than 2 m below the typical water table, a permanent drainage system was installed at the beginning of the '80. This system is still constantly operating in the area, maintaining it substantially dry, although due to the lack of maintenance it has modified its original functionality, creating local settlements and clear evidences of potential instability (see Figure 2A), especially around the tank area where the submerged pumps are located. Last time only in 2021, the pumping system failed, producing the subsequent flooding of the area and the related damages to the Roman mosaics and the archaeological structures (see Figure 2B). Preliminary studies and investigations were recently carried out within the actions of the European project H2020 SHELTER, with the main aim of understanding and monitoring the effects of the existing drainage system, also identifying the local hydrogeological and geotechnical characteristics. Such pieces of information, analysed in the context of the land subsidence that has long affected the area, can provide valuable data for its maintenance and preservation.

Figure 1A Aerial view of the Archaeological Area of Santa Croce in Ravenna (Italy) and the Monumental zone of S. Vitale and Galla Placidia. B) View of the Santa Croce Church from the street. C) View of the Church and the archaeological remains located at the bottom of the excavated basin around the Church.

Figure 2A Land settlements and instability of the soil slope and of the old brick masonry walls, concentrated around the tank area. B) Drainage operations by Civil Protection of the flooded Archaeological Area of Santa Croce as a consequence of the temporary break down of the pumps (August 2021).

Land subsidence in Ravenna

The archaeologic site of Santa Croce was first seat of a Roman domus; later, in the V century, the original church started to be built and subsequently enlarged and substantially modified over the subsequent centuries. Archaeologists have estimated a difference between the current configuration and the ancient Roman floor of more than 3 m, mostly due to the natural subsidence of local highly stratified alluvial sediments (Cassanelli et al, 2013). In more recent times, the land settlement in the Ravenna city centre has passed from few millimetres per year (~5.5 mm/year in the period 1900-1957) to 80 mm/year between 1972-73 (Bertoni et al, 2005), primarily due to groundwater pumping for industrial and civil purposes and, to a lesser extent, to gas extractions from onshore and offshore reservoirs. Therefore, the archaeological area of Santa Croce experienced ~1.3 m of land subsidence in the period 1897-2002 (Teatini, 2015) (see Figure 3 left). The corrective actions taken by the Italian government starting in the ’60 eventually mitigated the problem. As a consequence, the settlement decreased to a rate of ~1.3 mm/y in the period 1998-2002 (see Figure 3 right), a value close to the natural subsidence rate (Bertoni et al, 2005). Although these data suggest that land subsidence evolution in the Ravenna city center do not currently represent a decisive factor (Bitelli et al, 2020), the cumulated anthropogenic settlement has seriously aggravated the environmental conditions of the investigated site and of the other contemporary monuments.

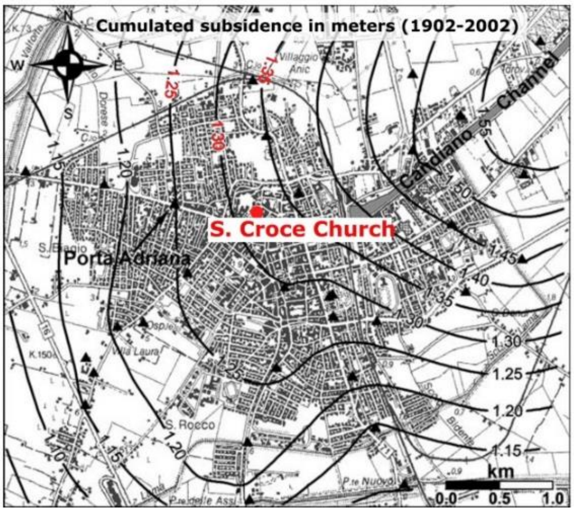

Average subsidence rate (mm/year)	
Time interval	**Historic Centre of Ravenna City**
1900-1957	5.5
1949-1972	2.5
1972-1973	80
1972-1977	60
1977-1982	13
1982-1986	5
1986-1992	5
1992-1998	4.5
1998-2002	1.3

Figure 3 Left: Cumulated land subsidence in the historic centre of Ravenna between 1902-2002 (image modified from Teatini et al, 2005). Right: Average subsidence rates in mm/year registered in the historic centre of Ravenna in the different time intervals, from Bertoni et al (2005).

The Area of S. Croce and the operating drainage system

In 1979 a permanent drainage system was built at the foot of the slope that surrounds the archaeological excavations of the Santa Croce site. The system still runs along two sides of the excavated perimeter. The reconstruction of the original system, as deduced from the documents collected in the Archives and field observations, is shown in Figure 4. The water that enters in the perforated pipe of the horizontal drainage starts from P1 and gets to a main well (C1 in Figure 4), where two submerged pumps lift the water into the public sewer. In 1984 a large concrete tank was built, to enhance the storage of the drained water. After more than 40 years from its installation, the drainage system, in particular the perforated drainage pipe, results completely obstructed and, as a consequence, water runs by gravity in the trench above it and it is only partially collected into the final concrete tank.

2022 Geotechnical investigations in the S. Croce area

In 2022 the subsoil underneath the archaeological site of Santa Croce and the Monumental area of S. Vitale and Galla Placidia have been investigated by means of two continuous coring boreholes, two cone penetration tests CPTu, one seismic CPTu, one dilatometer test, several SPT, dissipation and LeFranc permeability tests. The collected data, integrated with the results of previous investigations described in Ricceri (1992), enabled to define an accurate stratigraphic model of the site up to a depth of 35 m from the ground level. The subsoil is constituted by: an anthropic unit, ~5 m thick, rich in archaeological remains; a sandy layer, down to a depth of ~22 m (the shallowest Aquifer 1); a silty-clay layer, interposed between such first and the second aquifer, which ends at a depth of 33 m from the ground level. Below this unit, and up to the maximum investigated depth, a second fine grained material can be observed. During the same geotechnical campaign, 5 new standpipe piezometers were installed in the area for the continuous monitoring of the pore water pressure (pwp) distribution in the two aquifers, with the aim of quantifying the incidence of the drainage system and of local precipitations on the local hydrogeology. The recorded data from the two piezometers installed in the shallowest aquifer (Aquifer 1) close to the pumps show a marked drawdown, which reduces with the increasing distance from the pumps, as expected. At the same time, the analysis of additional preliminary data suggests that the drainage influence on the second aquifer is rather limited. The set of collected data and information will enable a well-calibrated design of a new drainage system or a renewal of the existing one. Both field investigations and subsequent possible interventions must guarantee the least disturbance of the archaeological site and of the surrounding monumental area, preserving its historic characteristics and integrity. The new challenge for the preservation of the site will be related not only to the installation and maintenance of the new drainage system but also to its required features for guiding the operation of pumping devices and for informing a related alert system. Together with the remotely-controlled drainage system, an emergency plan will be therefore defined to manage possibly arising critical situations.

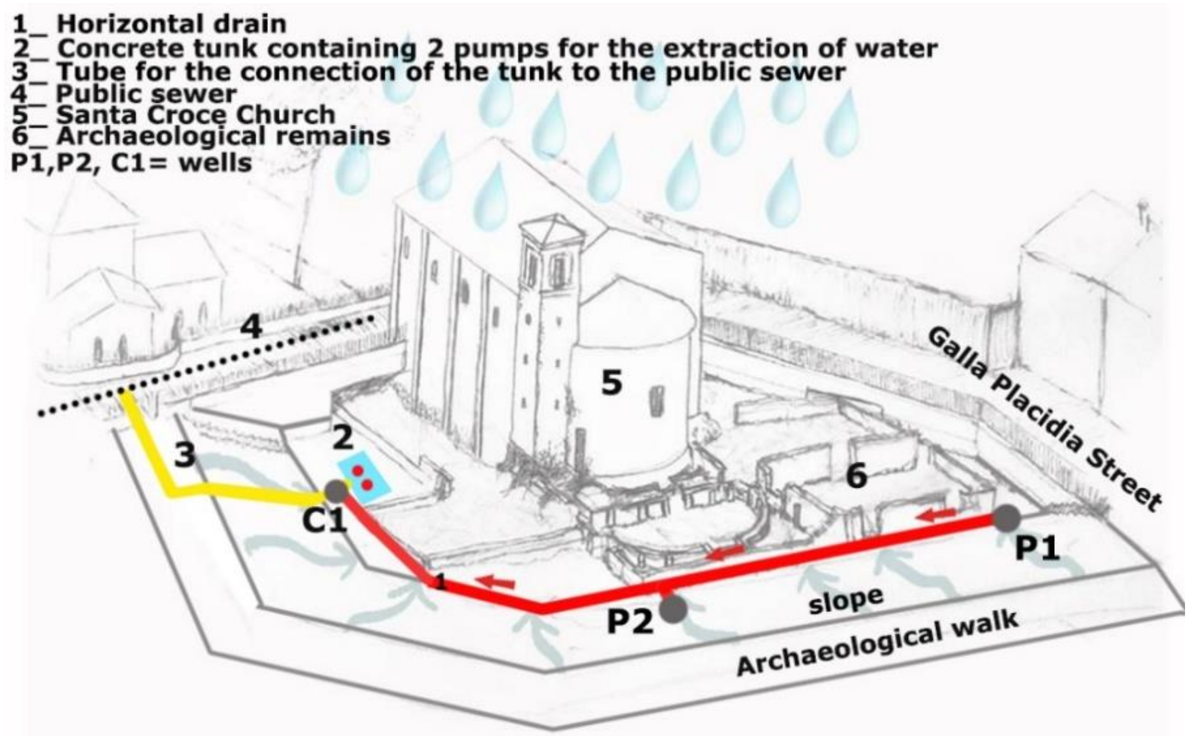

Figure 4 Schematic representation of the drainage system operating in the investigated area to keep dry the archaeological excavations around the church.

Conclusion

In the framework of H2020 SHELTER research project, the delicate situation and the numerous criticalities associated with the Archaeological Area of Santa Croce have been highlighted in relation to their effects on the historic heritage. Land subsidence and flooding are deeply interconnected natural hazards that threaten this unique area and require special care and attention in order to mitigate the related risks, making possible the preservation and future fruition of the entire complex. The performed geotechnical campaign together with the preliminary results of the on-site monitoring are a valuable source of information to understand the present context and design proper management strategies.

Acknowledgements

This research has received funding from the EU Horizon2020 under grant agreement n° 821282

References

Bertoni, W., Elmi, C. & Marabini, F. (2005). The subsidence of Ravenna. *Giornale di Geologia Applicata* 1, 23-32.

Bitelli, G., Bonsignore, F., Del Conte, S., Franci, F., Lambertini, A. et al (2020). Updating the subsidence map of Emilia Romagna regioni (Italy) by Integration of SAR interferometry and GNSS time series: the 2011-2016 period. *Proceedings of IAHS,* 32, 39-44.

Cassanelli, R., Cirelli, E., Crociati, E., Civiletti, J.P. et al (2013). *La Basilica di Santa Croce: nuovi contributi per Ravenna tardo-antica*. Curated by David M. Edizioni del Girasole.

Ricceri, G. (1992*). Studi e ricerche nell'area di S.Vitale Galla Placidia e Santa Croce in Ravenna. SGEditoriali*, Padova (Italia).

Teatini, P., Ferronato, M., Gambolati, G., Bertoni, W., Gonella, M. (2005). A century of land subsidence in Ravenna, Italy. *Environmental Geology*, 47,831-846.

Greenhouse gas emissions from incubated peat cores under dynamic groundwater conditions

Erne Blondeau[1], Anneke Stam[1], Gerard Velthof[2], Jan van den Akker[3], Marius Heinen[3], Jan Willem van Groenigen[1]

1 Soil Biology Group, Wageningen University and Research, Wageningen, The Netherlands
2 Team Sustainable soil management, Wageningen Environmental Research, Wageningen University and Research, Wageningen, the Netherlands
3 Team Soil, Water and Land Use, Wageningen Environmental Research, Wageningen University and Research, Wageningen, the Netherlands

erne.blondeau@wur.nl

Session: Mechanisms and understanding of land subsidence
Societal focus: Peatlands and GHG emissions

Introduction

In 2021, 19% of grasslands in the Netherlands were situated on drained peat soils, a large part of which is in use for grazing and grass production in dairy farming (Arets et al., 2022). To accommodate for this use of peat soils, groundwater levels (GWL) are maintained relatively deep (-40 to -90 cm below soil surface). Prolonged drainage of peat soils ultimately leads to subsidence as it stimulates both compaction and oxidation of the soil material (Erkens et al., 2016). Additionally, aerobic oxidation under drained conditions releases the greenhouse gases CO_2 and N_2O to the atmosphere, while, to a lesser extent, CH_4 is produced from anaerobic oxidation under very wet conditions (Tiemeyer et al., 2016). Recently, national and international agreements on mitigating climate change require a substantial decrease in the emission of these greenhouse gases from peat soils (Ministerie van Landbouw, Natuur en Voedselkwaliteit, 2019). It is, therefore, essential to understand the mechanisms leading to GHG emissions from peat soils and the concurrent subsidence and how these are affected by management practices.

CO_2 emissions from several incubation experiments on peat soils show that a limited amount of air infiltration can be sufficient to stimulate microbial respiration, while extreme drying actually starts to constrain microbial activity (Berglund & Berglund, 2011; Norberg et al., 2018). Like CO_2, N_2O emissions are limited by both aeration and water content as they affect nitrification (and thus NO_3^- availability) and denitrification (Van Beek et al., 2010). Particularly dynamic groundwater conditions are favorable to N_2O production (Tiemeyer et al., 2016). High CH_4 emissions are generally not observed in drained peat soils (Van den Pol-Van Dasselaar et al., 1997). Rewetting a previously drained peat soil, however, can turn it back into a net CH_4 source (e.g. Karki et al., 2016; Van de Riet et al., 2013). Incubation or mesocosm studies on intact soil cores provide an opportunity to study peat mineralization in a controlled environment, while approaching the water retention and gas diffusion processes of the field situation as much as possible (Askaer et al., 2010; Berglund & Berglund, 2011; Karki et al., 2016; Regina et al., 2015; van de Riet et al., 2013). However, to our knowledge, there have been no peat column experiments, where replicated objects were subjected to a wide range of water table fluctuations.

Aims and hypotheses of this study

In this project, which is part of the Dutch research program Living On Soft Soils (LOSS), we aim to get a better understanding of the effects of GWL strategies on GHG emissions from Dutch peat soils. We included three Dutch pastures on peat soils with different compositions in our experiment to obtain a range of representative emission values, since we hypothesize that CO_2 and N_2O emissions are positively affected by type and contents of organic matter and N-contents of the soil and negatively by a clay cover on top of the soil. Secondly, we hypothesize that peat oxidation is higher under a low GWL and the strength of CO_2, N_2O and CH_4 emissions will result from a balance between oxygen limitation and water limitation. Therefore, intact peat cores from the upper 5 - 110 cm of the soil are treated with GWL treatments, ranging from 0 to -100 cm below the sample surface. Finally, since we hypothesize that CO_2 and N_2O production depend on abundance and composition of organic matter, smaller cores derived from the different soil horizons were incubated and emissions were measured at varying moisture conditions.

Methods

Field sampling

We measured greenhouse gas emissions from large and small soil cores in a laboratory environment. Large soil columns were sampled in transparent plexiglass tubes (120 cm long, 24 cm inner diameter) from three peat meadows used for dairy farming in The Netherlands of varying soil composition. The first soil profile near the municipality of Zegveld consists of a clayey anthropogenic layer on top of forest and sedge peat. The second sampling took place near Vlist, in an area of forest peat with a peaty clay top layer. The soil from the third field near Aldeboarn contains a thick clay layer on top and sphagnum peat beneath. These three locations are all part of the Dutch national research program on greenhouse gas emissions from peat pastures (NOBV). Three replicates were sampled by cutting off the top grass layer (5 cm) in the field and carefully pushing the tubes vertically down into the soil. Additionally, we sampled one column per location with vegetation, to check for the effect of the living grass on N_2O and CO_2 emissions. In addition to the large columns, small intact cores (5 cm length, 5.1 cm diameter) were sampled in metal rings, out of each soil horizon down to 120 cm below the soil surface.

Laboratory setup peat columns

After sampling, the large columns were brought to a climate-controlled room (16°C, 70% relative humidity), where they stayed until the start of and during the experiment. The bottom 10 cm of the soil was replaced with a layer of fine sand after which the bottom of the tube was closed air tight with a PVC cap and the column was placed on a 50 cm high platform. Two drainage pipes were installed in each column, through which a groundwater level could be imposed by applying a pressure head at a specific place below in the soil. The first drain in the bottom of the peat soil was used for positive pressure heads (at the drain location) and the second in the sand layer was used to apply a suction to the entire peat core. The distance of the applied pressure head to the soil surface was then used as a proxy for the achieved GWL.

Groundwater level fluctuation and GHG flux measurements

Biological and physical soil processes are studied in two drying-wetting cycles taking place between January 2022 and January 2023. During the first drying-wetting cycle, the pressure head of the drain in the peat layer was changed weekly for eleven weeks to fluctuate the GWL between 0 cm and -100 cm below soil surface. Fluxes of CO_2, N_2O and CH_4 were measured twice a week (on the first and the last day of a GWL step) using dark closed chambers connected to a Gasera One photo acoustic gas monitor (Gasera Ltd, Finland). Three measurements over a closure time of 24 minutes were used to calculate flux values, assuming a linear concentration change between the measurement points.

Setup and measurements small soil cores

Four replicates per soil horizon and location of the field moist intact core samples were taken and placed on a sandbox located in the same climate room (16°C, 70% relative humidity) to saturate over two weeks. After reaching saturation, the samples were taken from the sand box and placed in open polyethylene jars, to dry to the air over a period of 3.5 weeks. Fluxes of CO_2, N_2O and CH_4 were measured 2-3 times a week, by closing the jars and measuring their headspace concentration at 27 minutes using the Gasera One photo acoustic gas monitor. A linear concentration increase between the first (background concentration) and second measurement point was assumed and checked occasionally. The mass of these ring samples was recorded before each flux measurement and after drying at 105°C, at the end of the experiment, from which volumetric water contents and water holding capacity were calculated at each measurement time.

Statistical analyses

The statistical software R was used for all data analyses (v4.1.2; R core Team 2021). Cumulative CO_2-C and N_2O-N fluxes from the large columns were calculated assuming linear changes between two measurement instances and log transformed in the case of N_2O-N. An analysis of variance was used to test for the effect of soil type on cumulative emissions from the bare columns.

Results and discussions

Moisture effect

CO_2 fluxes in the large columns showed an increase within the first groundwater step (Figure 1a). Further GWL changes during the drying and wetting of the columns did not result in clear effects on CO_2 emissions, until the columns were rewetted close to the surface again. From -40 cm below soil surface onwards, CO_2 emissions decreased slightly. As expected, CO_2 fluxes were higher in the grass columns than the bare columns from the corresponding locations. The difference can be attributed to grass and roots respiration (photosynthesis is assumed to be absent in the dark flux chambers). The CO_2 flux values from our grass columns were comparable in size to those from the grass-vegetated peat columns of Van de Riet et al. (2013). In contrast to the observations in the columns, CO_2 emission peaks were measured in the small cores near saturation (100% of WHC), which quickly dropped during the first days of evaporation (Figure 2).

N_2O emissions in the large columns peaked during near-saturation (GWL at 0 cm) both at the start of the drying track and at the end of the rewetting track (Figure 1b). The latter followed our expectations that N_2O emissions will be strongest during consecutive aerobic and anaerobic conditions. Similarly, the peaks during the initial saturation condition may be caused by denitrification during anaerobicity after an extra application of water to the columns, which was applied to fully saturate them. N_2O emissions from the small cores were very high from all layers and locations during saturation at the first measurement event (83- 2117 mg N_2O-N m^{-2} day^{-1}), but had decreased to 0-22 mg m^{-2} day^{-1} by the second measurement day. Saturation may have caused high denitrification rates, while the small core size may have prevented full reduction to N_2. CH_4 emissions in the large columns were generally low or slightly negative (Figure 1c), even during near-saturated conditions. During low GWL steps, any produced CH_4 is likely to have been oxidized before reaching the surface. Under high GWL, methanogenesis was potentially limited by labile carbon sources. High CH_4 emissions were only found in one of the bare Aldeboarn columns, during the GWL of -40 to -60 in the drying track. Possibly, the high clay content of the top layer caused a delay in aeration of this column, making it possible for produced CH_4 to diffuse upwards without oxidizing.

Soil type effect
Mean cumulative CO_2-C emissions over 75 days were higher from the Zegveld and Aldeboarn soils than from Vlist (respectively 0.2 and 0.3 ton ha^{-1}), but the soil type effect was not significant ($p = 0.09$). A soil type effect was not clearly seen in the small cores either, though the CO_2 peak was lower in the Zegveld samples than those from Vlist or Aldeboarn.

The mean cumulative N_2O flux from the Aldeboarn columns was over two or three times as high as the mean from the Vlist and Zegveld soils. However, the variation in N2O emission between replicates was large and there were no significant differences in N2O emissions between the three soils ($p = 0.06$).

Continuation of the experiment
A second, longer drying-wetting cycle in the large soil columns is taking place at present (October 2022). Herein, the time steps for the different water levels are extended to two weeks and the columns are drained down to a water level of -160 cm below surface. The outcomes of this cycle will help us to understand the potential effect of incubation time on the measured GHG fluxes, as well as respiration during very dry conditions. Additionally, biochemical as well as soil physical variables, which remained undiscussed in this abstract, are recorded in drying-wetting cycles 1 and 2. By analyzing these together, we aim to improve our understanding of the coupled processes of groundwater dynamics, water retention, peat mineralization and shrinkage.

Acknowledgements

The research presented in this paper is part of the project Living on soft soils: subsidence and society (grantnr.: NWA.1160.18.259). This project is funded by the Dutch Research Council (NWO-NWA-ORC), Utrecht University, Wageningen University, Delft University of Technology, Ministry of Infrastructure & Water Management, Ministry of the Interior & Kingdom Relations, Deltares, Wageningen Environmental Research, TNO-Geological Survey of The Netherlands, STOWA, Water Authority: Hoogheemraadschap de Stichtse Rijnlanden, Water Authority: Drents Overijsselse Delta, Province of Utrecht, Province of Zuid-Holland, Municipality of Gouda, Platform Soft Soil, Sweco, Tauw BV, NAM.

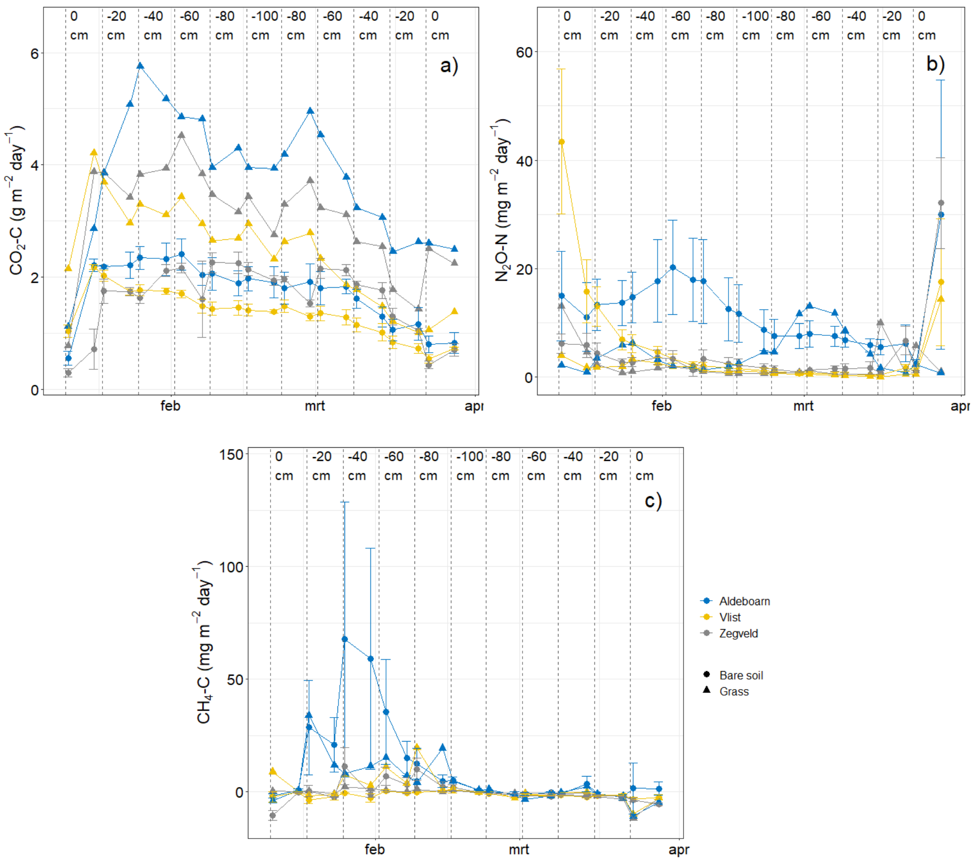

Figure 1 Fluxes of CO_2-C (a), N_2O-N (b) and CH_4-C (c) from the peat columns (with, n=1, and without, n = 3, grass sod) during the drying-rewetting cycle from January 12 – March 27 2022, with a GWL ranging between 0 and -100 cm below soil surface.

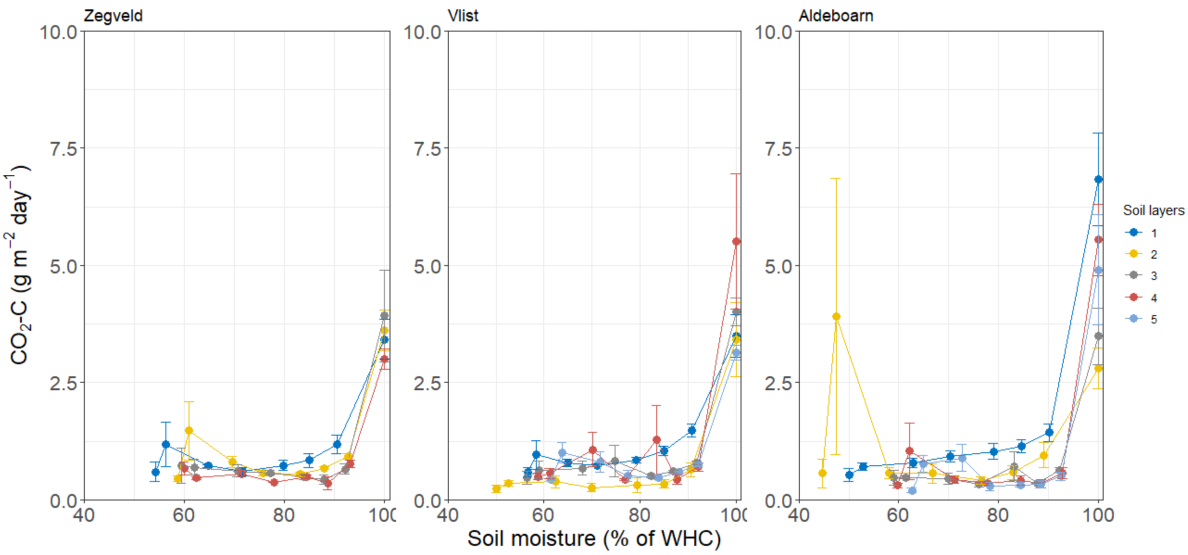

Figure 2 Fluxes of CO_2-C in the small soil cores against the moisture content of the samples. Samples originate from one of the four (Zegveld) or five (Vlist, Aldeboarn) soil horizons of which the upper 120 cm in the sampling location was composed, where 1 is the shallowest and 5 the deepest layer. Moisture content is represented by the percentage of the samples' initial water holding capacities.

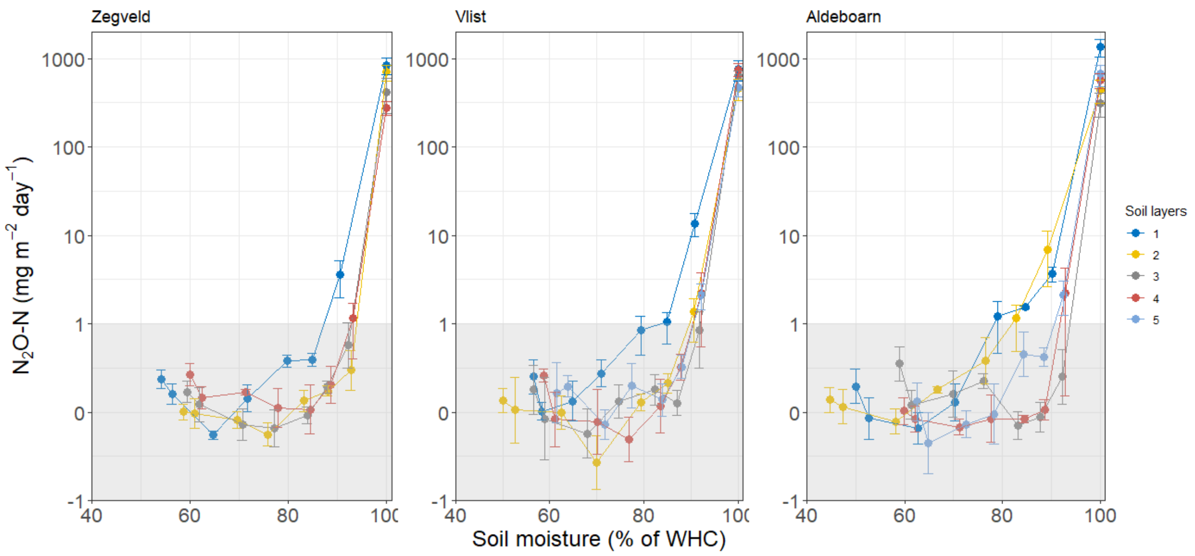

Figure 3 Fluxes of N_2O-N in the small soil cores against the moisture content of the samples. Samples originate from one of the four (Zegveld) or five (Vlist, Aldeboarn) soil horizons of which the upper 120 cm in the sampling location was composed, where 1 is the shallowest and 5 the deepest layer. Moisture content is represented by the percentage of the samples' initial water holding capacities. The y-axis values are log(10) transformed, except for the grey area, where the y-axis is scaled linearly.

References

Arets, E.J.M.M., S.A. van Baren, H. Kramer, J.P. Lesschen & M.J. Schelhaas (2022). *Greenhouse gas reporting of the LULUCF sector in the Netherlands; Methodological background, update 2022*. Wettelijke Onderzoekstaken Natuur & Milieu, WOt-technical report 217.

Askaer, L., Elberling, B., Glud, R. N., Kuhl, M., Lauritsen, F. R., & Joensen, H. R. (2010). Soil heterogeneity effects on O-2 distribution and CH4 emissions from wetlands: In situ and mesocosm studies with planar O-2 optodes and membrane inlet mass spectrometry. *Soil Biology & Biochemistry*, 42(12), 2254-2265. doi:10.1016/j.soilbio.2010.08.026

Berglund, O., & Berglund, K. (2011). Influence of water table level and soil properties on emissions of greenhouse gases from cultivated peat soil. *Soil Biology & Biochemistry*, 43(5), 923-931. doi:10.1016/j.soilbio.2011.01.002

Erkens, G., van der Meulen, M.J., Middelkoop, H. (2016). Double trouble: subsidence and CO2 respiration due to 1,000 years of Dutch coastal peatlands cultivation. *Hydrogeology Journal*, 24 (3), pp. 551-568

Karki, S., Elsgaard, L., Kandel, T. P., & Laerke, P. E. (2016). Carbon balance of rewetted and drained peat soils used for biomass production: a mesocosm study. *Global Change Biology Bioenergy*, 8(5), 969-980. doi:10.1111/gcbb.12334

Ministerie van Landbouw, Natuur en Voedselkwaliteit. (2019). *Klimaatakkoord- C4 Landbouw en Landgebruik*. Den Haag

Norberg, L., Bergiund, O., & Bergiund, K. (2018). Impact of drainage and soil properties on carbon dioxide emissions from intact cores of cultivated peat soils. *Mires and Peat*, 21. doi:10.19189/MaP.2017.OMB.284

R Core Team (2021). R: A language and environment for statistical computing. R Foundation for Statistical Computing, Vienna, Austria. URL https://www.R-project.org/.

Regina, K., Sheehy, J., & Myllys, M. (2015). Mitigating greenhouse gas fluxes from cultivated organic soils with raised water table. *Mitigation and Adaptation Strategies for Global Change,* 20(8), 1529-1544. doi:10.1007/s11027-014-9559-2

Tiemeyer, B., Borraz, E. A., Augustin, J., Bechtold, M., Beetz, S., Beyer, C., . . . Zeitz, J. (2016). High emissions of greenhouse gases from grasslands on peat and other organic soils. *Global Change Biology,* 22(12), 4134-4149. doi:10.1111/gcb.13303

van Beek, C. L., Pleijter, M., Jacobs, C. M. J., Velthof, G. L., van Groenigen, J. W., & Kuikman, P. J. (2010). Emissions of N2O from fertilized and grazed grassland on organic soil in relation to groundwater level. *Nutrient Cycling in Agroecosystems*, 86(3), 331-340. doi:10.1007/s10705-009-9295-2

van de Riet, B. P., Hefting, M. M., & Verhoeven, J. T. A. (2013). Rewetting Drained Peat Meadows: Risks and Benefits in Terms of Nutrient Release and Greenhouse Gas Exchange. *Water Air and Soil Pollution*, 224(4). doi:10.1007/s11270-013-1440-5

Van den Pol-Van Dasselaar, A., Van Beusichem, M. L., & Oenema, O. (1997). Effects of grassland management on the emission of methane from intensively managed grasslands on peat soil. *Plant and Soil*, 189, 1–9

Investigating land subsidence trend in the major coastal cities of Europe

R. Bonì[1], P. Teatini[2], C. Zoccarato[2], P. Minderhoud[2,3], L. Tosi[4], M. Béjar-Pizarro[5], C. Guardiola-Albert[5], G. Bru[5], P. Ezquerro[5], G. Herrera[5], R. Tomás[6], M.I. Navarro-Hernández[6]

1 Department of Pure and Applied Sciences, University of Urbino "Carlo Bo", Urbino, Italy.
2 Department of Civil, Environmental and Architectural Engineering, University of Padua, Padua, Italy.
3 Soil Geography and Landscape Group, Wageningen University, Wageningen, The Netherlands
4 Institute of Geosciences and Earth Resources, National Research Council, Padova, Italy
5 Geohazards InSAR Laboratory and Modeling Group, Instituto Geológico y Minero de España, Madrid, Spain.
6 Universidad de Alicante, Dpto. de Ingeniería Civil, Escuela Politécnica Superior de Alicante, Alicante, Spain.

Correspondence to: Roberta Bonì (roberta.boni@uniurb.it)
Session: Measuring and Monitoring of land subsidence

Abstract

Major coastal cities in the world are threatened by land subsidence due to natural and anthropogenic causes. These phenomena can exceed global sea-level rise by one order of magnitude. While sea-level rise has received great consideration by the scientific community, land subsidence and its effect on the relative sea-level rise in coastal cities have not. The aim of this work is to show the comparison of the recent trends of land subsidence in the major coastal cities of Europe by exploiting the advanced differential interferometric SAR (A-DInSAR) data provided by the European Ground Motion Service (EGMS) developed by the European Union's Earth observation programme. The results will be exploited to investigate the driving forces of the different land subsidence mechanisms.

Keywords: land subsidence; coastal areas; A-DInSAR; EGMS; relative sea-level rise

Introduction

Land subsidence is a worldwide problem as reported by a recent study that has evaluated how 90% of the global population may face a high probability of subsidence (Herrera et al., 2021) with an increasing exposure to sea-level rise. Different authors have evaluated the risk associated to future coastal flood in Europe due to global warming and socioeconomic development (e.g., Paprotny et al., 2018; Vousdoukas et al., 2018).

It is well known that the combined effect of land subsidence and sea level rise increases flood risk and that several coastal cities, such as Jakarta in Indonesia (Abidin et al. 2011), Shanghai in China (Yue et al. 2015), along with many other densely populated areas in the world (Yan et al. 2022), are sinking faster than the sea level is rising. However, information on current land subsidence dynamics and rates at a global scale is often not available. In addition, the spatio-temporal variability of the coastal land subsidence, due to the different causes, makes the integration of its contribution to future relative sea-level rise challenging.

In 2016, a European initiative was developed to provide A-DInSAR measurements at a continental scale (Crosetto et al. 2020). This service, named European Ground Motion Service (EGMS), represents the most important wide-area deformation monitoring system ever developed. The aim of this work is to give insight into i) the use of the EGMS products (displacement time series and average velocities) for the monitoring of land subsidence in 16 coastal metropoles in Europe characterized by a population over one million, and ii) the interpretation of the driving mechanisms using cross-correlations with subsurface geospatial information (e.g., geology, hydrogeology, etc.).

Data and Methods

Major coastal cities selected in Europe

In the selected coastal cities/metropoles, more than 1 million people are at risk from climate change and natural hazards (Figure 1). Thirteen cities were considered as the most vulnerable in Europe as of 2005 (Hallegatte et al., 2013) and three more were lately included (Antwerp, Oslo and Valencia) as they have surpassed 1 million inhabitants in recent years (Siegel, 2020).

Land subsidence is triggered by a variety of factors, many of which are related to hydrogeologic processes. Some natural processes causing land subsidence are influenced by human activities related to land and water use and by climatic variability (Galloway et al., 2016). To interpret the land subsidence in the selected cities, these drivers were investigated through a literature review and cross-correlation with subsurface geospatial information.

From the climatic point of view, six cities are localized in the maritime North climatic zone (i.e., Dublin, London, Rotterdam, Amsterdam, Antwerp, Hamburg), seven cities in the Mediterranean climatic zone (i.e., Porto, Lisbon, Valencia, Barcelona, Marseille, Naples, Athens), two cities (i.e., Oslo and Helsinki) are in the nemoral climatic zone, and one (i.e., Copenhagen) in the continental climatic zone (EEA, 2022).

Most of the cities (i.e., Athens, Barcelona, Marseille, Valencia, Hamburg) are sit above highly productive aquifers low and moderately productive aquifers (i.e., London, Lisbon, Amsterdam, Rotterdam). One and two cities are located in regions with highly (i.e., Copenhagen) and low to moderately productive *fissured* aquifers (i.e., Napoli, Dublin), respectively.

Non-aquiferous rocks characterized the regions of Oslo and Helsinki, with Porto and Antwerpen placed above locally aquiferous rocks (Figure 1).

Available scientific literature suggests the selected cities are experiencing land subsidence due to natural and/or anthropogenic causes. In some cases, the main cause of the detected subsidence could be due to excessive groundwater extraction, but detailed studies are lacking.

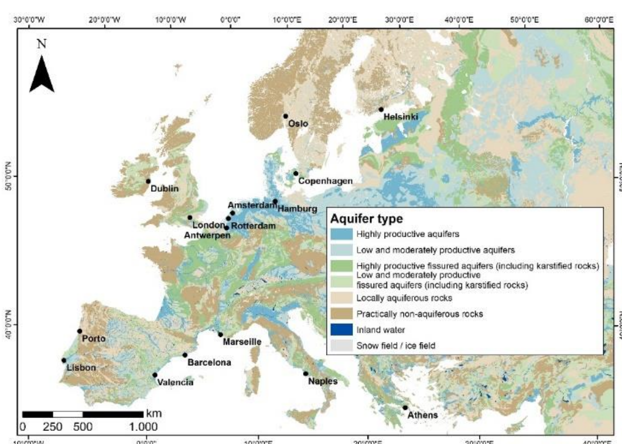

Figure 1. Location of the selected coastal cities positioned on the hydrogeological map of Europe (modified from Duscher et al. 2015).

EGMS dataset

The land subsidence rates have been investigated in the 16 cities using the EGMS products. This is a service developed by Copernicus, the European Union's Earth observation programme, that provides A-DInSAR data obtained using SAR images acquired by the Sentinel-1 satellites in ascending and descending geometries over Europe in the period from 2016 to 2020 (Figure 2).

The vertical displacement rates for each city were extracted from the EGMS Viewer by using the available "Ortho" level of product. The values represent absolute displacements, with the A-DInSAR outcome calibrated using GNSS records. Additional information about the dataset is available through the dedicated webpage (https://land.copernicus.eu/pan-european/european-ground-motion-service).

The tool "Compute average" was used to extract the mean velocity, the standard deviation associated to the mean velocity, the average displacement times series and the associated standard deviation in areas of the city most affected by land subsidence as detected by visual inspection.

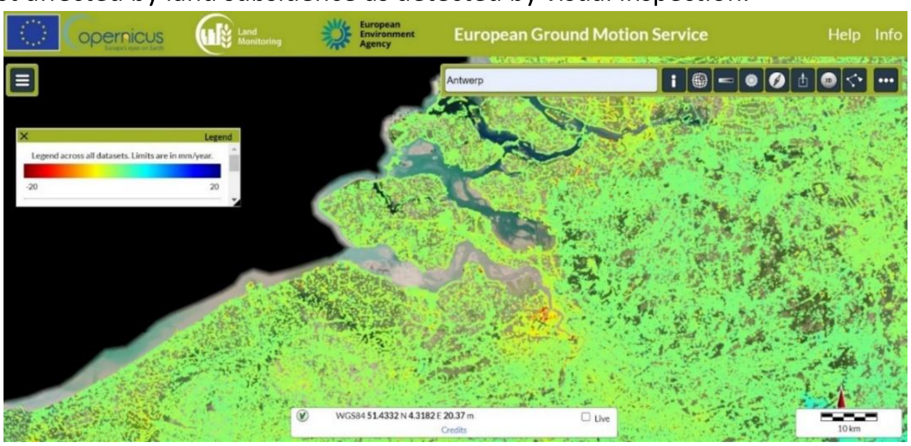

Figure 2. View of the EGMS products for Antwerp in Belgium. Negative and positive values stand for land subsidence and uplift, respectively.

Results and discussion

The results show that the mean velocity of studied cities ranges from -0.48 mm/yr up to -4.89 mm/yr. The highest values were detected for the cities of Antwerp, Hamburg, Barcelona and Rotterdam (Figures 3 and 4).

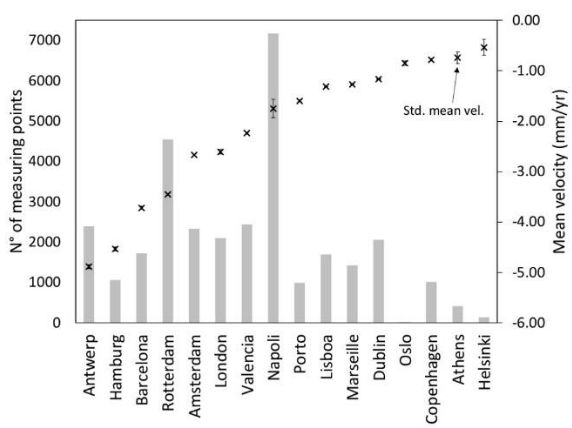

Figure 3. Mean velocities for the major coastal cities of Europe extracted in areas of interest. The grey columns and the black crosses represent the number of measuring points and the mean velocity, respectively. The standard deviation of the mean velocity and the number of measuring points for each area is also reported. Oslo shows only very local vertical movements and

21 measuring points were selected.

The highest subsidence rate is measured in Antwerp (Belgium), which is located in the alluvial plain of the Scheldt River where fluvial deposits are overlain by human-made landfills. The recent intensive urbanization could be the primary cause of the consolidation of these compressible deposits (Declercq et al., 2021). A similar land subsidence mechanism is reported for the port of Barcelona (Spain), which was built on Quaternary and Tertiary River alluvial compressible deposits of the Llobregat river delta (Pros et al., 2014).

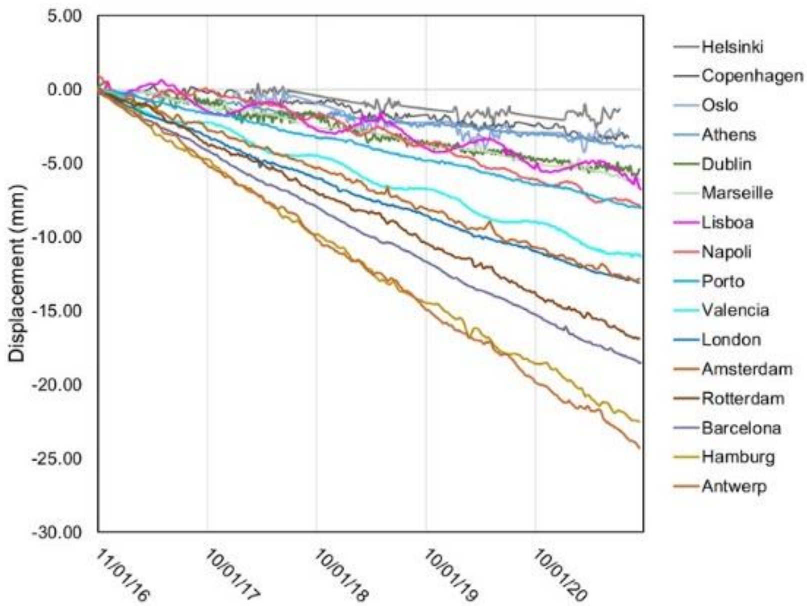

Figure 4. Average displacement time series for the selected areas of the coastal cities of interest.

High subsidence rates are observed also in Hamburg (Germany). In this case, the subsidence is due to the dynamics of evaporites (Kersten et al., 2017). Volcanic inflation/deflation is the main mechanism responsible for the movements in Napoli (Italy) although other causes were identified (Terranova et al., 2015). Athens (Greece) experiences land subsidence due to mining activities (Parcharidis et al. 2006). Land subsidence in Amsterdam and Rotterdam (The Netherlands) is due to compaction and oxidation depending on the subsurface lithology, the loading and groundwater table history (Koster et al., 2018; Van Asselen et al., 2018). Subsidence due to groundwater withdrawal is observed in London (UK) (Bonì et al., 2016) and suggested for Valencia (Spain) (Ruiz-Armenteros et al., 2018). The cities of Lisbon and Porto (Portugal) show movements probably due to the natural compaction of alluvial deposits and anthropogenic materials (Catalao et al., 2011; Sousa et al., 2012), although subsidence may also be due to aquifer overexploitation. Further studies and groundwater monitoring data are required to understand the cause of the detected movements in these cities. It is worth noting that Copenhagen (Denmark), Helsinki (Finland) and Oslo (Norway) show low subsidence rates in reclaimed areas and restricted zones where aquifer drainage operations for underground construction were carried out (Dehls and Nordgulen, 2004). In Dublin (Ireland), local compaction of unconsolidated shallow sediments such as peat or lacustrine deposits due to the load induced by the recent construction of roads and buildings could be the main cause of the observed phenomena (Fiaschi et al., 2019). Low subsidence rates are observed in Marseille (France).

Conclusions

This work shows the preliminary results of an investigation aimed at quantifying land subsidence in major coastal cities in Europe using EGMS products and understanding its potential driving mechanisms using geomatic layers such as geological, and hydrogeological maps. The approach could be applied to identify hotspots of land subsidence that will require further investigations to disentangling the governing mechanisms and implementing mitigation strategies and sustainable land management plans. Future studies will be performed to simulate projections of future subsidence trends and variabilities and to combine these measurements into relative sea-level rise scenarios with the final aim to estimate the flooding potential in these densely populated areas.

Acknowledgments

The activity has been developed within the scientific collaboration of the UNESCO Land Subsidence International Initiative (LaSII, https://www.landsubsidence-unesco.org/). This is a contribution of the IGCP-663 project of the IUGS and UNESCO, and SARAI project (Project PID2020-116540RB-C22 funded by MCIN/ AEI /10.13039/501100011033).

References

Abidin, H. Z., Andreas, H., Gumilar, I., Fukuda, Y., Pohan, Y. E., & Deguchi, T. (2011). Land subsidence of Jakarta (Indonesia) and its relation with urban development. *Natural hazards*, 59(3), 1753-1771.

Bonì, R., Cigna, F., Bricker, S., Meisina, C., & McCormack, H. (2016). Characterisation of hydraulic head changes and aquifer properties in the London Basin using Persistent Scatterer Interferometry ground motion data. *Journal of Hydrology*, 540, 835-849.

Catalao, J., Nico, G., & Conde, V. (2011, April). Detection of ground subsidence in the city of Lisbon: comparison of InSAR and topographic measurements. *In 2011 Joint Urban Remote Sensing Event* (pp. 417-420). IEEE.

Crosetto, M., Solari, L., Mróz, M., Balasis-Levinsen, J., Casagli, N., Frei, M., ... & Andersen, H. S. (2020). The evolution of wide-area DInSAR: From regional and national services to the European Ground Motion Service. *Remote Sensing*, 12(12), 2043.

Declercq, P. Y., Gérard, P., Pirard, E., Walstra, J., & Devleeschouwer, X. (2021). Long-term subsidence monitoring of the Alluvial plain of the Scheldt river in Antwerp (Belgium) using radar interferometry. *Remote Sensing*, 13(6), 1160.

Dehls, J. F., & Nordgulen, Ø. (2004). Evaluation of the use of PSInSAR for the monitoring of subsidence in Oslo region.

Duscher, K., Günther, A., Richts, A., Clos, P., Philipp, U., & Struckmeier, W. (2015). The GIS layers of the “International Hydrogeological Map of Europe 1: 1,500,000” in a vector format. *Hydrogeology journal*, 23(8), 1867-1875.

EEA, 2022. https://www.eea.europa.eu/data-and-maps/figures/observed-climate-zones-in-the

Fiaschi, S., Holohan, E. P., Sheehy, M., & Floris, M. (2019). PS-InSAR analysis of Sentinel-1 data for detecting ground motion in temperate oceanic climate zones: a case study in the Republic of Ireland. *Remote Sensing*, 11(3), 348.

Galloway, D. L., Erkens, G., Kuniansky, E. L., & Rowland, J. C. (2016). Preface: Land subsidence processes. *Hydrogeology Journal*, 24(3), 547-550.

Hallegatte, S., Green, C., Nicholls, R. J., & Corfee-Morlot, J. (2013). Future flood losses in major coastal cities. *Nature climate change*, 3(9), 802-806.

Herrera-García, G., Ezquerro, P., Tomás, R., Béjar-Pizarro, M., López-Vinielles, J., Rossi, M., ... & Ye, S. (2021). Mapping the global threat of land subsidence. *Science*, *371*(6524), 34-36.

Kersten, T., Kobe, M., Gabriel, G., Timmen, L., Schön, S., & Vogel, D. (2017). Geodetic monitoring of subrosion-induced subsidence processes in urban areas. *Journal of Applied Geodesy*, 11(1), 21-29.

Koster, K., Stafleu, J., & Stouthamer, E. (2018). Differential subsidence in the urbanised coastal-deltaic plain of the Netherlands. *Netherlands Journal of Geosciences*, 97(4), 215-227.

Paprotny, D., Sebastian, A., Morales-Nápoles, O., & Jonkman, S. N. (2018). Trends in flood losses in Europe over the past 150 years. *Nature communications*, 9(1), 1-12.

Parcharidis, I., Lagios, E., Sakkas, V., Raucoules, D., Feurer, D., Le Mouélic, S., ... & Cooksley, G. (2006). Subsidence monitoring within the Athens Basin (Greece) using space radar interferometric techniques. *Earth, planets and space*, 58(5), 505-513.

Pros, F., Gonzalez-Lopez, S., Martínez-Benjamin, J. J., Palau, V., & Duro, J. (2014, July). Breakwater settlement monitoring with InSAR data. *In 2014 IEEE Geoscience and Remote Sensing Symposium* (pp. 414-417). IEEE.

Ruiz-Armenteros, A. M., Manuel Delgado, J., Ballesteros-Navarro, B. J., Lazecky, M., Bakon, M., & Sousa, J. J. (2018, July). Deformation monitoring of the northern sector of the Valencia Basin (E Spain) using Ps-InSAR (1993–2010). *In IGARSS 2018-2018 IEEE International Geoscience and Remote Sensing Symposium* (pp. 2244-2247). IEEE.

Siegel, F. R. (2020). An example of coastal cities hazard exposure and economics. *In Adaptations of coastal cities to global warming, sea level rise, climate change and endemic hazards* (pp. 63-69). Springer, Cham.

Sousa, J. J., Bastos, L. C., Ruiz, A. M., Hooper, A. J., & Hanssen, R. (2012). Detection Of Ground Deformation In The Oporto Metropolitan Area With Multi-Temporal Interferometry (MTI). *Fringe 2011*, 697, 92-9092.

Terranova, C., Ventura, G., & Vilardo, G. (2015). Multiple causes of ground deformation in the Napoli metropolitan area (Italy) from integrated Persistent Scatterers DinSAR, geological, hydrological, and urban infrastructure data. *Earth-science reviews*, 146, 105-119.

Van Asselen, S., Erkens, G., Stouthamer, E., Woolderink, H. A., Geeraert, R. E., & Hefting, M. M. (2018). The relative contribution of peat compaction and oxidation to subsidence in built-up areas in the Rhine-Meuse delta, The Netherlands. *Science of the Total Environment*, 636, 177-191.

Vousdoukas, M. I., Mentaschi, L., Voukouvalas, E., Bianchi, A., Dottori, F., & Feyen, L. (2018). Climatic and socioeconomic controls of future coastal flood risk in Europe. *Nature Climate Change*, 8(9), 776-780.

Yan, X., Xu, Y., Yang, T., Tosi, L., Stouthamer, E., Minderhoud, P., ... & Bonì, R. (2022). Sustainable development of coastal cities through control of land subsidence: activities of IGCP Project 663 in Jakarta. *Episodes Journal of International Geoscience*, 45(1), 101-108.

Yue, L. U. O., Shujun, Y. E., Jichun, W. U., Xun, J. I. A. O., & Hanmei, W. A. N. G. (2015). Characterization of land subsidence during recovery of groundwater levels in Shanghai. *Geological Journal of China Universities,* 21(2), 243.

Using Video Surveys to Evaluate Land Subsidence Damage to Water Wells in the Sacramento Valley, California

J. Borchers, Water Matters LLC, Davis, California, USA (USGS, ret.)

hydrogeobro@gmail.com

Background

Down-well video surveys are used by well-service companies to determine the cause of reduced production or other problems with water wells in California. In subsiding areas, videotapes commonly show that well casings were compressed vertically and broken, collapsing telescopically into themselves. Videotapes of 317 down-well video surveys from wells in the Sacramento Valley that were collected from cities, water districts, and well drilling and pump contractors were used to 1) characterize well-casing damage, 2) to determine if they could provide information on the amounts and location of historical subsidence (subsidence occurring prior to extensive surveying or satellite-based monitoring), and 3) if damage was related to well construction methods, age of well casing, amounts of fine-grained sediment, or water-level history. Post-Eocene continental rocks and deposits that commonly contain freshwater range in thickness from 730 m in the northern part of the Sacramento Valley to more than 975 m in the southern Sacramento Valley. All scanned wells are shallower than 450 m.

Methods

Down-well video scans were collected on video tape in three formats— ¾-in, Beta, and VHS. Tapes were reviewed to determine the type of damage to well casings, depth of damage, and the amount of vertical compression on broken casings. The amount of vertical compression at each casing break was estimated by differencing the distance between casing joints as indicated by the camera depth indicator on the video tape and the original length of each casing joint as shown on Well Completion Reports submitted to California Department of Water Resources by drilling contractors. These reports also provided information on the alluvial texture of sediments penetrated by wells, and well-construction details. Reports by the California Department of Water Resources provided groundwater-level data during the time the wells were in service.

The number of damaged wells and intact wells drilled in the southwestern Sacramento Valley by three drilling contractors and three drilling methods were compared to evaluate if construction techniques influenced damage susceptibility. Relations between the integrity of well casings and well depth, well age, sediment texture, and groundwater-level change were examined statistically by comparing a group of 80 damaged wells with a group of 88 intact wells. The Mann-Whitney rank sum test was used to determine if the two samples of data come from populations that differ significantly (p-values <0.05) in the median value of the tested variable. The Mann-Whitney p-value, the smallest level of significance that allows the null hypothesis, 'the median value of the variable for damaged and intact wells is the same," to be rejected. Rejection of the null hypothesis at $p < .05$ implies that the variable may be related to subsidence damage. Additionally, Empirical Distribution Functions were prepared for damaged and intact wells to visually determine if the distribution range of values for each variable were similar in the two groups.

Results and discussion

All wells damaged by vertical compression are in the southwestern part of the Sacramento Valley, and all except one lie between the Sacramento River and the easternmost outcrop of the Tehama Formation (fig. 1). Damaged wells are in a wide north-south band from north of Zamora through Woodland and Davis, to just east of Dixon (fig. 1). This area extends to the west, north, and south of the area that other investigators have described as a regional trough of subsidence in the southwestern Sacramento Valley. All scanned wells are located in alluvium or flood-basin deposits (fig. 1) of Quaternary age and are completed in the underlying Tehama Formation of Pliocene-Pleistocene age. All substantial damage occurred to parts of the casing string within the Tehama Formation. The median depth to the top of the Tehama Formation in the damaged wells is 28.7 m below land surface. Therefore, the Quaternary alluvium and flood-basin deposits are relatively thin in the subsiding area. A thickness (and mass) of compacting and settling aquifer materials greater than that of these deposits alone probably is required to exert compressive forces that exceed the strength of steel well casing. Where spirit leveling had quantified subsidence near damaged wells, subsidence magnitude during the life of the well always exceeded the total estimated vertical offset (shortening) of broken casing.

Most damage occurs as broken casings (119), but casing ripples (18), ovaled casing (4), and crushed or spiraled well screens (13) also were observed (fig. 2). Most casing breaks and other compressive features occur at weak points in the casing string, such as perforations and slots (68), screens (13), or joints (38). However, the number of casing breaks in blank casing (25) is relatively high. The median depth, in meters below land surface, of ruptures at casing joints (68) and casing openings (73) is about the same, but, oddly, the median depth of ruptures in blank casing is significantly shallower (48 m). The vertical offset on most compressive features was estimated to be less than 0.15 m. The greatest estimated vertical offset on a single compressive feature is 0.91 m. There is no apparent relation between the amount of vertical offset and the depth of a compressive feature below land surface. Most wells have only one compressive feature although one well was found to have six separate casing ruptures.

Nonparametric statistical analysis of quantitative factors that might be related to subsidence indicated that the following have a greater than 95 percent chance of being significantly different between a group of 80 damaged wells and a group of 88 intact wells: age of a well at the time it was scanned; maximum change in hydraulic head and the decline of the preconsolidation head during the active life of the well; year the well was drilled; year the well was scanned; fatigue factor (a measure of potential strain hardening and embrittlement calculated by multiplying the days in service by the average annual change of hydraulic head). Other factors, such as well depth, texture (meters of fine-grained sediment), relative texture (percent fine-grained sediment), altitude of land surface, and average annual change of hydraulic head were not significantly different between the groups, implying these factors likely were unrelated to subsidence that damaged wells.

The categorical variables drilling method and drilling contractor were examined by comparing the number of damaged wells with the number of intact wells in each category, as shown in table 1. A relation between drilling contractor and well damage might be inferred from table 1. For contractor I, the numbers of intact and damaged wells are about equal; for contractor II, most wells sustained damage; and for contractor III, most wells remained intact. Other factors being equal, this might indicate contractor III drills good wells. However, a comparison of broken and intact wells by drilling method (table 1) implies that reverse rotary wells are less likely to be damaged than wells drilled by other methods, and that a relation between drilling method and well damage may be the underlying reason for the apparent relation between drilling contractor and well damage. That is, wells drilled by contractor II that were mostly damaged were drilled primarily by the conventional-rotary method.

To determine if the apparent relation between drilling method and well damage is real or coincidental, data on hydraulic-head change and well age were analyzed separately for wells drilled by cable-tool, conventional-rotary, and reverse-rotary methods. In addition, and because of the relative abundance of data for conventional-rotary wells, data from damaged and intact wells drilled by this method were used preferentially to determine if well age or change in hydraulic head were related to well damage (table 2).

As a group, the cable-tool and conventional rotary wells are older than those drilled by the reverse-rotary method (table 2), which is a newer technique. However, because there seems to be little difference in the length of time that damaged and intact conventional rotary wells have been in service it is likely unimportant that the age of cable-tool and conventional-rotary wells (median for both methods, about 6200 days) greatly exceeds the age of reverse-rotary wells (median, 2900 days, table 2). The apparent relation between well age and damage probably reflects a relation between well damage and the timing of subsidence, rather than a weakening of well casing by corrosion or other time-dependent process.

Similarly, the fatigue factor is higher for cable tool and conventional rotary wells than for reverse rotary wells, but because there is not a statistical difference in this variable between damaged and intact wells drilled by the conventional rotary method ($p=0.209$, table 2) it is likely that strain weakening of well casing is not significantly related to the occurrence of damage.

The average annual change of hydraulic head at wells drilled by the conventional rotary method also is not significantly different in damaged and intact conventional-rotary wells and therefor this variable likely is unrelated to well damage.

Likewise, the median maximum change in hydraulic head during the service time of damaged conventional-rotary wells is slightly higher than that for intact wells in the same group (median, 19.5 and 18 m, respectively; table 2), but the differences are not statistically significant at the 0.05 level ($p = 0.0975$). Hydraulic-head variables in table 2 are not independent. The weak relation between the average annual change of hydraulic head or the maximum change in hydraulic head, and damaged wells likely results from a more direct relation between well damage and decline of the preconsolidation head.

Preconsolidation head is the hydraulic head (groundwater level) that triggers inelastic, permanent compaction of aquifer sediments and initiation of substantial subsidence. For the aquifer system in the study area the preconsolidation head is roughly equivalent to the lowest hydraulic head aquifer sediments have experienced. The aquifer near damaged, conventional-rotary wells has undergone a significantly greater decline in preconsolidation head than has the aquifer near intact conventional-rotary wells during the time the wells were in service (median, 6.1 and 0.91m, respectively, $p = 0.0148$; table 2, fig. 2). The decline of the preconsolidation head during the service time of wells drilled by the conventional-rotary and cable-tool methods is greater than that for wells drilled by the reverse-rotary method (fig 3.). In fact, the preconsolidation head in the aquifer near most reverse-rotary wells has not declined between the date the wells were constructed and the date they were scanned (median = 0 m, table 2; fig.3).

Conclusions

Data gleaned from video tapes of downwell video surveys suggests that the drilling method has little effect on ability of a well to resist subsidence. However, because most reverse-rotary wells probably have not been subjected to the high rates and amounts of subsidence that have occurred near many wells drilled by other methods, the ability of reverse-rotary wells to resist vertical compression has not been adequately tested in the field. Therefore, relations between drilling method and well damage cannot be evaluated until more data are available to describe the reaction of reverse-rotary wells to compressive forces in actively subsiding areas. The decline of preconsolidation head in the aquifer system is likely the primary cause of inelastic subsidence that exerted downward compressive force on well casings that was sufficient to collapse casings telescopically into themselves, bending, ripping, and shortening casing strings. Conclusions relating vertical shortening of the casing string to subsidence magnitude are subject to error because neither casing protrusion or subsidence rate have been considered in the analysis.

Table 4. Number of Damaged and Intact Wells Constructed by Three Drilling Contractors

	Drilling Method*			
	All Three Methods	Rev. Rotary	Conv. Rotary	Cable Tool
Contractor I				
Intact Wells	17	8	8	1
Damaged Wells	21	1	17	3
Contractor II				
Intact Wells	2	0	2	0
Damaged Wells	13	0	13	0
Contractor III				
Intact Wells	10	6	3	1
Damaged Wells	3	2	1	0

*Rev. Rotary = reverse-rotary drilling method, Conv. Rotary = conventional-rotary drilling method.

Table 2 Comparison of Water-Level and Well-Age Variables Between Wells Drilled by All Three Drilling Methoas and Between Damaged and Intact Wells Drilled by the Conventional Rotary Method (No. of wells in ().)

	Cable Tool Median Value All Wells	Reverse Rotary Median Value All Wells	Conventional Rotary Median Values All Wells	Conventional Rotary Median Values Intact Wells	Conventional Rotary Median Values Damaged Wells	Mann-Whitney *p*-Value
Year Well Drilled	1959 (12)	1977 (21)	1964 (53)	1968 (16)	1962 (37)	0.0501
Well Age (days)	6166 (9)	3827 (18)	6173 (51)	5471 (14)	6269 (37)	0.5616
Average Annual Change of Hydraulic Head (m)	4.6 (10)	6.9 (16)	6.7 (51)	22 (14)	6.7 (37)	0.2457
Fatigue Factor (day-m*)	25,600 (10)	19,700 (16)	45,000 (51)	30,600 (14)	48,400 (37)	0.2092
Maximum Change ot Hydraulic Head (m)	14.9 (10)	16.3 (16)	18.6 (51)	18 (14)	19.5 (37)	0.0975
Decline of Preconsolidation Head (m)	1.7 (10)	0 (16)	3.7 (51)	0.9 (14)	6.1 (37)	0.0148

Table 1 & 2 1) Number of damaged and intact wells constructed by three drilling contractors, 2) Comparison of water-level and well-age variables between wells drilled by all three drilling methods and between damaged and intact wells drilled by the conventional rotary method.

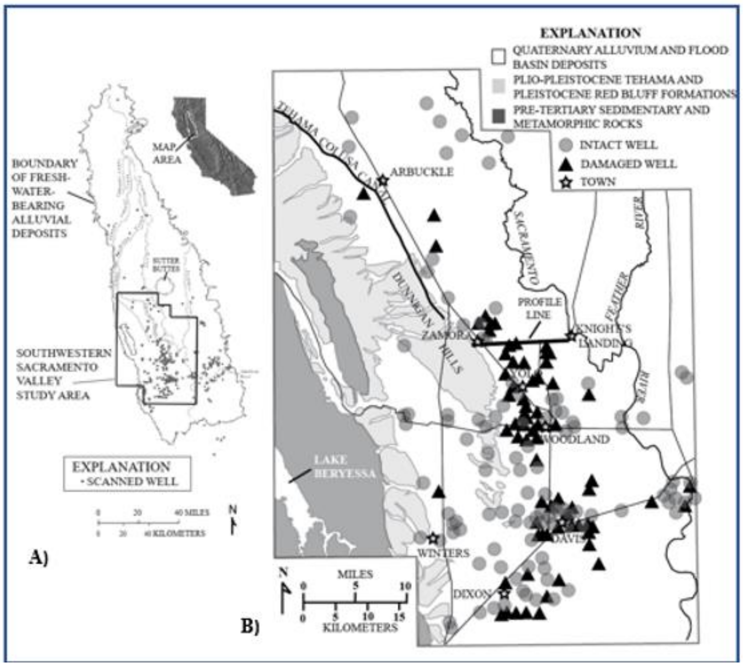

Figure 1 A) Location of the study area and video scanned wells, and B) Geology and location of damaged and intact wells.

Figure 2 A) Ovaling and rippling, B) Ripping and tearing, C) Crushing/Spiraling of well screen.

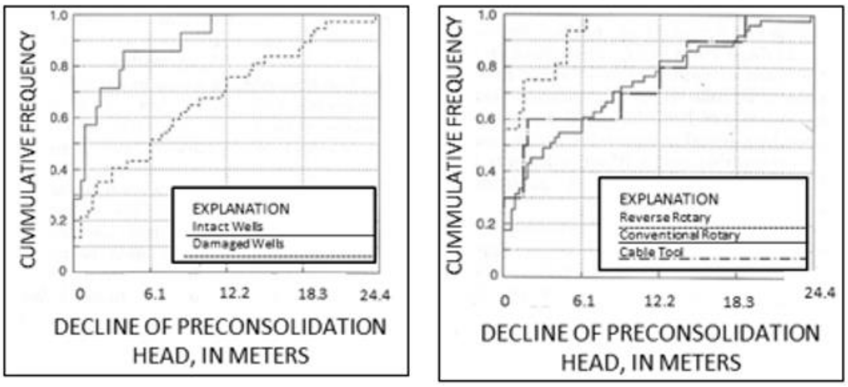

Figure 3 & 4 3) Empirical distribution functions of the decline of the preconsolidation head in the aquifer near damaged and intact wells drilled by the conventional rotary method, 4) Empirical distributions functions of the decline of the preconsolidation head in the aquifer near wells drilled by the reverse-rotary conventional rotary, and cable-tool methods.

Holocene stratigraphy and land subsidence: Understanding the subsidence of the Volturno River alluvial plain by combining geological and geotechnical modelling

Carla Buffardi[1], Daniela Ruberti[1]

1 Department of Engineering - University of Campania L. Vanvitelli, Via Roma, 9, 81031 - Aversa (CE), Italy 6

carla.buffardi@unicampania.it

Session: Mechanisms and Understanding of land subsidence

Introduction

Recently most of the world's major river deltas are sinking due to both accelerations in global sea level rise and subsidence rates. Other effects of subsidence can be aquifer salinization, inundation of lowlands, and coastal erosion, among others (Bagheri-Gavkosh et al., 2021; Herrera-García et al., 2021). In coastal and delta areas, subsidence can have natural causes related to the recent formation and composition of the geological substrate. The latter is often consisting of alternating layers of sand and more compressible materials, like clay and peat.

In the Mediterranean area, there are several alluvial coastal plains affected by subsidence (Yan et al., 2020). The aim of the present study is the definition of the substrate architecture and its correlation with the ground deformation trends of an alluvial coastal plain along the eastern Tyrrhenian Sea. The study area is the plain of the Volturno River, located in the northern Campania coastal area (Southern Italy), developed after the Holocene transgression.

In this area the base of the Holocene deposit is represented by a volcaniclastic unit (the Campania Grey Tuff - CGT) originated by the Campi Flegrei caldera 39 ka eruption, that covered all the previous marine-transitional settings on the whole alluvial and coastal plain. In response to the Last Glacial Maximum sea-level drop, a paleovalley originated from the paleo-Volturno River fluvial downcutting, about 15-20 km wide and up to 30 m deep in the depocenter (Ruberti et al., 2022).

Materials and methods

The reconstruction of the subsoil relies on more than 1500 shallow borehole stratigraphies (mostly up to 20-30 m in depth) and CPTs located along the Volturno plain. The facies analysis and the lithostratigraphic study allowed the reconstruction of the Late-Pleistocene-Holocene stratigraphic architecture; moreover, the 3D graphic restoration of the LGM incised valley morphology, engraved in the CGT deposits, provided the outline of the reference surface for the Holocene sedimentation. The litho-stratigraphic data were compared with the coefficients obtained from the elaboration of CPTs, in order to characterize also the geotechnical properties of the different layers.

The next step involved a preliminary correlation between subsidence rates and the geological and geotechnical composition of the subsurface. A cumulative vertical ground displacement map was used, estimated during 1992-2010, based on Matano et al., 2018 (Fig. 1A).

In order to understand if and how the different lithologies recognized are related to the distribution of subsidence rates, post-CGT deposits were further classified and gathered on the basis of the main lithological facies such as sands, clays and peat as they represent the more compressible materials and subjected to secondary consolidation. For each stratigraphic log, the thicknesses of these lithologies were compared to the total thickness of the post-CGT deposit. Different coefficients were developed and hierarchized to establish the relationships between the analyzed characteristics of geotechnical weak horizons and the variability of subsidence rates, that range between 0 and -20 mm/yr in an area of about 750 kmq across the Volturno River and that shows places with apparently anomalous localized subsidence.

The overlay with data on settlements, road and rail networks and floodable areas represents a first step towards a risk analysis.

Results and discussions

Among the main outputs of the research, the reconstruction of the upper surface of the CGT is of valuable interest. It provides the picture of the palaeomorphology at the LGM through a 3D Digital Surface Model (DSM). The reconstructed surface actually suggests the occurrence of a complex network of incisions that supports the reconstruction of a channel entrenchment on the plain and especially towards the coastline, which at that time was located ca. 13 km offshore (Ruberti et al., 2022). Above this surface, large remobilization of volcaniclastic material took place during the re-establishment of the fluvial system, witnessed by the abundance of reworked pyroclastic ash and clasts recognized in the alluvial deposits of the medium-upper part of the valley fill. Transitional and marine deposits occur in the lower and coastal plain. There, medium-coarse sand and gravel intercalate to silty sand and grey-blue clay and silt very rich in organic material and peat (Fig. 1 C).

The spatial analysis, conducted by a GIS software, highlighted the relationship between major ground deformation and the filling of the incised paleo-valley, corresponding to the Holocene alluvial/transitional deposits that overlies a compaction-free Pleistocene basement, and this is consistent with the hypothesis that compaction of deeper Holocene strata is still significant (Fig. 1 A). Inside this general trend, differential compaction was detected proceeding from the coastal zone towards the interior (Fig. 1 B). This can be explained given the more recent age of the sediments in the inner part of the plain, the ones corresponding to the maximum ingression of the sea during the Holocene transgression. This can be confirmed by the consideration that most of the compaction of peat, in fact, occurs during the formation phase, mainly due to microbiological and chemical processes in wet environments. Thus, the deepest peat deposits (the oldest ones) have already compacted in the first stage of the Holocene transgression (van Asselen et al., 2009).

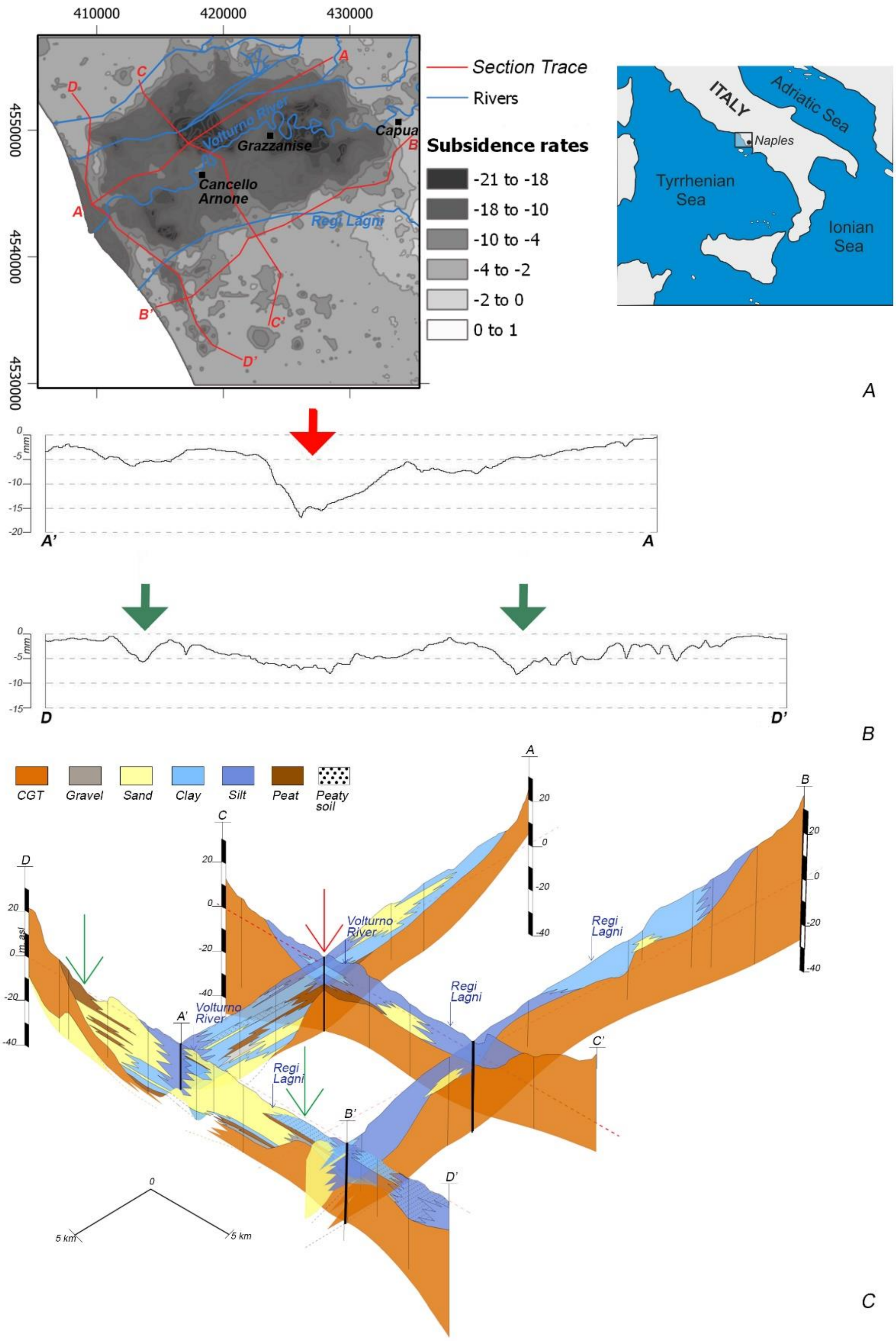

Figure 1 A) Cumulative vertical ground displacement map estimated during 1992-2010 (based on Matano et al., 2018). Location map of the study area. B) Subsidence profiles of the sections AA' and DD' are shown as representative of the general trend across the plain. Red and green arrows indicate negative peaks, discussed in the text and displayed on the 3-D lithostratigraphic reconstruction in (C).

Rates of subsidence due to the compaction of Holocene sediments have been documented in several floodplains and deltaic coastal plains around the world (Higgins, 2015; Teatini et al., 2011), due to the compaction of compressible sediments such as peat and clay. It is clear that compaction does not occur equally throughout the stratigraphic sequence, but may depend on stratigraphic position (i.e. age and depth) or thickness

Our findings confirm that the viscous component of these materials plays an important role in their behavior: the geologically younger soils are still subject to secondary subsidence while the older ones have already undergone much consolidation also because of the lithostatic load, and the inclusion of a significant amount of peat and organic matter clearly reflects high values for the coefficient of secondary compression.

In this respect, in order to characterize the geomechanical behaviour of each horizon, a detailed reconstruction of the Holocene fill appears to be of fundamental importance.

Conclusion

The analysis of the relationship between ground deformation and stratigraphic architecture have demonstrated the strong correspondence major vertical displacements and high thicknesses of compressible materials. Furthermore, the stratigraphic position of these layers assumes a significant role since the consolidation is time-dependent (Buffardi et al., 2021). With the aim to sharing research results, the future goal could be to export the methodology developed in this study to other coastal contexts in the Mediterranean area.

References

Amorosi, A., Pacifico, A., Rossi, V., Ruberti, D., 2012. Late Quaternary incision and deposition in an active volcanic setting: The Volturno valley fill, southern Italy. *Sediment. Geol*. 282, 307–320. https://doi.org/10.1016/j.sedgeo.2012.10.003

Bagheri-Gavkosh, M., Hosseini, S. M., Ataie-Ashtiani, B., Sohani, Y., Ebrahimian, H., Morovat, F., & Ashrafi, S., 2021. Land subsidence: A global challenge. *Science of The Total Environment*, 778, 146193. https://doi.org/10.1016/j.scitotenv.2021.146193

Buffardi, C., Barbato, R., Vigliotti, M., Mandolini, A., & Ruberti, D., 2021. The holocene evolution of the volturno coastal plain (Northern campania, southern italy): Implications for the understanding of subsidence patterns. *Water (Switzerland*), 13(19). https://doi.org/10.3390/w13192692

Herrera-García, G., Ezquerro, P., Tomás, R., Béjar-Pizarro, M., López-Vinielles, J., Rossi, M., Mateos, R.M., Carreón-Freyre, D., Lambert, J., Teatini, P., Cabral-Cano, E., Erkens, G., Galloway, D., Hung, W.-C., Kakar, N., Sneed, M., Tosi, L., Wang, H. and Ye, S., 2021. Mapping the global threat of land subsidence. *Science*, 371(6524), 34–36. https://doi.org/10.1126/science.abb8549.

Higgins, S.A., 2015. Review: Advances in delta-subsidence research using satellite methods. *Hydrogeol. J*. 24, 587–600. https://doi.org/10.1007/s10040-015-1330-6

Matano, F., Sacchi, M., Vigliotti, M. & Ruberti, D., 2018. Subsidence Trends of Volturno River Coastal Plain (Northern Campania, Southern Italy) Inferred by SAR Interferometry Data. *Geosciences,* 8, 8. https://doi.org/10.3390/geosciences8010008.

Ruberti, D., Buffardi, C., Sacchi, M., & Vigliotti, M., 2022. The late Pleistocene-Holocene changing morphology of the Volturno delta and coast (northern Campania, Italy): Geological architecture and human influence. *Quaternary International*, 625(September 2021), 14–28. https://doi.org/10.1016/j.quaint.2022.03.023

Sacchi, M., Molisso, F., Pacifico, A., Vigliotti, M., Sabbarese, C., Ruberti, D., 2014. Late-Holocene to recent evolution of Lake Patria, South Italy: An example of a coastal lagoon within a Mediterranean delta system. *Glob. Planet. Change* 117, 9–27. https://doi.org/10.1016/j.gloplacha.2014.03.004

Teatini, P., Tosi, L., Strozzi, T., 2011. Quantitative evidence that compaction of Holocene sediments drives the present land subsidence of the Po Delta, Italy. *J. Geophys. Res. Solid Earth* 116, 8407. https://doi.org/10.1029/2010JB008122

van Asselen, S., Stouthamer, E., van Asch, T.W.J., 2009. Effects of peat compaction on delta evolution: A review on processes, responses, measuring and modeling. *Earth-Science Rev.* 92, 35–51. https://doi.org/10.1016/j.earscirev.2008.11.00

Yan, X., Yang, T., Yan, X.U., Tosi, L., Stouthamer, E., Andreas, H., Minderhoud, P., Ladawadee, A., Hanssen, R., Erkens, G., Teatini, P., Lin, J., Bonì, R., Chimpalee, J., Huang, X., Da LIO, C., Meisina, C. and Zucca, F. ,2020. Advances and Practices on the Research, Prevention and Control of Land Subsidence in Coastal Cities. *Acta Geologica Sinica*, 94(1), 162–175. https://doi.org/10.1111/1755-6724.14403

Analysis of Surface Deformation Patterns Affecting Taiwan's High-Speed Rail System near Tuku, Yunlin County, Taiwan

T.J. Burbey[1]

1 Virginia Tech, USA

tjburbey@vt.edu

Background

West-central Taiwan continues to experience excessive land subsidence due to the overexploitation (3.3 billion cubic meters annually) of the Choshui River alluvial aquifer system in support of its extensive agriculture and aquaculture economies in Chunghwa and Yunlin Counties (Lee, Yu et al. 2018). Taiwan's high speed rail (HSR) system extends north-south through one of the country's most severe land subsidence bowls near Tuku in Yunlin County, south of the Choshui River (Fig 1). The pillars near Tuku that support the HSR reside along the eastern flank of the most severe subsidence bowl in the region, causing the pillars to subside, move laterally westward and tilt eastward (Taiwan HSR, personal commun, 2020). The eastward tilt is contrary to logical thinking and a perplexing problem when subsidence is viewed as a one-dimensional problem. This research shows that when viewed in a three-dimensional framework, the motions occurring along the HSR near Tuku can be readily explained through examination of the surface motions from the GNSS network, understanding the influence of the aquifer-system boundary conditions and careful analysis of results from an E-W plane-strain aquifer flow and deformation model of the individual aquitards and aquifers encountered vertically by the foundation of the pillars.

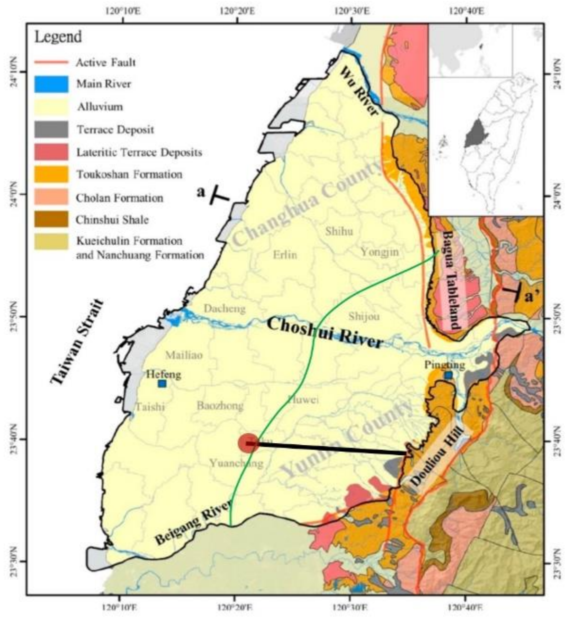

Figure 1 Location of study area in Yunlin County. Black line shows extent of plane-strain numerical model. Green line is the high-speed rail (HSR) system and red circle is the subsidence bowl impacting the HSR.

Study area

Chunghwa and Yunlin counties in west-central Taiwan cover 1,800 km2 with the Choshui river bisecting the counties and flowing westward from the highlands in the east (100 m amsl) to the coast bordering the Taiwan Strait (Fig 1) (Tatas, Chu et al. 2022). The aquifer system is composed of sands, silts and clays eroded from the sedimentary and metamorphic rocks along the eastern boundary of the aquifer system (Fig 1). The uppermost 200m of aquifer system in the study are is composed of three aquifers (ranging in thickness from 42m to 95m in the mid fan but decreasing westward) and two intervening aquitards that vary in thickness from zero along the eastern margin to more than 100m in thickness along the coast where the clays dominate (Fig 2) (Ali, Chu et al. 2021). The major subsidence bowl near Tuku in Yunlin county is in the mid fan part of the aquifer system. Aquifer two (AQ2) is the primary producing unit leading to most of the land subsidence in the area and occurs within the uppermost 200m of the system (Chu, Ali et al. 2021). The distance from the pumping center in Tuku to the eastern boundary is approximately 25 km.

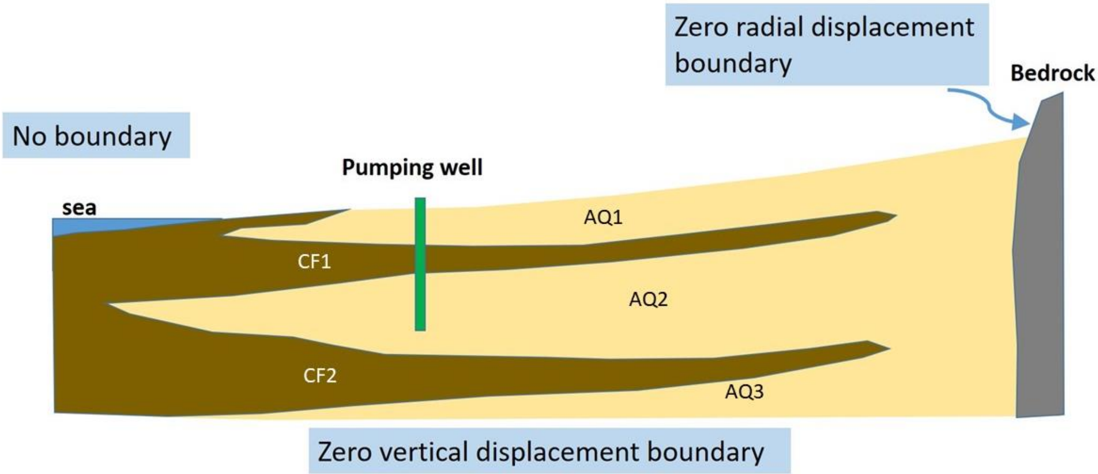

Figure 2 Conceptual model along east-west section near Tuku (black line in Fig 1) showing aquifers (AQ) and aquitards (CF) in the uppermost 200 m of the system. The numerical model extends from the pumping well to the eastern bedrock boundary (25km).

Methods

Taiwan has one of the most widespread GNSS networks in the world (Hung, Hwang et al. 2010). However, all motions on Taiwan are typically measured relative to a station in Penghu, an island off the coast in the Taiwan Strait. This results in the general motion of mainland Taiwan to move westward or northwestward, particularly those stations situated within the study area due to the overall plate motion on which Taiwan resides. However, because the aquifer is free to move from pumping-induced deformation relative to bedrock and plate motion, the GUKN station within the bedrock just east of the Choshui alluvial aquifer system is chosen as the reference frame for this investigation. This changes the direction of motions within the aquifer system to an eastward orientation; that is, toward to only fixed boundary condition within the aquifer system. This eastward motion is attributed to extensive groundwater pumping in the mid fan region (near Tuku in the study area).

A two-dimensional plane strain Biot model (Hsieh 1996) was constructed to simulate groundwater flow and vertical and horizontal aquifer deformation in the region from the pumping center near Tuku to the eastern fixed hardrock boundary (no radial displacement, Fig 2), a distance of about 25 km. The model is free to subside vertically on the lateral boundaries. The eastern lateral boundary has an outward flux in the zone representing aquifer two but this boundary is free to move horizontally and vertically. The bottom boundary is allowed to freely move horizontally but is fixed vertically. The total thickness of the model is 200 m, representing the uppermost sediments and active zone of pumping. The model simulates flow and deformation in a three aquifer—two aquitard model using hydraulic and poromechanical properties obtained from pumping tests, drilling logs, laboratory testing and previous investigations.

Results

Numerical modeling results support the GNSS surface deformations when using GUKN as the reference frame. When excessive groundwater pumping occurs in the mid-fan region, the fixed eastern boundary causes the continuous deformable aquifer system to be pulled toward it (Fig 3). Furthermore, greater surface deformation occurs toward the east and is dampened with depth, particularly through the clay confining layers, which, according to numerical results from the Biot model, tends to impede horizontal motion causing a shearing effect (Fig 4). Horizontal deformation through each aquifer is constant at a particular location with the uppermost aquifer experiencing the greatest eastward deformation and the third aquifer (150-200m depth) experiencing the least. This pattern explains why the pillars are tilting toward the east and not toward the west, which would be the case if a draping effect were dominating the deformation. Pillar foundations extend 60 m into the aquifer system; deep enough to experience the lessening eastward horizontal motion with depth (Fig 5). In addition, the pillars near the Tuku subsidence bowl are actually moving eastward at a lower rate than the pillars north and south of the subsidence bowl. This slower rate is hypothesized to be due to the larger thickness of clays in the vicinity of the subsidence bowl and extending eastward. This hypothesis is supported by the drilling logs when the pillars were installed.

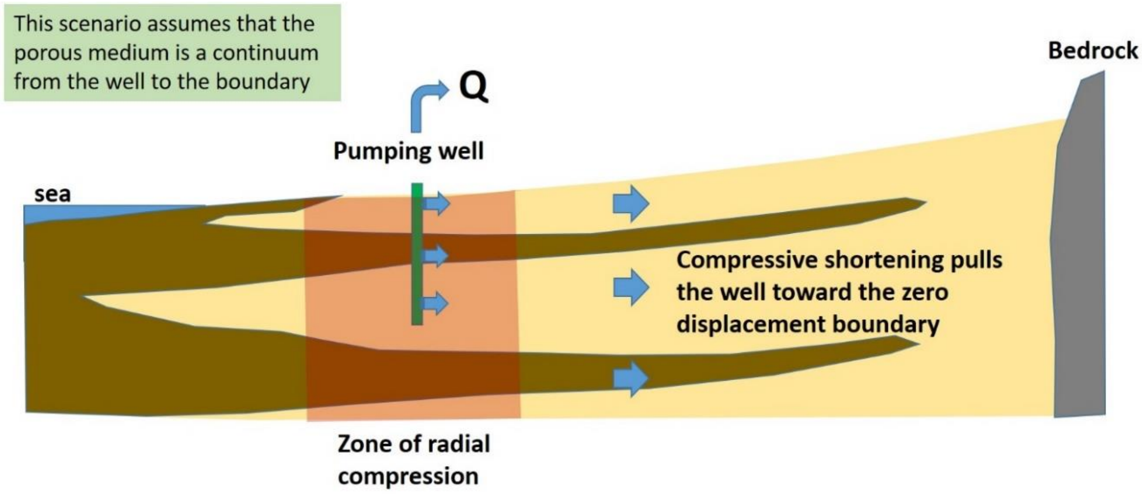

Figure 3 Although a region of radial compression occurs in the vicinity of the subsidence bowl, the overall motion of the aquifer is drawn toward the eastern boundary because the aquifer behaves as a continuum.

These findings reveal the vital role of fixed boundary conditions in large-scale deformation modelling and the role that excessive groundwater pumping and aquifer heterogeneity play in influencing both surface and subsurface three-dimensional deformation patterns. This understanding is important for managing and mitigating the deleterious effects of groundwater pumping on Taiwan's HSR system.

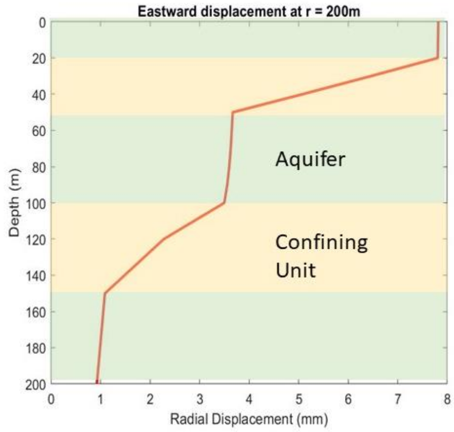

Figure 4 Numerical results showing that clay units dampen horizontal motion causing a shearing that causes a decrease in eastward motion with depth

Conclusions

Excessive groundwater exploitation in Chunghwa and Yunlin counties in west-central Taiwan has led to continuous and widespread land subsidence. An extensive GNSS network reveals that surface deformations from pumping are eastward toward the "fixed" mountains. Taiwan's HSR runs north-south along the flank of Taiwan's largest subsidence bowl. Numerical modeling reveals that eastward motion is dampened with depth through the topmost three aquifers and leads to an eastward tilt of the pillars near the subsidence bowl.

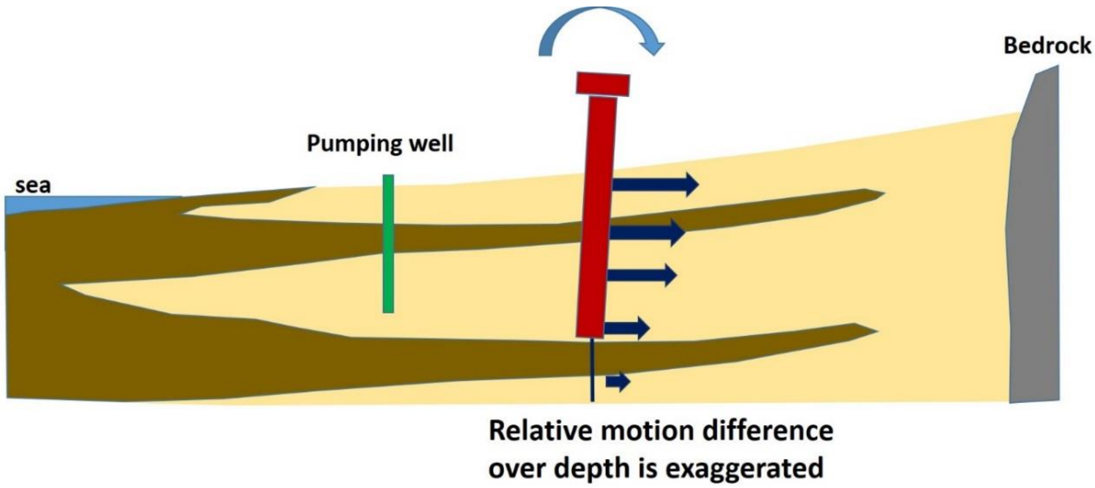

Figure 5 The pillars are deep enough to be influenced by the dampening eastward horizontal motion causing the pillars to tilt eastward away from the pumping center near Tuku.

References

Ali, M. Z., et al. (2021). "Spatio-temporal estimation of monthly groundwater levels from GPS-based land deformation." *Environmental Modelling & Software* 143: 105123.

Chu, H.-J., et al. (2021). "Spatio-temporal data fusion for fine-resolution subsidence estimation." *Environmental Modelling & Software* 137: 104975.

Hsieh, P. A. (1996). "Deformation-induced changes in hydraulic head during ground-water withdrawal." *Ground Water* 34(6): 1082-1089.

Hung, W.-C., et al. (2010). "Monitoring severe aquifer-system compaction and land subsidence in Taiwan using multiple sensors: Yunlin, the southern Choushui River Alluvial Fan." *Environmental Earth Science* 59: 1535-1548.

Lee, M., et al. (2018). "Water-energy Nexus for multi-criteria decision making in water resource management: A case study of the Choshui River Basin in Taiwan." *Water* 10(12).

Tatas, et al. (2022). "Estimating future (next-month's) spatial groundwater response from current regional pumping and precipitation rates." *Journal of Hydrology* 604: 127160.

Proc. IAHS, 382, 571–576, 2020
https://doi.org/10.5194/piahs-382-571-2020

Tenth International Symposium on Land Subsidence (TISOLS)

Factors that condition physical vulnerability to ground fracturing in Mexico City

Dora Carreon-Freyre[1], Raul I. Gutierrez-Calderon[2], Mariano Cerca[1], and Carlos F. Alcantara-Duran[2]

[1]Centro de Geociencias, Universidad Nacional Autónoma de México, Santiago de Querétaro, PC 76230, Mexico
[2]Coordinación de Evaluación de Riesgo, Iztapalapa, Mexico City, PC 09000, Mexico

Correspondence: Dora Carreon-Freyre (freyre@geociencias.unam.mx)

Published: 22 April 2020

Abstract. In spite of subsidence being a well-studied geological phenomenon in Mexico City, its effects and risks for urban infrastructure and inhabitants have been neglected. Damage in the short, medium and long term implies maintenance and important mitigation costs. There are not systematic studies that address methodologies for the estimation of physical vulnerability of the geological media to fracture. In this work, factors conditioning the deformation and susceptibility to fracturing are analyzed using a deterministic approach. The identified physical variables were mapped, measured and integrated into a database that allowed for an adequate correlation of the parameters that condition fractures spatial distribution. A methodology for estimating a vulnerability index to fracturing (VIF) useful for decision making is proposed in this work.

1 Introduction

According to historical reports, earth fissures and ground fractures affected the Mexico City subsoil before 1900 and have been studied since the mid-twentieth century. The persistent subsidence and the associated differential (Gayol, 1925) deformation have caused damage to housing and urban infrastructure, mainly to roads, water pipes and drainage. The first subsidence measurements and ground fractures developed after the beginning of groundwater extraction in the central part of the lacustrine plain were reported in 1925. Since then, a total subsidence of 13 m has been reported at the center of Mexico City. Land subsidence was first numerically associated with groundwater extraction in the 1950s. The local authorities began to restrict groundwater pumping in the most affected areas nevertheless, and by the 1970s groundwater extraction was translated to the eastern side of the city (around the remnants of Lake Texcoco). With a fast-growing population and an increased need of water, ground fractures also developed in this zone, and by the 1990s fractures propagated and covered a larger area (Fig. 1).

Land subsidence has been widely studied in Mexico City during the last 5 decades (Zeevaert, 1953); nevertheless its effects in the mid and long term and risks for urban infrastructure and inhabitants have not yet been assessed properly. Damages in the long term implies maintenance and important mitigation costs (Carreon-Freyre et al., 2019). There are not systematic studies that address a methodology for the estimation of physical vulnerability to the fracture of the geological media. In this work, factors conditioning the deformation and susceptibility to fracturing are analyzed using a deterministic approach. A total subsidence of 13 m has been reported at the center of the lacustrine plain in Mexico City (Cabral-Cano et al., 2008; López-Quiroz et al., 2009).

Brittle fracturing of the near-surface clayey sediments of the lake has been attributed to subsidence related to high groundwater exploitation rates (Carrillo, 1947; Carreón-Freyre et al., 2006; Ovando-Shelley et al., 2012). Surficial deformation features can be related to shallow groundwater flows, and, consequently, fractures open and close seasonally (Carreón Freyre, 2010; Carreon-Freyre et al., 2016; Aguilar-Pérez et al., 2006). Moreover, a generalized consolidation state of thick clayey sequences related to deep groundwater depletion has been established; deep ground fracturing is a non-dilatant fracture in silts and clay sequences and may propagate through weak planes associated with lithological

(a) (b)

Figure 1. **(a)** Camarón Street fracture, Tláhuac, Mexico City. **(b)** Fracture in Albarradas, Iztapalapa, Mexico City.

contacts or major structural features from depth to the surface. A complex pattern of ground fractures dissects the lacustrine plain of Mexico City, which threatened the urban infrastructure. Recently the map of fractures was integrated into the Mexican *National atlas of risks* (Carreón Freyre et al., 2017) (Fig. 2).

2 Physical variables conditioning physical vulnerability of the media to fracture development

The general concept of physical vulnerability that considers a "degree of damage" can be defined differently in each discipline; for this work we consider the physical vulnerability as the "characteristic of the geological media that describes its susceptibility (or resistance) to the impact of the hazard of fracturing" in agreement with the definitions stated by the glossary presented in Schmidt-Thomé et al. (2007) and Kappes et al. (2012). The evaluation of physical vulnerability requires the implementation of an interdisciplinary methodology including: (a) the review of groundwater management, especially in urban areas; (b) detailed geological, hydrogeological and morphological characterization; and (c) the monitoring of groundwater piezometric evolution, land subsidence and ground differential displacements. The interdisciplinary analysis allows for a better understating of the triggering mechanisms of differential settlements, the generation and the propagation of ground fracturing (Ochoa-González et al., 2018).

According to previous studies ground fracturing is generated by the interaction of different factors (Carreon-Freyre et al., 2019): (1) geological preexisting discontinuities caused by variations in the depositional environment (Carreón-Freyre et al., 2006); (2) stress history due to climate changes determining the geometry of early fracturing; (3) variations in the compressibility and permeability of geological materials that control short-term and local-scale deformation (Carreon-Freyre et al., 2016); and (4) the exhaustive exploitation of aquifers causing a decline of the pore water pressure leading to subsidence and creating vertical and horizontal tensile stresses (Carrillo, 1947; Rivera and Ledoux, 1991; Holzer, 1984; Juárez-Badillo and Figueroa Vega, 1984). The propagation of fractures is conditioned by the interaction of physical variables that can be mapped, measured and integrated into a database. Coexistence of one or several of the mentioned factors determines the mechanism of fracturing at diverse scales.

3 Estimation of the vulnerability index to fracturing

We have followed a deterministic approach and the indicator-based methodology proposed by Kappes et al. (2012) for the study of multiple variables that can be mapped, measured and integrated into a database for spatial correlation analysis. For the development of the vulnerability index to fracturing (VIF) a weighted numerical analysis was performed to determine the potential areas of Mexico City that are prone to subside, develop ground fractures and/or present severe differential deformation (Fig. 3). Susceptibility of the variables was estimated and normalized for each variable that includes the addition of the weighted values: terrain slope from the geomorphologic map (W_{gm}), piezometric descent (W_{pd}), gradient of subsidence (W_{gs}), fracture type (W_{f}) and lithological variations or contacts (W_{lit}), as shown in the following equation:

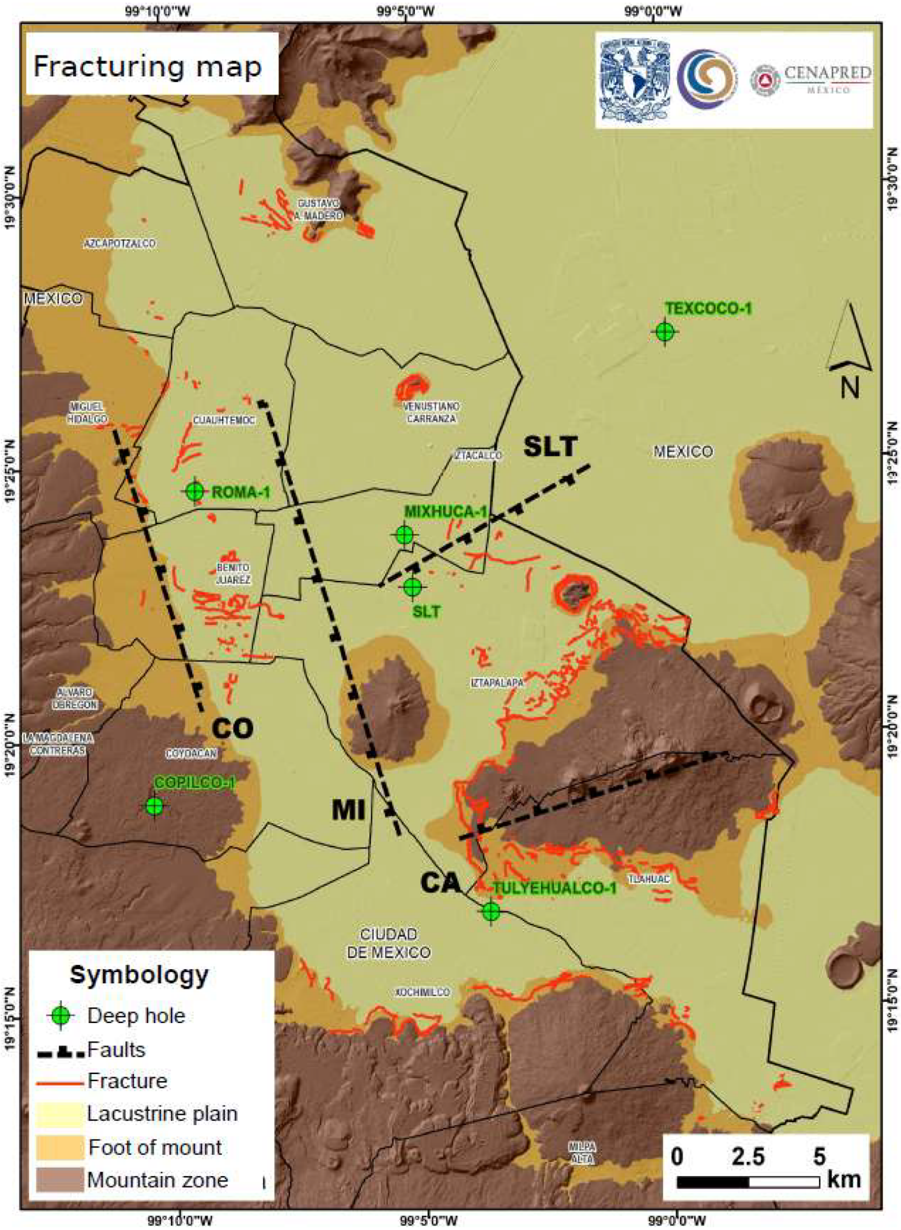

Figure 2. Ground fractures distribution in Mexico City (red lines) and main regional geological reported faults (black dotted lines) (Carreón Freyre et al., 2017).

$$\mathrm{VIF} = \left[\sum_{i=0}^{n} W_{\mathrm{gm}} + W_{\mathrm{pd}} + W_{\mathrm{gs}} + W_{\mathrm{f}} + W_{\mathrm{lit}}\right] / n\,, \tag{1}$$

where n is the number of variables.

The assignation of the weighted values considered a different percentage of the total amount recorded in the study area. For example, to estimate the "gradient of subsidence" (g_{s}), two tables were defined for absolute (Table 1) and weighted values (Table 2).

The spatial correlation of the physical variables allowed for identifying zones of fracture generation and estimating

Table 1. Rated values for the gradient of subsidence (g_{s}) in Mexico City.

Gradient of subsidence	Assigned value
Low (< 4 cm)	0 %
Medium (4–12 cm)	65 %
High (> 12 cm)	35 %
Total assigned value	100 %

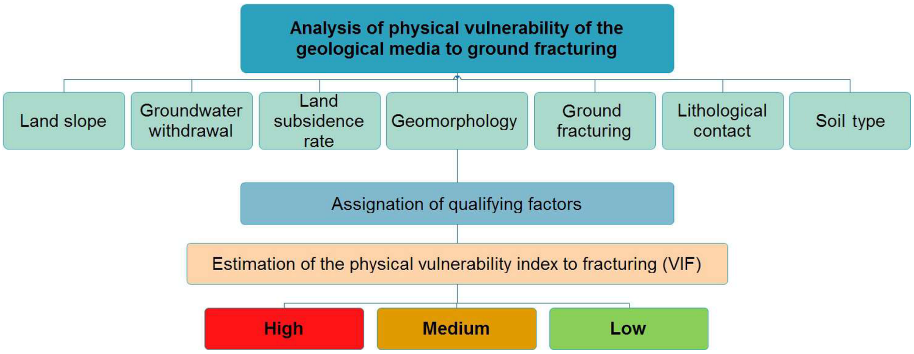

Figure 3. Flowchart for the determination of the physical vulnerability index to fracturing.

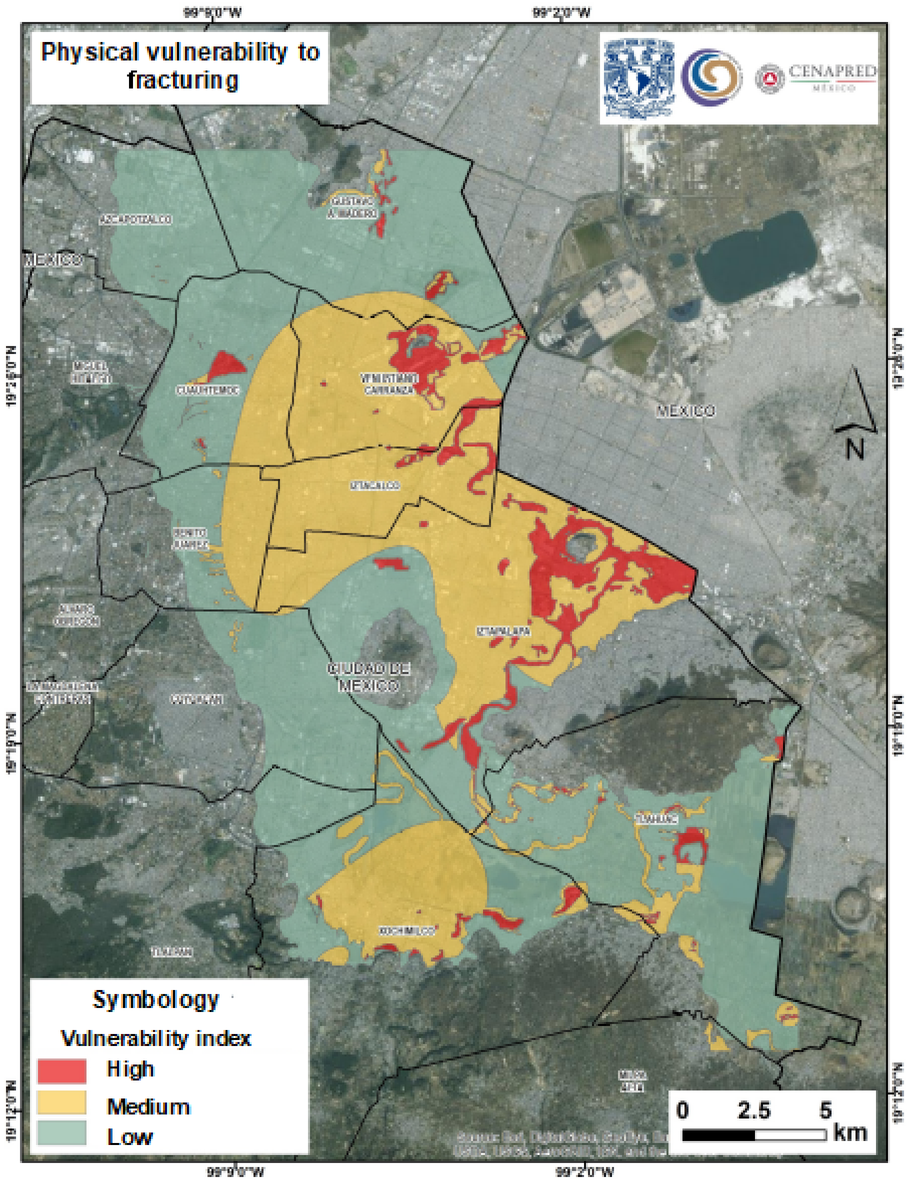

Figure 4. Mexico City distribution map of the physical vulnerability index to fracturing (Carreón Freyre et al., 2017).

Table 2. Weighted values for the gradient of subsidence (g_s).

Gradient of subsidence	Weighted value W_{gs}
Low (< 4 cm)	0 %
Medium (4–12 cm)	9.75 %
High (> 12 cm)	5.25 %
Weight of the variable	15 %

Table 3. Rates of physical vulnerability to fracturing in the Mexico City area.

Vulnerability level	Surface (km^2)	Percentage
High	23.9	3.9
Medium	143.8	23.6
Low	215.1	35.3
No subsidence	226.8	37.2
Total	609.6	100

propagation conditions (Fig. 4). The proposed vulnerability index to fracturing is easy to use for decision making and helps in the zoning of risk areas.

4 Results: map of distribution of VIF in Mexico City

The results of the analysis were integrated in a geographic information system and presented as a map defining three zones in Mexico City with values ranging from high to low physical vulnerability:

– High vulnerability represents a surface of 23.9 km^2 (3.9 % of the area of Mexico City) located mainly at the eastern part of the city, with minor areas downtown and to the southern part.

– Medium vulnerability covers a surface of 144 km^2 downtown and in the eastern and southern parts of Mexico City.

– Low vulnerability, with a surface of 215.1 km^2, corresponds mainly to the rocky highlands of the western part of the city (Table 3).

5 Conclusions

Overexploitation of the aquifer has caused a continuous piezometric water level decline reaching about 50 m and up to 13 m of land subsidence in the central part of Mexico City. Consequently, the intensity of fracturing has increased and caused numerous problems to urban infrastructure. Estimations of infrastructure damage are in the order of several billion US dollars. This represents a great challenge for land and groundwater management in Mexico. We propose a deterministic methodology for the estimation of a vulnerability index to fracturing which is easy to use for zoning. The presented results are qualitative and cannot be analyzed statistically; nevertheless the VIF has shown to be very useful for decision making. The map can be a useful tool when assessing the related geological risk in Mexico City. The accuracy of the results should be improved with a larger database. Additionally, the VIF can be useful for the design of adequate monitoring systems aimed at the optimization of mitigation measures in the damaged sites.

Data availability. The database of the fracture map of Mexico City can be consulted at the CENAPRED public web site, in the section "Aplicaciones: Sistema de Información de Riesgos. Ciudad de México" http://www.atlasnacionalderiesgos.gob.mx/portal/fenomenos/ (CENAPRED, 2020).

Author contributions. DCF and RGC designed the proposed methodology. MC supervised the analysis of geological information, and CAD created the map database. DCF prepared the paper with contributions from all co-authors.

Competing interests. The authors declare that they have no conflict of interest.

Special issue statement. This article is part of the special issue "TISOLS: the Tenth International Symposium On Land Subsidence – living with subsidence". It is a result of the Tenth International Symposium on Land Subsidence, Delft, the Netherlands, 17–21 May 2021.

Acknowledgements. The obtained results are part of the *National atlas of risks* developed by the Centro Nacional de Prevención de Desastres (National Center of Disaster Prevention; CENAPRED) in Mexico and of the activities supported by the UNESCO IGCP 641 project.

Financial support. This research has been supported by the CENAPRED (grant no. CNPC/1183/2015).

References

Aguilar-Perez, L. A., Ortega-Guerrero, M. A., Lugo-Hubp, J., and Ortiz-Zamora, D.: Análisis numérico acoplado de los desplazamientos verticales y generación de fracturas por extracción de agua subterránea en las proximidades de la Ciudad de México, Revista Mexicana de Ciencias Geológicas, 23, 247–261, ISSN 2007-2902, 2006.

Cabral-Cano, E., Dixon, T. H., Miralles-Wilhelm, F., Sánchez-Zamora, O., Díaz-Molina, O., and Carande, R. E.: Space Geodetic Imaging of Rapid Ground Subsidence in México City, Bull. Geol. Soc. Am., 120, 1556–1566, https://doi.org/10.1130/B26001.1, 2008.

Carreón Freyre, D.: Keynote. Land subsidence processes and associated ground fracturing in Central Mexico, in: Land Subsidence, Associated Hazards and the Role of Natural Resources Development (Proceedings of EISOLS 2010, Querétaro, México), Red Book Series Publication 339, edited by: Carreón Freyre, D., Cerca, M. and Galloway, D. L., IAHS Press, CEH Wallingford, UK, 149–157, ISBN 978-1-907161-12-4, ISSN 0144-7815, 2010.

Carreon-Freyre, D., Cerca, M., Ochoa-Gonzalez, G., Teatini, P., and Zuñiga, R.: Shearing along faults and stratigraphic joints controlled by land subsidence and piezometric gradients in the Valley of Queretaro, Mexico, Hydrogeol. J., 24, 657–674, https://doi.org/10.1007/s10040-016-1384-0, 2016.

Carreón Freyre, D., Cerca Martinez, M., Gutierrez Calderón, R., and Alcántara Durán, C.: Análisis de vulnerabilidad física a la subsidencia, hundimiento y agrietamiento en la Ciudad de México, Report, National Atlas of Risks Centro Nacional de Prevención de Desastres (CENAPRED), Aplicaciones/Sistema de Información sobre Riesgos/Ciudad de México, available at: https://cordis.europa.eu/project/id/511208 (last access: 30 March 2020), 2017.

Carreon-Freyre, D., Cerca, M., Gutierrez-Calderon, R., Alcantara-Duran, C., Strozzi, T., and Teatini, P.: Land Subsidence and associated ground fracturing in urban areas, Study cases in central Mexico, in: Proceedings of the XVI Pan-American Conference on Soil Mechanics and Geotechnical Engineering, Cancun, México, 17–20 November 2019, 9 pp., 2019.

Carreón-Freyre, D. C., Hidalgo-Moreno, C., and Hernández-Marín, M.: Mecanismos de fracturamiento de depósitos arcillosos en zonas urbanas. Caso de deformación diferencial en Chalco, Estado de México, Boletín de la Sociedad Geológica Mexicana, Número Especial de Geología Urbana, Tomo, LVIII, 237–250, 2006.

Carrillo, N.: Influence of artesial wells in the sinking of Mexico City, in: Volumen Nabor Carrillo: El hundimiento de la Ciudad de México y el Proyecto Texcoco, Com. Impulsora y Coordinadora de la Investigación Científica Anuario, 47, 7–14, 1947.

Centro Nacional de Prevención de Desastres (CENAPRED): Atlas Nacional de Riesgos, available at: http://www.atlasnacionalderiesgos.gob.mx/portal/fenomenos/, last access: 30 March 2020.

Gayol, R.: Estudio de las perturbaciones que en el fondo de la Ciudad de México ha producido el drenaje de las aguas del subsuelo, por las obras del desagüe y rectificación de los errores a que ha dado lugar una incorrecta interpretación de los efectos producidos, Revista Mexicana de Ingeniería y Arquitectura, III, 96–132, 1925.

Holzer, T. L.: Ground failure induced by groundwater withdrawal from unconsolidated sediments, Rev. Eng. Geol., 6, 67–105, 1984.

INEGI: Intercensal Survey (Encuesta Intercensal 2015). Instituto Nacional de Estadistica y Geografia, 96 pp., available at: https://www.inegi.org.mx/programas/intercensal/2015/ (last access: 30 March 2020), 2015.

Juárez-Badillo, E. and Figueroa Vega, G. E.: Stresses and displacements in an aquifer due to seepage forces (one dimensional case), J. Hydrol., 73, 259–288, 1984.

Kappes, M. S., Papathoma-Köhle, M., and Keiler, M.: Assessing physical vulnerability for multi-hazards using an indicator-based methodology, Appl. Geogr., 32, 577–590, https://doi.org/10.1016/j.apgeog.2011.07.002, 2012.

López-Quiroz, P., Doin, M. P., Tupin, F., Briole, P., and Nicolas, J. M.: Time series analysis of Mexico City subsidence constrained by radar interferometry, J. Appl. Geophys., 69, 1–15, https://doi.org/10.1016/j.jappgeo.2009.02.006, 2009.

Ochoa González, G. H., Carreón-Freyre, D., Franceschini, A., Cerca, M., and Teatini, P.: Overexploitation of groundwater resources in the faulted basin of Querétaro, Mexico: A 3D deformation and stress analysis, Eng. Geol., 245, 192–206, https://doi.org/10.1016/j.enggeo.2018.08.014, 2018.

Ovando-Shelley, E., Lermo-Samaniego, J., Auvinet, G., and Méndez-Sánchez, E.: Microtremor measurements to identify zones of potential fissuring in the basin of Mexico, Geofísica Internacional, 51-2, 143–156, 2012.

Rivera, A. and Ledoux, E.: Non-Linear modeling of groundwater flow and total subsidence in the Mexico City aquifer-aquitard system, in: P. Fourth Int. Symp. Land Subsidence, IAHS, 12–17 May 1991, Houston, Texas, USA, 45–58, 1991.

Schmidt-Thomé, P., Klein, J., Aumo, R., and Hurstinen, J.: Report: Technical Glossary of a Multi Hazard Related Vulnerability and Risk Assessment Language – Final version, Armonia Project, Contract No. 511208, Applied Multi-Risk Mapping of Natural Hazards for Impact Assessment, Geological Survey of Finland (GTK), available at: https://www.umweltbundesamt.de/en/topics/climate-energy/climate-change (last access: 30 March 2020), 2007.

Zeevaert, L.: Stratigraphy and engineering problems in the lacustrine clayey deposits of Mexico City, Memoria del Congreso Científico Mexicano, 5, 58–70, 1953.

Assessment of potential recharge lakes by absolute gravimetry in regions of severe land subsidence in Taiwan

K. Chen[1], C. Hwang[1]

1 Department of Civil Engineering, National Yang Ming Chiao Tung University, Taiwan

khc@nycu.edu.tw

Session: Measuring and Monitoring

Reducing groundwater withdrawal and increasing groundwater levels from clay layers can alleviate land subsidence. A sandy aquifer in a clay-dominated region can store groundwater and serve as a recharge lake for water management. However, identifying an appropriate location for constructing a recharge lake can be costly. At a test site, the representative region of existing hydrogeological parameters such as infiltration and storage coefficients is limited to only a few meters around the site. Finding valid hydrogeological parameters for a sufficiently large coverage around a potential recharge lake over a heterogeneous aquifer system can be challenging, but this task is in urgent need in the regions of severe land subsidence in Taiwan.

A microgal-level terrestrial gravimeter is sensitive to mass migration in a near-surface area. Repeated gravity measurements using such a gravimeter can be used to estimate groundwater mass balances in a shallow sandy aquifer. After correcting the environment-induced temporal gravity effects and vertical displacements, time-variable gravity changes at a gravity site reflect the groundwater mass balance. Ground-based gravimetry has several advantages over existing methods, particularly in land subsidence-hit regions. First, ground-based gravimetry can sense the groundwater balance in an unconfined sandy aquifer, where groundwater recharge and extraction result in only small (mm-level) ground deformation. Second, ground-based gravimetry does not require the distribution of storage coefficients in an unconfined aquifer (i.e., specific yield) and groundwater levels for groundwater mass change estimations. Third, gravity changes reflect the average mass change over a region of tens to a hundred meters. Thus, the use of repeat gravity measurements may eliminate the requirements needed in numerous typical hydrogeological tests. In addition, the time of repeated measurements can be manually designed according to events of interest. These advantages are important when constructing recharge lakes in land subsidence-hit regions, especially about the efficiency of acquiring critical hydrogeological parameters.

Groundwater change and vertical displacement lead to gravity changes. Gravity value declines when groundwater is withdrawn or when the surface elevation increases. According to equivalent water height (EWH) used in gravity interpretation, a layer of pure water in thickness of five centimeters can induce 2µgal (10-8 m/s2) of gravity change. Also, one centimeter of vertical displacement leads to 2µgal of gravity change. However, an excessive withdrawal of groundwater is accompanied by compaction of a clay aquifer. In some particular cases, gravity values experience only small fluctuations when the site is subsiding. Therefore, a gravity correction for vertical displacement is required before estimating groundwater storage change by gravimetry.

This study takes advantage of dense, diversified ground deformation measurements at the Choshui River Alluvial Fan (CRAF) in central Taiwan. Continuous GNSS data are used for correcting the gravity effect of land motion at a site, and regional ground deformation is derived from multilayer compaction well (MLCW), leveling, and InSAR observations at different time and space scales. We set up seven absolute gravity sites at CRAF in 2021, five of which are located in regions of severe land subsidence. We measured absolute gravity values in different seasons and focused on capturing groundwater storage change before and after rainy seasons. In 2021, the vertical displacement at the gravity sites of STES and JJES reached -10 cm due to a serious drought in the first half of 2021 in Taiwan. A residual gravity change of 26.6 μgal and a vertical displacement of -4.2 cm (relative to the values in March) in May were detected at STES in 2021. The patterns of the gravity changes at the sites located in the subsidence-hit regions are similar to the gravity change patterns at the sand-dominated aquifers in the proximal region of CRAF, revealing the existence of regional unconfined aquifers (RUAs) in the regions affected by land subsidence.

A site experiencing significant gravity changes can be a site with a high groundwater storage change, and thus can be a potential site to build a recharge lake. A test using gravity changes could be a preliminary test to identify a potential RUA in a clay-dominated aquifer. As such, the measured gravity changes in 2021 can be used to rank the priority of the potential sites for recharge lake construction. In addition, we conducted an electrical resistivity imaging (ERI) survey in 2022 to confirm the existence of a RUA discovered by absolute gravimetry in 2021. We continue to measure gravity changes in 2022 at the sites STES, JJES and TKJH for studies such as detecting interannual changes in water balance of the sandy aquifers and making use of gravity data to assist land subsidence prevention.

First Results of Dutch Peatland Subsidence Observations Using InSAR

P. Conroy*, S.A.N. van Diepen, F.J. van Leijen, R.F. Hanssen

1 Department of Geoscience and Remote Sensing, Delft University of Technology

p.n.conroy@tudelft.nl

Introduction

Land subsidence in the Netherlands is becoming an increasingly critical issue as it is closely linked with sea level rise, flooding risks and greenhouse gas emissions due to peat oxidation (Erkens et al., 2016; Erkens et al., 2016). Despite the importance of this issue, it is very difficult to accurately assess subsidence levels across the country. SAR Interferometry (InSAR) is a very promising technique for monitoring land surface motion at large spatial scales with frequent temporal sampling. While InSAR techniques employing stable point scatterers (PS) have been successfully used to monitor subsidence in the Netherlands (Caro Cuenca & Hanssen, 2008; Caro Cuenca et al., 2011; Hanssen et al., 2018), these PS points are usually founded at greater depths and the movement of the surrounding landscape has had to be indirectly inferred.

So far, it has been impossible to directly observe land surface motion using distributed scatterer (DS) techniques in the Netherlands because rapid soil movement, seasonal land use changes and high noise levels result in sudden losses of interferometric coherence, rendering any such attempt extremely challenging (Morishita & Hanssen, 2015; Heuff & Hanssen, 2020).

We present a first test of a novel methodology for InSAR processing which makes use of contextual data and machine learning techniques to robustly estimate a surface motion time series using C-band Sentinel-1 InSAR at the parcel scale. To our knowledge, this is the first accurate InSAR time series of a Dutch grassland polder region.

Methods

Contextual Data Integration

We assemble a database of combined public cadastral parcel delineations and land cover data, soil maps, and groundwater management zones, available: PDOK. These factors play a critical role in either the movement of the land surface, the scattering properties which affect the radar observation, or both. By cross-referencing this data with the SAR imagery, we can assign each pixel to a known parcel ID with known soil, land use and land cover (LULC), and groundwater parameters. This ensures that we are processing homogeneous observations which are representative of the same land surface movement phenomena.

Parcel Multilooking and Phase Estimation

After the dataset of contextual data is prepared, we multilook the native 5×20 meter Sentinel-1 observations according to the parcel delineations of the contextual dataset. This is a natural division to make, as the land cover, soil type, and groundwater are approximately consistent within a parcel. This also ensures a high multilooking degree of approximately 100 equivalent looks (although this varies with each parcel according to its shape and size) which aids in suppressing noise (Hanssen, 2001). Following the multilooking step, we perform phase estimation using the EMI method (Ansari et al., 2018).

Segmentation and Temporal Phase Ambiguity Resolution

Rapidly changing displacement phases and noise make the application of standard phase unwrapping algorithms very unreliable, and often large movements in one direction are misinterpreted as smaller movements in the opposite direction (Alshammari et al., 2018; Tampuu et al., 2022). This motivated the development of a machine-learning aided phase unwrapping algorithm, described in Conroy et al (2022). The algorithm uses rainfall and temperature data to anticipate large subsidence and uplift events in order to guide phase ambiguity resolution in the temporal domain.

The second major hurdle preventing successful InSAR estimations are the sudden losses of coherence in the time series. Especially during the (late) summer period, coherence levels can often drop to such low levels that there is essentially no useful information retained in the interferograms with even the shortest temporal baseline (6 days). Whenever this occurs, we designate the event as a “Loss-of-Lock” and divide the time series into separate segments. While we can unwrap each individual temporal segment with a satisfactory degree of reliability, the segments themselves are disconnected, and an unknown vertical shift exists between segment (Conroy et al., 2022). We can reconnect the segments by observing neighbouring parcels. While each parcel follows a similar general pattern, the actual date during which coherence drops below the useable threshold is different in each case. Thus by using contextual information to group similar parcels together, we can use the aggregate of all segments in a group to fully span the incoherent periods with coherent observations.

This is accomplished by fitting a kinematic model to the unwrapped segments. For this purpose, we use a simple seasonal plus linear (SL) model, which can be used to approximately estimate the mean position of a segment without making many assumptions. The total number of segments in a group is N = (Num. SAR tracks) × (Num. parcels per group) × (Num. segments per parcel). The SL model is parameterized by the vector θ, and given N segments, there are N + 3 parameters to estimate:

$$\boldsymbol{f_g}(\boldsymbol{\theta}, t) = \begin{cases} \theta_1 \cos(2\pi f_a t + \theta_2) + \theta_3 t + \theta_4, & \text{for } i = 1 \\ \theta_1 \cos(2\pi f_a t + \theta_2) + \theta_3 t + \theta_5, & \text{for } i = 2 \\ \quad\vdots & \\ \theta_1 \cos(2\pi f_a t + \theta_2) + \theta_3 t + \theta_{N+3}, & \text{for } i = N \end{cases} \tag{1}$$

where t is the independent variable representing time, and fa denotes an annual frequency. The vector θ contains all the estimated parameters of the displacement model: θ1 is the amplitude of the annual periodic component, θ2 is the phase offset of the annual periodic component, θ3 is the linear rate and θi+3 is the estimated vertical shift of the ith segment. Note that the parameters [θ1, θ2, θ3] are the same for every segment in a given group g characterized by the model fg. The model is fit by minimizing the mean squared error between the model and the segment during the coherent period.

Spatial Ambiguity Resolution

High noise levels in the individual parcels make applying a geodetic network approach to spatial ambiguity resolution very challenging (van Leijen, 2014). However, a less strict spatial ambiguity constraint is applied by considering the phase changes between consecutive interferograms of a given parcel, Δϕ, versus its corresponding group mean, $\Delta\bar{\phi}$:

$$\Delta\phi_{new} = \begin{cases} \Delta\phi_{\text{old}} + 2\pi, & \text{for } |\Delta\phi_{\text{old}} + 2\pi - \Delta\bar{\phi}| < |\Delta\phi_{\text{old}} - \Delta\bar{\phi}| \\ \Delta\phi_{\text{old}} - 2\pi, & \text{for } |\Delta\phi_{\text{old}} - 2\pi - \Delta\bar{\phi}| < |\Delta\phi_{\text{old}} - \Delta\bar{\phi}| \\ \Delta\phi_{\text{old}}, & \text{otherwise.} \end{cases} \tag{2}$$

Each parcel is checked and the ambiguities are adapted according to equation (2). The group mean is recalculated once the spatial unwrapping procedure is completed for all parcels.

Results

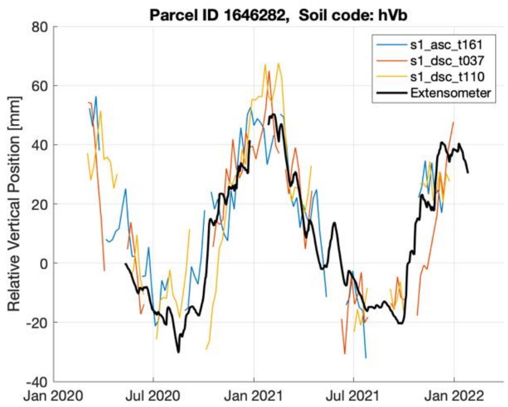

(a)

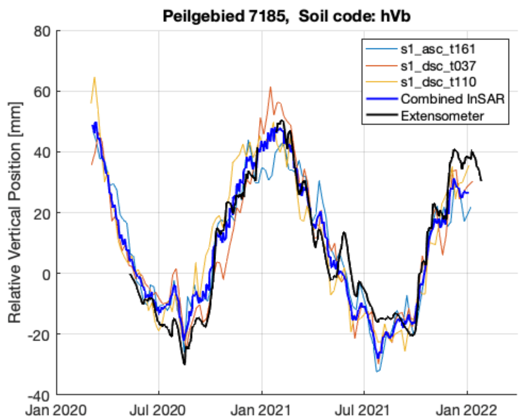

(b)

Figure 1 (a) Parcel example of a grassland polder where a peat soil is covered by up to 15 cm clay/peat. Three independent Sentinel-1 track results are shown relative to the reference extensometer. (b) Group time series estimations plotted against validation data obtained from the Zegveld test site.

Time Series Validation Against Ground Truth

We validate the approach described in Section 2 against in-situ measurements taken by an extensometer, which provides hourly measurements of Holocene soil displacement at a given location (van Asselen et al., 2020). A 10x10 km study area surrounding Zegveld, the Netherlands is observed between Apr. 1, 2020 and Jan. 15, 2022. These dates are chosen as they correspond with the installation of an Integrated Geodetic Reference Station (IGRS) with corner reflectors which is used as the reference point, and the failure of the Sentinel-1b satellite in early 2022, respectively.

Two types of output are available: partial time series estimations per parcel (shown in Figure 1a) and full time series estimations per group (Figure 1b). It should be noted that while the extensometer provides measurements at one point, the InSAR time series is a spatial average of many points, and will therefore differ from the extensometer as some short term variations are filtered out of the result. Note that this spatial filtering effect will be stronger for the group result. The validation parcel belongs to a larger group of 51 parcels, which, based on the contextual data available, we expect to behave in a broadly similar fashion. A wholly continuous time series of the group can be estimated by taking the median of all time series segments. This has the benefit of strongly reducing the effects of noise and phase unwrapping errors at the cost of reduced spatial resolution.

Initial Spatial Results

A spatial plot showing the estimated linear deformation rate per parcel is shown in Figure 2. The time series used in this study is too short to provide accurate estimates of linear irreversible subsidence rates, however, we can assess both the spatial correlation of the result and compare the order of magnitude to the expected level.

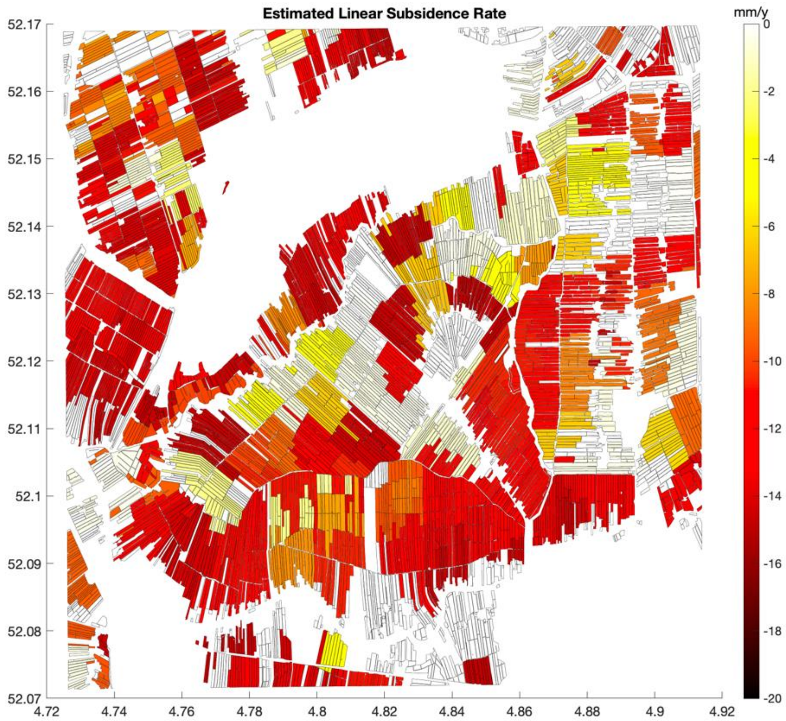

Figure 2 Zegveld linear displacement rate map. Uncoloured parcels indicate that no estimation is made at that location.

Conclusion

We demonstrate a new methodology for estimating the ground motion of cultivated peatlands using DS time series InSAR. Our initial results show that the approach is promising, and we have been able to successfully validate our result against the ground truth data we have available. To our knowledge this is first accurate InSAR measurement of peatland surface motion in the Netherlands. Following this successful test, we plan to process a longer time series in order to obtain more accurate long-term subsidence estimates and to allow for comparison between seasons as a response to climatic stimuli.

Acknowledgement

This research is part of the Living on Soft Soils (LOSS): Subsidence and Society project, and is supported by the Dutch Research Council (NWO-NWA-ORC), grant no.: NWA.1160.18.259, URL: nwa-loss.nl

References

Erkens, G., van der Meulen, M. J., Middelkoop, H. (2016). "Double trouble: Subsidence and CO2 respiration due to 1,000 years of Dutch coastal peatlands cultivation," *Hydrogeology Journal*, vol. 24, no. 3, pp. 551–568

Erkens, G., Bucx, T., Dam, Lange, R. D., Lambert, J.G. (2016). Sinking Cities: An Integrated Approach to Solutions, In: The Making of a Riskier Future: How Our Decisions Are Shaping Future Disaster Risk. *World Bank*.

Caro Cuenca, M., Hanssen, R. F. (2008). "Subsidence due to peat decomposition in the Netherlands, kinematic observations from radar interferometry," in Proc. *ESA Fringe Workshop*, (Frascati, Italy), pp. 1–6.

Caro Cuenca, M., Hanssen, R. F., Hooper, A., Arikan, M. (2011). "Surface deformation of the whole Netherlands after PSI analysis," in Proc. *ESA Fringe Workshop*, (Frascati, Italy), pp. 19–23.

Hanssen, R. F., Van Leijen, F. J., Erkens, G., Stouthamer, E., Cohen, K., Lange, Meulen, Akker and Others (2018). *"Land motion service of the Netherlands*,".

Morishita, Y., Hanssen, R. F. (2015). "Deformation parameter estimation in low coherence areas using a multisatellite InSAR approach," *IEEE Transactions on Geoscience and Remote Sensing*, vol. 53, no. 8, pp. 4275–4283.

Heuff, F. M., Hanssen, R. F. (2020). "InSAR phase reduction using the remove-compute-restore method," in 2020 *IEEE International Geoscience and Remote Sensing Symposium*, pp. 786–789.

"Publieke Dienstverlening Op de Kaart (PDOK*)." www.pdok.nl.*

Hanssen, R. F. (2001). *Radar Interferometry: Data Interpretation and Error Analysis*. Dordrecht: Kluwer Academic Publishers.

Ansari, H., De Zan, F., Bamler, R. (2018). "Efficient phase estimation for interferogram stacks," *IEEE Transactions on Geoscience and Remote Sensing*, vol. 56, no. 7, pp. 4109–4125.

Alshammari, L., Large, D. J., Boyd, D. S., Sowter, A., Anderson, R., Andersen, R., Marsh, S. (2018). "Long-term peatland condition assessment via surface motion monitoring using the ISBAS DInSAR technique over the flow country, Scotland," Remote Sensing, vol. 10, no. 7.

Tampuu, T., De Zan, F., Shau, R., Praks, J., Kohv, M., Kull, A. (2022). "Reliability of sentinel-1 InSAR distributed scatterer (DS) time series to estimate the temporal vertical movement of ombrotrophic bog surface," *in EGU General Assembly*, vol. EGU22-2387, (Vienna, Austria).

Conroy, P., Van Diepen, S. A. N., Van Asselen, S., Erkens, G, Van Leijen, F. J., Hanssen, R. F. (2022). "Probabilistic estimation of InSAR displacement phase guided by contextual information and artificial intelligence," *IEEE Transactions on Geoscience and Remote Sensing*, vol. 60, pp. 1–11.

Conroy, P., Van Diepen, S. A. N., Van Leijen, F. J., Hanssen, R. F. (2022) "Hybrid InSAR processing for rapidly deforming peatlands aided by contextual information," *in 2022 IEEE International Geoscience and Remote Sensing Symposium*.

Van Leijen, F. (2014). Persistent Scatterer Interferometry based on geodetic estimation theory. *PhD thesis*, TU Delft.

Van Asselen, S., Erkens, G., De Graaf, F., (2020). "Monitoring shallow subsidence in cultivated peatlands," *Proceedings of the International Association of Hydrological Sciences*, vol. 382, pp. 189–194.

Vulnerability of tidal morphologies to relative sea-level rise in the Venice lagoon (Italy)

M. Cosma[1], C. Da Lio[1], S. Donnici[1], T. Strozzi[2], P. Teatini[3], C. Zoccarato[3], L. Tosi[1]

1 Institute of Geosciences and Earth Resources, National Research Council, Padova, 35131, Italy
2 Gamma Remote Sensing, Gümligen, 3073, Switzerland
3 Dept. of Civil, Environmental and Architectural Engineering, University of Padova, Padova, 35131, Italy

Session: Theme: Impacts and Hazards – Topics: Coastal areas; Deltas & Sea Level Rise

Abstract
Tidal morphologies in coastal lagoons are forced to keep pace with accelerated sea-level rise, and their survival relies on delicate feedbacks between surface and subsurface processes. Quantifying the vulnerability of tidal morphologies to relative sea-level rise should be one of the fundamental pieces of information for planning appropriate conservation strategies for lagoon areas. Most assessments of lagoon vulnerability to sea-level rise focus on intertidal environments, e.g., saltmarshes, and neglect the effects of sea-level rise on subtidal flats. This contribution proposes a vulnerability analysis of tidal morphologies in the Venice lagoon (Italy) to past, ongoing and future relative sea-level rise based on the concept that both intertidal and subtidal zones are sensitive to this process. Vulnerability is assessed by combining sensitivity and hazard maps properly generated from a series of indicators such as sea-level rise trends, land subsidence, morphological setting, and stratigraphic characteristics of Holocene deposits.

Introduction
Lagoons are part of unique wetland environments with both submerged and emerged morphologies that provide valuable ecosystem services worldwide (e.g., Barbier et al., 2011). Because their survival is strictly dependent on vertical elevation, there is broad consensus on the high susceptibility of tidal environments to the adverse effects of relative sea-level rise (RSLR), i.e. sea-level rise plus land subsidence, resulting in loss of morphological structure and consequently geo- and bio-diversity.

Despite the extreme fragility of tidal morphologies, quantification of their vulnerability to RSLR is still poorly developed, even though it is a fundamental starting point for guiding conservation and adaptation processes that will become increasingly critical in light of projected mean sea level rise by 2050. Most vulnerability assessments of lagoons and wetlands generally focus on the emerged sectors and neglect the potential effects that RSLR may also have on the submerged zones, especially the tidal flats that form a morphological continuum with saltmarsh platforms. Furthermore, these assessments rarely consider the heterogeneity of shallow deposits and the variability of land subsidence when calculating the RSLR.

This work aims at evaluating the vulnerability of tidal morphologies to RSLR in the Venice Lagoon, Italy (Figure 1). It provides a high spatial resolution analysis that downscales the framework proposed by Tosi et al. (2020), and combines relevant indicators describing the sensitivity and hazard status of tidal morphologies. Among the sensitivity indicators, the thickness of the main Holocene depositional units was considered because most of land subsidence in the Venice lagoon depends on the stratigraphic architecture of the shallow deposits (Tosi et al., 2009). Different hazard scenarios are used accounting for past, ongoing, and future SLR trends measured in the north Adriatic over the last decades and projected to 2050.

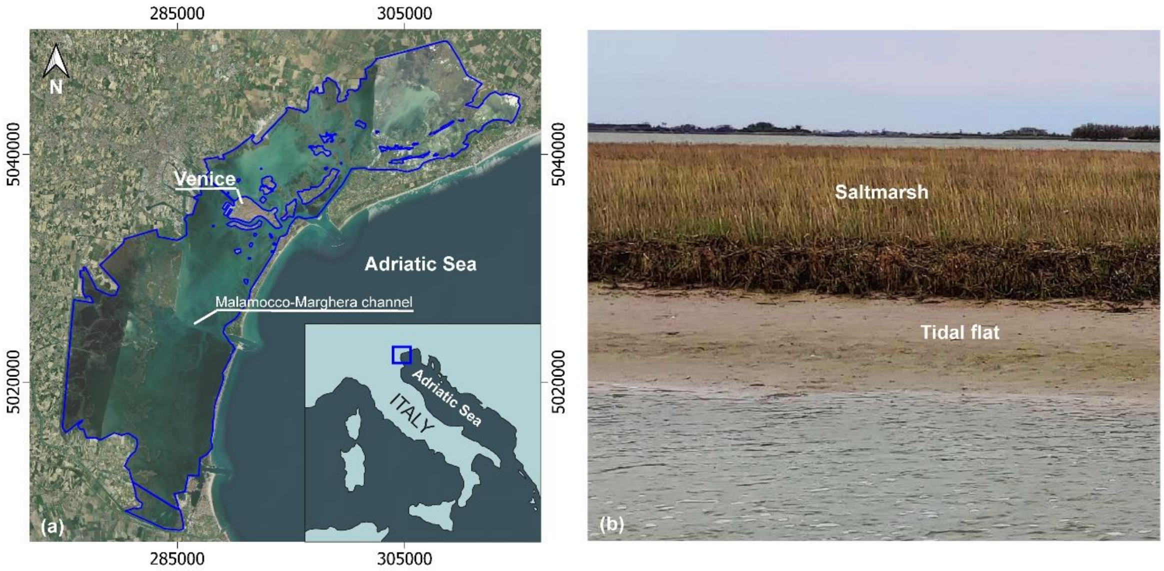

Figure 1. (a) Satellite image of the Venice lagoon facing the northern Adriatic Sea, Italy. (b) Typical tidal environment at low-tide condition with vegetated saltmarshes and bare tidal flats.

Methods

The vulnerability of tidal morphologies to RSLR was assessed according to an index-based model that combines the following indicators: land subsidence, sea-level rise, ground elevation of emerged and submerged areas, and stratigraphic architecture. Land subsidence was obtained from Sentinel-1 images acquired between 2015 and 2019 (Tosi et al., 2020) and processed using the Interferometric Point Target Analysis (IPTA) PSI chain. Three scenarios referred to the past (1990s), ongoing (2020s), and future (2050s) conditions were developed under different morphological settings and sea-level rise trends. The rates of past (1.5 mm/yr) and ongoing (3.5 mm/yr) sea-level rise were computed through time series analysis of the tide-gauge station located in Trieste, whose data are provided by Permanent Service for Mean Sea Level (https://www.psmsl.org/). The rate of projected sea-level rise (6.5 mm/yr) by 2050 was derived from the IPCC RCP8.5 scenario (Oppenheimer et al., 2019). The ground elevation indicator consists of a digital terrain model, which was obtained by merging three datasets to cover both the emerged and submerged lagoon areas. Specifically, LiDAR, bathymetric (https://idt2.regione.veneto.it/idt/downloader/download) and TanDEM-X data were properly homogenized and referred to the surface elevation conditions of the three scenarios. The stratigraphic architecture was derived from a simplified model of the Holocene depositional units mapped in Tosi et al. (2007a; b) and Fabbri et al. (2013). Specifically, three stratigraphic indicators were selected to account for the thickness of two muddy units with different degrees of consolidation, and the thickness of a sandy unit.

The index-based model approach followed these main steps: (i) set-up of the datasets related to each indicator (i.e., the thematic layers); (ii) classification of the thematic layers, i.e. each dataset was classified into 5 classes with scores ranging from 0 to 4 representing an increasing contribution to vulnerability; (iii) weighting of the sensitivity indicators; (iv) linear combination of sensitivity and hazard classified thematic layers to compute the vulnerability index.

Results

The result of the classification of the thematic layers is shown in Figure 2. All adopted sensitivity indicators show strong contributions of spatial variability to vulnerability.

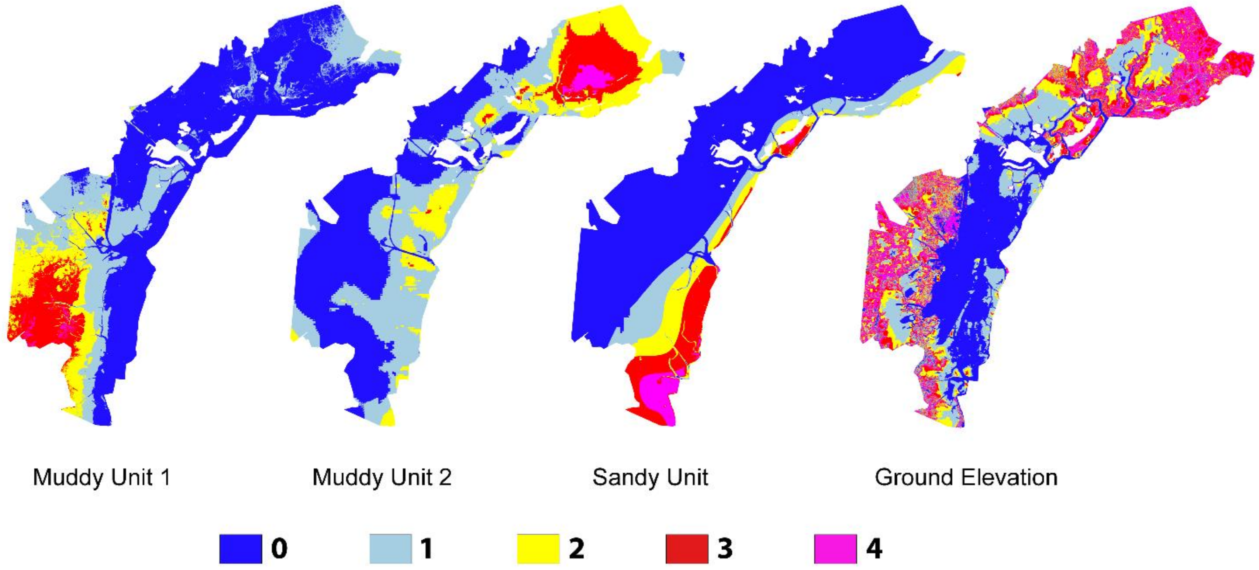

Figure 2. Classification of the thematic layers. Score from 0 to 4 identify low-to-high contributions to vulnerability.

The maps of the sensitivity, hazard, and vulnerability of lagoon morphologies (Figure 3) are provided here for the ongoing scenario as an example of the outcomes from this work.

The sensitivity map (Figure 3a) shows that tidal morphologies fall mostly in the negligible class (about 40%), while the marginal and moderate classes are rather similar at 35% and 25%, respectively. The hazard map (Figure 3b) highlights that 60% of the lagoon area is marginally threatened, whereas it is moderately and strongly threatened for 35 and 5 %, respectively.

The vulnerability map (Figure 3c), obtained from the appropriately weighted combination of sensitivity and hazard maps, depicts a large spatial heterogeneity, resulting from the variability of ground elevation of the emerged and submerged areas and the stratigraphic architecture associated with land subsidence and sea-level rise. Specifically, strong and moderate vulnerability affects nearly 30% of the lagoon basin, whereas marginal and negligible totals 70%.

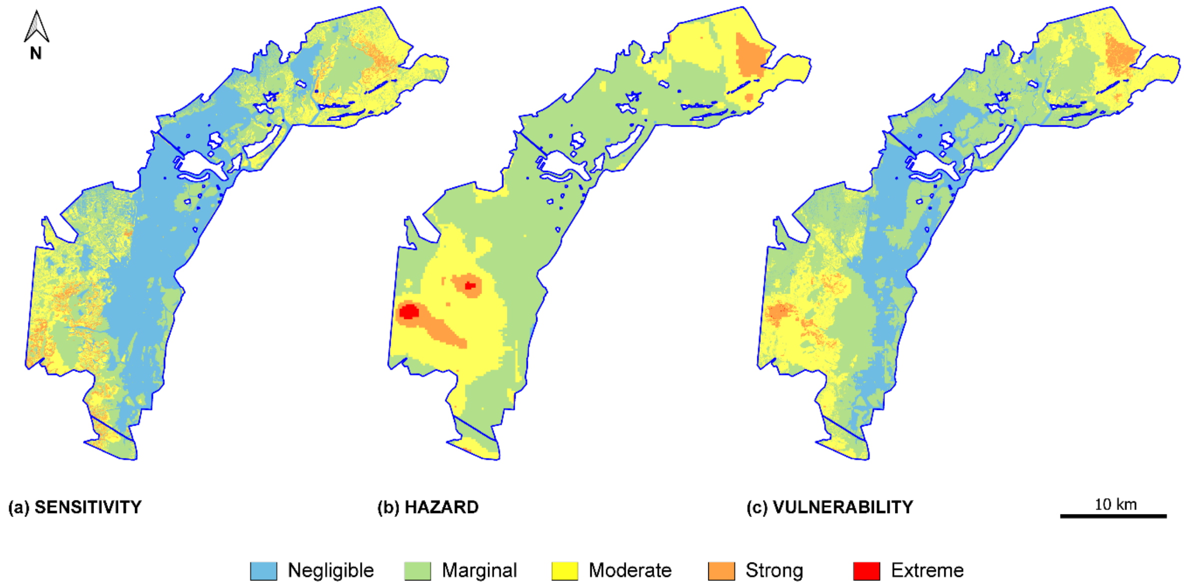

Figure 3. Maps of sensitivity, hazard, and vulnerability of tidal morphologies in the Venice lagoon under the ongoing scenario.

In general, there is a sharp increase in the vulnerability of emerged and submerged morphologies from past to future scenarios. The northeastern and the southwestern areas of the lagoon are the most threatened, while the central basin is relatively lower in vulnerability. In the 2050 scenario, 30% of the lagoon area is expected to be in strong and extreme vulnerability conditions.

Conclusion

The result of this work highlights the lagoon areas that need more attention. The worst ongoing conditions mainly affect saltmarshes in the northeastern and southwestern lagoon and reflect the occurrence of thicker fine-grained Holocene units and the higher land subsidence rates. Conversely, the relatively lower vulnerability classes refer to the central and southeastern lagoon areas where tidal flats and sandy unit prevail and sinking rates are lower. However, many of the present-day subtidal flats in these areas are the result of strong erosional and sinking processes caused by land subsidence due to groundwater exploitation in the industrial area (1950s-1960s) and the excavation of the Malamocco-Marghera navigation channel (1970s), which led to a transformation of lagoon morphologies from intertidal to subtidal. Therefore, in the ongoing scenario, the most vulnerable intertidal morphologies that occurred in the past have already disappeared.

It is expected that the vulnerability analysis will be a valuable aid to the management authorities in decision-making for the planning of measures aimed at safeguarding the Venice lagoon, among all, the reconstruction of the lost saltmarshes.

Acknowledgements

This work was supported by VENEZIA-2021 Research Programme, Topic 3.1, funded by the "Scientific activity performed in the Research Programme Venezia2021, coordinated by CORILA, with the contribution of the Provveditorato for the Public Works of Veneto, Trentino Alto Adige and Friuli Venezia Giulia". This article is also a contribution to the International Geoscience Programme Project 663 "Impact, Mechanism, Monitoring of Land Subsidence in Coastal Cities" and "Vulnerability of the Northwestern Adriatic coastal areas to relative sea level rise" DLR TanDEM-X Project DEM_HYDR1975.

References

Barbier, E.B., Hacker, S.D., Kennedy, C., Koch, E.W., Stier, A.C. and Silliman, B.R. (2011) The value of estuarine and coastal ecosystem services. *Ecol. Monogr*., 81, 169–193.

Fabbri, P., Zangheri, P., Bassan, V., Fagarazzi, E., Mazzuccato, A., Primon, S. and Zogno, C. (2013) Sistemi idrogeologici della provincia di Venezia - acquiferi superficiali. *Provincia di Venezia, Università degli Studi di Padova,* 127 pp.

Oppenheimer, M., Glavovic, B.C., Hinkel, J., van de Wal, R., Magnan, A.K., Abd-Elgawad, A., Cai, R., Cifuentes-Jara, M., DeConto, R.M., Ghosh, T., Hay, J., Isla, F., Marzeion, B., Meyssignac, B. and Sebesvari, Z. (2019) Sea Level Rise and Implications for Low-Lying Islands, Coasts and Communities. In: *IPCC Special Report on the Ocean and Cryosphere in a Changing Climate* (Ed. H.-O. Pörtner, D.C. Roberts, V. Masson-Delmotte, P. Zhai, M. Tignor, E. Poloczanska, K. Mintenbeck, A. Alegría, M. Nicolai, A. Okem, J. Petzold, B. Rama, and N.M. Weyer), Cambridge University Press, Cambridge, UK and New York, NY, USA, 321–445.

Tosi, L., Da Lio, C., Donnici, S., Strozzi, T. and Teatini, P. (2020) Vulnerability of Venice's coastland to relative sea-level rise. Proc. Int. *Assoc. Hydrol. Sci*., 382, 689–695.

Tosi, L., Rizzetto, F., Bonardi, M., Donnici, S., Serandrei-Barbero, R. and Toffoletto, F. (2007a) Note illustrative della Carta Geologica d'Italia alla scala 1:50.000, Foglio 128 "Venezia". *APAT, Dip. Difesa del Suolo, Servizio Geologico d'Italia, SystemCart, Roma,* pp. 164. 2 Maps.

Tosi, L., Rizzetto, F., Bonardi, M., Donnici, S., Serandrei-Barbero, R. and Toffoletto, F. (2007b) Note Illustrative della Carta Geologica d'Italia alla scala 1:50.000, Foglio 148-149, "Chioggia-Malamocco". *APAT, Dip. Difesa del Suolo, Servizio Geologico d'Italia, SystemCart, Roma*, pp. 164. 2 Maps.

Tosi, L., Teatini, P., Carbognin, L. and Brancolini, G. (2009) Using high resolution data to reveal depth-dependent mechanisms that drive land subsidence: The Venice coast, Italy. *Tectonophysics*, 474, 271–284.

Management of groundwater in the Nobi Plain that modeled groundwater use for earthquake disasters and environmental preservation

K. Daito[1]

1 Department of Integrated Informatics, Daido University, 457-8530, 10-3 Takiharu-cho, Minami-ku, Nagoya, Japan

Kenji Daito (daito@daido-it.ac.jp)

Introduction

Daito(2020) in the paper of TISOLS2020, the well is set up in the place of refuge specified in each municipality in the Nobi Plain, and the groundwater drawn up usually assumed use as the water of environmental preservation, and assumed use as the drinking water and daily life water at the disaster. The state of groundwater and the ground change were forecast by using the three-dimensional groundwater flow analysis and the perpendicular one-dimension consolidation subsidence analysis, and what should be of the large area groundwater management was examined.

As a result, it was thought that an important subsidence was not generated if it was a pump discharge of 100L or less a person/the day in each place of refuge. However, it has been understood that the decrease in the groundwater level is large in the vicinity of Nagoya City on which the place of refuge and the population have concentrated compared with other regions.

In this report, it proposed to decrease some pump discharges in the vicinity of Nagoya City. Moreover, it proposed to increase the pump discharge in the vicinity of Ogaki City with little decrease in the groundwater level even if groundwater was pumped. And, the decrease in the groundwater level was suppressed by transporting the shortfall of water to the vicinity of Nagoya City at the disaster, and the possibility of the subsidence became lower. This is a better management of the large area groundwater.

Moreover, it proposes how to use the groundwater drawn up effectively actually. Even when the disaster occurs, the groundwater of about 100L/day a person which corresponds to the volume of water of washing and cooking and washing can be pumped in each place of refuge. This groundwater becomes the source of the river of environmental prevention water to aim to attempt the improvement of the metropolitan environment in each municipality because it is possible to use it for the environmental sustainability in the water park etc. and the water quality purification by discharge to the river, etc.

Methods and results

The result of the groundwater level in the vicinity of Ogaki City has been extracted from the result of the three-dimensional groundwater flow analysis of Daito(2020). There is little decrease in the groundwater level even if a lot of groundwater is pumped from each aquifer as shown in Figure 1-3. Moreover, it is thought that it is common to all aquifers and the groundwater level is not steady from the 1965's to the 1975's because the change in the pump discharge of each year appears in the change in the groundwater level.

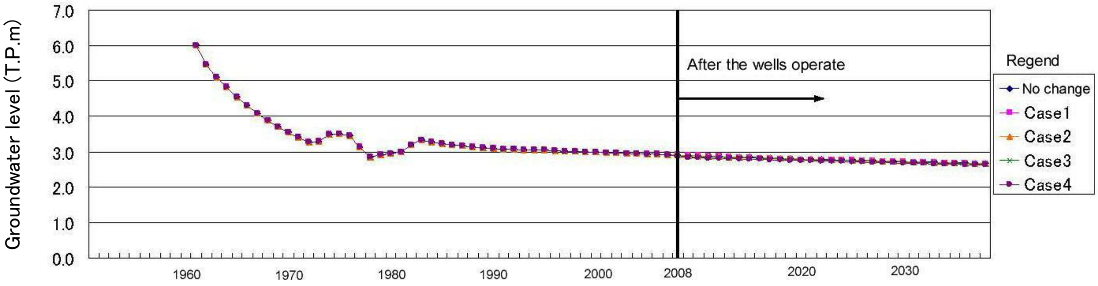

Figure 1 Annual change of groundwater in the vicinity of Ogaki observation well (G1 aquifer)

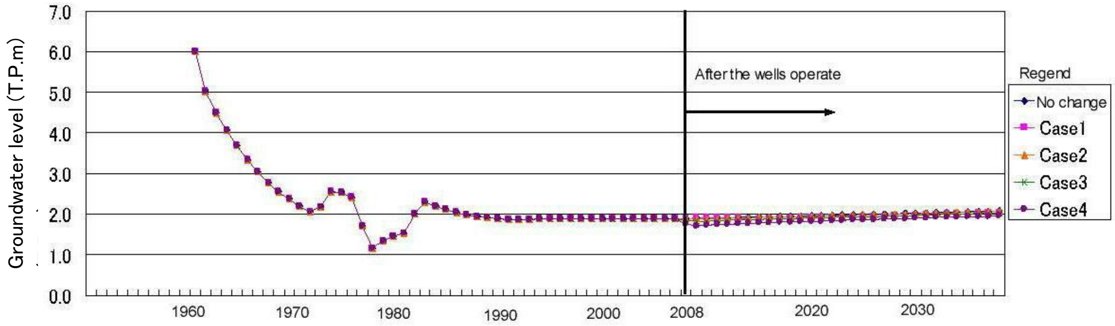

Figure 2 Annual change of groundwater in the vicinity of Ogaki observation well (G2 aquifer)

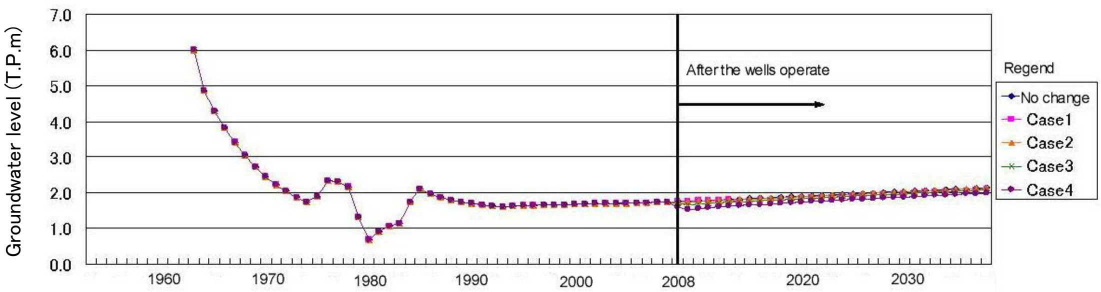

Figure 3 Annual change of groundwater in the vicinity of Ogaki observation well (G3 aquifer)

The groundwater drawn up in each place of refuge is usually used as environmental preservation water. Here, it proposes how to use it actually based on the case with the groundwater exploitation in Ichinomiya City and the Kita-ku of Nagoya City.

First of all, to secure water quality purification of the pond and an excellent landscapes, the groundwater of 350m3/day (amount of the permission pumping) is drawn up in the Aasaiyama Park in Ichinomiya City. The groundwater of about 2,419m3/year is pumped in the case of Case1, the groundwater of about 16,124m3/year is pumped in the case of Case2, the groundwater of about 80,622m3/year is pumped in the case of Case3, and the groundwater of about 201,555m3/year is pumped in the case of Case4 in the place of refuge in Ichinomiya City as shown in Table 2 of Daito(2020).

About eight places of refuse are necessary in Case2, and about two places of refuse are necessary in Case3 to cover the groundwater of 350m3/day. There are the six places of refuge from the Asaiyama Park within 1km in the radius as showing in Figure 4. A necessary amount of groundwater cannot be covered with Case2 though a necessary amount of groundwater can be covered in Case3. However, it is thought that it is possible to make up a shortfall by increasing some pump discharges a place in the place of refuge because pumping to 100L/day a person is possible.

Moreover, there are 173 places of refuges in Ichinomiya City. Therefore, it is thought that it leads to the town improvement by effectively using groundwater for a new water park etc.

Figure 4 Distribution of the places of refuge in the vicinity of Aasaiyama Park

Next, the underground water that sprang up by the Kamiiida tie line construction work in the Kita-ku of Nagoya City would be discharged 18.6 millionm3 (6.2 millionm3/year) to Horikawa River in three years of 1998 - 2001, and be useful for the water quality purification. However, discharge was discontinued with the end of construction. However, there is time when the raw water transmission cannot be done for the environmental sustainability of the Shonai River at fish's egg laying time etc. In the places of refuge in Kita-ku of Nagoya City, the groundwater of about 3,640m3/year is pumped in Case1, the groundwater of about 24,266m3/year is pumped in Case2, the groundwater of about 121,330m3/year is pumped in Case3, and the groundwater of about 303,326m3/year will be pumped in Case4 when assuming that the groundwater drawn up is used as alternative water at this time as shown in Table 2 of Daito(2020) .

There are 31 places of refuge in Kita-ku of Nagoya City, and 11 places of refuge are from Horikawa River within 1km in both shores as showing in Figure 5. Everything cannot be covered by the groundwater drawn up, because there are a lot of volume of water from the Shonai River .

However, it is thought it is useful for Horikawa's water quality purification and environmental sustainability, etc. by throwing groundwater from these 11 places of refuge to Horikawa River though the volume of water is few.

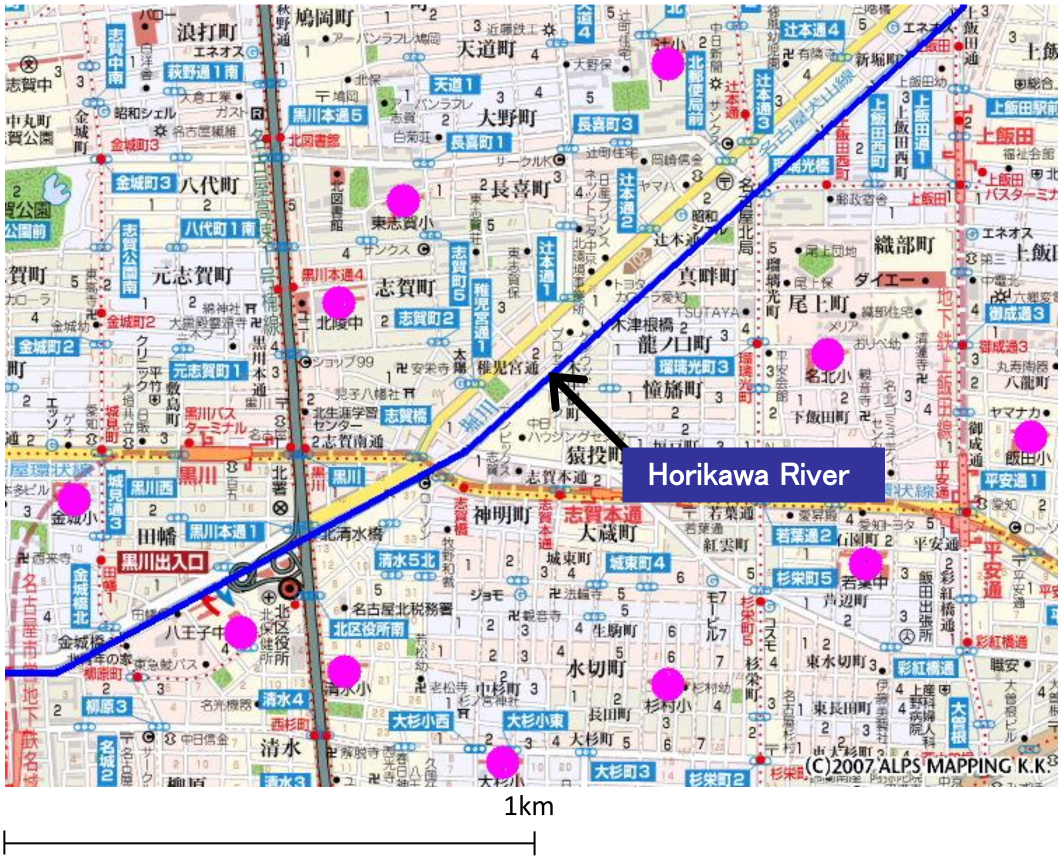

Figure 5 Distribution of the places of refuge in the vicinity of Horikawa River

Conclusion

In this report, it proposed the method of managing the large area groundwater at the disaster. It is to increase the pump discharge in the vicinity of Ogaki City with little decrease in the groundwater level even if underground water is pumped, and to decrease some pump discharges in the vicinity of Nagoya City. And, the decrease in the groundwater level in the vicinity of Nagoya City is suppressed by transporting underground water to the vicinity of Nagoya City as a shortfall of daily life water, and the possibility of the subsidence becomes lower.

Moreover, it proposes how to use the groundwater drawn up effectively actually. Even when the disaster occurs, the groundwater of about 100L/day a person which corresponds to the volume of water of washing and cooking and washing can be pumped in each place of refuge. This groundwater becomes the source of the river of environmental prevention water to aim to attempt the improvement of the metropolitan environment in each municipality because it is possible to use it for the environmental sustainability in the water park etc. and the water quality purification by discharge to the river, etc.

References

Daito, K. (2020). Management of groundwater in the Nobi Plain that modeled groundwater use for earthquake disasters and environmental preservation. Proc. *Tenth International Symposium on Land Subsidence*(TISOLS),727-731.

Surface motion at different spatial and temporal scales: measurement approaches and first results of a German-wide monitoring programme

U. Dettmann[1,2], R. Seidel[1], A. Piayda[1], S. Frank[1], M. Minke[1], D. Lempio[1] and B. Tiemeyer[1]

1 Thünen Institute of Climate-Smart Agriculture, Bundesallee 65a, 38116 Braunschweig, Germany
2 Institute of Soil Science, Leibniz University Hannover, Herrenhäuser Str. 2, 30419 Hannover, Germany

ullrich.dettmann@thuenen.de

Introduction

Worldwide, surface motion is observed in peatlands (Howie and Hebda, 2018; Evans et al., 2021). On a long-term basis, surface heights in pristine and near-natural peatlands are increasing due to the formation of peat, while in drained peatlands surface heights are mainly decreasing due to the decomposition of peat and the concomitant emissions of carbon dioxide (CO_2).

Among other goals, the project 'Implementation of the German peatland monitoring programme for climate protection (MoMoK) - Part 1: Open Land' aims to estimate CO_2 emissions and uptake by surface motion in German peatlands. Therefore, the spatial distribution of surface heights at 198 field sites will be measured annually by elevation surveys in order to quantify the long-term trend of surface motion. At selected field sites, short-term trends of surface motion (e.g. caused by shrinkage and swelling in dependence on moisture conditions) will be measured on a higher temporal scale (hourly) with level recorders (extensometers) or pressure differences between a 'fixed' and 'moving' pressure transducer (ΔP).

Here, we show preliminary results of surface motion measurements obtained with three different measurement approaches. We (1) compare data of a level recorder with those of a 'fixed' and 'moving' pressure transducer, (2) compare surface motion data of three extensometer which are installed close to each other (distance ~3 m) with water table depths and (3) show how well different spatial and temporal scales can fit together.

Methods

Site selection

In the 'MoMoK' project, 198 sites were selected in order to represent the German-wide distribution of different organic soil types, peat substrates and thickness, land-use types and water management approaches. Organic soil types were classified into fen, bog, peat-derived organic soil, covered organic soil, and deep-ploughed organic soil following the classification scheme of Wittnebel el al. (2021). Land use types were separated into cropland, grassland and wet peatlands (paludiculture, near-natural and re-wetted). Table 1 shows the number of sites for each organic soil and land use type combination. To date (2022-08-22), 46 sites are installed.

	Fen peat soil	Bog peat soil	Peat-derived organic soil	Covered organic soil	Deep-ploughed organic soil	**Sum**
Cropland	12	3	12	6	6	**39**
Grassland	57	12	21	15	6	**111**
Wet peatland	36	12	0	0	0	**48**
Sum	**105**	**27**	**33**	**21**	**12**	**198**

Table 1 Number of 'MoMoK' sites separated into organic soil and land use types.

Measurement approaches

Surface motion is measured at different spatial and temporal scales. All measurements are performed in reference to the top of a fixed rod which is installed firmly in the mineral subsoil at all sites. The spatial distribution of surface motion is measured by a yearly repeated elevation survey (level-meter or tachymeter) on a 50 x 50 m grid with approximately 200 Points. At 12 sites, elevation surveys are performed at a higher temporal resolution of two months.

At selected sites, surface motion is measured in an hourly resolution either by level recorder (extensometer, constructed within the project by the Thünen Institute of Climate-Smart Agriculture) or by the pressure difference between a 'fixed' and 'moving' pressure transducer (ΔP) within one monitoring well for peat water levels (Frank et al., 2022). Thereby, one pressure transducer is fixed to the pipe of the monitoring well, and the second pressure transducer is attached to a pipe that is placed over the pipe of the monitoring well, free to move with the surface (op de Beek et al., 2018). Extensometers will be installed at 52 sites (to date, extensometers are installed at 26 sites) distributed proportionally to the organic soil types and land use types of the 198 'MoMoK' sites. 'Fixed' and 'moving' pressure transducer will be installed additionally at all wet peatland sites without extensometer.

Results

Hourly measurements: extensometer vs. ΔP

Figure 1 shows relative surface heights measured with an extensometer and ΔP at a deep drained bog used as grassland. Both measurement approaches showed similar results with a root mean square error (RMSE) of 0.004 m. Slight differences could be attributed to soil heterogeneity or differences in measurement technique, mostly by different contact of the measurement equipment to the moving soil surface.

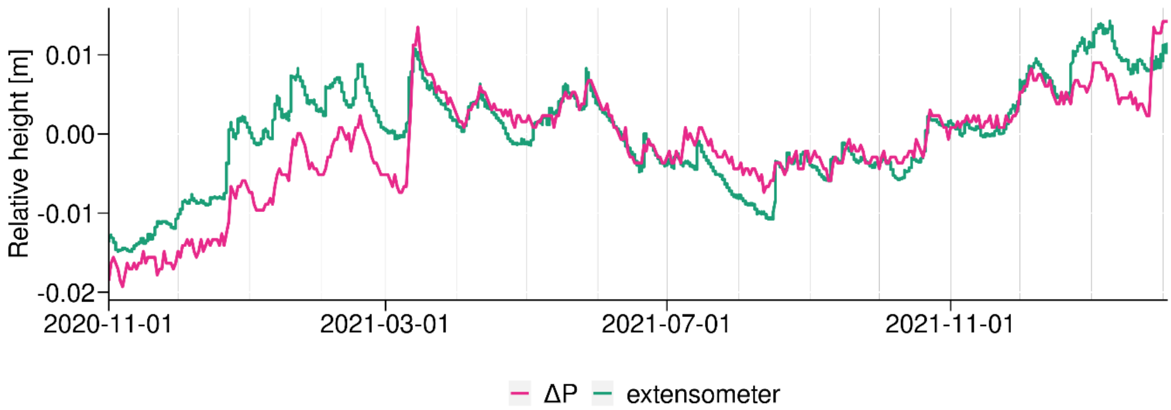

Figure 1 Relative heights measured with an extensometer and a 'fixed' and 'moving' pressure transducer (ΔP).

Replicate measurements with three extensometers

Water table dynamics and relative surface heights at a drained bog under grassland use are shown in Figure 2. The lowest water tables (~0.6 m below surface) were observed from mid-August to mid-October (Fig. 2a). In winter, water tables were close to the surface. The relative surface heights were strongly dependent on the water table dynamics (Fig. 2). As expected, the lowest relative surface heights were measured at the driest period at the end of summer, followed by continuously increasing relative surface heights at mid-October with maximum values at the end of February. The amplitude between minimum and maximum measured values was approximately 0.06 m. All three extensometers showed similar results over the measurement period of approximately one year (Fig. 2b).

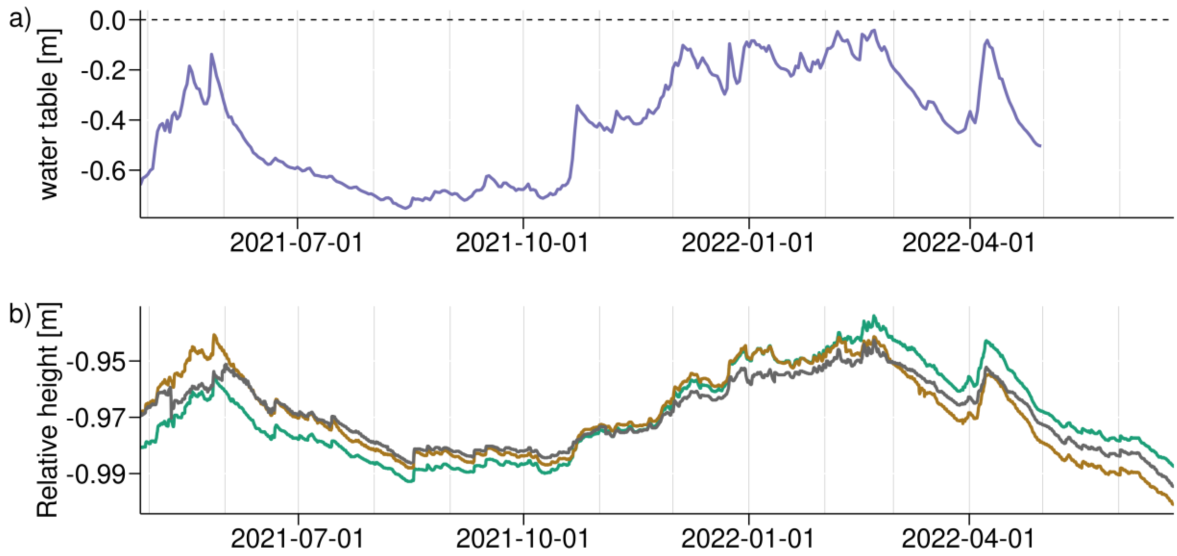

Figure 2 a) Water table and b) relative surface heights measured with three extensometers.

Elevation survey vs. extensometer

Figure 3 shows the heights of repeated elevation surveys and the mean ± standard deviation of three extensometer measurements at a deep drained bog used as grassland. Heights measured with the extensometers are in the same range as the median heights determined by the elevation survey. As the elevation survey covers a larger spatial area, a larger variability of the heights within one measurement date is to be expected and not reflecting a lower precision of the data. The quality of the data is reflected by the distributions of the elevation surveys (boxplots in Figure 3) remaining constant over the repeated measurements.

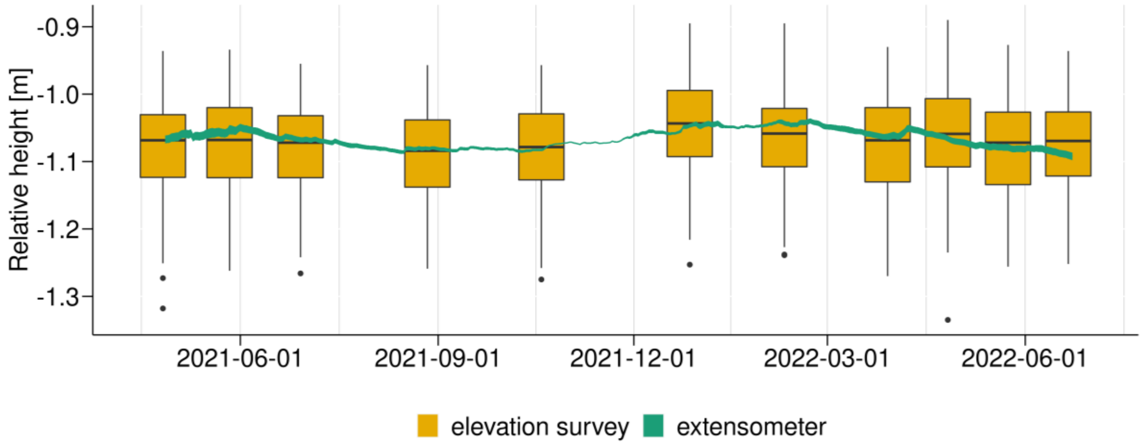

Figure 3 Extensometer measurements (standard deviation of three extensometer) and repeated elevation surveys (boxes define the 25-75% quartiles, whiskers are 1.5 times the quartile, points represent values outside this interval).

Conclusion

The results show that different measurement approaches can lead to similar results. At an hourly resolution, reliable surface heights may both be obtained by extensometer and ΔP. Data of high temporal resolution are necessary for process understanding and can support model development or parameterisation, in order to predict surface motion in dependence on different drivers (e.g. soil moisture conditions). The disadvantage is that surface motion of only a small area is measured, neglecting microtopography as well as soil and field heterogeneity. Elevation surveys are suited to capture the spatial variability of field sites, but lack on the temporal resolution. Here, we showed that surface motion measured on a small spatial, but high temporal scale (extensometer or ΔP) can be combined with elevation surveys which capture a larger spatial, but lower temporal scale.

References

Evans, C.D., Callaghan, N., Jaya, A., Grinham, A., Sjogersten, S., Page, S.E., Harrison, M.E., Kusin, K., Kho, L.K., Ledger, M., Evers, S., Mitchell, Z., Williamson, J., Radbourne, A.D. and Jovani-Sancho, A.J. 2021. A Novel Low-Cost, High-Resolution Camera System for Measuring Peat Subsidence and Water Table Dynamics. Frontiers in Environmental Science 9, 1-18.

Frank, S., Dettmann, U., Heidkamp, A., Piayda, A., Oehmke, W. and Tiemeyer, B. 2022. Methodenhandbuch zu den Gelände- und Laborarbeiten für den Aufbau des deutschlandweiten Moorbodenmonitorings für den Klimaschutz (MoMoK) - Teil 1: Offenland. Version 1.0, Thünen Working Paper 199. https://literatur.thuenen.de/digbib_extern/dn065255.pdf (accessed on 2022-12-02).

Howie, S.A. and Hebda, R.J. 2018. Bog surface oscillation (mire breathing): A useful measure in raised bog restoration. Hydrological Processes 32(11), 1518-1530.

op de Beeck, M., Gielen, B., Merbold, L., Ayres, E., Serrano-Ortiz, P., Acosta, M., Pavelka, M., Montagnani, L., Nilsson, M., Klemedtsson, L., Vincke, C., De Ligne, A., Moureaux, C., Marañon-Jimenez, S., Saunders, M., Mereu, S. and Hörtnagl, L. 2018. Soil-meteorological measurements at ICOS monitoring stations in terrestrial ecosystems. International Agrophysics 32, 619-631. doi: https://doi.org/10.1515/intag-2017-0041

Wittnebel, M., Tiemeyer, B. and Dettmann, U. 2021. Peat and other organic soils under agricultural use in Germany: Properties and challenges for classification. Mires and Peat 27, 19, 1-24.

Groningen data driven subsidence forecast – addressing aquifer depletion uncertainty in a Bayesian framework

Rob van Eijs[1], Onno van der Wal[1], Stijn Bierman[2], Hermann Bähr [1], Gini Ketelaar[1], Anke Jannie Landman[1]

1 Nederlandse Aardolie Maatschappij, Assen
2 Shell Global Solutions International B.V., Amsterdam

rob.vaneijs@shell.com

Abstract

After the discovery of the Groningen gas field in 1959, land subsidence due to gas production was recognized as a potential threat to water management in the Province of Groningen. During the 60 years of gas production from the field, the cemented reservoir sandstone has compacted with tens of centimetres due to the decrease of the pressure. The resulting land subsidence has been monitored frequently over the past 60 years by geodetic measurements (optical levelling, InSAR, GNSS). In this study, subsidence models were calibrated using a Bayesian Monte Carlo-Markov chain approach. Subsidence forecasts are based on the short-term production scenarios, the long-term pressure equilibration phase in the gas field and connected lateral aquifers.

Introduction

The Groningen gas field is the largest gas field in Europe with a gas volume of around 2900 billion cubic meters (De Jager and Visser, 2017). A large part of the Groningen province lies below the sea level, an area that requires active water management. Significant compaction and subsidence due to gas production can be regarded as a threat to constant groundwater levels with possible consequences for land usage and infrastructure like dikes and bridges. Large additional subsidence volumes require additional efforts from water boards to preserve the usage of the land as it is today.

This subsidence threat has long been recognised, which resulted in many studies (e.g., van Thienen-Visser and Fokker, 2017 and van Eijs and van der Wal, 2017). These studies all had the objective to match a geomechanical model to the available geodetic data. Subsequently, the history matched model is then used for forecasting the future subsidence.

Besides the impact on groundwater levels, reservoir compaction has also been correlated to the occurrence of induced seismicity (Bourne et al. 2014). Although induced seismicity is mainly caused by poro-elastic effective stress changes, it is observed that the highest frequencies and magnitudes of earthquakes occur in areas where the compaction is highest. Because of the seismic activity, the minister of Economic Affairs and Climate Policy decided to end the production from the Groningen field in 2022. This decision will stop further depletion of the main reservoir layer and hence subsidence of the field at large. However, it does not imply that further compaction and subsidence will cease immediately. Both visco-plastic compaction and pressure redistribution will lead to moderate amounts of further subsidence above the gas field. Another potential source for further compaction is the pressure decline in the aquifers that are laterally connected to the gas field. Because there are no wells in these aquifers, the pressure cannot be measured directly and can only be estimated from calibration and/or inversion of the geodetic data.

Methods

There are multiple possibilities to calibrate a model to measured data. In the past, deterministic models were manually fitted to the data. These methods are prone for non-uniqueness and often lack a proper quantification of the uncertainty. A stochastic approach would circumvent these drawbacks where data is used to find both the optimal match and its uncertainty. In this study, analytical and therefore fast models are used in the statistical methodology for matching and forecasting the subsidence above the Groningen field. This method is described in detail by Bierman and Towe (2020). The method distinguishes the model uncertainty (Σ_{emp}) and geodetic measurements uncertainty (Σ_{geod}) that in total provide a description of the prediction interval. The probability is based on the goodness of fit expressed by the value for the negative log-likelihood (NLL).

Furthermore, the workflow is designed to address the following additional questions:

- Can we find properties, based on well or seismic data, that correlate to rock mechanical data to create prior spatial compressibility maps?
- What is the most likely aquifer realization using the geodetic data?
- How improve the spatial and temporal match with the geodetic data?

To obtain the answers to these questions, the following workflow was constructed (Figure 1). A description of the steps, including the results for each step is presented in the next sections.

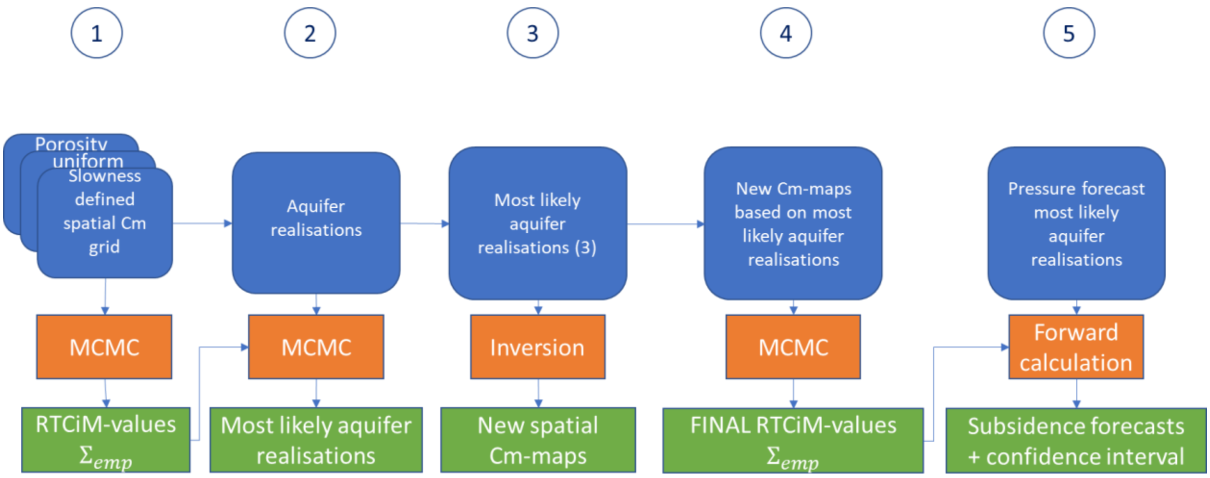

Figure 1 Scheme of the 5-step workflow. Input of each step in blue, the orange boxes visualize the calculation method and in green, the results per step.

Step 1: Generation of the prior rock compressibility grids and calculate a first set of compaction model and uncertainty parameters:

The following correlations were used as a prior input in the calculations: Cm – porosity, Cm – slowness (1/sonic velocity) and a uniform Cm (uniaxial compressibility) grid for the area above the gas field. The porosity, derived from core and logs, and the sonic slowness, derived from seismic data, are used to build spatial maps for the Cm values that are used in the Rate Type Compaction Model (De Waal and Smits, 1988, Pruiksma et al., 2015). This compaction model allows for a description of stress rate dependent compaction. In short, the model describes a first direct strain response, ε_d, to a change of the loading rate (e.g. caused by the gas production), followed by a more gradual response referred to as the secular strain, ε_s. The total strain is defined as the sum of a direct part and a time dependent secular part:

$\varepsilon = \varepsilon_d + \varepsilon_s$. More details of the implementation of the RTCiM, where the i stands for an isotachen formulation, can be found in NAM (2020).

For these spatial maps the most likely RTCiM parameters and uncertainty parameters are found using a Monte Carlo-Markov Chain (MCMC) method. This inversion procedure uses the geodetic data and converges to a compaction scenario with the lowest value for the negative log likelihood and calculates the value for the model uncertainty (Σ_{emp}). Knowing the thickness and the pressure, the most likely RTCiM parameter values can be calculated. In step 1, only geodetic benchmarks above the gas field are used in the calibration, because of the well constrained pressure input in the workflow coming from the Groningen reservoir model.

Step 2, selection of the aquifer realisations

Using the obtained results for the uncertainty (Σ_{emp}) and RTCiM parameters from step 1, the objective of step 2 is to test the aquifer realisations in combination with the spatial Cm grids. To test multiple aquifer scenarios in the southwestern aquifer, box-models that allow for multiple pressure profiles per box over the length of the box, were created. Box-models are defined by fault structures (long edges of the box) and the boundaries of the gas fields at the western short edges of the boxes. The boundaries of the boxes are controlled by the gas pressures in the Groningen field and the pressures of the smaller gas fields to the west of Groningen. Combining the defined box-models and legacy reservoir models, 3126 possible aquifer realisations for each prior compressibility grid, are tested to obtain a value for the NLL. The computational effort is relatively small because of the fixed values for the model uncertainty (Σ_{emp}) and RTCiM parameters from step 1 that are assigned to both the gas field and aquifer reservoir rock properties. The geodetic benchmarks above the aquifers are used to assess the modelled subsidence fit to the measurements. The most likely realisation, defined by the NLL, for each of the possible spatial Cm grids is selected, resulting in three modelled subsidence scenarios.

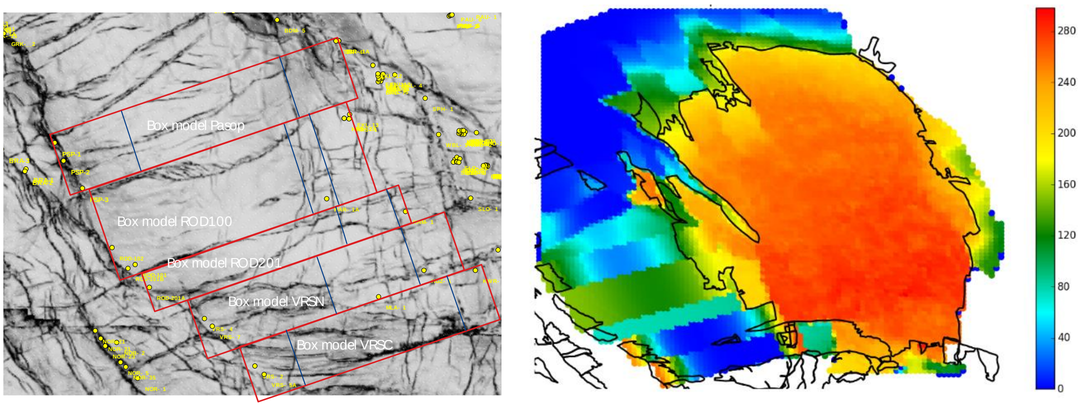

Figure 2 left: box models in the southwestern aquifer. Right: an example of a pressure depletion realization that shows the boundaries of the box-models as well in the southwestern part of the figure.

Step 3, inversion to obtain optimal spatial Cm grids

To reduce local higher residuals in the three subsidence scenarios, step 3 uses an inversion scheme to give more weight to the measurements in these areas. Rather than using a smoothing parameter, the spatial Cm maps of step 1 are used as a prior input into the inversion scheme where the weight of the prior is set by a penalty factor. A trade-off between the goodness of fit, provided by the negative log likelihood and the outcome of a geologically reasonable distribution, guided by the prior spatial map, concluded the value of the penalty factor. Step 3 results in 3 new spatial compressibility maps for each of the three subsidence scenarios shown in Figure 3.

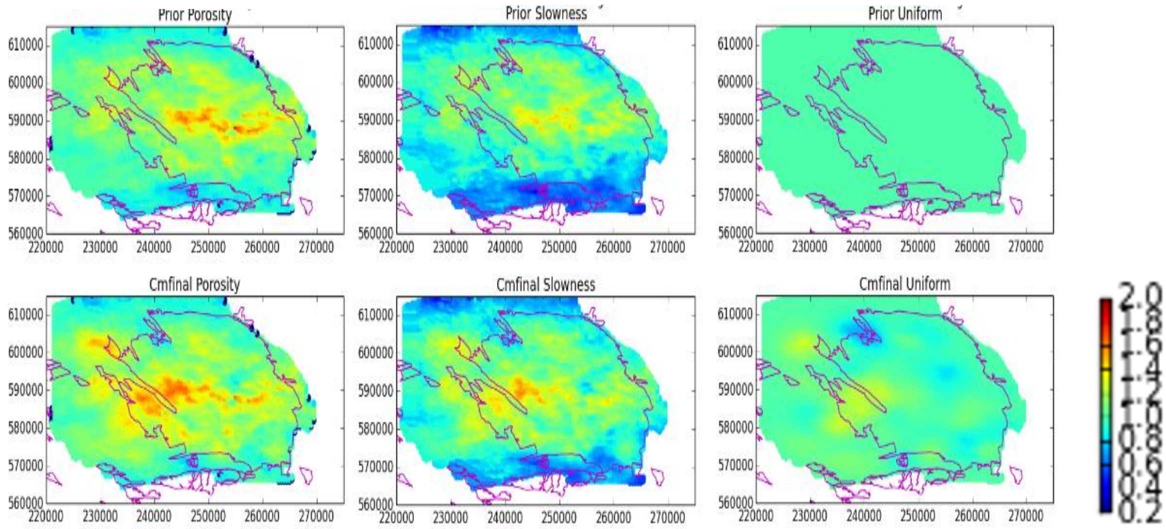

Figure 3   Results for the spatial Cm inversion using a value for the penalty factor of 5. The columns indicate the prior Cm grid. The top row shows the prior Cm grids and the bottom row the resulting spatial Cm grids.

Step 4, improve the temporal fit to the data, by adjusting the RTCiM parameter values

In step 3, local spatial mismatches are decreased. In step 4 the match to the temporal signal from the measurements is improved including a new assessment of the Σ_{emp}. New values for the RTCiM parameters are derived after the application of the MCMC statistical workflow and using the new spatial Cm maps from step 3. This step resulted in adjusted posterior values for the RTCiM parameters and the parameter values that describe the Σ_{emp}. Figure 4 shows a coverage plot for the most likely subsidence scenario. The blue vertical lines in the left graph show the bandwidths of the predicted displacements. The red points in the same graph show the measured displacements. The horizontal axis is defined by the rank of the median predicted displacements (more than 10000 data points). With a perfect model, the coverage would be 95%, implying that 95 % of the measurements fall into their respective prediction intervals. The result after step 4 is close to this value (92%), a value that improved when compared to the results after running step 1. More important is the improvement of the coverage per benchmark (map on the right in Figure 4). No local or regional clusters of benchmarks with a poorer coverage are observed. The adjusted Cm grid in step 3 contributed most to this improvement.

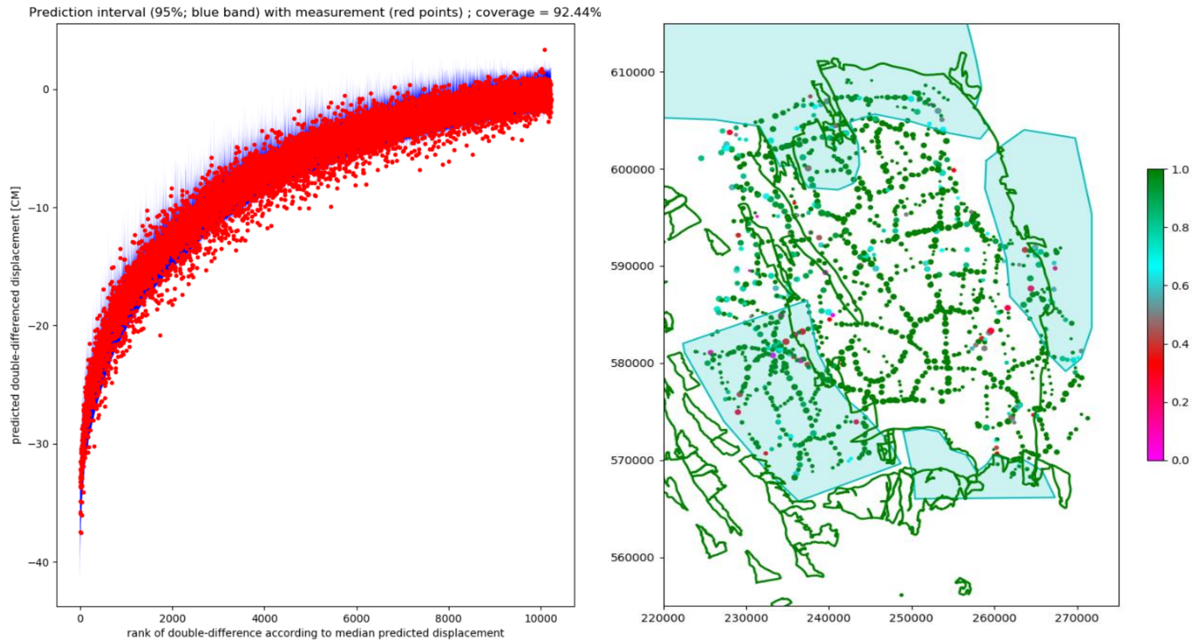

Figure 4 Prediction interval and coverage (left graph). Right picture: coverage per benchmark. The size of the dot indicates the number of measurements that are linked to the benchmark. The colour indicates the fraction of measurements that are inside the prediction interval. Dark green means that all measurements in time linked to the specific benchmark are inside the prediction interval.

Step 5, subsidence forecasts

Step 5 executes the forward calculation to obtain the forecast for the most likely subsidence scenario including its uncertainty. The estimated parameters for the Σ_{emp} provide the uncertainty of the forecast, i.e. the confidence interval. Figure 5 shows for five locations above the field the model results with the historical data and the subsidence forecast, including a 95% confidence interval of the model.

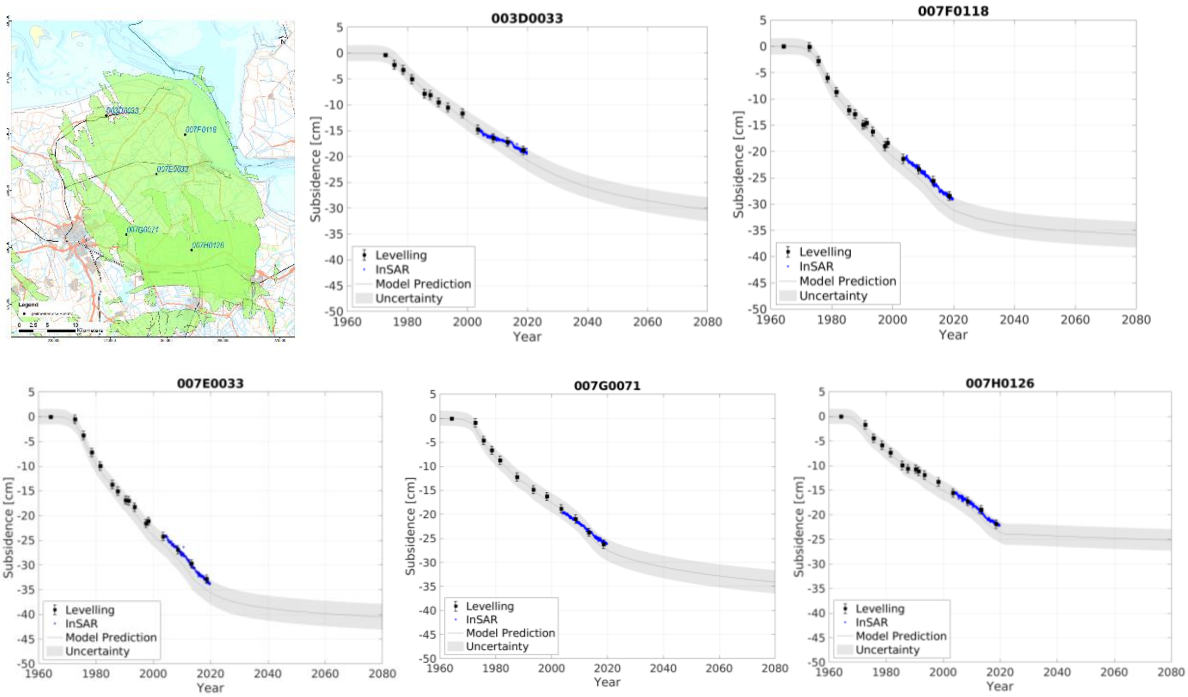

Figure 5 Subsidence at benchmark locations till 2080: dark grey line is the predicted subsidence, grey is the P95 confidence interval, black squares are levelling measurements plus uncertainty, the blue dots are the InSAR measurements.

References

Bierman S., & Towe, R. (2020) Statistical methodology for fore casting of subsidence above the Groningen gas field For the Rate Type Compaction isotach Model (RTCiM) for reservoir compaction. *Shell report* SR.20.00973 (link)

Bourne, S.J., Oates, S.J., van Elk, J. & Doornhof, D., (2014). A seismological model for earthquakes induced by fluid extraction from a subsurface reservoir. *Journal of Geophysical Research* 119 (12): 8891–9015. doi: 10.1002/2014JB011663

Van Eijs, R., & Van der Wal, O. (2017). Field-wide reservoir compressibility estimation through inversion of subsidence data above the Groningen gas field. *Netherlands Journal of Geosciences*, 96(5), S117-S129. doi:10.1017/njg.2017.30 (link)

De Jager, J., & Visser, C. (2017) Geology of the Groningen field – an overview. *Netherlands Journal of Geosciences*, 96(5), S3-S15. doi:10.1017/njg.2017.22

NAM (2020) Groningen long term subsidence forecast. *NAM report* EP202008201822 (link)

Pruiksma, J.P., Breunese, J.N., Thienen-Visser, K., & De Waal, H. (2015) Isotach formulation of the rate type compaction model for sandstone. *International Journal of Rock Mechanics and Mining Sciences*. 78. 127-132. 10.1016/j.ijrmms.2015.06.002.

Van Thienen-Visser, K., & Fokker, P. (2017). The future of subsidence modelling: Compaction and subsidence due to gas depletion of the Groningen gas field in the Netherlands. *Netherlands Journal of Geosciences*, 96(5), S105-S116. doi:10.1017/njg.2017.10

De Waal, J.A. and Smits, R.M.M. (1988) Prediction of reservoir compaction and surface subsidence-field application of a new model. *SPE Formation Evaluation* 3 (02): pp.347–356. Paper Number: SPE-14214-PA

Land subsidence due to the overexploitation of the aquifers in arid regions. The case of Remah and Al Wagan areas, Al Ain, UAE.

M. Elkamali[1], C. Loupasakis[2]*, I. Papouptsis[3], A. Abuelgasim[1]

1 National Water & Energy Center, Geography & Unban Sustainability, United Arab Emirates University
2 The National Technical University of Athens, School of Mining & Metallurgical Engineering, Dept. of Engineering Geology & Hydrogeology
3 Institute for Astronomy, Astrophysics, Space Applications & Remote Sensing, National Observatory of Athens

*Corresponding author: Cloupasakis@metal.ntua.gr

Introduction

United Arab Emirates (UAE) characterised by arid climate with limited resources of fresh water and high-water demand in sectors of domestic, agriculture, and industry. Water resources in the UAE can be classified into conventional water resources (seasonal floods, springs, falajs, and groundwater) and non-conventional water resources (desalination water and Treated wastewater) (Rizk & Alshahran, 2003). Due to this limitation in water resources, sustainable groundwater practices are required to maintain the available resources to diminish. One of the most crucial groundwater practices are monitoring of groundwater dynamics, in quality and quantity, and the implications of unsustainable groundwater usage.

Al Ain region is located at the eastern part of Abu Dhabi Emirate, UAE at the border with Sultanate Oman. It is characterised by arid climate with scarce rainfall in winter and high annual evapotranspiration. The region is geomorphologically consists of Jabal Hafit and Oman mountains, a gravel plain at the western side of Oman Mountains known as Al Jaww Plain, and large Sand Dunes. Groundwater aquifers in the UAE can be classified into limestone aquifers, ophiolite aquifers, gravel aquifers, and sand dune aquifers (Elmahdy & Mohamed, 2015). Groundwater system of the Al Ain region is composed of the last two aquifers with dominant of the sand dune aquifers. This region occupies 50% of the Abu Dhabi Emirate agricultural activities consumes huge amount of groundwater with annual discharge more than 200 million m^3.

The current study aims at investigating the deformations occurring at the site due to the overexploitation of the aquifers by combining SAR satellite data, with ground water level measurements and ground truth surveys for the verification of the deformations.

Synthetic Aperture Radar (SAR) is a radar satellite system which transmits its own signal and measure the backscatter signal, stores in amplitude and phase signal, to satellite sensor. SAR satellite system differs from the optical satellite system due to its independence of sun and weather. SAR Interferometry (InSAR) technique has the capability to measure the effect groundwater dynamics on land surface with millimetric resolution (Ferretti et al. 2007). InSAR techniques have been utilised to detect land surface deformations occurred due to extraction of subsurface materials such as groundwater, oil, and gas. InSAR techniques rely mainly on measuring the phase difference between two SAR scenes acquired from different orbit location or at different time. Monitoring of land surface deformations require implementing InSAR technique with a time-series SAR scenes acquired over the area of interest. The interferometry depends on identifying targets with stable phase during the period of the study known as Permanent or Persistent Scatterers (PS) such as buildings, rocks, pavement roads, etc. In the last two decades, many InSAR approaches have been developed in order to process InSAR time-series data, includes Persistent Scatterer Interferometry (PSI) (Ferretti et al. 2001), Small Baseline Subset (SBAS) (Berardino et al. 2002), and Stanford Method for PSI (StaMPS) (Hooper et al. 2004).

Applications of the InSAR technique for surface deformations in the UAE are limited due to the wide coverage of the sand dunes (more than 70% of the country) where the SAR signal experiences temporal decorrelation and there is a significant drop in interferometric coherence. Coarse-resolution investigation for the Al Ain region using SBAS technique and ENVISAT (C-band) data aimed to detect regional land surface deformations in the eastern part of Abu Dhabi Emirate (Cantone et al., 2013). This investigation delineated a significant subsidence in the Remah and Al Wagan areas. The coarse resolution in combination with the coherence change of the sand limited the reliability of this study.

Methods

As already mentioned, this study was conducted by combining SAR satellite data, with ground water level measurements and ground truth surveys for the verification of the deformations. Sentinel-1 data, provided by the European Space Agency (ESA), were used to process the SAR interferometry over the study area. Water level data were provided by the Environment Agency of Abu Dhabi (EAD), and they were used to determine zones affected by groundwater overexploitation. Land surfaced subsidence evidences were identified in the field, confirming the deformations identified by the SAR interferometry data. The dataset used consists of 37 Sentinel-1A Single Look Complex (SLC) images acquired along the ascending orbit from path 130 and frames 73 and 75, for a time span between February 2015 and May 2019. The image acquired on 22 October 2017 was selected as a primary, or master, image to increase the expected coherence due to it is minimum spatial and temporal baselines.

The water level dataset indicated an extensive depression cone covering the area under investigation (Figure 1). The extended network of irrigation wells has systematically affected the unconfined sand dune aquifers unit and resulted in lowering the groundwater level with a maximum drawdown at its centre of approximately 40 to 50 m. As expected, at the perimeter of the cone, the ground water lowering gradually decreases in relation to the distance from the centre of the cone. The great discharge from the aquifer, more than 240 million m^3, along with a very low hydraulic conductivity of the aquifer resulted in a low annual groundwater recharge.

Land surface deformations were observed during the field visit and can be summarized as follow; leaning of some fracture walls caused by the differential settlements of their foundations, well casings experienced protrusion due to the land surface subsidence, and dislocated electrical pillars with the wires tensioned due to the differential surface movements (Figure 2).

The performed SAR interferometry analysis was the Parallelized Persistent Scatterer Interferometry (P-PSI) an open-source software implementing a distributed processor for fully automated and computational efficient for detecting land surface velocities along line-of-sight (LOS) via PSI and long time-series dataset of Sentinel-1. The P-PSI uses two main software packages, Interferometric Scientific Computing Environment (ISCE) and Stanford Method for Persistent Scatterer Interferometry (StaMPS). ISCE was implemented with topsStack processor for creating a stack of co-registered SLC images. Then it has been utilised for interferogram generation, coherence maps, differential interferogram generation, and spatial subset. After that, StaMPS was implemented for the time-series interferometric analysis and computation of land surface velocities. The topographic incorporated phase was estimated and removed using an external Digital Elevation model, while phase noise was corrected by removing all pixels exceeding 1.0 interferometric phase standard deviation. The Atmospheric Screen Phase (APS) was estimated and removed by applying the open-source Toolbox for Reducing Atmospheric InSAR Noise (TRAIN). Finally, after removing all incorporated phase components the phase of land surface displacement remains and was used to estimate the annual ground displacement.

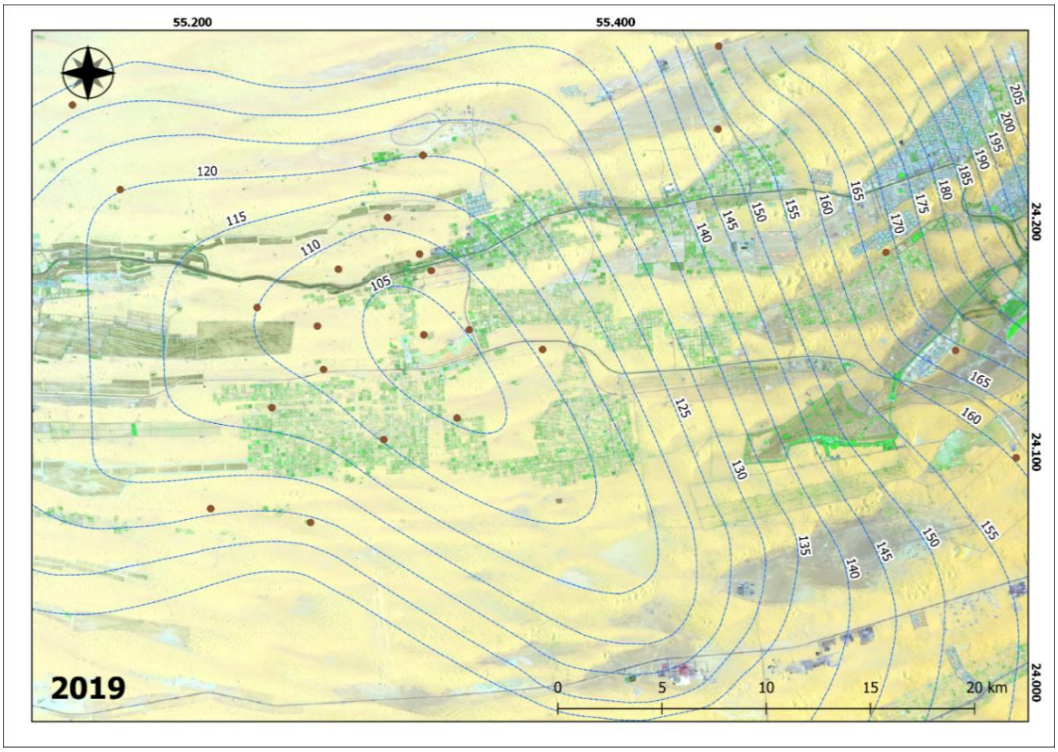

Figure 1 Groundwater level contours, blue doted lines, indicate the depression cone during 2019. The brown dots indicate the monitoring water wells.

Figure 2 Land surface subsidence evidences. On the left the leaning wall, at the middle the protrusion well casing, and on the left the leaning of electrical pillars.

Conclusions

This study showed an extensive land surface subsidence with a rate of 40 mm/year in the period between 2015 and 2019. The cone of depression for the water level drawdown in the study area was found in spatial correlation with the detected land surface subsidence bowl. This can be concluded that the land surface subsidence was triggered by the groundwater over extraction.

Furthermore, it was proved that the repeat-pass satellite SAR interferometry can provided substantial information about the actual extent of the land subsidence phenomenon. Space-based technologies are cost effective, providing high spatial coverage. So, they are able to fill the data and knowledge gaps and reduce the uncertainties by providing high spatial and temporal valuable information about the extend and the progress of the subsidence.

Finally, it should be noted that the detection of the phenomenon at an initial stage is extremely important, as further expansion of the affected area and damages on settlements and infrastructure can be prevented. The information provided by these studies can give rise to focused geotechnical and hydrogeological studies.

Acknowledgements

This work was supported by a grant from the United Arab Emirates University (UAEU) National Center for Water and Energy under grant number 31R155-Research Center-NWC-3-2017.

References

Berardino, P., Fornaro, G., Lanari, R., Sansosti, E., 2002. A new algorithm for surface deformation monitoring based on small baseline differential SAR interferograms. IEEE Trans. *Geosci. Remote Sens*. 40, 2375 –2383. https://doi.org/10.1109/TGRS.2002.803792.

Cantone, A., Riccardi, P., Baker, H.A., Pasquali, P., Closson, D., Abou Karaki, N., 2013. *Monitoring Small Land Subsidence Phenomena in the Al-Ain Region by Satellite SAR Interferometric Stacking*. https://doi.org/10.3997/2214-4609.20131906.

Elmahdy, S.I., Mohamed, M.M., 2015. Groundwater of Abu Dhabi Emirate: a regional assessment by means of remote sensing and geographic information system. *Arabian Journal of Geosciences*. 8, 11279-11292. https://doi.org/10.1007/s12517-015-1932-2.

Ferretti, A., Prati, C., Rocca, F., 2001. Permanent scatterers in SAR interferometry. *IEEE Transactions on Geoscience and Remote Sensing*. 39, 8–20. https://doi.org/10.1109/36.898661.

Ferretti, A., Savio, G., Barzaghi, R., Borghi, A., Musazzi, S., Novali, F., et al., 2007. Submillimeter Accuracy of InSAR Time Series: Experimental Validation. *IEEE Transactions on Geoscience and Remote Sensing*. 45, 1142-1153. https://doi.org/10.1109/TGRS.2007.894440.

Hooper, A., Zebker, H., Segall, P., Kampes, B., 2004. A new method for measuring deformation on Volcanoes and other natural terrains using InSAR Persistent Scatterers. *Geophyiscal Research Letters*. 31, 1-5. https://doi.org/10.1029/2004GL021737.

Rizk, Z.S., Alsharhan, A.S., 2003. Water resources in the United Arab Emirates. In: Alsharhan AS, Wood WW, editors. *Developments in Water Science.* 50. Elsevier, pp. 245-264.

Proc. IAHS, 382, 733–740, 2020
https://doi.org/10.5194/piahs-382-733-2020

Open Access PIAHS

The 6M approach to land subsidence

Gilles Erkens[1,2] **and Esther Stouthamer**[2]

[1]Deltares Research Institute, Daltonlaan 600, 3584 BK, Utrecht, the Netherlands
[2]Faculty of Geosciences, Utrecht University, 3584 CB, Utrecht, the Netherlands

Correspondence: Gilles Erkens (gilles.erkens@deltares.nl)

Published: 22 April 2020

Abstract. Though global awareness of land subsidence has increased over recent years, subsidence remains an ongoing and largely unsolved problem, which is exemplified by frequent discoveries of apparently new subsiding areas. This means that for many of these areas there is a continuous and growing need to provide guidance to decision makers on how to tackle this global problem. This paper presents a comprehensive, step-by-step approach to address land subsidence, illustrated by best practise examples from around the world. The approach places emphasis on the long-term sustainability of resources, whose development is related to the subsidence problems. We identified 6 steps, collectively referred to as the 6M approach, that are crucial to tackle subsidence: Measuring, understanding Mechanisms, Modelling, Money, Measures and Monitoring. This paper offers guidance for implementing the 6M approach, and the lessons learned from the real-life examples provide valuable information and inspiration for decision makers and experts to address subsidence. The focus is on subsidence in deltaic and coastal areas where subsidence contributes to relative sea level rise. It is expected that the 6M approach will contribute to lowering the threshold to act on subsidence. The 6M approach is also used as a guiding principle for the thematic subdivision of TISOLS, providing a meaningful linkage between subsidence science and the societal response to subsidence problems.

1 Introduction: land subsidence, a wicked problem

In many coastal and delta cities land subsidence exceeds absolute sea level rise, in some places as much as a factor of ten (e.g. Erkens et al., 2016a). Increased flood risk and other widespread impacts of subsidence result in damage totalling billions of dollars per year (Bucx et al., 2015, 2019). Much of this land subsidence is caused by human activities, such as groundwater extraction or draining and loading of soft soils (e.g. Galloway et al., 2016). Addressing subsidence in these vulnerable coastal areas has proven to be challenging. Generally, land subsidence is a slowly progressing, hidden threat, often not leading to a sense of urgency. In many cases, technical options to mitigate and adapt to subsidence are readily available, but formulating a subsidence strategy is difficult, let alone implementing its strategic measures. This is because land subsidence presents complex technical and societal issues involving many stakeholders with wide-ranging interests, and generally poor technical understanding of the underlying processes (Bucx et al., 2019). This paper offers guidance in the form of a step-wise 6M approach to help overcome these impediments to deal with land subsidence.

2 The land subsidence lock-in

Throughout history, in coastal areas adaptation to land subsidence has been the preferred strategy to manage subsidence hazards. For instance, the raising of embankments has traditionally been the response to lowered land elevations and the consequent increased flood risk. Subsidence that resulted in reduced drainage capacity of the surface water and overall wetter conditions, has often been addressed by the installation of pumps, which led to further subsidence (e.g. Erkens et al., 2016b for the Dutch situation). There are sparse examples of subsidence mitigation measures from the past. In fact, it was not until the 1960s that the first mitigation measures were taken (Bucx et al., 2015). The dominance of experiences with adaptation measures have led to an optimisation of subsidence adaptation strategies. This applies to the technical aspects (for example, the building of embankments for

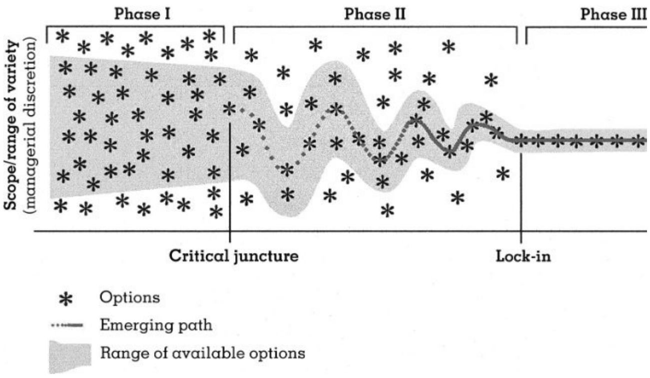

Figure 1. Path dependency leads to a lock-in situation at the end. This is currently the situation for land subsidence in many coastal areas, where an adaptation strategy is preferred over a mitigation strategy (The constitution of an organisational path figure from Sydow et al., 2009).

flood protection and pumping stations that drain the land), but also to the institutional and financial aspects. Institutions that have implemented these adaption measures and strategies have strengthened as they have acquired the requisite technical skills and knowledge, and the necessary vast financial resources (Seijger et al., 2018). As a result, over time it was increasingly easy to implement an adaptation strategy to subsidence problems. This development of a single strategy to manage subsidence problems, can be viewed as a path-dependent process, where future managerial discretion in terms of choices or options depends on the choices made in the past (Fig. 1). The end stage of path dependency, when managerial discretion is limited and a single management option is fully dominating, is called a lock-in. Sinking coastal and deltaic areas can thus be regarded as being trapped in a dual lock-in condition as the dominating adaptation strategy in terms of the applied technologies and the principal institutions act as constraints to moving toward a more long-term sustainable strategy (Seijger et al., 2018), one that may also include measures to mitigate subsidence.

3 Emerging from the lock-in

The lock-in condition means that it is difficult to choose alternative management options, as this conflicts with existing interests and breaks with the long-standing traditional approach to managing the subsidence. If the societal and financial benefits of alternative management approaches are fully known, a different action perspective may be proffered to decision makers. For these management alternatives a sound and shared knowledge base is required in terms of an in-depth understanding of the physical problems, the financial perspectives (what are the costs and benefits of different options?) and governance and legal capabilities (who is responsible and are there sufficient capabilities to implement the management measures?). When these conditions are satisfied, the threshold to act on an alternative management strategy will become lower.

Emerging from the lock-in is becoming increasingly urgent in subsiding coastal and deltaic areas. On the one hand, awareness of subsidence and its consequences has increased, exemplified by increased media coverage and scientific studies over the recent years. On the other hand, the sense of urgency has increased because as land subsidence accumulates, new problems arise, and existing problems worsen. Exposure to land subsidence is also still increasing, as population growth, ongoing urbanisation and economic growth seems to be focussed in coastal and deltaic areas. Finally, the realisation that land subsidence is interconnected with absolute sea level rise, both contributing to relative sea level rise, and the increasingly grim predictions of future climate warming induced absolute sea level rise increase the urgency to deal with subsidence in coastal and deltaic areas. In this light, land elevation needs to be viewed as an economic asset, and therefore loosing elevation as a liability.

4 A strategic framework

Realising that a sound and shared knowledge base is required to facilitate decision making to emerge from the lock-in, the question of where to start arises. Bucx et al. (2015) gathered real-life examples of best practises from around the world where land subsidence has been addressed. This was further elaborated and put into a framework by Erkens et al. (2015). Over the last years, the framework has evolved to what is presented in this paper: 6 steps that need to be taken to facilitate decision making with scientific knowledge. In contrast to many existing studies that describe how knowledge may be used in decision making (for instance Van Hardeveld, 2019 for land subsidence in the Netherlands), this study uses examples to document how this is done in practise and is therefore more anecdotal.

A step-wise approach is elaborated along the stages of the policy cycle, with clear steps that need to be taken (Fig. 2). The policy cycle is a tool that is used to analyse the development of a policy item and has been used for decades in political sciences. For each of the steps identified, there are questions that need to be addressed, and commonly both technical and governance aspects need to be considered to answer the questions. Because the steps are sequential, they offer a step-wise path on how to proceed. In total 6 steps were identified that provide the required information when starting to tackle subsidence, that all include the letter M (hence the 6M approach, Fig. 2): Measuring of land subsidence, understanding land subsidence Mechanisms, predictive Modelling of land subsidence, Monetary aspects of land subsidence (cost-benefit analyses [CBA]), implementation of Measures, and Monitoring and evaluation. Although these steps are meant to be sequential, in real life short-cuts are being taken be-

Figure 2. The 6M approach to land subsidence. The six steps are meant to be taken sequentially in a repeating loop, if necessary. CBA = cost benefit analyses. Image design by Welmoed Visser.

tween different steps, for instance when measurements (M1) from the first step show the urgency of the situation and measures are directly implemented (M5). If measures are proposed (M6) inspired by a best practise example elsewhere, sometimes the steps (Fig. 2) are followed in reverse order, specifically when locally-based substantiation is required to justify proposed measures.

Once the circle of the 6M approach is completed and monitoring and evaluation is in place, it is likely that evaluation leads to new research questions and the 6Ms start over. To ensure application of the gathered knowledge in other areas or for other sources of subsidence, preferably the monitoring data, analytical results and best practice examples (of the various 6M steps) are stored in a central database.

5 The 6M approach and TISOLS

The 6M approach is also used as a guiding principle for the thematic subdivision of TISOLS, providing a meaningful linkage between subsidence science and the societal response to subsidence problems.

6 Real-life examples of the 6 M's

6.1 M1 Measuring land subsidence

In coastal or deltaic areas where there is no apparent indication of subsidence, the first step (M1) is to establish whether a certain area is in fact subsiding and if so, at what rate. The occurrence of subsidence may not be obvious from casual observation, particularly when subsidence is non-differential and no structural damage (cracks, tilting) is observed in buildings or infrastructure. Typically, the loss of elevation compared to local sea level is mistaken for sea level rise as a result of climate warming. The aim of the measurements is to obtain insight into the current status of the land subsidence in terms of spatial and temporal trends. This may also include obtaining insight on the governance situation or the legal framework related to land subsidence.

An example where land subsidence measurements were the first step to establish the problem and create awareness is Jakarta in Indonesia. Land subsidence was recognized in 1926 in northern Jakarta from optical levelling, but first reports of subsidence-related impacts to infrastructure and flooding date from 1978 (Abidin et al., 2001). Dedicated land subsidence measurements started in the late 1990s with the installation of GPS stations by the Technical University of Bandung and resulted in research publications that basically served the academic community (Bucx et al., 2019). After Jakarta was hit by the most severe flooding in three centuries in 2007 when the seawall was overtopped during high tide and seawater flooded 40 % of the city, awareness progressively grew among authorities that land subsidence posed a problem that required further measuring (Bucx et al., 2015).

In contrast to geodetic surveys typically consisting of sparse point measurements, such as the aforementioned GPS stations, remotely sensed LIDAR (light detection and ranging) and InSAR (Interferometric Synthetic Aperture Radar) images can provide spatially detailed ground displacement maps. InSAR images date back to the early 1990s and can now be used to establish subsidence rates and patterns since then. Application of this technique in soft soil areas is for the moment limited to the built-up environment, as a result of the need for stable reflectors (targets). Ideally, multiple observation techniques are combined, for instance absolute measurements from GPS and optical levelling can be combined with remotely sensed data, for example, the relative displacement measurements from InSAR. In this way, spatially resolved subsidence maps with respect to a global geodetic reference frame can be produced. Heuff et al. (2019) published the first operational nation-wide spatially resolved subsidence map of the Netherlands with absolute deformation rates based on Persistent Scatterer InSAR, GNSS and gravimetry measurements (https://bodemdalingskaart.nl/, last access: 26 January 2020). This map shows that a large part of the Netherlands is indeed subsiding (Fig. 3).

6.2 M2 understanding subsidence Mechanisms

Land subsidence may be the result of different contributing processes. Often there are both natural and human-induced causes for land subsidence at the same location. Discriminating between these different sources by understanding the underlying mechanisms is relevant as natural subsidence rates

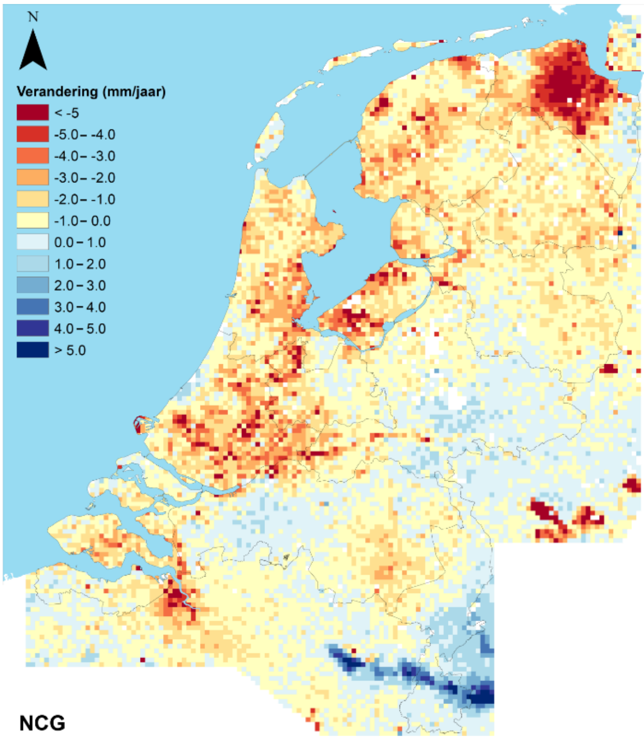

Figure 3. Land subsidence rates in the Netherlands (2015–2018). This product is an example where multiple measurement techniques were combined, in this case Persistent Scatterer InSAR, GNSS and gravimetry. Map downloaded in 2019 from https://bodemdalingskaart.nl/ and produced by the Nederlands Centrum voor Geodesie en Geo-Informatica (Dutch Geodetic Centre, NCG). Verandering (mm/jaar) = Deformation (mm/year).

are mainly limited to tens of mm per year. Human induced subsidence rates can easily reach cm's per year, to even tens of cm's per year. For policy development this distinction between natural and human-induced subsidence is important: while it is worthwhile to implement mitigation measures to reduce human-induced subsidence, for natural subsidence only adaptation measures may be taken (Erkens et al., 2015).

Van Asselen et al. (2018) show that subsidence of streets and gardens in the Dutch urban area's on peat soils is the result of many different components, and that the contribution of these components may vary over time and space. In this example, in the urban areas the loading of the peat with anthropogenic fill is the dominant cause for the observed land subsidence. The oxidation of peat (biogeochemical process of soil organic matter decomposition by micro-organisms) is hampered because the peat has subsided below the groundwater level which is often situated within the fill (Fig. 4). Just outside the urban area, where the fill is absent, peat oxidation is the dominant factor causing subsidence. This shows that step M2 is relevant to select the right measure (M5): in this case raising the groundwater level would reduce subsidence by peat oxidation in the rural area but would be less effective in preventing subsidence in the urban area.

Unravelling components contributing to subsidence is essential to understand the underlying subsidence mechanisms. In-situ observations, for instance obtained with extensometers, may be used to unravel the total subsidence signal. Extensometers are used to measure compaction worldwide (e.g. Poland, 1984). Extensometers can be used to derive point measurements of vertical movement of different (sub)surface levels at mm-scale accuracy, and to determine the contribution of different layers, and in some cases processes, to total subsidence. Another approach that can be followed is inverse modelling, whereby with the use of a careful inversion scheme, the available knowledge on the geology and hydrological dynamics of a system can be quantitatively constrained with subsidence observations (e.g. Fokker et al., 2007). Observational data linked to a single subsidence process form essential input for step M3: subsidence modelling. This data may be used to validate process-based numerical subsidence models.

6.3 M3 predictive Modelling of land subsidence

In the third step M3, once the causes for land subsidence have been established, predictions can be made to gain insight into future land subsidence. Integrated land subsidence models that include multiple subsidence processes are still rare. Most numerical models describe a single land subsidence process, and there are in fact multiple models that predict compression of the subsurface soils and geologic materials, but all are focussed on applications at different depth ranges (for example, shallow soft soils, shallow to deep aquifer systems and deeper natural gas reservoirs).

An example where numerical modelling is used to predict future subsidence for different scenario's is the low-lying Mekong delta, largely located in Vietnam. As a first step (M1), Erban et al. (2014) used InSAR (Interferometric Synthetic Aperture Radar) to determine land subsidence rates of 10–40 mm yr^{-1} between 2006–2010 over large areas in the Mekong Delta. Secondly (step M2), groundwater overexploitation has been proposed to be the main driver of subsidence in the Mekong Delta (Erban et al., 2014).

Thirdly (step M3), groundwater extraction-induced subsidence over the coming 80 years in the Mekong Delta was quantified using a numerical model (Minderhoud et al., 2020). The model consisted of two parts: a hydrological (groundwater) model (MODFLOW, USGS), and a one-way coupled geo mechanical land subsidence model SUB-CR (Kooi et al., 2018). The groundwater model simulates groundwater drawdowns and extraction-induced subsidence in six mitigation and non-mitigation extraction scenarios on a delta-wide scale (Fig. 5). The model provided important insights. It shows the extent of lag effects in land subsidence after changes in the groundwater extraction. Important is the notion that if groundwater extraction is allowed to increase

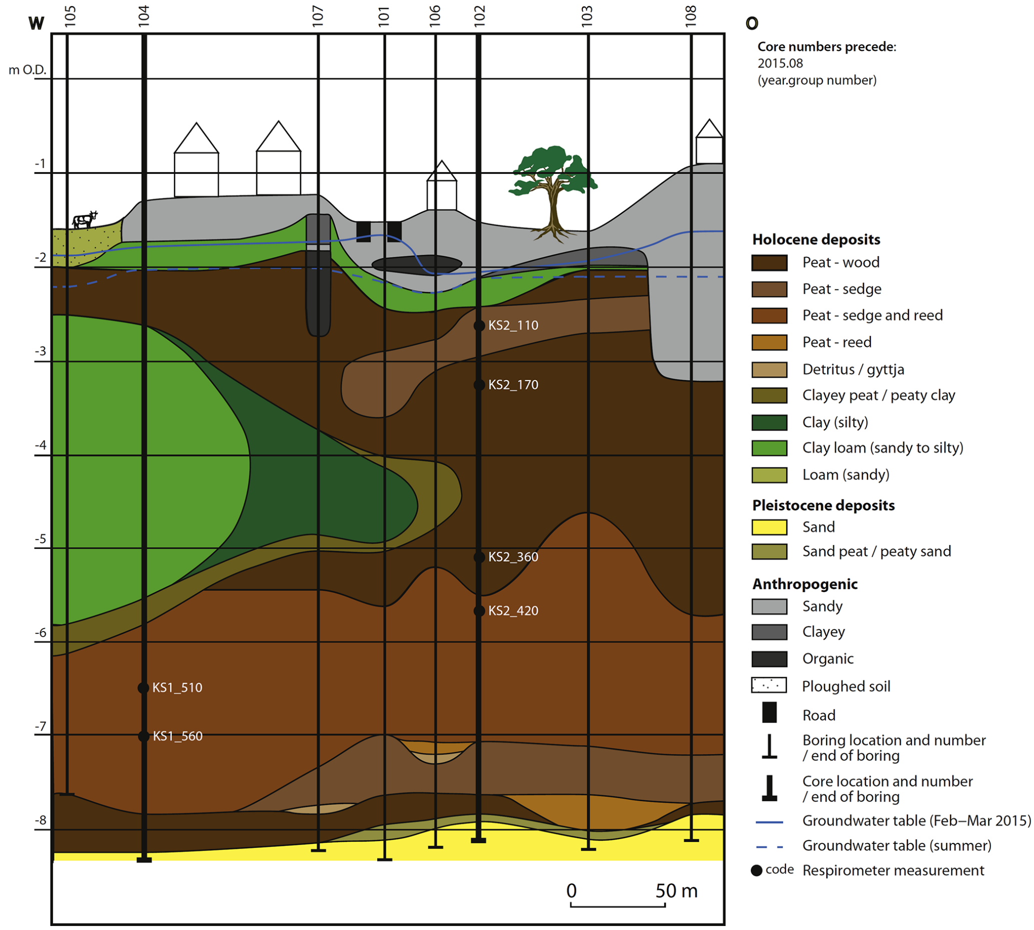

Figure 4. Cross-section from Van Asselen et al. (2018) showing that the groundwater level (blue line) is situated within the anthropogenic fill (coloured grey). This means that peat oxidation is limited in the urban area. Ouside the urban area, at the left end of the picture, the groundwater level is in the peat (coloured brown). Here, peat oxidation is the dominant process causing subsidence.

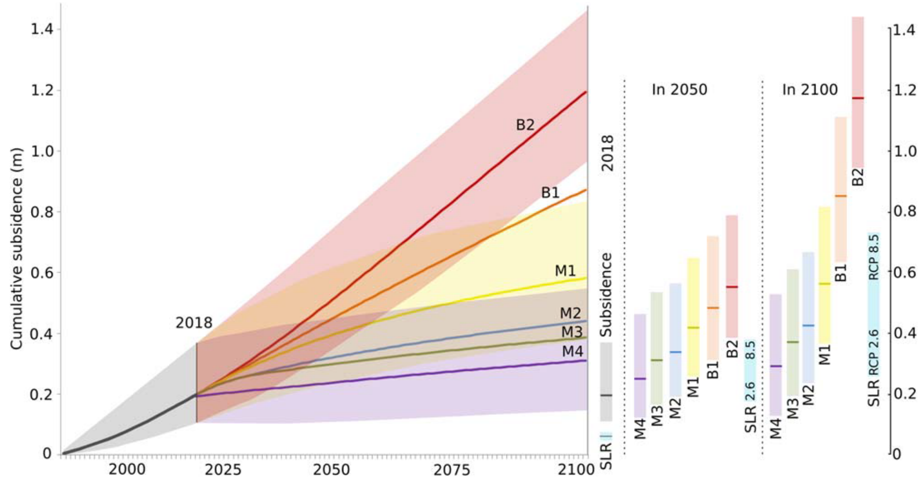

Figure 5. Average cumulative subsidence of the Mekong delta for different groundwater extraction pathways since 2018 (from Minderhoud et al., 2020). This modelling study shows the potential of limiting subsidence when more mitigative pathways are followed (scenarios M1–4 in the figure).

continuously, as it did over the past decades, extraction-induced subsidence has the potential to drown the Mekong delta before the end of the century (Minderhoud et al., 2020). A positive note is that the outcomes also reveal the potential for mitigation measures to reduce subsidence by limiting groundwater exploitation (Fig. 5).

Modelling of land subsidence has some important added value compared to subsidence measurements. As useful as the InSAR measurements may be, the data only cover parts of the delta because of the paucity of stable reflectors in the rural areas. Model outcomes for historical scenario's (also for eras predating measurements) do provide spatially resolved insights and may be used in conjunction with InSAR results (e.g. Minderhoud et al., 2017). Furthermore, interpolation of measurements to retrieve future scenarios of land subsidence is not producing accurate results, as the spatial heterogeneity of the delta subsurface and variability in the hydrogeological situation, remain unaccounted for. Temporal variations in extraction amounts and more complex scenarios that include relocation of groundwater extractions throughout the delta can never be captured by simply extrapolating current observed rates. More refined modelling can provide the required spatially resolved subsidence predictions under various possible and realized future conditions.

6.4 M4 Monetary aspects of land subsidence

With subsidence predictions for different management scenarios available (M3), the next step is that for each scenario the cost (damage) and benefits (usually avoided damage/costs) need to be established as part of a cost-benefit analysis. Estimating subsidence-related costs is notoriously complex. Subsidence is a "hidden threat" because in practice, the actual costs appear on financial sheets as ad hoc investments or planned maintenance schemes but typically are not identified as damage costs related to subsidence (Erkens et al., 2015). Dedicated damage estimates can help to raise awareness among policymakers and initiate policy development. For subsidence, being a gradual process, usually mitigation measures are costly in the short term, but cost-effective only in the long term (Erkens et al., 2015). Cost-benefit analyses could provide insight into these hidden costs and potential benefits of mitigation measures in a quantitative way.

A recent example where a cost-benefit analyse was executed is the city of Gouda in the Netherlands (Kok, 2017). The historic city centre of Gouda is subsiding by approximately 3–5 $\mathrm{mm\,yr^{-1}}$. Many older historical buildings have shallow foundations and subside at similar rates. Damp conditions and groundwater flooding in these buildings necessitated a repeated lowering of the groundwater level over the last centuries. Further lowering of the groundwater level however, might cause rotting of wooden foundations of buildings elsewhere in the city. This balance between damage costs to buildings with a shallow foundation and buildings with a wooden pile foundation is reflected in the cost-benefit analyses (Kok, 2017). The results show that in the reference scenario (business as usual), where groundwater levels are further lowered in the future, the expected damage costs from subsidence is between EUR 26–40 million before 2100. These are costs incurred to replace the wooden pile foundations that rot and to mitigate subsidence in the public space. If the groundwater level is not lowered, approximately EUR 4–11 million of these damage costs to wooden pile foundations may be prevented, but the damage costs due to the expensive reconstruction of shallow foundations add up to a disproportionate EUR 130 million. An alternative scenario, in which the groundwater levels would still be lowered, but at the same time measures are implemented to reduce the damage at the structures would cost EUR 7–16 million. However, the prevented damage in this scenario is approximately EUR 13–20 million, making this the economically most rational option.

This example shows how cost-benefit analyses, based on subsidence model outcomes, may inform decision makers, helping them to unlock the lock-in. It also provides a rationale for investing upfront in measures to realize long-term benefits. However, from a political perspective, this has the potential disincentive of incurring costs under one political administration only to have the benefits realized under another administration. Lastly, it shows how costs and benefits are different for different stakeholders. In the example above in the different scenarios, the costs and benefits are different for the owners of buildings with shallow foundation and the owners of buildings with wooden pile foundations. This may thus lead to demands for financial compensation measures or mitigative measures to be enforced to reduce costs for a certain stakeholder group.

6.5 M5 implementation of Measures

Implementation of measures follows cost-benefit analyses and the informed decision making. Implementation of measures often include governance and legal aspects (who is responsible?) and financial aspects (who is paying for the measures, and who is gaining the benefits?).

There are generally two policy strategies for subsiding areas: mitigation and adaptation – analogue to climate change policy discussions. A successful strategy, however, probably includes both (Erkens et al., 2015). Mitigation only works for human-induced subsidence (see M2). For the human-induced subsidence that cannot be mitigated, owing either to technical difficulties, or to financial constraints (i.e. the mitigation costs are too high), an adaptation strategy should be considered. This is also true for latent or lagging subsidence (see M3) occurring after a particular set of mitigation measures have been implemented or for natural subsidence, for which mitigation does not apply. Whereas mitigation focusses on the hazard element within the risk equation, adaptation measures focus on reducing the impact of subsidence, by decreasing the vulnerability of a certain asset to the negative impacts of subsidence and/or by decreasing the exposure of assets to subsidence.

For most cities that pursue an active policy on subsidence, mitigation measures are uncommon, but successful examples do exist. The examples of Tokyo (Japan) and Bangkok (Thailand) provide an interesting contrast (Erkens et al., 2015). In Tokyo, land subsidence was arrested after strict regulations restricting groundwater use were implemented. The restrictions started from the early 1950s and were subsequently extended to a larger area and to a larger group of stakeholders. This gave stakeholders time to adjust and to develop alternative water sources. For instance, surface water availability was enhanced as dams were constructed in several river basins that were designated for water resources development. In Bangkok, Thailand, regulation of groundwater extraction have successfully reduced the land subsidence. A main element of the measures was the taxation of groundwater use. Groundwater-use charges were first implemented in 1985 and have gradually increased. In Bangkok, currently only about 10 % of the total water use is derived from groundwater extractions, mainly for industrial use. Whereas Tokyo followed a path of restriction in a top-down way, Bangkok followed a path of self-regulation using taxation. It is encouraging to see that both strategies have worked and share some similarities. In both cases, the costs of the measures were high, and impacted households and businesses, alike. In both cities, the implementation of measures was accompanied by investing in development of databases containing measurement data (step M1) and predictive model outcomes (step M3). There were heavy investments in city-wide monitoring systems (step M6). Lastly, in both cases the federal government played an important role in the final decision making, bypassing the local decision-making structures.

6.6 M6 Monitoring and evaluation of subsidence measures

For all measures taken to reduce land subsidence and its impacts, it is important that the effectiveness of the measures is monitored. This implies that a subsidence monitoring network needs to be installed before the measures are implemented. Often, the monitoring network will be based on the same techniques or methods that was used to initially measure land subsidence (M1). Monitoring of the results of the implemented measures will enable the adjustment of these measures in due course.

Shanghai, China is an example of a city with a successful subsidence mitigation strategy and a robust operational monitoring system. The city has experienced severe land subsidence as a result of excessive groundwater extraction for domestic and industrial use (e.g. Ye et al., 2016a, b). Land subsidence in Shanghai was reported as early as 1921. Average subsidence rates since are approximately 26 mm yr^{-1}. In the 1960s, a series of countermeasures were taken (Ye et al., 2016a), including a resolution restricting groundwater use, the implementation of artificial recharge of groundwater, and the partial transfer of groundwater withdrawal to deeper aquifers. This resulted in decreased rates of land subsidence in the Shanghai urban area. Currently, the maximum allowed land subsidence in Shanghai is 6 mm yr^{-1}. If this is exceeded, extra measures are implemented, such as stricter restrictions on groundwater extraction amounts. Generally, the consequences of the (lower) land subsidence rates are considered acceptable, but additional subsidence mitigation measures may be implemented if required. An essential element of this strategy is the monitoring network. Land subsidence in Shanghai is traditionally monitored by means of extensometers, benchmarks and groundwater observation wells (Ye et al., 2016a). The oldest parts of the monitoring systems have been installed in the 1960s to monitor the accelerating subsidence rates occurring at that time and have been operational ever since. Numerical land subsidence models supported the detailed mitigation measures implemented in Shanghai. Monitoring results are coevally used to continuously evaluate the performance of the subsidence mitigation strategy.

The city of Shanghai works with a safe level of land subsidence. The is the level of land subsidence at which the damage is still acceptable and perhaps compensable. The appointment of the acceptable remaining rates of subsidence and associated damage is foremost a policy issue, and heavily relies on accurate damage estimates (M4) which are often rare. But, the establishment of a "safe" level of land subsidence is a crucial step in mitigating and controlling subsidence. This level will most likely not be zero: a reasonable small amount of subsidence (geologically or naturally caused for instance) has to be accepted in all cases.

7 Concluding remarks

The 6M approach and framework fulfils two needs. On the one hand, it guides decision makers through steps that are required for informed decision making based on best practise examples from elsewhere. Land subsidence is a relative slow hazard, and is often considered an urgent, but not immediate threat. It therefore requires a long-term perspective, which this step-by-step framework offers. This framework may be applicable to implementing measures for other hazards as well.

On the other hand, the 6M approach provides scientists with an applied, uniform context for their research. By identifying subsidence research as a component of one or more of the 6 steps, researchers can better focus their research and more effectively compare, share and communicate results within the scientific community. It may also help in communicating scientific results to decision makers and stakeholders. Because this type of communication is a key element of the Tenth International Symposium on Land Subsidence in the Netherlands in 2021, the 6M framework is used as the guiding principle for the thematic subdivision of TISOLS.

Data availability. All data used in this review paper is published and available through the cited papers in the reference list.

Author contributions. GE designed the 6M approach, provided the literature review and wrote the paper. ES helped in further developing the research approach and tested the approach in practise

Competing interests. The authors declare that they have no conflict of interest. Gilles Erkens is member of the editorial board of this special issue but has not reviewed this paper, nor has he influenced the publication decision process.

Special issue statement. This article is part of the special issue "TISOLS: the Tenth International Symposium On Land Subsidence – living with subsidence". It is a result of the Tenth International Symposium on Land Subsidence, Delft, the Netherlands, 17–21 May 2021.

Acknowledgements. We sincerely thank Devin Galloway (United States Geological Survey) for his constructive comments on a draft version of this paper. During his time as chair of the UNESCO working group on land subsidence, Devin Galloway promoted to link land subsidence science to society and valued practical application of scientific results. Encouraged by this, this paper seeks to contribute to this science-policy interaction within the land subsidence community.

References

Abidin, H. Z., Djaja, R., Darmawan, D., Hadi, S., Akbar, A., Rajiyowiryono, H., Sudibyo, Y., Meilano, I., Kasuma, M. A., Kahar, J., and Subarya, C.: Land Subsidence of Jakarta (Indonesia) and its Geodetic Monitoring System, Nat. Hazards, 23, 365–387, 2001.

Bucx, T., Erkens, G., Dam, R., De Lange, G., and Lambert, J.: Sinking Cities, Deltares brochure, Delft, the Netherlands, 12 pp., 2015.

Bucx, T., Erkens, G., Hommes, S., Kok, S., Ellen, G. J., Kooi, H., and Van de Guchte, C.: Sinking cities II – example cases, Deltares brochure, Delft, the Netherlands, 25 pp., 2019.

Erban, L. E., Gorelick, S. M., and Zebker, H. A.: Groundwater extraction, land subsidence, and sea-level rise in the Mekong Delta, Vietnam, Environ. Res. Lett., 9, 084010, https://doi.org/10.1088/1748-9326/9/8/084010, 2014.

Erkens, G., Bucx, T., Dam, R., de Lange, G., and Lambert, J.: Sinking coastal cities, Proc. IAHS, 372, 189–198, https://doi.org/10.5194/piahs-372-189-2015, 2015.

Erkens, G., Bucx, T., Dam, R., De Lange, G., and Lambert, J.: Sinking Cities: An Integrated Approach to Solutions, in: The Making of a Riskier Future: How Our Decisions Are Shaping Future. Disaster Risk, edited by: Global Facility for Disaster Reduction and Recovery, World Bank, Washington, D.C., USA, Case Study C 90-99, 2016a.

Erkens, G., van der Meulen, M. J., and Middelkoop, H.: Double trouble: subsidence and CO_2 respiration due to 1,000 years of Dutch coastal peatlands cultivation, Hydrogeol. J., 24, 551–568, 2016b.

Fokker, P. A., Muntendam-Bos, A.-G., and Kroon, I. C.: Inverse modelling of surface subsidence to better understand the Earth's subsurface, First Break, 25, 101–105, https://doi.org/10.3997/1365-2397.25.1110.27601, 2007.

Galloway, D. L., Erkens, G., Kuniansky, E. L., and Rowland, J. C.: Preface: Land subsidence processes, Hydrog. J., 24, 547–550, 2016.

Heuff, F., van Leijen, F., Mulder, G., Samiei-Esfahany, S., and Hanssen, R.: Observations of Dutch Peat Soils during dry summer of 2018 and its consequences for CO_2 emissions, Geophysical Research Abstracts, Vienna, Austria, 21, 1 p., 2019.

Kok, S.: Quick scan MKBA bodemdaling binnenstad Gouda, Deltares report, Utrecht, the Netherlands, 2017 (in Dutch).

Kooi, H., Bakr, M., de Lange, G., den Haan, E., and Erkens, G.: User guide to SUB-CR; a MODFLOW package for land subsidence and aquifer system compaction that includes creep, Deltares internal report 11202275-008, Utrecht, the Netherlands, 2018.

Minderhoud, P. S. J., Erkens, G., Pham, V. H., Bui, V. T., Erban, L., Kooi, H., and Stouthamer, E.: Impacts of 25 years of groundwater extraction on subsidence in the Mekong delta, Vietnam, Environ. Res. Lett., 12, 064006, https://doi.org/10.1088/1748-9326/aa7146, 2017.

Minderhoud, P. S. J., Middelkoop, H., Erkens, G., and Stouthamer, E.: Groundwater extraction may drown mega-delta: projections of extraction-induced subsidence and elevation of the Mekong delta for the 21st century, Environ. Res. Commun., 2, 011005, https://doi.org/10.1088/2515-7620/ab5e21, 2020.

Poland, J. F.: Guidebook to Studies of Land Subsidence Due to Ground-water Withdrawal, UNESCO report, Paris, France, ISBN 92-3-102213-X, 1984.

Seijger, C., Ellen, G. J., Janssen, S., Verheijen, E., and Erkens, G.: Sinking deltas: trapped in a dual lock-in of technology and institutions, Prometheus, 35, 193–213, 2018.

Sydow, J., Schreyögg, G., and Koch, J.: Organisational Path Dependence: Opening the Black Box, Acad. Manage. Rev., 34, 689–709, 2009.

Van Asselen, S., Erkens, G., Stouthamer, E., Woolderink, H. A. G., Geeraert, R. E. E., and Hefting, M. M.: The relative contribution of peat compaction and oxidation to subsidence in built-up areas in the Rhine-Meuse delta, The Netherlands, Sci. Total Environ., 636, 177–191, 2018.

Van Hardeveld, H.: Informed science–policy interactions: Advancing the support of collaborative management of social–ecological systems, PhD thesis, Utrecht University, Utrecht, the Netherlands, 170 pp., 2019.

Ye, S., Xue, Y., Wu, J., Yan, X., and Yu, J.: Progression and mitigation of land subsidence in China, Hydrogeol. J., 24, 685–693, 2016a.

Ye, S., Luo, Y., Wu, J., Yan, X., Wang, H., Jiao, X., and Teatini, P.: Three-dimensional numerical modeling of land subsidence in Shanghai, China, Hydrogeol. J., 24, 695–709, 2016b.

The relation between land subsidence and CO_2 emission in peatlands

G. Erkens[1,2], S. van Asselen[1]

1 Deltares Research Institute, Utrecht, The Netherlands
2 Department of Physical Geography, faculty of Geosciences, Utrecht University, Utrecht, The Netherlands

gilles.erkens@deltares.nl

Abstract

There are two crucial factors that need to be considered when using land subsidence data to establish CO_2 emissions from drained peatlands: i) not all land subsidence is the result of microbial decomposition of peat, and ii) a conversion value to express land subsidence (volume change) in CO_2 emissions (mass). This paper assesses how previous studies have dealt with these two factors and supplements existing values and experiences with new data and insights gathered over the last couple of years.

Introduction

Drainage of peatlands leads to double trouble: it causes land subsidence and carbon dioxide (CO_2) emission (cf. Erkens et al., 2016). The former increases local flood risk in these often already wet and flood-prone environments, whereas the latter contributes to the increased levels of greenhouse gasses in the atmosphere and thus to global climate warming.

Land subsidence and CO_2 emission are not just happening both in drained peatlands, in fact a relation exists between land subsidence and CO_2 emission. Both originate from the same process, namely the decomposition of organic matter by microorganisms such as bacteria, archaea, and fungi (Stephen and Johnson, 1951). This happens mostly under the influence of oxygen that can enter the unsaturated part of the soil following drainage. Carbon dioxide is a product of the decomposition process of organic material by microorganism. The same decomposition results in mass loss by itself which may lead to volume reduction which is noticeable as land subsidence at the surface. Additionally, decomposition of the organic matter forming matrix may lead to a decreased strength of the peat layer. When the loss of strength is severe, it may result in compaction of the layer and thus to land subsidence.

A relation between the degradation of peat layers, greenhouse gas emissions, and subsidence by volumetric loss was already identified by Neller (1944). Using this relation, land subsidence has been used as a proxy for greenhouse gas emission from drained peatlands (Hooijer et al., 2012; Erkens et al., 2016), or the other way around (Deverel et al., 2016). Particularly for studies on larger spatial scale, land subsidence has been used as a proxy, because methods to measure land subsidence over larger areas were readily available, such as spirit levelling or extensometers, whereas regional or nation-wide measurements of greenhouse gas emission are more complex and demanding. For the Netherlands for instance, the official national LULUCF (Land Use, Land Use Change and Forestry) reporting of CO_2 emission from peatlands (Arets et al., 2019) is based on a relation between measured land subsidence and CO_2 emission (Van den Akker et al., 2008a).

There are two crucial factors that need to be considered when using land subsidence data to establish CO_2 emissions from drained peatlands: i) not all land subsidence is the result of microbial decomposition of peat, and ii) a conversion value to express land subsidence (volume change) in CO_2

emissions (mass). This paper assesses how previous studies have dealt with these two factors and supplements existing values and experiences with new data and insights gathered over the last couple of years. The results contribute to the increasing need to establish large-scale greenhouse gas emission values from drained peatlands, driven by the greenhouse gas reduction aims agreed on in the Paris Agreement (2015).

Methods

This study mainly used existing published results from previous studies from around the world. These are put in the context of the Netherlands, where land subsidence is used as a proxy for CO_2 emissions in the national reporting. Results from published studies are complemented with recently acquired results from the Netherlands Research Programme on Greenhouse Gas Dynamics of Peatlands and Organic Soils (NOBV). The NOBV is measuring and monitoring land subsidence and CO_2 emissions from the drained Dutch peatlands and collects data on relevant soil parameters (Erkens et al., 2021).

Results

A major issue when converting land subsidence values into CO_2 emission values for drained peatlands is that not all land subsidence is related to the decomposition of peat and thus to emissions. There are four steps that need to be taken to convert land subsidence data to CO_2 emissions: i) isolate the deeper-rooted subsidence below the soft soil layer from the total subsidence, ii) discriminate between permanent and non-permanent processes in the soft soil layer, iii) establish how much subsidence is related to physical processes and how much to peat decomposition, iv) use a conversion factor to calculate CO_2 emissions from land subsidence as a result of peat decomposition. These steps will be presented in this section.

First, we distinguish between land subsidence processes that happen below the soft soil layer (peat, clay) and land subsidence processes that happen within the soft soil layer. Naturally occurring land subsidence and human-induced land subsidence rooted in deeper layers below the soft soil deposits, for instance because of extraction of water, gas, salt, or oil or isostatic and tectonic movements, need to be isolated from the total land subsidence at the surface (e.g. Erkens et al., 2015; Minderhoud et al., 2015) as these components are unrelated to the decomposition of peat. Usually this is possible when land subsidence in peatlands is measured opposed to a benchmark or reference level that is rooted in the underlying (Pleistocene) deposits. In this way all movement as a result of the processes below the soft soil layer are also in the reference level.

More complex is the discrimination between other processes that lead to land subsidence within the (Holocene) peat layer itself or surrounding (Holocene) soft soil deposits (clay). Processes that lead to permanent soil deformation happen both in the unsaturated and saturated zone (Table 1).

In the unsaturated zone increased stresses by suction (negative pore water pressure) will cause permanent shrinkage. In the saturated zone, increased effective stress, either by reduced pore water pressure or increased total stress, may cause consolidation and viscous behavior of the material under constant pressure conditions (creep) leads to compaction. These three physical processes lead to volume reduction and compaction of the deposits, but not to greenhouse gas emissions. Peat decomposition and the occurrence of physical processes leading to soil deformation may be linked, because decomposition of organic matter may impact the supportive skeleton consisting of plant material and fibers, decreasing strength of the peat, and eventually causing peat compaction. This relationship still needs to be established with laboratory geotechnical testing on samples in their original form and decomposed form.

Result	Position in subsurface	Process	Driver	Causing CO_2 respiration?
Permanent deformation	Unsaturated zone	Organic matter (peat) decomposition	Microbial activity	Yes
		Shrinkage (irreversible)	Pore water suction	No
	Saturated zone	Consolidation	Effective stress	No
		Viscous behaviour (creep)	Viscosity	No
Non-permanent deformation	Unsaturated zone	Shrink/swell behavior (reversible)	Pore water suction	No
	Saturated zone	Poro-elastic behaviour	Effective stress	No

Table 1 Processes leading to deformation in drained peatlands. Only one of the identified processes leading to land subsidence is related to CO_2 emissions

Reference	Location	Reported value of contribution of physical compaction	Timescale of study
Erkens et al., 2016	Netherlands, peatlands	28%	1000 years
Van Asselen et al., 2018	Netherlands, urban/rural environment	17-65%	10-1000 years
Schothorst, 1977	Netherlands, rural	35-48%	6 years
Stephens et al. 1984)	Everglades, Florida, USA	47%	years-decades
Van den Akker et al., 2008a,b	Rural peatlands, Netherlands	0% (at 1,00 m depth), ~10% overall	30 years
Hooijer et al., 2012	Southeast Asia	25% (5 years); 8% (18 years)	20 years
Deverel & Leighton, 2010	Sacramento Delta, California, USA	43/45/69%	80 years (modelled)
Kasimir-Klemedtsson et al., 1997	Sweden, the Netherlands	30%	years

Table 2 Reported contribution of physical compaction to total land subsidence. The selected studies are focusing on peat layers at the surface.

Contributions of physical compression processes versus peat decomposition to total land subsidence of stacks of peat and clay layers have been reported in literature (Table 2).

The values reported in Table 2 show that the contribution of physical processes to total land subsidence may differ substantially. Note that shrinkage, happening in the unsaturated part of the soil, is often neglected as the shrunk soil will experience decomposition after shrinkage. There is however an overall trend observed that on longer time scales the contribution of physical processes to total land subsidence decreases. This is the result of the short-term nature of shrinkage and consolidation (but not of creep) that happen specifically during the first years following an increase in effective stress, for example due to a drainage event (see results from Hooijer et al., 2012 and van Asselen et al., 2018 in Table 2). After a single drainage event, the contribution of physical processes will become small after decades. In case of multiple consecutive drainage or loading events, like in the Netherlands, this contribution may remain higher, as shown by Erkens et al. (2016). Overall, the contribution of physical processes to land subsidence in drained peatlands will be larger than 0%, and most studies indicate a contribution of ~20-50%. For the Netherlands, the value of ~30% on the time scale of decades seems realistic (Table 2).

In the NOBV research programme, several extensometers have been installed to monitor land movement over time (hourly measurement) in Dutch drained peatlands. Figure 1 shows a preliminary result for a drained peatland in Zegveld, the Netherlands, that there is highly dynamic surface movement over the 2,5-year measurement period (see also Van Asselen et al., 2020). Permanent deformation let alone the contribution of peat decomposition to total deformation, is not clear from these measurements. This is the result of the difference in scale and magnitude of the non-permanent processes shrink/swell and poro-elastic response (Table 1) over permanent deformation processes. Note that this measurement field has a long-lasting history of drainage and did not see a recent change in drainage depth. With total land movement of up to 10 cm over a year (Figure 1), it will take years (minimum 5 years) before permanent deformation (in the order of mm per year) may be derived from such measurements. This shows the great challenges that using land subsidence measurements as a proxy for CO_2 emissions brings. The most practical measurements to isolate land subsidence due to microbial decomposition are long-lasting (> 5 years) land movement measurements, preferably with an extensometer, that enables separating the saturated from the unsaturated zone processes (Van Asselen et al., 2020), in a situation wherein the drainage depth remains constant over time (so non-permanent processes remain as constant as possible).

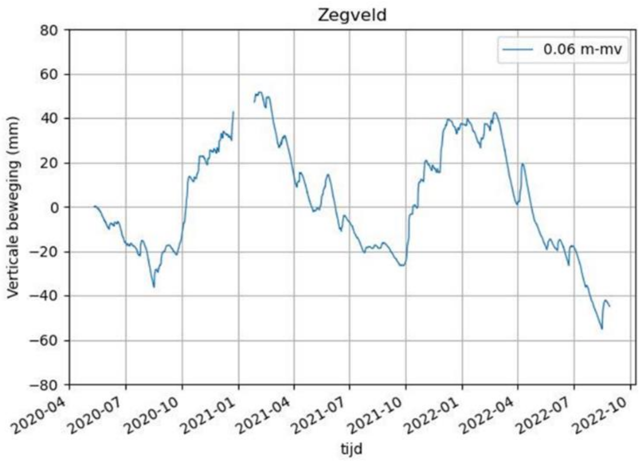

Figure 1 Preliminary results of the extensometer from Van Asselen et al (2020). Reported contribution of physical compaction to total land subsidence. The selected studies are focusing on peat layers at the surface.

To convert land subsidence attributed to organic matter decomposition to CO_2 emissions, a conversion factor needs to be established. The factor depends on the fraction of carbon in the organic matter (not discussed in this paper), the bulk density and the organic matter fraction (Van den Akker et al., 2008b). Erkens et al. (2016) found that there is no relation between the relative organic matter content and organic matter density for peats (>20% weight organic matter; Figure 2). Erkens et al. (2016) derived an average organic matter density of 103 kg/m^3 for all peats in the Netherlands, but the range in Figure 2 is considerable. This range is mainly the result of compaction of peat layers that increased their organic matter density. Van den Akker et al. (2008b) found that the organic matter density at 30 cm depth in a drained peat layer was 207 kg/m^3, whereas at 120 cm depth this was only 112 kg/m^3. These are unfortunately just two samples, whereas the values from Erkens et al (2016) are based on almost 1000 samples, but these are taken from many different depths. In order to convert land subsidence to CO_2 emission, there is therefore a need for an updated value. The NOBV research programme sampled per 5 cm 15 research sites throughout the Dutch peatlands (mostly drained). The average organic matter density for the upper 120 cm (considered the interval where peat decomposition happens) from the ca 360 samples is 147 kg/m^3. It is suggested that this value is used in the Netherlands for the conversion from land subsidence to CO_2 emissions. Using the formula from Van den Akker et al (2008b), we arrive at a value of 2965 kg CO_2 per ha per yr per 1 mm land subsidence due to peat decomposition, higher than the previously reported value of 2259 kg CO_2 per ha yr per mm land subsidence (Van den Akker et al., 2008b)

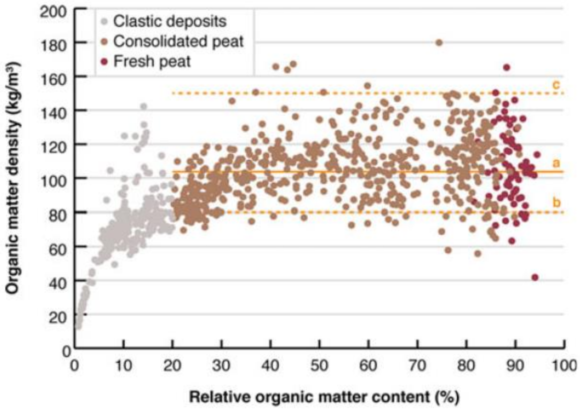

Figure 2 Relation from Erkens et al (2016) between relative organic matter content and the organic matter density. Above relative organic matter content of 20%, there is no relation with organic matter density, because for these samples the clastic content does not contribute to the volume of the sample.

Conclusion

- When land subsidence measurements are to be used as proxy for CO_2 emissions, it is imperative to separate the land subsidence rooted below the soft soil layer and to discriminate between permanent and non-permanent land deformation processes within the soft soil layer. The following step is to further subdivide the permanent deformation processes into physical processes and microbial decomposition, which is related to CO_2 emission. Research suggests that on longer timescales ~30% of the land subsidence in drained peatlands is the result of physical processes and may thus not be correlated to CO_2 emissions.
- Based on new data, the average organic matter density of the upper 120 cm of the drained Dutch peatlands contain 147 kg/m^3 organic matter. This value should be used, at least in the Netherlands, when using land subsidence rates as a proxy for CO_2 emissions by organic matter decomposition. When applied to the Netherlands, we arrive at a value of 2965 kg CO_2 per ha per year per 1 mm land subsidence to organic matter decomposition.

References

Arets, E. J. M. M., van der Kolk, J. W. H., Hengeveld, G. M., Lesschen, J. P., Kramer, H., Kuikman, P. J., & Schelhaas, M. J. (2019). Greenhouse gas reporting of the LULUCF sector in the Netherlands. Methodological background, update 2019, *Wettelijke Onderzoekstaken Natuur & Milieu, WOt-technical report* 146, 113 pp.

Deverel, S.J. & Leighton, D.A. (2010). Historic, Recent, and Future Subsidence, Sacramento-San Joaquin Delta, California, USA. *San Francisco Estuary and Watershed Science*, 8(2), 25 pp.

Deverel, S.J., Ingrum, T., Leighton, D. (2016). Present-day oxidative subsidence of organic soils and mitigation in the Sacramento-San Joaquin Delta, California, USA. *Hydrogeol Journal* 24, 569–586.

Erkens, G., Bucx, T., Dam, R., De Lange, G., Lambert, J. (2015). Sinking coastal cities Proc. *IAHS*, 372, 189–198.

Erkens, G., Van der Meulen, M.J., Middelkoop, H. (2016). Double trouble: subsidence and CO2 respiration due to 1,000 years of Dutch coastal peatlands cultivation. *Hydrogeol Journal* 24, 551–568

Erkens et al. (2021). Nationaal Onderzoeksprogramma Broeikasgassen Veenweiden (NOBV) – Data-analyse 2020-2021 (in Dutch), *NOBV report*, 241 pp.

Hooijer, A., Page, S., Jauhiainen, J., Lee, W.A., Lu, X.X., Idris, A., Anshari, G. (2012). Subsidence and carbon loss in drained tropical peatlands. *Biogeosciences* 9, 1053–1071.

Kasimir-Klemedtsson, A., Klemedtsson, L., Berglund, K., Martikainen, P., Silvola, J. & Oenema, O. (1997). Greenhouse gas emissions from farmed organic soils: a review. *Soil Use and Management* 13, 245-250

Minderhoud P.S.J., Erkens, G., Pham, V.H., Vuong, B.T., Stouthamer, E. (2015). Assessing the potential of the multi-aquifer subsurface of the Mekong Delta (Vietnam) for land subsidence due to groundwater extraction. *Proc. IAHS* 372, 73–76.

Neller, J.R. (1944). Oxidation loss of lowmoor peat in fields with different water tables. *Soil Science* 58, 195-204.

Schothorst, C.J., 1977. Subsidence of low moor peat soils in the western Netherlands. *Geoderma* 17 (4):265–291.

Stephens, J.C., Allen Jr., L.H., Chen, E., 1984. Organic soil subsidence*. Rev. Eng. Geol*. VI, 107–122.

Stephens, J.C. & Johnson, L., 1951. Subsidence of organic soils in the Upper Everglades region of Florida. *Proceedings of Soil Science Society Florida*, 191-237.

Van Asselen, S., Erkens, G., Stouthamer, E., Woolderink, H.A.G., Geeraert, R.E.E., Hefting, M.M. (2018). The relative contribution of peat compaction and oxidation to subsidence in built-up areas in the Rhine-Meuse delta, The Netherlands. *Science of the Total Environment* 636, 177–191.

Van Asselen, S., Erkens, G., De Graaf, F. (2020). Monitoring shallow subsidence in cultivated peatlands. *Proc. IAHS* 382, 189-194.

Van den Akker, J.J.H., Beuving, J., Hendriks, R.F.A., Wolleswinkel. R.J. (2008a). 5510 - Maaivelddaling, afbraak en CO_2-emissie van Nederlandse veenweidegebieden (in Dutch). *Leidraad Bodembescherming* 83, 30 pp.

Van den Akker, J.J.H., Kuikman, P.J., De Vries, F., Hoving, I., Pleijter, M., Hendriks, R.F.A., Wolleswinkel, R.J., Simões, R.T.L. & C. Kwakernaak (2008b). *Emission of CO2 from agricultural peat soils in the Netherlands and ways to limit this emission.* In: Farrell, C and J. Feehan (eds.), 2008. Proceedings of the 13th International Peat Congress After Wise Use – The Future of Peatlands, Vol. 1 Oral Presentations, Tullamore, Ireland, 8 – 13 june 2008. International Peat Society, Jyväskylä, Finland. ISBN 0951489046. pp 645-648

Nationwide deformation monitoring with SqueeSAR® using Sentinel-1 data

A. Ferretti[1], C.A. Bischoff[1], A. Rucci[1], A. Uttini[1], C. Giannico[1], F. Meloni[1]

1 TRE ALTAMIRA s.r.l., Milano, 20143, Italy

alessandro.ferretti@tre-altamira.com

Abstract

Subsidence and other surface deformation phenomena can now be routinely mapped on a national scale thanks to ESA's Sentinel-1 sensors and advanced InSAR algorithms. To be integrated into existing monitoring programmes, InSAR datasets should be calibrated with GNSS measurements. The dense spatial coverage of multi-temporal InSAR datasets captures local deformation phenomena and, with appropriate calibration, can advance the understanding of regional deformation trends. The regular and reliable SAR image acquisitions by Sentinel-1, as well as significant improvements in the scalability of InSAR processing chains allow regular updates of deformation maps on a national scale. Filtering the large amount of data for relevant information is achieved by using proper data screening tools, which have become extremely important for taking advantage of the unique amount of information provided by millions of measurement points.

Introduction

Despite the failure of Sentinel-1B in December 2021, which has immediately triggered a speed up of all project phases for the launch of Seninel-1C, the Sentinel-1 constellation, operated by the European Space Agency (ESA), has been acquiring SAR images all over the globe since late 2014. This constellation is the first of its kind, specifically designed for monitoring surface deformation over large areas, and it is creating a revolution in satellite geodesy.

The availability of a reliable satellite data source and the adoption of cloud computing solutions for data processing today allow regular updates of nationwide InSAR deformation maps with unprecedented accuracy. In fact, when calibrated with GNSS measurements, InSAR data provides a unique layer of information not only for scientists, but also for decision-makers and even the general public, as recently demonstrated - in the framework of the Copernicus program - by the European Ground Motion Service (EGMS, 2023).

In this paper, we report some results obtained by the SqueeSAR® processing chain, which has been lately updated to include specific algorithms for wide area processing (WAP).

Methodology

SqueeSAR® is a proprietary multi-interferogram technique (Ferretti et al., 2011; Ferretti, 2014), providing high precision measurements of ground displacement by processing multi-temporal satellite SAR images acquired over the same area, from the same acquisition geometry. By means of a statistical analysis of amplitude and phase data, the SqueeSAR® technique can select a sparse grid of image pixels, which can be used as a "natural geodetic network" to study and monitor slow surface deformation phenomena, with a precision of a few millimetres (Ferretti, 2014).

2-D Displacement Data

As any other InSAR analysis, the SqueeSAR® technique measures the projection of the displacement vector affecting each radar target along the satellite's line of sight (LOS) (Ferretti et al., 2011). However, a proper combination of SqueeSAR® results obtained from two different acquisition geometries (i.e. ascending and descending), acquired over the same area in the same temporal period, allows one to obtain an estimation of 2-D measurements, along vertical and east-west direction.

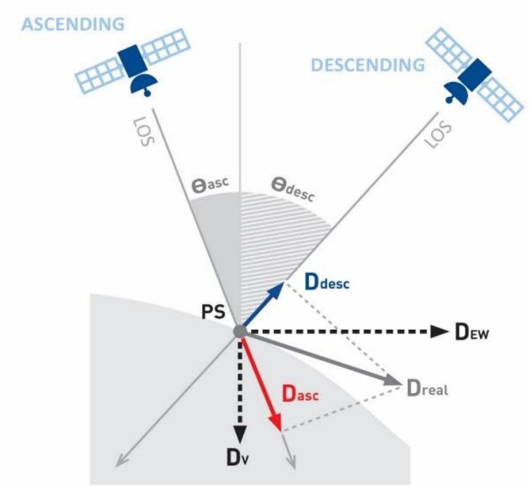

Figure 1 Decomposition of LOS displacements into vertical and horizontal components from images acquired in ascending and descending orbits.

This methodology requires the motion in north-south direction to be negligible or to be provided by other information sources (e.g. GNSS data). Whenever the (relative) motion of a measurement point in north-south direction is significant and no prior information is available, a bias will appear in the estimation of target motion, affecting mostly the vertical component of the displacement (Brouwer and Hanssen, 2021).

It should be noted that 2-D measurements are possible only whenever the same target is visible from both ascending and descending orbits: a condition not met very often in real-life scenarios. To overcome this limitation, the constraint of the radar target is relaxed: the area of interest is split into small patches of terrain and the measurements of all measurement points within the same cell are averaged, creating just one "pseudo-PS". The combination of the results and the estimation of the 2-D displacement time series is then performed for each cell containing data from both acquisition geometries (Ferretti, 2014; Teatini et al., 2011).

Since the acquisition dates usually differ from one dataset to another, the displacement measurements of each "pseudo-PS" are interpolated and re-sampled on a common temporal grid. For Sentinel-1 data, the spatial grid used for the estimation of 2-D displacement data is typically 100 x 100 m, while the sampling step in time is usually kept equal to 6 or 12 days.

Wide area monitoring with InSAR

Compared to InSAR analyses over areas of interest of hundreds or a few thousand square kilometres, Wide Area Processing (WAP) is characterized by three main challenges (Ferretti et al., 2019):

- Atmospheric effects – It is well known that the variance of atmospheric effects increases with the distance from a reference point (Ferretti, 2014; Hanssen, 2001). Moreover, ionospheric effects can become more significant. It is then extremely important, for the generation of high quality InSAR results over wide areas, to reduce the impact of this kind of disturbances, by using prior information (e.g. using GNSS data) or numerical weather models (Parizzi et al., 2020).

- Data mosaicking – in WAP, it is mandatory to deal with data mosaicking, to avoid introducing inconsistencies in combining results obtained from several independent “processing sites”. As a minimum, for Sentinel-1 data acquired in TOPS mode, the processing algorithm should not introduce any phase variations passing from one burst to another (Yague-Martinez et al., 2016).
- Computational burden – It is somewhat obvious that what is feasible when running a multi-interferogram approach on 30 images acquired over an area of interest of 100 km2 can become extremely challenging, if not impossible, when extended to 300,000 km2 covered by thousands of SAR images. Requirements on data storage, processing times, number of CPUs involved, and speed for data transfer can change by orders of magnitude. Although cloud computing can indeed be the solution, it is worth recalling that a proper and efficient use of the cloud requires bespoke software development, at least for complex processing chains, which can have major impact on processing costs.

All three points mentioned above, were carefully considered when developing the new processing chain for wide area processing used to generate the InSAR results presented in this paper, as well as the results provided by TRE ALTAMIRA in the framework of the European Ground Motion Service (EGMS, 2023).

InSAR data calibration using GNSS data

In order to validate and incorporate regional InSAR datasets into existing monitoring programs, it is crucial to calibrate using "absolute" measurements like GNSS data. To minimize the influence of possible misleading regional trends on the estimated displacement data (due, for instance, to atmospheric leakage or wrong satellite ephemerides), it is highly recommended to use GNSS data. An example of the calibrated SqueeSAR® results for the Denmark national deformation map is shown in Figure 2, with the GNSS stations marked in red. Even a limited number of stations can strongly improve the quality of InSAR measurements and mitigate the impact of low-wavenumber spurious signal components.

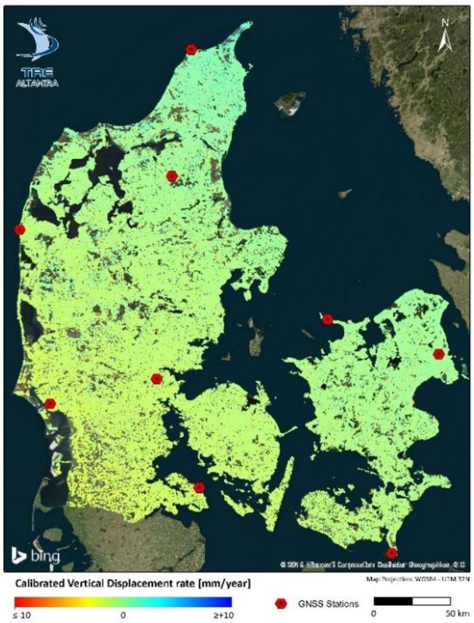

Figure 2 GNSS calibrated vertical deformation over Denmark. GNSS stations are shown in red.

The calibration methodology can be applied to both LOS measurements and the derived vertical and east-west components. The following outlines the main steps in the calibration procedure:

1) Time series filtering: GNSS time series are usually filtered using a moving average to reduce noise in the measurements. The time series of SqueeSAR® measurement points within a certain radius of each GNSS station (e.g. 200 m) are averaged.
2) Large-scale low frequency phase patterns are then removed from InSAR data, to avoid biases caused by uncompensated atmospheric components. To recover low frequency patterns due to real motion, first the difference in average velocity (linear trend) between each average SqueeSAR® time series and the corresponding filtered GNSS station time series is calculated. These differences are then used to estimate a first order surface (plane), which is subtracted from the SqueeSAR® data. This ensures that SqueeSAR® measurement points now also contain the low frequency component of the motion that was removed during the initial SqueeSAR® processing.
3) Absolute calibration: this step ties the two measurement techniques together and references the relative SqueeSAR® measurements to the absolute reference of the GNSS network. The procedure involves the generation of a time series of residuals, which is derived from comparing the averaged SqueeSAR® time series to the corresponding GNSS time series for each GNSS station. All the time series of residuals are then averaged to define a common time series of residuals (cRTS). This cRTS represents the movement of the local SqueeSAR® reference points with respect to the absolute GNSS reference frame. The cRTS was then removed from every SqueeSAR® measurement point time series.

The flow chart in Figure 3 is a summary of these steps is.

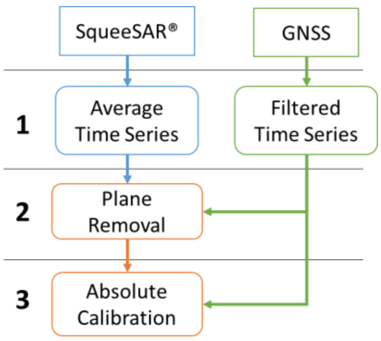

Figure 3 Overview of the steps in the calibration procedure.

Results

The following examples are taken from the national SqueeSAR® map for California (US), where InSAR data was calibrated and validated using GNSS measurements, from the national SqueeSAR® map for Japan (not calibrated with GNSS data, since the main focus was on local phenomena) and from the SqueeSAR® monitoring service provided to the region of Tuscany (Italy), where the main target of the service is landslide monitoring and where ascending and descending InSAR data are updated every 12 days all over the region (22,985 km2).

Aquifer related subsidence in California (US)

Nationwide ground deformation maps can deliver unique information by constraining the spatial extent of large-scale ground deformation phenomena, such as the subsidence in San Joaquin Valley, California, shown in Figure 4. This data was processed under contract with the California Department of Water Resources (DWR).

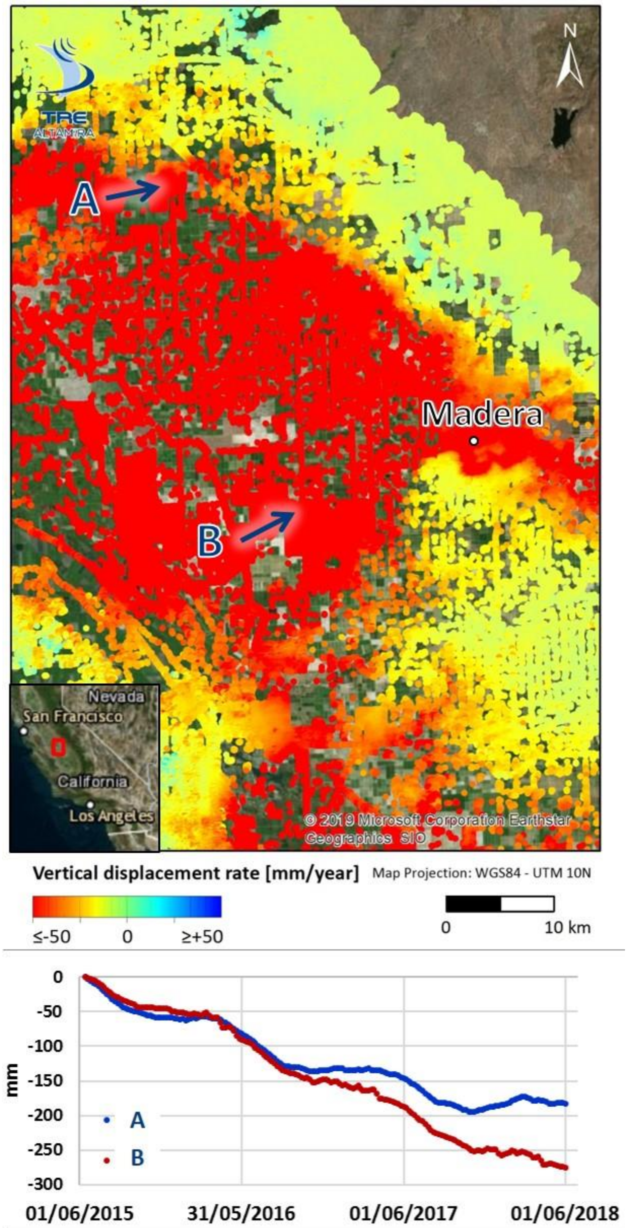

Figure 4 Map of the subsidence observed over California's St Joaquin Valley. Location is indicated on the overview map in the bottom left corner. Time series in the graph below show the difference in subsidence behaviour at location A compared to location B.

It is well established that land subsidence in San Joaquin valley is a danger to infrastructure, such as bridges, and that it has been caused by a combination of anthropic and natural factors, such as water pumping for agriculture and droughts (Faunt et al., 2016). In fact, water overdraft and the subsequent land subsidence over San Joaquin Valley already started in the 1920s, and became a widespread concern in the 1950s, when the water levels were lowered at unprecedented rates (Ireland et al., 1981). Since land use, surface-water availability and aquifer recharge vary, land subsidence across the valley is heterogenous, which makes monitoring crucial for managing the risk posed to infrastructures (Faunt et al., 2016).

The nationwide ground deformation map created with SqueeSAR®, based on Sentinel-1 SAR images, reveals these heterogenous patterns. The vertical displacement time series in Figure 4 demonstrate the different subsidence behaviours at two locations, which appear to be influenced by varying degrees of aquifer recharge.

Integration with data provided by 231 permanent GPS stations spread all over the state allowed the accurate estimation of vertical displacement components. The update of InSAR data over California is currently carried out every quarter over more than 100,000 km2. This data has become a timely, actionable, subsidence information that local, state, and federal agencies can use for decision making.

Post-seismic subsidence in Japan

As already mentioned, monitoring ground deformation on a large spatial scale using satellite SAR data can benefit from GNSS calibration, allowing one to better estimate low frequency spatial components of the motion. However, if no GNSS data are available, interesting patterns of motion can still be detected at medium scales, such as the deformation occurring in the aftermath of the earthquakes in April 2016 in Kumamoto, Japan, shown in Figure 5. This example was taken from the SqueeSAR® national deformation map for Japan, which is based on Sentinel -1 SAR images (Ferretti et al., 2019).

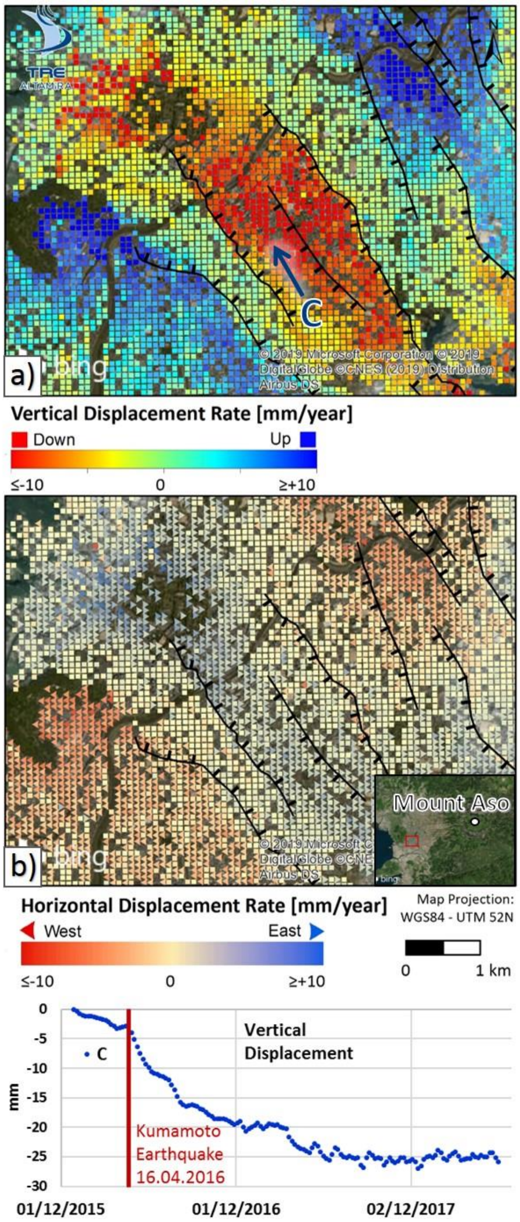

Figure 5 Maps showing a) vertical and b) east-west displacement rates between December 2015 – June 2018 over Kumamoto, Japan. The location is indicated on the overview map in bottom right corner. Black lines show faults inferred from ALOS-2 SAR interferometry by Fujiwara et al. (2016). The time series shows vertical displacement at location C, indicated in map a).

The ground displacement patterns shown in Figure 5 match well with the results of ALOS-2 interferometry published by Fujiwara et al. (2016). The structures shown in Figure 5 are secondary faults interpreted from the results of ALOS-2 interferograms. According to the authors, these faults form a graben group and are not directly related to the main faults on which the earthquakes occurred. The SqueeSAR® time series in Figure 5 shows that there is approximately −15 mm vertical displacement between April and December 2016. A second phase of relatively fast vertical displacement started in March 2017, however the cause for this is unknown (see time series in Figure 5). From June 2017 onwards, the area appears to stabilise.

Fujiwara et al. (2016) point out that there remains a question as to whether these secondary fault systems could become "primary" earthquake faults in the future.

While there is currently no concrete answer for this, Fujiwara et al. (2016) suggest that preparing for the possibility is important. Routinely monitoring displacement using InSAR may help to better understand and predict the behaviour of these structures.

Local subsidence in the region of Tuscany (Italy) automatically detected by a trend change algorithm

Despite the benefits of a dense spatial coverage of SqueeSAR® measurement points over wide areas, filtering the data for relevant information can become challenging. This is especially important if deformation maps are updated more regularly, such as for the service provided to the region of Tuscany (Italy), where SqueeSAR® deformation maps based on Sentinel-1 SAR images are updated every 12 days. This continuous monitoring generates a stream of data that needs to be filtered for significant changes in the displacement trends. This task is currently performed by an automatic trend change detection algorithm. Variables such as the magnitude of the trend change deemed significant, or the time period considered, can be changed depending on the phenomena of interest (Del Soldato et al., 2019).

The map in Figure 6 shows the displacement rate along ascending LOS, over an industrial area in the Montemurlo Municipality, Tuscany.

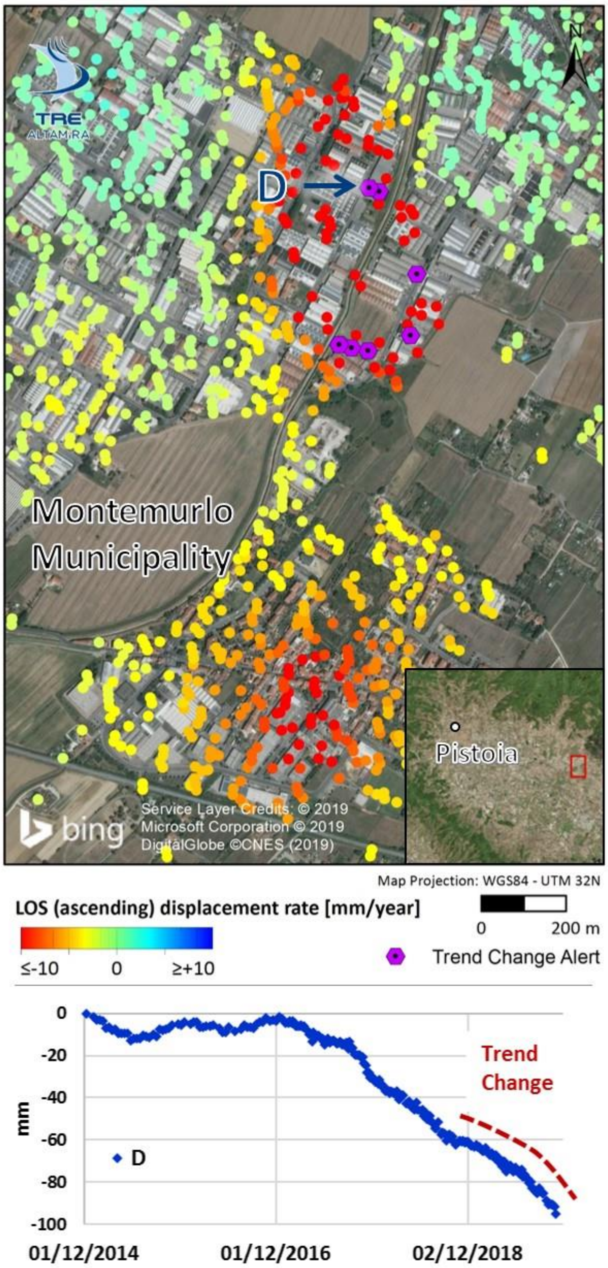

Figure 6   LOS deformation map from the continuous monitoring service provided to the region of Tuscany (Italy). The location is indicated on the overview map in bottom right corner. The violet markers highlight SqueeSAR® measurement points that display a significant recent trend change in their displacement. The time series is an example of a measurement point highlighted by the trend change algorithm.

The time series in the graph in Figure 6 shows that after negative displacement started in December 2016, there has been another trend change in 2018, which was highlighted by the trend change algorithm.

The negative displacement in LOS shown in Figure 6 is likely to be related to the over-pumping of water to meet the needs of local textile factories, which are numerous in the Montemurlo Municipality (Del Soldato et al., 2019). The displacement pattern observed in this industrial estate (see Figure 6) is discussed as a case study in more detail by Del Soldato et al. (2019).

Conclusions

Surface deformation phenomena can now be mapped routinely on a national scale with the frequent and reliable coverage provided by ESA's Sentinel-1 SAR sensors. Producing these maps is possible with bespoke cloud-based software using advanced InSAR algorithms, such as SqueeSAR®, which allows scalable processing of large SAR data stacks.

Recently, the publication of the results of the European Ground Motion Service (EGMS), in the framework of the Copernicus program, has shed new light on the potential of satellite radar data for detecting and monitoring surface deformation phenomena over wide areas. Radar images acquired by Sentinel-1 sensors can be used not only for nationwide analyses, but at continental scale. This can allow users to obtain synoptic views of subsidence phenomena, especially along coastal areas, over thousands of kilometres.

The availability of a growing number of InSAR datasets have also highlighted the importance of data calibration with GNSS measurements, especially for regional analyses and the estimation of vertical and east-west components. In fact, the bias of vertical displacement data estimated from ascending and descending satellite orbits, introduced by neglecting north-south displacement components, can be largely compensated for, at least whenever the spatial density of GNSS stations is high enough to capture the main components of the displacement field affecting the area of interest.

Recent InSAR analyses over wide areas, have emphasized the importance of data screening tools too, supporting users in the identification and selection of measurement points affected by a particular behaviour (e.g., acceleration, abrupt changes, etc.). To this end, machine learning algorithms are gaining momentum, due to their flexibility and their capacity to deal with big data. In general, due to the ever-increasing cardinality of InSAR datasets, anomaly detection algorithms will become a key element in any future monitoring program based on satellite radar data.

Finally, even if not presented in this paper, recent analyses based on Sentinel-1 data have shown the complementarity of large-scale InSAR results with what can be obtained using high-resolution (HR) radar imagery. In fact, HR data are much more suitable for monitoring individual assets, such as a building or a bridge, and can allow users to increase the temporal sampling of the phenomenon of interest.

References

Brouwer, W.S. and Hanssen, R.F., 2021, July. An Analysis of Insar Displacement Vector Decomposition Fallacies and the Strap-Down Solution. *In 2021 IEEE International Geoscience and Remote Sensing Symposium IGARSS* (pp. 2927-2930). IEEE.

EGMS - European Ground Motion Service – *Algorithm Theoretical Basis Document*. 2023. Available on-line: https://land.copernicus.eu/pan-european/european-ground-motion-service

Faunt, C.C., Sneed, M., Traum, J. and Brandt, J.T., 2016. Water availability and land subsidence in the Central Valley, California, USA. *Hydrogeology Journal*, 24(3), p.675.

Ferretti, A.*: Satellite InSAR Data - Reservoir Monitoring from Space*, EAGE Publications, 2014.

Ferretti, A., Fumagalli, A., Novali, F., Prati, C., Rocca, F. and Rucci, A.: A new algorithm for processing interferometric data-stacks: SqueeSAR, *IEEE Trans. Geosci. Remote Sens.,* 49(9), 3460–3470, doi:10.1109/TGRS.2011.2124465, 2011.

Ferretti, A., Novali, F., Giannico, C., Uttini, A., Iannicella, I. and Mizuno, T.: “A SqueeSAR database over the entire Japanese territory”, in *IGARSS 2019*, IEEE, Yokohama., 2019.

Fujiwara, S., Yarai, H., Kobayashi, T., Morishita, Y., Nakano, T., Miyahara, B., Nakai, H., Miura, Y., Ueshiba, H., Kakiage, Y. and Une, H., 2016. Small-displacement linear surface ruptures of the 2016 Kumamoto earthquake sequence detected by ALOS-2 SAR interferometry. *Earth, Planets and Space*, 68, pp.1-17.

Hanssen, R.F., 2001. *Radar interferometry: data interpretation and error analysis* (Vol. 2). Springer Science & Business Media.

Ireland, R.L., Poland, J.F. and Riley, F.S., 1984. *Land subsidence in the San Joaquin Valley, California, as of 1980* (Vol. 437). US Government Printing Office.

Parizzi, A., Brcic, R. and De Zan, F., 2020. InSAR performance for large-scale deformation measurement. *IEEE Transactions on Geoscience and Remote Sensing*, 59(10), pp.8510-8520.

Del Soldato, M., Solari, L., Raspini, F., Bianchini, S., Ciampalini, A., Montalti, R., Ferretti, A., Pellegrineschi, V. and Casagli, N., 2019. Monitoring ground instabilities using SAR satellite data: A practical approach. *ISPRS International Journal of Geo-Information*, 8(7), p.307.

Teatini, P., Castelletto, N., Ferronato, M., Gambolati, G., Janna, C., Cairo, E., Marzorati, D., Colombo, D., Ferretti, A., Bagliani, A. and Bottazzi, F., 2011. Geomechanical response to seasonal gas storage in depleted reservoirs: A case study in the Po River basin, Italy. *Journal of Geophysical Research: Earth Surface*, 116(F2).

Yagüe-Martínez, N., Prats-Iraola, P., Gonzalez, F.R., Brcic, R., Shau, R., Geudtner, D., Eineder, M. and Bamler, R., 2016. Interferometric processing of Sentinel-1 TOPS data. *IEEE transactions on geoscience and remote sensing*, 54(4), pp.2220-2234.

Proc. IAHS, 382, 463–467, 2020
https://doi.org/10.5194/piahs-382-463-2020

Elasto-viscoplastic modeling of subsidence above gas fields in the Adriatic Sea

Fabrizio Gemelli[1], **Anna Corradi**[1], **Giorgio Volonté**[2], **Stefano Mantica**[1], **and Michela De Simoni**[1]

[1]Eni S.p.A., Geomechanics Technologies Dept., San Donato Milanese, 20097, Italy
[2]Eni S.p.A., Geomechanics Laboratory, San Donato Milanese, 20097, Italy

Correspondence: Fabrizio Gemelli (fabrizio.gemelli@eni.com)

Published: 22 April 2020

Abstract. From the analysis of GPS monitoring data collected above gas fields in the Adriatic Sea, in a few cases subsidence responses have been observed not to directly correlate with the production trend. Such behavior, already described in the literature, may be due to several physical phenomena, ranging from simple delayed aquifer depletion to a much more complex time-dependent mechanical response of subsurface geomaterials to fluid withdrawal. In order to accurately reproduce it and therefore to be able to provide reliable forecasts, in the last years Eni has enriched its 3D finite element geomechanical modeling workflow by adopting an advanced constitutive model (Vermeer and Neher, 1999), which also considers the viscous component of the deformation. While the numerical implementation of such methodology has already been validated at laboratory scale and tested on synthetic hydrocarbon fields, the work herein presents its first application to a real gas field in the Adriatic Sea where the phenomenon has been observed. The results show that the model is capable to reproduce very accurately both GPS data and other available measurements. It is worth remarking that initial runs, characterized by the use of model parameter values directly obtained from the interpretation of mechanical laboratory tests, already provided very good results and only minor tuning operations have been required to perfect the model outcomes. Ongoing R&D projects are focused on a regional scale characterization of the Adriatic Sea basin in the framework of the Vermeer and Neher model approach.

1 Introduction

In the last two decades Eni S.p.A. has been developing a robust modeling methodology for production-induced subsidence (Capasso and Mantica, 2006). It is based on 1-way hydro-mechanical coupling (Gambolati et al., 2005) and elasto-plastic modified Cam-Clay model (MCCM, Roscoe and Burland, 1968). Though taking into account inelastic strains is instrumental for describing compaction in clastic reservoirs (Pijnenburg et al., 2019) and the MCCM keeps providing accurate reproduction of monitoring data gathered from almost all the gas fields in the Adriatic Sea (e.g. Gemelli et al., 2015), a further constitutive modeling effort has been recently required for a few of them showing a certain delay between production trend and GPS data – a phenomenon broadly described in the literature (e.g. Hettema et al., 2002).

The modeling approach has been enhanced by adopting the elasto-viscoplastic model proposed by Vermeer and Neher (1999, VNM), capable to describe the viscous response of reservoir sands and derived from the extended overstress theory (Olszak and Perzyna, 1970; Yin et al., 2010).

The VNM has been recently implemented in different finite element (FE) codes (Nguyen et al., 2016; Cremonesi et al., 2019; Isotton et al., 2019), before also in Plaxis®.

Then, having the implementation already been validated at laboratory scale and tested at reservoir scale on synthetic hydrocarbon fields (Volonté et al., 2017; Musso et al., 2020), this paper presents a first application of the enhanced approach to the production-induced subsidence analysis of a real gas field in the Adriatic Sea, the GPS data of which exhibit a delay of about 1.5 year (Fig. 1).

Herein, because of confidentiality issues, field data have been anonymized and analysis results normalized.

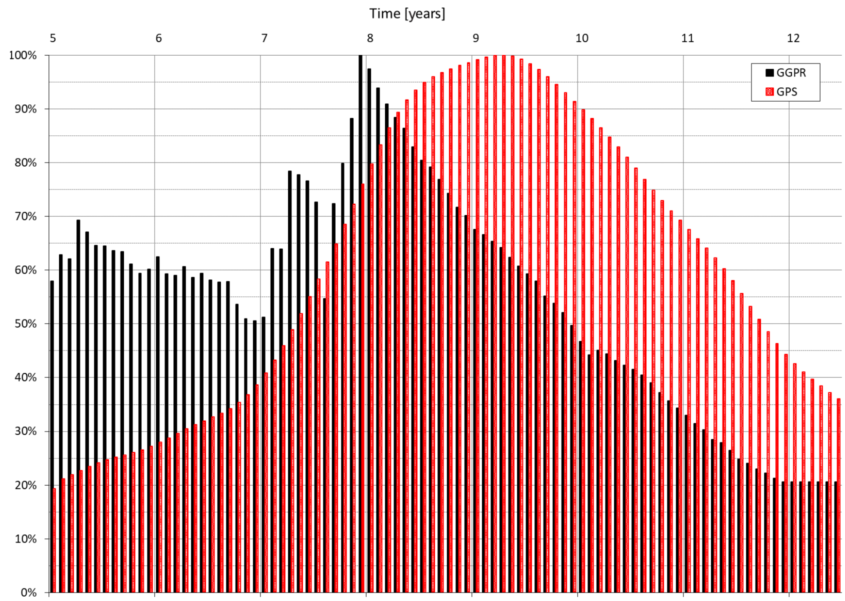

Figure 1. Monthly data for platform B: gas production rate (GGPR) versus GPS rate filtered from seasonal component.

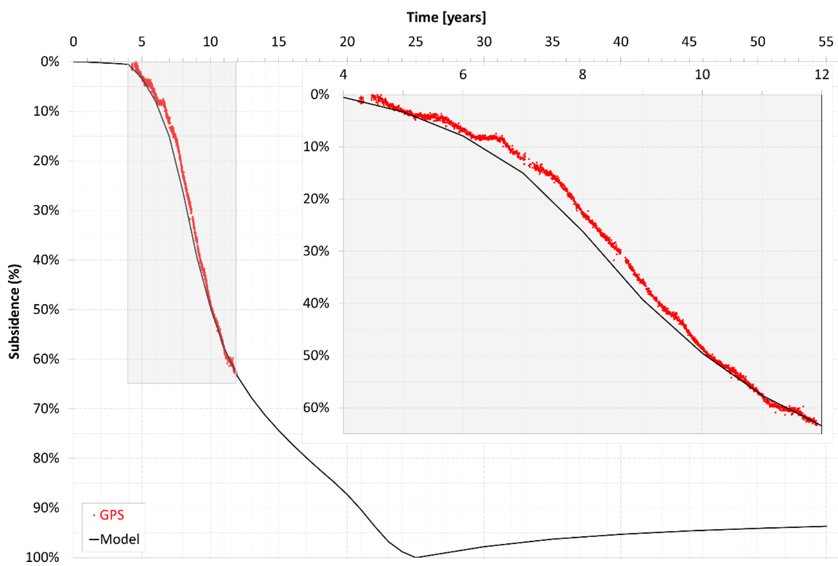

Figure 2. Time evolution of subsidence at platform B: GPS data versus model estimate, with magnification.

2 Field and production

The off-shore gas field studied herein is located in the Adriatic Sea, at about 60 km from the Italian coastline, where the average water depth is around 60 m.

The sandy reservoir layers lie from 900 to 1800 m s.s.l. and are produced by 28 wells, connected to platforms A and B.

According to the Intersect® fluid-dynamic model, the gas volume originally in place is approximately 30 GSm^3 and the recovery factor expected at forecast end is about 50 %.

3 Geomechanical modeling

The subsidence analysis has been performed by means of a 3D FE model built with the commercial code Abaqus®.

Input data about geometry, geology and petrophysics, of both reservoir layers and hydraulically connected aquifers, have been provided by the fluid-dynamic model, the same for pore pressure distribution and time evolution.

The domain has been discretized with about 5.5×10^5 finite elements. The model has around 2×10^6 degrees of freedom.

For the 6 input parameters of the VNM (Volonté et al., 2017; Musso et al., 2020), a preliminary estimate has been

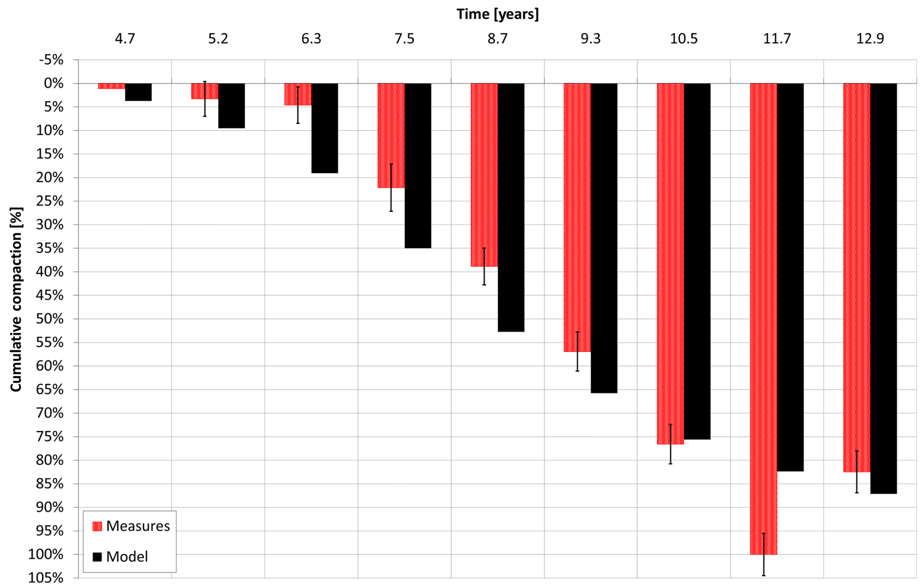

Figure 3. Time evolution of compaction along the monitoring well of platform B: markers data versus model estimates.

Table 1. VNM parameter values (post-calibration and dimensionless).

κ^*	elastic compliance	6.19×10^{-3}
ν	Poisson's ratio	0.3
λ^*	elasto-plastic compliance	5.75×10^{-2}
M	CSL slope	1.33
μ^*	creep index	1.06×10^{-3}
POCR	pseudo-OCR	1.339

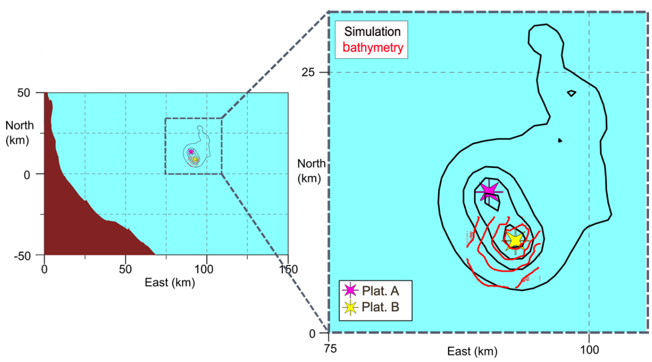

Figure 4. Subsidence developed in the 7 year time interval elapsed between two bathymetric surveys, perfomed at year 3 and 10 after the production start. Comparison between corresponding iso-subsidence lines: model estimates versus survey data.

directly obtained from an experimental campaign of tailored laboratory oedometric compression tests, characterized by a creep phase and carried out on samples of bottom hole cores from the same field. An initial geomechanical simulation has been performed with these preliminary values of the parameters. Then, in order to accurately reproduce the GPS data recorded at platform B, a calibration operation has been performed (Fig. 2), obtaining the final values of the parameters (Table 1). This step has required only a very minor tuning of the creep index μ^* (less than 4 % variation), that is compatible with the uncertainty associated to interpretation of laboratory tests. All other parameters have been left unchanged.

4 Results

While GPS data from platform B have been used to calibrate the VNM parameters, other available data from the same platform are useful for evaluating the capability of the geomechanical model to accurately simulate the hydro-mechanical response of the field to gas withdrawal.

To this purpose, Figs. 3 and 4 present comparisons in terms of reservoir compaction and iso-subsidence lines, respectively, for platform B.

In particular, Fig. 3 shows the cumulative compaction observed at reservoir depth along a well of platform B, where almost yearly a special logging tool is run for monitoring the distance between the radioactive markers. The comparison with the corresponding model estimates is very satisfactory: in fact, except for the measure acquired at year 11.7, which is out of trend, all the others are reproduced within the error bar or slightly overestimated.

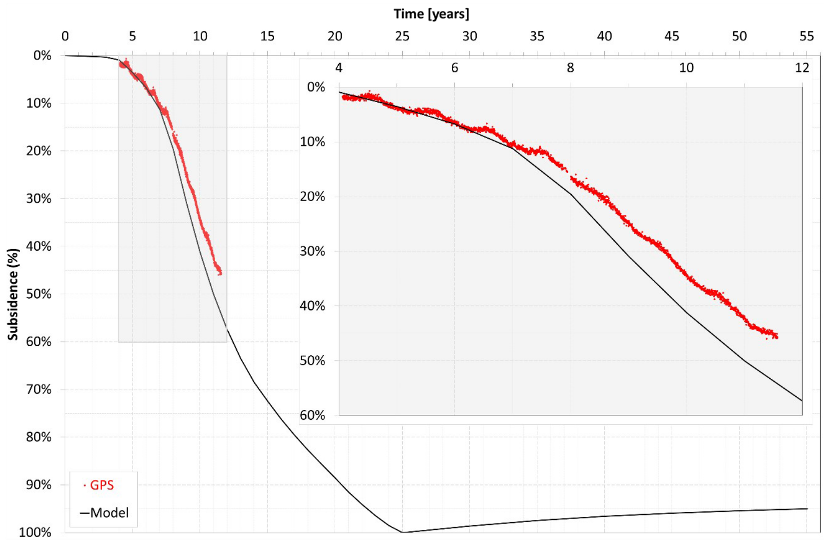

Figure 5. Time evolution of subsidence at platform A: GPS data versus model estimate, with magnification.

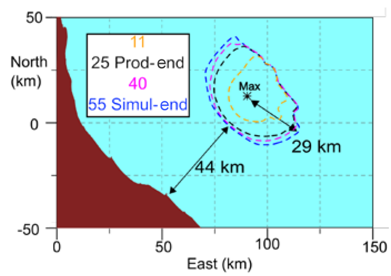

Figure 6. Maps with time evolution of 2 cm iso-subsidence line. At simulation-end (30 years after the production-end), minimum distance from coastline and maximum areal extent of the subsidence bowl.

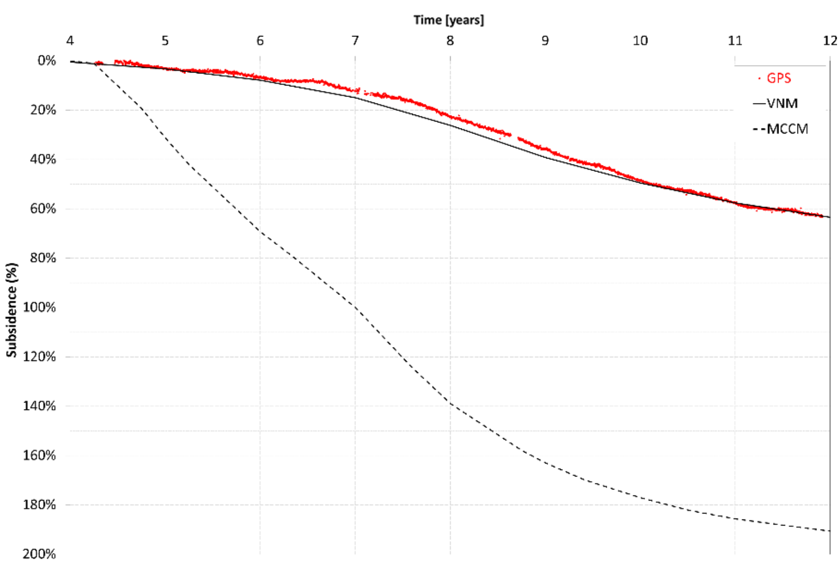

Figure 7. Time evolution of subsidence at platform B: comparison between GPS data, VNM and MCCM estimates.

Figure 4 shows the good agreement in terms of subsidence developed in the 7 year interval time elapsed between 2 bathymetric surveys performed around platform B, at year 3 and 10, respectively, after the production start.

Figure 5 shows the expected subsidence evolution at platform A. Even if calibrated on data from platform B, the model reproduces properly the subsidence rate recorded at the GPS station installed on platform A.

Figure 6 shows time evolution of the 2 cm iso-subsidence line, plus values of minimum distance from the coastline and maximum extent at simulation-end, which is usually set 30 years after the production-end.

Finally, Fig. 7 shows subsidence estimates provided by both VNM and MCCM, this latter with parameter values from lab tests and 1.2 overconsolidation ratio.

5 Concluding remarks

The subsidence analysis presented herein is the first application to a real gas field of the Eni's enhanced 3D finite element geomechanical workflow. The results show a very accurate reproduction of the monitoring data and the significative improvement obtained by adopting the VNM.

Data availability. Data sets have been used but can not be published for a matter of confidentiality.

Author contributions. FG performed and supervised the whole work. AC provided support on numerical modelling and implementation of constitutive laws, GV on rock mechanics laboratory testing, GV and SM on constitutive modelling, SM also on subsidence monitoring data assessment and MDS on fluid-dynamic modelling.

Competing interests. The authors declare that they have no conflict of interest.

Special issue statement. This article is part of the special issue "TISOLS: the Tenth International Symposium On Land Subsidence – living with subsidence". It is a result of the Tenth International Symposium on Land Subsidence, Delft, the Netherlands, 17–21 May 2021.

Acknowledgements. The authors gratefully thank Eni S.p.A. for the authorization to publish this work.

References

Capasso, G. and Mantica, S.: Numerical simulation of compaction and subsidence using Abaqus, Proc. Abaqus Users' Conference, Boston, USA, 125–144, 2006.

Cremonesi, M., Ghisi, A., Perego, U., Corradi, A., Gemelli, F., and Mantica, S.: A numerical study on explicit vs. implicit time integration of the Vermeer-Neher constitutive model, edited by: Carcaterra, A., Paolone, A., and Graziani, G., Proceedings of XXIV AIMETA Conference 2019, AIMETA 2019. Lecture Notes in Mechanical Engineering, Springer, Cham, 1245–1256, 2019.

Gambolati, G., Teatini, P., and Ferronato, M.: Basic conceptual guidelines for a sustainable gas/oil field development, Proc. 7th International Symposium on Land Subsidence, Vol. II, Shanghai, China, 919–924, 2005.

Gemelli, F., Monaco, S., and Mantica, S.: Modelling methodology for the analysis of subsidence induced by exploitation of gas fields, Second EAGE Workshop on Geomechanics and Energy, Celle, Germany, ISBN 978-94-6282-161-3, 2015.

Hettema, M., Papamichos, E., and Schutjens, P.: Subsidence delay: field observation and analysis, Oil Gas Sci. Technol., 57, 443–458, 2002.

Isotton, G., Teatini, P., Ferronato, M., Janna, C., Spiezia, N., Mantica, S., and Volonté, G.: Robust numerical implementation of a 3D rate-dependent model for reservoir geomechanical simulations, Int. J. Numer. Anal. Methods Geomech., 43, 2752–2771, 2019.

Musso, G., Volonté, G., Gemelli, F., Corradi, A., Nguyen, S. K., Lancellotta, R., Brignoli, M., and Mantica, S.: Evaluating subsidence above gas reservoirs with an elasto-viscoplastic law: laboratory evidences and case histories, submitted to Geomechanics for Energy and the Environment, Elsevier, 2020.

Nguyen, S. K., Volonté, G., Musso, G., Brignoli, M., Gemelli, F., and Mantica S.: Implementation of an elasto-viscoplastic constitutive law in Abaqus/Standard for an improved characterization of rock materials, Abaqus Users' Conference, Boston (USA), Natural Resources, 710, 710–724, 2016.

Olszak, W. and Perzyna, P.: Stationary and non-stationary viscoplasticity, McGraw-Hill, New York, 53–75, 1970.

Pijnenburg, R. P. J., Verberne, B. A., Hangx, S. J. T., and Spiers, C. J.: Inelastic deformation of the Slochteren sandstone: stress-strain relations and implications for induced seismicity in the Groningen gas field, J. Geophys. Res.-Sol. Ea., 124, 5254–5282, 2019.

Roscoe, K. H. and Burland J. B.: On the generalized stress-strain behaviour of "wet" clay, Engineering Plasticity, Cambridge Univ. Press, 535–609, 1968.

Vermeer, P. A. and Neher, H. P.: A soft model that accounts for creep, Beyond 2000 in Computational Geotechnics, Rotterdam, Netherlands, ISBN 905809040X, 1999.

Volonté, G., Gemelli, F., Nguyen, S. K., Musso, G., Lancellotta, R., Brignoli, M., and Mantica, S.: Advances in geomechanical subsidence modeling: effects of elasto-visco-plastic constitutive behaviour, 51st US Rock Mechanics Symposium, San Francisco, USA, 3635–3642, 2017.

Yin, Z.-Y., Chang, C. S., Karstunen, M., and Hicher, P. Y.: An anisotropic elastic–viscoplastic model for soft clays, Int. J. Solids Struct., 47, 665–677, 2010.

Subsidence-induced damage to the built environment: a new research program focusing on challenges and needs

C.P.W. Geurts[1], T. Candela[3], K. Koster[4], D. Moretti[1], S. Osinga[3], J.P. Pruiksma[1], P.A. Fokker[3], A.T. Slobbe[2], J. Brouwer[5], R.A. Huijbregts[5]

1 Department of Structural Dynamics, TNO - Buildings, Infrastructure and Maritime
2 Department of Structural Reliability, TNO - Buildings, Infrastructure and Maritime
3 Department Applied Geosciences, TNO - Geological Survey of the Netherlands, Utrecht, the Netherlands
4 Department Geomodelling, TNO - Geological Survey of the Netherlands, Utrecht, the Netherlands
5 TNO - Strategic Analysis and Policies, Utrecht, the Netherlands

chris.geurts@tno.nl

Introduction

Damage inflicted to the built environment as a result of anthropogenic induced subsidence is a hazard that has been reported all over the world. This primarily occurs in low-lying urbanized coastal zones such as Venice, New Orleans, and Jakarta, but has also been observed in upland urban conglomerates like Tehran and Mexico City.

In the Netherlands, subsidence induced damage is estimated to exceed over €20 billion in the coming decades (Van den Born et al., 2016). Besides damage to buildings, subsidence can compromise the integrity of critical infrastructures, such as flood protection structures, (rail)roads, pipelines, and underground cables. The built environment can be damaged by subsurface activities ranging from groundwater level management to deep resource extraction. Besides existing subsurface activities, there are multiple anticipated changes that can exacerbate subsidence-induced structural damage in the Netherlands: (i) housing shortage, forcing to build in our most subsidence prone areas; (ii) the transition to renewable energies (geothermal and Aquifer Thermal Energy Storage, ATES) which can lead to additional subsidence; (iii) the closing of the Groningen gas field, forcing gas production at other locations; and (iv) increased drinking water extraction accelerating local subsidence processes.

At present in the Netherlands, damage induced to the built environment is dealt with only after its occurrence. This leads to often unresolved issues with respect to the contribution of subsidence to the damage which has been observed. This reactive approach stems from the lack of knowledge and lack of tools to accurately assess the causal relationship between subsidence and damage. In this contribution, we present the outline and preliminary results of a new multi-disciplinary research program 'Subsidence and Building Damage' currently in progress at TNO, which aims to fill in these gaps to predict subsidence and the related damage to the built environment.

From subsidence to building damage: the Model Chain approach

The main goal of the 'Subsidence and Building Damage' research program is to establish causal relationships between the sources of subsidence and inflicted damage to the built environment. The core of the research program is to develop the know-how necessary to generate a model chain for subsidence induced damage to the built environment. The aim of this model chain is to identify per subsidence cause the probability of damage, given the type of construction and given the location. To achieve this goal a number of knowledge gaps need to be overcome, which are illustrated in Figure 1.

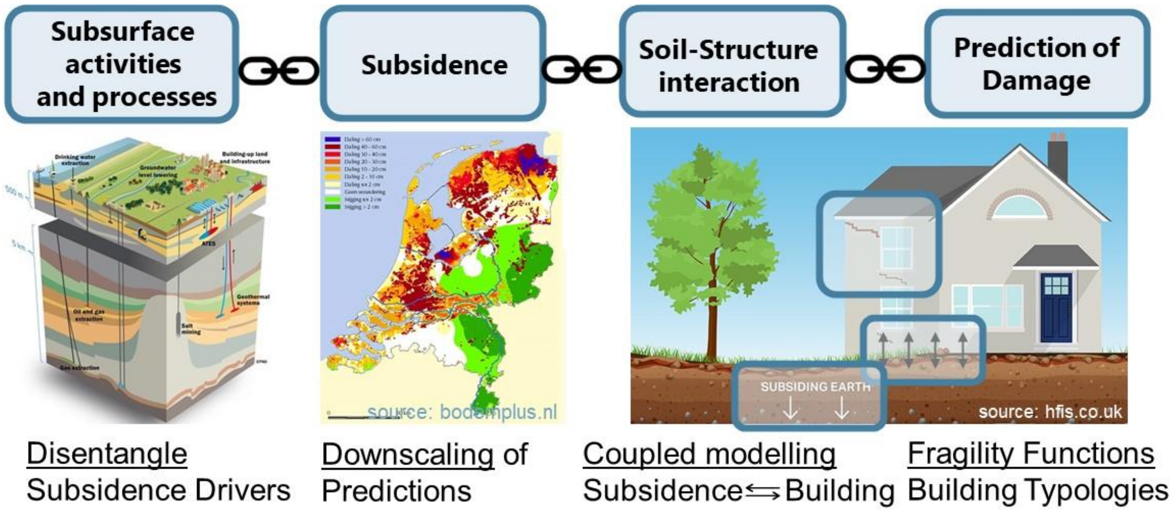

Figure 1 From subsidence to building damage prediction. The chain in the upper panel of the figure illustrates the different steps in the model chain. The lower panel indicates the knowledge gaps within each model step.

The chain of models starts with the description of the subsurface activities which form the drivers behind subsidence (Candela and Koster, 2022). Based on these drivers, probabilistic predictions of subsidence are made. The next step deals with the description of the interaction between soil and structure. Soil behavior influences the structure on top, and vice versa. Finally, the damage risks should be assessed. This is conducted by developing fragility functions for a range of selected typologies. These typologies are defined such that they properly describe the building behavior under subsidence loads and so that these are representative of a large group of buildings.

Research lines

This section delineates the key research questions to be answered within six research lines.

Research line 1: Subsidence predictions

This research line answers the research question: *How to disentangle multiple sources of subsidence and downscale our subsidence predictions to the building-scale?* Physics-based models fed by laboratory-derived constitutive equations and coupled with AI algorithms are developed to disentangle the contribution of each superposed source of subsidence and to downscale our subsidence predictions.

Research line 2: Soil Structure Interaction

This research line answers the research question: *What is the influence of soil-structure interaction on the subsidence induced damage of the built environment?* To provide answer(s) first we develop physics-based coupled models of the soil-structural interaction (finite element models). Ultimately the goal is to create accurate and computationally cheap models (i.e. surrogate models) that are used as components in the structural modelling of civil engineering assets and their damage.

Research line 3: Damage predictions

This research line answers the research question: *How to derive fragility functions that predict structural damage under subsidence?* To answer this question, we develop physics-based structural models (finite element models) fed by the subsidence predictions. The nonlinear finite element models are parametric, which allows to programmatically vary parameters and to couple them with probabilistic models that represent uncertainties in material properties, loading, dimensions, etc. Finally, we devise novel methodologies to derive fragility functions.

Research line 4: Model validation and calibration
To trust models, they must be validated against real world observations. This validation/calibration step is performed for each model component and the entire model chain as well. The main research question is: *How to satisfactorily validate a model when existing observations can be scarce and/or attached to a low signal-noise ratio and collecting new observations can be time consuming?*

A combination of diverse type of data (satellite-based such as InSAR; cone penetration tests; damage assessments by experts; etc.) coupled with adapted data assimilation procedures and conformance methodology is developed.

Research line 5: Software development
Within this research line we develop software that implements the model chain. The research question is: *How to effectively link models which describe different physical processes, and how to account for uncertainties, to allow for model calibration, to be maintainable and expandable when new knowledge is obtained?* The software should be fast enough to allow scenario studies, sensitivity studies, and probabilistic forecasts.

Research line 6: Societal impact and user involvement
This research line answers the research question*: How to increase the societal impact of the model chain and to connect it to the relevant users and their contexts*? A knowledge brokerage process is set up between potential users of the model chain and researchers who are involved in its development. AI learning capabilities to assist planning and decision making are explored. The objective is to enhance the understanding and use of the model in the selected user contexts. Finally, guidance are developed for different user groups, such as policy makers, banks, insurance companies, and house owners.

Outlook

Figure 2 illustrates the level zero model chain which enables:

(A) to provide probabilistic predictions of differential settlement at the building scale;
(B) to use (A) to estimate probabilities of damage for existing masonry buildings.

The large-scale subsidence is computed combining geological and groundwater realizations with InSAR observations. The small-scale differential subsidence is computed combining large subsidence predictions with spatial correlations of lithologies. The probability of damage is computed combining the small-scale differential subsidence with fragility curves.

Although not all uncertainties and complexities were accounted for, as until now only a single source of subsidence (phreatic groundwater level lowering) was considered, this proof-of-concept has shown its value: we are able to couple our subsurface and structural modelling capabilities with the potential to model the causal relationship between subsidence and building damage.

The success of this ‘Subsidence and Building Damage’ research program will be supported by the active interaction between TNO and external parties.

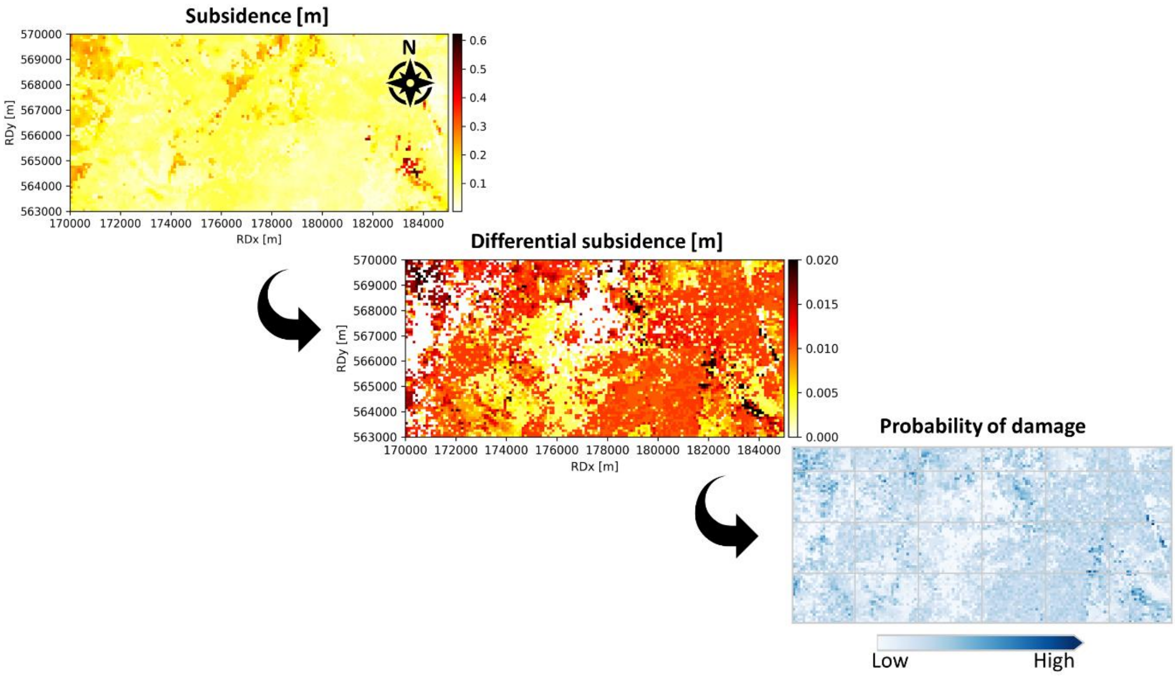

Figure 2 From large-scale subsidence to differential subsidence at the building scale to building damage prediction. These results of the level zero model chain correspond to an arbitrary area of interest in the Netherlands. The large-scale subsidence map (top) corresponds to the mean of the ensemble of multiple realizations. The small-scale differential subsidence (middle) corresponds to the P90 of the ensemble of multiple realizations.

References

Candela, T., Koster, K. (2022). The many faces of anthropogenic subsidence. *Science*, 376 (6600), 1381-1382.

Van den Born, G.J., Kragt, F., Henkens, D., Rijken, Van Bemmel, B. and Van der Sluis, S. (2016). *Dalende bodem, stijgende kosten (in Dutch).* PBL, Den Haag, pp. 94.

Towards a legal strategy fitting today's challenge of reducing impacts of subsidence in the Netherlands

M. van Gils[1], E. Stouthamer[2], F. Groothuijse[1]

1 Utrecht University Centre for Water, Oceans and Sustainability Law
2 Department of Physical Geography, Utrecht University

m.m.w.vangils@uu.nl

Abstract

This abstract is an update of an accepted paper in the TISOLS 2020 proceedings (https://doi.org/10.5194/piahs-382-825-2020). The paper describes how the legal framework might be improved, so that it can contribute to the development of effective policies to reduce (the impacts of) soil subsidence. The update provides a concise overview of the paper and further elaborates on its findings, based on new research. The paper best suits the theme **measures and coping strategies: mitigation and adaptation** and is linked to the societal foci of **strategies & pathways** and **peatlands & GHG emissions.**

Introduction

Reducing the impacts of soil subsidence is one of the main societal challenges for the physical environment in the Netherlands (Rli, 2020). In order to reduce (the impacts of) subsidence, either by mitigation or adaptation, governments should develop effective policies in various policy domains, implemented by financial, legal and factual measures. Policies are changing – a good example is the reduction of CO_2 emissions from peatlands by 1 Megaton laid down in the National Climate Agreement – but the change is often too incremental to effectively address the challenge of soil subsidence. That is not surprising: there are various governance and legal obstacles for effective policy change to reduce (the impacts of) soil subsidence, often flowing from the cross-sectoral nature of the challenge of soil subsidence and the fragmented nature of the Dutch legal system.

Methods

The paper and the update are based on a review of legislation, jurisprudence and legal and governance literature. References to these sources are included in the paper as published in 2020. The update is based on new research, including publications by the authors, to which references are included in this update.

Results

Subsidence as a legal challenge

Soil subsidence is not only a societal challenge, but also a *legal* challenge. First, to fulfil international, EU and national obligations for the reduction of greenhouse gas emissions, the CO_2 emissions from peatlands must be reduced drastically in the (near) future. These reduction targets are enacted in the

Paris Agreement and the Dutch Climate Act. Furthermore, EU Regulation 2018/841 (LULUCF Regulation) obliges member states to ensure that emissions from land use, including emissions from managed peatlands, do not exceed removals from other land use sectors. Second, in so far soil subsidence has or could have significant effects on protected species and habitats in protected nature areas, the Birds and Habitats Directives require that appropriate steps are taken. These legal requirements do not address subsidence as such but do require governments to reduce some of its negative impacts. That in turn means that the underlying processes, most importantly peat oxidation, must be (strongly) mitigated in certain areas. That entails drastic policy changes with considerable societal impact.

Obstacles for effective policy- and decision-making

There are, however, various governance and legal obstacles for such policy changes, which often flow from the cross-sectoral nature of soil subsidence as well as the fragmentation of the Dutch legal system, characterized by a sectoral division of responsibilities over different governments (Van Gils a.o., 2020; Van den Ende, 2022). Soil subsidence intersects with various policy domains, most importantly spatial planning, nature protection and water management. Reducing (the impacts of) subsidence therefore requires policy changes in different policy areas, for which different governments are responsible in the Dutch legal system. Municipalities are primarily responsible for spatial planning, provinces are responsible for nature protection; the governments mainly responsible for water management are the regional water authorities (RWAs) for regional waters and the national government for national waters, whereas municipalities are responsible for some aspects of water management in the built environment (an overview is provided in the paper).

The fragmented nature of the legal system provides obstacles for effective policy change: for example, since RWAs can only make decisions aimed at water-related interests, they cannot reduce drainage in peatlands to reduce CO_2 emissions for the reason of mitigating climate change (Van Gils & Groothuijse, 2021). Even if the legal system does not directly provide such obstacles, its fragmentation could still pose obstacles related to the governance of subsidence, such as a lack of procedural and substantive coordination of policies.

Conclusion: improving the legal framework

What is needed are legal mechanisms or the strengthening thereof that enable effective policy change within the fragmented legal system. Such strategies should not, or not mainly, be aimed at reducing the fragmentation of the legal framework as such. The sectoral division of responsibilities is an integral part of the Dutch legal and constitutional system. Furthermore, different policy domains will always require different policies and these conflicting interests cannot be resolved by institutional changes alone. Possible legal mechanisms that might effectuate policy change are the establishment of a goal regarding the reduction of soil subsidence or CO_2 from peatlands, either in national or provincial legislation or as an environmental value and changing sectoral environmental legislation so that it requires that soil subsidence and its impacts are taken into account in all relevant public decisions, especially spatial planning.

References

Gils, M.M.W. van, Groothuijse, F.A.G., Stouthamer, E. & Van Rijswick, H.F.M.W. (2020). Bodemdaling in Nederlandse veengebieden: Knelpunten voor solide beleid en besluitvorming. *Milieu en Recht*, 2021(2).

Gils, M.M.W. van & Groothuijse, F.A.G. (2021). Juridisch instrumentarium voor de reductie van CO2-emissie uit veengebieden: gefundeerd op slappe bodem? *Tijdschrift voor Bouwrecht 2021* (115).

Raad voor de leefomgeving en infrastructuur (2020). *Stop bodemdaling in veenweidegebieden. Het Groene Hart als voorbeeld.*

Van den Ende, M., Driessen, P., Hegger, D., & Mees, H. (2021). *Governance challenges to wicked land-use related sustainability problems: A framework of analysis with empirical illustrations from soil subsidence in peatland areas in the Netherlands (forthcoming).*

Proc. IAHS, 382, 291–296, 2020
https://doi.org/10.5194/piahs-382-291-2020

Analysis of land subsidence changes on the Beijing Plain from 2004 to 2015

Lin Guo[1,2], Huili Gong[1,2], Xiaojuan Li[1,2], Lin Zhu[1,2], Wei Lv[3], and Mingyuan Lyu[1,2]

[1]College of Resource Environment and Tourism, Capital Normal University, Beijing 100048, China
[2]Beijing Laboratory of Water Resources Security, Capital Normal University, Beijing 100048, China
[3]Chinese Academy of Calligraphy Culture, Capital Normal University, Beijing 100048, China

Correspondence: Huili Gong (4039@cnu.edu.cn) and Lin Zhu (hi-zhulin@163.com)

Published: 22 April 2020

Abstract. Land subsidence, as a surface response to the development, utilization and evolution of underground space, has become a global and multidisciplinary complex geological environment problem. Since the 1960s, land subsidence has been developing rapidly in the Beijing Plain area. Against the backdrop of the integration of Beijing, Tianjin and Hebei in addition to "southern water" (South-to-North Water Diversion Project, SNWDP) entering Beijing, the systematic study of the evolution mechanism of land subsidence is of great significance for the sustainable development of the regional economy. Firstly, this study used ENVISAT ASAR and RADARSAT-2 data to obtain surface deformation information for the Beijing Plain area from 2004 to 2015 and then verified the results. Secondly, the study area was divided into units using a 960 m $\times$ 960 m grid, and the ground settlement rate of each grid unit from 2004 to 2015 was obtained. Finally, the Mann–Kendall test was performed on the grid to obtain the mutation information for each grid unit. Combined with hydrogeology and basic geological conditions, we have attempted to analyze the causes of the mutations in the grid. The results show that 2347 grid cells were mutated in a single year, with most of these distributed across the Yongding River alluvial fan and the middle and lower parts of the Chaobai River alluvial fan. A total of 1128 grid cells were mutated in multiple years, with the majority of these cells mainly distributed across the upper-middle area of the alluvial fan, near the emergency water source and at the edge of the groundwater funnel. This study aims to provide favorable technical support and a scientific basis for urban construction in Beijing.

1 Introduction

At present, more than 150 countries and regions have suffered land subsidence, which has caused huge security risks and economic losses (Gong et al., 2018). Land subsidence in China mainly occurs in the North China Plain (Gao et al., 2018), the Yangtze River Delta (Yin et al., 2016), the Fenwei Basin (Xue et al., 2005) and the Pearl River Delta (Ye et al., 2015), and it presents significant regional differences. Among these differences, the continuous land subsidence in the North China Plain continues to increase (Zhang et al., 2016), the Yangtze River Delta region's subsidence has been effectively controlled and the Fenwei Basin region's subsidence is still developing rapidly.

From the perspective of land subsidence monitoring technology, interferometric synthetic aperture radar (InSAR) has become a new ground observation technique over the past 20 years (Ferretti et al., 2000). Compared with traditional technology, InSAR has the advantages of a wide monitoring range and high monitoring accuracy and has been widely used in ground subsidence monitoring research by experts and scholars (Castellazzi et al., 2016; Albano et al., 2016; Amighpey et al., 2016; Dehghani et al., 2013; Ge et al., 2014; Da Lio and Tosi, 2018?). In 2002 and 2004, Berardino and Lanaride et al. proposed the small baseline set interferometry–interferometric synthetic aperture radar (SBAS-InSAR) technique, which is more suitable for long time, slow deformation surface monitoring (Berardino et al., 2002; Lanari et al., 2004). Subsequently, experts and schol-

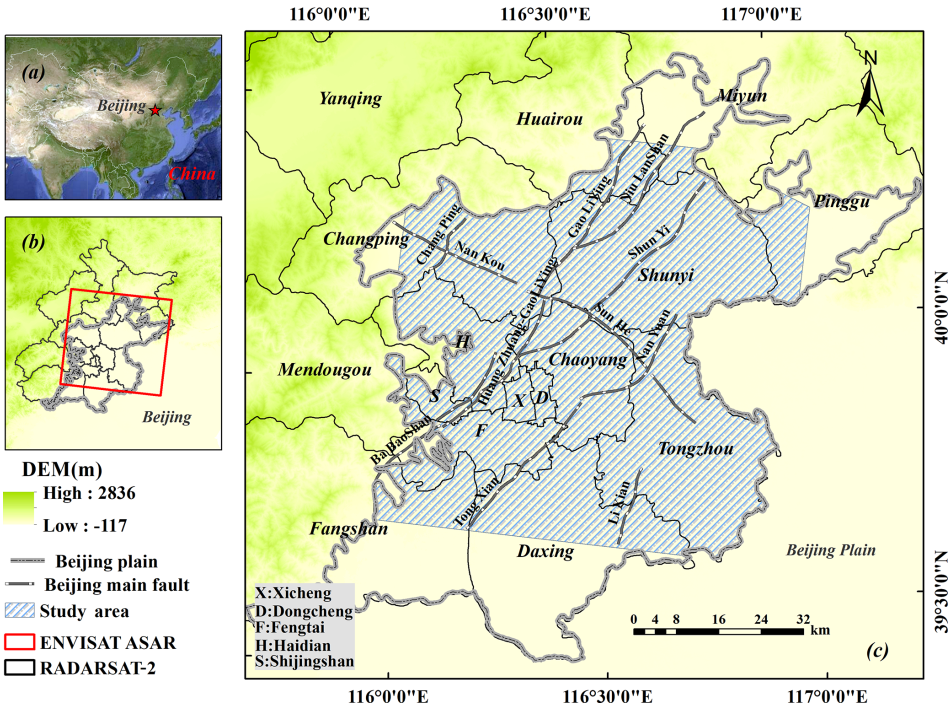

Figure 1. Geographical location of the study area.

ars have used this technology to select multisource SAR data, such as ENVISAT ASAR and COSMO-SkyMed, and have used these data to monitor the surface deformation of the Gulf of Naples (Solari et al., 2018), Los Angeles (Chilingar and Endres, 2005), Central Mexico and other areas (Castellazzi et al., 2016). From the perspective of the evolution mechanism of ground subsidence, the causes of the occurrence and evolution of ground subsidence include both natural and anthropogenic factors. For a long time, experts and scholars have focused more on ground subsidence caused by human factors, including groundwater exploitation, mining, dynamic load and so on (Zhu et al., 2015). Against the backdrop of strong manual intervention in regional water circulation, the identification of land subsidence changes in Beijing can provide technical support for the rational allocation of water resources.

2 Materials and methods

2.1 Study area

Beijing, as the capital of China, is the center of national politics, economy and culture and is an international metropolis with a population of nearly 20 million people (Zhou et al., 2017). In general, the surface elevation in Beijing is between 8 and 2303 m, and it is higher in the northwest and lower in the southeast (Zhou et al., 2017) (Fig. 1). The locations and the hydrogeological conditions of the study region are described in detail in a previous study (Guo et al., 2019). The ground subsidence in Beijing began in 1935, and the main subsidence regions were located in Xidan and Dongdan. Since the 1970s, land subsidence rates on the Beijing Plain have significantly increased due to the pumping of underground water. In general, the subsidence area is divided into two major areas – "North" and "South" – as well as seven subsidence centers. The North area is located in the east and north of Beijing and includes the Chaoyang, Tongzhou, Changping, Haidian and Shunyi districts. Among them, the Chaoyang and Tongzhou subsidence areas in the east of the plain are contiguous and are Beijing's fastest (with respect to change) and largest subsidence regions. The subsidence rates of the four subsidence centers in the urban areas of Chaoyang (Jinzhan, Heizhuanghu and Sanjianfang) and Tongzhou have exceeded 100 mm yr^{-1} for many years. The subsidence center in the north of the plain comprises the Changping Baxianzhuang and Haidian Xi Xiaoying areas. In the South area, which is mainly located in Daxing, the primary subsidence center is Lixian. On the whole, the land subsidence rates in the east of the plain are highest, followed by the northern region. Subsidence in the South area mainly occurs in the vicinity of Hebei.

2.2 Processing of SBAS-InSAR and PS-InSAR data from the Beijing Plain from 2004 to 2015

This study used 47 ENVISAT ASAR data from June 2003 to October 2010 and 48 RADARSAT-2 data from November 2010 to December 2015. The Doris-StaMPS algorithm

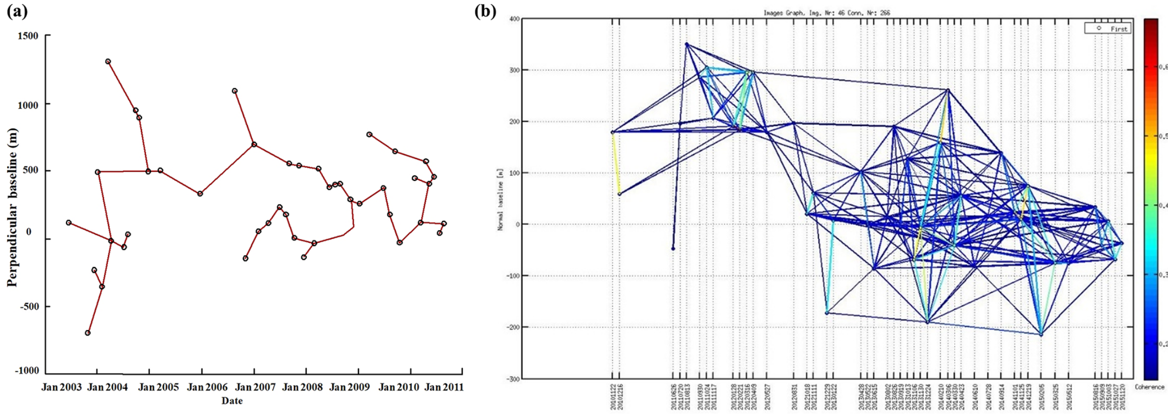

Figure 2. Panel **(a)** shows the small baseline segment from 2003 to 2010 obtained using SBAS-InSAR. Panel **(b)** shows the small baseline set from 2010 to 2015 obtained using Quisin-PSInSAR.

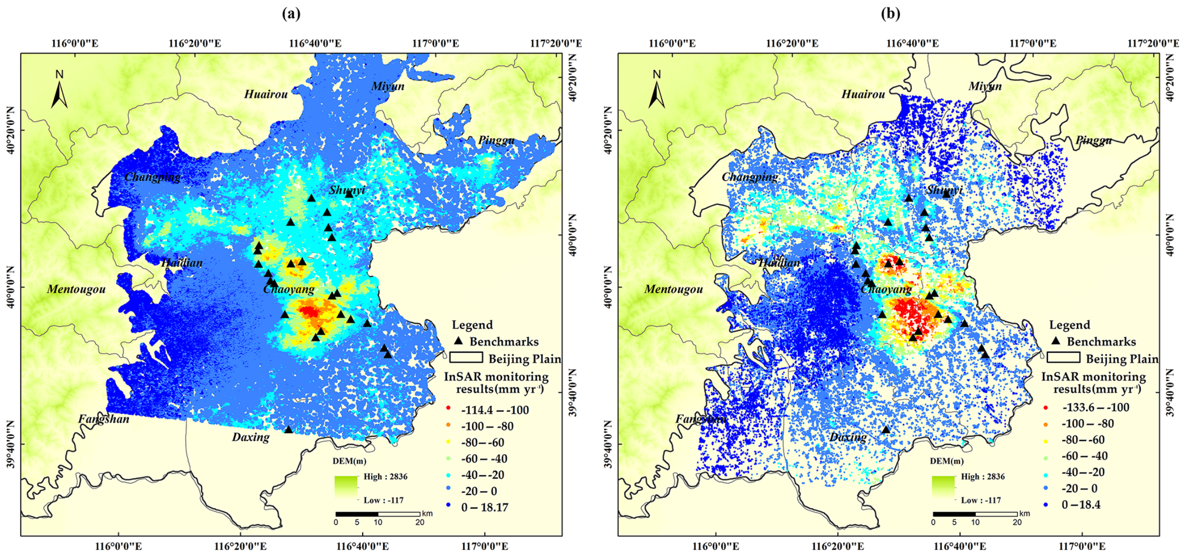

Figure 3. The average land subsidence rate map of the Beijing Plain from 2004 to 2015. Panel **(a)** is the average rate from 2004 to 2010, and panel **(b)** is the average rate from 2010 to 2015.

and commercial SARPROZ software were used to analyze the SAR data. The small baseline segments are shown in Fig. 2.

3 Results and discussion

3.1 Acquisition of the land displacement information for the Beijing Plain from 2004 to 2015

Based on the surface deformation monitored by SBAS-InSAR and Quisin-PSInSAR, and using the ArcGIS spatial analysis platform, the displacement rate map of the Beijing Plain area was obtained (Fig. 3). From 2004 to 2010, the average deformation rate ranged from -114.4 to $+18.17\,\mathrm{mm\,yr^{-1}}$. The area where the subsidence rate exceeded $25\,\mathrm{mm\,yr^{-1}}$ reached $1078.5\,\mathrm{km^2}$, which accounted for 17.2 % of the total area of the Beijing Plain. From 2011 to 2015, the average deformation rate ranged from -133.57 to $18.44\,\mathrm{mm\,yr^{-1}}$.

3.2 InSAR validation

The benchmarks from 2003 to 2013 were selected for validation (Fig. 4). The benchmarks were taken as the original point, and all of the monitoring points within a radius of 150 m were extracted. As can be seen from Fig. 4, the correlation coefficient for the InSAR monitoring results and the level monitoring results from 2003 to 2010 is 0.95. From 2011 to 2013, the correlation coefficient for the InSAR monitoring results and the level monitoring results is 0.99.

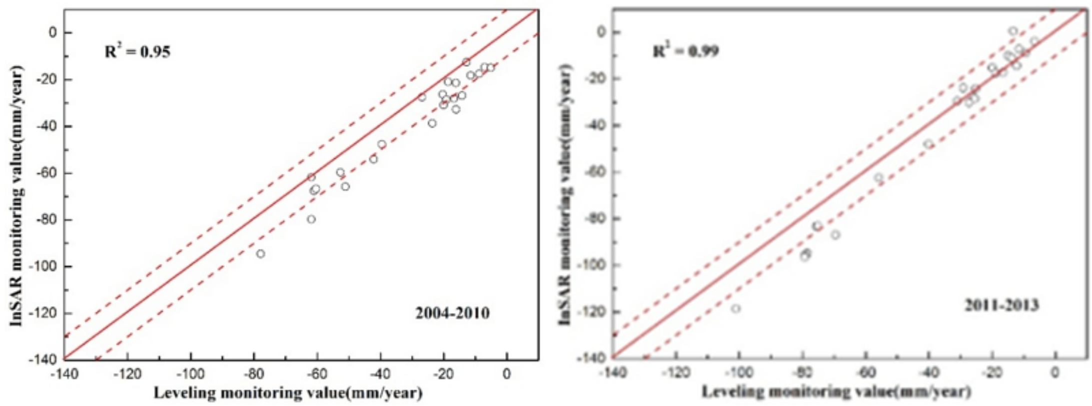

Figure 4. The validation map between InSAR and benchmarks from 2003 to 2013.

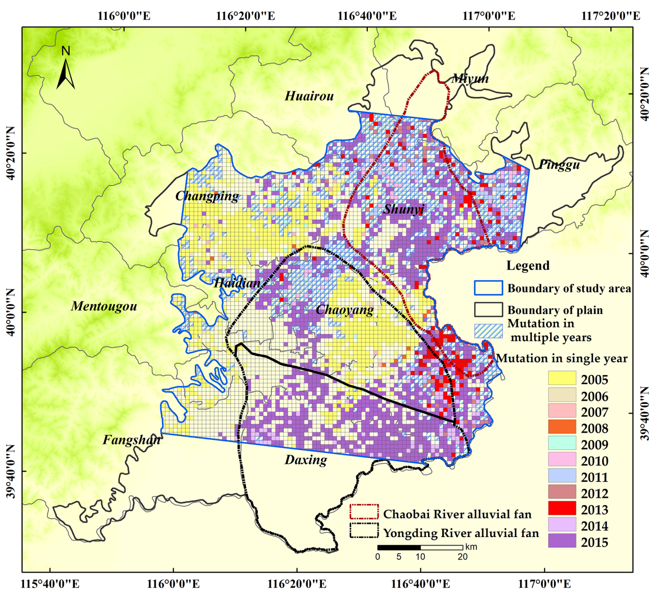

Figure 5. Land subsidence changes (land subsidence rate) results for the Beijing Plain from 2004 to 2015.

3.3 The Mann–Kendall test for land subsidence on the Beijing Plain

In this research, the Mann–Kendall test was used to detect the trend change in land subsidence on the Beijing Plain. Firstly, the research area was divided into a 960 m × 960 m grid using the Create Fishnet tool in ArcGIS. Secondly, according to the information from the persistent scatterer (PS) points from 2004 to 2015 that were acquired using InSAR technology, the displacement information from each grid was obtained by utilizing the Spatial Join function in ArcGIS. Finally, the Mann–Kendall test was performed on each grid using Python, and the changes in land subsidence on the Beijing Plain were obtained (Fig. 5).

3.4 Discussion

Figure 5 shows that the grid with single-year mutation is mostly distributed in the middle and the lower part of the Chaobai River alluvial–diluvial fan and the Yongding River alluvial–diluvial fan, and that the grid with multiple-year mutations is mostly distributed at the top of the alluvial–diluvial fan. The reason for this may be that the main factor causing land subsidence on the Beijing Plain is drastic drops in the groundwater level of the Quaternary system, which result in a decrease in the pore water pressure in the overburden layer and a loss of water in the soil layer due to the pumping of underground water. However, in the middle and upper part of the alluvial fan, the deposits have a good permeability, and the groundwater level fluctuates greatly due to the influence of precipitation. The rainfall in different years and the rainfall intensity during the flood season have some different characteristics that may cause the groundwater level in the middle and upper part of the alluvial fan to significantly fluctuate; therefore, the grid with sudden ground subsidence may be more variable. On the other hand, the four emergency water sources are all located in the middle and upper part of the alluvial fan. Affected by the exploitation, the groundwater level changes markedly, resulting in greater fluctuations in land subsidence. Furthermore, at the edge of the Quaternary groundwater drop funnel, the grid with mutation in the land subsidence rate is very variable. This shows that the boundary of the groundwater funnel is the place where the groundwater level changes most, and the land subsidence is relatively fragile and unstable.

4 Conclusions

The main conclusions of this study are as follows:

1. From 2004 to 2015, the maximum land subsidence rate was $-141\,\mathrm{mm\,yr^{-1}}$.

2. The single-year mutation cells were mainly distributed in the middle and lower parts of the alluvial–diluvial fans of the Yongding and Chaobai rivers. The multiple-year grid mutations were mainly distributed in the middle and upper parts of the alluvial fan, near the emergency water source and at the edge of the underground water funnel.

Data availability. No data sets were used in this article.

Author contributions. LG performed the experiments, analyzed the data and wrote the paper. HG, XL and ZZ provided crucial guidance and support throughout the research. LW and YM contributed significantly to the validation work and data interpretation.

Competing interests. The authors declare that they have no conflict of interest.

Special issue statement. This article is part of the special issue "TISOLS: the Tenth International Symposium On Land Subsidence – living with subsidence". It is a result of the Tenth International Symposium on Land Subsidence, Delft, the Netherlands, 17–21 May 2021.

Acknowledgements. We thank both the European Space Agency (ESA) and the Canadian Space Agency for their great efforts in developing and distributing the remotely sensed SAR data. We also thank the China Geological Survey (CGS) for the leveling data released to the public. Moreover, we are grateful to the National Aeronautics and Space Administration (NASA) for making the SRTM DEM data available. Finally, we acknowledge the creators of the Python computer language and ArcGIS software as well as the Doris/SARPROZ and StaMPS/QPS data processing software.

Financial support. This work was supported by the National Natural Science Foundation of China (grant nos. 41930109/ D010702 and 41771455/ D010702) and the General Scientific Research Plan project of the Beijing Municipal Commission of Education (grant no. KM202010028011).

References

Albano, M., Polcari, M., Bignami, C., Moro, M., Saroli, M., and Stramondo, S.: An innovative procedure for monitoring the change in soil seismic response by InSAR data: Application to the Mexico City subsidence, Int. J. Appl. Earth Obs. Geoinf., 53, 146–158, https://doi.org/10.1016/j.jag.2016.08.011, 2016.

Amighpey, M. and Arabi, S.: Studying land subsidence in Yazd province, Iran, by integration of InSAR and levelling measurements, Remote Sens. Appl. Soc. Environ., 4, 1–8, https://doi.org/10.1016/j.rsase.2016.04.001, 2016.

Berardino, P., Fornaro, G., Lanari, R., and Sansosti, E.: A new algorithm for surface deformation monitoring based on small baseline differential SAR interferograms, IEEE T. Geosci. Remote, 40, 2375–2383, https://doi.org/10.1109/TGRS.2002.803792, 2002.

Castellazzi, P., Arroyodomínguez, N., Martel, R., Calderhead, A. I., Normand, J. C. L., Gárfias, J., and Rivera, A.: Land subsidence in major cities of Central Mexico: Interpreting InSAR-derived land subsidence mapping with hydrogeological data, Int. J. Appl. Earth Obs. Geoinf., 47, 102–111, https://doi.org/10.1016/j.jag.2015.12.002, 2016.

Chilingar, G. V. and Endres, B.: Environmental hazards posed by the Los Angeles Basin urban oilfields: an historical perspective of lessons learned, Environ. Geol., 47, 302–317, https://doi.org/10.1007/s00254-004-1159-0, 2005.

Da Lio, C. and Tosi, L.: Land subsidence in the Friuli Venezia Giulia coastal plain, Italy: 1992–2010 results from SAR-based interferometry, Sci. Total Environ., 633, 752–764, https://doi.org/10.1016/j.scitotenv.2018.03.244, 2018.

Dehghani, M., Zoej, M. J. V., Hooper, A., Hanssen, R. F., Entezam, I., and Saatchi, S.: Hybrid conventional and Persistent Scatterer SAR interferometry for land subsidence monitoring in the Tehran Basin, Iran, ISPRS J. Photogramm., 79, 157–170, https://doi.org/10.1016/j.isprsjprs.2013.02.012, 2013.

Ferretti, A., Prati, C., and Rocca, F.: Nonlinear subsidence rate estimation using permanent scatterers in differential SAR interferometry, IEEE T. Geosci. Remote, 38, 2202–2212, https://doi.org/10.1109/36.868878, 2000.

Gao, M., Gong, H., Chen, B., Li, X., Zhou, C., Min, S., Yuan, S., Zheng, C., and Duan, G.: Regional Land Subsidence Analysis in Eastern Beijing Plain by InSAR Time Series and Wavelet Transforms, Remote Sens., 10, 365, https://doi.org/10.3390/rs10030365, 2018.

Ge, L., Ng, H. M., Li, X., Abidin, H. Z., and Gumilar, I.: Land subsidence characteristics of Bandung Basin as revealed by ENVISAT ASAR and ALOS PALSAR interferometry, Remote Sens. Environ., 154, 46–60, https://doi.org/10.1016/j.rse.2014.08.004, 2014.

Gong, H., Yun, P., Zheng, L., Li, X., Lin, Z., Chong, Z., Huang, Z., Li, Z., Wang, H., and Zhou, C.: Long-term groundwater storage changes and land subsidence development in the North China Plain (1971–2015), Hydrogeol. J., 26, 1417–1427, https://doi.org/10.1007/s10040-018-1768-4, 2018.

Guo, L., Gong, H. L., and Zhu, F.: Analysis of the Spatiotemporal Variation in Land Subsidence on the Beijing Plain, China, Remote Sens., 11, 1170, https://doi.org/10.3390/rs11101170, 2019.

Lanari, R., Mora, O., Manunta, M., Mallorquí, J. J., Berardino, P., and Sansosti, E.: A small-baseline approach for investigating deformations on full-resolution differential SAR interferograms, IEEE T. Geosci. Remote Sens., 42, 2375–2383, https://doi.org/10.1109/TGRS.2004.828196, 2004.

Solari, L., Del Soldato, M., Bianchini, S., Ciampalini, A., Ezquerro, P., Montalti, R., Raspini, F., and Moretti, S.: From ERS 1/2 to Sentinel-1: Subsidence monitoring in Italy in the last two decades, Front. Earth Sci., 6, 149, https://doi.org/10.3389/feart.2018.00149, 2018.

Xue, Y. Q., Yun, Z., Ye, S. J., Wu, J. C., and Li, Q. F.: Land subsidence in China, Environ. Geol., 48, 713–720, https://doi.org/10.1007/s00254-005-0010-6, 2005.

Ye, S., Xue, Y., Wu, J., Yan, X., and Yu, J.: Progression and mitigation of land subsidence in China, Hydrogeol. J., 24, 1–9, https://doi.org/10.1007/s10040-015-1356-9, 2015.

Yin, J., Yu, D., and Wilby, R.: Modelling the impact of land subsidence on urban pluvial flooding: A case study of downtown Shanghai, China, Sci. Total Environ., 544, 744–753, https://doi.org/10.1016/j.scitotenv.2015.11.159, 2016.

Zhang, Y., Wu, H. A., Kang, Y., and Zhu, C.: Ground Subsidence in the Beijing-Tianjin-Hebei Region from 1992 to 2014 Revealed by Multiple SAR Stacks, Remote Sens., 8, 675, https://doi.org/10.3390/rs8080675, 2016.

Zhou, C., Gong, H., Chen, B., Li, J., Gao, M., Zhu, F., Chen, W., and Liang, Y.: InSAR time-series analysis of land subsidence under different land use types in the Eastern Beijing Plain, China, Remote Sens., 9, 380, https://doi.org/10.3390/rs9040380, 2017.

Zhu, L., Gong, H., Li, X., Rong, W., Chen, B., Dai, Z., and Teatini, P.: Land subsidence due to groundwater withdrawal in the northern Beijing plain, China, Eng. Geol., 193, 243–255, https://doi.org/10.1016/j.enggeo.2015.04.020, 2015.

Zooming in on CO_2 emissions of adaptive peatland management

H. van Hardeveld[1]

1 Waternet, Amsterdam, the Netherlands

henk.van.hardeveld@waternet.nl

Abstract

Financial compensation for the reduction of greenhouse gas emissions would enhance the implementation of adaptive peatland management strategies. To broker such deals, high spatio-temporal resolution impact assessments are needed. The added value of the SOMERS method for such endeavors was tested. SOMERS was shown better suited to assess the impacts of adaptative strategies on CO_2 emissions than previous methods based on empirical relations with groundwater tables. The method can be further refined by considering seepage conditions.

Introduction

Previously, an integrated impact assessment with the RE:PEAT tool on the Tygron Geodesign Platform (TGP) demonstrated that pressurized field drains and/or higher water levels could enhance the sustainable management of a Dutch peatland polder, but none of the stakeholders would be able to singlehandedly cover the implementation costs (Van Hardeveld et al., 2020). However, if a financial bonus would be granted for the reduction of greenhouse gas emissions, the implementation of pressurized field drains and/or higher water levels would become feasible. To broker such deals, integrated impact assessments with high spatio-temporal resolution are needed, as well as more certainty regarding the impacts of the adaptations on greenhouse gas emissions.

In recent years, many scholars have focused on methods to estimate greenhouse gas emissions from peat soils. For instance, Van den Akker et al. (2008) derived CO_2 emissions from soil subsidence assessments which reflected an empirical relation with the average lowest annual groundwater table, and Couwenberg et al. (2011), Tiemeyer et al. (2020) and Evans et al. (2021) all used empirical relations between mean annual groundwater tables and CO_2 emissions. Although all these relations show that in general, higher groundwater tables lead to less CO_2 emissions, the magnitude of the emissions estimates varies.

To contribute to a better understanding of peatland CO_2 emissions, a group of Dutch scientists is developing SOMERS (Subsurface Organic Matter Emission Registration System), an estimation method which is more sophisticated than mere regression formulas of groundwater statistics. They combine monitoring results of multiple Dutch peatland sites with detailed Hydrus-2D modelling to assess the potential aerobic microbial respiration rate of peatland parcels on a daily basis (Boonman et al. 2021). The first version of SOMERS allows users to access their results and estimate CO_2 emissions for a range of settings, using a lookup table with soil type, ditch water level and parcel width as variables. The question this paper seeks to answer is: what is the added value of the SOMERS method for impact assessments of adaptive peatland management strategies?

Methods

The SOMERS method was compared to an adaption of the method of Van den Akker et al. (2008) that was used in the RE:PEAT tool (Van Hardeveld et al. 2019). For this comparison, the lookup table of the SOMERS method was reconstructed as a mapping tool with high spatio-temporal resolution on the TGP. Both methods were used to assess the impacts of three management strategies in Polder de Ronde Hoep, an agricultural peatland polder of 11.9 km² near Amsterdam: (1) current surface water levels, maintained at 30 cm below the ground surface along the border of the polder, and 10 cm below the ground surface in the center of the polder, (2) raised surface water levels, maintained everywhere at 10 cm below the ground surface, and (3) pressurized field drains which maintain the groundwater table at 30–40 cm below the ground surface.

Results

For the strategy with current surface water levels, the average CO_2 emission assessed by the SOMERS method (8,8 10^3 kg ha^{-1} yr^{-1}) and the RE:PEAT tool (8,5 10^3 kg ha^{-1} yr^{-1}) differed only slightly. The strategy with raised water levels revealed more pronounced difference, with the SOMERS method estimating 4,7 10^3 kg ha^{-1} yr^{-1} and the RE:PEAT tool 3,1 10^3 kg ha^{-1} yr^{-1}. In both strategies, differences were most pronounced at some parcels in the north and along the southern border with strong downward seepage conditions. The strategy with pressurized field drains resulted in the lowest emission estimates, ranging from 3,9 10^3 kg ha^{-1} yr^{-1} according to the SOMERS method to nothing at all according to the RE:PEAT tool.

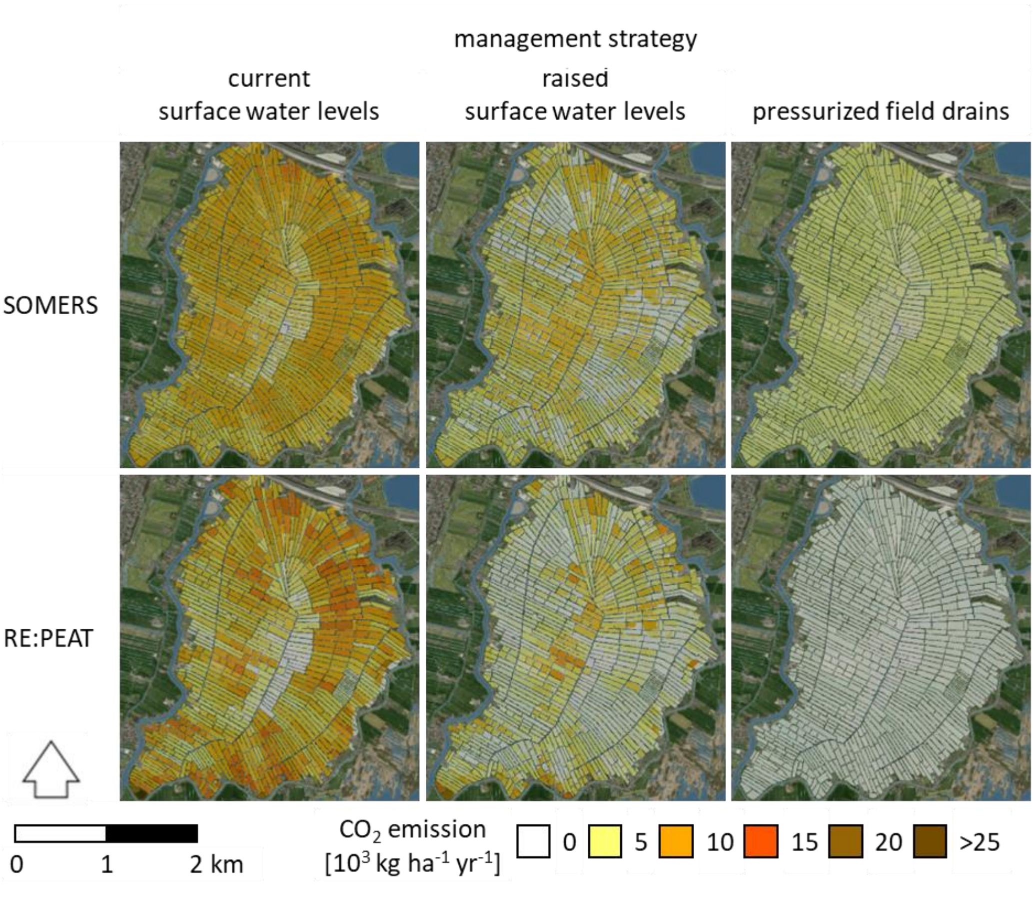

Figure 1 CO2 emissions in the research area resulting from the three management strategies.

Discussion

Polder de Ronde Hoep is a polder with marked downward seepage. Therefore, lowest annual groundwater tables are relatively low compared to similar polders with less seepage, i.e., the conditions which reflect the original empirical relation of the Van den Akker method. In the RE:PEAT tool, the slope of the empirical relation of the Van den Akker method was adjusted, so that estimated soil subsidence in the current situation would better match the recorded long term soil subsidence in polder de Ronde Hoep. As a result, groundwater tables at 30–40 cm below the ground surface result in zero soil subsidence and therefore, zero CO_2 emission. This does not match with emission measurements at monitoring sites with similar conditions. The SOMERS method, which is derived from these measurements, is far more trustworthy on that account. In fact, as many stakeholders involved in policy processes commented on the unlikeliness of the results, the SOMERS method has now replaced the previous method to assess CO_2 emission in the RE:PEAT tool. However, further refinements regarding seepage conditions are still needed. Assessments based on the potential aerobic microbial respiration rate are very well suited to consider the full range of these conditions. Therefore, the next version of the SOMERS method might very well be of even more added value for impact assessments of adaptive peatland management strategies.

References

Boonman, J., Hefting, M.M., van Huissteden, C.J.A., van den Berg, M., van Huissteden, J., Erkens, G., Melman, R., and van der Velde, Y.: Cutting peatland CO2 emissions with water management practices. *Biogeosc*. Discuss. https://doi.org/10.5194/bg-2021-276, 2021.

Couwenberg, J., Thiele, A., Tanneberger, F., Augustin, J., Bärisch, S., Dubovik, D., Liashchynskaya, N., Michaelis, D., Minke, M., Skuratovich, A., and Joosten, H.: Assessing greenhouse gas emissions from peatlands using vegetation as a proxy, *Hydrobiol.* 674, 67–89, https://doi.org/10.1007/s10750-011-0729-x, 2011.

Evans, C. D., Peacock, M., Baird, A. J., Artz, R. R. E., Burden, A., Callaghan, N., Chapman, P. J., Cooper, H. M., Coyle, M., 815 Craig, E., Cumming, A., Dixon, S., Gauci, V., Grayson, R. P., Helfter, C., Heppell, C. M., Holden, J., Jones, D. L., Kaduk, J., Levy, P., Matthews, R., Mcnamara, N. P., Misselbrook, T., Oakley, S., Page, S., Rayment, M., Ridley, L. M., Stanley, K. M., Williamson, J. L., Worrall, F., and Morrison, R.: Overriding water table control on managed peatland greenhouse gas emissions, *Nature,* https://doi.org/10.1038/s41586-021-03523-1, 2021.

Tiemeyer, B., Freibauer, A., Borraz, E. A., Augustin, J., Bechtold, M., Beetz, S., Beyer, C., Ebli, M., Eickenscheidt, T., Fiedler, 900 S., Förster, C., Gensior, A., Giebels, M., Glatzel, S., Heinichen, J., Hoffmann, M., Höper, H., Jurasinski, G., Laggner, A., Leiber-Sauheitl, K., Peichl-Brak, M., and Drösler, M.: A new methodology for organic soils in national greenhouse gas inventories: Data synthesis, derivation and application, *Ecol. Indic*., 109, 105838, https://doi.org/10.1016/j.ecolind.2019.105838, 2020.

Van den Akker, J. J. H., Kuikman, P. J., de Vries, F., Hoving, I., Pleijter, M., Hendriks, R. F. A., Wolleswinkel, R. J., Simões, R. T. L., and Kwakernaak, C.: Emission of CO2 from Agricultural peat soils in the Netherlands and ways to limit this emission, in: Proceedings of the 13th International Peat Congress After Wise Use – The Future of Peatlands, Vol. 1 Oral Presentations, Tullamore, Ireland, 8–13 June 2008, edited by: Farrell, C. and Feehan, J., *International Peat Society*, Jyväskylä, Finland, 645–648, 2008.

Van Hardeveld, H. A., Driessen, P. P. J., Schot, P. P., and Wassen, M. J.: How interactive simulations can improve the support of environmental management? Lessons from the Dutch peatlands, *Environ. Model. Softw.,* 119, 135–146, https://doi.org/10.1016/j.envsoft.2019.06.001, 2019.

Van Hardeveld, H.A., de Jong, H., Knepflé, M., de Lange, T., Schot, P.P., Spanjers, B., and Teurlincx, S.: Integrated impact assessment of adaptive management strategies in a Dutch peatland polder. *Proc. IAHS*, 97, 1–5, https://doi.org/10.5194/piahs-97-1-2020, 2020.

Long-term Analysis of Peatland Subsidence in two intensive agricultural used lowlands in Northern Germany

A. Herrmann[1], T. Martens[2], J. Schrautzer[2], M. Trepel[2], J. Zeitz[1]

1 Humboldt-Universität zu Berlin, Faculty of Life Sciences, Albrecht Daniel Thaer-Institute of Agricultural and Horticultural Sciences, Department of Soil Science
2 Christian-Albrechts-Universität zu Kiel, Faculty of Mathematics and Natural Sciences, Institute for Ecosystem Research, Department of Applied Ecology and Paleoecology

andreas.herrmann.1@agrar.hu-berlin.de

Introduction

Intensive drainage measures for agricultural use led to a progressive peatland subsidence in addition to the release of greenhouse gas (GHG) emissions. For example, in the Netherlands, approximately 2 to 4 m of peatland soil has disappeared since the Middle Ages (Van Asselen, 2018). In contrast to the growth rate of peat, the loss rate is relative quick. Studies have shown that the subsidence rate of peatlands is approximately between 0,7 and 1,5 cm per year (Nieuwenhus & Schokking, 1997; Van den Akker, 2008; Van den Akker, 2017). The loss corresponds to high GHG emissions, high costs for water management and major damage to infrastructure (Van Hardeveld, 2018).

Peatland subsidence and high GHG emissions in degraded peatlands is also an ongoing problem in Germany, because of an intensive agricultural tradition for decades and centuries. In the context of global climate change the federal states, e.g. Schleswig-Holstein and Brandenburg face different challenges in the near future. On the one hand the local farmers and authorities have to deal with a higher sea level related with investments for higher pump capacity and on the other hand they have to deal with a loss of productive land due to a continued progressive drainage infrastructure, leading to further peatland degradation. For future water management strategies valid information on these processes are needed, but reliable statements are not yet or only partially available.

In the presented study we estimated the loss of organic soils in two project regions in northern Germany and assess the small-scale heterogeneity of this process for the future. We also assumed, that there are some factors, which affect the peatland subsidence, e.g. the drainage depth, but also the peat thickness, the presence or absence of a mineral top layer as well as the underlying substrates.

Study area

Eider-Treene-Sorge (ETS) Lowland (Schleswig-Holstein)

The Eider-Treene-Sorge Lowland is located about 50 km western of Kiel and covers an area of about 45.000 ha. The Lowland was formed after the last glaciation due to the runoff of meltwater. Peat growth was initiated during the Holocene by predominantly paludification processes. The geologic bedrock is characterized by mainly holocenic sands and scattered occurrence of basin clay and organic or mineral gyttja. Due to high precipitation rates (800-900 mm) fens and raised bogs occur naturally peat thickness ≤ 50 dm are widespread. The ETS is dominated by intensively agricultural dairy farming with up to 5 cuts per year. These intensively used peatlands show strongly degradation in the uppermost layers. Large parts of the lowland are below the sea level and are actively drained by pumping stations; in higher areas, ditches and other pumping systems ensure drainage and thus the agricultural usability of the peat soils.

Upper Rhinluch (UR) (Brandenburg)

The Upper Rhinluch is situated ca. 60 km northwest of Berlin and covers an area of 14.000 ha. The landscape was formed in the late glacial period as a result of paludification processes. The geologic bedrock is composed of holocenic sands and calcareous gyttja. The organic soils are characterized by shallow peat layers, in general the thickness is no more than 5 to 7 dm. The annual precipitation amounts to ca. 500 mm and the mean annual air temperature is 9,6 °C.

Due to intensive drainage the peatland soils are very degraded and show strongly earthified peat in the topsoil related with an aggregated subsoil with shrinking cracks. Land use is dominated by large dairy farms and in some extensive suckler cow husbandry. Due to the drier climate the mowing intensity does not exceed 3 cuts per year.

Methodical approach

In this study, we investigated the long-term change of agriculturally used peatlands with special focus on soil stratigraphic data like peat thickness, underlying bedrock and peat substrates. First, we analysed historical soil recordings contained in a database provided by the regional State Offices and selected all profiles older than 30 years, with a full description up to the underlying substrate and a constant grassland use. In total we extract 24.000 soil profiles in the ETS and ca. 10.000 profiles in the Upper Rhinluch. Then, we calculated probability distribution focused on soil types (according to German Soil Classification), peat thickness as well as the presence and thickness of mineral top layers. Finally, we derived typical model soil profile classes, which are characteristic for the different regions and area-representative.

After that we selected randomly historical profile sets, which are evenly distributed across all model soil profile classes for some reference drilling campaigns, which was carried out in 2020 and 2021 very close to the historical points (accuracy amounted about 3 meter). In total we resume 111 soil profiles in the ETS and 164 profiles in the UR. During these surveys we recorded different soil parameter such as peat thickness, horizon and substrate sequences, decomposition status. Additionally, we took soil samples to determine physical and chemical parameters, like bulk density, pH-values and carbon content, among others.

The difference of the historical and the current peat thickness gives an indication of the specific subsidence rates of the previously model soil classes. The data will apply into a thickness alteration model, integrating two components: 1.) the alteration due to compression of organic substrates within the aeration zone and 2.) a constant loss due to postglacial isostatic compensation movement or due to higher loads of upper layers because of former drainage. A similar approach could be found by Hoogland et al., 2012.

Results

We confirm that all investigated peatland profile pairs under agricultural use are subject to subsidence and the process does not end by a certain peat thickness. The mean calculated subsidence rate amounts to 0,7 cm per year with some difference between the project regions. In the ETS the rates vary between 0,37 and 1,44 cm per year, while in the Upper Rhinluch the rates are some lower with 0,33 and 0,86 cm per year. Further it becomes clear, that these subsidence rates differ within the peat thickness (Fig. 1). Peatland soils with a lower former total thickness class (< 30 or 30-70 cm) show subsidence rates of 0,30 to 0,48 cm per year, respective. In contrast, peatland soils with a higher former thickness class (120-200 or >200 cm) exhibit higher subsidence rates of 1,02 to 1,25 cm per year. Similar results could be found if we consider only the first meter of the aerated zone. Figure 2 shows the alteration of peat thickness as a function of the different proportion of peat in the first profile meter. Light different rates appear with 0,20 cm per year in peaty soils with an amount of 20 percent and 0,85 cm per year in soils with 100 percent peat in the first meter. However significant differences are found only between the lower former peat thickness (<120 cm) and the higher ones (>120 cm).

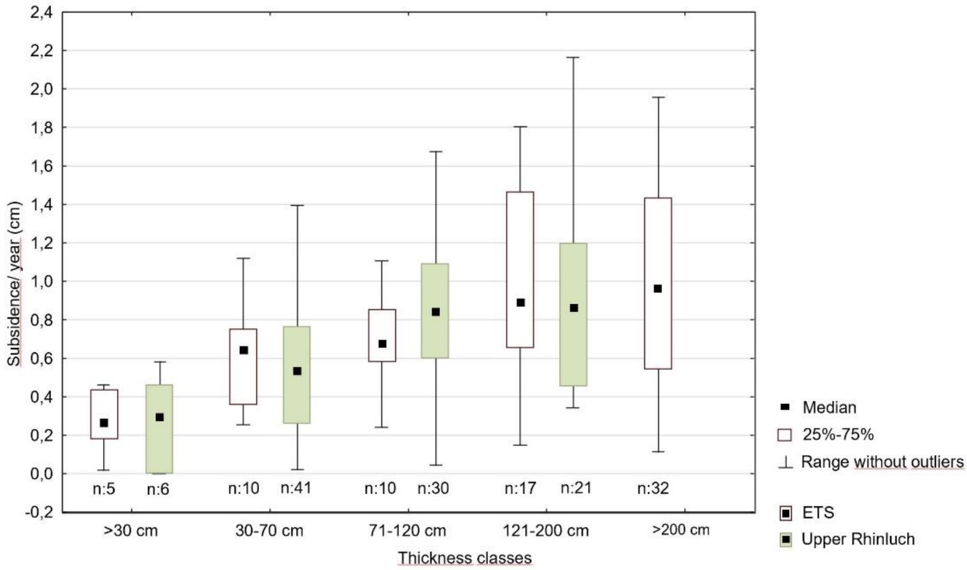

Figure 1 Subsidence rates differentiated by former peat thickness classes and project regions

We could not find a significant dependence between the subsidence rates and the underlying substrate. We also find a slight trend between the presence/absence of a mineral top layer and the subsidence. The mean rate with a mineral top layer amounts to 0,76 cm per year, in contrast 0,68 cm without a mineral cover.

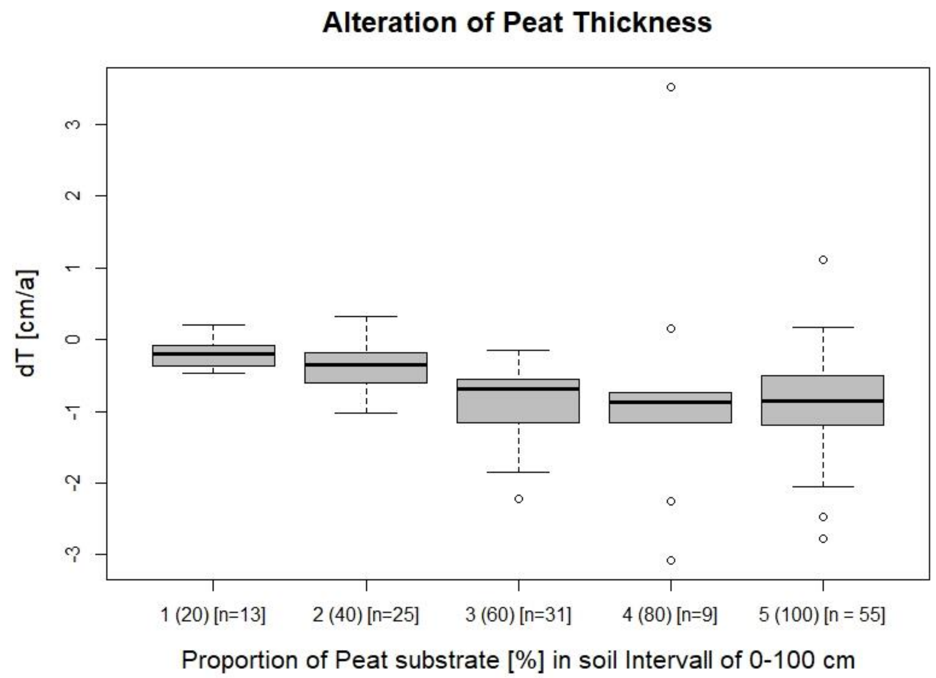

Figure 2 Alteration of peat thickness for different portion of peat substrate; comparison between historical pedological data and soil-geological reference surveys; sample size in brackets

Conclusions

By comparing the pedologic profile records with the historical profile records, there are rather low rates of subsidence over time at the sites with particularly shallow peat layers. When comparing the current profile information with the historical data, it also becomes clear that the composition of the peat at these sites has changed. Significantly, higher proportions of mineral components (sand, silt) are present in these profiles today. These higher proportions of mineral components could also be a reason for the lower subsidence rates in these profiles.

References

HOOGLAND, T., VAN DEN AKKER, J. J. H., BRUS, D. J. (2012). Modelling the subsidence of peat soils in the Dutch coastal area. *Geoderma* 171: 92-97

NIEUWENHUS, H.S., SCHOKKING F. (1997). Land subsidence in drained peat areas of the Province of Friesland, The Netherlands. *Quarterly Journal of Engineering Geology and Hydrogeology* 30 (1): 37-48

VAN ASSELEN, S., ERKENS, G., STOUTHAMER, E., WOOLDERINK, H.A.G., GEERAERT R.E.E., HEFTING, H.M. (2018). The relative contribution of peat compaction and oxidation to subsidence in built-up areas in the Rhine-Meuse delta, The Netherlands. *Science of the total Environment* 636: 177-191.

VAN DEN AKKER, J.J.H., KUIKMAN, P.J., DE VRIES, F., HOVING, I., PLEIJTER, M., HENDRIKS, R.F.A., WOLLESWINKEL, R.J., SIMÕES, R.T.L. & KWAKERNAAK, C. (2008): Emission of CO2 from agricultural peat soils in the Netherlands and ways to limit this emission. In: Farrell, C and J. Feehan (eds.). *Proceedings of the 13th International Peat Congress After Wise Use – The Future of Peatlands*, Vol. 1 Oral Presentations, Tullamore, Ireland, 8 - 13 june 2008. – International Peat Society; Jyväskylä, Finland. pp 645-648.

VAN DEN AKKER, J.J.H., HENDRIKS, R.F.A. (2017). Diminishing peat oxidation of agricultural peat soils by infiltration via submerged drains. *GLOBAL SYMPOSIUM ON SOIL ORGANIC CARBON*, Rome, Italy, 21-23 March 2017

Economic analyses of urban subsidence in Gouda and Amsterdam, the Netherlands

Saskia Hommes-Slag[1], Sien Kok[1],Daan Rooze[1] and Mark de Bel[2]

1 Urban Soil and Groundwater Management, Deltares, 3508 AL Utrecht, the Netherlands. Correspondence: Saskia Hommes-Slag (saskia.hommes@deltares.nl)
2 Water Resources and Delta Management, Deltares.

Abstract

This paper presents the updated research on an approach and outcomes of two exploratory economic analyses of subsidence: 1) in the inner city of Gouda, the Netherlands; 2) in five areas in the city of Amsterdam, the Netherlands. Results from the Gouda case study indicate that especially the mitigation strategy focusing on reducing damage, rather than a strategy aiming to halt subsidence altogether, might have a positive economic rationale. Results from the Amsterdam case study show that there is no single approach that works for all areas and other neighborhoods in the municipality of Amsterdam. The methodological framework for economic analysis in a subsidence context does however help to quantify and compare the main expected damages for each research area.

Introduction

In the Netherlands, subsidence of clay and peat soils is mainly caused by artificial lowering of phreatic groundwater levels, and soft-soil loading by buildings and infrastructure. Expected damages are significant: estimated at EUR ~ 22 billion until 2050 (van den Born et al., 2016). As in the Netherlands land subsidence is mostly human-induced, much of this damage may be prevented: the rate of subsidence can be reduced, and/or structural or non-structural measures can be taken to minimize the negative effects of land subsidence. As subsidence mechanisms and asset exposure characteristics differ across rural and urban areas, but also within urban areas (e.g. new urban developments versus historic city centers), the optimal approach needs to be targeted to local circumstances.

Kok & Hommes-Slag (2020) demonstrate how the economic rationale for interventions in a subsidence context was determined in the case of Gouda, the Netherlands. Although economic estimates in the analysis are specific to the context of a subsiding historic urban zone with a mix of shallow and piled foundations, the methodological framework used is applicable to other subsidence contexts as well. In this update, an extra economic rationale (quick scan) is added for five research areas in the city of Amsterdam, the Netherlands.

Methods

The quick scan carried out for the city of Amsterdam consists of two parts: 1) an analysis when 'tipping points' can be expected to be reached affecting the quality of life in an area; 2) Indication of economic effects of subsidence. This paper focuses on the second part of the quick scan. This part uses the same methodological framework that was used in the case of Gouda (Kok & Hommes-Slag, 2020).

Results

The results from the quick scan for the city of Amsterdam show a differentiated picture between the five research areas. The various causes and aspects of the subsidence problem of the five areas are reflected in the economic damage. In areas where buildings are founded on piles and where the ground level drops significantly, a lot of damage is expected to cable & pipe connections and reduced accessibility of buildings. In the research area, where buildings are built on shallow foundations, the decreasing drainage depth with consequent frequent groundwater flooding of buildings is the dominant problem. However, the slight subsidence in this area only has a small effect on the aggravation of this problem. In one of the research areas a variety of problems plays a role. The main process is damage to foundations due to the low groundwater level due to the proximity of a low-lying park. Decline of cultural heritage (monumental buildings and trees) calls for urgent action in this area.

On a methodological level, we can conclude that the framework that is used for the cost-benefit analysis in Gouda and Amsterdam is helpful in pointing out the main expected economic effects.

Conclusion

Unfortunately, there is no single approach that works for all areas and other neighborhoods in the municipality of Amsterdam that provides a ready-made answer to subsidence. Therefore, further research is needed to adapt the approach to local circumstances.

The quick scan does show that all areas will have to deal with subsidence. The extent to which differs per research area. It is recommended to further investigate the level of subsidence in the area, the groundwater levels and subsidence of the buildings. It is also recommended to build a detailed and validated groundwater and subsidence model of the entire city. Together with a detailed description of the (geotechnical) properties and structure of the subsoil, more well-founded statements can be made about changes in the future (e.g. due to climate change) and the effect on the expected damage.

In any case, this quick scan shows that subsidence can be a serious problem in parts of the built environment of Amsterdam, next to the parks and rural peat meadow areas, which are already on the agenda for dealing with subsidence. What this exactly means for the whole of the municipality of Amsterdam requires a further analysis of both the problem and the possible solutions and the responsibilities of the different parties.

References

Deltares (2022), *Quick scan bodemdaling in Amsterdam - Verkenning van omslagpunten leefbaarheid en economische impact in 5 pilotgebieden*, 11207290-002-BGS-0002

Kok, S., Hommes-Slag, S. (2020), Cost-benefit analysis of urban subsidence mitigation strategies in Gouda, the Netherlands, *Proc. IAHS*, 382, 761-766, 2020, https://doi.org/10.5194/piahs-382-761-2020

Proc. IAHS, 382, 747–753, 2020
https://doi.org/10.5194/piahs-382-747-2020

Tenth International Symposium on Land Subsidence (TISOLS)

Investigating the effectiveness of drain infiltration to minimize peat oxidation in agricultural fields in Flevoland, the Netherlands

Frouke Hoogland, Arjen S. Roelandse, Beatriz de La Loma González, Maarten J. Waterloo, Perry W. Mooij, Sabine A. Verhagen, and Jouke Velstra

Acacia Water B.V., van Hogendorpplein 4, Gouda, 2805BM, the Netherlands

Correspondence: Frouke Hoogland (frouke.hoogland@acaciawater.com)

Published: 22 April 2020

Abstract. In the Province of Flevoland, the Netherlands, land subsidence poses a problem to agriculture and water management. The peat layers in the soil are susceptible to compression and oxidation causing further subsidence. Applying subirrigation through the tile drain system to maintain saturation of the peat may be a measure to slow down subsidence. A study was therefore carried out at two sites, Nagele and Zeewolde, to assess the impact of subirrigation in the peat on the seasonal variation in soil moisture content, and corresponding redox conditions. Bacterial community analysis was carried out to verify the hydrochemical observations. Subirrigation proved to be an efficient measure to maintain a high water level in the peat soil as long as the permeability in the upper part of the peat was sufficient to allow transmission of water into the inter-drain area and when the peat layer extended enough below the minimum regional water level to prevent drainage to the sand layer underneath. The peat showed dual porosity and water levels could well be maintained by subirrigation at the Nagele site. At the Zeewolde site, the variability in the thin peat layer allowed drainage to occur in the sand layer, preventing subirrigation to maintain high water levels. However, at both sites the peat layer remained close to saturation throughout the summer, which may be caused by the fine-grained mineral layer isolating the peat from water extraction via evapotranspiration. Nitrate concentrations of up to $100\,\mathrm{mg\,L^{-1}}$ were observed were high ($>50\,\mathrm{mg\,L^{-1}}$) in the oxic mineral top layer but were low in the peat ($0.3\,\mathrm{mg\,L^{-1}}$) at both Nagele and Zeewolde sites. Sulphate concentrations also showed a decrease with depth in the peat at Nagele, indicating a transition from sub-oxic above 1.5 m depth to anoxic conditions at 3.5 m depth. The hydrochemical observations in the soil moisture in the peat at Nagele confirmed that conditions were sub-oxic in the upper part of the peat (0.7 m below soil surface) to anoxic at greater depth (3.5 m). Soil microbe analyses showed few nitrification bacteria in the peat, whereas communities specialised in denitrification and ammonification were present, as well as sulphate reducing bacteria and methanogenic species. This confirmed the sub-oxic to anoxic conditions in the peat deduced from the hydrochemical observations. At Zeewolde, conditions remained sub-oxic throughout the profile.

1 Introduction

The Flevoland polders were reclaimed in the mid-20th century from the former Zuiderzee, which was closed off from the North Sea to form the fresh water IJsselmeer lake. The land surface is currently about 3–4 m below sea level, and subsidence continues (Fokker et al., 2015) posing a significant threat to agricultural practices (Vogelenzang et al., 2019), complicating water management and threatening water quality by increased upward seepage of saline water. Main causes of subsidence were the loss of pore pressure following reclamation and subsequent gradual lowering of phreatic water levels by the Water Board to create and maintain favourable conditions for agriculture. This resulted in compression and compaction of the clayey top soil layer and the peat layer underneath. An important factor for continued subsidence is the oxidation and permanent shrinkage of shallow humic clay and peat layers (Fokker et al., 2015). Peat oxidation can account to up to 68 % of loss in volume (Leifeld et al., 2011) and is fastest at high oxygen availability and high soil temperatures. Peat oxidation conditions are therefore most favourable during summer when phreatic levels decrease in response to evapotranspiration and near-surface peat layers partially dry out. Land use in Flevoland is mainly agricultural. About 71 % of agricultural land is used for intensive arable farming of potatos, wheat, sugar beet and onions, which requires phreatic levels of at least 0.8 m below the surface. Peat meadows for production of grass or corn fodder cover about 21 % (Vogelenzang et al., 2019). For arable farming, tile drain systems and regulation of the regional water level by the Water Boards keep groundwater levels low, even during high rainfall events. Inter-drain distances are typically between 12 and 30 m. In peat meadows, drainage is accomplished by a system of shallow ditches dug at typical inter-distances of more than 30 m (Couwenberg, 2018).

In summer, the lowering of the regional water level by the Water Board and high crop evapotranspiration cause a decline in phreatic water level, thereby allowing oxygen to enter the soil pores causing potential for enhanced decomposition and shrinkage of peat. A possible method to reduce the risk of subsidence in agricultural areas with shallow peat layers is to adapt the tile drain system for subirrigation, such as to allow active infiltration into the peat and maintain a higher water level in the soil. This requires transmission of water from the drains into the inter-drain space. The degree of success of subirrigation therefore depends on if the infiltration capacity is high enough to balance the extraction of soil moisture in the inter-drain space for evapotranspiration. Peat often exhibits dual porosity, with higher permeability in interconnected macropores and low permeability in the matrix (Rezanezhad et al., 2016). Permeability generally decreases with depth and low permeabilities require small inter-drain distances to maintain moist conditions in the area between the drains. Within the "Spaarwater Flevoland" project the effects of active tile drain infiltration on phreatic water levels and soil moisture content between drains and on peat oxidation processes were investigated at two agricultural plots in the dry summers of 2018 and 2019. The objectives were to assess the rate of infiltration through the tile drain system to maintain a uniform phreatic level, and if subirrigation could prevent the soil water from becoming oxic. The latter was studied using hydrochemical and microbiological analyses.

2 Site description

Soils in Flevoland show considerable heterogeneity due to temporal and spatial variations in the depositional environments in the Holocene. Sand and peat deposits occurred in tidal marshes, which were overlain by fine-grained deposits

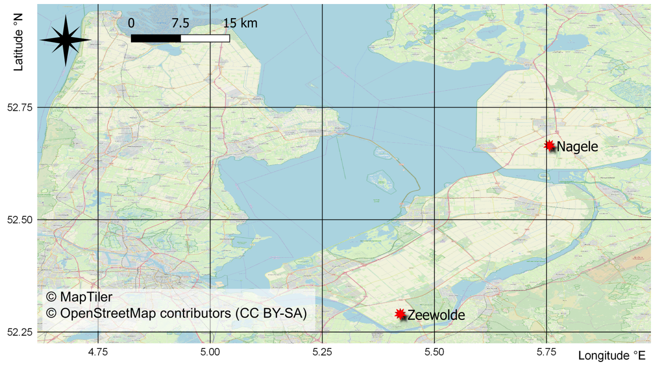

Figure 1. Locations of the Zeewolde and Nagele sites in the Flevoland Province, east of Amsterdam, in the Netherlands. © MapTiler and © OpenStreetMap contributors 2020. Distributed under a Creative Commons BY-SA License.

of varying thickness. The soil in Flevoland is characterised by a sequence of a fine-grained mineral top layer on a peat layer formed on sand. Two pilot sites were selected with different soil layering and thickness of the peat layers. The locations of the Zeewolde and Nagele pilots are presented in Fig. 1.

2.1 Nagele site

The soil at the Nagele site (52°39′55″ N, 5°45′22″ E, −4 m a.s.l.) is characterised by a 0.3–0.5 m deep top layer of silty clay underlain by about 2.5 m of peat formed on sand (Velstra et al., 2015). The tile drains were at a depth of 0.8–0.9 m below the surface with an inter-drain spacing of 12 m. New tile drains were installed between the original drains in the peat layer, applying a sand filling on the drain up to the surface. This brought the inter-drain distance to 6 m in both experimental and reference fields. In dry summers, such as those of 2018 and 2019, the farmer applies subirrigation by setting up water level in the ditch above the drain outlets to reach a maximum water level of 0.7 m below the soil surface. The crop rotated between grass in 2017, to potatoes in 2018, and onion in 2019. Crop roots were not observed in the peat layer. The subsidence in this area has been estimated at 2–3 mm yr^{-1} (Source: Bodemdalingskaart.nl, Nederlands Centrum voor Geodesie en Geo-informatica (NCG)).

2.2 Zeewolde site

The soil at the Zeewolde site (52°17′22″ N, 5°25′25″ E, −4 m a.s.l.) showed more spatial variation in the layering. The top layer of silt/clay, with a thickness of 0.5–1.1 m, was deposited on a 0.05 m thin sand layer. A peat layer of varying thickness (0.2–1.1 m) and with a thin clay layer at its base was subsequently observed. The base layer consisted of sand at 1.2–1.6 m below the surface (Velstra et al., 2015). The tile drains were at a depth of 0.8–0.9 m below the surface with an inter-drain spacing of 16 m. New tile drains were again installed between the original drains in the clay/peat layers, applying sand filling up to the surface, which brought the inter-drain distance to 8 m. Crop rotation was typical for Flevoland including sugar beet, onions and potatos. Crop roots were not observed in the peat layer. The subsidence in this area was somewhat lower at about 1 mm yr^{-1} (NCG).

3 Methods

For subirrigation, the tile drains were connected to a collector drain and buffer tank, in which provisions were made to allow fixing water levels at 0.1 m level increments, independent of the ditch water level. A solar pump was used to supply water to the buffer tank from the ditch to maintain a set water level. Percolating rain water was removed by overflow in the drain well to the ditch. This system allows subirrigation in the experimental plot to be better regulated and at higher water levels than possible in the regular ditch approach. Flows into and out of the drains were continuously monitored with flow meters (Octave; Arad, Israel). Phreatic water level measurements were made in transects perpendicular to tile drain directions. Piezometers were installed next to the drains and at 0.5–1.0 m intervals in the inter-drain space for continuous phreatic water level measurements (CTD-10; Decagon, USA). Soil moisture content profiles were measured (GS3; Decagon, USA) down to a depth of 0.75 m. Soil moisture and groundwater samples were extracted at two-week intervals using rhizons (Rhizosphere Research Products, the Netherlands) installed at 0.25, 0.50. and 0.75 m depths. Deeper groundwater was sampled at 1.5 and 3.5 m depth (sand layer) from piezometers, which were duly flushed before sampling. Samples were filtered (0.2 µm PES) and analysed at the laboratory of Acacia Water for major cat- and anions using ion chromatography (Aquion; Dionex, USA). Fe and Mn ion concentrations were determined colorimetrically (DR900; Hach, USA).

Bulk soil samples (three locations at Nagele) for identification of bacterial communities in view of their potential to reduce nitrate and sulphate were taken at depths of 0.7 and 2.2 m in the peat layer. Sampling was carried out at the end of the winter season (6 March 2019) in prepared sample bottles and were analysed using next generation sequencing (ORVIdecode) at Orvion (the Netherlands). This procedure allows characterization of DNA and identification of bacteria populations.

4 Results

4.1 Groundwater level and soil moisture content

Ground water level measurements at Nagele showed discharge towards the drain from the inter-drain space in the winter period, with higher water levels in the piezometer between the drains than that at the drain (Fig. 2). In the summer of 2018, the pump was not capable to supply enough water to the drains and the water level between the drains decreased following the deeper regional trend. In the summer of 2019, the farmer decided to increase the water level to the bottom of the clay layer at about 0.5 m below the surface and infiltration occurred such that the peat remained saturated despite the decrease in the regional ground water level. The situation in summer 2019 showed that the peat layer was permeable enough at drain depth (Ks = 0.1–0.2 m d^{-1}) to allow flow of water into the inter-drain spacing. In addition, the thickness of the peat layer and permeability at depth were such that leakage to the deeper sand layer seemed minimal, allowing for a stable higher water level in the peat than in the sand layer below. The soil moisture content θ at a depth of 0.7 m remained close to saturation, varying between 0.71 and 0.75, except for the period between 20 June and 25 August 2018 when not enough water could be supplied to the drains and θ gradually decreased to 0.61. This suggests that the peat at this depth became unsaturated and in contact with oxygen.

In Zeewolde, where the peat layer was less deep and the drains were locally in the base sand layer, it was not possible to supply enough water to maintain a high level in the peat layer because of leakage to the regional groundwater system through the sand layer. The water levels in the peat layer therefore followed the regional trend (Fig. 3).

The decline in phreatic level during the dry period did not have a large effect on θ at a depth of 0.7 m in the peat (Fig. 4). The moisture content in peat at Zeewolde reference showed very little variation between winter and summer seasons, even though the summer of 2018 was extremely dry. Moisture content at the Nagele reference site showed seasonal variation in the first year, but less in the second year as the farmer decided to use tile drain subirrigation to keep the peat moist in summer.

In Zeewolde, the experimental site showed a fluctuating moisture content, peat being saturated in wet periods ($\theta = 0.77$), followed by a fast drop to $\theta = 0.75$. This pattern suggests rapid draining of macropore space (about 2 %), with remaining moisture staying immobile in the peat matrix. The soil moisture content in the peat of the experimental plot in Nagele maintained its high moisture content until the water supply to the tile drains was interrupted by mid-June 2018. This was followed by a decline in θ to 0.61 by August. In the summer of 2019, the water content remained high, except during short periods when the pump malfunctioned. The fast decrease in θ after pump failure also suggest draining of the macropore space, rather than of the matrix. The top fine-grained mineral soil layer, with its relatively high plant available water, provided most of the moisture for evapotranspiration. Roots were not observed in the peat layer, presumably also because of the continuously high moisture content. The peat layer at Zeewolde seemed also to be isolated from the sand layer below due to the thin impermeable clay layer at its base preventing drainage. The small ranges in observed θ

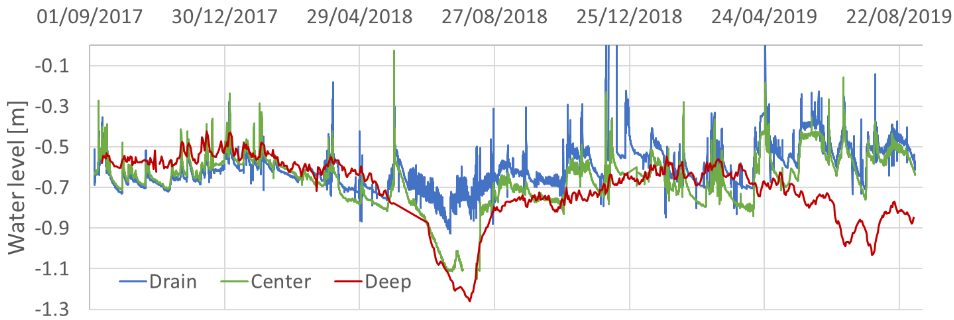

Figure 2. Groundwater levels in the experimental field at Nagele, where the drain well was used to maintain fixed water levels in summer. Drain is on the drain, centre is between the drains and deep is the groundwater level in the deep sand layer (regional). Note that the piezometers were dry at water levels below 1.1 m.

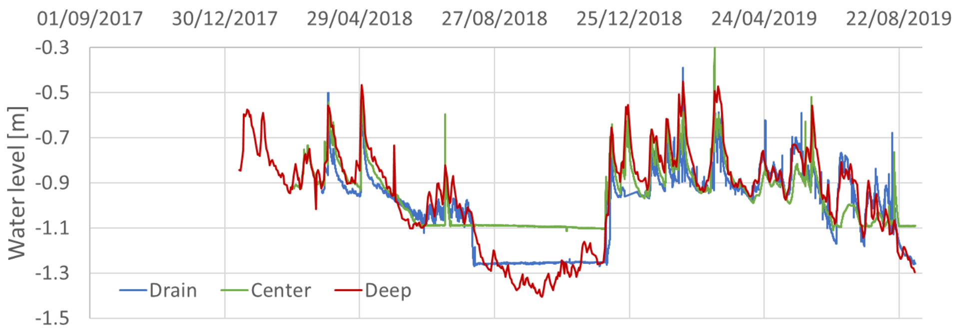

Figure 3. Groundwater levels in the experimental field at Zeewolde, where the drain well was used to maintain fixed water levels in summer. Drain is on the drain, centre is between the drains and deep is the groundwater level in the deep sand layer (regional). Note that the piezometers were dry at water levels below 1.1 m.

indicate that the soil moisture tensions remained low at above -50 hPa (pF $= 1.7$).

4.2 Hydrochemistry

Electrical conductivity of soil moisture in the peat at 0.75 cm depth was relatively high at 2743 ± 839 uS cm^{-1} in the reference plot and 2031 ± 487 uS cm^{-1} in the subirrigated plot, which may reflect the saline environment from which the land was reclaimed. The corresponding pH values ranged from 5.53–7.65 in the reference plot to consistently higher values of 5.90–8.70 in the subirrigation plot. Both plots showed seasonal variation in pH, with the highest values observed in the summer season. Atmospheric oxygen has to travel through the fine-grained top layer before reaching the peat. This is mainly by diffusion, although cracks formed during drying in summer and could have formed preferential gas flow paths towards the peat layer. If the macropores in the peat drain oxygen may enter but may not reach the peat matrix regions where moisture is immobile. When oxygen is present, this is preferably used in the decomposition process by bacteria. Stuyfzand (1993) and Mendizabal (2011) have defined different redox zones in soils related to the presence of certain ions (e.g. NO_3, SO_4) or dissolved gases (e.g. O_2, H_2S) in groundwater. Analyses of water extracted from different depths in the peat therefore provides information on the redox status. At a depth of 0.5 m in the top layer of fine-grained soil nitrate concentrations were observed up to concentrations of 100 mg L^{-1}, with an average of 43 ± 45 mg L^{-1}. As the surface layer is unsaturated and exposed to the atmospher the conditions ca be considered oxic. In the peat layer below, NO_3 concentrations were low, averaging to 0.3 ± 0.5 and 0.07 ± 0.29 mg L^{-1} at 0.75 and 1.5 m depths, respectively. NO_3 concentrations did not increase in peat in response to the decreasing moisture content in June–August 2018, suggesting sampling of water from immobile regions in the peat with the rhizons. SO_4 concentrations, however, did increase in the samples during the dry period, indicating that SO_4 was produced at 0.75 m depth. With SO_4 concentrations of well over 500 mg L^{-1} (and generally low Fe and Mn ion concentrations) the redox conditions at 0.75 and 1.5 m depth could be classified as sub-oxic. Nitrate was also absent in samples taken from the piezometer at 3.5 m depth, and SO_4 concentrations were strongly reduced to an average of 12 ± 12 mg L^{-1}. Furthermore, the release of H_2S gas was observed during sampling at depths below 2 m. The water chemistry in the peat layer in Nagele therefore indicated that the redox environment changed from sub-oxic at 0.75–1.5 m to anoxic/deep anoxic at 3.5 m depth.

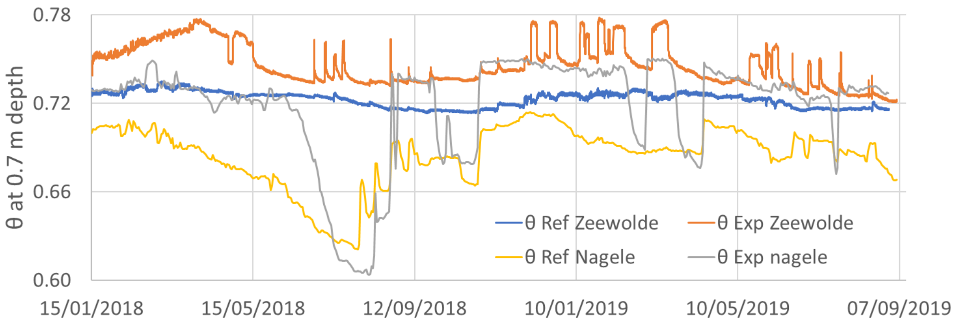

Figure 4. Variation in soil moisture content (θ) at 0.7 m depth in peat for reference (Ref) and experimental (Exp) plots in Zeewolde and Nagele.

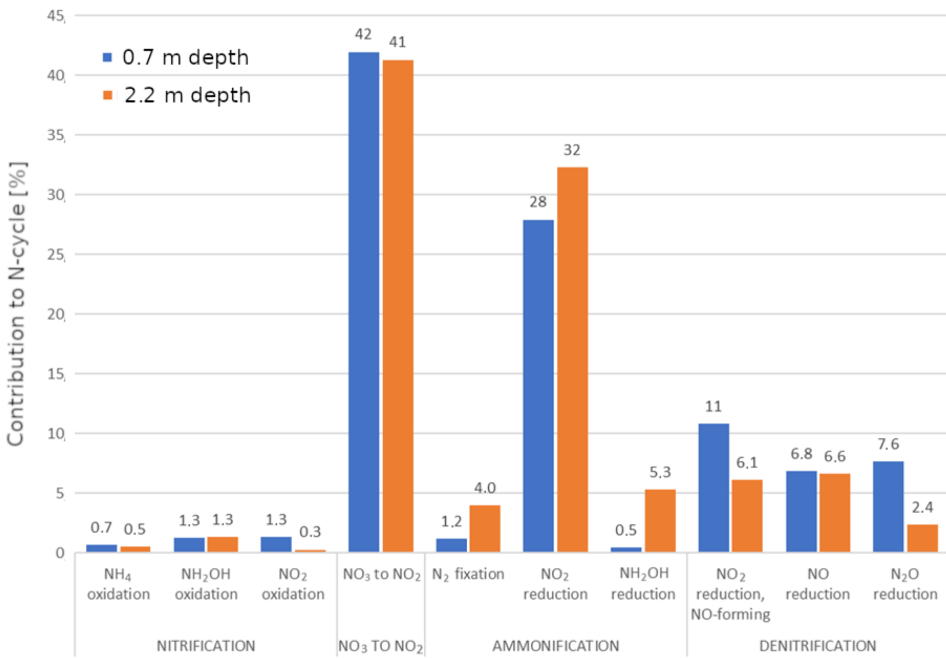

Figure 5. Contribution of bacterial communities to nitrogen transformation processes in the peat layer at depths of 0.7 m (sub-oxic) and 2.2 m (anoxic) in Nagele, March 2019.

The peat decomposition process is slowed down with depth as the electron donors change with depth from initially NO_3 to finally SO_4. Similarly, low NO_3 concentrations were observed in the peat in Zeewolde, but SO_4 concentrations were much higher throughout the peat/sand profile and the conditions therefore remained sub-oxic.

4.3 Analyses of bacterial communities in peat

Salinity and redox status influence the microbial biomass and metabolic activity related to the mineralization of carbon in peat, with pH being an important factor controlling the microbial diversity (DeAngelis et al., 2010; Preston et al., 2012; Tecon and Or, 2017). In the upper part of the peat oxygen seems to be absent, but nitrate percolating down from the unsaturated top layer can provide the oxygen used for decomposition by nitrate reducing bacteria. Lower in the profile, nitrate has been consumed and the bacterial population could change to include species that specialise in the reduction of, for instance, sulphate. At Nagele, the analysis indicated that bacteria were present in much larger numbers in the shallow suboxic peat sample than in the deeper anoxic sample. In both samples proteobacteria were dominant accounting for 70 % of the population DNA, with alpha- and betaproteobacteria accounting for about 50 %. Terrabacteria groups (mainly actinobacteria) accounted for another 10 %. Differences were observed in the presence of *Gemmatimonadetes* at 2 % in the sub-oxic sample and at 0.8 % in the anoxic region. *Chloroflexi* and *Firmicutes* bacteria increased from 0.3 % and 0.4 % in the sub-oxic region to 2 % and 1 % in the anoxic region, respectively. *Planctomycetes*, known to perform nitrite reduction and ammonium oxidation anaerobically (Dong et al., 2009; Fuerst, 2017), was present at about 1.0 % in both samples. The analyses showed that nitrificating bacterial communities typical for oxic conditions were virtually absent (Fig. 5), supporting the observation that dissolved oxygen concentration remained low in the peat.

The fractions of bacteria specialised in denitrification (mainly $NO_3 \rightarrow N_2$) were only slightly lower in the anoxic region, but the fractions of ammonification bacteria species were higher than those in the suboxic region. The latter suggests increased limitations in the availability of nitrate with depth. Sulphate reducing bacteria (*Desulfarcales*, *Desulfobacterales*, *Desulfovibrionales* and *Desulfuromonadales* from the deltaproteobacteria class) were also observed in both samples, making up 0.7 % of the total population in the sub-oxic region and 1.9 % in the anoxic region. The percentages of methano-microbia were low but increased with depth from 0.03 % to 0.11 % of the DNA present.

5 Conclusions

The study shows that several conditions need to be met for keeping a peat layer saturated through subirrigation by infiltration of water through the tile drain system. The first condition is that the inter-drain distance is proportional to the permeability of the peat. The present study showed that the 6 m inter-drain distance was sufficiently low to cause a fast response of the phreatic level at the centre of the drains. Soil moisture measurements suggested a dual porosity system that would allow relatively fast transfer of water through the peat. The second condition is that leakage towards the lower regional phreatic level should be limited, which requires a low permeability layer to extend below the minimum water level. This condition was not met at Zeewolde, allowing the supplied water to infiltrate in the sand layer below the peat and causing the water level to drop. In spite of this, the moisture content remained high in the peat layer at both sites, even though 2018 was an exceptionally dry year. The fine-grained mineral layer capping the peat seems to have provided sufficient moisture to the crop for evaporation, while largely preventing the extraction of moisture from the peat underneath. The thin layer of sand on top of the peat layer at Zeewolde may have prevented upward flow through capillary rise, whereas drainage to the sand layer may have been minimized by the low permeability of the peat/clay layer at the base of the peat. Cracks formed in the top soil but were not deep enough to reach the peat layer. Furthermore, the farmer aims to keep cracks at minimum through surface irrigation to avoid tilt damage, in particular to onion crop.

Both the biogeochemistry and the bacterial community analyses indicated that oxygen levels in the peat remained low even in the dry summer season (sub-oxic – anoxic conditions), with very low nitrate concentrations being observed in the peat, and a decrease of sulphate concentrations observed with depth. The bacterial analysis supported the hydrochemical observations confirming the absence of nitrification microbes and indicating that decomposition of peat in the absence of oxygen is through nitrate and sulphate reducing bacteria. The lower DNA count at depth, relative to that in the shallow sub-oxic region, suggests a decrease in the rate of peat mineralisation with depth.

Data availability. Measured groundwaterlevels are publicly accessable at http://flevoland.acaciadata.com/ (Acacia Water BV, 2017). Further data are available upon request from the authors.

Author contributions. FH and AR are responsible for the hydrological data analyses, AR is the projectleader. BLG and MW are responsible for the geochemical data analyses. MW and FH did the text writing and editing. SV performs the lab analysis of waterquality. PM performs the field measurements and installation of equipment. JV provided assistance for data analyses.

Competing interests. The authors declare that they have no conflict of interest.

Special issue statement. This article is part of the special issue "TISOLS: the Tenth International Symposium On Land Subsidence – living with subsidence". It is a result of the Tenth International Symposium on Land Subsidence, Delft, the Netherlands, 17–21 May 2021.

Acknowledgements. We are grateful to Aleida de Vos from Orvion for the contribution towards the interpretation of the microbial diversity in the soil. Stijn Groeneweg and Saline Verkerk are thanked for their assistance with analyses of water samples.

Financial support. This research has been supported by the Province of Flevoland (decision no. 1957339, file no. 1947426), LTO Noord Fondsen (project no. 16.29) and Zuiderzeeland Reigonal Water Authority (case nos. 479411 and 519214)

References

Acacia Water BV: available at: http://flevoland.acaciadata.com/, 2017.

Couwenberg, J.: Some facts on submerged drains in Dutch peat pastures, IMCG Bulletin, June/July, 9–21, 2018.

DeAngelis, K. M., Silver, W. L., Thompson, A. W., and Firestone, M. K.: Microbial communities acclimate to recurring changes in soil redox potential status, Environ. Microbiol., 12, 3137–3149, https://doi.org/10.1111/j.1462-2920.2010.02286.x, 2010.

Dong, L. F., Smith, C. J., Papaspyrou, S., Stott, A., Osborn, A. M., and Nedwell, D. B.: Changes in Benthic Denitrification, Nitrate Ammonification, and Anammox Process Rates and Nitrate and Nitrite Reductase Gene Abundances along an Estuarine Nutrient Gradient (the Colne Estuary, United Kingdom), Appl. Environ. Microbiol., 75, 3171–3179, https://doi.org/10.1128/AEM.02511-08, 2009.

Fokker, P. A., Gunnink, J., de Lange, G., Leeuwenburgh, O., and van der Veer, E.G.: Compaction parameter estimation using surface movement data in Southern Flevoland, Proc. IAHS, 372, 183–187, https://doi.org/10.5194/piahs-372-183-2015, 2015.

Fuerst, J. A.: Planctomycetes – New Models for Microbial Cells and Activities, chap. 1, in: Microbial Resources, From Functional Existence in Nature to Applications, edited by: Kurtböke, I., Academic Press, 1–27, 354 pp., 2017.

Leifeld, J., Müller, M., and Fuhrer, J., Peatland subsidence and carbon loss from drained temperate fens, Soil Use Manage. 27, 170–176, https://doi.org/10.1111/j.1475-2743.2011.00327.x, 2011.

Mendizabal, I.: Public supply well fields as a valuable groundwater quality monitoring network, PhD thesis, Vrije Universiteit, Amsterdam, 119 pp., 2011.

Preston, M. D., Smemo, K. A., McLaughlin J. W., and Basiliko, N.: Peatland Microbial Communities and Decomposition Processes in the James Bay Lowlands, Canada, Front. Microbiol., 3, 1–15, https://doi.org/10.3389/fmicb.2012.00070, 2012.

Rezanezhad, F., Price, J. S., Quinton, W. L., Lennartz, B., Milojevic, T., and van Cappellen, P.: Structure of peat soils and implications for water storage, flow and solute transport: A review update for geochemists, Chem. Geol., 429, 75–84, 2016.

Stuyfzand, P. J.: Hydrochemistry and hydrology of the coastal dune area of the Western Netherlands, PhD Thesis Vrije Universiteit, Amsterdam, 362 pp., 1993.

Tecon, R. and Or, D.: Biophysical processes supporting the diversity of microbial life in soil, FEMS Microbiol. Rev., 41, 599–23, https://doi.org/10.1093/femsre/fux039, 2017.

Velstra, J., Burger, S., van der Gaast, J., and Verbruggen, M.: Spaarwater Flevoland – Verkennen, Acacia Institute Report, 42 pp., 2015.

Vogelzang, T., Smit, B., Kuiper, P. P., and Gillet, C.: Grond in beweging; Ontwikkelingen in het grondgebruik in de provincie Flevoland in de periode tot 2025 en 2040., Wageningen Economic Research, Report 2019-00, 86 pp., 2019.

Proc. IAHS, 382, 103–109, 2020
https://doi.org/10.5194/piahs-382-103-2020

Tenth International Symposium on Land Subsidence (TISOLS)

IoT technology and big data processing for monitoring and analysing land subsidence in Central Taiwan

Wei-Chia Hung[1,2], **Yi-An Chen**[1], **and Cheinway Hwang**[2]

[1]Green Environmental Engineering Consultant Co. LTD., Hsinchu, Republic of China
[2]Department of Civil Engineering, National Chiao Tung University, Hsinchu, Republic of China

Correspondence: Wei-Chia Hung (khung@itrige.com.tw)

Published: 22 April 2020

Abstract. Over 1992–2018, groundwater overexploitation had caused large-scale land subsidence in the Choshui River Alluvial Fan (CRAF) in Taiwan. The Taiwan High Speed Railway (THSR) passes through an area of severe subsidence in CRAF, and the subsidence poses a serious threat to its operation. How to effectively monitor land subsidence here has become a major issue in Taiwan. In this paper, we introduce a multiple-sensor monitoring system for land subsidence, including 50 continuous operation reference stations (CORS), multi temporal InSAR (MT-InSAR), a 1000 km levelling network, 34 multi-layer compaction monitoring wells and 116 groundwater monitoring wells. This system can monitor the extent of land subsidence and provide data for studying the mechanism of land subsidence. We use the Internet of Things (IoT) technology to control and manage the sensors and develop a bigdata processing procedure to analyse the monitoring data for the system of sensors. The procedure makes the land subsidence monitoring more efficient and intelligent.

1 Introduction

Due to the continuous growth of population and economy in Taiwan, more water resources are needed. The use of the groundwater resources is inevitable when the surface water sources become insufficient. Groundwater overexploitation may result in land subsidence and other disasters. In coastal areas, sea water can intrude the water-bearing stratum and result in soil salinization. The salinization can degrade the vital functions of the soil and the salinized land can no longer support industry developments are downgraded. The underground water resources will no longer be utilized. These land subsidence problems will increase the social cost. Selected cases of land subsidence (Tosi et al., 2007; Tomás et al., 2010; Hung et al., 2011).

Taiwan is located in the subtropical monsoon region, and the climate of Taiwan is oceanic tropical and subtropical. The rainfall is plentiful; the annual rainfall reaches up to 2500 mm, which is 2.5 times of the average world rainfall. However, Taiwan is a country suffering from severe water shortage due to a number of reasons. Taiwan is highly populated, with foothills and high mountains over 2/3 of the island. Because of the steep terrains, the discharge times of major rivers to the oceans are short. As Taiwan's economy continues to grow the total water consumption continues to rise rapidly. As a result, groundwater now has become a major water source. Overexploitation of the groundwater is common in the suburban areas. In particular, severe land subsidence has occurred in the southwestern coastal areas, especially over Choushui River Alluvial Fan (CRAF) in recent years.

CRAF is the most important agricultural area in western, central Taiwan, with elevations ranging from 0 to 100 m. CRAF covers a total area of 2000 km^2 and is bounded by Wu River (north), Pekang Creek (south), Douliu Mound (east) and Taiwan Strait (west). Figure 1 shows the geographical location of CRAF, which is centered at 24.0° N and 120.5° E.

Choshui River is the longest river in Taiwan. The sediments in CRAF originate from rock formations in the the river's upstream watershed, including slate, metamorphic quartzite, shale, sandstone, and mudstone (Fig. 2). Sediment loads composed of weathered rock fragments of different sizes gradually settled on the riverbed, floodplain, and seabed to form CRAF. The head of CRAF contains mainly gravel

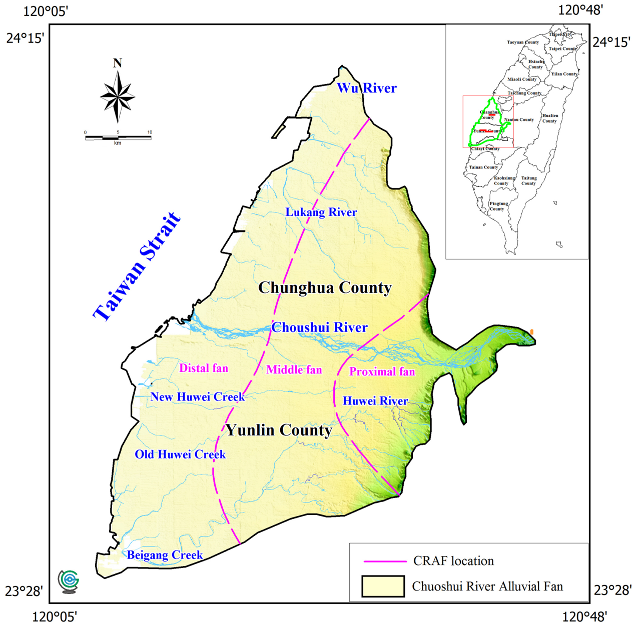

Figure 1. Geographical location of Choushui River Alluvial Fan (CRAF).

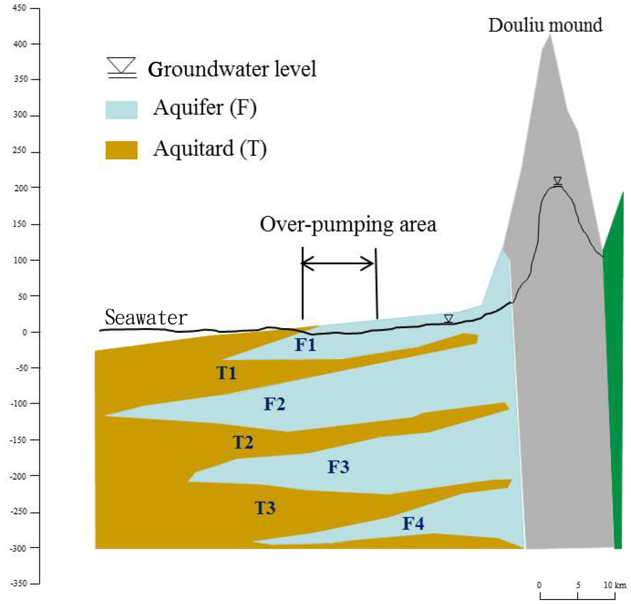

Figure 2. Geological settings of Choshui River Alluvial Fan (modified from Central Geological Survey of Taiwan, http://www.moeacgs.gov.tw/, last access: December 2019).

and coarse sand, and theproximal CRAF is a delta covered by fine sand. Because the upstream watershed area of Choshui River is wide and infiltrative, surface water in the head of the fan penetrates the ground to recharge the sub-surface aquifers over CRAF.

According to the statistics of Water Resource Agency of Taiwan, the extracted groundwater in Yunlin is 94 metric tons per day, and is 305 million tons per year. Without enough recharge, the withdrawal of groundwater can decrease the water level and consequently reduce the porous pressure and increase the effective stress, inevitably leading to land subsidence. The Taiwan High Speed Rail (THSR) passes through Yunlin, where subsidence poses a serious threat to its operation (Hung et al., 2011).

2 Synergy of monitoring sensors

In order to investigate the mechanism of land subsidence in central Taiwan, a multi-sensor monitoring system is installed. The system includes InSAR, GPS, leveling, multi-layer compaction monitoring well and Piezometer. Figure 3 shows a conceptual picture of the multi-sensor monitoring system. These sensors complement each other in spatial and temporal resolutions, and the results from these sensors can be compared for validation of the observed land subsidence. With a good spatial correlation and proper environmental corrections for Sentinel images, the method of Small Baseline Subset Differential (SBAS) will deliver areal vertical displacements accurate to few cm at a 25 m spatial resolution and at a time scale equivalent to the satellite repeat period. At the continuous GPS stations, the accuracy of vertical displacements is about 1 cm from the daily solutions. With precision levels and adequate correction models, leveling can deliver point-wise vertical displacements accurate to few mm at the leveling benchmarks. Figure 4 shows the distributions of leveling networks, continuously operating reference Stations (CORS) of GPS, groundwater monitoring wells and multi-layer compaction monitoring wells used in this paper.

In this study, leveling and InSAR results were used to detect the land subsidence area and calculate land subsidence rate in CRAF. In the center of the bowl-shaped subsidence area, the data from the CORS GPS stations and multi-layer compaction monitoring wells were used to analyze the mechanism of land subsidence.

3 Monitoring result of CRAF

3.1 Leveling

The length of the leveling network in the CRAF monitoring system is 1000 km (Fig. 4). The accuracy requirement for the leveling is a $3\sqrt{K}$ mm misclosure in any double run, where K is the distance between two neighboring benchmarks in km. At each leveling setup, the distances to the foresight and back sight were measured by an electronic distance measurement (EDM) device to ensure the two are nearly identical. Corrections for collimation error, atmospheric refraction and the earth's curvature were applied to the differential heights. Because the cumulative differences between foresight and backsight distances do not exceed 10 m, residual

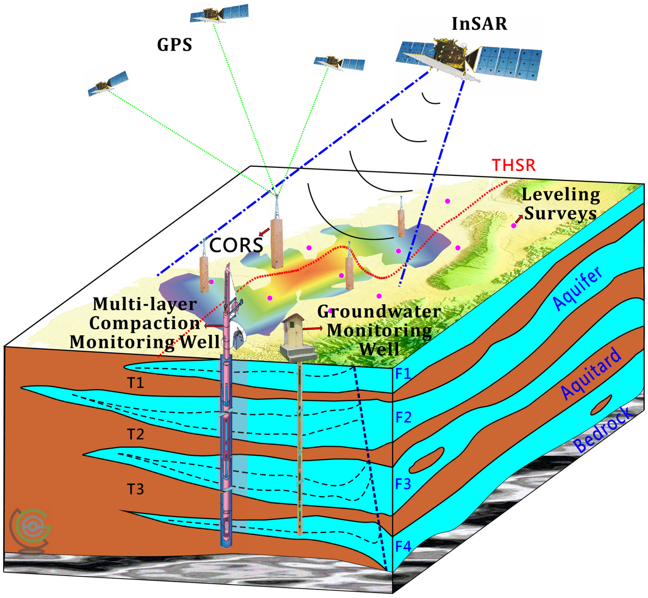

Figure 3. A conceptual picture of the multi-sensor land subsidence monitoring system in central Taiwan.

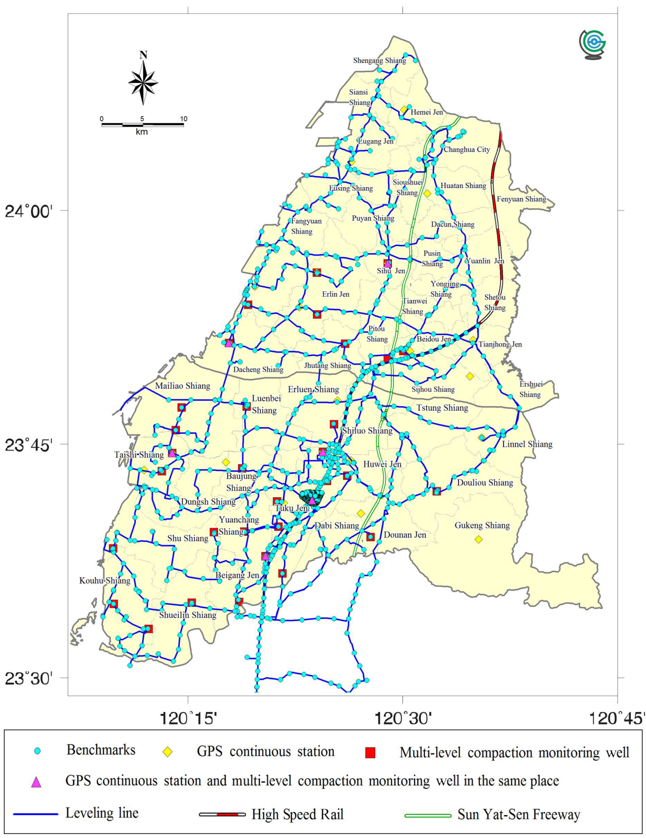

Figure 4. Distributions of leveling benchmarks, monitoring wells and CORS GPS stations in CRAF, the names of townships in Yunlin County and Changhua County are shown here.

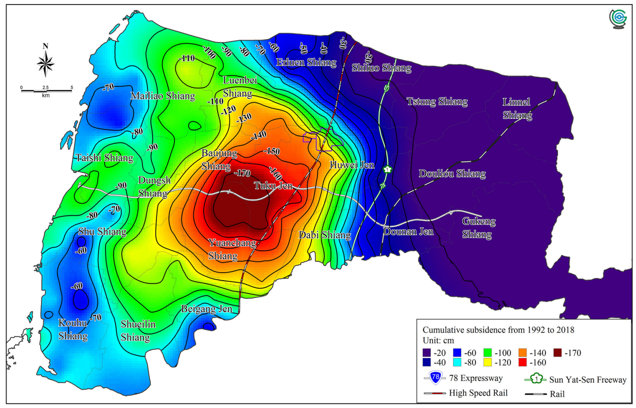

Figure 5. Cumulative subsidence derived from leveling over 1992–2018.

collimation errors, the earth's curvature and atmospheric effects were negligible. Figure 5 shows the contours of cumulative subsidence based on the interpolations using Kriging. In the past two decades, the maximum cumulative subsidence is over 170 cm and the contours of subsidence show a basin-like pattern centering at Huwei, Tuku, and Yuanchang Townships. THSR nearly passes through the center of this basin (Fig. 5), and it would have a major safety concern resulting from the subsidence.

3.2 Continuously Operating Reference Stations based on GPS

The GPS network used in the study (Fig. 6) consists of 50 GPS stations. The Bernese software (Version 5.2), developed by Bern University, was used to compute the horizontal and vertical coordinates of the stations using an automatic data processing procedure. This procedure was used to establish a cloud GPS early warning system for surface deformation, which can show ongoing land subsidence values in central Taiwan at a short latency. The system was established on the Amazon Web Services (AWS), which receives the GPS measurements from the GPS stations to perform coordinate computations, analyse coordinate changes and store the results using a highly automatic procedure. The final graphic results of land subsidence are broadcasted automatically through the internet for early warning. This warning system takes advantage of the internet-based cloud service for a large-scaled monitoring of ongoing land subsidence in central Taiwan.

The GPS-derived vertical displacement rates in Fig. 6 (from January 2018 to December 2018) indicate that a section of THSR passes through the main subsidence area in Yunlin County, and this is consistent with the result in Fig. 5. The major subsidence in Yunlin occurs from February to May during the dry season of Taiwan, followed by October. The major land subsidence (February–May) concurred with the 1st rice plantation in central Taiwan, when the rainfall

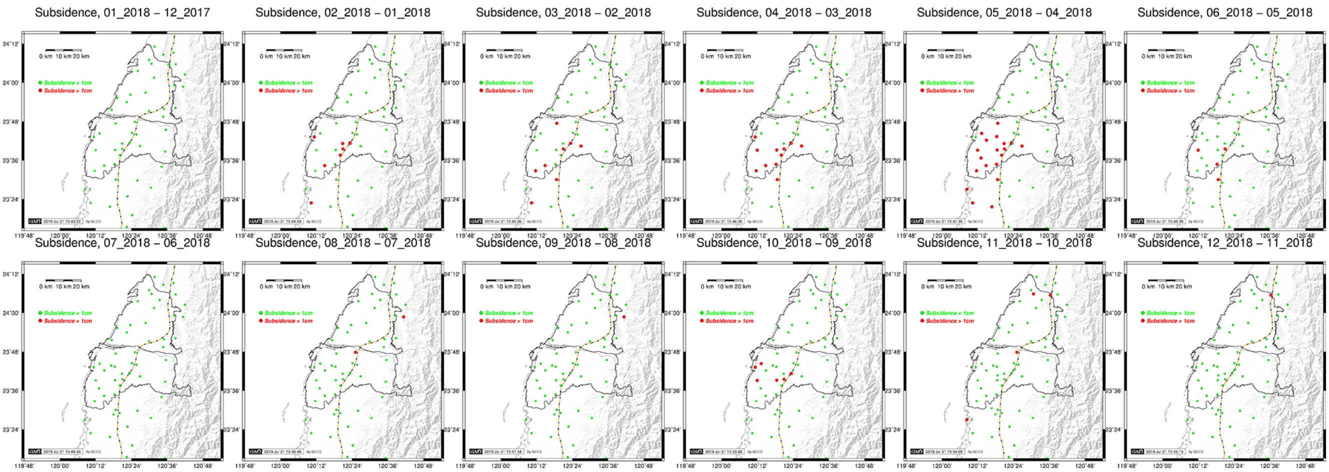

Figure 6. Distributions of continuous GPS stations in CRAF and vertical displacement rates from GPS over January 2018–December 2018.

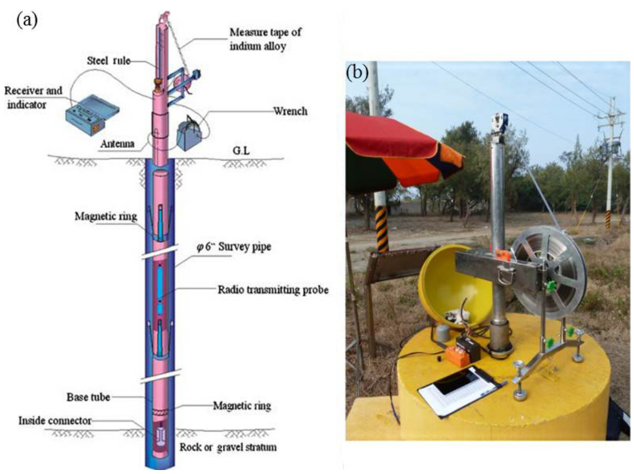

Figure 7. Sample pictures of a multi-layer compaction monitoring well.

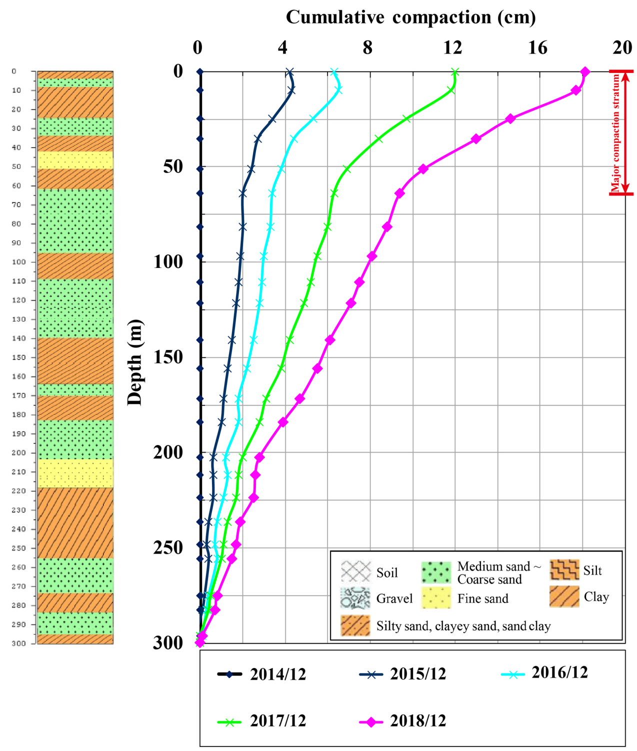

Figure 8. Layers of sediments (column on the left) and cumulative compactions from 2014 to 2018 at STES.

was the least and the plantation area was the largest. During the wet season (June to September), land subsidence here is less significant thanks to relatively large rainfall and small amount of groundwater extraction.

3.3 Multi-layer compaction monitoring well

As mentioned in Sect. 1, the subsurface deposits in the aquifer system of CRAF are heterogeneous, with different hydraulic and mechanical properties across the different layers of deposits. In order to well understand the mechanism of subsidence seen in Figs. 5 and 6, multi-layer compaction monitoring wells (Hung et al., 2012) were installed to measure compactions at different stratigraphic intervals within the aquifer system (Fig. 7).

A multi-layer compaction monitoring well is able to measure the depths of magnetic rings with respect to the bottom of the well (300 m depth) at a mm accuracy, which are then used to determine the depth variations at all the ring locations. That is, the difference between the depths measured at two successive epochs at the same ring is the compaction between the two epochs occurring in the stratigraphic section of the ring . The total compaction is the sum of the compactions at all rings. In general, 20 to 26 magnetic rings are anchored in in a well, depending on the stratigraphic types determined from drilling data near the well. The depths of the

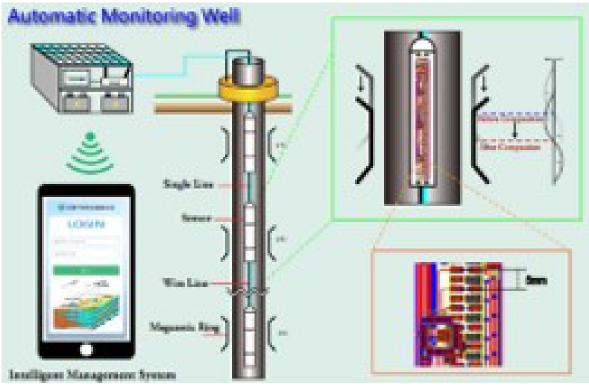

Figure 9. Automatic Multi-layer Compaction Monitoring Well.

rings are measured at a one-month interval. The variations in the ring depths at a well are accurate to 1 mm and the depth measurements are stable (Hung et al., 2012). Currently, we have installed 34 multi-layer compaction monitoring wells in CRAF (Fig. 4).

Figure 8 shows the cumulative compactions from 2014 to 2018 at the STES monitoring well, located in the most severe subsidence area along the rail of THSR. The aquifers near STES contains highly compressible sand and clay in alternations, resulting in the major and the secondary compactions at depths 0–60 m and 60–200 m, respectively. The compactions at different strata of a monitoring well like STES can be used to infer the source of the main groundwater use. For example, if a major compaction over a shallow stratum indicates that the source of the groundwater use is agriculture, for which shallow groundwater is preferred for concerns of energy consumption. In contrast, a major deep-aquifer compaction indicates potential sources from municipal and industrial groundwater uses. As such, measurements from a compaction monitoring well can be used to detect the sources of major compactions, thereby mitigating the problems causing the compactions (land subsidence).

In 2019, we developed a new automatic system to collect data at a multi-layer compaction well (Fig. 9). The new system consists of 36 sensors that can automatically detect the magnetic forces every 10 min from the anchored magnetic rings in the well. The system then transforms the forces to the depths of the rings to calculate the compactions at the rings. Using the IoT technology, we transmit the compaction time series to a control center for an intelligent monitoring of land subsidence. In addition, we installed this IoT device at each of the groundwater monitoring stations in central Taiwan to transmit groundwater levels every 10 min to the control center for real-time monitoring of groundwater use. We used the methods of FFT and wavelet analyses to detect the frequency and amplitude of groundwater withdrawals, which help to identify the timing and purpose of ground-water pumping (Fig. 10). Our analyses show that daytime pumping is mostly for agriculture use, while nighttime pumping is for industrial

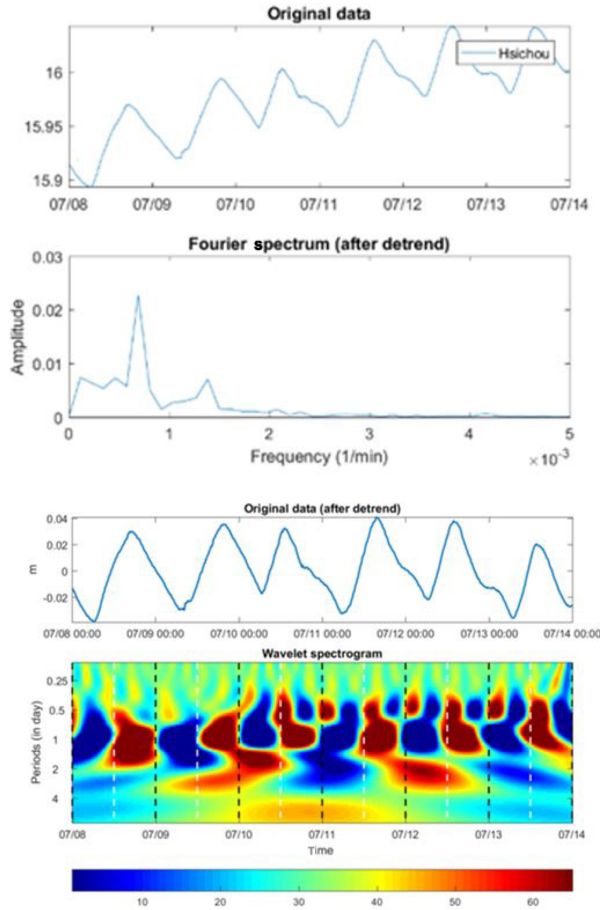

Figure 10. Groundwater levels transmitted by the IOT (top two rows) and their Fourier spectrum (left bottom) and time-frequency spectrum (right bottom).

use. Using this intelligent IoT monitoring equipment and a big-data processing method, we can monitor land subsidence in real time and act to mitigate it.

3.4 Areal subsidence by Multi Temporal InSAR (MT-InSAR)

In the past decades, synthetic aperture radar interferometry (InSAR) has been proved to be a powerful and effective geodetic technique for measuring surface deformation. InSAR can produce subsidence rates with high spatial resolutions and sub-centimeter accuracy. However, changes in surface attributes and variations in water vapor stratification between image acquisition times can cause spatial decorrelations in conventional SAR interferometry can cause errors in deformation measurements. Such errors in DInSAR may be mitigated by using the multi-temporal InSAR (MT-InSAR) technique. The InSAR literature shows that three MT-InSAR methods have been used to monitor land subsidence in Taiwan, namely the methods of persistent scatterers InSAR (PSI) (Hooper et al., 2004), Small Baseline Subset

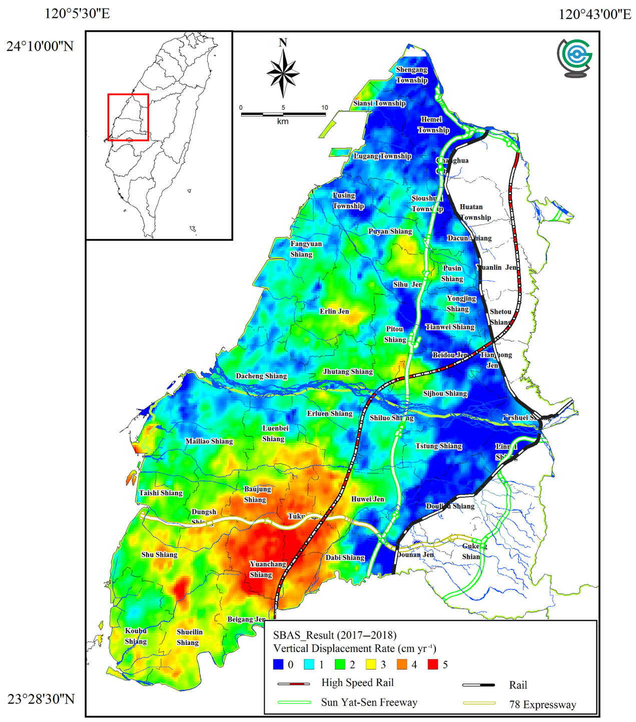

Figure 11. Vertical displacement rate from SBAS over 2017–2018.

Differential (SBAS) (Berardino et al., 2002) and temporarily coherence point InSAR (TCPInSAR) (Zhang et al., 2011).

In this paper, we used the SBAS method to determine surface deformations in CRAF from 2017 to 2018, which were then compared with the deformations from precise leveling. The pixel density over CRAF from SBAS is 89 pixels km^{-2}, compared to 0.2 points km^{-2} in the leveling network. The vertical displacements inferred from SBAS are consistent with those from leveling to 8 mm yr^{-1} (RMS). Furthermore, for a data fusion we computed a smooth correction surface for the SBAS result using the differences between the leveling and InSAR displacements (Hung et al., 2011). Figure 11 shows the vertical displacement rates after the data fusion from 2017 to 2018.

The deformation pattern in Figure 11 is in good agreement with the pattern from leveling. The major subsidence areas are located western of Sun Yat-Sen Freeway, e.g., in the middle fan and distal fan of CRAF (Fig. 1). The combined displacement field is more representative of the overall deformation characteristics than the SBAS-only or the leveling-only field, providing more land subsidence information for to better assess the impact of land subsidence over CRAF.

4 Discussion and conclusion

The long-term land subsidence in central Taiwan can damage infrastructure such as THSR and threaten lives. The multi-sensor system developed in this paper, including GPS, MT-InSAR, Leveling, monitoring well, and groundwater well, can effectively monitor such land subsidence from space, ground, and underground. This system collects subsidence data for understanding the magnitude and major sources of groundwater uses in shallow and deep aquifers, which can be used for decision making in industrial developments. The result from the system can help to reduce the rate and area of land subsidence. This system will be enhanced by extending the monitoring area and using an improved automation. About 400 GPS CORSs around Taiwan will be included in the system enhancement to determine three dimensional surface deformations. Combining deformations from InSAR, GPS, and leveling allow to effectively determine the space-time evolutions of land subsidence. The Internet of Things (IoT) technology developed in this paper allows to control and manage the monitoring sensors for intelligent monitoring of land subsidence.

Data availability. In this study, the continuous GPS data, leveling, multi-layer compaction monitoring well and groundwater data are provided by Water Resource Agency (WRA), Dept of Economics, Taiwan, R.O.C.

Author contributions. WCH produced the leveling, GPS, multi-layer compaction monitoring well and InSAR data, developed the automatic multi-layer compaction monitoring well system, drafted and revised the manuscript. YAC prepared the Sentinel-1A data, produced InSAR and the multi-layer compaction monitoring well data and revised the manuscript. CH provided the professional reference suggestion and revised the manuscript. All authors read and approved the final manuscript.

Competing interests. The authors declare that they have no conflict of interest.

Special issue statement. This article is part of the special issue "TISOLS: the Tenth International Symposium On Land Subsidence – living with subsidence". It is a result of the Tenth International Symposium on Land Subsidence, Delft, the Netherlands, 17–21 May 2021.

Acknowledgements. This study is supported by Water Resource Agency, Dept of Economics, Taiwan, R.O.C.

Financial support. This research has been supported by the Water Resource Agency (project no. MOEAWRA1080322).

References

Berardino, P., Fornaro, G., Lanari, R., and Sansosti, E.: A new algorithm for surface deformation monitoring based on small baseline differential SAR interferograms, IEEE Trans. Geosci. Remote Sens., 40, 2375–2383, 2002.

Hooper, A., Zebker, H., Segall, P., and Kampes, B.: A new method for measuring deformation on volcanoes and other natural terrains using InSAR persistent scatterers, Geophys. Res. Lett., 31, L23611, https://doi.org/10.1029/2004GL021737, 2004.

Hung, W.-C., Hwang, C., Chen, Y.-A., Chang, C.-P., Yen, J.-Y., Hooper, A., and Yang, C.-Y.: Surface deformation from persistent scatterers SAR interferometry and fusion with leveling data: A case study over the Choushui River Alluvial Fan, Taiwan, Remote Sens. Environ., 115, 957–967, 2011.

Hung, W.-C., Hwang, C., Liou, J.-C., Lin, Y.-S., and Yang, H.-L.: Modeling aquifer-system compaction and predicting land subsidence in central Taiwan, Eng. Geol., 147, 78–90, 2012.

Tomás, R., Herrera, G., Delgado, J., Lopez-Sanchez, J. M., Mallorquí, J. J., and Mulas, J.: A ground subsidence study based on DInSAR data: Calibration of soil parameters and subsidence prediction in Murcia City (Spain), Environ. Geol., 111, 19–30, 2010.

Tosi, L., Teatini, P., Carbognin, L., and Frankenfield, J.: A new project to monitor land subsidence in the northern Venice coastland (Italy), Environ. Geol., 52, 889–898, 2007.

Zhang, L., Ding, X., and Lu, Z.: Ground settlement monitoring based on temporarily coherent points between two SAR acquisitions, ISPRS J. Photogramm. Remote Sens., 66, 146–152, 2011.

Insights into increasing land subsidence along Nigeria's Gulf coast

Femi Emmanuel Ikuemonisan[1,2,*], Philip S.J. Minderhoud[3,4,5], Leon Hauser[6], Vitalis Chidi Ozebo[1], Roberta Boni[7], Claudia Zoccarato[4], Marie-Noëlle Woillez[8], Pietro Teatini[4]

1 Department of Physics (Geophysics Research Group), University of Lagos, Nigeria
2 School of Pre-Degree Studies (Physics Unit), Lagos State University, Lagos, Nigeria *Correspondence to Femi Ikuemonisan (femi.ik@yahoo.com),
3 Soil Geography and Landscape Group, Wageningen University, Wageningen, The Netherlands,
4 Department of Civil, Environmental and Architectural Engineering, University of Padova, Padova, Italy,
5 Department of Subsurface and Groundwater Systems, Deltares Research Institute, Utrecht, The Netherlands
6 Leiden University (check), Leiden, The Netherlands,
7 University of Urbino, Urbino, Italy,
8 French Development Agency (AFD), Paris, France

Session: Measuring and Monitoring of land Subsidence
Focus: Coastal areas

Abstract

Land subsidence is a threat to environmental sustainability and can pose greater dangers with a proportionate rise in bordering sea levels. Nigerian low-lying coastal region and the various economic activities around the coast are vulnerable to rising sea level because of global warming. However, no existing study has examined sea-level rise combined with land subsidence. This study reviews available literature on land subsidence and consequential relative sea-level rise along Nigerian coastlines and identifies research gaps. Subsidence occurs, at least, in four Nigerian coastal cities – Lagos, Port Harcourt, Uyo, and Warri. The highest observed subsidence (up to 520 mm/year) is found in the Harcourt area, which is likely due to continued groundwater pumping and oil and gas extraction.

Keywords: Subsidence; Relative sea-level rise; InSAR; Nigeria; Gulf of Guinea; Port Harcourt

Introduction

Nigeria is bounded to the south by the Atlantic Ocean and has the longest coast among the countries in the Gulf of Guinea, with an approximate length of 853 km. The country has one of the largest populations in the World, with an estimated 212 million inhabitants and a projected growth rate of 3.1% per year (United Nations, 2019). With this projection, Nigeria will become the third largest country by population within the next three decades. Most of country's industries are situated along the Gulf of Guinea, including seaports and harbors a significant number of facilities to develop oil fields. This has led to a dramatic increase in population. Consequently, the rate of groundwater pumping and swampland reclamation, which are known causes of land subsistence worldwide, are accelerating dramatically.

Subsidence is a major environmental issue impacting coastal cities of the World and threatening environmental sustainability. Efficient modelling of RSLR, i.e. the combined impact of sea-level rise (SLR) and land subsidence, is a critical step to mitigate the risk of RSLR-induced hazards in coastal cities, as continuous monitoring and observation are cost-prohibitive and time-consuming. Both monitoring and modelling raise awareness for environmental authorities and residents about the hazards of the contribution of land subsidence to rising sea levels. In addition, modelling can provide significant insights into future trends (Shirzaei et al., 2021).

This study synthesizes previous topical research work relating to land subsidence evolution and sea-level change in the Nigerian low-lying coast to identify knowledge gaps and for further studies. In addition, this study reveals recent subsidence trends in the Port Harcourt area, which is one of the areas where the highest subsidence rates have been estimated over the last years using recently acquired Sentinel-1 data.

Study area and approach

Nigeria coastline runs along Africa west coast in the Gulf of Guinea. The coast is situated in a low-lying elevation between latitude 4°10′–6°20′ N and longitude 2°45′–8°32 E. The elevation map of the study area is shown in Figure 1. The Nigeria low-lying coast can be classified as the western coast and the eastern coast, spanning eight southern Nigerian States and is host to several coastal cities. These include Lagos, one of the world most rapidly expanding megacities, Warri and Port Harcourt, located in the Niger Delta region and home to Nigeria's oil and gas sector. Across the Niger Delta region, there are over 900 oil and gas field establishments in various towns and communities, with nearly 800 operational oil wells. Available literature is reviewed following the five-stage review framework by Arksey and O'Malley (2005). For the Port Harcourt case study, 217 Sentinel-1 images (Track 30, Ascending orbit) were processed on the Geohazard Thematic Exploitation Platform (Geohazard TEP) using the Parallel Small BAseline Subset (P-SBAS) algorithm (Casu et al., 2014) to generate a map of average land displacement and displacement time series.

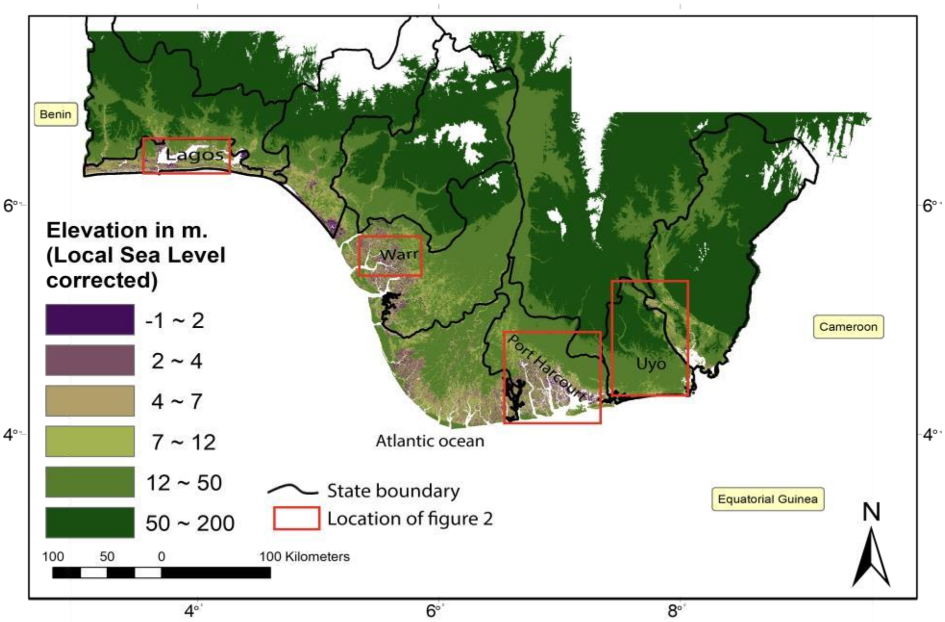

Figure 1 Elevation map of the study area

Results and discussions

The literature review yielded few studies reporting on land subsidence for four major areas along the Nigerian low-lying coast: Port Harcourt, Lagos, Warri, and Uyo, see Figures 1 for their location. Figure 2 shows the spatial distribution of land subsidence in these areas and Table 1 presents a summary on the temporal coverage and methods used to monitor land subsidence.

Land subsidence in the Port Harcourt area

The Port Harcourt area experiences the highest land subsidence rates presently known along the Nigerian coast (Figure 2a). Land subsidence rates at selected oil well locations in this area accelerated dramatically from 33 mm/year in 1982 to 550 mm/year in 2000 (Abija et al., 2020). In a related study by Uko et al. (2018), land subsidence in the Port Harcourt area varied between 67 to 200 mm/year at some levelling sites in 2018. The observed high subsidence rate is attributed to reservoir compaction caused by hydrocarbon production in the area. The compaction of onshore oil fields is predicted to reach staggering 15.5 m at near optimal reservoir pressure drawdown, with a possibility to extend significant land subsidence toward the coastline (Abia & Abam, 2022). As shown in Figure 1, the elevation of this area is approximately 4 m above msl.

S/N	Location	Temporal coverage	Method: data	Max. Subsidence rate (mm/year)	References
1	Lagos	2002 – 2011	InSAR: Envisat-ASAR	7.0	Mahmud et al. (2016)
		2002 – 2019	InSAR: Sentinel-1, TerraSAR-X, COSMOSkyMed	9.5	Cian et al. (2019)
		2015 – 2019	InSAR: Sentinel-1	94.0	Ikuemonisan et al. (2021)
2	Port Harcourt area	1988 – 2003	Analytical modelling, Leveling, GPS	520.0 (expected estimate) 200	(Abia & Abam, 2022) Uko et al. (2018) Uko & Otugo (2016)
3	Uyo area	-	Modelling: Groundwater extraction	Very High (qualified in classes)	Udoh & Udofia (2014)
4	Warri	2006 - 2010	InSAR: Envisat-ASAR	5.0	Mahmud et al. (2016)

Table 1 Summary of land subsidence observations in Nigerian coastal cities

Land subsidence in the Lagos area

Various methods and satellite data have been deployed to monitor subsidence in Lagos. The maximum known subsidence rate as estimated by InSAR in the Lagos area is 94 mm/year, and is predicted to increase by over 20% in the coming years partly due to groundwater over-exploitation (Ikuemonisan et al., 2021). However, none of the methodologies provides exactly the same results. The observations cover consecutive time periods and show an accelerating trend towards present. InSAR-based study shows high subsidence rates for the southern part of Lagos, notably the areas along the Atlantic Ocean coast and the Lagos lagoons. As shown in the Figure 2b, approximately 340 km^2 of Lagos experiences severe subsidence, about 68% of the city's area. Major subsidence bowls developed across the Lagos causing frequent flooding as water inundates subsiding areas when precipitation exceeds infiltration.

Although various factors have been attributed to cause land subsidence in Lagos, a linear regression analysis between subsidence and groundwater level change (as estimated by Gravity Recovery and Climate Experiment (GRACE)) indicates a fair correlation between the two parameters (Ikuemonisan et al., 2021). The statistical correlation coefficient is in the order of ≈ 0.45, suggesting that groundwater extraction is one of the causes of land subsidence in Lagos. It is worth mentioning that GRACE provides coarse resolution of groundwater level change. Other drivers of land subsidence in this area may include natural compaction of unconsolidated sediments and compaction of the reclaimed wetland due to the weight of the overburden structure, as Lagos is predominantly set on a sedimentary formation.

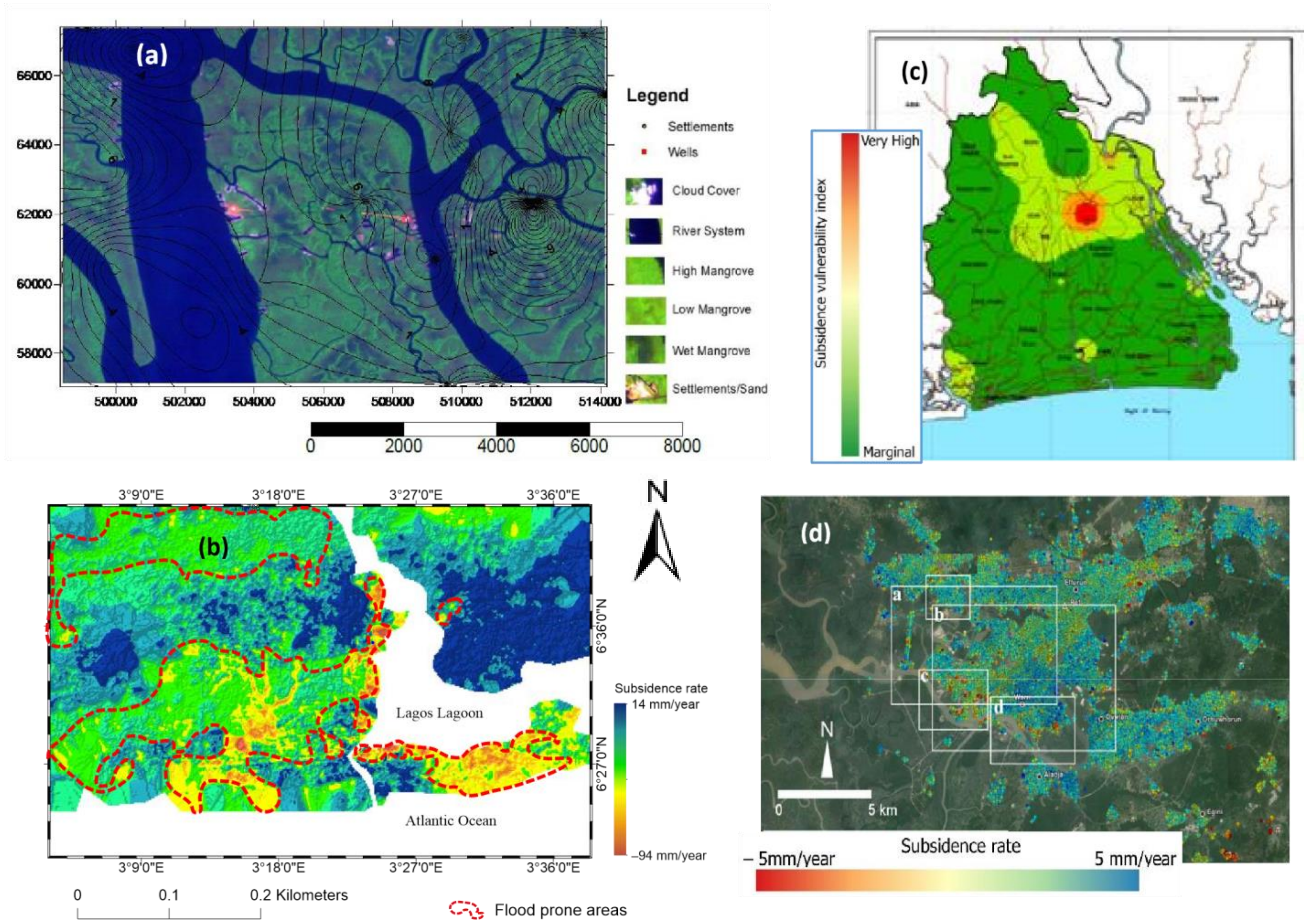

Figure 2 Spatial distribution of land subsidence in Nigerian low-lying coasts: (a) subsidence rate over baseline map of 1988 in the Port Harcourt area, southeast Niger Delta [After Uko et al., 2016]; (b) land displacement in Lagos as estimated by Sentinel-1 satellite between 2015 and 2020, showing subsidence bowls [Modified after Ikuemonisan et al., 2021]; (c) land subsidence in the Uyo area [After Udoh & Udofia (2014); (d) land displacement in the Warri area as estimated by Envisat-ASAR (2002 –2011) [After Mahmud et al., 2016].

Land subsidence in the Warri and Uyo areas

Previous studies also focused on land subsidence in the Warri and Uyo areas. Time series analysis of InSAR images acquired over Warri between 2006 and 2010 indicates that average subsidence amounts 5 mm/year. Subsidence in the area can predominantly be ascribed to excessive groundwater pumping and oil and gas extraction (Mahmud et al., 2016). In the Uyo area, land subsidence vulnerability has been assessed by Udoh and Udofia (2014) using water extraction data collected at the scale of the Akwa Ibom State. The study found that the Uyo area, particularly the built-up areas, are mostly vulnerable to land subsidence due to groundwater depletion, as shown in Figures 2(c) and (d).

InSAR study of the Port Harcourt area

Port Harcourt city has progressively grown in population over the last ten years, causing a rapid expansion of physical infrastructure, including high-rise buildings, housing, and industrial estates. In addition, Port Harcourt has a relatively low surface elevation, ranging from 4 m to 7 m (Figure 1). Figure 3 shows the spatial distribution of land subsidence as estimated by InSAR in the Port Harcourt area. The Sentinel-1 spatiotemporal analysis showed widespread coastal subsidence in the area. The maximum subsidence rate projected in the vertical axis is 50 mm/year. In general, subsidence rates range in coastal regions from 50 mm/year above the oil production areas to 26 mm/year in industrial areas. The southern coastal areas of Port Harcourt city, Onne, which is home to a major Nigerian seaport with adjoining oil fields has the highest subsidence rate. The displacement time series for the Port Harcourt area is depicted in Figure 3(b). The largest cumulative subsidence amounted to 370 mm over the last 7 years. Calibration of InSAR results would require the availability of independent absolute measurements, generally made available through GNSS stations. Only one station (RUST) was located in the study area and the record was processed at the Nevada Geodetic Laboratory. Unfortunately, the recorded time series is short (from 2011 to 2013) with two considerable gaps, making it impossible to derive a reliable trend of land movement.

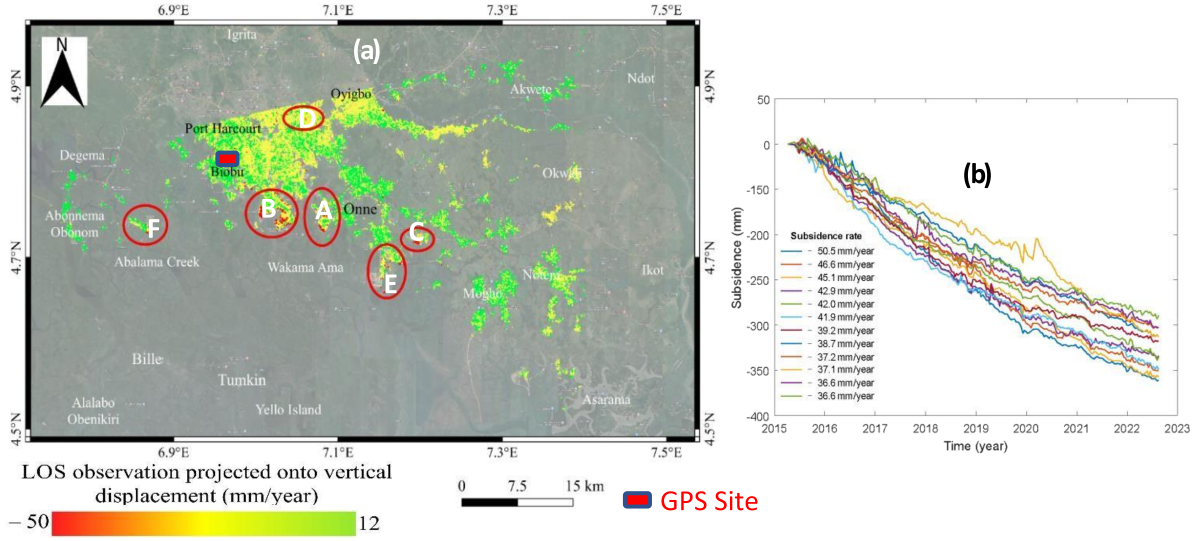

Figure 3 Spatial and temporal trend of land displacement in the Pot Harcourt area: (a) velocities based on Sentinel-1 observation (most subsided areas are highlighted with red ellipses). Features are underlain by a Google Earth map; (b) Displacement time series of the ten most subsided areas. Time series with subsidence rates of 50.5 mm/year and 46.6 mm/year belong to the ellipse A; time series with subsidence rates of 45.1 mm/year, 42.9 mm/year, and 42.0 mm/year belong to the ellipse B; time series with subsidence rates of 41.9 mm/year and 39.2 mm/year belong to the ellipse C; time series with subsidence rates of 38.7 mm/year belong to the ellipse D; time series with subsidence rates of 37.2 mm/year, 37.1 mm/year, and 36.6 mm/year belong to the ellipse E; time series for the ellipse F also have a subsidence rate of 36.6 mm/year.

Knowledge gaps and future research

A few previous studies revealed widespread land subsidence in parts of Nigeria's lowly coastal cities, but no detailed study provides useful information on the contribution of land subsidence to rising sea levels or the future trend of RSLR. The lack of operational GNSS stations to calibrate and validate InSAR measurements makes the entire InSAR outcome somewhat uncertain. Another significant knowledge gap is the lack of records of groundwater withdrawals and piezometric evolution over the last decades, which are necessary for efficient quantification of the role of groundwater depletion on land subsidence. For accurate local SLR projection and RSLR estimation, up-to-date observational studies are essential to assess the local sea-level changes and continuous piezometric measurements. Combined measurements of the recent sea-level changes with vertical land motion and piezometric data will significantly improve our capability to predict land subsidence and RSLR over the next decades.

Funding

This project is funded by the France Development Agency (AFD).

The Sentinel-1 datasets used for the Port Harcourt case study were processed on the Geohazard Thematic Exploitation Platform (Geohazard-TEP), supported by the European Space Agency (ESA) Network of Resources Initiative (NoR)''

References

Abija, F. & Abam, T. (2022). Predicting Ground Subsidence Due to Long Term Oil/Gas Production in A Niger Delta Basin, Nigeria: Implications for CO2 EOR and Geosequestration, (Preprint) https://doi.org/10.21203/rs.3.rs-357959/v1

Abija, F.A. Abam, T.K.S. Teme, S.C. Eze, C.L, (2020) Relative Sea Level Rise, Coastline Variability and Coastal Erosion in the Niger Delta, Nigeria: Implications for Climate Change Adaptation and Coastal Zone Management. J Earth Sci Clim Change 2020 11:9.

Casu, F., Elefante, E., Imperatore, P., Zinno, I., Manunta, M., De Luca, C., Lanari, R. (2014) SBAS-DInSAR Parallel Processing for Deformation Time Series Computation. IEEE JSTARS, doi: 10.1109/JSTARS.2014.2322671

Ikuemonisan, F. E., Ozebo, V. C., & Olatinsu, O. B. (2021). Investigation of Sentinel-1-derived land subsidence using wavelet tools and triple exponential smoothing algorithm in Lagos, Nigeria. *Environmental Earth Sciences*, 80(21). https://doi.org/10.1007/s12665-021-10020-1.

Mahmud, M. U., Yakubu, T. A., Adewuyi, T. O., Sousa, J. J., Ruiz-Armenteros, A. M., Bakoň, M., … Perissin, D. (2016). Subsidence monitoring in the coastal region of Nigeria using multi temporal interferometric synthetic aperture radar (MT-Insar). *In European Space Agency, (Special Publication)* ESA SP (Vol. SP-740). European Space Agency.

Shirzaei, M., Freymueller, J., Törnqvist, T. E., Galloway, D. L., Dura, T., & Minderhoud, P. S. J. (2020). Measuring, modelling and projecting coastal land subsidence. Nature Reviews Earth & Environment, 2(1), 40–58. https://doi.org/10.1038/s43017-020-00115-x

Udoh, F., & Udofia, E. (2014). Land Subsidence Monitoring Using Geographic Information System (GIS) Techniques in Akwa Ibom State, Nigeria. *Current World Environment Journal*, 9(1), 1–6. https://doi.org/10.12944/cwe.9.1.01.

Uko, E. D., Famuyibo, D. A., & Okiongbo, K. (2018). Estimation of Land Surface Subsidence Induced by Hydrocarbon Production in the Niger Delta, Nigeria, Using Time-Lapse Orthometric Levelling Data. *SSRN Electronic Journal*. https://doi.org/10.2139/ssrn.3214967.

United Nations, Department of Economic and Social Affairs, Population Division (2019). World Population Prospects 2019: Data Booket. ST/ESA/SER.A/424.

Extended abstract TISOLS:
Quantifying land subsidence due to shallow-depth subsurface processes in the Groningen gas field area- The Netherlands; a new monitoring site

Chayenne Janssen[1] , Hans Middelkoop[1], Esther Stouthamer[1]

1 Departement of Physical Geography, Utrecht University, The Netherlands

Session: Mechanisms and Understanding of land subsidence
Foci: Coastal areas, Delta & Sea Level Rise

Email: c.j.e.janssen@uu.nl

Introduction

Land subsidence due to natural and human induced processes occurs on different time scales and depth intervals. The Groningen gas field area in the northeast of the Netherlands (Fig. 1) experiences considerable land subsidence of up to 60 cm since 1960. This is caused by different drivers operating at shallow subsurface depth (excessive land drainage: upper 15 m), intermediate depth (extraction of groundwater from Pleistocene aquifers: tens to hundreds of meters), and kilometer(s) depth (extraction of hydrocarbons since 1959: reservoir-depth). The negative impacts of land subsidence are manifold, affecting amongst others the built environment, infrastructure and water management. Especially since general land use in this area is agricultural, water levels need to be regulated for favourable conditions which in turn impacts subsurface movements. The design of efficient measures mitigating land subsidence requires quantification of the individual processes that contribute to total (sub)surface movement, as well as the development of reliable techniques for monitoring surface elevation changes at high spatial and temporal resolution.

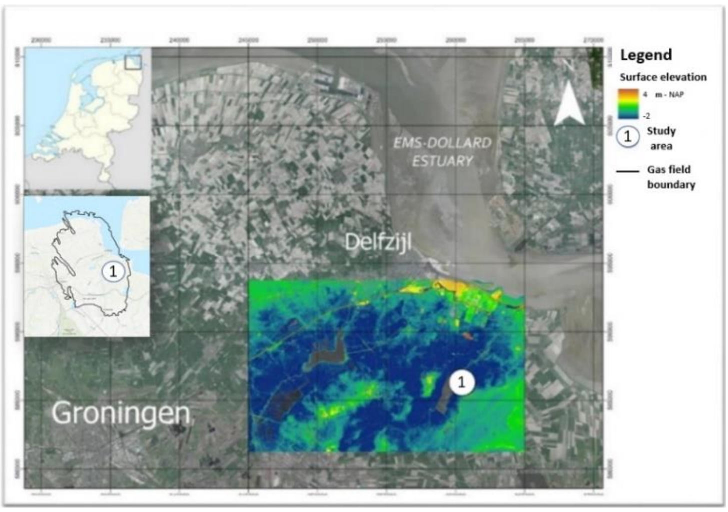

Figure 1 Study area Nieuwolda Groningen, lowly elevated surface within the Groningen gas field area. Coordinates are according to the Dutch national RD-grid (EPSG:28992).

The goal of this research is to quantify the shallow subsurface processes occurring in the Holocene sequence of the Groningen gas field area. The main causes of shallow (sub)surface deformation in the upper 15 meter are initial, primary and secondary compression, oxidation of organic matter and shrinkage and swelling of clay and peat layers (Brouns et al., 2014; van Asselen et al., 2009) (Fig. 2). These processes are driven by changes in internal and exterior stresses mainly caused by loading and changes in phreatic groundwater level. Main boundary conditions determining the vulnerability of the subsurface for these processes and their impact involve subsurface lithology, soil texture, initial porosity, organic matter content and water content (Van Asselen et al., 2009).

In this abstract, two monitoring sites are presented along with preliminary results. The monitoring sites were designed and installed in the area of Nieuwolda (Fig. 1, location 1), in the east of the Groningen gas field area to provide independent, reliable, frequent and precise time series of observed changes in the boundary conditions (such as water content, porosity and organic matter content), and relative vertical distance between several benchmarks, at a location that is expected to show significant temporal variability.

Geological setting and monitoring sites

The (sub)surface of the Groningen gas field area is unique to the Netherlands, in its formation, build-up and post-depositional development. Therefore, two monitoring sites are developed in the town of Nieuwolda. The subsurface lithology for both sites is characterized by alternating, meters thick, Holocene clay (Naaldwijk Fm. – shallow marine/tidal deposits) and peat layers (Nieuwkoop Fm.), positioned on top of the Pleistocene sand layer (Boxtel Fm. – mainly aeolian transported cover sand) that are assumed to be stable with regard to shallow subsurface processes causing (sub)surface movement.

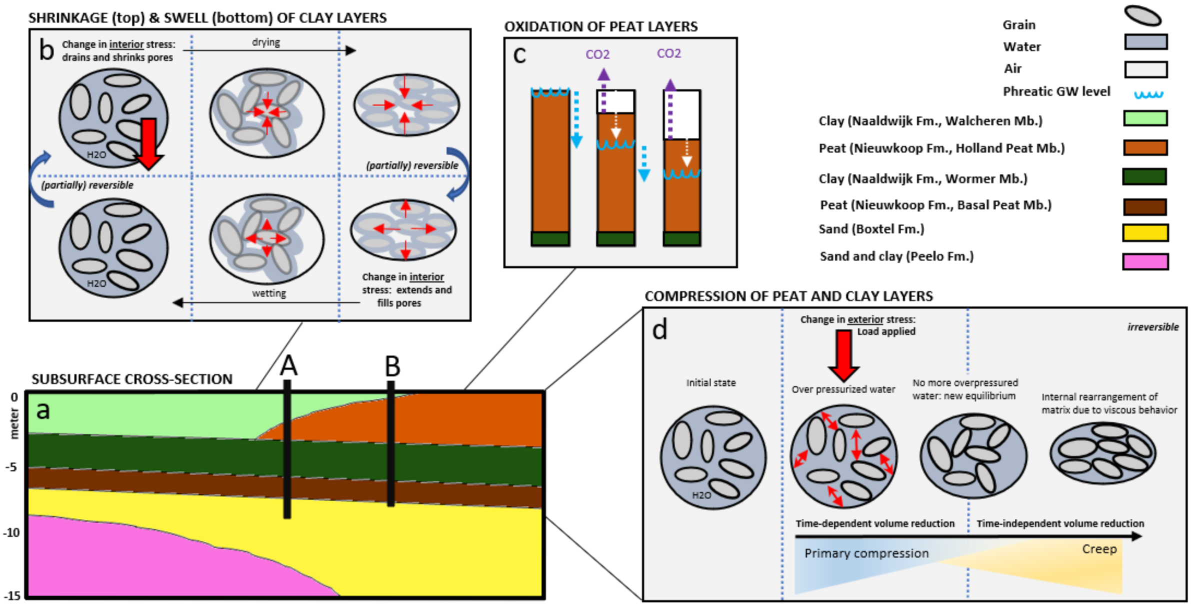

Figure 2 Subsurface processes inducing vertical (sub)surface movement in the upper 15 m of the Holocene sequence. a) Schematic subsurface build-up (approximately 3 km wide), consisting of Holocene and Late Pleistocene deposits, similar to the shallow subsurface of the Groningen gas field area. Location A and B indicate the locations of the surficial clay and peat extensometer. b) Schematic overview of shrinkage and swelling in saturated surficial clay layers induced by changes in interior stresses (red arrows indicate hydraulic stress). c) Schematic overview of lowering of the phreatic groundwater level inducing decomposition of peat layers and subsequent subsidence and CO2 release. d) Schematic overview of compression in peat and clay layers induced by changes in exterior stresses.

The two extensometers were installed penetrating a surficial clay layer (Naaldwijk Fm. – Walcheren Mb.) on top of a peat layer (Nieuwkoop Fm. – Holland Peat Mb.), locally alternated with a clay layer containing numerous plant remains (mainly reed), and a consecutive vertical lithological sequence of a clay layer (Naaldwijk Fm. – Wormer Mb.) on top of a basal peat layer (Nieuwkoop Fm. – Basal Peat), ending in the Pleistocene Boxtel Fm. basement consisting of sand (Fig. 3). The extensometers were designed to document the relative vertical movement of the layers between the anchors in response to changing boundary conditions such as fluctuating groundwater levels. Installation of the extensometers involved several steps and components. At each location, a cone penetration test was performed to determine the initial (t=0) cone resistance for locating the lithological boundaries and the depth of the stable sand layer, followed by the placement of the deepest (reference) anchor into the top of the stable Pleistocene Boxtel Fm. A steel casing was anchored in cement at the bottom of each extensometer borehole along which several (Borros) anchors that were positioned at geohydrological boundaries. The different anchors measure the changes in thickness of the layers between the anchors, with a precision range on millimetre scale (STOWA, 2020).

On extensometer A, several anchors (II, III, IV) were installed within the first two meters beneath the surface. Due to the absence of organic material above the average lowest groundwater level, aerobic oxidation will not occur, and the deformation measured by anchors II and III can only be caused by shrinkage, swell and compression of the clay layer. Additional anchors (IV and V) positioned deeper beneath the surface and the lowest groundwater level will monitor the compression of peat and (organic) clay layers.

Extensometer B, at the site where peat occurs at shallow depth, monitors the combined effect of oxidation of the peat layers above the average lowest groundwater level with anchors II and III, and shrinkage and swelling that occurs in these layers. Since the amount of shrinkage and swelling in peat layers is significantly different compared to shrinkage and swelling of clay layers (Camporese et al., 2006; Oleszczuk et al., 2003) it is important to measure these processes in both a clay (extensometer A) and clay on top of peat (extensometer B) sequence. Furthermore, previous monitoring studies of peatlands throughout the Netherlands showed that peat layers in the saturated zone experience a remarkable amount of deformation (e.g. Van Asselen, 2011; NOBV, 2020). Therefore, anchor IV was placed to monitor the compression of peat in the saturated zone. Anchor V is positioned at the base of the Holocene sequence to monitor the total deformation of the sequence. It is assumed that most deformation between anchor IV and V will occur within the Wormer Mb. of the Naaldwijk Fm., as the basal peat (Nieuwkoop Fm.) has already been mostly compacted.

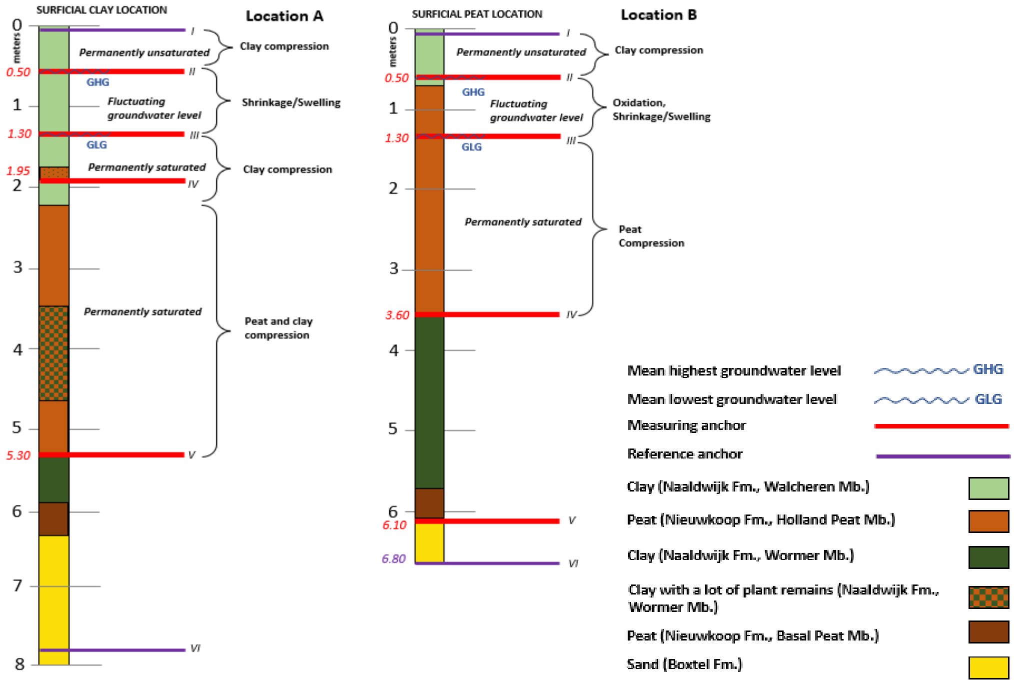

Figure 3 Schematic overview of the lithological build-up and the two extensometer sequences (in meters below the land surface), with their anchor positions and corresponding measuring purposes. The surface level of the surficial clay location is elevated 1.48 m below mean sea level. The surface level of the surficial peat location is elevated 2.40 m below mean sea level.

One of the most prominent boundary conditions that influences the vertical (sub)surface movement processes is phreatic groundwater level fluctuation. To document this, three monitoring wells have been installed for each site, including a 1) phreatic groundwater well at 2 m below the surface near extensometer A with the surficial clay and 1.75 m below the surface near extensometer B where peat occurs at shallow depth (55 cm below surface), 2) a deep groundwater well to monitor hydraulic head, extending into the Pleistocene sand layer founded at a depth of 8 m below surface for location A, and 7 m below surface for location B (first confined aquifer), and 3) a groundwater well in the nearby ditches to monitor the effect of the ditch water level on the measuring sites. Automatic data loggers were installed in all the monitoring wells and extensometers.

First results

The monitoring sites were installed early May 2022. The extensometer measurements and groundwater levels (hydraulic heads shown in the confined aquifer and phreatic groundwater levels in the unconfined aquifer) for both locations over the period of May 5th until July 24th are shown in figure 4. Groundwater levels in general decreased over this period due to a progressively dry weather period with some occasional peaks as a result of precipitation. However, towards the end of the monitoring period, groundwater levels are rising again. Over the same period, the upper four extensometer anchors for location A show an upward trend, describing elevation of the (sub)surface with the exception of the anchor at a depth of 5.30 below surface. For location B a fluctuation in anchor movement is observed with the exception of the anchor nearest to the surface. The surficial anchors are extremely susceptible to events at the surface, such as irrigation, local or temporal loading, and ploughing. Long-term measurements are needed to clarify the elevating trend of the surficial anchors.

The extensometer measurements of the Nieuwolda sites show clear correlations between groundwater fluctuations and anchor movements, although long-term measurements are required to draw more reliable conclusions. However, a short sharp rise in groundwater levels in the order of centimeters, can be correlated to vertical anchor movements in the range of several millimeters as shown for location A for the end of May. Clearly, measurements covering a full year, including the wetter winter period will better reveal the relations between shrinkage, swell, oxidation and compression for both locations, and provide a better understanding of their causing mechanisms and boundary conditions.

Additional quantification devices and modelling

To understand more direct relations between weather conditions, water level management and land use, future additions to the monitoring sites will consist of weather stations, incorporating pluviometers measuring precipitation, radiation monitors, soil moisture measuring devices and thermometers. In addition, transponders will be positioned on both monitoring sites to enable the correlation to InSAR measurements and to work towards improvement of the implementation of shallow (sub)surface processes in the InSAR algorithms.

To quantify shallow subsurface processes over time on a regional scale, we will deploy compression modelling based on the a,b,c isotache method (Den Haan, 1994) and oxidation modelling (based on organic versus mineral content) over the period from 1959 until present to quantify the amount of surface deformation and its net effect due to processes and also specifically water management strategy applied to the Groningen gas field area over time. This enables determining the contribution of these shallow subsurface processes to total land subsidence in this area. For parameter estimation, samples on both sites will be analysed in the lab for organic content and additional lithological properties. The Nieuwolda measurements will serve as validation for these models and quantification at a local scale.

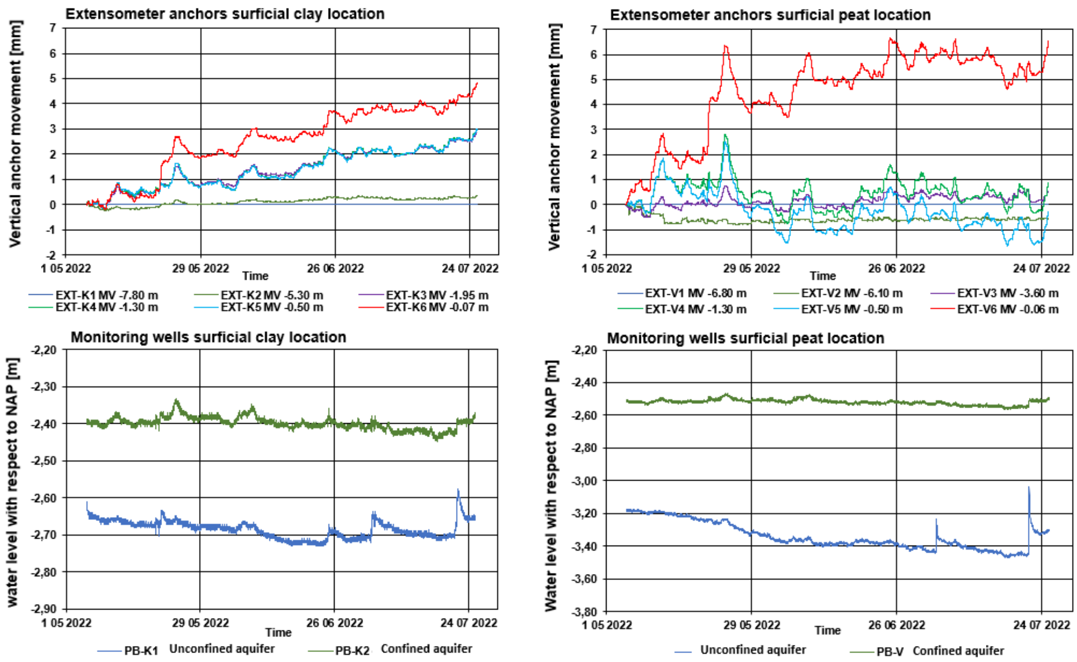

Figure 4 First extensometer results and groundwater level results. Vertical anchor movements in meters are with respect to the original measurement. Anchor positions are with respect to the surface level which is respectively 1.48 m below the mean sea level for location A with surficial clay and 2.40 m below mean sea level for location B with surficial peat.

Conclusion

To quantify the shallow (sub)surface processes occurring in the Groningen gas field area in the northeast of the Netherlands, two measuring sites were developed. The measuring sites govern different lithological build-ups consisting of Holocene clay and peat layers on top of the Pleistocene sand layer, assumed to be stable with regard to shallow subsurface processes resulting in deformation of the (sub)surface. Extensometers were installed at a surficial clay location and at a location with peat occurring at shallow depth, measuring the vertical movement of several anchors at geohydrological boundaries. Additionally, three groundwater monitoring wells were installed on each location consisting of a phreatic groundwater level well, a deeper well reaching into the Pleistocene sand layer for monitoring of the hydraulic heads, and a monitoring well in the nearby ditches to monitor ditch water level.

First order results show correlations between fluctuating groundwater levels and anchor movements. However, yearly measurements are required for reliable conclusions and quantification of the separate processes. Future results in combination with additional measuring devices such as weather station information and InSAR data, will provide more insights into the shallow (sub)surface deformation processes, their response to changing boundary conditions and the effect on the surface of the Groningen gas field area.

Funding

The research presented is part of the DeepNL project 'Monitoring and Modeling the Groningen Subsurface based on integrated Geodesy and Geophysics: improving the space-time dimension' (grantnr. DEEP. NL.2018.052) funded by the Dutch Research Council and NAM.

References

Brouns, K., Eikelboom, T., Jansen, P. C., Janssen, R., Kwakernaak, C., van den Akker, J. J. H., Jos, & Verhoeven, T. A. (n.d.). Spatial Analysis of Soil Subsidence in Peat Meadow Areas in Friesland in Relation to Land and Water Management, Climate Change, and Adaptation. https://doi.org/10.1007/s00267-014-0392-x

Camporese, M., Ferraris, S., Putti, M., Salandin, P., & Teatini, P. (2006). Hydrological modeling in swelling/shrinking peat soils. https://doi.org/10.1029/2005WR004495

Den Haan, E. J. (1994). Vertical compression of soils. http://resolver.tudelft.nl/uuid:b8dc88e0-f400-4d86-9a2e-4e00b68d0472

NOBV (2020). Nationaal Onderzoeksprogramma Broeikasgassen Veenweiden (NOBV) jaarrapportage 2019-2020. 1–171.

Oleszczuk, R., Bohne, K., Szatylowicz, J., Brandyk, T., & Gnatowski, T. (2003). Influence of load on shrinkage behavior of peat soils. *Journal of Plant Nutrition and Soil Science* 166(2):220 – 224 DOI:10.1002/jpln.200390032

Peng, X., & Horn, R. (n.d.). Anisotropic shrinkage and swelling of some organic and inorganic soils. https://doi.org/10.1111/j.1365-2389.2006.00808.x

STOWA, 2020. Deltafact Bodemdaling versie 3.1, 2020. https://www.stowa.nl/deltafacts/ruimtelijke-adaptatie/adaptief-deltamanagement/bodemdaling

Van Asselen, S., Stouthamer, E., & van Asch, T. W. J. (2009). Effects of peat compaction on delta evolution: A review on processes, responses, measuring and modeling. *In Earth-Science Reviews* (Vol. 92, Issues 1–2, pp. 35–51). Elsevier. https://doi.org/10.1016/j.earscirev.2008.11.001

Van Asselen, S. (2011). The contribution of peat compaction to total basin subsidence: Implications for the provision of accommodation space in organic-rich deltas, Basin Res., 23, 239–255, 2011.

Assessment of Subsidence Risk Associated with Aquifer Storage and Recovery in the Coastal Lowlands Aquifer System, Houston, Texas, USA

Van Kelley[1], Michael Turco[2], Neil Deeds[1], Ashley Greuter[2], Chris Canonico[2]

[1]INTERA, Inc., Austin, Texas, 78757, USA
[2]Harris-Galveston Subsidence District, Friendswood, Texas, 77058, USA

Correspondence to: Van Kelley (vkelley@intera.com)

Abstract. In the Houston, Texas region, groundwater use is regulated by the Harris-Galveston Subsidence District (District) because of historical regional subsidence from groundwater development. The District regulates groundwater production in the Coastal Lowlands Aquifer System (CLAS) to mitigate subsidence through the implementation of District Groundwater Regulatory Plan. The District has successfully reduced groundwater pumping as a percent of demand regionally while controlling subsidence through the implementation of alternative water supplies. Aquifer Storage and Recovery (ASR) is an alternative water supply strategy that provides a means to store water underground and increase water supply more cost effectively than traditional storage expansion strategies. Groundwater users in the District are interested in the many potential benefits of ASR as a water supply strategy. Little is known about the potential effects on compaction and land surface subsidence resulting from ASR operations. Recognizing this, the District funded research on the potential subsidence risk associated with ASR. Two hypothetical, though representative, ASR projects were developed and analysed: (1) an industrial ASR project meant to provide water supply during a drought of record (DOR), and (2) a municipal ASR project designed to provide an annual municipal summer peaking water supply. Simulations of groundwater hydraulics and subsidence were performed at three potential locations within the CLAS to provide insight into variability associated with location and aquifer depth. Theoretical simulations confirmed the potential for subsidence associated with the application of ASR in the CLAS, although operating an ASR for summer peaking needs has less potential risk of subsidence than the DOR scenario in the scenarios simulated. The study simulations provide insight into how an ASR project may be designed and operated to minimize compaction and potential subsidence. Based on this study, ASR operated to address summer peaking showed the greatest potential to reduce additional compaction verses sourcing all water from groundwater. This theoretical study provides a basis for future research on subsidence associated with ASR and provides a framework for consideration for the regulation of ASR within the District.

Introduction and Statement of Research Needs

In response to regional subsidence in the Houston Region, the Texas Legislature created the Harris-Galveston Subsidence District (District) in 1975 to provide for the regulation of groundwater withdrawal throughout Harris and Galveston counties in south-east Texas for the purpose of preventing land subsidence. The District's jurisdictional area includes the City of Houston, surrounding municipalities, and the industrial and port complex of the Houston Ship Channel and Galveston Bay.

Historically, the Coastal Lowlands Aquifer System (CLAS) in the District had been the primary water source for the region's municipal, industrial, and agricultural water supply. The Chicot, Evangeline, and Jasper aquifers are the three primary water bearing units of the aquifer system, with the Chicot being the shallowest (youngest) and the Jasper being the deepest (oldest). Historical reliance on groundwater from the Chicot and Evangeline aquifers in the Harris-Galveston Subsidence District (District) led to significant regional subsidence occurring by the 1970s (**Kasmarek and others, 2016**) in response to regional lowering of aquifer water levels.

Since 1975, groundwater regulations set forth by the District has resulted in increased aquifer water-levels and slowing and/or cessation of subsidence in regulatory areas closest to the Gulf of Mexico. The potentiometric water-levels (water levels) in the CLAS in the District have rebounded greater than 200 feet from the historical minimum water-level in response to pumping curtailment. To meet the District's regulations, water providers are required to develop alternative water supplies (primarily treated surface water). Water providers in the region have begun considering Aquifer Storage and Recovery (ASR) as a potential alternative water supply strategy that offers redundancy of supply during periods of drought or other natural disasters (ie., floods).

ASR is a proven water supply strategy to increase the availability of either groundwater or surface water through the storage of water in an aquifer using a well or wells (**Pyne, 2005**). Just as surface water reservoirs are routinely used to increase surface water availability for the future, ASR uses an aquifer to increase availability of either stored surface water, groundwater or reuse water. A properly designed ASR project will define a yield (storage volume) that the ASR project will supply over some time horizon. **Figure 1** is a schematic of a hypothetical ASR well showing the stored water, often referred to as "the bubble," the buffer zone which represents a volume of mixed recharge and native aquifer groundwater and the target storage volume which encompasses both the bubble and the buffer zone.

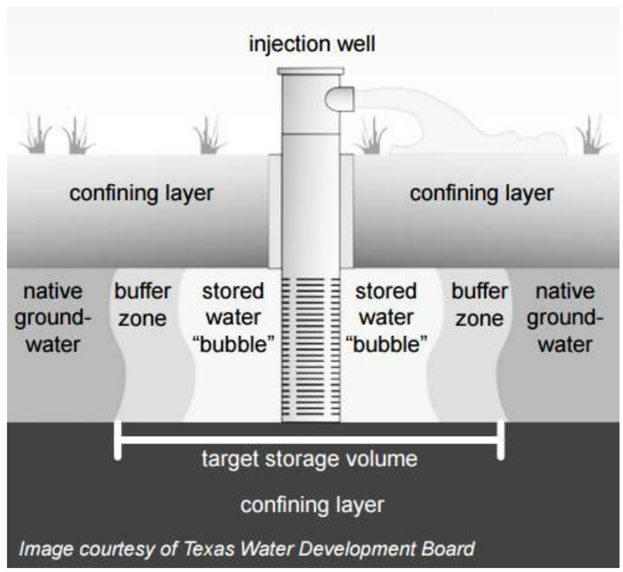

Figure 1: Schematic of an ASR well at the end of recharge and prior to recovery showing the stored water and the buffer zone (after Pyne, 2005)

A typical ASR project includes periods of recharge when water is being stored within the aquifer and periods of recovery when water is being pumped from the aquifer. During recharge periods the water level at and near the well will rise greater than it was prior to recharge (static water level). During recovery periods the water level will fall below static water levels just as occurs in standard well pumping. The duration of recharge and recovery periods can vary significantly depending upon the volume of water stored and the needs of the project. Because ASR includes periods of pumping during recovery of stored water, it can cause compaction and subsidence.

This study contains three key elements; a literature review of ASR in subsidence prone environments, numerical simulations of representative hypothetical ASR projects and a discussion of key considerations to support the future management and potential regulation of ASR in the District. Because of the theoretical nature of the study, recommendations were also made for future research and data needs to better constrain our understanding of ASR and associated potential subsidence.

Mechanisms of Subsidence and Relevance to ASR

The CLAS is composed of a complex sequence of sands and clays. Compaction and resulting subsidence in the CLAS in the study area is caused by the reduction of the pore pressure in the clay beds as a result of groundwater pumping. This decline in pressure in the aquifer leads to a decrease in pore pressure within the numerous clay lenses, which then begin to compact due to increased effective stress (**Poland and Davis, 1969**). This permanent compaction of the sediments, caused by groundwater withdrawal, is the largest contributor to land subsidence throughout the region.

Compaction can be a slow process and the time it takes for compaction to occur within a clay bed depends on several clay characteristics. Generally, the thickness of the clay beds, the percentage of clay deposits relative to the total thickness of the aquifer, and the depth of burial of the deposits determine the potential for compaction and risk for subsidence.

Historical subsidence in the District has regionally exceeded 6 feet and locally exceeded 10 feet in the District region. The District, in cooperation with other agencies and institutions in the region regularly monitors groundwater production, groundwater levels and subsidence in the region. The United States Geological Survey (USGS) monitors water levels and operates 11 extensometers in the District. The District and the University of Houston operate a land surface deformation monitoring network with over 200 stations located within the District Region.

Because ASR requires pumping in addition to recharge, there is potential for an ASR project to induce compaction and potentially contribute to subsidence in the CLAS.

Five ASR case studies (Kelley and Deeds, 2019) were reviewed for this study: San Juaquin Valley, CA; Santa Clara Valley, CA; Antelope Valley, CA.; Las Vegas, NV; and Shanghai, China. The literature review showed that well-documented case studies for Managed Aquifer Recharge (MAR) in subsidence prone aquifers significantly outnumbered ASR case studies. There are limited publicly documented case studies of subsidence associated with ASR. ASR case studies reviewed were the Las Vegas ASR and MAR project and the Antelope Valley, California ASR cycle test performed by the USGS. In both cases, measurable subsidence occurred in the vicinity of the ASR projects during their operation or testing.

A review of the case studies also found that in aquifers which have historically undergone significant regional subsidence, such as the CLAS in the District, the rate of subsidence can increase in response to increased effective stress caused by subsequent pumping, even when pumping water levels remain above the historical minimums. This has been documented in several areas of California and has been observed in the District in response to renewed pumping during a regional drought in 2011. Therefore, maintaining water levels above historical lows during withdrawal does not guarantee that the cessation of compaction of the aquifer and subsidence. These facts complicate the prediction of potential subsidence from ASR projects in aquifers that have experienced significant regional subsidence such as the CLAS in the District.

Because the pressure reduction in lower conductivity clay interbeds is inherently transient, compaction occurs over years if not decades and the effective stress controlling further subsidence in an aquifer with a complex history of water level decline, rebound and subsidence is very uncertain. Stated differently and in context to the ASR problem, what level of additional drawdown during recovery will re-initiate higher subsidence rates? The literature has shown that in aquifers with significant subsidence, the effective stress on the aquifer does not represent the effective stress predicted by the lowest observed water levels. This raises a complicating question when considering additional pumping or ASR in the shallow portions of the CLAS that have undergone significant historical compaction and where groundwater levels have significantly rebounded.

To account for the uncertainty in the current effective stress of the system, simulations performed in this study assume that the initial static water level prior to the ASR project operation defines the preconsolidation state or effective stress on the aquifer. This assumption is regulatorily conservative by preventing overestimation of the benefit of ASR to mitigate subsidence.

Hypothetical ASR Cases and Simulation of Resulting Compaction

Two hypothetical ASR projects (cases) that vary in their recharge and recovery time periods and periodicity were considered; a drought of record (DOR) strategy and a seasonal-peaking strategy. The DOR project assumes recharge of excess contract water over a 5 year period followed with the withdrawal of the total storage volume over a period of 5 years during a period of drought when it is assumed the availability of contract water will be limited. Alternatively, the seasonal-peaking strategy (a common strategy for municipal ASR projects) assumes excess water supply in the winter is recharged in the project with the total storage volume withdrawn during the summer months when need is highest.

The initial location for the hypothetical DOR ASR project is termed the base case location and is located near the city of Texas City, TX, USA. To investigate hydrogeologic variability inherent in the CLAS, two additional project locations were considered: one on Galveston Island (downdip site) and one just southeast of Houston, TX in the far northwest edge of HGSD Regulatory Area 1 (updip site). **Figure 2** shows the location of the three hypothetical ASR project areas.

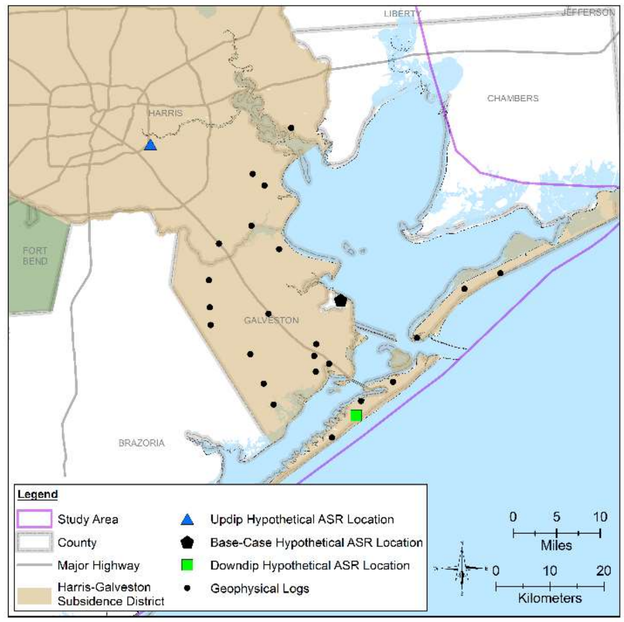

Figure 2: Location of the three hypothetical ASR project sites simulated (Kelley and Deeds, 2019).

A numerical groundwater flow model was developed to estimate compaction associated with the hypothetical ASR projects operating with the two water management strategies. The numerical model was developed using the United States Geological Survey (USGS) code MODFLOW-NWT (**Niswonger and others, 2011**) which supports the USGS subsidence (SUB) package (**Höffmann and others, 2003**).

The water source for the hypothetical ASR projects simulated was assumed to be treated surface water sourced from the Brazos River. An analysis of geochemical compatibility of the source water with groundwater was performed based upon measured groundwater quality data and inferred formation mineralogy. Results of the geochemical analysis suggest that there could be potential for calcite precipitation which could reduce the ability of the aquifer to store and transmit water. Additionally, there could be potential for other chemical reactions as result of mixing the source water with groundwater which could mobilize arsenic and other metals, increasing the total dissolved solids of the recovered water. Pre-recharge treatment of the injected water and proper design of an ASR buffer zone can mitigate any potential water quality issues identified in this study though good mineralogic data is a data gap which would require coring within the recharge intervals and the overlying and underlying confining units.

Potential of Subsidence Induced by Compaction from ASR in the Chicot and Evangeline Aquifers

Compaction was simulated for the DOR case and the summer peaking case at each of the three hypothetical sites. In addition, a simplified hypothetical ASR model was developed simulating a single ASR well completed in one hydrogeologic unit to isolate how various aquifer characteristics and ASR operational parameters can affect compaction.

Figure 3 plots maximum predicted compaction versus time in the immediate vicinity of the ASR well for the hypothetical DOR case and the summer peaking case at the base-case location (blue lines). **Figure 3** also plots maximum predicted compaction versus time for both sites from only production of an equal volume of groundwater as recovered in the ASR well (dashed lines). The difference in predicted compaction between the two curves provides one measure of the relative benefit of ASR over just groundwater pumping for an equal volume of groundwater. Model simulations predict that approximately 0.24 feet of maximum compaction would occur for the DOR case at the base-case location after one operational cycle (**Figure 4)**. At a radial distance of 1,000 feet from the ASR well(s), predicted compaction ranged from 25 to 30% of predicted compaction in the immediate vicinity of the ASR well(s). For both the DOR and summer peaking cases, ASR results in less compaction than production with no recharge. For the hypothetical DOR case, the benefit of ASR versus only groundwater production is a 50% reduction in compaction after the first year of recovery, and approximately 3% reduction in total compaction at the end of a 5-year recovery period

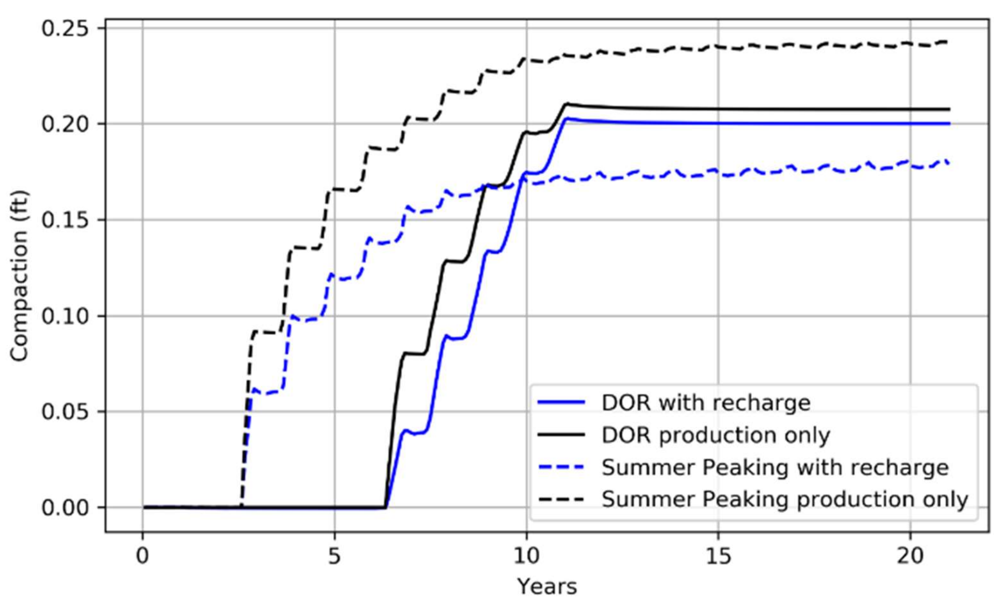

Figure 4: Compaction versus time for the DOR and summer peaking projects, comparing ASR simulations (recharge and production) to simulations with only production.

(**Figure 3**). In the summer peaking case, the benefit of ASR versus only groundwater pumping is greater than a 30% reduction in compaction after 20 cycles of annual operation (**Figure 3**).

The simulations performed to date are limited in scope and are for hypothetical projects. Potential subsidence associated with an actual ASR project will be dependent on the specific operational details and location of the project. As a result, future proposed ASR projects in the District will require a site-specific analysis of their potential benefits as compared to traditional groundwater pumping based upon that project's operational details and the detailed hydrogeology at the site. Model simulation results show that properly designed ASR projects can reduce the "effective drawdown" on the aquifer for a given groundwater yield and thus result in less compaction and potential subsidence. Results suggest that optimal cycling of recharge and withdrawal can reduce the "effective drawdown" and thereby reduce subsidence.

Designing an ASR project to minimize the potential for subsidence presents another design constraint to those traditionally considered. Model results suggest that an ASR project can be designed and operated to minimize potential compaction. Key components of an ASR project that may be modified to limit the potential compaction are: (1) maximizing the well spacing; (2) decreasing the recovery rate(s); (3) decreasing recovery duration prior to the next recharge cycle; and (4) targeting high transmissivity, low clay content intervals as the storage formation(s).

Relevance and Potential Impact on Future Regulations

This study is the first District study of the potential for subsidence from the implementation of ASR and provides new insights for how compaction may occur with the development of an ASR project in the Chicot and Evangeline aquifers. The results of this study have led to the development of recommendations for future data and research requirements for ASR projects in the District as well as recommendations for future District rule modifications and regulatory provisions.

Acknowledgements

The authors would like to acknowledge the following contributors to this study: Mr. Fred Blumberg and Ms. Ashley Evans of ARCADIS; Mr. David Pyne and Richard Glanzman of ASR Systems; Dr. Zhuping Sheng of Texas A&M El Paso; Mr. Scott Marr of HDR, Inc. and Mr. Bill Mullican.

References

Höffmann, J., Leake, S.A., Galloway, D.L., and Wilson, A.M., 2003, MODFLOW-2000 Ground-Water Model--User Guide to the Subsidence and Aquifer-System Compaction (SUB) Package: U.S. Geological Survey Open-File Report 03-233, 44 p.

Kasmarek M.C., Ramage, J.K., and Johnson, M.R., 2016. Water-Level Altitudes and Water-Level Changes in the Chicot, Evangeline and Jasper Aquifers and Compaction 1973-2015 in the Chicot and Evangeline Aquifers, Houston-Galveston Region, Texas, U.S. Geological Survey Scientific Investigations Map 3365, 2016.

Kelley, V. and Neil Deeds, 2019. Assessment of Subsidence and Regulatory Considerations for Aquifer Storage and Recovery in the Evangeline and Chicot Aquifers, Report prepared for the Harris-Galveston Subsidence District, 188 p.

Niswonger, R.G., S. Panday, and M. Ibaraki. 2011. MODFLOW-NWT, A Newton formulation for MODFLOW-2005: U.S. Geological Survey Techniques and Methods 6-A37, 44 p.

Poland, J.F., and Davis, G.H., 1969. Land subsidence due to withdrawal of fluids, in Varnes, D.J., Reviews in engineering geology, v. II: Boulder Colorado, Geological Society of America, p. 187-268.

Pyne, R.D.G., 2005. Aquifer Storage Recovery – A Guide to Groundwater Recharge Through Wells, Second Edition, ASR Press, 608 p.

Proc. IAHS, 97, 1–7, 2020
https://doi.org/10.5194/piahs-97-1-2020

Integrated monitoring of subsidence due to hydrocarbon production: consolidating the foundation

Gini Ketelaar[1], Hermann Bähr[1], Shizhuo Liu[1], Harry Piening[1], Wim van der Veen[1], Ramon Hanssen[2], Freek van Leijen[2], Hans van der Marel[2], and Sami Samiei-Esfahany[2]

[1]Nederlandse Aardolie Maatschappij B.V., Assen, the Netherlands
[2]Department of Geoscience and Remote Sensing, Delft University of Technology, Delft, the Netherlands

Correspondence: Gini Ketelaar (gini.ketelaar@shell.com)

Published:

Abstract. This paper describes several geodetic studies that consolidate the reliability and precision of monitoring subsidence due to hydrocarbon production: the deployment of Integrated Geodetic Reference Stations (IGRS); the application of high resolution InSAR; the comparison of different GNSS processing methodologies; the implementation of an efficient InSAR stochastic model, and the framework of integrated geodetic processing (levelling, GNSS, InSAR). The advances that have been made are applicable for any other subsidence monitoring project.

1 Introduction

Since the start of hydrocarbon production in the Netherlands, the Nederlandse Aardolie Maatschappij (NAM) has performed subsidence monitoring over its gas and oil fields, following Dutch legislation and the commitment to produce in a safe and responsible manner. Innovative geodetic acquisition techniques for subsidence monitoring (GPS/GNSS, InSAR) have been actively investigated and deployed over the past decades, as well as state-of-the-art processing and geodetic testing techniques. The solid foundation that has been established for subsidence monitoring has been reinforced towards the future by incorporating the latest (scientific) developments. This paper addresses recent results from the geodetic studies that are part of the production plan of the Groningen gas field:

- The deployment of Integrated Geodetic Reference Stations (IGRS).
- The application of high-resolution InSAR.
- Improvement of the InSAR stochastic model.
- Comparison of GNSS processing methodologies.
- Integrated geodetic processing of levelling, GNSS and InSAR measurements (concept).

2 Integrated Geodetic Reference Stations

To further improve the subsidence monitoring network over the Groningen gas field, NAM has deployed 25 Integrated Geodetic Reference Stations (IGRS) since 2018 (Hanssen, 2017; Kamphuis, 2019). The IGRS consist of a GNSS receiver, two InSAR corner reflectors (for ascending and descending tracks) and several levelling benchmarks, all mounted on the same deeply founded monument (Fig. 1). The advantage of the IGRS is that the accuracy of levelling, GNSS and InSAR deformation estimates can be cross-validated directly, since the measurements are with respect to the same monument and hence reflect the same deformation cause. Also, spatially-dependent biases and noise can be assessed and mitigated.

The IGRS support minimizing subsurface uncertainties and optimizing future subsidence predictions. The density and location of the IGRS have been chosen such that the areas with the largest uncertainty in subsurface behaviour are captured (e.g. areas with potential aquifer depletion that do not contain wells). These areas are primarily located at the edge of the Groningen gas field, where horizontal movements are expected to be the largest. The IGRS target density was chosen such that the expected horizontal deformation signal can be reconstructed, considering the GNSS noise structure.

Tenth International Symposium on Land Subsidence (TISOLS)

Figure 1. IGRS; design by Delft University of Technology.

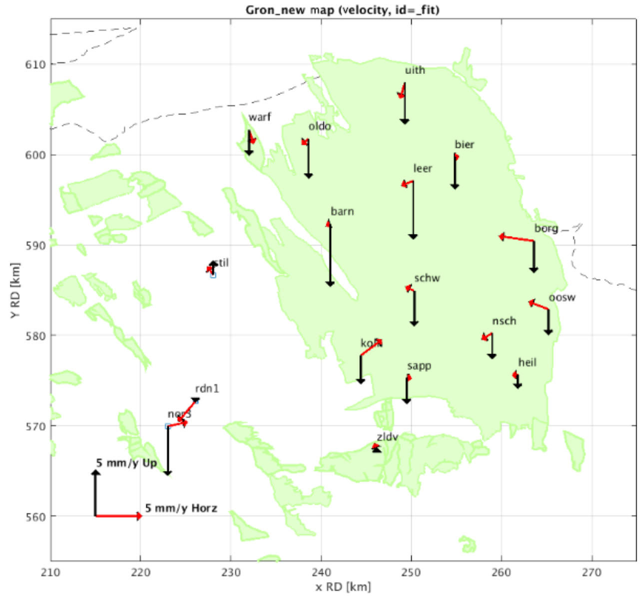

Figure 2. Horizontal and vertical deformation in mm yr^{-1} for the IGRS that are operational more than 1 year, from start of deployment until mid 2019. The green areas depict the gas fields. The station "nor3" contains a fluctuating component due to gas injection and extraction.

From the three geodetic techniques, only GNSS delivers all 3D deformation components (East, North, Height) with high precision. GNSS measurement precision (1σ) of the height component is 2 mm (Nederlandse Aardolie Maatschappij B.V., 2017), which implies that movements larger than 4 mm can be detected with 95 % confidence level. The precision of the horizontal components is slightly better.

Figure 2 depicts the latest analysis results of the vertical and horizontal movements of the Groningen IGRS. Based on geomechanical predictions, horizontal deformation rates are expected 0 in the center of the gas field, and ~ 2 mm yr^{-1} at the edges of the field in the direction towards the center. All IGRS have been connected to the 2018 Northern Netherlands leveling campaign. IGRS InSAR time series processing will be performed in late 2019.

3 High-resolution InSAR

Three TerraSAR-X tracks (two descending and one ascending) have been processed by SkyGeo B.V. for NAM covering the time period 2013–2019 (Qin et al., 2019). The high spatial and temporal resolution enables near-realtime building and infrastructure stability monitoring. Furthermore, a more detailed insight into horizontal movements is possible. However, due to the almost north–south oriented orbit, only the east–west component of the horizontal movements can be estimated well from the TerraSAR-X results. Figure 3 shows the horizontal movements over the Groningen gas field in the direction of the ascending look direction projected on the horizontal plane (almost east-west oriented, $\sim 10^\circ$ angle). Also clearly visible is the horizontal deformation signal in the salt mining areas (near Veendam and Winschoten). The horizontal movements over the Groningen gas field in the recent year are as expected still below measurement precision; there is not yet a strong correlation with the IGRS processing results. However, the time series of the GNSS stations that have been operational from 2013/2014 have been cross-validated with the TerraSAR-X data (Line-of-Sight) and have shown agreement at millimeters level.

The high-resolution InSAR processing results have also been used to investigate whether it is possible to discriminate between shallow and deep (at hydrocarbon reservoir level) deformation. Two methodologies can be used for this: separation based on the deformation histogram of neighbouring Persistent Scatterers (PS), and PS separation based on height above ground level. The latter turned out to be the most effective for high-resolution InSAR and has led for the first time to a localized clear shallow deformation pattern (up to 2 mm yr^{-1} rates) in Groningen that correlates with soil composition (Fig. 4).

4 InSAR Stochastic Model

Despite the successful application of InSAR in practice, one of the main concerns is that the quality description of InSAR deformation measurements in terms of precision is not adequate. Often, the error structure is simplified such as neglecting the spatio-temporal correlation between InSAR deformation measurements. The unrealistic quality description could negatively affect decision-making based on the InSAR results.

In order to describe the quality of the InSAR data in terms of precision, it is needed to mathematically describe the spatio-temporal variability of noise components in the data. It should be noted that, in the context of deformation

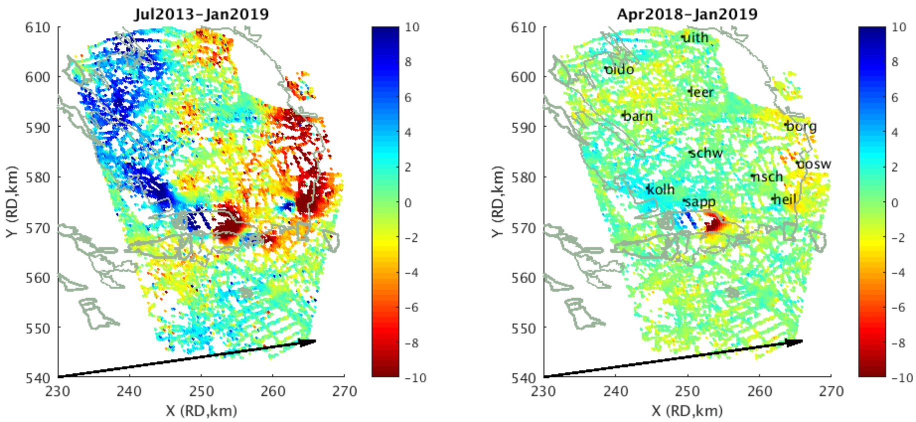

Figure 3. Horizontal deformation (mm) in the direction of the ascending look direction projected on the horizontal plane (arrow) for the time periods 2013–2019 and 2018–2019, including the location of the IGRS that are operational minimal from April 2018. The outlines of the gas fields are depicted in grey.

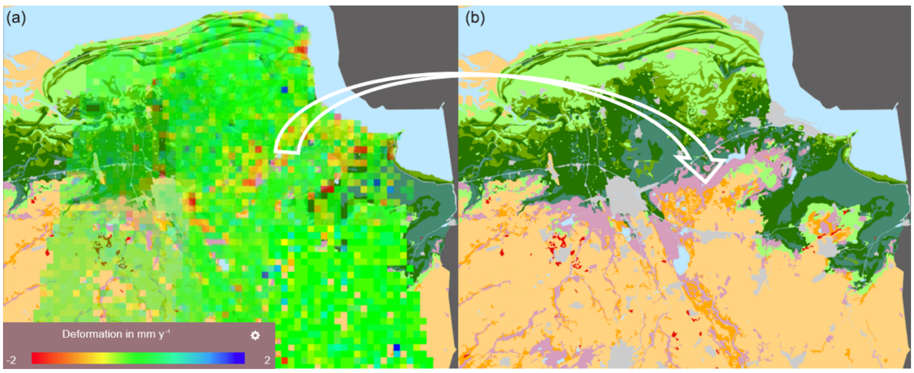

Figure 4. Shallow compaction rates (mm yr^{-1}) computed by PS separation based on height above ground level **(a)**, and soil composition **(b)**. The strip with shallow compaction rates of 1–2 mm yr^{-1} corresponds with the location of peat layers (pink). Source: SkyGeo B.V.

monitoring and modeling, the term *noise* not only comprises the uncertainty of the measurements itself (scattering and atmospheric noise in InSAR), but it also subsumes all signal (or deformation) components in InSAR observations that are not related to the signal of interest. Therefore, we distinguish two noise components: *measurement noise*, and *idealization noise* (level to which the measurements are representative for the signal of interest). Here, the main focus is on the stochastic modeling (covariance matrix) of the InSAR measurement noise (Van Leijen et al., 2020).

In order to evaluate the spatio-temporal variability of the measurement noise, an InSAR dataset over an assumedly signal-free area ($\sim 20 \times 20$ km) in northern Netherlands has been used. A RadarSAT-2 dataset containing 98 radar images acquired between 2009 and 2016 was used for the study. It should be noted that, although the selected area is assumed to be affected minimally by deep and shallow sources, it still could be affected by some residual deformation. In order to isolate the effect of measurement noise, the potential contribution of residual deformation should be subtracted from the data. To do so, for each InSAR point, a linear trend and a periodic annual signal has been estimated and subtracted from the timeseries of InSAR observations. The remaining can be assumed to contain only measurement noise.

From the obtained timeseries of all the points in the selected area, the spatio-temporal empirical variograms are computed using robust algorithms (Cressie and Hawkins, 1980; Genton, 1998) in order to reduce the sensitivity to outliers. The results are visualized in Fig. 5. By visual/qualitative analysis of this figure, we can recognize three different types of behavior: (i) a nugget effect (lower bound of $\sim 10\,\mathrm{mm}^2$), (ii) a spatially correlated signal, and (iii) a temporally correlated signal.

To combine these three effects in a generic model, the following exponential variogram model has been used:

$$\gamma(\Delta t, \Delta d) = \sigma_0^2 + \sigma_\mathrm{t}^2 \left(1 - e^{\frac{-\Delta t}{R_\mathrm{t}}}\right) + \sigma_\mathrm{s}^2 \left(1 - e^{\frac{-\Delta d}{R_\mathrm{s}}}\right), \qquad (1)$$

where, Δt and Δd are time difference and spatial distance, $\gamma(\Delta t, \Delta d)$ is the variogram as a function of Δt and Δd , σ_0^2 is the variance of the nugget effect, σ_t^2 and σ_s^2 are the variance of the temporal and the spatial components, and R_t and

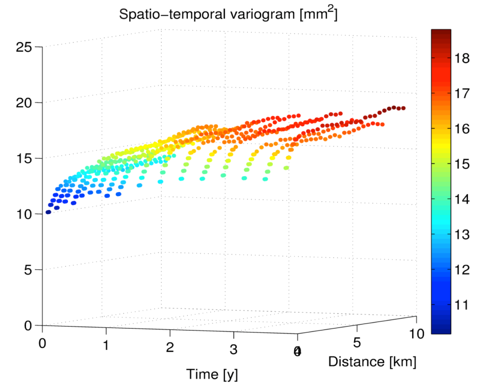

Figure 5. Spatio-temporal variograms computed from RadarSAT-2 InSAR data over the assumed stable area.

Table 1. Estimated variogram model parameters.

	σ_0^2 (mm^2)	σ_t^2 (mm^2)	R_t (yr)	σ_s^2 (mm^2)	R_s (km)
Estimated parameters	7.93	5.5	0.67	3.9	1.11

R_s are the correlation length of the temporal and the spatial components, respectively. The results of the parameter estimation are summarized in Table 1.

Using the estimated variogram model, it is possible to construct the full covariance matrix of measurement noise for the spatio-temporal InSAR data (Yaglom, 1962). Note that the large volume of InSAR data (usually consisting of tens of thousands of points with tens to hundred epochs) result in a huge covariance matrix that is not practically useful due to the computational and numerical limitations. In this regard, a proper data reduction is usually required for InSAR data. Therefore, the covariance matrix of the full dataset should be propagated to the covariance matrix of the reduced dataset. In the context of InSAR processing in Groningen, reduction techniques have been used based on averaging in time and space (e.g. see Samiei-Esfahany and Bähr, 2015). As the averaging-based data reduction can be formulated as a linear operator (e.g., as $y_{\text{reduced}} = \mathbf{A}\, y_{\text{full}}$), the covariance matrix of the full dataset can be propagated to the reduced covariance matrix using the linear error-propagation as

$$\mathbf{Q}_{\text{reduced}} = \mathbf{A}\,\mathbf{Q}_{\text{full}}\,\mathbf{A}^{\mathrm{T}}. \quad (2)$$

As an example of the reduced dataset, Fig. 6 shows the reduced InSAR timeseries over Groningen area, with spatial averaging over grids of 5×5 km and temporal averaging over 6 month intervals. Note that, in this example of data reduction, the full dataset of 371 890 point-targets and 98 epochs (i.e., in total 36 445 220 observations), has been reduced to 455 spatial grids and 15 epochs (i.e., in total 6825 observations).

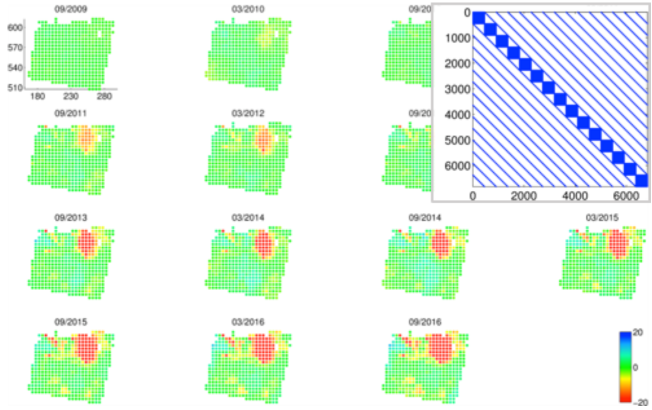

Figure 6. Reduced InSAR timeseries over the Groningen area, with spatial averaging over grids of 5×5 km and temporal averaging over 6 month intervals, and the structure of the covariance matrix (upper right). Blue areas show the non-zero elements, which are an indication of both spatial and temporal correlation in the data.

With the proposed approach, a reduced InSAR dataset is delivered to the subsurface community, including its full covariance matrix, incorporating both spatial and temporal correlation of data measurement noise. The covariance matrix can be further used as a quality descriptor of the InSAR data, as well as a proper weight matrix in geomechanical and subsurface modeling.

5 GNSS processing methodologies

In the NAM GNSS processing methodologies project (Van der Marel, 2020) different methodologies have been investigated with the aim to obtain transparent time series estimates to support conclusions on subsidence rates with realistic confidence levels. The three different processing methodologies that have been investigated are: state-space modeling (SSR), baseline network processing (BSW), and Precise Point Positioning (PPP). An overview of the main characteristics of each method is given in Table 2.

Besides the NAM monitoring and NAM reference stations (of which the coordinates are kept fixed – with incremental updates – in the SSR processing), IGS and EUREF stations have been included in the BSW and PPP processing, as well as the Dutch AGRS and NETPOS stations in the BSW processing.

The time series results have been decomposed into components: a long term trend using a spline function, annual and semi-annual components, temperature influence, atmospheric loading, time series steps (e.g. due to antenna changes), and residuals. In the estimation of the temperature influence and atmospheric loading, temperature and pressure data from the Royal Netherlands Meteorological Institute (KNMI) is used. During a first iteration also two common mode components are estimated, the common mode in

Table 2. GNSS processing methodologies. SSR processing has been carried out by 06-GPS using Geo++ software (Wübbena et al., 2001); BSW by the Dutch Cadastre using the Bernese GNSS software (Dach et al., 2015); PPP by Nevada Geodetic Laboratory (NGL) using Gipsy/Oasis software (Blewitt et al., 2018).

Name	Methodology	Main Characteristics	Reference Frame
SSR	State-Space Representation Kalman Filter	Undifferenced processing; local reference stations; state-space modelling	Constrained to local reference stations with incremental coordinate updates
BSW	EUREF standard regional network processing	Receiver-satellite double differences; Ionosphere free linear combination; ZTD estimation; IGS/EPN reference stations; IGS orbits.	Unconstrained (undistorted) best fit to selected IGS/EUREF reference stations in ITRF2008
PPP	Precise Point Positioning	Undifferenced processing; IGS orbits and clocks; Ionosphere free linear combination; ZTD estimation	ITRF2008 provided through the orbits and clocks

the residuals (residual stack), and common mode of the periodic parameters (harmonics, temperature influence, and atmospheric loading). For the estimation of the common mode a subset of the stations is used. The common mode is removed in the second iteration.

All three processing chains estimate, after removal of the common mode, a similar annual, semi-annual, temperature influence and atmospheric loading for each station. The periodic common mode signals themselves are however very different for each solution; the common modes in the BSW and PPP solutions are significantly larger than the common mode in the SSR solutions.

The agreement between the estimated trend signals of the BSW and PPP is good, which is what should be expected because both solutions use ITRF2008 as reference frame. For the final results, the known tectonic motion of the Eurasian plate has been removed in the horizontal component (conversion to ETRS89), but heights stay in ITRF2008. This is because the conversion to ETRS89 introduces a small extra vertical velocity component in the results ($\sim 1\,\mathrm{mm\,yr^{-1}}$). The cause of this effect lies in the choices that were made for the definition of the transformation between ITRF and ETRS89.

When comparing the BSW and PPP solutions with respect to the SSR solutions, the overall patterns in the time series are similar, however – for some stations – small deviations are present. Figures 7, 8 and 9 show the East, North and

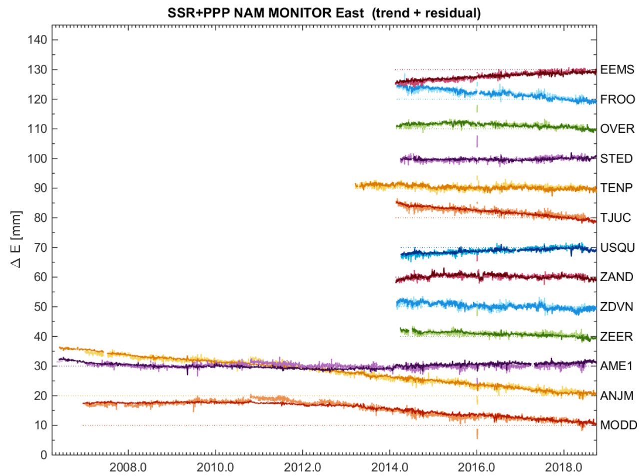

Figure 7. GNSS time series East component (relative, mm), PPP (light) and SSR (dark) solution.

Height/Up time series for a selection of Groningen and Wadden Sea GNSS continuous monitoring stations, for the SSR and PPP solution. The BSW solution is similar to the PPP solution, but with a lower noise level.

The reason for the differences lies in the reference stations. The SSR solution is computed in a local reference network. The reference station coordinates are checked periodically by relaxing the coordinate constraints. In case movement is detected in one or more reference stations, the coordinates of the reference stations are updated. For the BSW and PPP, ITRF2008 is used as reference frame. For ITRF2008, reference stations are used that lie well outside the area of interest.

The results indicate that there may be a possibility to further optimize the procedure for the reference stations in the SSR solution. Instead of incremental corrections of a local set of reference station coordinates, the results of the BSW and/or PPP processing could be utilized to strengthen the solution over longer periods. However, a local reference network stays key for high precision local deformation monitoring.

6 Integrated Geodetic Processing

The available observations acquired by the different techniques (levelling, GNSS, InSAR, but potentially also gravity, tilt) are complementary to each other due to their spatial density and coverage, temporal density and coverage, and sensitivity (1D versus 3D). Because of this complementary nature, an integration of the techniques to generate an optimal output product is desirable. However, the differences between the techniques make this integration non-trivial. Conventional geodetic processing methodologies require for instance measurements at common locations (e.g., benchmarks). Therefore, geodetic adjustment and testing procedures are typi-

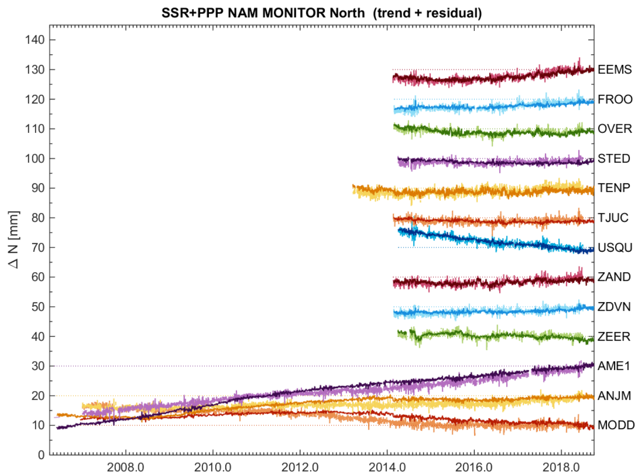

Figure 8. GNSS time series North component (relative, mm), PPP (light) and SSR (dark) solution.

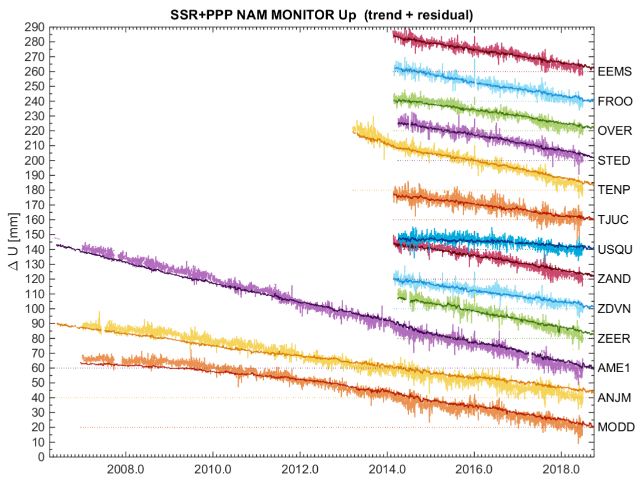

Figure 9. GNSS time series Height/Up component (relative, mm), PPP (light) and SSR (dark) solution.

cally applied for each technique/dataset separately, followed by a final integration step.

The Integrated Geodetic Processing (IGP) approach enables the adjustment and testing of the various observation types simultaneously. Hereby, the complementary nature of the techniques is better used. The overall concept of the IGP approach is shown in Fig. 10. The approach meets a number of pre-defined requirements. For instance, the user is able to select the area and period of interest, together with the signal of interest (e.g., surface motion due to deep causes, shallow causes, or the total). Furthermore, various output products can be generated. Before the integration, each dataset is pre-processed to account for certain technique-dependent error sources, such as benchmark identification errors in case of levelling data. Each dataset is accompanied with its covariance matrix. Within the integration step, possible differences between the geodetic datums is accounted for.

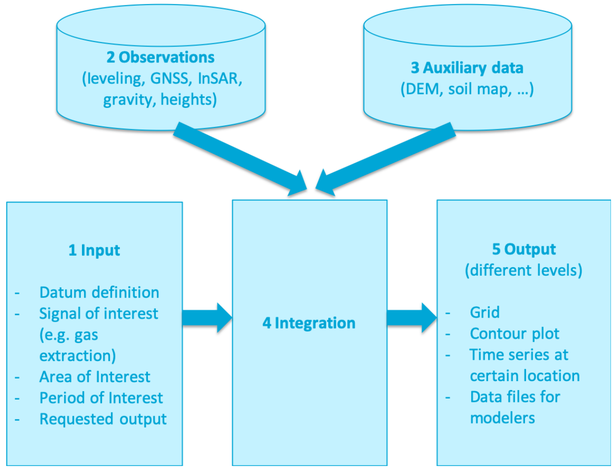

Figure 10. Overall concept of the Integrated Geodetic Processing approach.

7 Conclusions

Multiple advances have been made in the recent years on monitoring subsidence due to hydrocarbon production in the Netherlands. Integrated Geodetic Reference Stations (IGRS) enable to cross-validate levelling, GNSS and InSAR independent of the deformation cause, and will contribute to minimizing subsurface uncertainties. The application of high-resolution InSAR has quantified shallow deformation components in the Groningen area. The comparison of different GNSS processing methodologies has strengthened the confidence in the information that can be derived from the measurements. The InSAR stochastic model has been improved to incorporate correlated noise structures in an efficient way. All these “ingredients” have consolidated the foundation for integrated geodetic processing for future subsidence monitoring.

Data availability. Subsidence monitoring data that is publicly available can be accessed via https://www.nlog.nl/geodetische-meetregisters-en-gps-metingen (NLOG, 2020). The geodetic studies described in this paper are covered in the project reports for NAM in the references.

Author contributions. All authors have participated in the collaboration projects between NAM and Delft University of Technology, and contributed to the paper. Particular contributions have been made by SSE on the InSAR stochastic model, by HvdM on GNSS processing methodologies, and by SL on high resolution InSAR in cooperation with SkyGeo B.V.

Competing interests. The authors declare that they have no conflict of interest.

Special issue statement. This article is part of the special issue "TISOLS: the Tenth International Symposium On Land Subsidence – living with subsidence". It is a result of the Tenth International Symposium on Land Subsidence, Delft, the Netherlands, 17–21 May 2021.

Acknowledgements. The studies described in this paper have been made possible by the contributions from the following parties: high-resolution InSAR processing by SkyGeo B.V.; placement and processing of GNSS receivers by 06-GPS B.V.; GNSS regional network processing by the Dutch Cadastre, and GNSS Precise Point Positioning processing by Nevada Geodetic Laboratory.

References

Blewitt, G., Hammond, W. C., and Kreemer, C.: Harnessing the GPS data explosion for interdisciplinary science, EOS T. Am. Geophys. Un., 99, https://doi.org/10.1029/2018EO104623, 2018.

Cressie, N. and Hawkins, D. M.: Robust estimation of the variogram: I. Mathematical Geology, 12, 115–125, Springer Berlin Heidelberg, 1980.

Dach, R., Lutz, S., Walser, P., and Fridez, P. (Eds.): Bernese GNSS Software Version 5.2. User manual, Astronomical Institute, University of Bern, 2015.

Genton, M. G.: Highly Robust Variogram Estimation, Mathematical Geology, 30, 213–221, Springer Berlin Heidelberg, 1998.

Hanssen, R.: IPC No. P115850NL00. A radar retroreflector device and a method of preparing a radar retroreflector device, Patent No. 2019103, 2017.

Kamphuis, J. C.: Co-location of geodetic reference points: On the design and performance of an Integrated Geodetic Reference Station, MSc thesis, Delft University of Technology, the Netherlands, 2019.

Nederlandse Aardolie Maatschappij B.V.: Ensemble Based Subsidence application to the Ameland gas field – long term subsidence study part two (LTS-II) continued study, 2017.

NLOG: Geodetische meetregisters en GPS metingen, available at: https://www.nlog.nl/geodetische-meetregisters-en-gps-metingen, last access: 13 March 2020.

Qin, Y., Salzer, J., Maljaars, H., and Leezenberg, P. B.: High resolution InSAR in the Groningen area, project report for NAM, SkyGeo B.V., 2019.

Samiei-Esfahany S. and Bähr, H.: Research and development project for geodetic deformation monitoring, for long-term study on anomalous time-dependent subsidence in the Wadden sea region, Tech. rep., Nederlandse Aardolie Maatschappij B.V., Assen, the Netherlands, 2015.

Van der Marel, H.: Comparison of GNSS Processing Methodologies for Subsidence Monitoring, project report for NAM, Delft University of Technology, 2020.

Van Leijen, F. J., Samiei-Esfahany, S., Van der Marel, H., and Hanssen, R. F.: Improving the Functional and Stochastic Model of InSAR, project report for NAM, Delft University of Technology, 2020.

Wübbena, G., Bagge, A., and Schmitz, M.: RTK networks based on Geo++ GNSMART – Concepts, Implementation, Results, Proceedings of the National Technical Meeting of the Satellite Division of the Institute of Navigation, ION GPS/2001, September 2001, Salt Lake, USA, 368–378, 2001.

Yaglom, A. M.: An Introduction to the Theory of Stationary Random Functions, Series of selected Russian publications in the mathematical sciences, Prentice-Hall, 1962 (revised English edition translated and edited by Richard A. Silverman, Dover Publications, Mineola, New York, 2004).

Proc. IAHS, 382, 493–498, 2020
https://doi.org/10.5194/piahs-382-493-2020

Modelling subsidence due to Holocene soft-sediment deformation in the Netherlands under dynamic water table conditions

Henk Kooi[1] **and Gilles Erkens**[1,2]

[1]Deltares Research Institute, P.O. Box 85467, 3508 AL Utrecht, the Netherlands
[2]Faculty of Geosciences, Utrecht University, P.O. Box 80115, 3508 TC Utrecht, the Netherlands

Correspondence: Henk Kooi (henk.kooi@deltares.nl)

Published: 22 April 2020

Abstract. Local and regional governments in The Netherlands are increasingly faced with the question how to adjust and optimize groundwater table conditions in urban areas to minimize ongoing subsidence and its consequences. To help addressing this question, a model was developed that includes soft-soil deformation by creep. In this paper, a study is presented in which the model was used to investigate and intercompare the effectiveness of measures that (a) prevent anomalous water table drop during a drought, (b) suppress the seasonal variability of the water table, and (c) involve a permanent rise of the mean water table.

1 Introduction

Urban areas in the western part of The Netherlands commonly show persistent subsidence over multiple decades at rates between 0–10 mm yr^{-1}. At the same time, buildings with a foundation in Pleistocene strata usually show much smaller to negligible subsidence, indicating that the land surface subsidence is mainly caused by slow deformation of clay and peat deposits in the Holocene strata. In contrast to areas with peat oxidation, in urban areas, the persistent nature of the subsidence is thought to be the expression of viscous behaviour (creep) of the subsurface, under periodic addition of fill at the surface to compensate for elevation loss and/or water table lowering. The subsidence causes damage to pipes and cables, damage to buildings and infrastructure without pile foundation, damage to buildings due to decay of wooden pile foundations if the water table is lowered, nuisance flooding, and high maintenance costs of public space functions. Because (ground)water level change can provoke subsidence, and local and regional governments are responsible for groundwater levels in the public space, these governments are faced with the question how to adjust and optimize water table conditions to minimize the subsidence and its consequences. To be able to choose among potential measures, questions they seek answers to include: How much subsidence can be prevented by:

a. preventing excessive water table lowering during an occasional drought;

b. permanent damping of seasonal water table variations;

c. raising of the mean water table?

In this study, modelling was used to address these questions.

2 Methods

2.1 Model formulation

A 1-dimensional mathematical model was built that quantifies the concepts depicted in Fig. 1. The model domain consists of Holocene peat and clay layers. Coupled groundwater flow and deformation (consolidation/swelling) are calculated in these layers, resulting in vertical land movement relative to the underlying Pleistocene aquifer. The natural Holocene stack is overlain by an anthropogenic cover layer (fill), generally consisting of debris and sand that was added in the course of history. The phreatic water table sits within the cover layer and varies in response to weather conditions and

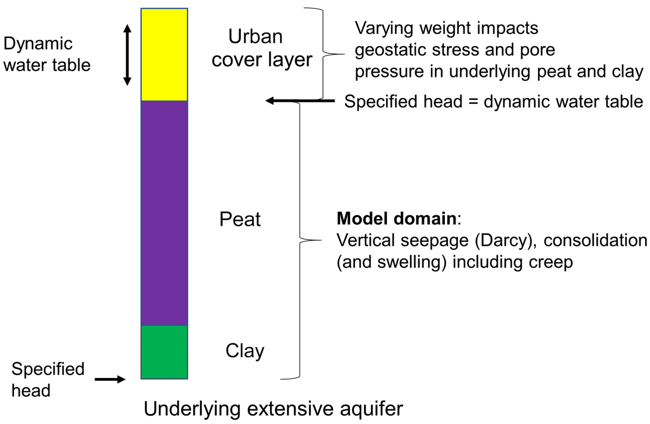

Figure 1. Conceptual model.

human interference. The water table variations directly impact the pore pressure and the geostatic stress in the underlying layers due to the changes in cover layer weight (water content change), and indirectly impact pore pressures by the changing head at the base of the cover layer, which acts as the upper drainage boundary for consolidation and swelling in the peat and clay stack.

Deformation is calculated employing an isotache-based, viscoelastic compression model that is used in certified geotechnical software for settlement modelling in The Netherlands and other countries. The viscous deformation is referred to as creep. The creep strain in the isotache model is a generalization of, and therefore replaces, the ideal-plastic deformation of Terzaghi's classical elastoplastic compression model. That is, all irreversible deformation in the isotache model is caused by creep. The model uses three compression parameters: swelling constant a, compression constant b, secondary compression constant c; and an (initial) overconsolidation ratio OCR. For a given set of values of the compression parameters, the momentary viscous (creep) time rate of (natural) strain ε_{cr} is a function of OCR:

$$\frac{d\varepsilon_{cr}}{dt} = \frac{c}{\tau} \qquad \tau = \tau_{ref}\mathrm{OCR}^{\frac{b-a}{c}} \tag{1}$$

where $\tau_{ref} = 1$ d. τ is intrinsic time, which can be taken as an apparent age of the clay or peat, where young age corresponds to high, and old age to low creep rates. For a comprehensive description of the model, see Den Haan (1994) or Kooi et al. (2018). The model equations are solved with FlexPDE 6.50, a scripted finite element solution environment for partial differential equations.

The model does not account for shrink and swell associated with seasonal desiccation and wetting of clay-rich units in the unsaturated zone (e.g., te Brake et al., 2013).

2.2 Parameter values

Table 1 lists the parameter values that were used for peat, clay and the anthropogenic cover layer in the calculations presented here. Deformation of the cover layer is assumed to be negligible. Hydraulic conductivity of peat and clay was assigned a fixed value of 5 mm d^{-1}. These are representative values that provide a fair impression of the impacts of the water table scenarios. The values of OCR were varied (by specifying τ) in order to vary the background (initial) subsidence rate by creep. A comprehensive sensitivity analysis is beyond the scope of this paper.

Table 1. Parameter values per lithology.

	a (–)	b (–)	c (–)	γ_{sat} (kN m^{-3})	γ_{unsat} (kN m^{-3})
anthropogenic	–	–	–	20.4	18.4
peat	0.017	0.13	0.009	11.5	–
clay	0.005	0.065	0.003	18.5	

Table 2. Scenarios for the perturbation applied to the reference ground water table condition.

scenario	description
drought	amplitude +1.0 m *in* dry season year 8
damping	amplitude −0.4 m applied *after* year 9
raising	annual mean +0.5 m applied *after* year 9

2.3 Model runs

The model was run for the three-layer configuration shown in Fig. 1, with a thickness of 3, 7 and 2 m for the anthropogenic, peat and clay layer, respectively. This layering approximates subsurface conditions in the city of Gouda (Van Laarhoven, 2017). Seasonal water table variations are represented by a sine-function. In reference runs, the mean annual water table is 1 m below land surface and the amplitude 0.5 m. Table 2 summarizes the three modified water table scenarios "dry summer", "damping", and "raising" that were used to study their impacts. The magnitude of the applied perturbations is rather large compared to what is generally feasible in practice. This was done to bring out the impacts more clearly.

Note that for "drought" the reference and the scenario should formally be swapped to evaluate the impact of mitigation measures that prevent excessive water table lowering during the drought. In the runs hydraulic head at the base of the clay is kept constant and equal to the mean ground water table. A period of 25 years is simulated.

To study how impacts of water table scenarios vary as a function of the background (or initial) subsidence rate, values of 10, 20 and 100 years were assigned to the initial intrinsic time τ for both the peat and clay layer. These τ values can be converted to corresponding values of OCR using Eq. (1) and the parameter values listed in Table 1.

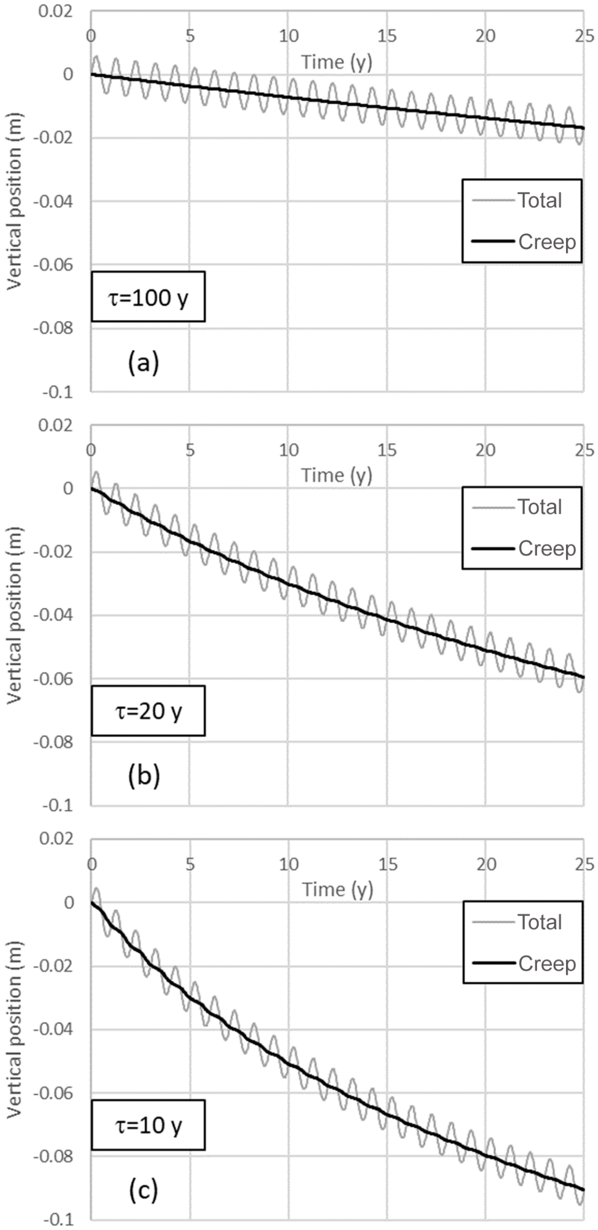

Figure 2. Calculated subsidence for the reference runs.

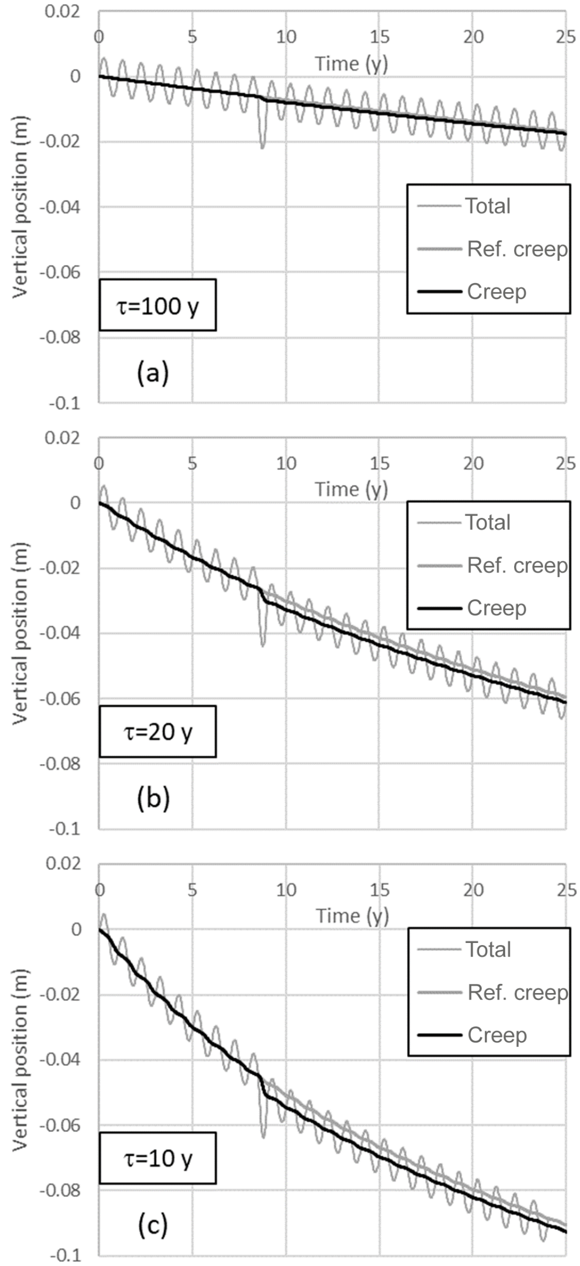

Figure 3. Calculated subsidence for scenario "dry summer". The creep of the reference runs is depicted as "ref. creep".

3 Results

Figure 2 presents the calculated vertical land movement of the reference runs. τ values of 100, 20 and 10 years yield initial subsidence rates of about 1, 3 and 5 mm yr^{-1}, respectively. The total movement includes oscillations with an amplitude of about 5 mm that are predominantly caused by the elastic response of the peat and the clay to the seasonal stress changes. The accumulated irreversible, inelastic subsidence is labelled "creep". It includes subtle seasonal variations indicating that the creep rate accelerates (with some delay) when the water table declines and decelerates when the water table rises.

Figures 3–5 present the calculated vertical land movement for the three water table scenarios. To visualize the impact of the changed conditions, the creep component of the reference runs (Fig. 2) is shown for reference.

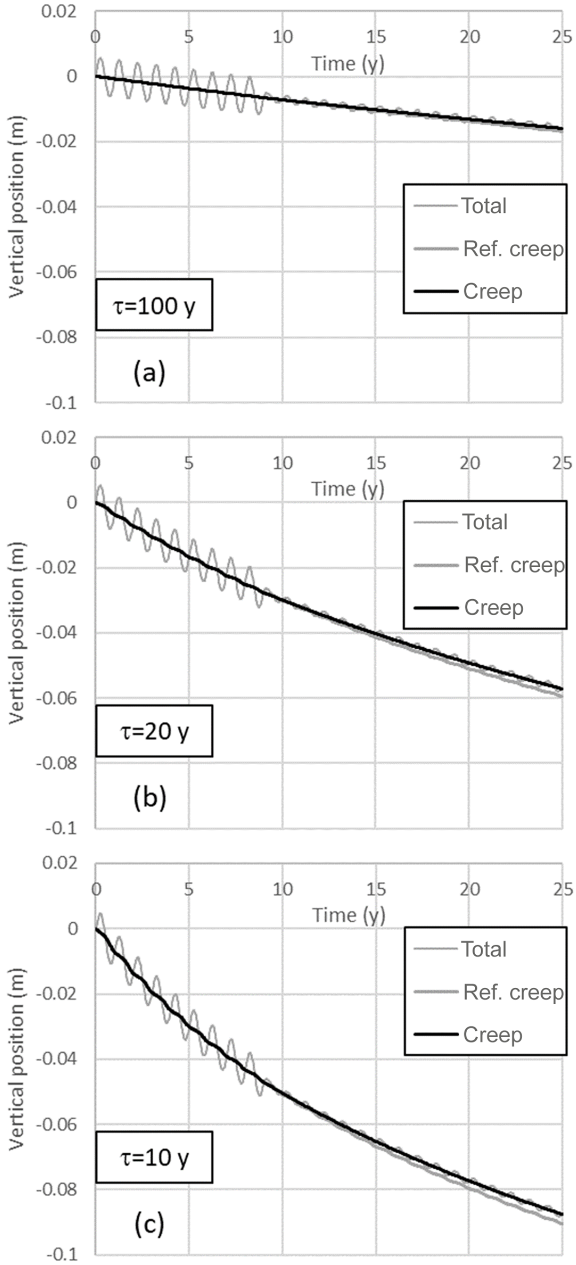

Figure 4. Calculated subsidence for scenario “damping”. The creep of the reference runs is depicted as “ref. creep”.

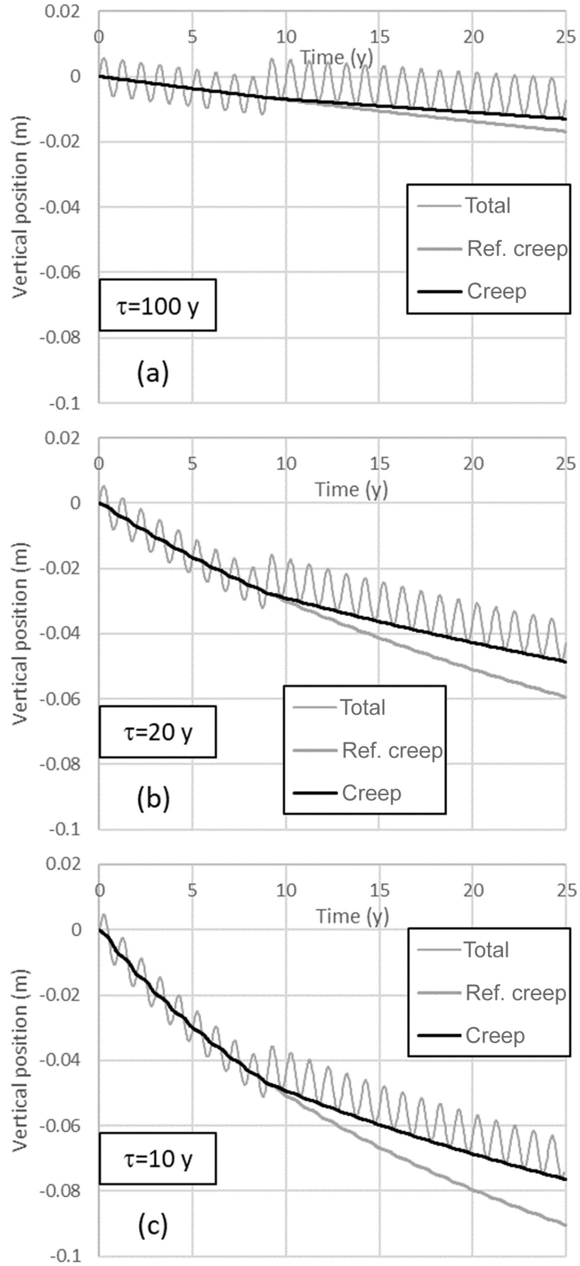

Figure 5. Calculated subsidence for scenario “raising”. The creep of the reference runs is depicted as “ref. creep”.

4 Discussion and conclusions

4.1 Elucidation of results of the scenarios

4.1.1 Drought scenario

Figure 3 shows that a single dry season with 1 m extra water table lowering, has a distinct subsidence impact (up to about 1 cm). However, most of this subsidence is due to elastic deformation and is recovered by the end of the drought. The net impact of the drought – defined here by the difference between the “creep” and “ref. creep” curves – is induced by enhancement of the rate of creep during the period in which the water table is anomalously low. The duration of this period (6 months in the simulation), therefore, is an important factor that determines the magnitude of the post-drought impact. The results further show that the impact is more significant for low values of τ (low OCR and high background subsidence rate). Furthermore, the loading and unloading caused by the drought and its recovery leaves the peat and clay mildly overconsolidated after the drought. That is, the OCR is slightly enhanced, and the creep rate slightly reduced after the drought. This is visible in Fig. 3c where the "creep" and "ref. creep" curve very slowly converge over the years after the drought. The net impact of the drought is very small relative to the background subsidence.

4.1.2 Damping scenario

The reduction of the amplitude of seasonal water table variation by 0.4 m (80 %) moderates the seasonal variation of the total land surface movement by approximately the same amount, and the annual average creep rate is slightly reduced (Fig. 4). The impact of the latter, in terms of millimetres of subsidence prevented, takes many years to decades to develop. The reduction of the annual creep rate is the result of opposing contributions of the wet and the dry season. The raised water table during the dry period compared to the reference condition, reduces the creep rate in that season. However, during the wet season, the lower water table compared to the reference condition enhances the creep rate during that time. The contribution of the dry season prevails in the net impact. This indicates that the effectiveness would be larger if only the dry season water table would be raised, and the wet season water table would be left untouched. The net impact of the drought is very small relative to the background subsidence.

4.1.3 Raising scenario

The permanent increase of the mean water table by 0.4 m has both a direct and a secular effect on the land surface elevation (Fig. 5). The direct effect consists of elastic uplift/heave of about 5 mm. The secular effect consists of the reduction of the creep rate. The reduction of the creep rate is permanent and applies to both the wet and the dry season (the amplitude of water table variation is not modified in this scenario). Comparison with Figs. 3 and 4 reveals that the impact of permanently raising of the water table is larger than for the other two scenarios. The greater impact is due to the permanent reduction of the creep rate. However, since water tables are already maintained at rather shallow depth in parts of The Netherlands that contain Holocene soft-soils, localities where water table can be raised by several decimetres or more without causing damage are probably very limited.

4.2 Need for field- and laboratory testing

The isotache model employed in this study, includes modern-day concepts of the soil mechanics of Holocene peat and clay. This model has been developed for the modelling of, and is primarily tested against, settlement caused by large loads such as dikes, and surcharge that is applied in areas where new residential areas are being built. It is presently unclear to what extent the model also accurately represents creep rates and creep behaviour for the small loads associated with the water table scenarios considered in this manuscript. Dedicated field- and laboratory tests are needed to shed more light on creep rates and creep behaviour for effective stress levels at or below the preconsolidation stress, and to test the validity of presented results.

4.3 Conclusions

Modelling employing an isotache-based viscoelastic compression model adopted from certified geotechnical software for settlement modelling allows quantitative assessment of the subsidence impact of interferences in water table conditions in urban areas.

Model results indicate that:

- The absolute subsidence impact of measures increases with increasing background subsidence rate.
- The effectiveness of measures increases with the duration of the period during which water tables are raised. That is, permanent raising tends to be more effective than periodic or occasional prevention of water table drops.
- For conditions that exist in urban areas in The Netherlands, water table interventions are predicted to prevent a fraction of the subsidence that would have occurred without the intervention.

Data availability. No data sets were used in this article.

Author contributions. HK conceptualized the analysis, developed the model scripts, conducted the experiments and wrote the original draft of the manuscript. GE reviewed and edited the draft manuscript.

Competing interests. Co-author Gilles Erkens is member of the editorial board of the special issue but was not responsible for the acceptance of the manuscript for publication.

Special issue statement. This article is part of the special issue "TISOLS: the Tenth International Symposium On Land Subsidence – living with subsidence". It is a result of the Tenth International Symposium on Land Subsidence, Delft, the Netherlands, 17–21 May 2021.

References

Den Haan, E. J.: Vertical Compression of Soils, PhD Dissertation, Technical University of Delft, 96 pp., 1994.

Kooi, H., Bakr, M., de Lange, G., den Haan, E., and Erkens, G.: User guide to SUB-CR; a MODFLOW package for land subsidence and aquifer system compaction that includes creep, Deltares internal report 11202275-008, available at: http://publications.deltares.nl/11202275_008.pdf (last access: 25 February 2020), 2018.

te Brake, B., van der Ploeg, M. J., and de Rooij, G. H.: Water storage change estimation from in situ shrinkage measurements of clay soils, Hydrol. Earth Syst. Sci., 17, 1933–1949, https://doi.org/10.5194/hess-17-1933-2013, 2013.

Van Laarhoven, S.: Influence of loading history on subsurface architecture and subsidence potential for the historical city of Gouda, The Netherlands, MSc Thesis, Utrecht University, 159 pp., 2017.

Systematic assessment of damage to buildings due to groundwater lowering-induced subsidence: methodology for large scale application in the Netherlands – update with results from the Dutch nationwide model

M. Korff[1,2], S. Kok[1], E. Smyrniou[1]

1 Deltares, Delft, 2600 MH, The Netherlands
2 TU Delft, Delft, 2628 CN, The Netherlands
Correspondence to: Mandy Korff (mandy.korff@deltares.nl)

Abstract

Subsidence of peat and clay soils due to (artificial) lowering of the groundwater table and loading of soft soils is commonplace in the Netherlands, causing extensive damage to exposed and vulnerable assets. In Costa et al (2020) a methodology is presented for the systematic regional or countrywide assessment of two subsidence-related damage mechanisms to buildings: differential settlement of buildings on a shallow foundation, and timber pile degradation due to low groundwater levels. The methodology is set up in a modular, systematic way – initially based on expert judgement and validation with available local detailed information - which allows for future improvements. In this update we present results of the model that can be a valuable input for public or private decision making, e.g. in awareness raising and evaluating interventions.

Introduction

In the Netherlands, subsidence of peat and clay soils due to (artificial) lowering of the groundwater table and loading of soft soils is commonplace, causing extensive damage to exposed and vulnerable assets. Improved risk assessment of subsidence-related damage to buildings would inform public and private actors from national to local scale on current and future risks and stimulate them to address this issue. In Costa et al. (2020) the authors proposed a methodology for systematic regional or countrywide assessment of two subsidence-related damage mechanisms to buildings: timber pile degradation due to low groundwater levels and differential settlement of buildings on shallow foundations. In this update the results of the corresponding model are presented.

Methodology recap and additional detail

The risk assessment is constructed in a modular, systematic way that allows for continuous improvement. Modules are built based upon the conceptual framework of Hazard (H) – Exposure (E) – Vulnerability (V) according to the definitions by the UNISDR (2016). Figure 1 and Figure 2 illustrate the methodology for the calculation of damages due to the two damage mechanisms. Details of the modules are given in Costa et al. (2020).

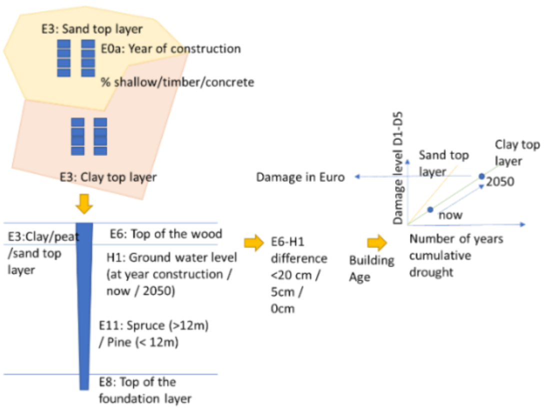

Figure 1 Schematic for the calculation of damages due to timber pile degradation induced by low groundwater levels.

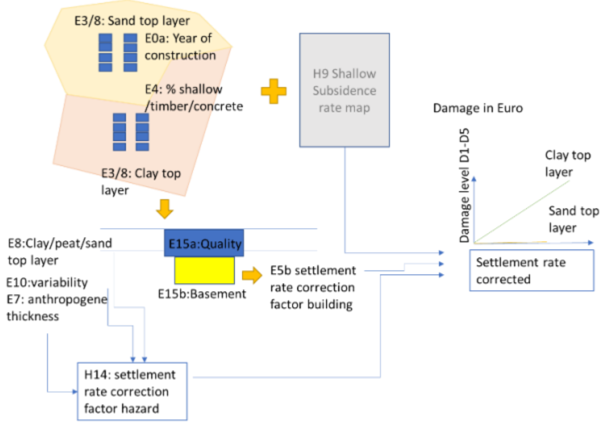

Figure 2 Schematic for the calculation of damages due to differential settlement of buildings on shallow foundations.

The exposure characterizes the buildings that are at risk. Key indicators for the exposure are the foundation types, characteristics and location, see Figure 3. Regional areas of typically similar foundations based on historical practice each have a foundation type probability per building, per year, per area and per soil type based on the expert sessions and local inventories made in some locations. For both damage mechanisms, the damage level is expressed in classes ranging from 1-5, (Burland and Wroth 1974). Damage classes for shallow foundations are assigned based on the rate of settlement with correction for factors of local hazard, shown in Table 1.

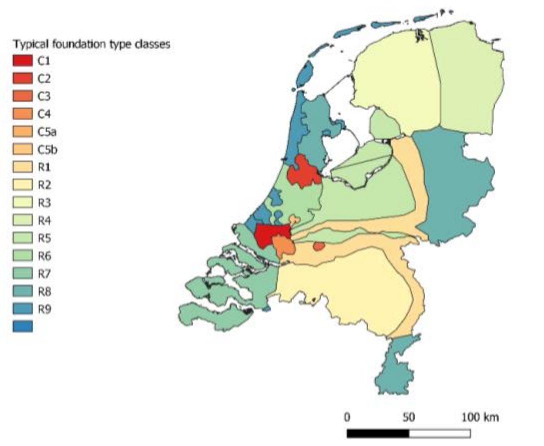

Figure 3 Map with regional areas of typical foundation types.

Table 1 Relationship between settlement rate and damage class.

Corrected settlement rate [mm/year]	Damage class
< 0.1	D0
0.1-1	D1
1-2	D2
2-3	D3
3-4	D4
>4	D5

Sensitivity analysis of model

A sensitivity analysis was executed on the impact of underlying assumptions on the hazard correction factors (e.g. the impact of a sand, clay or peat soil type at the foundation layer on the susceptibility of a building to differential settlement) as described in Costa et al (2020): Figure 4 shows the impact of alternative underlying assumptions on the resulting corrected subsidence rate in mm/year (which affects the expected damage level) against the number of buildings in the database. Similar analyses were done on several of the hazard and exposure parameters for the shallow foundation model, and the vulnerability function for the timber pile model. The shallow foundation model is most sensitive to assumptions regarding impact of heterogeneity in the subsurface and the type of soil at the foundation level. The timber pile model is quite sensitive to the assumed shape of the vulnerability function. These parameters will be focus of further study to reduce uncertainty in the model.

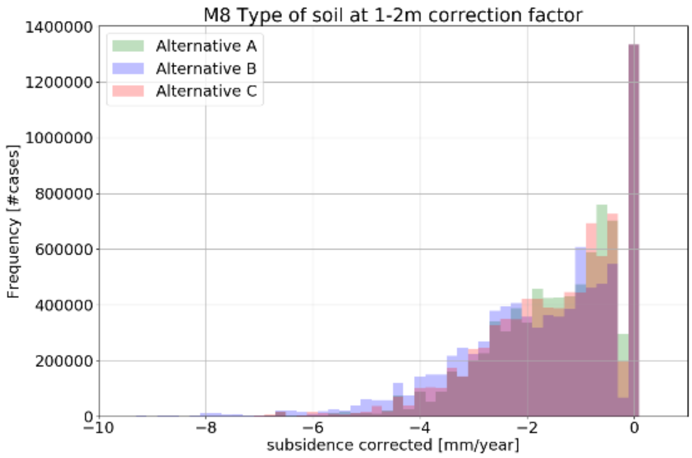

Figure 4 Number of buildings and their resulting subsidence rate including correcting factors as described in Costa et al (2020) for three different soil types (A, B, C).

Results of the model

To arrive at a national level estimate of expected damage in 2050, all information and indicators are collected at the building level in the model, with aggregated results presented in Figures 5 and 6.

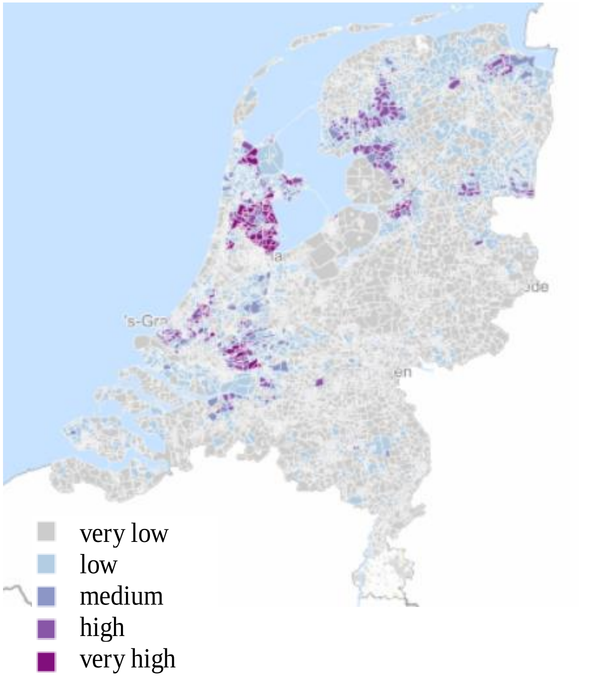

Figure 5 Shallow foundation risk per area; 2050 scenario with high climate change effects (very low: risk score <1; low: <5; medium: <10; high: <25; very high: <100)

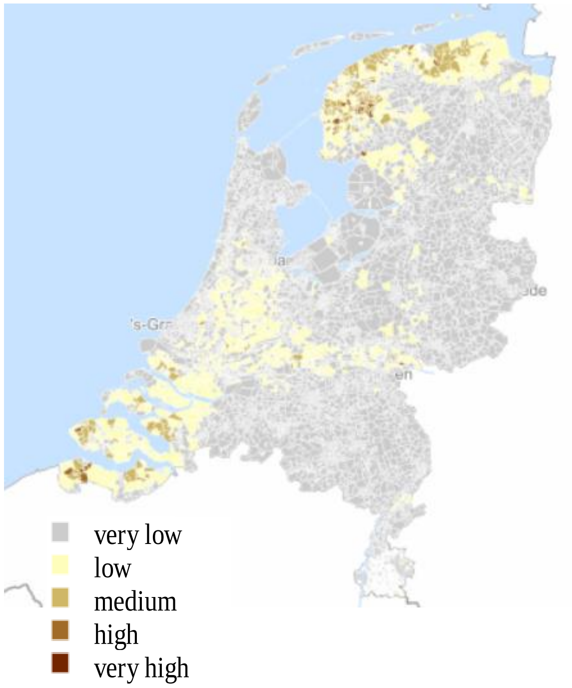

Figure 6 Timber pile foundation risk per area; 2050 scenario with high climate change effects (very low: risk score <1; low: <3; medium: <6; high: <15; very high: <41; medium: <10; high: <25; very high: <100)

Aside from this visual application of the model, the model was also run to derive an estimate of total risk (in number of buildings/ damage class and nominal € restoration cost) in the Netherlands until

2050 (see Figure 7, Table 2). As opposed to the previous version of the model of which results were used in the Klimaatschadeschatter (2019), this run was based on updates in vulnerability functions for both timber pile and shallow foundations, updated baseline subsidence map and updated shallow soil type map to better reflect sensitivity to shrink-swell behavior of clays, and new low groundwater level maps. Results show that total damages will be in the order of €9 to €40 billion until 2050. Most of the damage is to be expected in buildings with shallow foundations: in particular the small selection that is expected to reach damage level 5 and require full restoration. It should be noted that uncertainty in the model outcomes is still very high.

Conclusions and future work

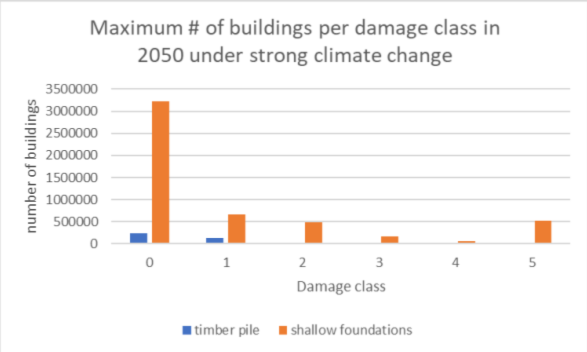

Figure 7 Maximum amount of buildings in each damage class by 2050 under strong climate change.

Table 2 Total restoration costs until 2050 for strong climate change scenario.

	Total restoration costs until 2050 per damage class in € *mln under strong CC			
	timber pile		shallow foundations	
Damage class	min	max	min	max
1	135	241	0	0
2	56	1038	115	1147
3	36	658	164	819
4	55	562	220	1323
5	11	310	8573	34291
	293	**2809**	**9072**	**37579**

This paper shows results and sensitivity of the damage assessment due to subsidence and drought to shallow foundation and foundations with timber piles. The approach relies heavily on the quality of the data. At this moment the model is being converted to a fully probabilistic model as to enable better propagation and assessment of uncertainties. The probabilistic model will be used to assess the sensitivity of the parameters in more detail. Also, ongoing research in the NWA-Loss project (nwa-loss.nl) on fragility functions for building damage will be implemented (see Prosperi, 2023 in this conference).

References

Burland, J. B., & Wroth, C. P. (1974). “Settlement of Buildings and Associated Damage.” Settlement of Structures, Proceedings of the Conference of the British Geotechnical Society (January 1975): 611–764.

Costa, A., Kok, S., & Korff, M. (2020). Systematic assessment of damage to buildings due to groundwater lowering-induced subsidence: methodology for large scale application in the Netherlands. In Tenth International Symposium on Land Subsidence.

Kok, S., Angelova, L., Impact droogte op funderingen; Deltares report 11205062-002 d.d 09-09-2020 (in Dutch)

Klimaateffectatlas.nl (2021) viewer drought foundation settlement and timber pile degradation (accessed on July 25, 2022) - including link to technical background report

Klimaatschadeschatter.nl (2019) viewer compiled drought risk per municipality (accessed on August 9, 2022).

Prosperi, A., Longo, M., Korswagen, P.A., Korff, M., Rots, J.G. (2023). Shape matters: Influence of varying settlement profiles due to multicausal subsidence when modelling damage in a masonry façade. Tisols 2023

UNISDR. 2016. A/71/644 Report of the Open-Ended Intergovernmental Expert Working Group on Indicators and Terminology Relating to Disaster Risk Reduction.

1D compaction modelling for subsidence prediction in California's San Joaquin Valley

M. M. Lees[1], R. Knight[1], W. Neely[1], M. Malenda[1]

1 Stanford University, Department of Geophysics.
Contact: mlees@stanford.edu

Abstract

We used 1D compaction models, which simulate the time-dependent drainage of subsurface clays, to aid with subsidence management in California's San Joaquin Valley. We applied models at two locations, calibrated over the period 1950s- present, and then made subsidence predictions through 2080. We found that our modelling was a significant improvement over existing approaches which either do not consider any physical-based modelling or consider simplified, elastic models with no time-dependent clay drainage. While remaining simplifications in our modelling approach limit the accuracy of subsidence predictions, 1D compaction modelling represents a promising direction to reliably simulate subsidence for groundwater management with the potential for further important scientific contributions to be made to meet management needs.

Introduction and background

Subsidence in California's San Joaquin Valley (SJV) has long been amongst the most dramatic in the World and in 2020 continued to occur at rates exceeding 20 cm/yr (Figure 1a). In 2014, California passed the Sustainable Groundwater Management Act, which requires groundwater managers to make plans to avoid 'undesirable results' of groundwater extraction, including excessive subsidence (Dickinson, 2014). A number of the first round of the so-called Groundwater Sustainability Plans (GSPs) were rejected as inadequate, with the lack of rigorous modeling of subsidence one reason for rejection. At present, GSPs either do not use physical subsidence models at all and assume that stabilization of heads will lead to cessation of subsidence, or they use elastic modeling, which assumes all subsidence occurs instantaneously with a head drop.

Here, we summarize a recent project where we worked in the Kaweah subbasin and applied 1D compaction modelling to simulate subsidence for their revised GSP. 1D compaction modelling solves for the time-dependent drainage of clays in response to head drops in sands, based on the aquitard drainage model, but has seen limited use in the SJV (Helm, 1975). We took the study of Lees et al. (2022), which developed and calibrated a 1D compaction model of historic subsidence at the South Hanford site in the basin, and extended it in two ways. First, we applied the workflow to a second location (the Tulare Irrigation District or TID site); and secondly, we extended the modelling to include future projections. The locations of both sites are displayed in Figure 1a.

Methods

The conceptual model we used at both sites is shown in Figure 1b. We separated the subsurface into an unconfined and a confined aquifer separated by the Corcoran Clay, where each aquifer consists of an interconnected coarse-matrix with clay interbeds. The variable d_i represents the depth of the lower aquifer below the deepest well. The number and thickness of the interbeds were determined using electrical-resistivity logs and lithology data. We used head measurements to determine the effective stress in the coarse-grained matrices, and used this effective stress as the temporally-varying boundary condition to solve for the evolution of effective stress in clays (Equation 1, Lees et al., 2022). It is this step capturing the time-dependent drainage of clays which is omitted in elastic models. We then converted the effective stress changes into compaction (Equation 3, Lees et al., 2022); this step is the same as in elastic models. We solved for compaction many times using different parameter values until we obtained a good match between simulated deformation and observed subsidence. The methodology is described in detail for the South Hanford site in Lees et al. (2022).

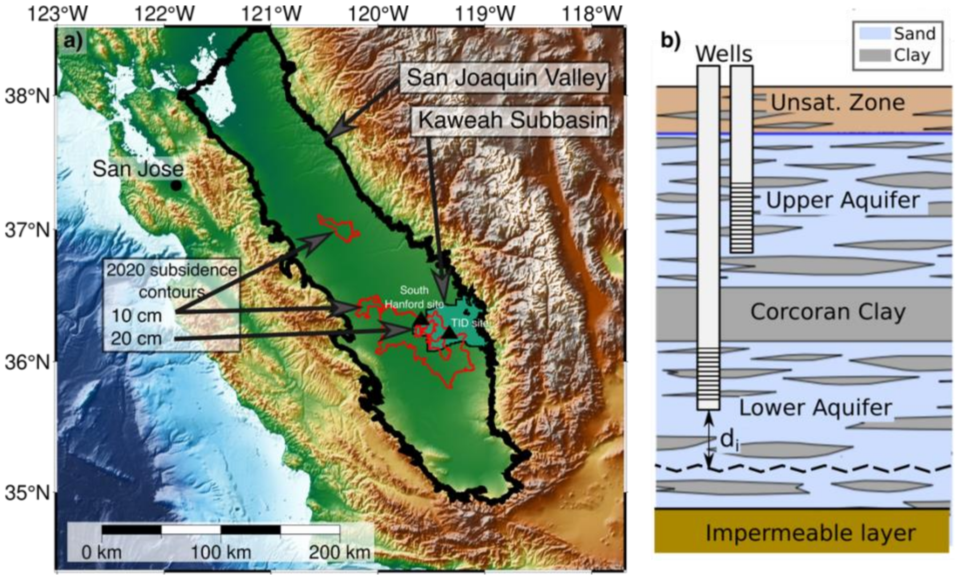

Figure 1 a) Map showing the Kaweah subbasin in relation to the San Joaquin Valley and 2020 subsidence, with 10 and 20 cm contours labelled. Subsidence contours come from TRE Altamira InSAR data, available at https://data.cnra.ca.gov/dataset/tre-altamira-insar-subsidence. The TID site and South Hanford site locations are shown by black triangles. b) the conceptual model we used for subsidence modelling.

To expand the modelling to the TID site, we gathered model inputs in a similar fashion to the South Hanford site. We took head records from seven wells to reconstruct a record of head in the coarse-matrices and we used a resistivity log and a lithology log to estimate the number and thickness of clay interbeds. Compaction models were assessed and calibrated using InSAR measurements from 2015-21 and a levelling survey from 1962-1970. To project future subsidence at both sites, we continued our models to 2080 using the projected upper and lower aquifer head pathways contained within the GSP.

Results

The simulated subsidence for both sites, as well as the historic and projected head, are shown in Figure 2. While a perfect fit was obtained with calibration data for the South Hanford site, as described in Lees et al. (2022), there was a small residual misfit at the TID site. At the South Hanford site, we projected approximately 7.8 m of subsidence between 2020-2040, and an additional 7.2 m from 2040-2080. At the TID site, we projected approximately 3.7 m of subsidence between 2020-2040, and an additional 2.9 m from 2040-2080.

Discussion

Our modeling represents a significant improvement over previous approaches used in GSPs. We include residual compaction, which is an important component as evidenced by the high rates of subsidence we simulate during 2040-80. Our simulations are based on the aquitard drainage model, which is long-established and gives physical basis to our simulations. Finally, our models are data-driven, which gives them a good physical grounding.

One downside is the limited spatial sampling: only two locations within an entire subbasin. The number of locations was low because the modelling required a large effort per site. This effort included both the collection of high-quality input data and the computational burden of the modelling itself[1]. Spatial sampling could be improved by embedding 1D compaction models into regional groundwater models, yet this would lead to lower reliability, as the compaction would be driven by modelled rather than measured head, and it would exacerbate the computational intensity. In our case, higher spatial sampling was required for the purposes of the GSP, and Montgomery & Associates took our two models and used a scheme to interpolate the results, although the accuracy of this approach was not tested (Montgomery & Associates, 2022).

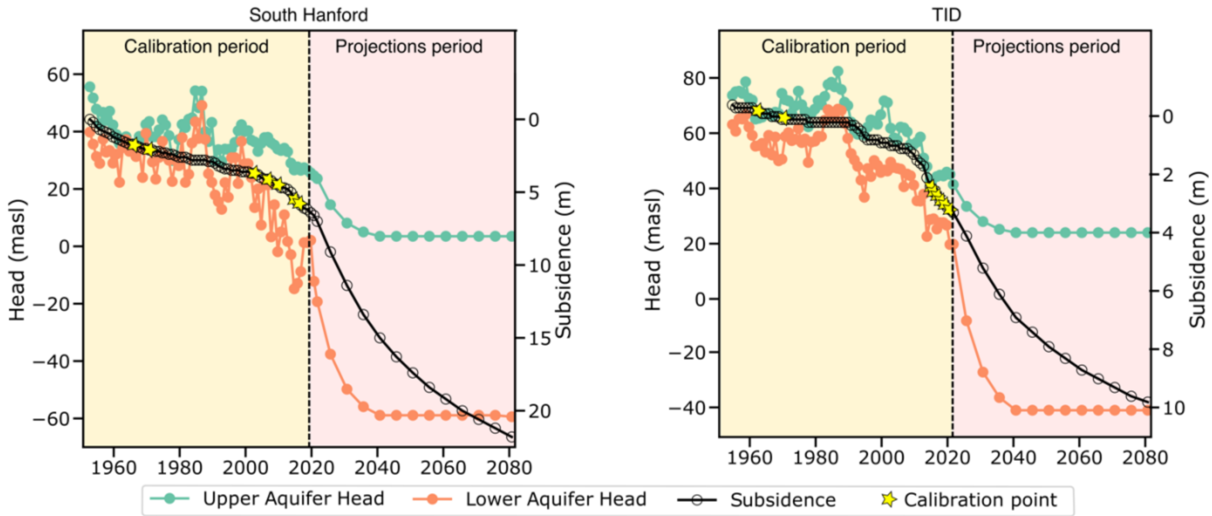

Figure 2 The input head and simulated subsidence for the two sites. The calibration period is where we used measurements of input head, tweaking input parameters until the simulated subsidence matched observations at calibration points. The projections period is where head was based on GSP-predictions and subsidence was simulated using calibration period parameters.

There remain aspects of the modeling which reduce our confidence in the predictions made. Foremost is the assumption of constant parameters. In the 1970s, Helm suggested that it is unlikely that S_{skv} will be constant with time as it is a function of stress (Helm, 1975, 1976). Nonetheless, he also found that a relatively good result could be obtained using a constant value. Helm's finding was relevant to a 20-year period, and it is unclear whether constant parameters remain a good approximation when considering the ~100+ years of subsidence required today. This may be a reason we could not perfectly fit the calibration data at the TID site. If, as is likely, S_{skv} decreases significantly between 1952 and 2080, our simulations will over-estimate subsidence.

[1] It took tens-to-hundreds of hours to run 100,000s of models at a site. This large number of models was needed to explore the parameter space for inputs such as K_v, S_{skv}, d_i and others in order to match the observed subsidence. Each model, containing up to 10 layers of different thickness clays, took 1-2 minutes.

Additionally, concerns include the lack of in-situ measurements of model inputs such as S_{skv} and K_v, which leads to a reliance on sweeping over large regions of parameter space to calibrate parameters. Finally, pumping now extends deeper than it did in the 1970s, and the lower aquifer is commonly >100 m thick. This begs the question of whether it might be necessary to divide the lower aquifer into multiple layers, each with a different head in the interconnected matrix, which could alter the results of projections.

Conclusions

1D compaction modelling for sustainable groundwater management in the SJV is a powerful tool likely to gain increasing attention in coming years. Despite its proven potential, there are important avenues of investigation and advancement for the scientific community to make in order to fully meet the management need.

Acknowledgements

Funding for this study was provided by Montgomery & Associates under contract to the Mid-Kaweah, East-Kaweah and Greater Kaweah Groundwater Sustainability Agencies (GSAs), and the Gordon and Betty Moore Foundation. We thank Dennis Mills of Kings County Water District, Larry Dotson of Kaweah Delta Water Conservation District, Eric Osterling from Greater Kaweah GSA and Aaron Fukuda from Tulare Irrigation District for assisting with local datasets. We thank Derrik Williams and Georgina King (both of Montgomery & Associates) and Aaron Fukuda for detailed discussions throughout the study.

References

Dickinson. Assembly Bill No. 1739 (2014). Retrieved from https://leginfo.legislature.ca.gov/faces/billTextClient.xhtml?bill_id=201320140AB1739

Helm, D. C. (1975). One-dimensional simulation of aquifer system compaction near Pixley, California: 1. Constant parameters. *Water Resources Research*, *11*(3), 465–478. https://doi.org/10.1029/WR011i003p00465

Helm, D. C. (1976). One-dimensional simulation of aquifer system compaction near Pixley, California: 2. Stress-Dependent Parameters. *Water Resources Research*, *12*(3), 375–391. https://doi.org/10.1029/WR012i003p00375

Lees, M., Knight, R., & Smith, R. (2022). Development and Application of a 1D Compaction Model to Understand 65 Years of Subsidence in the San Joaquin Valley. *Water Resources Research*, *58*(6), e2021WR031390. https://doi.org/10.1029/2021WR031390

Montgomery & Associates. (2022, July 27). Technical Approach for Developing Subsidence Sustainable Management Criteria in the Kaweah Subbasin.

Quantifying shrinkage of marine and fluvial clay deposits by means of soil-shrinkage curves

Bente Lexmond[1], Marc Nijboer[1,2], Cjestmir de Boer[2], Jasper Griffioen[1,2], Gilles Erkens[1,3], Esther Stouthamer[1]

1 Utrecht University
2 TNO Geological Survey of The Netherlands
3 Deltares
Corresponding author: Bente Lexmond (b.r.lexmond@uu.nl)
Theme: Mechanisms and Understanding of land subsidence; Foci: Coastal areas, Deltas & Sea Level Rise

Abstract

Shrinkage and swelling due to moisture content changes in clay-rich expansive soils are well-known and notorious phenomena, as they cause damage to infrastructure and change the hydrological and mechanical characteristics of the soil. Irreversible soil shrinkage also induces land subsidence. Shrinkage behaviour is often described by a soil-shrinkage curve, which relates the void ratio to the moisture content. The shape of these curves depends on sampling method, sample size and type, and is related to the soil and porewater composition, soil density and its stress history. The aim of this research project is a) to acquire understanding of clay deformation due to drying and chemical changes and b) to quantify the interacting processes in situ such as compaction and shrinkage in a soil column. To do so, an adapted soil-shrinkage curve methodology was devised, combining several types of measurements. With the use of the methodology clear differences in soil-shrinkage curves can be identified. Organic fluviatile clay samples show relatively more shrinkage during the first phase of shrinkage, compared to inorganic marine clay samples. The organic clay samples also show an increasingly dominant vertical deformation during drying.

Introduction

Damage to infrastructure and changing hydrological and mechanical soil properties are notorious phenomena as a result of volume change of expansive soils. When unconsolidated soft deposits are dried irreversible shrinkage can take place, leading to (enhanced) land subsidence. Both reversible and irreversible soil shrinkage have been studied extensively for over 70 years (e.g., Stirk, 1954; Davidson & Page, 1956; Yule & Ritchie, 1980; Cornelis et al., 2006) using diverse methods and sample types. An important tool in understanding shrinkage and swelling is a soil-shrinkage curve, which relates the void ratio to the moisture content of a soil.

Traditionally, four shrinkage phases are defined in a shrinkage curve; (1) structural shrinkage, (2) proportional shrinkage, (3) residual shrinkage and (4) zero shrinkage (e.g., Peng & Horn, 2007). Structural shrinkage can occur during the first phase of drying in which macropores dry, but the volume loss is not equal to the volumetric water loss. After the structural shrinkage, proportional shrinkage occurs when volume loss equals moisture loss. Thereafter, the residual and finally zero shrinkage phases take place, when the loss of moisture yields little to no shrinkage. Not all phases are present in every soil-shrinkage curve: small (aggregate size) or remoulded samples lack the structural shrinkage phase as large macro pores are not present in the samples (Peng & Horn, 2013). However, the structure of a soil also changes during the zero shrinkage-phase, as intraparticle space is transferred to interparticle layers, which does not necessarily cause a change in the bulk density (Bruand and Prost, 1987). A change in the structure of the soil can cause permanent changes in the 2 soils' hydrological and mechanical behaviour. To capture the shrinkage behaviour in phases two to three, Lu & Dong (2017) proposed an alternative soil-shrinkage curve that focusses on the properties of the water that is transferred during drying. Two main regimes were identified: capillary and adsorption, in which the capillary phase encompasses water that can flow freely, and adsorption is the phase in which soil particle surfaces start to dehydrate.

The shrinkage curve and the field shrinkage limit (maximum amount of shrinkage at a suction of -1600 hPa; Bronswijk & Evers-Vermeer, 1990) has been correlated with soil characteristics such as expansive clay content (Crescimanno & Provenzano, 1999; Mishra et al., 2008), organic matter content (Peng & Horn, 2007;), soil density, specific surface area, cation exchange capacity (Gray & Allbrook, 2002) and maximum adsorbed water content (Lu & Dong, 2015). These characteristics can be related to the soil water retention curve (SWRC, or pF-curve), which related the water content to the soil water suction. Greene-Kelly (1974) also found a significant correlation between expansive mineral content and shrinkage for remoulded samples, but not for samples that have been exposed to drying and wetting cycles, indicating the effect of stress history on the shrinkage behaviour. Rasa et al. (2009) studied the effect of land use on shrinkage and found a difference of 4.8% in total shrinkage when a clay soil was managed differently, whereas on average shrinkage was 10% in these soils. These results highlight the importance of studying natural undisturbed samples to identify shrinkage governing soil characteristics.

The aim was to create a non-disturbing continuous volume change measurement set-up while also measuring soil water suction and the weight of the sample, in order to create soil-shrinkage curves during air drying of natural undisturbed samples. The method and preliminary results are described and assessed in the following sections.

Methodology

The first step in the project was measuring the soil-shrinkage curves of marine and fluviatile undisturbed clay-rich samples from the Netherlands, using a basic measurement set-up. These results are summarized in the next section. After confirming the sample size to be suitable to measure all shrinkage phases, a measurement method was devised that measures soil shrinkage, evaporation and soil water suction, continuously in controlled conditions. This set-up is used to measure the shrinkage of clay-rich samples from all over the Netherlands, focusing on differences in organic matter content, clay mineralogy, porewater salinity and stress history, to be able to understand the influence and quantify the effect of soil composition and stress history on soil shrinkage.

Two sampling sites were selected based on depositional environment (marine and fluvial), texture, organic matter content and practical considerations with regard to land use and accessibility. Both the sampling sites are located in the western Netherlands: near the villages Abbenes (marine deposit) and Montfoort (fluvial deposit) (Figure 1). Samples were extracted by using a ring sampler to minimize disturbance. In the laboratory the samples were transferred from the stainless-steel sample rings to latex pouches, to be able to measure both height and diameter changes. Water samples were collected from the same sampling depth in nearby (50 cm) boreholes to determine the local groundwater composition at both sampling sites.

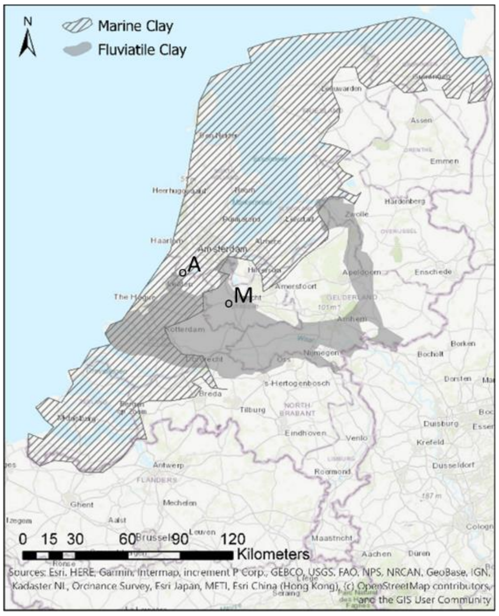

Figure 1 Sample locations Montfoort (M) and Abbenes (A) and an indication of the marine and fluviatile Holocene clay deposits in the Netherlands.

Sample preparation and characteristics

The soil samples were left to dry in a climate-controlled room for up to 20 days, while the height and diameter of the samples were measured with the use of a digital caliper twice a day (9:30 and 16:30), with exception of weekends. The top of the samples was not covered by the latex cover, creating an evaporative surface. The measurements were terminated when no volume loss was detected for at least two days. After the measurements samples were analyzed on textural composition (pipette method; Gee & Bauder, 1986), organic matter content (loss on ignition; Heiri et al., 2001) and CaCO3 content (Schleiber method; Eijkelkamp). The sample characteristics are shown in table 1.

Table 1 Composition of the organic fluvial (Montfoort) and inorganic marine (Abbenes) clay soils in terms of calcium carbonate content, organic matter content, and grain size distribution. All values are given in weight percentages.

Soil ID	**Sample depth**	**$CaCO_3$**	**Organic matter**	**<2 µm**	**2-8 µm**	**8-16 µm**	**16-32 µm**	**32-63 µm**	**>63 µm**
Organic clay 1	95 cm	0.19	26.81	47.74	18.76	3.72	0.51	2.12	0.07
Organic clay 2	95 cm	0.19	29.63	41.12	21.4	3.93	2.66	0.91	0.21
Inorganic clay 1	185 cm	2.40	6.65	44.85	29.43	13.56	4.09	0.91	0.0
Inorganic clay 2	185 cm	0.56	7.37	39.77	32.22	10.31	9.39	0.46	0.0

Measured and fit shrinkage curves

The measurement method is suitable to measure differences in the soil-shrinkage curves of the different samples, with a measurement interval of twice a day (Figure 2). The fluviatile samples (Organic clay 1 and 2) have significantly higher initial moisture contents and void ratios than the marine samples (Inorganic clay 1 and 2). The different shrinkage phases were identified on the representative inflection points and are shown in Figure 2. The fluvial samples also show a more extensive structural shrinkage phase than the marine samples, responsible for 14-18% of the total shrinkage (Table 2).

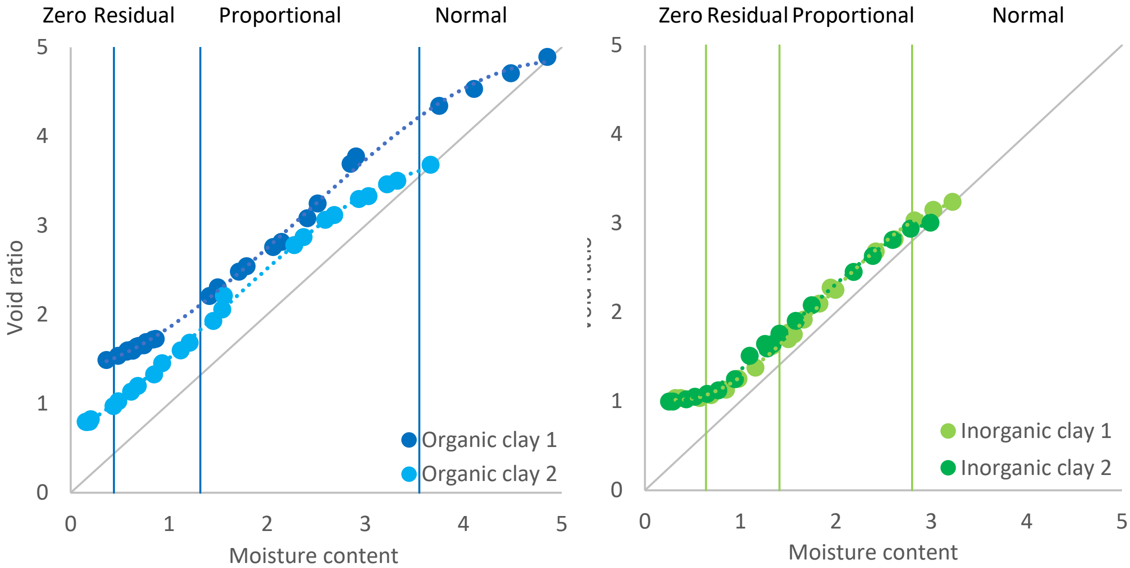

Figure 2. Soil shrinkage curves of organic fluviatile and inorganic marine samples, measured during air drying. Including indications of the transition between shrinkage phases for organic clay 1 and inorganic clay 1.

Table 2. The moisture content loss (ϑ) and decrease in void ratio (e) as per sample during the structural (s), proportional (p), residual (r) and zero (z) shrinkage phases.

Sample	ϑ_s**(%)**	ϑ_p**(%)**	ϑ_r**(%)**	ϑ_z**(%)**	e_s**(%)**	e_p**(%)**	e_r**(%)**
Organic clay 1	27.40	45.60	18.00	9.00	14.11	43.15	11.45
Organic clay 2	27.99	50.82	18.75	2.45	17.94	47.01	14.67
Inorganic clay 1	13.58	42.90	23.77	19.75	7.92	43.54	14.31
Inorganic clay 2	13.62	44.52	25.91	15.95	8.21	43.14	16.43

Shrinkage can be measured volumetrically and is often assumed to be isotropic. The measured shrinkage is not completely isotropic in these samples. Relatively, the marine inorganic clay samples show a larger height decrease during the first phase of shrinkage, followed by a more dominant decrease of radius in a later stage of the shrinkage (Figure 3). The organic fluviatile samples show a relatively larger height decrease during all phases of the shrinkage.

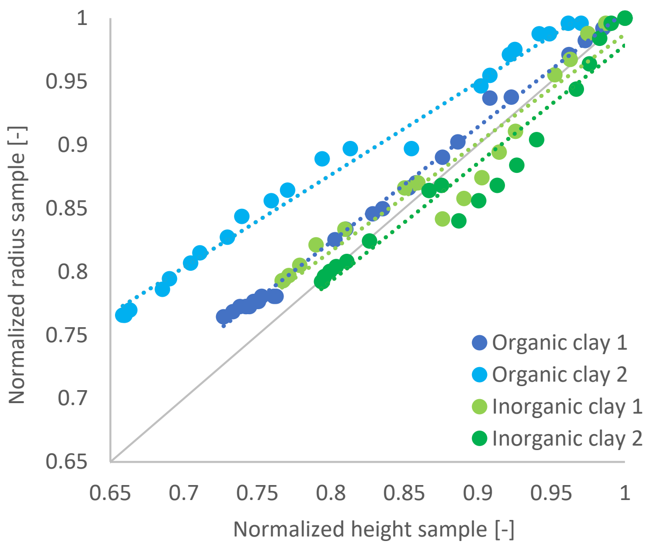

Figure 3. The normalized radius over the normalized height of the sample during shrinkage.

Conclusion and outlook

The base set-up that was devised for measuring the shrinkage of undisturbed natural clay samples is sufficient to capture the four shrinkage phases occurring during air-drying clay rich samples. The methodology would benefit when volume measurements are carried out more frequently, with regard to identifying the different shrinkage phases in the soil-shrinkage curves.

The differences in shrinkage behaviour that are identified for the four analyzed samples are a combined effect of differences in the composition, structure and density of the samples. However, the relatively larger decrease in the height of the fluviatile organic rich clay samples can be explained by the structure of the clay as a result of the depositional environment. The clay particles are deposited mostly horizontal in plate form in fluviatile low-energy deposits, whereas the high ion content in salt or brackish water causes the clay particles to flocculate and deposit in a card-house structure in marine depositional environments (Gibbs, 1983). The laminar platelets can create a denser structure than the card-house structured platelets, especially in the vertical direction.

To be able to understand and quantify the shrinkage behaviour of Holocene clay deposits in the Netherlands a larger database is needed. The aim of this research project is to create that dataset and to incorporate the results in soil shrinkage simulations. Both horizontal and vertical shrinkage can add to land subsidence, either via exposing buried organic-rich deposits to oxygen via cracks, or because of irreversible shrinkage in unripe clay layers.

Funding

The research presented is part of the project Living on soft soils: subsidence and society (grantnr.NWA.1160.18.259). This project is funded by the Dutch Research Council (NWO-NWA-ORC), Utrecht University, Wageningen University, Delft University of Technology, Ministry of Infrastructure & Water Management, Ministry of the Interior & Kingdom Relations, Deltares, Wageningen Environmental Research, TNO Geological Survey of The Netherlands, STOWA, Water Authority: Hoogheemraadschap de Stichtse Rijnlanden, Water Authority Drents Overijsselse Delta, Province of Utrecht, Province of Zuid-Holland, Municipality of Gouda, Platform Soft Soil, Sweco, Tauw BV, NAM.

References

Bruand, A., & Prost, R. (1987). Effect of water content on the fabric of a soil material: an experimental approach. *Journal of Soil Science*, *38*(3), 461-472.

Cornelis, W. M., Corluy, J., Medina, H., Diaz, J., Hartmann, R., Van Meirvenne, M., & Ruiz, M. E. (2006). Measuring and modelling the soil shrinkage characteristic curve. *Geoderma*, *137*(1-2), 179-191.

Crescimanno, G., & Provenzano, G. (1999). Soil shrinkage characteristic curve in clay soils: Measurement and prediction. *Soil Science Society of America Journal*, *63*(1), 25-32.

Davidson, S. E., & Page, J. B. (1956). Factors influencing swelling and shrinking in soils. *Soil Science Society of America Journal*, *20*(3), 320-324.

Gebhardt, S., Fleige, H., & Horn, R. (2012). Anisotropic shrinkage of mineral and organic soils and its impact on soil hydraulic properties. *Soil and tillage research*, *125*, 96-104.

Gee, G. W., Bauder, J. W., & Klute, A. (1986). Methods of soil analysis, part 1, physical and mineralogical methods. *Soil Science Society of America, American Society of Agronomy*.

Gibbs, R. J. (1983). Coagulation rates of clay minerals and natural sediments. *Journal of Sedimentary Research*, *53*(4), 1193-1203.

Gray, C. W., & Allbrook, R. (2002). Relationships between shrinkage indices and soil properties in some New Zealand soils. *Geoderma*, *108*(3-4), 287-299.

Greene-Kelly, R. (1974). Shrinkage of clay soils: A statistical correlation with other soil properties. *Geoderma*, *11*(4), 243-257.

Heiri, O., Lotter, A. F., & Lemcke, G. (2001). Loss on ignition as a method for estimating organic and carbonate content in sediments: reproducibility and comparability of results. *Journal of paleolimnology*, *25*(1), 101-110.

Lu, N., & Dong, Y. (2017). Correlation between soil-shrinkage curve and water-retention characteristics. *J. Geotech. Geoenviron. Eng*, *143*(9), 04017054.

Mishra, A. K., Dhawan, S., & Rao, S. M. (2008). Analysis of swelling and shrinkage behavior of compacted clays. *Geotechnical and Geological Engineering*, *26*(3), 289-298.

Peng, X., Horn, R., & Smucker, A. (2007). Pore shrinkage dependency of inorganic and organic soils on wetting and drying cycles. *Soil Science Society of America Journal*, *71*(4), 1095-1104.

Peng, X., & Horn, R. (2013). Identifying Six Types of Soil Shrinkage Curves from a Large Set of Experimental Data. *Soil Science Society of America journal*.

Rasa, K., Horn, R., Räty, M., Yli-Halla, M., & Pietola, L. (2009). Shrinkage properties of differently managed clay soils in Finland. *Soil use and management*, *25*(2), 175-182.

Stirk, G. B. (1954). Some aspects of soil shrinkage and the effect of cracking upon water entry into the soil. *Australian Journal of Agricultural Research*, *5*(2), 279-296.

Yule, D. F., & Ritchie, J. T. (1980). Soil shrinkage relationships of Texas Vertisols: I. Small cores. *Soil Science Society of America Journal*, *44*(6), 1285-1291.

Proc. IAHS, 382, 505–510, 2020
https://doi.org/10.5194/piahs-382-505-2020

Land subsidence modelling using a long short-term memory algorithm based on time-series datasets

Huijun Li, Lin Zhu, Huili Gong, Hanrui Sun, and Jie Yu

Laboratory Cultivation Base of Environment Process and Digital Simulation,
Capital Normal University, Beijing, 100048, China

Correspondence: Lin Zhu (hi-zhulin@163.com)

Published: 22 April 2020

Abstract. With the rapid growth of data volume and the development of artificial intelligence technology, deep-learning methods are a new way to model land subsidence. We utilized a long short-term memory (LSTM) model, a deep-learning-based time-series processing method to model the land subsidence under multiple influencing factors. Land subsidence has non-linear and time dependency characteristics, which the LSTM model takes into account. This paper modelled the time variation in land subsidence for 38 months from 2011 to 2015. The input variables included the change in land subsidence detected by InSAR technology, the change in confined groundwater level, the thickness of the compressible layer and the permeability coefficient. The results show that the LSTM model performed well in areas where the subsidence is slight but poorly in places with severe subsidence.

1 Introduction

The continuous over-pumping of groundwater can result in dramatic drawdown and regional land subsidence, threatening the living environment. Land subsidence is often related to anthropogenic factors that can cause economic losses and casualties, such as municipal infrastructure damage, cracks in transport facilities, and building fractures.

Land subsidence is a complex process influenced by the interaction of anthropogenic activities and the hydrogeological environment. It often develops unevenly and seasonally and can display hysteresis depending on the soil mechanical properties (Ezquerro et al., 2014; Miller and Shirzaei, 2015; Bonì et al., 2016; Gao et al., 2018; Haghighi and Motagh, 2019).

Previous studies on the mechanism of land subsidence were based on the well-understood constitutive model, and the numerical simulation model was established to simulate the future displacement. However, explicit description of hydrogeological information which may have space–time sparseness is required to do so accurately. This constrains its application for large areas. The grey model (GM) based on grey theory is an alternative model to predict the short-term land subsidence, but it ignores the non-linear characteristic of land subsidence. Some researchers proposed the modified GM model combined with artificial neural network (ANN) or other algorithms to deal with the non-linear features (Li et al., 2007). These methods can have a good short-term prediction and perform well when data volume is small, while the deep information cannot be mined when the data volume is large and cannot be used in long-term prediction.

The long short-term memory (LSTM) model is a deep-learning method that can process a large volume of time-series data and forecast the value of the next moment. It constructs a multilayer neural network to excavate the temporal dynamic features of historical data, considering the non-linearity and temporal dependency characteristics. The prediction period depends on the time interval of the input data. It has been successfully applied to $PM_{2.5}$ concentration forecasting, which is a temporal–spatial phenomenon (Qi et al., 2019), but no research used this method to simulate the land subsidence.

With the rapid growth of land subsidence data volume obtained by InSAR technology, the application of deep-learning

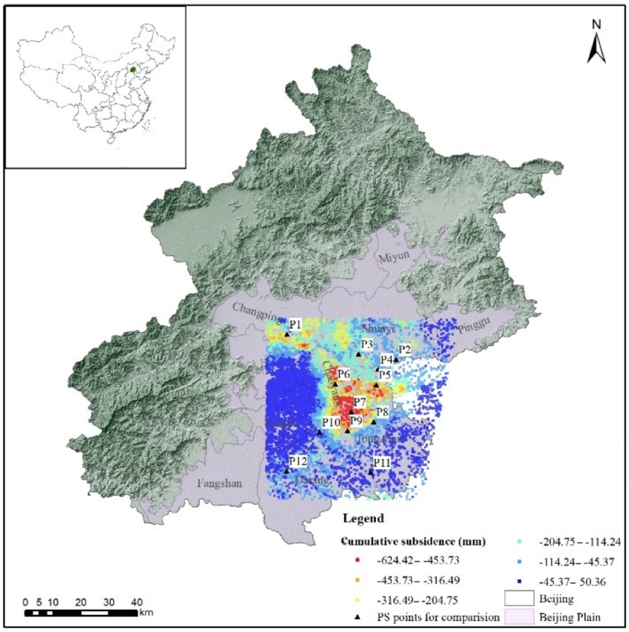

Figure 1. The location of the study area and land subsidence from 2011 to 2015 derived from RadarSat-2 images (the digital elevation model data are from the Shuttle Radar Topography Mission – SRTM – website).

methods of recent studies shows its potential in time-series land subsidence modelling (Yu et al., 2018). In this paper, we utilized the LSTM method to model the land subsidence under multiple influencing factors.

2 Study area and datasets

2.1 Study area

The study area is located in the Beijing Plain, where the largest cumulative land subsidence from 2011 to 2015 had been reached at 624.42 mm, as shown in Fig. 1. Due to urban sprawl and groundwater extraction, land subsidence in Beijing has become a matter of concern and is threatening the sustainable development of the city.

2.2 Available datasets

As noted in the literature, excessive exploitation of groundwater is the main trigger of land subsidence, and compressible layers are geologically responsible for the land subsidence in the Beijing Plain region (Zhu et al., 2015, 2017; Chen et al., 2016). This study considered these two aspects to be the influencing factors of land subsidence. The available datasets include the confined groundwater level, the thickness of the compressible layer, the permeability coefficient, and the cumulative land subsidence from 2011 to 2015 derived from 38 RadarSat-2 descending images. Constrained by accessible groundwater data, we got 16 487 persistent scatterer (PS) points. Therefore, we have in total 626 506 samples recording the LOS subsidence and the related influencing factors to simulate the land subsidence.

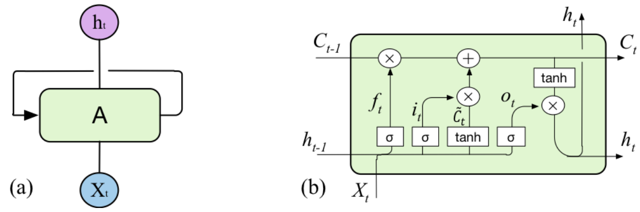

Figure 2. Diagram of an RNN network and LSTM computing cell (from Wikipedia).

2.3 Data processing

The confined groundwater level observed by the monitoring stations was interpolated using the kriging interpolation method into a raster with a 20 m × 20 m grid size by a batch process. The thickness of the compressible layer and the permeability coefficient of the study area were both represented by a contour. So, they were converted into points and interpolated using the kriging method. The change in the confined groundwater level was calculated and used as the input variable of the LSTM model together with the other two factors. The cumulative land subsidence was also converted into the variation to eliminate its tendency. All the data were normalized using the min–max scaling method. All these attributes were extracted to the PS points by a spatial analysis tool in ArcGIS.

3 Methodology

3.1 InSAR technology

InSAR technology records the phase and amplitude of the electromagnetic waves of ground objects. The phase information is used to inversely determine the extent of land subsidence. PS-InSAR (PSI) is the most common and effective method for detecting regional time-series land subsidence by calculating the differential interferometric phase and generating lots of PS points. PSI technology overcomes the problems of temporal and geometrical decorrelation and minimizes the atmospheric and noise phase contributions. The outputs include (1) the coordinates of land subsidence points, (2) the LOS cumulative land subsidence and (3) the land subsidence rate. Increasing availability of the long-term and large amount of land subsidence data detected by InSAR technology has provided the chance for data-driven modelling.

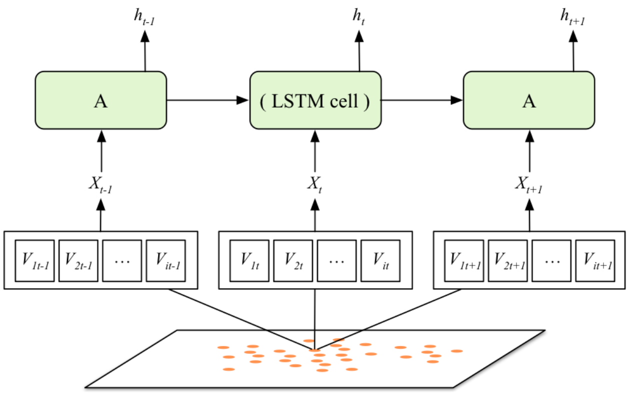

Figure 3. The LSTM model structure of this study.

Table 1. Details of the experimental settings.

Parameter	Value
Number of records	626 506
Training set	70 %
Test set	30 %
Time series	2010–2015, 38 months
Learning rate	0.001
Batch size	38
Hidden layers	8
Input size	4
Output size	1
Optimization function	Gradient descent optimizer

3.2 LSTM algorithm

A RNN (recurrent neural network) is a kind of deep neural network for processing sequence data considering the impact of last moments on the present. Parameter sharing on a time domain with a loop structure is its important character. As shown in Fig. 2a, $\boldsymbol{X}_t$ represents the input characteristics at time t, A is the computing unit which is also known as the hidden layer, and $\boldsymbol{h}_t$ is the output value. The hidden layer controls the information conversion process of the sequence data. It fits the mapping relations between the input multidimensional features and the labels and learns the weight matrix and bias to calculate the corresponding output value. However, RNN suffers from vanishing gradient or gradient explosion problems when dealing with long-term time-series data.

The LSTM proposed by Hochreiter and Schmidhuber (1997) is a computing unit in a RNN structure. It introduced a gating function to avoid the long-term dependency problem. As shown in Fig. 2b, $\boldsymbol{f}_t$, $\boldsymbol{i}_t$, and o_t are three nonlinear gate functions and named the forget gate, input gate, and output gate in each memory block, respectively. The key to the LSTM is the cell state $\boldsymbol{C}_t$, which has only a small amount of linear interaction during the entire operation. It can effectively record history information for a long time

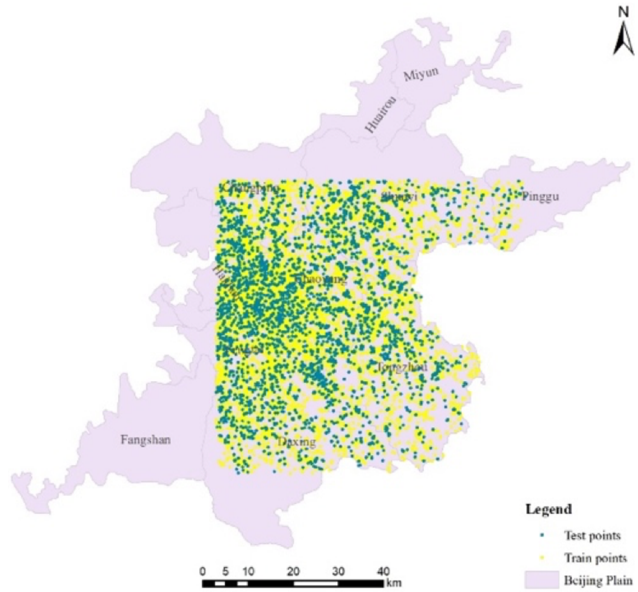

Figure 4. The distribution of the train and test data (the administrative map is from the Beijing Institute of Geo-Environment Monitoring).

through the three gates. For an input vector $\boldsymbol{x}_t$, the calculation equations for an LSTM unit with the three gates are as follows:

$$\boldsymbol{f}_t = \sigma(\mathbf{W}_\mathrm{f}\cdot[\boldsymbol{h}_{t\text{-}1}, \boldsymbol{x}_t] + \boldsymbol{b}_\mathrm{f}), \tag{1}$$

$$\boldsymbol{i}_t = \sigma(\mathbf{W}_\mathrm{i}\cdot[\boldsymbol{h}_{t\text{-}1}, \boldsymbol{x}_t] + \boldsymbol{b}_\mathrm{i}), \tag{2}$$

$$\boldsymbol{o}_t = \sigma(\mathbf{W}_\mathrm{o}\cdot[\boldsymbol{h}_{t\text{-}1}, \boldsymbol{x}_t] + \boldsymbol{b}_\mathrm{o}), \tag{3}$$

$$\boldsymbol{C}_t = \boldsymbol{f}_t \times \boldsymbol{C}_{t\text{-}1} + \boldsymbol{i}_t \times \tilde{\boldsymbol{C}}_t, \tag{4}$$

$$\tilde{\boldsymbol{C}}_t = \tanh\,(\mathbf{W}_\mathrm{C}\cdot[\boldsymbol{h}_{t\text{-}1}, \boldsymbol{x}_t] + \boldsymbol{b}_\mathrm{C}), \tag{5}$$

$$\boldsymbol{h}_t = \boldsymbol{o}_t \times \tanh\,(\boldsymbol{C}_t), \tag{6}$$

where $\mathbf{W}_\mathrm{f}$, $\mathbf{W}_\mathrm{i}$, $\mathbf{W}_\mathrm{o}$, and $\mathbf{W}_\mathrm{C}$ are the weight matrices for input vectors and $\boldsymbol{b}_\mathrm{f}$, $\boldsymbol{b}_\mathrm{i}$, $\boldsymbol{b}_\mathrm{o}$, and $\boldsymbol{b}_\mathrm{C}$ are the bias vectors at time t, respectively. $\tilde{\boldsymbol{C}}_t$ is the cell state of $\boldsymbol{x}_t$ involving the hidden state value $\boldsymbol{h}_{t\text{-}1}$ from a previous block at time t-1. $\boldsymbol{C}_t$ is the current unit state controlled by $\boldsymbol{f}_t$ and $\boldsymbol{i}_t$. h_t is the current output value controlled by the output gate and the current unit state. σ and tanh are the activation functions, a non-linear calculation process.

3.3 Subsidence modelling

The LSTM model structure established in this study was drawn in Fig. 3. The orange dots are the PS points, which record the time-series land subsidence derived from synthetic aperture radar (SAR) images and corresponding attributes that influence the land subsidence. The green block which contains the LSTM computing cell is the memory block of the RNN model. $\boldsymbol{X}_t = \{V_{1t},\ V_{2t},\ V_{it}\}$ are the input data at time t. V_{it} is the ith attribute of each PS point at time t. The

Table 2. The RMSE of the 14 validation points.

Test points	P1	P2	P3	P4	P5	P6	P7	P8	P9	P10	P11	P12
RMSE	15.77	13.95	16.69	12.60	15.19	16.07	16.32	11.30	13.49	10.01	5.97	4.48

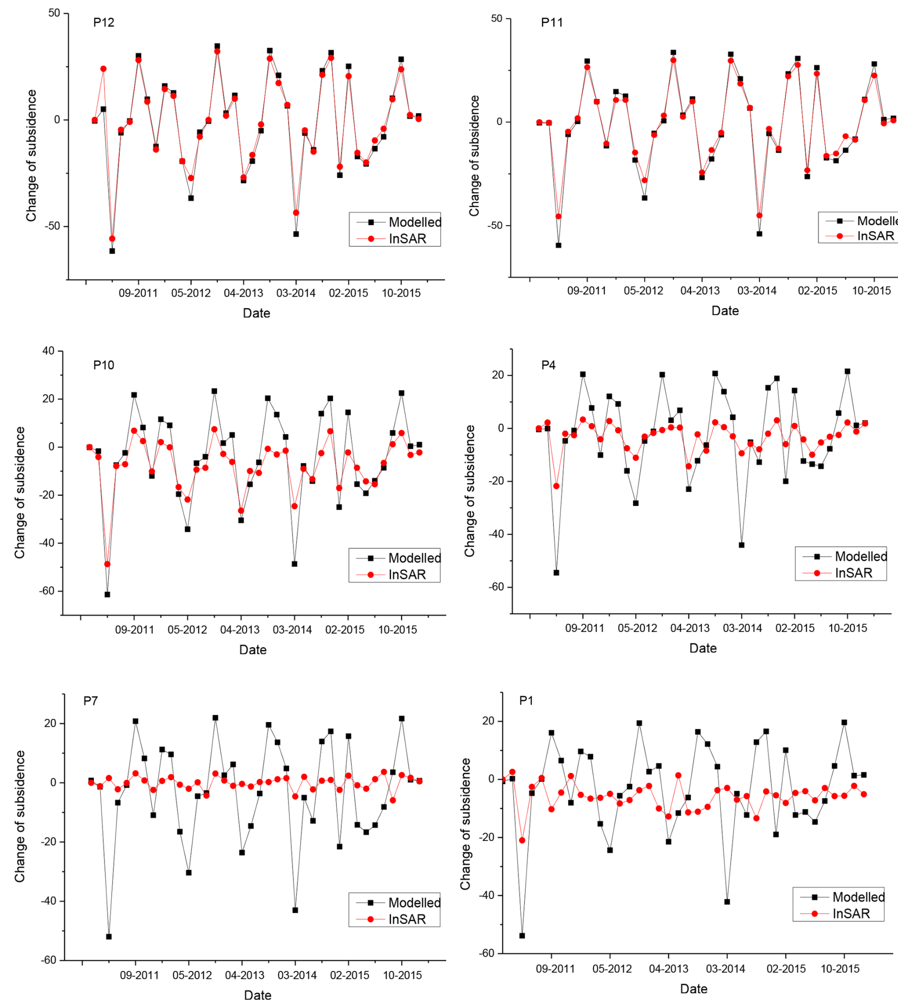

Figure 5. The fit curve between modelled and InSAR-derived change in land subsidence.

model would extract the characteristics of the multiple attributes through the time-series data from the input samples.

In this study, $X_t = \{V_{1t}, V_{2t}, V_{3t}, V_{4t}\} = \{$the change in land subsidence, the change in confined groundwater level, compressible layer thickness, permeability coefficient$\}$. It was a four-dimensional vector. The subsidence data were as the input labels and the attribute data were as the input features in the model-learning period. The model simulates the relationships between the change in subsidence and influencing factors.

4 Results and discussion

4.1 Experimental settings

The detailed experimental settings are listed in Table 1. The datasets were randomly divided into 70 % for the training set and 30 % for the test set to verify the accuracy of the model. The distribution of these data is shown in Fig. 4. The model training stage used the sum of variance between the modelled and accurate values to calculate the loss. The gradient descent optimizer was used for the parameter optimization. The activation function was the common one Tanh. Limited by the data volume, the learning rate was set to 0.001 and

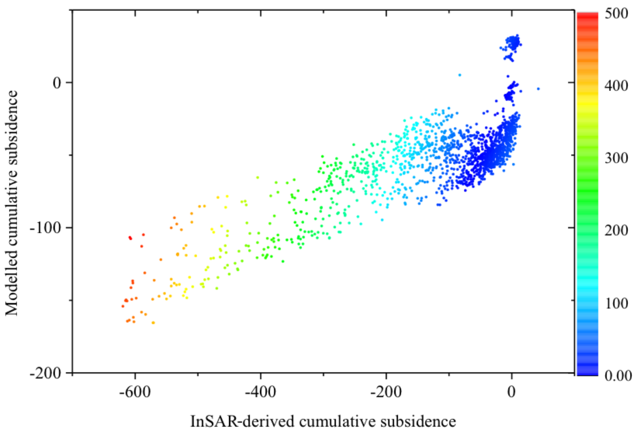

Figure 6. The deviation between the modelled and InSAR-derived cumulative land subsidence at the last moment.

the hidden layers were set to eight. A higher value can be set when the data volume is larger.

4.2 Experimental results

We got 13 190 points, in total 501 220 records as the training data, and 3297 points, in total 125 286 records, to test the model.

4.2.1 Results of LSTM modelling

To evaluate the performance of the model, 12 PS points were selected randomly as the validation point (the black triangle legend in Fig. 1). We compared the modelled land subsidence with the InSAR-derived results and evaluated the errors with root-mean-square error (RMSE). As shown in Table 2, the southern points (P11, P12) with less of a cumulative subsidence have a small error, while those points located in the severe land subsidence areas (P1, P3, P5, P6, P7) have a high RMSE.

To evaluate the impact of land subsidence severity on the model results, we chose P11 and P12 located in the southern area where the subsidence is small, P4 and P10 at the edges of the subsidence regions and P1 and P7 in the severe land subsidence areas. The fitting curves between the modelled and InSAR-derived land subsidence of these points were plotted in Fig. 5.

The results show that the LSTM model performed well in areas where the subsidence is slight but poorly in places with severe subsidence.

Overall, the RMSE and MAE are 14.412 and 10.539, respectively. Notably, the results recorded the change in land subsidence, which means that the RMSE represented the error of the change in land subsidence.

We calculated the change amount of land subsidence back to a cumulative quantity to assess the accuracy of the modelled cumulative land subsidence. The RMSE is 67.599. Figure 6 plotted the deviation between the modelled and InSAR-derived cumulative land subsidence. The deviation is small when the cumulative land subsidence is less than 100 mm. As the land subsidence increases, the deviation increases.

4.2.2 Analysis of the error source

As the results show, the severe land subsidence regions got a poor fit. These are areas of intense human activities (e.g. urban construction) and complex hydrogeological conditions, which are not reflected completely in the model.

There are two main error sources. One comes from inaccurate data and the selection of the input variables. In this study, we chose the confined groundwater level, the compressible layer thickness and the permeability coefficient as the influencing factors. The input groundwater level data were interpolated by the kriging method which may ignore the influence of the geological environment. The permeability coefficient has very little impact on the result. The selection of the input variables should include the main factors that affect land subsidence, such as the compressibility. These data are unpublished in our study area. It may be inverse to geotechnical test and geophysical methods in the future.

The other comes from the imperfect method. The LSTM model can process the time-series data well, but cannot deal with spatial phenomena. However, besides the groundwater level, the other two factors are almost constant in the time domain and spatially heterogeneous. This may be solved by combining the convolutional neural network (CNN) model which can extract spatial characteristics. In addition, the LSTM extracts characteristics from data, ignoring the physical process of land subsidence. This may also reduce its accuracy.

5 Conclusion and future work

This study constructed an LSTM model to simulate the land subsidence using the PS data detected by InSAR technology. Three factors were considered, which are the change in confined groundwater level, compressible layer thickness, and permeability coefficient. The model performed well in the southern areas where the subsidence is slight but poorly in the northern places with severe land subsidence. Land subsidence is a temporal–spatial phenomenon, and the LSTM model is a data analysis method with no consideration of physical mechanisms. In the future, we should combine the CNN model to solve the spatial heterogeneity and consider the physical process such as the consolidation theory in the model. Compared with the numerical simulation model and other grey models, this method requires fewer hydrogeological parameters and can be used for long-term large-area land subsidence modelling.

Data availability. The data used in this study will be available from the corresponding author on reasonable request.

Author contributions. HJL completed the experiment and paper, LZ and HLG provided rigorous guidance to the thesis, HRS processed part of the datasets, JY revised the paper.

Competing interests. The authors declare that they have no conflict of interest.

Special issue statement. This article is part of the special issue "TISOLS: the Tenth International Symposium On Land Subsidence – living with subsidence". It is a result of the Tenth International Symposium on Land Subsidence, Delft, the Netherlands, 17–21 May 2021.

References

Bonì, R., Cigna, F., Bricker, S., Meisina, C., and McCormack, H.: Characterisation of hydraulic head changes and aquifer properties in the London Basin using Persistent Scatterer Interferometry ground motion data, J. Hydrol., 540, 835–849, 2016.

Chen, M., Tomaìs, R., Li, Z. H., Motagh, M., Li, T., Hu, L. Y., Gong, H. L., Li, X. J., Yu, J., and Gong, X. L.: Imaging land subsidence induced by groundwater extraction in Beijing (China) using satellite radar interferometry, Remote Sens., 8, 468–489, 2016.

Ezquerro, P., Herrera, G., Marchamalo, M., Tomás, R., Béjar-Pizarro, M., and Martínez, R.: A quasi-elastic aquifer deformational behavior: Madrid aquifer case study, J. Hydrol., 519, 1192–1204, 2014.

Gao, M. L., Gong, H. L., Chen, B. B., Li, X. J., Zhou, C. F., Shi, M., Si, Y., Chen, Z., and Duan, G. Y.: Regional Land Subsidence Analysis in Eastern Beijing Plain by InSAR Time Series and Wavelet Transforms, Remote Sens., 10, 365–382, 2018.

Haghighi, H. M. and Motagh, M.: Ground surface response to continuous compaction of aquifer system in Tehran, Iran: Results from a long-term multi-sensor InSAR analysis, Remote Sens. Environ., 221, 534–550, 2019.

Hochreiter, S. and Schmidhuber, J.: Long short-term memory, Neural Comput., 9, 1735–1780, 1997.

Li, G. D., Yamaguchi, D., and Nagai, M.: A GM(1,1)–Markov chain combined model with an application to predict the number of Chinese international airlines. Technological Forecasting and Social Change, Technol. Forecast. Soc. Change, 74, 1465–1481, 2007.

Miller, M. M. and Shirzaei, M.: Spatiotemporal characterization of land subsidence and uplift in Phoenix using InSAR time series and wavelet transforms, J. Geophys. Res.-Solid Earth, 120, 5822–5842, 2015.

Qi, Y., Li, Q., Karimian, H., and Liu, D.: A hybrid model for spatiotemporal forecasting of PM2.5 based on graph convolutional neural network and long short-term memory, Sci. Total Environ., 664, 1–10, https://doi.org/10.1016/j.scitotenv.2019.01.333, 2019.

Yu, B., Yin, H., and Zhu, Z.: Spatio-Temporal Graph Convolutional Networks: A Deep Learning Framework for Traffic Forecasting, https://doi.org/10.24963/ijcai.2018/505, 2018.

Zhu, L., Gong, H. L., Li, X. J., Wang, R., Chen, B. B., Dai, Z. X., and Teatini, P.: Land subsidence due to groundwater withdrawal in the northern Beijing plain, China, Eng. Geol., 193, 243–255, 2015.

Zhu, L., Gong, H., Dai, Z., Guo, G., and Teatini, P.: Modeling 3-D permeability distribution in alluvial fans using facies architecture and geophysical acquisitions, Hydrol. Earth Syst. Sci., 21, 721–733, https://doi.org/10.5194/hess-21-721-2017, 2017.

Bayesian inversion of piezometric and displacement data to characterize aquifer properties

Yueting Li[1], Claudia Zoccarato[1], Lorenzo Tamellini[2], Chiara Piazzola[2], Pablo Ezquerro[3], Guadalupe Bru[3], Carolina Guardiola-Albert[3], Roberta Bonì[4], and Pietro Teatini[1]

1 Department of Civil, Environmental and Architectural Engineering, University of Padova, Padova, Italy
2 Istituto di Matematica Applicata e Tecnologie Informatiche "E. Magenes", Consiglio Nazionale delle Ricerche, Pavia, Italy
3 Geohazards InSAR Laboratory and Modeling Group (InSARlab), Geological Survey of Spain (IGME), CSIC, Madrid, Spain
4 Department of Pure and Applied Sciences, University of Urbino "Carlo Bo", Urbino, Italy
Session: Modelling and Matching of land subsidence
Contact: yueting.li@studenti.unipd.it

Introduction

The Alto Guadalentín Basin is one of the most important agricultural areas in Spain (Figure 1a). The exploitation of groundwater started in the 1960s to compensate for the scarcity of water and reached the maximum in the 1980s following the increasing anthropogenic activities. The over-exploitation of groundwater led to a significant decline of the piezometric level. Although new regulations have restricted the extraction of groundwater since 1989, these efforts had limited effects. The piezometric level in the vicinity of some active wells has declined up to 200 m from 1960 to 2012. As a direct consequence of such a large drawdown, the basin is experiencing one of the greatest rates of subsidence in Europe, with local rates exceeding 10 cm/yr. In the last decades, a series of studies have been conducted including geological surveys, subsidence monitoring, and deterministic numerical modeling (Cerón García 1995; Bonì et al. 2015; Ezquerro et al. 2017) providing investigations and explanations of the ongoing processes.

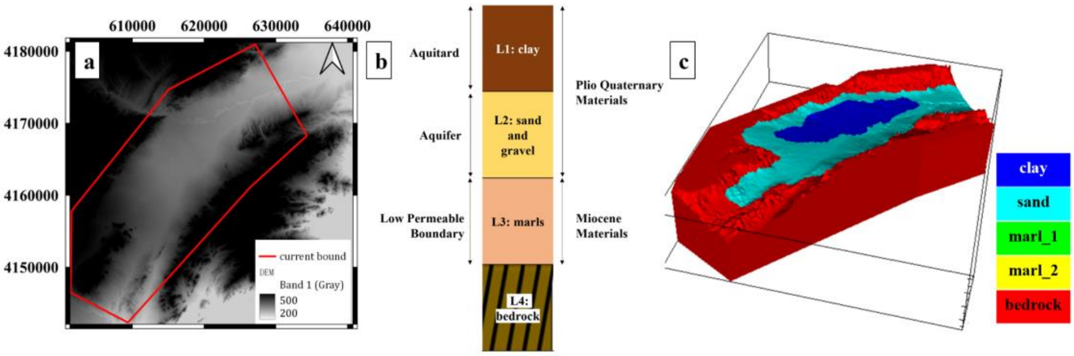

Figure 1 The Alto Guadalentín Basin. (a) Location of the aquifer system and digital elevation model showing the 2D model boundary, (b) Lithostratigraphic model of the aquifer system, and (c) 3D model domain with spatial distribution of the sedimentary bodies.

The aquifer system is composed of three main stratigraphic units (Figure 1b-c). The top clay layer is an aquitard but highly compressible, so this layer accounts for a large proportion of subsidence. The underlying sand and gravel layer is the main productive aquifer. The bottom of the aquifer system is mainly constituted by marls. There is some minor extraction within this layer even though it is much less permeable than the sand and gravel unit. However, it is challenging to perform history-matching, or even predict the aquifer system response to the human-induced stress. Indeed, from the hydraulic and geomechanical point of view, the behaviors of aquifer systems are governed by key parameters such as hydraulic conductivity and compressibility. On the other hand, these parameters are affected by high uncertainty, either because they are naturally heterogenous or because of inadequate observations. Overlooking these uncertainties may cause biased estimations of soil properties and compromised numerical results. Therefore, a Bayesian-based scheme is here implemented to reduce the uncertainty of hydraulic conductivity and compressibility by minimizing the residuals of the model outcomes with respect to the available measurements. This investigation focuses on two variables, namely the compressibility of the clay unit C_{mc} and the hydraulic conductivity of the sandy aquifer K_s, owing to their major contributions to land subsidence and groundwater production.

Methodology

The proposed framework intends to take advantage of several novel techniques including land surface deformation measurements by satellite remote sensing, an advanced numerical model that couples unsaturated groundwater flow with three-dimensional geomechanics, and the estimation of the system uncertainty by surrogate-based approaches. A 3D coupled variably-saturated groundwater flow-geomechanical model is applied to describe the interactions between hydrogeology and geomechanics (Nardean et al. 2021). This model allows to simulate how, in deformable porous media, the pore space in the reference bulk volume varies with the displacement of the solid grains and the pressure of the wetting phase. Then, a Bayesian-based method is employed to calibrate the parameters of interest by using piezometric records available over the period from 1960 to 1989 and displacement data obtained by Advanced Differential radar Interferometry (A-DInSAR) technique (Bonì et al. 2015) over the interval between 1992 and 2012.

The simulation is split into two periods for the purpose of model parameters estimation. First, the groundwater flow (GW) simulator is activated alone to compute the piezometric level from 1960 to 1989. In this time window, the calibration of K_s is conducted by using piezometric records from several monitoring wells. Displacement data are not available in this time frame. Then, the coupled model is run for the second time window (1992-2012) to simulate the piezometric and the displacement fields. Here, the compressibility C_{mc} is calibrated by assimilation of both land displacements and piezometric records.

In this framework, the model parameters are characterized by log-uniform prior probability density functions (pdfs) where $log(K_s/2) \sim U[-2, 0]$ m/d and $log(K_s/2) \sim U[-2, 0]$ KPa^{-1}). We initially tested the Markov Chain Monte Carlo (MCMC) method, a sampling algorithm, which calls for the simulation of the full problem multiple times. Since the computational cost associated with this strategy was unaffordable, we employed a surrogate-based approach where the full problem was replaced by a simpler, and much faster proxy to evaluate. In this work, the surrogate is based on the sparse grid approach given the tradeoff of accuracy and the training cost. This numerical technique is designed to compute the integral or interpolant of high dimensional functions from a set of collocation knots. Specifically, Leja knots are sampled from the parameter space to reach a fast convergence (Piazzola and Tamellini 2022). Besides, Leja knots have a nested structure where the knots from lower interpolation levels are a subset of higher levels, so the existing knots can be used in a step-by-step approach to gradually increase the accuracy of the surrogate. Prior to performing the Bayesian inversion by MCMC, the goodness of surrogate model is validated by evaluating the mean square error (MSE) indicator $E_{mse} = \sqrt{\frac{1}{I}\sum_{i=1,\cdots,I}^{I} \quad \frac{U_\Lambda(K_i)-U(K_i)}{U(K_i)}}$, where I is the number of validation points, U_Λ and U are solutions of the surrogate model and the numerical model respectively.

Preliminary result

GW outcome in the time window 1960-1989 results in a drawdown which mainly concentrates in the southeast and partially northwest portions of the basin. This pattern is consistent with the distribution of pumping wells. Along the vertical direction, the drawdown mainly occurs within the sand and gravel layer and marl layer. The maximum decline reaches more than 100 m over three decades where the saturation degree also experiences a pronounced reduction in the shallowest soil. The pressure head within the clay layer presents a lag response and ends up with a drop around 20 m. The computed drawdown reasonably matches the piezometric records at wells in the southwestern part of the basin but reaches a half of recorded values to the northeast. These differences should be shrunk after the parameter calibration.

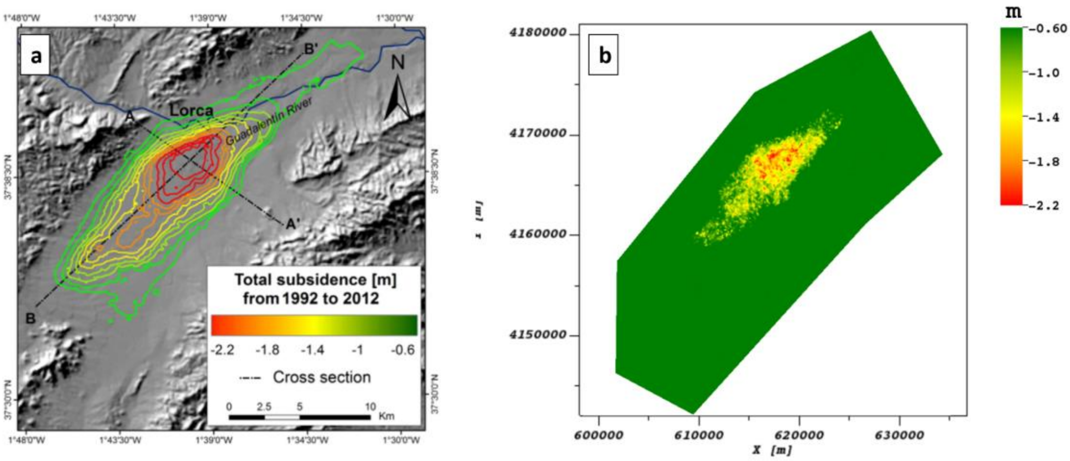

Figure 2 Land subsidence over the Alto Guadalentín Basin. (a) Total subsidence from 1992 to 2012 as obtained with the A-DInSAR technique (Bonì et al. 2015) (b) Model results from the 3D variably-saturated groundwater flow coupled with geomechanics in the time window between 1960 and 1992. Assuming K_s=0.2 m/d and C_{mc}=1e^{-4} .

The coupled model is also preliminary run over this time window to compute the amount of land displacements during the first 30 years of aquifer exploitation. The drawdown obtained by the coupled model has a similar pattern, but in the main productive area the piezometric decline is 10 m greater than the values obtained by the GW model when running alone. This difference is mainly caused by the variation of porosity, and consequently of aquifer storage, that is accounted for in the coupled formulation but neglected in GW simulations. In fact, aquifer storage is constant in the GW model while it varies in the coupled model decreasing as the aquifer compacts. The numerical results in terms of land subsidence agree with the spatial behavior of the A-DInSAR data. Although the simulation and A-DInSAR data span different time series, the shape and maximum value of the subsidence bowls look consistent (Figure 2). The coupled model also suggests the horizontal displacement is below 0.4 m.

The surrogate of the GW model for the first time window was obtained by testing an increasing number of knots and, thus, evaluating the accuracy of the surrogate solution. A final number of 9 knots are chosen as the MSE is on the order of centimeters. The response surfaces obtained with the surrogate for most of the monitoring wells are smooth and show the expected piezometric level decline over time, particularly over the years with a greater withdrawal (Figure 3). For the same year, the piezometric level is generally lower with a smaller K_s as expected (Figure 3a). The remaining response surfaces have an abnormal rising when K_s is close to the lower threshold, likely due to the narrower drawdown bowl that develops when the hydraulic conductivity decreases (Figure 3b). Undoubtedly, this surrogate model based on sparse grids provides highly reliable approximations of the numerical model.

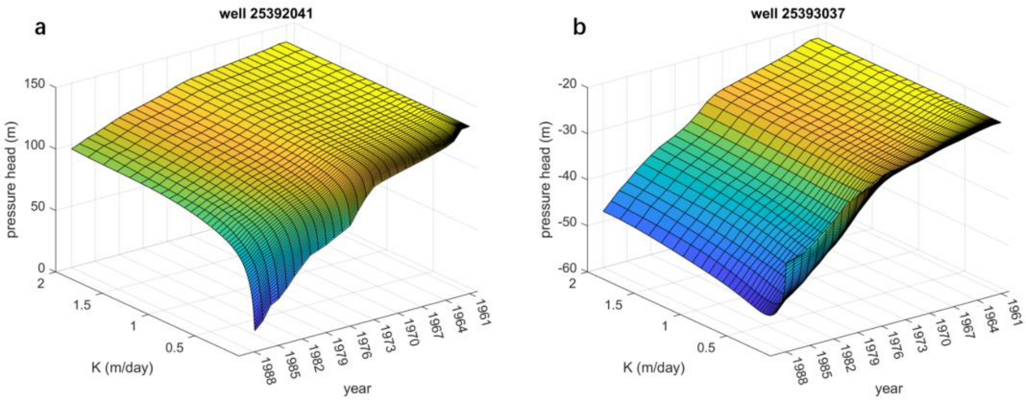

Figure 3 The response surfaces obtained by the surrogate model at two monitoring wells. (a) Well 25392041 represents the kind of wells which are in the main productive area, the pressure head is positively related to K_S (b) Well 25393037 is a bit far away from the productive wells. Wells like 25393037 are less affected by drawdown when K_S is low.

Conclusions

The proposed numerical model is capable of describing land subsidence caused by the groundwater withdrawal in a variably saturated aquifer system. In addition, the sparse grid approach used to reduce the computational burden presents a good ability on approximating the numerical results in terms of accuracy and cost. Inverse parameter estimation for K_S with the piezometric data for the first period is ongoing. Once Bayesian inversion will be validated with a proper posterior distribution of K_S, this study will move to the second period calibration by using the coupled model and A-DInSAR outcomes.

References

Bonì, Roberta, Gerardo Herrera, Claudia Meisina, Davide Notti, Marta Béjar-Pizarro, Francesco Zucca, Pablo J. González, et al. (2015). “Twenty-Year Advanced DInSAR Analysis of Severe Land Subsidence: The Alto Guadalentín Basin (Spain) Case Study.” Engineering Geology 198 (November): 40–52. https://doi.org/10.1016/j.enggeo.2015.08.014.

Cerón García, Juan Carlos, (1995). “Estudio hidrogeoquímico del acuífero del alto guadalentín (Murcia).” https://digibug.ugr.es/handle/10481/55814.

Ezquerro, Pablo, Carolina Guardiola-Albert, Gerardo Herrera, José Antonio Fernández-Merodo, Marta Béjar-Pizarro, and Roberta Bonì, (2017). “Groundwater and Subsidence Modeling Combining Geological and Multi-Satellite SAR Data over the Alto Guadalentín Aquifer (SE Spain).” Geofluids 2017: 1–17. https://doi.org/10.1155/2017/1359325.

Nardean, S., M. Ferronato, Y. Zhang, S. Ye, X. Gong, and P. Teatini, (2021). “Understanding Ground Rupture Due to Groundwater Overpumping by a Large Lab Experiment and Advanced Numerical Modeling.” Water Resources Research 57 (3). https://doi.org/10.1029/2020WR027553.

Piazzola, Chiara, & Lorenzo Tamellini, (2022). “The Sparse Grids Matlab Kit -- a Matlab Implementation of Sparse Grids for High-Dimensional Function Approximation and Uncertainty Quantification.” arXiv. http://arxiv.org/abs/2203.09314.

Improving Subsidence Modelling of Different Depth Domains in the Mekong Delta

P.S.J. Minderhoud[1,2,3],*, A. Guzy[2,5], S. Baldan[2], R. Xotta[2], B.R. Lexmond[4], C. Zoccarato[2], P. Teatini[2]

1 Soil Geography and Landscape Group, Wageningen University, Wageningen, The Netherlands
2 Department of Civil, Environmental and Architectural Engineering, University of Padova, Padova, Italy
3 Department of Subsurface and Groundwater Systems, Deltares Research Institute, Utrecht, The Netherlands
4 Department of Physical Geography, Utrecht University, Utrecht, The Netherlands
5 Faculty of Geo-Data Science, Geodesy and Environmental Engineering, AGH UST, Cracow, Poland
* Correspondence to Philip.Minderhoud@wur.nl
Session: Modelling and Matching of land subsidence – Deltas and sea-level rise

Introduction

The Mekong delta, one of the largest deltas in the world, is densely populated and important for food production. As the delta plain is lowly elevated, less than a meter on average above local sea level (Minderhoud et al. 2019), it is vulnerable to sea-level rise and land subsidence. The delta experiences high rates of natural compaction at its coast (Lovelock et al., 2015; Zoccarato et al, 2018) while human activities associated with land-use change (Minderhoud et al., 2018), urbanisation (de Wit et al., 2021) and intensified groundwater exploitation are accelerating subsidence further (Minderhoud et al., 2017; 2020a). At present the delta experiences high rates of land subsidence, with a delta-wide average rate exceeding 10 mm/yr and local rates as high as 60 mm/yr (Copernicus, 2019; Minderhoud et al., 2020b). As a result, the relative sea-level rise in the Mekong delta is dominated by land subsidence and forms an existential threat to the delta (Kondolf et al., 2022).

Deltaic subsidence is the cumulative effect of various drivers and processes in the subsurface (Tosi et al., 2009, Shirzaei et al., 2021), that can be both of natural and anthropogenic origin (Candela & Koster, 2022). As a result, subsidence can be both spatially and temporally highly variable within a delta. Subsidence caused by natural processes is unavoidable and can only be countered by adaptation, such as managed sedimentation strategies to build elevation through sediment deposition (Dunn & Minderhoud, 2022), while human-induced subsidence can be reduced or mitigated following a proper strategy (e.g. Erkens & Stouthamer, 2020).

In recent years the number of studies on subsidence in the Mekong delta has increased considerably, from direct measurements at a few locations in the delta using relative surface elevation tables (SETs, Lovelock et al., 2015) and dedicated subsidence monitoring stations (Karlsrud et al., 2017, 2020) delta-wide InSAR estimates (Erban et al., 2014; Copernicus, 2019). These estimates, combined with land-use change detection, revealed the spatial-temporal evolution and land-use change impacts on subsidence (Minderhoud et al., 2018) and detailed analyses of differential, depth-dependent subsidence in urban areas in the delta (De Wit et al. 2021). Two different numerical models were created targeting distinct subsidence processes: 1) groundwater extraction-induced aquifer-system compaction (Minderhoud et al., 2017), consequently used to create future elevation projection under different extraction scenarios (Minderhoud et al., 2020a), and 2) natural compaction of shallow sediments following Holocene delta progradation (Zoccarato et al., 2018). This contribution provides an overview of past and ongoing numerical advances in subsidence modelling in the Mekong delta and provides an outlook for future work.

Past numerical advances

A delta-wide 3D hydrogeological model of the Mekong delta was created to simulate groundwater extraction and consequent aquifer-system compaction based on datasets on delta geology, hydro(geo)logy, geomechanics and groundwater extractions (Minderhoud et al., 2017). The hydrogeological model was calibrated using hydraulic head monitoring data. A 1D compaction module, SUB-CR (Kooi et al., 2020) was used to simulate aquifer-system compaction using a viscoelastic compression theory following the isotache concept (Suklje, 1957; Bjerrum, 1967). In the first model version groundwater extraction and consequent aquifer-system compaction were simulated from 1991 to 2015 (Minderhoud et al, 2017). The simulated subsidence was calibrated using InSAR estimates for 2006-2009 (Erban et al., 2014) and revealed an acceleration in aquifer-system compaction in the delta, which was later confirmed by InSAR estimates from 2014-2019 (Copernicus 2019; Minderhoud et al., 2020b). Consequently, the model was updated by including an explicit surface water system and the past extraction rate simulated in the model was improved based on hydraulic head analysis (Minderhoud et al., 2020a). The updated model was used with scenarios of future groundwater use to project aquifer-system compaction until the end of the 21th century (Fig. 1).

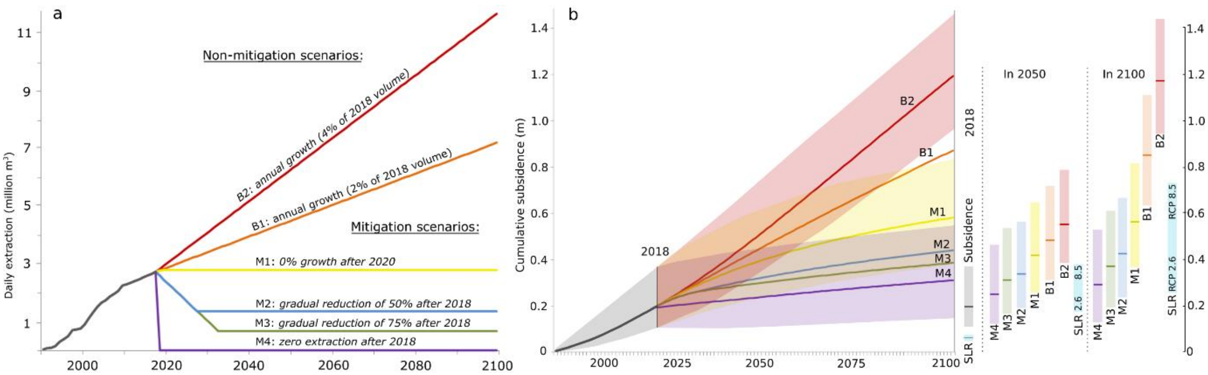

Figure 1 a) Scenarios of groundwater extraction for the Mekong delta. b) Cumulative delta-average subsidence for each modelled scenario. The results are placed in comparison to global sea-level rise as projected in various RCP scenario (IPCC) specifically for the Mekong delta (modified after Minderhoud et al., 2020a, reproduced under CC BY 3.0).

The large Mekong delta has prograded rapidly in the second half of the Holocene shoreline advances up to 50 m/yr (Tamura et al., 2020). Rapid sedimentation of fine-grained sediments is followed by high rates of natural compaction resulting from delayed dissipation of overpressure under its own weight. To simulate this for the Mekong delta, Zoccarato et al. (2018) applied NATSUB-2D, a novel finite-element, groundwater flow model coupled to a 1D compaction module with a compressible mesh, able to simulate the large deformations (with a Lagrangian approach) happening in these young, highly porous and compressible deposits (Zoccarato & Teatini, 2017). The simulation of the last 4000 years of delta progradation along a transect towards the South revealed the potential occurrence of present unprecedented high natural compaction rates at the coast, up to several cm/yr. These values match direct measurements of shallow compaction in this area with SETs (Giao et al., 2014; Lovelock et al., 2015) in mangrove forests and subsidence monitoring stations (Karlsrud et al., 2020) and demonstrated that a large part of the shallow near-coastal subsidence can be of natural origin and a product of fast delta progradation. The transect results were combined with the spatial occurrence of Holocene clays to provide a first estimate of delta-wide natural compaction following delayed overpressure dissipation assuming homogeneous clay deposits (Minderhoud, 2019).

The combined effect of extraction-induced aquifer-system compaction and natural compaction on future elevation evolution in the delta (Fig. 2) shows the critical situation and potential drowning of the Mekong delta in the near future under high rates of relative sea-level rise. It also reveals the importance of the described numerical models that enable the forecasting of future compaction and create relative sea-level rise projections to inform policymakers and steer mitigation efforts.

Ongoing advances to improve subsidence models for the Mekong delta

The described models represent the past advances in subsidence models for the Mekong delta that go beyond 1D calculations and were in revealing the high subsidence in the Mekong delta and informing policymakers (Kondolf et al., 2022). Here we describe ongoing efforts to improve these models and subsidence quantifications for the delta via code development and model advancement (Figure 3).

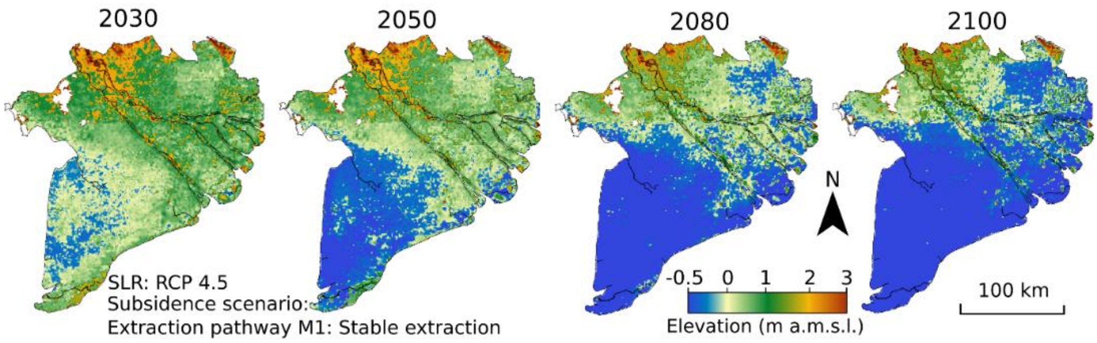

Figure 2 Elevation projections for the Mekong delta under extraction-induced compaction (scenario M1, Fig. 1), sea-level rise (SLR) following RCP 4.5 and natural compaction, assuming it is no longer compensated by sedimentation (modified after Minderhoud et al., 2020a, supplement, CC BY 3.0, elevation data Minderhoud et al., 2019b).

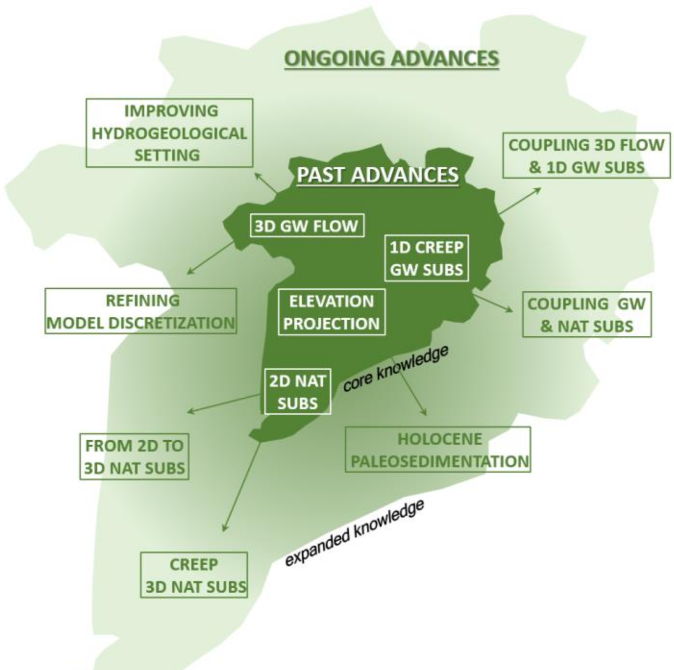

Figure 3 Past and ongoing advances in numerical modelling of subsidence in the Mekong. The modelling advances encompass both natural (NAT) and groundwater (GW) extraction-induced subsidence (SUBS), processes acting in different depth domains under different drivers.

Advances in modelling hydrogeological aquifer-system compaction

Improving hydrogeological schematization. In the present schematisation, the aquitards are discretized as a single layer, which makes it unable to simulate delayed groundwater pressure propagation within the aquitard. The effect is assessed by creating and comparing with several additional models in which the aquitard discretization is refined (Lexmond et al., submitted).

Quantify the impact of the deterministic modelling approach on compaction. The hydrogeological model has a deterministic model parameterization, calibrated to hydraulic head time series. To determine the impact of this deterministic modelling approach on simulated compaction, stochastic modelling of hydrogeological parameters is performed (Lexmond et al., submitted).

Improve parameter consistency between hydrogeology and geomechanics. Since the groundwater model and the geomechanical module were initially parameterized and calibrated independently, there is an inconsistency between the hydrogeological model parameterization (i.e. specific storage) and the geomechanical parameterization (i.e. compression index), as Pham et al. (2022) also pointed out. To overcome this drawback, an iterative procedure is implemented to calibrate specific storage and compression index consistently for each individual layer using piezometric and InSAR records. This is accomplished with InSAR-retrieved land subsidence datasets covering the years 2006 to 2010 (Erban et al., 2014) and 2016 to 2019 (Minderhoud et al., 2020b). Since these datasets span varying time intervals, they allow for the capture of non-linear deformation behaviour and, as a result, further improvements in the accuracy of land subsidence estimations. Consequently, the recalibrated model simulates a larger decrease in hydraulic head in the most heavily pumped aquifers and thus higher values of land subsidence in vulnerable areas when compared to the initial model (Guzy et al., in prep).

Advances in modelling of natural compaction

Upgrade the numerical domain to 3D. The 2D simulator (Zoccarato & Teatini, 2017) is expanded to a 3D spatial domain, i.e. NATSUB3D (Xotta et al., 2022). The 1D compaction module is coupled to a 3D groundwater flow module and the finite element code can generate a 3D tetrahedral grid that deforms over time with sediment compaction. The new code allows for properly simulating sediment accretion and compaction with time for 3D landform evolution, by updating the mesh following compaction and recomputing the hydrogeological and geomechanical parameters dependent on the strain.

3D subsurface model development based on paleo-sedimentation of Holocene deposits. The current hydrogeological and geomechanical state of the subsurface is influenced by its recent sedimentation history which can be simulated using the NATSUB3D code. To properly simulate and quantify present shallow compaction in the Mekong delta in the NATSUB3D code, a new approach is developed to retrieve spatial and temporal information on paleo-sedimentation rates from lithological data. The approach combines lithological bore logs, sediment geochronology (i.e. datings), spatial interpolation and geomechanical parametrization of representative lithologies to create maps of paleo-sedimentation during the Holocene delta evolution. Based on these maps that represent sediment accumulation in the last 4000 yrs of the Holocene delta evolution, a first 3D lithological model was simulated that enables computation of present-day natural compaction rates for the coastal part of the Mekong delta (Fig. 4).

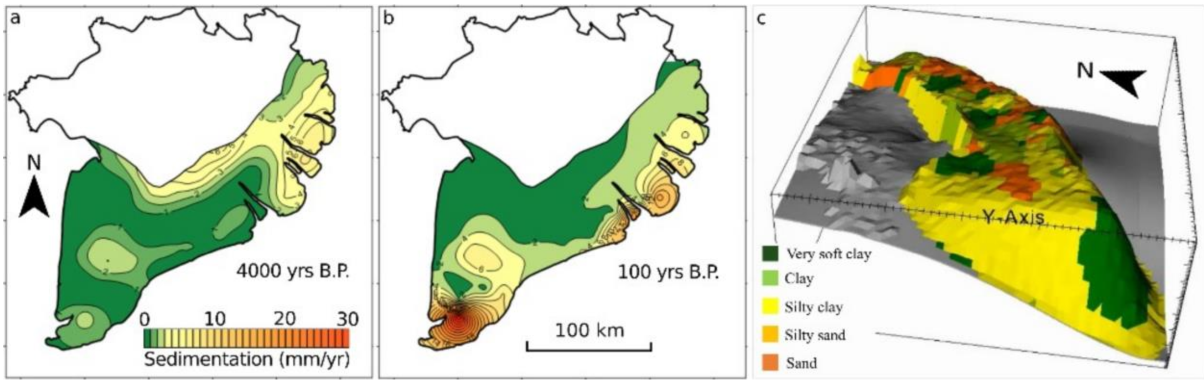

Figure 4 a-b) Example of paleo-sedimentation rate maps. Sedimentation rate maps were derived for each lithological class over 100-yr intervals spanning from 4000-0 yrs B.P. When more lithologies were deposited in the same interval, the model assumed spatio-linear mixing of the lithologies and computes hydro-geomechanical properties of the deposits according to the ratio of each lithological class. c) Simulated present 3D lithology of the Holocene deposits (4000 yr B.P to present) in the Mekong delta (Baldan et al., in prep).

Coupling aquifer depletion with shallow natural subsidence. The effect of deeper groundwater extraction on subsidence in the shallow subsurface is evaluated by linking two numerical models. The present and future effects of groundwater extraction (i.e. water level drop), computed with the calibrated 3D hydrogeological model of the Mekong delta, is used as input for the upgraded NATSUB3D model (Baldan et al., in prep.) This will allow quantifying the impact of extractions on shallow subsidence in the Mekong delta (Guzy et al., in prep.).

Adding a visco-elastic approach to NATSUB3D. In addition to the existing elastoplastic approach, a visco-elastic approach is added to the NATSUB3D code to enable the simulation of time-dependent creep (i.e. secondary compression) following the isotache approach. In this approach, compaction is no longer only driven by stress (i.e. load increase following sediment deposition), but also becomes time-dependent (i.e. creep), causing compaction to continue also in the absence of dissipation of porewater overpressure. With this update, NATSUB3D can also be applied to investigate the effect of creep compaction in young sedimentary settings (Xotta et al., in prep.).

Acknowledgements

P.S.J.M. received funding from the European Union's Horizon 2020 research and innovation program under the Marie Skłodowska-Curie Grant No. 894476—InSPiRED—H2020-MSCA-IF-2019. P.S.J.M., A.G. and P.T. received funding from the Dutch Science Foundation (NWO-WOTRO) under the WOTRO Impact and Innovation Grants (I&IG 2020), Project No. 481.20.139 titled "Conserve water or drown in the consequences: Sustaining the sinking Mekong delta". A.G. received funding from the National Science Center of Poland under the Preludium-17 Grant No. 2019/33/N/ST10/00724 titled "Modeling of land surface movements due to rock mass drainage".

References

Baldan, Minderhoud, Teatini, Xotta, Zoccarato. Data-driven 3D modelling of long-term delta evolution accounting for sediment compaction: The Mekong Delta. Earth Surface Processes and Landforms, in preparation.

Bjerrum, L. (1967). Engineering geology of Norwegian normally consolidated marine clays as related to settlements of buildings. Géotechnique, 17(2): 81-118.

Candela, B. T., & Koster, K. (2022). The many faces of anthropogenic subsidence. Science, 376(6600).

Copernicus (2019). EMSN-062: Assessing changes in ground subsidence rates, Mekong Delta, Vietnam FINAL REPORT https://emergency.copernicus.eu/mapping/list-of-components/EMSN062.

de Wit, K., Lexmond, B. R., Stouthamer, E., Neussner, O., Dörr, N., Schenk, A., Minderhoud, P. S. J. (2021). Identifying causes of urban differential subsidence in the Vietnamese Mekong delta by combining InSAR and field observations. Remote Sensing, 13(2), 1–33. doi.org/10.3390/rs13020189.

Dunn, F. E., & Minderhoud, P. S. J. (2022). Sedimentation strategies provide effective but limited mitigation of relative sea-level rise in the Mekong delta. Communications Earth and Environment, 3(1). https://doi.org/10.1038/s43247-021-00331-3.

Erban, L. E., Gorelick, S. M., & Zebker, H. A. (2014). Groundwater extraction, land subsidence, and sea-level rise in the Mekong Delta, Vietnam. Environmental Research Letters, 9(8), 084010.

Erkens, G., & Stouthamer, E. (2020). The 6M approach to land subsidence. Proceedings of the International Association of Hydrological Sciences, 382, 733–740. https://doi.org/10.5194/piahs-382-733-2020.

Giao, P. H., Thoang, T. T., Thuyen, L. X. & Vu, N. H. H. (2014). Geotechnical characterization of the subsoil profile underlying the land subsidence monitoring points in Southern Vietnam Delta. 9th Int. Symp. Lowl. Technol. 1, 429–436, https://doi.org/10.1017/CBO9781107415324.004.

Guzy, Minderhoud, Teatini, et al. Revising modelling predictions of anthropogenic land subsidence in the Mekong delta by a one-way coupled model. Science of the Total Environment, in preparation.

Guzy, Teatini, Zoccarato, Minderhoud. Aquifer depletion can contribute to Holocene compaction in the Mekong delta. Communications Earth & Environment, in preparation.

Hoang, T. M., van Lap, N., Oanh, T. T. K., & Jiro, T. (2016). The influence of delta formation mechanism on geotechnical property sequence of the late Pleistocene–Holocene sediments in the Mekong River Delta. Heliyon, 2(11). https://doi.org/10.1016/j.heliyon.2016.e00165.

Karlsrud, K., Vangelsten, B. V., and Frauenfelder, R. (2017): Subsidence and shoreline retreat in the Ca Mau Province – Vietnam. Causes, consequences and mitigation options, Geotechnical Journal of the SEAGS & AGSSEA, 48, ISSN 0046-5828, 2017a.

Karlsrud, K., Tunbridge, L., Khanh, N. Q., & Dinh, N. Q. (2020). Preliminary results of land subsidence monitoring in the Ca Mau Province. Proceedings of the International Association of Hydrological Sciences, 382, 111–115. https://doi.org/10.5194/piahs-382-111-2020.

Tamura, T., Nguyen, V. L., Ta, T. K. O., Bateman, M. D., Gugliotta, M., Anthony, E. J., Nakashima, R., & Saito, Y. (2020). Long-term sediment decline causes ongoing shrinkage of the Mekong mega delta, Vietnam. Scientific Reports, 10(1), 4–10. https://doi.org/10.1038/s41598-020-64630-z.

Kooi, H. and Erkens, G.: Creep consolidation in land subsidence modelling; integrating geotechnical and hydrological approaches in a new MODFLOW package (SUB-CR), Proc. IAHS, 382, 499–503, https://doi.org/10.5194/piahs-382-499-2020, 2020.

Lexmond, B.R., Torfs, P.J.J.F., Stouthamer, E., Guzy, A., Teatini, P., Minderhoud, P.S.J. (2021). The Effect of Discretization and Conductivity Uncertainty on Subsidence Simulation of the Vietnamese Mekong Delta. Submitted.

Lovelock, C. E., Cahoon, D. R., Friess, D. A., Guntenspergen, G. R., Krauss, K. W., Reef, R., Rogers, K., Saunders, M. L., Sidik, F., Swales, A., Saintilan, N., Thuyen, L. X., & Triet, T. (2015). The vulnerability of

Indo-Pacific mangrove forests to sea-level rise. Nature, 526(7574), 559-U217. https://doi.org/10.1038/nature15538.

Minderhoud, P. S. J., Erkens, G., Pham, V. H., Bui, V. T., Erban, L., Kooi, H., & Stouthamer, E. (2017). Impacts of 25 years of groundwater extraction on subsidence in the Mekong delta, Vietnam. Environmental research letters, 12(6), 064006.

Minderhoud, P. S. J., Coumou, L., Erban, L. E., Middelkoop, H., Stouthamer, E., & Addink, E. A. (2018). The relation between land use and subsidence in the Vietnamese Mekong delta. Science of The Total Environment, 634, 715-726.

Minderhoud, P. S. J. (2019). The sinking mega-delta: Present and future subsidence of the Vietnamese Mekong delta. Utrecht Studies in Earth Sciences, vol. 168 (Doctoral dissertation, Utrecht University).

Minderhoud, P. S. J., Coumou, L., Erkens, G., Middelkoop, H., & Stouthamer, E. (2019a). Mekong delta much lower than previously assumed in sea-level rise impact assessments. Nature communications, 10(1), 1-13.

Minderhoud P.S.J., Coumou L., Erkens G., Middelkoop, H. and Stouthamer E. (2019b). Digital elevation model of the Vietnamese Mekong delta based on elevation points from a national topographical map. PANGAEA, https://doi.org/10.1594/PANGAEA.902136.

Minderhoud, P.S.J., Middelkoop, H., Erkens, G., & Stouthamer, E. (2020a). Groundwater extraction may drown mega-delta: projections of extraction-induced subsidence and elevation of the Mekong delta for the 21st century. Environmental Research Communications, 2(1), 011005.

Minderhoud, P.S.J., Hlavacova, I., Kolomaznik, J., & Neussner, O. (2020b). Towards unravelling total subsidence of a mega-delta–the potential of new PS InSAR data for the Mekong delta. Proceedings of the International Association of Hydrological Sciences, 382, 327-332.

Pham, H., Sass, I., Nguyen, O. (2022). Concerns Related to Modelling Land Subsidence of Mekong Delta. In: Ha-Minh, C., Tang, A.M., Bui, T.Q., Vu, X.H., Huynh, D.V.K. (eds) CIGOS 2021, Emerging Technologies and Applications for Green Infrastructure. Lecture Notes in Civil Engineering, vol 203. Springer, Singapore. https://doi.org/10.1007/978-981-16-7160-9_102.

Shirzaei, M., Freymueller, J., Törnqvist, T. E., Galloway, D. L., Dura, T., & Minderhoud, P. S. J. (2021). Measuring, modelling and projecting coastal land subsidence. Nature Reviews Earth & Environment, 2(1), 40–58. https://doi.org/10.1038/s43017-020-00115-x.

Suklje, L. (1957). The analysis of the consolidation process by the isotaches method. Proceedings of the 4th International Conference on Soil Mechanics and Foundation Engineering 1 201–206.

Candela, B. T., & Koster, K. (2022). The many faces of anthropogenic subsidence. Science, 376(6600).

Tamura, T., Nguyen, V. L., Ta, T. K. O., Bateman, M. D., Gugliotta, M., Anthony, E. J., Nakashima, R., & Saito, Y. (2020). Long-term sediment decline causes ongoing shrinkage of the Mekong mega delta, Vietnam. Scientific Reports, 10(1), 4–10. https://doi.org/10.1038/s41598-020-64630-z.

Tosi, L., Teatini, P., Carbognin, L., & Brancolini, G. (2009). Tectonophysics using high-resolution data to reveal depth-dependent mechanisms that drive land subsidence: The Venice coast, Italy. Tectonophysics, 474(1–2), 271–284. https://doi.org/10.1016/j.tecto.2009.02.026.

Xotta, R., Zoccarato, C., Minderhoud, P.S.J., & Teatini, P. (2022). Modelling the role of compaction in the three-dimensional evolution of depositional environments. Journal of Geophysical Research – Earth Surface, accepted.

Zoccarato, C., & Teatini, P. (2017). Numerical simulations of Holocene salt-marsh dynamics under the hypothesis of large soil deformations. Advances in Water Resources, 110(October), 107–119. https://doi.org/10.1016/j.advwatres.2017.10.006.

Zoccarato, C., Minderhoud, P.S.J., & Teatini, P. (2018). The role of sedimentation and natural compaction in a prograding delta: insights from the mega Mekong delta, Vietnam. Scientific reports, 8(1), 1-12.

A summary review based on case studies of the challenges related to the comparison of displacements measured by PS-InSAR and simulated by geomechanical coupled to groundwater models

A. Moreau[1], A. Choopani[1,2], P-Y. Declercq[2], P. Orban[1], X. Devleeschouwer[2], A. Dassargues[1]

1 Hydrogeology & Environmental Geology, Urban and Environmental Engineering unit, University of Liège, Liège (Belgium)
2 Royal Belgium Institute of Natural Sciences, Geological Survey of Belgium, Rue Jenner 13, 1000 Brussels (Belgium)
Contact: aline.moreau@uliege.be
Keywords: Consolidation, PS-InSAR, Coupled equations, Leuven, Antwerp.

Abstract

Land subsidence is currently a great challenge for regions densely populated lying over compressible sediments. Mexico City (Ortega-Guerrero et al., 1999; Ortiz-Zamora et al., 2010), Hanoi (Nguyen et al., 2022), Huwei (Tsai et al., 2018 ; Chu et al., 2021), Houston (Kearns et al., 2015 ; Area et al., 2012 ; Miller et al., 2019), Tehran (Mahmoudpour et al., 2016), Las Vegas (Yan, 2007; Burbey, 2002), CanTho (Van Ty et al., 2021), Florence (Ceccatelli et al., 2021) and Lorca (Fernandez-Merodo et al., 2021) are only a few example of cities with subsidence issues. Exploitation of groundwater is the most cited cause of subsidence. Groundwater production creates a decrease of water pressure in the saturated geological medium and based on the Terzaghi principle, any increase of the effective stress can cause consolidation in a porous medium, in confined as in unconfined conditions (Dassargues 2018).

Interferometric Synthetic Aperture Radar (InSAR) technology is used to map the displacement patterns and quantify surface motion over time. It has been shown that InSAR provides an extremely cost-effective means of measuring ground surface displacement over large areas with a fine spatial resolution and precision within the centimeters under ideal conditions (Peng et al., 2022). Persistent Scatterer InSAR Interferometry (PS-InSAR) (Ferretti et al., 2000; Ferretti et al., 2001; Ferretti et al., 2002; Ferretti et al., 2007) technique is one of the most prevalent InSAR algorithms developed mostly for overcoming the decorrelation. Integration and comparison of PS-InSAR-derived displacement measurements with simulated displacement by geomechanical models coupled to groundwater flow models is broadly used for better understanding of the subsurface consolidation mechanisms. However, the practical implementation of such application still has its own challenges, which has received less attention in the literature. Developments in the use of InSAR results have involved inverse modeling (i.e., with groundwater flow and geomechanical models) providing values for aquifers properties (Chaussard et al. 2014; Gualandi and Liu 2021; Jiang et al. 2018; Miller and Shirzaei 2015; Miller et al. 2017; Motagh et al. 2017).

Using PS-InSAR processing, multiple localized land subsidences have been identified in the Antwerp and Leuven areas. On the right bank of the river Scheldt, within the borders of the city of Antwerp, the harbor of Antwerp was gradually developed leading to dock excavations in the estuary polders environment. PS-InSAR was used to detect, map and study the ground displacements (Declercq et al., 2021). Those parts of the subsurface that were disturbed by human activity are referred as 'anthropogenic layers' and are very compressible. However, other possible consolidation drivers such as consolidation of the most compressible sublayers induced by groundwater drainage and pumping are considered (Choopani et al., 2021).

The city of Leuven lies on a multilayer aquifer system called 'Brulandkrijt', consisting of interbedded chalk and sandy aquifers with clayey aquitards. Two areas of significant subsidence have been detected in the North of Leuven showing possibly a delayed consolidation process of the compressible low permeability aquitards.

Using these two case studies as examples, we show how PS-InSAR-derived subsidence observations can be compared to results of hydrogeological and geomechanical modeling. The general methodological workflow with the different steps of a groundwater model construction is described in detail in Dassargues (2018). In the most common case, which is the simulation of subsidence caused by groundwater withdrawal, the most widely used conceptual approach consists in simulating the groundwater flow problem in fully 3D conditions. The water pressure results from this 3D flow model are then prescribed at each time step in the different nodes of a 1D geomechanical model.

One of the most used software code on a regional scale is MODular groundwater FLOW model (MODFLOW). Many 1D-geomechanical model have been developed to simulate land subsidence caused by groundwater withdrawal. The SUB package, which is developed for simulating regional compaction of semi-permeable layers using MODFLOW is the most used software for land subsidence simulations (Hoffmann et al., 2003; Leake et al., 2007; Kooi et al., 2018; Leake et al., 2010). In the workflow of SUB package in MODFLOW, porous media flow is modeled in 3D, but compaction is simulated as a 1D process. An advantage of the SUB package is that it considers the assumption and the calculation of a delay for propagating water pressure decrease within the compressible beds, that are practically low permeability layers.

The current study is part of a more comprehensive work that focuses on the practical challenges of the comparison of simulated displacement in a fully coupled model to PS-InSAR observations. Following this methodology applied to the case studies of Antwerp and Leuven, the summary of the challenges is as follows.

A possible 'loss of coherence' corresponding to changes in physical characteristics (e.g., in vegetated areas) is the basic obstacle for InSAR applications leading us to use multi temporal technique such as PS-InSAR which are offering time series of deformation only at the location of Permanent Scatterers (PS). As a result, the fundamental limitation of PS-InSAR for land subsidence monitoring is that it cannot provide a spatially continuous map of displacements. Additionally, a time lag between radar dataset acquisitions is another constraint that prevents us from fully comparing simulated to observed time series of displacements.

The complexity and spatial variability of the geology and of the different hydrogeological and geotechnical processes that take place simultaneously in the subsoil mean that one measured value of subsidence may correspond to several possible causes. Hydraulic parameter characterization is required for groundwater flow modeling, compressibility values and preconsolidation stresses in all considered layers are required for geomechanical modeling. The assessment of their spatial variability and distribution can be very challenging and depending on the local sedimentological conditions. Parameter values from sample-based boreholes, which are often sparsely distributed, could not be a good representation of physical characteristics of the whole unit. The number of observation wells can be limited and not so regularly monitored.

Another conceptual challenge when dealing with most groundwater-geomechanical models is that the elastic and inelastic compressibility coefficients are most often assumed to be constant over the simulation period. This is not the case in the reality as the compressibility is dependent on the preconsolidation stress (i.e., the maximum stress that the layer has endured previously). In unconfined conditions, the effective stress is less increased by pumping or drainage than in confined conditions as the decrease in pore pressure is partially balanced by a decrease in the total stress addition when the water table drops (Dassargues 2018, Guzy and Malinowska, 2020).

Consequently, comparing PS-InSAR-derived displacement measurements to results from groundwater flow coupled to geomechanical models is never a simple process. There is no single model to represent every case of land subsidence. It takes many years and many studies to collect the adequate data to establish a representative coupled model of the surface deformation with an accurate understanding of the occurring processes.

References

Ortega-Guerrero, A., Rudolph, D. L., & Cherry, J. A. (1999). Analysis of long-term land subsidence near Mexico City: Field investigations and predictive modeling. Water resources research, 35(11), 3327-3341.

Ortiz-Zamora, D., & Ortega-Guerrero, A. (2010). Evolution of long-term land subsidence near Mexico City: Review, field investigations, and predictive simulations. Water Resources Research, 46(1).

Nguyen, M., Lin, Y. N., Tran, Q. C., Ni, C. F., Chan, Y. C., Tseng, K. H., & Chang, C. P. (2022). Assessment of long-term ground subsidence and groundwater depletion in Hanoi, Vietnam. Engineering Geology, 299, 106555.

Tsai, M. S., & Hsu, K. C. (2018). Identifying poromechanism and spatially varying parameters of aquifer compaction in Choushui River alluvial fan, Taiwan. Engineering Geology, 245, 20-32.

Chu, H. J., Ali, M. Z., & Burbey, T. J. (2021). Development of spatially varying groundwater-drawdown functions for land subsidence estimation. Journal of Hydrology: Regional Studies, 35, 100808.

Kearns, T. J., Wang, G., Bao, Y., Jiang, J., & Lee, D. (2015). Current land subsidence and groundwater level changes in the Houston metropolitan area (2005–2012). J. Surv. Eng, 141(4), 05015002.

Area, H., & Model, G. (2012). Hydrogeology and Simulation of Groundwater Flow and Land-Surface Subsidence in the Northern Part of the Gulf Coast AQ-Uifer System, Texas, 1891–2009. US Geological Survey: Reston, VI, USA.

Miller, M. M., & Shirzaei, M. (2019). Land subsidence in Houston correlated with flooding from Hurricane Harvey. Remote Sensing of Environment, 225, 368-378.

Mahmoudpour, M., Khamehchiyan, M., Nikudel, M. R., & Ghassemi, M. R. (2016). Numerical simulation and prediction of regional land subsidence caused by groundwater exploitation in the southwest plain of Tehran, Iran. Engineering Geology, 201, 6-28.

Yan, T. (2007). Effects of delayed drainage on subsidence modeling and parameter estimation (Doctoral dissertation, Virginia Tech).

Burbey, T. J. (2002). The influence of faults in basin-fill deposits on land subsidence, Las Vegas Valley, Nevada, USA. Hydrogeology Journal, 10(5), 525-538.

Van Ty, T., Minh, H. V. T., Avtar, R., Kumar, P., Van Hiep, H., & Kurasaki, M. (2021). Spatiotemporal variations in groundwater levels and the impact on land subsidence in CanTho, Vietnam. Groundwater for Sustainable Development, 15, 100680.

Ceccatelli, M., Del Soldato, M., Solari, L., Fanti, R., Mannori, G., & Castelli, F. (2021). Numerical modelling of land subsidence related to groundwater withdrawal in the Firenze-Prato-Pistoia basin (central Italy). Hydrogeology Journal, 29(2), 629-649.

Fernández-Merodo, J. A., Ezquerro, P., Manzanal, D., Béjar-Pizarro, M., Mateos, R. M., Guardiola-Albert, C., ... & Herrera, G. (2021). Modeling historical subsidence due to groundwater withdrawal in the Alto Guadalentín aquifer-system (Spain). Engineering Geology, 283, 105998.

Dassargues, A. (2018). Hydrogeology: groundwater science and engineering. CRC Press.

Peng, M., Lu, Z., Zhao, C., Motagh, M., Bai, L., Conway, B. D., & Chen, H. (2022). Mapping land subsidence and aquifer system properties of the Willcox Basin, Arizona, from InSAR observations and independent component analysis. Remote Sensing of Environment, 271, 112894.

Ferretti, A., Prati, C., & Rocca, F. (2000). Nonlinear subsidence rate estimation using permanent scatterers in differential SAR interferometry. IEEE Transactions on geoscience and remote sensing, 38(5), 2202-2212.

Ferretti, A., Prati, C., & Rocca, F. (2001). Permanent scatterers in SAR interferometry. IEEE Transactions on geoscience and remote sensing, 39(1), 8-20.

Ferretti A, M., & GuarnieriA, P. (2007). InSAR Principles: Guidelines for SAR Interferometry Processing and Interpretation.

Chaussard, E., Bürgmann, R., Shirzaei, M., Fielding, E. J., & Baker, B. (2014). Predictability of hydraulic head changes and characterization of aquifer-system and fault properties from InSAR-derived ground deformation. Journal of Geophysical Research: Solid Earth, 119(8), 6572-6590.

Gualandi, A., & Liu, Z. (2021). Variational Bayesian Independent Component Analysis for InSAR Displacement Time-Series with Application to Central California, USA. Journal of Geophysical Research: Solid Earth, 126(4), e2020JB020845.

Jiang, L., Bai, L., Zhao, Y., Cao, G., Wang, H., & Sun, Q. (2018). Combining InSAR and hydraulic head measurements to estimate aquifer parameters and storage variations of confined aquifer system in Cangzhou, North China Plain. Water resources research, 54(10), 8234-8252.

Miller, M. M., & Shirzaei, M. (2015). Spatiotemporal characterization of land subsidence and uplift in Phoenix using InSAR time series and wavelet transforms. Journal of Geophysical Research: Solid Earth, 120(8), 5822-5842.

Miller, M. M., Shirzaei, M., & Argus, D. (2017). Aquifer mechanical properties and decelerated compaction in Tucson, Arizona. Journal of Geophysical Research: Solid Earth, 122(10), 8402-8416.

Motagh, M., Shamshiri, R., Haghighi, M. H., Wetzel, H. U., Akbari, B., Nahavandchi, H., ... & Arabi, S. (2017). Quantifying groundwater exploitation induced subsidence in the Rafsanjan plain, southeastern Iran, using InSAR time-series and in situ measurements. Engineering geology, 218, 134-151.

Declercq, P. Y., Gérard, P., Pirard, E., Walstra, J., & Devleeschouwer, X. (2021). Long-term subsidence monitoring of the Alluvial plain of the Scheldt River in Antwerp (Belgium) using radar interferometry. Remote Sensing, 13(6), 1160.

Choopani, A., Declercq, P. Y., Orban, P., Devleeschouwer, X., & Dassargues, A. (2021, September). Land subsidence as revealed by PS-InSAR observations in the Antwerp area (Belgium): first steps towards the understanding and modelling. In IAH2021 48th IAH Congress' Inspiring Groundwater'.

Hoffmann, J., Leake, S. A., Galloway, D. L., & Wilson, A. M. (2003). MODFLOW-2000 ground-water model--User guide to the subsidence and aquifer-system compaction (SUB) package. Geological Survey Washington DC.

Leake, S. A., & Galloway, D. L. (2007). MODFLOW ground-water model: User guide to the subsidence and aquifer-system compaction package (SUB-WT) for water-table aquifers. US Geological Survey.

Kooi, H., & Yuherdha, T. (2018). A.: Updated subsidence scenarios Jakarta; MODFLOW SUB-CR calculations for Sunter, Daan Mogot and Marunda. Deltares internal report 11202275_008, available at: https://www. deltares. nl/en/publication/new-subsidence-prognoses-jakarta/(last access: 25 February 2020).

Leake, S. A., & Galloway, D. L. (2010, October). Use of the SUB-WT Package for MODFLOW to simulate aquifer-system compaction in Antelope Valley, California, USA. In Land Subsidence, Associated Hazards and the Role of Natural Resources Development: Proceedings of the Eighth International Symposium on Land Subsidence: Queretaro, Mexico, International Association of Hydraulic Sciences (pp. 61-67).

Guzy, A., & Malinowska, A. A. (2020). State of the art and recent advancements in the modelling of land subsidence induced by groundwater withdrawal. Water, 12(7), 2051.

Proc. IAHS, 382, 635–642, 2020
https://doi.org/10.5194/piahs-382-635-2020

Open Access PIAHS

The potential impact of measures taken by water authorities on greenhouse gas emissions

Anne Marieke Motelica-Wagenaar[1], Tim A. H. M. Pelsma[1], Laura Moria[1], and Sarian Kosten[2]

[1]Waternet, P.O. Box 94370, Amsterdam, the Netherlands
[2]Department of Aquatic Ecology and Environmental Biology, Institute for Water and Wetland Research, Radboud University, P.O. Box 9102, 6500 HC Nijmegen, the Netherlands

Correspondence: Anne Marieke Motelica-Wagenaar (anne.marieke.motelica@waternet.nl)

Published: 22 April 2020

Abstract. Water authorities responsible for water quantity and water quality management may strongly influence the magnitude of greenhouse gas emissions from the surface waters and the adjacent peat areas within their territories. Climate smart water management (reducing influx of organic matter and improving water quality) is therefore a potentially strong mitigation tool. We hypothesize that climate smart water management has a stronger mitigation potential than reducing emissions from the operational management of a Water Authority. Based on literature data on greenhouse gas emissions from ditches and agricultural peatlands, we present a case study of a Dutch Water Authority – Amstel, Gooi and Vecht (operated by Waternet). We estimate that greenhouse gas emissions from the 195 km^2 large peat area within its territory are 470 kt CO_2-eq per year. An additional 231 kt CO_2-eq yr^{-1} is emitted from the water bodies within the 102 km^2 large water area territory. Both emissions are considerably higher than the estimated climate footprint of the operational management of the water board ($\sim$ 62 kt CO_2-eq per year in 2017). While Waternet strives to have a net zero emission of greenhouse gases related to its operational management by 2020, we postulate that measures (to be taken before 2030) such as the prevention of organic matter and nutrients entering surface waters, the removal of organic carbon from ditches and higher groundwater levels in agricultural peatlands, may reduce greenhouse gas emissions in ditches and agricultural peat meadows with 26 and 27 kt CO_2-eq per year, respectively. Measures that are taken to reduce greenhouse gas emissions in water bodies are expected to have a positive impact on water quality as well.

1 Introduction

In line with the Paris agreement of 2015, the Dutch government aims to reduce greenhouse gas (GHG) emissions (Government of the Netherlands, 2019). The work of the Dutch water boards, responsible for water quantity and water quality management, influences aquatic and terrestrial GHG emissions. However, the Dutch water boards currently are not responsible for dealing with GHG emissions from the water systems they manage. Nevertheless, the Dutch waterboards support climate-change mitigation. The Dutch waterboards have set ambitious goals for energy efficiency (more than 30 % reduction in energy use in 2020 compared to 2005) and renewable energy production (the goal is to be 40 % self-supporting in 2020) (Goorts and Kolkuis Tanke, 2018). Waternet works for the regional water authority Amstel, Gooi and Vecht (AGV) and for the municipality of Amsterdam for water-tasks. Activities conducted by Waternet in the realm of the water cycle in and around Amsterdam result in GHG emissions. Waternet aims to become a net zero emitter of GHGs in 2020 (van der Hoek, 2012). In 2014 the climate footprint of Waternet was calculated as 50 kt CO_2-eq yr^{-1}. To realize the net zero emission ambition, it was decided that measures are required to lower the emissions or to compensate them.

In the climate footprint of the water boards, the emissions in the environment (water bodies and peatlands) are normally not taken into account. These emissions are potentially high. In 2017, the emissions from the decrease in carbon stored in peat soils and peaty soils in The Netherlands were reported as

6.4 Mt CO_2-eq, which represents 3.2 % of the CO_2-emission in the Netherlands (RIVM, 2019). The emissions of water bodies have not yet been included in the terrestrial GHG balance, but these are potentially high as well (Bastviken et al., 2011). Currently, the magnitude of the emission from inland water has a high uncertainty. In the Netherlands, the number of measurement locations is limited and the existing data is predominantly from peat areas (Koschorreck et al., 2020; Schrier-Uijl et al., 2011; Vermaat et al., 2011).

We hypothesize that climate smart water management has a stronger mitigation potential than reducing emissions from the operational management of a Water Authority. In this paper, a case study of Waternet's GHG emissions is investigated. Questions that are posed include: what are the present GHG emissions in ditches, shallow waters and peat meadows? What is an achievable possible reduction in GHG emissions by 2030 in the area of Water authority of Amstel, Gooi and Vecht? How do these reductions relate to their own company emissions and other emissions in the water management area?

2 Material and methods

2.1 Estimation of operational management related GHG emissions

The climate footprint of the business operations of AGV consists of Scope 1, 2 and 3 emissions. These emissions are derived from consumption of natural gas, transport fuels and process-related emissions (Scope 1), consumption of heat and electricity (Scope 2), consumption of chemicals, materials for building, transport of residuals, transport of employees (home-work and business transport by own cars or public transport), travelling by plane and outsourced maintenance of the water system (Scope 3). Methods applied in this paper are largely consistent with the "klimaatmonitor" of the Dutch water authorities (Goorts and Kolkhuis Tanke, 2018) and the calculation method developed for drinking water companies (Snip and Oesterholt, 2019). N_2O emissions are multiplied by a factor 265 ($g\,g^{-1}$ CO_2-eq/N_2O) and CH_4 emissions are multiplied by factor 28 CO_2-eq/CH_4 ($g\,g^{-1}$) comprise the global warming potential of a 100-year time horizon (IPCC, 2014).

The direct process related emissions at the waste water treatment plant (wwtp) and effluent of N_2O and CH_4 are based on measurements of N-load and Chemical Oxygen Demand (COD) and default emission intensities general numbers (Frijns et al., 2008). Besides, N_2O emissions are measured at wwtp Amsterdam-West.

2.2 Estimation of GHG emissions from surface waters

The total area of the water bodies within the territory of Waternet was derived from the national Dutch database (BGT watervlakken). Water types within the territory area (ditches, lakes, canals and ponds) are distinguished based on morphology, soil type and expert judgement in line with the Water Framework Directive (Elbersen et al., 2003). For these water types GHG emissions are estimated as described below. Methane emissions are estimated for all water types, carbon dioxide emissions are estimated for dirched, lakes and ponds only. No nitrous oxide emissions are estimated, due to a lack of data. For each type of water body, the total area is multiplied by an emission factor.

The emission factors of diffusive GHG emissions in ditches and lakes are determined based on the mean methane and carbon dioxide diffusive flux measurements in West-Netherlands by Schrier-Uijl et al. (2011). The mean day-time summer GHG diffusive emissions in these studies were 25 and 2.8 $mg\,CH_4\,m^{-2}\,h^{-1}$ and 124 and 53 $mg\,CO_2\,m^{-2}\,h^{-1}$ for ditches and lakes respectively on peat soils. Notably these emissions had a large standard deviation. These numbers are used for all soil types in our approach, though there may be differences in GHG emissions between soil types. Subsequently, we adjusted these day-time summer emission intensities to account for potential diel and seasonal variation as follows.

Diffusive methane and carbon dioxide emissions – Lower GHG emissions in the night and in the winter are expected due to decreased temperatures (Schrier-Uijl et al., 2011; Vermaat et al., 2011; Van der Nat et al., 1998; Xing et al., 2004). However, diffusive emissions have also been found to increase during the night (Harisson et al., 2005). To obtain a conservative estimate of average diel emissions we multiplied day-time diffusive fluxes with 2/3 (based on Schrier-Uijl et al., 2008). In addition, we assumed summer emissions to account for 70 % of total year-round CH_4 and CO_2 emissions in ditches (Schrier-Uijl et al., 2011). For lakes, these GHG emissions corrections are not performed, as the temperature in lakes is more stable than in ditches. Besides, higher CO_2 emissions were found in winter than in summer in lakes in Denmark (Trolle et al., 2012).

Ebullitive CH_4 emissions – the emission of methane through ebullition is often higher than diffusive emissions (Aben et al., 2017; Davidson et al., 2018; Van Bergen et al., 2019), but reliable data is scarce (Aben et al., 2017). To obtain a conservative estimate we assumed ebullition to account for 50 % of total methane emissions from ditches and lakes (Vermaat et al., 2011; Wu et al., 2019).

Total GHG fluxes from ditches and lakes are assumed to be 33 and 18 tCO_2-eq $ha^{-1}\,yr^{-1}$ respectively. These emission factors compare well with fluxes determined based on measurements in Dutch peatland water bodies of 35 $t\,CO_2$-eq $ha^{-1}\,yr^{-1}$ (Vermaat et al., 2011).

Methane estimated emissions from canals are based on general numbers of 11.6 $t\,CO_2$-eq $ha^{-1}\,yr^{-1}$ as provided by IPCC (2019).

GHG emissions from ponds were estimated with an emission factor of 34 $t\,CO_2$-eq $ha^{-1}\,yr^{-1}$, based on measurements in a Dutch urban pond in the province of Gelderland (Van Bergen et al., 2019).

2.3 Estimation of GHG emissions from agricultural peatlands

The estimated emissions in the agricultural grassland on peat are based on the relation with the average ground water levels and corrected for clay layer (Jurasinski et al., 2016; Troost et al., 2018).

2.4 Potential effect of water management measures to reduce GHG emissions

Mesocosm experiments show a distinct effect from nutrient loading, with a two-fold increase in (diffusive and ebullition) methane emissions from high nutrient lakes compared to low nutrient lakes (Davidson et al., 2018). Therefore, we assume that a reduction in nutrient loading can reduce methane emissions by 50 % in eutrophic water bodies.

We assume that ditch depth is inversely related to methane emission intensity, since the shallowing of ditches is almost always caused by the deposition of organic matter fueling methane production, either by strong run-off from the land and erosion or by a strong primary production or both, combined with a lack of ditch management. In most cases, areas with shallow peat ditches are also richer in phosphorus (Van Rotterdam et al., 2019). We assume that methane emissions in shallow eutrophic peat ditches can be reduced by 50 % by 2030 as a result of dredging and consequent deepening of the ditch. The residual emission of the organic matter/sludge removed from the ditch (and partly probably emitted as CO_2 instead of CH_4), is not taken into account.

The potential GHG emissions reduction by water management measures in other water bodies (lakes, canals and ponds) is not quantified.

The potential of lowering the emissions in agricultural peat meadows by 2030 are determined for four measures: a strong raise of groundwaterlevel up to 10 cm below surface (paludiculture), 20 cm higher ground water level from 1 April until 1 October, subsurface irrigation by submerged drains and nature development (for the latter measure, it is assumed that nature is a net-zero greenhouse gas emitter). The possible GHG emission reduction for each measure was derived from the relation of mean ground water level and GHG emission (Jurasinski et al., 2016; Troost et al., 2018). The total area where the measures can be taken are based on expert judgement at Waternet.

Table 1. Estimation of methane emissions in water bodies in the water management area of AGV.

Water body	Emission factor [t CO_2-eq ha^{-1} yr^{-1}]	Area [ha]	Total emission [kt CO_2-eq yr^{-1}]
Ditches	33	3540	118
Lakes	18	4753	88
Canals	11.6	1710	20
Ponds	34	171	6
Total		10 174	231

3 Results and discussion

3.1 Estimation of operational management related GHG emissions

As previously indicated the 2014 emission of AGV was estimated to be 50 kt CO_2-eq yr^{-1}. To become a net-zero emitter by 2020 the implementation of several measures are contemplated. It should be noted, however, that since 2014 it has become apparent that the actual emissions of AGV are higher than previously estimated. In 2017, the climate footprint is about 62 kt CO_2-eq (see Fig. 1). This is despite various measures like energy consumption reduction and solar energy production.

The overall emissions went up largely because of high N_2O emissions measured at wwtp Amsterdam-West. These emissions were high due to maintenance in this period (28 kt CO_2-eq). Besides, the analysis of emissions is updated and more complete in 2017 than it was in 2014. For the direct process related emissions, the analysis includes all wwtp's of AGV instead of only wwtp Amsterdam-West. Emission factors were used to estimate emissions from the other wwtp's of Waternet.

3.2 Estimation of GHG emissions from surface waters

Total GHG emissions from water bodies in the AGV water management area are estimated to be about 231 kt CO_2-eq yr^{-1} (see Table 1). The highest surface area of water bodies are lakes (both shallow and deep), but following our assessment, the majority of the methane emissions take place in ditches (see Table 1).

The water management area of AGV consists of about 35 million m^2 ditches (of which 24 million m^2 in peat areas and 11 million m^2 in sand/clay soil). The median water depth is 33 cm. GHG emissions in these ditches are estimated based on measurements in the West of Netherlands in peat ditches.

The IPCC Refinement of 2019 uses another standard emission factor for methane emissions from ditches (and canals) and ponds of 11.6 and 5.12 t CO_2-eq ha^{-1} yr^{-1}, respectively (which is 3 and 4-fold lower than our emission factors, re-

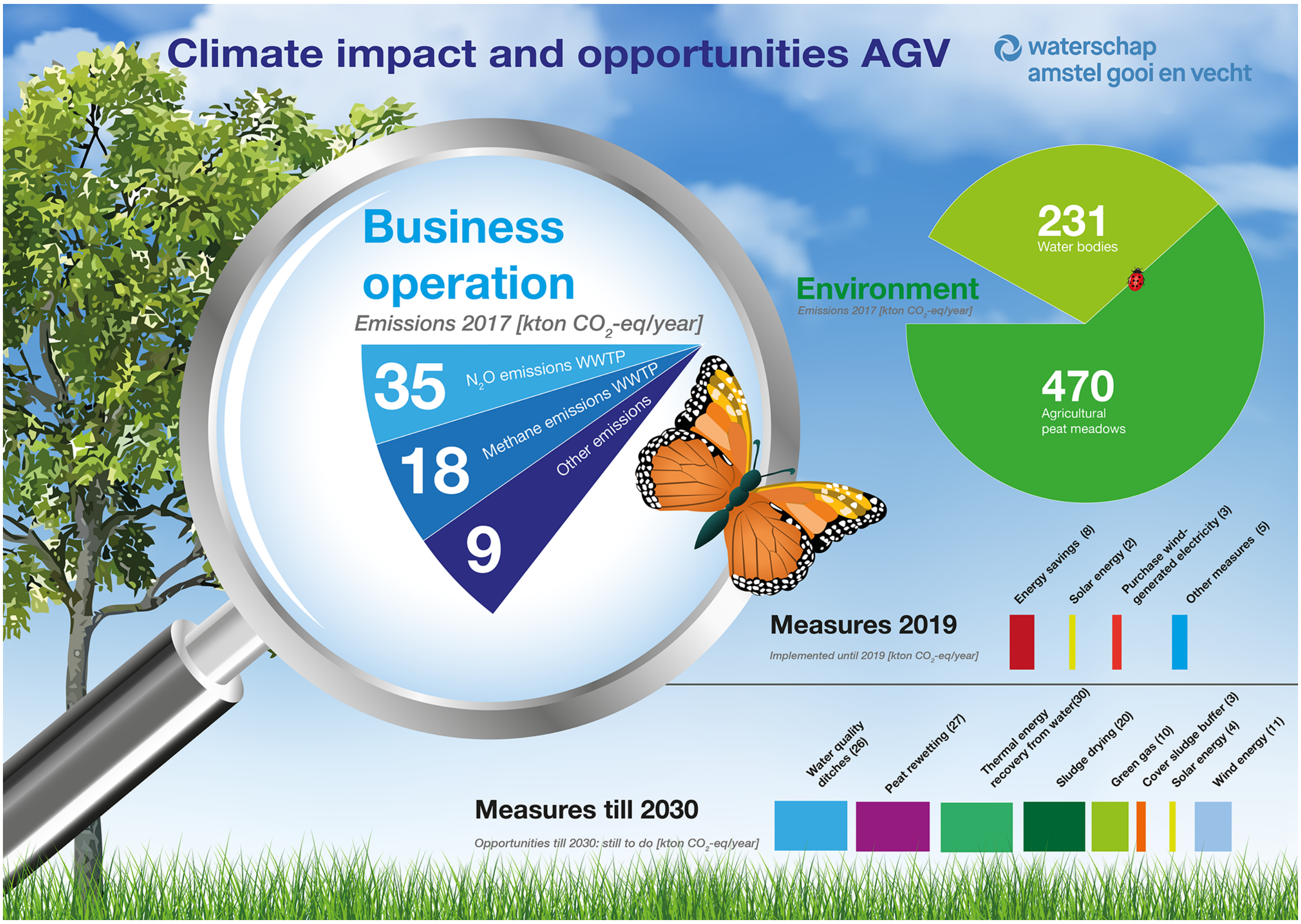

Figure 1. Climate impact and opportunities regional water authority Amstel Gooi and Vecht (AGV). Figure 1 was created by © Waternet.

spectively) (IPCC, 2019). These emission factors are used world-wide (IPCC, 2019). If these emission factors are used, the methane emissions of ditches and ponds in the water management area of AGV would be “only” 41 and 1 kt CO_2-eq yr^{-1}, respectively. However, in the IPCC Refinement, it is stated that good practice includes the development of country specific emission factors (IPCC, 2019). We argue, that the emission factors in this paper are more representative for the GHG emissions from ditches and ponds in the AGV water management area than the IPCC emission factors. The principle reason is that our emission factors are based on GHG emissions measurements in ditches and lakes in the West of the Netherlands and in a Dutch pond, whereas the IPCC emission factors are based on emissions from ditches and ponds worldwide.

More than half of the ditches in the area of Waternet are shallow eutrophic or hypertrophic. About 20 % of the ditches are hypertrophic (duckweed cover > 10 %). A 50 % reduction of methane emissions in half of the ditches may imply a reduction of about 26 kt CO_2-eq yr^{-1}.

Methane emissions can be reduced by removing the sludge, but a more sustainable plan would be preventing organic matter from reaching the ditches. This can be accomplished either by limiting fertilizers (from both sludge and from fields) and inflow of nutrient-rich water and thus limiting the primary production (plant growth, algae) in the ditches. In addition, it is important to slow down or stop the degeneration of nearby (peat) soils, which causes the ditch to fill over time (via run-off) with sludge. Improved submerged vegetation and increased depth will both cause a drop in the temperature of the water and will cause (more) oxygen to reach the sludge via the roots of the plants. All these factors are assumed to reduce the emissions of methane and CO_2.

As pointed out earlier, the estimation of methane emissions in ditches is still highly uncertain. To which extent the emissions can be reduced is even more uncertain.

Our assumption that methane emissions will be lowered due to measures targeting a reduction in nutrient loading, for instance, is based on mesocosm experiments (Davidson et al., 2018). In the field, however, so far no consistent differences in methane emissions from eutrophic and mesotrophic ditches have been found (Schrier-Uijl et al., 2011). We expect, that this lack of field evidence for the impact of trophic state is likely due to large spatial variations. Although we aimed to be conservative in our estimates, this example highlights that our estimated potential to lower the methane emissions may be overestimated. On the other hand, the temperature induced increase of methane emission will likely strongly increase future methane emissions (Davidson et al., 2018).

Although lakes and canals also fix carbon internally via photosynthesis, lake metabolism is generally a net source of CO_2 and CH_4 (Sanches et al., 2019; Huttunen et al., 2003). Environmental factors, such as the external organic and nutrient loads, temperature and precipitation act as important driving factors for CH_4 emissions. Higher emissions occur where nutrient loading and air temperature and precipitation are high (Sanches et al., 2019; Huttunen et al., 2003). Nutrient loading increases primary production in aquatic systems. Plant biomass decaying under anoxic circumstances in the sediment can increase CH_4 release from lakes to the atmosphere. The carbon dioxide fluxes are higher from reservoirs and lakes whose catchment areas are rich in peatlands or managed forests, and from eutrophic lakes in comparison to oligotrophic and mesotrophic sites (Huttunen et al., 2003; Deemer et al., 2016). Within the management area of AGV, numerous measures are implemented to reduce nutrient loading to lakes and canals and to improve their water quality. These measures will also reduce methane emissions from canals and lakes. However, this reduction is not quantified in this study.

Ponds constitute only about 2 % of the total water management area of AGV. However, the GHG emission factor used for this water body is relatively high, compared to lakes (see Table 1).

Urban ponds often receive a lot of organic matter (like drainage ditches) from run-off, street- and roof water, and adjacent water bodies. These ponds are subject to leaves, litter and dog/bird droppings and sometimes even sewage after heavy rainfall. Methane emissions can be reduced by improvement of the roof- and streetwater sewage system (reducing first flush in case of heavy rain).

3.3 Estimation of GHG emissions from agricultural peatlands

The water management area of AGV consists of about 19 400 ha agricultural peat meadows, which emit about 470 $ktCO_2$-eq yr^{-1} (mainly due to oxidation as a consequence of drainage) (Troost et al., 2018; Van den Born et al., 2016). The average emission for drained peat meadows is about 24 t CO_2-eq ha^{-1} yr^{-1}.

Higher groundwater levels in part of the management area of AGV (rewetting of peatland) may reduce these emissions by about 27 kt CO_2-eq yr^{-1} by 2030 (see Table 2).

Table 2. Calculation of total possible GHG reduction until 2030 for the agricultural peat meadow in the water management area of AGV.

Measure	GHG reduction [t CO_2-eq ha^{-1} yr^{-1}]	Area [ha]	Total GHG reduction [kt CO_2-eq yr^{-1}]
(1) Paludiculture	15	300	4.5
(2) Higher summer groundwater level	5	500	2.5
(3) Submerged drains	0.165	1500	0.25
(4) Nature	20	1000	20
Total			27.25

Transformation from normal agricultural land to paludiculture could be applied at the lowest parts of peat-polders. These lowest parts are in general equipped with extra pumps to keep the meadow dry. It would take little technical effort (mainly switching off the pumps and place some extra weirs) to start paludiculture here. It is estimated that 300 ha could be transformed to paludiculture. These areas have relatively low water levels with high GHG emissions. Therefore, the GHG reduction of 15 t CO_2-eq ha^{-1} yr^{-1} is a conservative estimate (Geurts and Fritz, 2018).

It is expected that a 20 cm higher groundwater level typically measured from 1 April until 1 October will lead to a 10 cm higher mean annual ground water level, which will lead to an emission reduction of about 5 t CO_2-eq ha^{-1} yr^{-1}. This could take place at about 500 ha which is a conservative estimate, though it would require changes in the current water management practice. Higher ground water levels are reached by higher water levels in ditches (sometimes water levels will have to be raised more than 20 cm, especially in infiltration areas, alternatively one could dig more irrigation ditches). This could lower the production of the grass and thus have impact on the business of the farmer.

The total potential area for subsurface irrigation by submerged drains has been determined to be about 4500 ha. In this analysis it is assumed that in 1/3 of the potential area these drains can be implemented. The estimation of the GHG reduction is small for this measure, as the potential is based on the difference of the mean annual groundwater level. The subsurface irrigation by submerged drains leads to higher groundwater levels in summer and lower groundwater levels in winter, therefore the mean annual groundwater level is hardly affected. If this irrigation is carried out with active pumping, the emissions of GHG may be reduced by as much as 63 % (Hoving et al., 2018). Subsurface irrigation with pumps has little or slight positive effect on the production on the grassland, but requires an investment of about EUR 2600 per ha (Hoving et al., 2018). Agricultural use remains unchanged.

The transformation of agricultural land to natural habitat is assumed to make the GHG emissions climate neutral. In the Dutch climate agreement ("klimaatakkoord 2019") it is stated that 10 000 ha agricultural land will be transformed to natural habitat. The water management area of AGV emits about 10 % of the national emission of agricultural peat meadow. Therefore, in this analysis, it is assumed that in the water management area of AGV, 1000 ha is transformed to natural habitat. It is assumed that the wetter peat soils (with lower GHG emissions than average) are first transformed to natural habitat, therefore the estimation of the GHG emission is assumed to be lower than 24 t CO_2-eq ha^{-1} yr^{-1} (which is the mean GHG emission of the agricultural peat meadow in the AGV water management area). In Table 2, we present a reduction of 20 t CO_2-eq ha^{-1} yr^{-1} in case of transformation to nature, which we derived from both "klimaatakkoord (2019)" and Schrier-Uijl et al. (2014). Schrier-Uijl et al. (2014) measured a reduction of 20.4 t CO_2-eq ha^{-1} yr^{-1}. They compared rewetted nature (net CO_2 sink) with traditional peat meadow (net emission).

For measures 2 and 3 (higher summer ground water level and the subsurface irrigation by submerged drains), the GHG reduction potential is underestimated because the reduction is calculated on the basis of annual ground water levels even though summer water levels are higher. The highest GHG emissions are normally taking place at higher temperatures (Moore and Dalva, 1993).

Measured phosphorous concentrations are higher in shallow ditches with higher groundwater levels in the water management area of AGV (Van Rotterdam et al., 2019). This indicates that rewetting of peat to reduce GHG emissions from the peatland can have side-effects. Wetting of peat, especially when water can run off from the fields or flow out of drainage pipes, could result in an increased phosphorus load tot the ditch. This is because phosphorus in (partly) decomposed peat will become available in anoxic conditions.

4 Conclusions

This investigation shows that GHG emissions in the territory of the water board AGV, which are influenced by the water management practices, are much greater than the emissions of the business operations of AGV. Therefore, it may be more effective to implement measures to reduce GHG emissions in the environment than it is to focus only on reduction of the climate footprint of the water company itself. GHG emissions in water bodies (especially ditches and lakes) and agricultural peat meadows are significant.

Water management measures that are aimed at lowering GHG emissions have an impact on water quality. This is especially true for those measures applied to water bodies because a synergy is expected between the lowering GHG emissions and water quality. Since water authorities are experts and have experience in implementing water management measures, water authorities are important stakeholders in lowering the emissions from water bodies and peatlands. For the implementation of practices aimed at reducing GHG emissions in the environment, cooperation with other stakeholders like farmers is important, since farmers are in most cases owner of the ditches.

Although there are various uncertainties to be addressed, like the origin of the sludge in peatland ditches and the need for more measurements of GHG emissions and the effect of water management measures on these emission, some measures can be taken right way as they are no-regret because besides having a likely positive climate effect they also have other positive effects. These measures on peatland are (in order of decreasing climate effect): improvement of water quality in the ditches, transfer agricultural land to wet nature, summer raise of the ditch levels, paludiculture and pump driven submerged drains.

Data availability. Underlying data is stored in a non-public database of Waternet. Datasets are available by contacting the correspondence author.

Author contributions. AMMW took the lead to write this paper. TAHMP, LM and SK contributed in writing the paper. AMMW is responsible for generating an overview of the climate footprint of Waternet and the measures that will or can be taken by Waternet in general to reduce greenhouse gas emissions. TAHMP made an estimation of the potential to lower the greenhouse gas emissions in peat areas. LM and TAHMP provided measures to reduce methane emissions in ditches. LM provided the specifications of the ditches and lakes of AGV (total surface area, depth, soil type). LM made an estimation of the potential to lower the greenhouse gas emissions in ditches. SK provided background literature to make the estimation of greenhouse gas emissions in surface waters.

Competing interests. The authors declare that they have no conflict of interest.

Special issue statement. This article is part of the special issue "TISOLS: the Tenth International Symposium On Land Subsidence – living with subsidence". It is a result of the Tenth International Symposium on Land Subsidence, Delft, the Netherlands, 17–21 May 2021.

Acknowledgements. The idea of this work was given by André Struker (commissioner). The infographic (Fig. 1) is drawn by Paul van Elk. The data that is provided to calculate the emissions is provided by different workers from Waternet. Hereby some are mentioned though not all: Marcel Zandvoort (N_2O emissions), Jacqueline de Danschutter (measures taken for k2020), Sara Giorgi (thermal energy recovery from water), Bram Konneman (wind energy). Finally the basis for the climate footprint is set by Theo Janse (who is now retired from Waternet).

References

Aben, R. C. H., Barros, N., van Donk, E., Frenken, T., Hilt, S., Kazanjian, G., Lamers, L. P. M., Peeters, E. T. H. M., Roelofs, J. G. M., de Senerport Domis, L. N., Stephan, S., Velthuis, M., Van de Waal, D. B., Wik, M., Thomton, B. F., Wilkinson, J., DelSontro, T., and Kosten, S.: Cross continental increase in methane ebullition under climate change, Nat. Commun., 8, 1682, https://doi.org/10.1038/s41467-017-01535-y, 2017.

Bastviken, D., Tranvik, L. J., Downing, J. A., Crill, P. M., and Enrich-Prast, A.: Freshwater methane emissions offset the continental carbon sink, Science, 331, 50, 2011.

Davidson, T. A., Audes, J., Jeppesen, E., Landkildehus, F., Lauridsen, T. L., Søndegaard, M., and Syväranta, J.: Synergy between nutrients and warming enhances methane ebullition from experimental lakes, Nature Clim. Change, 8, 156–160, 2018.

Deemer B. R., Harrison, J. A., Li, S., Beaulieu, J. J., DelsSontro, T., Barros, N., Bezerra-Neto, J. F., Powers, S. M., Dos Santos, M. A., and Vonk, J. A.: Greenhouse gas emissions from reservoir water surfaces: A new global synthesis, Bioscience, 66, 949–964, https://doi.org/10.1093/biosci/biw117, 2016.

Elbersen, J. W. H., Verdonschot, P. F. M., Roels, B., and Hartholt, J. G.: Definitiestudie Kaderrichtlijn Water (KRW), I. Typologie Nederlandse Oppervlaktewateren, Alterra-rapport 669, available at: https://library.wur.nl/WebQuery/wurpubs/320649 (last access: 24 February 2020), 2003.

Frijns, J., Mulder, M., and Roorda, J.: Op weg naar een klimaatneutrale waterketen, STOWA 2008-17, ISBN 978.90.5773.411.3, available at: https://pdfs.semanticscholar.org/dfde/639a3a184fc107ea6c213064bd8a681f0cee.pdf?_ga=2.70582483.278089143.1582543929-197030730.1582543929 (last access: 24 February 2020), 2008.

Geurts, J. and Fritz, C.: Paludiculture pilots and experiments with focus on cattail and reed in the Netherlands. Technical report CINDERELLA project, FACCE-JPI ERA-NET Plus on Climate Smart Agriculture, available at: https://www.veenweiden.nl/wp-content/uploads/2018/08/Rapportage-Paludicultuur-Radboud-Universiteit.pdf (last access: 24 February 2020), 2018.

Goorts, C. and Kolkhuis Tanke, R.: Klimaatmonitor waterschappen, Verslagjaar 2017, available at: https://www.uvw.nl/wp-content/uploads/2018/12/Klimaatmonitor-waterschappen-2017.pdf (last access: 24 February 2020), 2018.

Government of the Netherlands: Klimaatakkoord, available at: https://www.klimaatakkoord.nl/documenten/publicaties/2019/06/28/klimaatakkoord (last access: 24 February 2020), 2019.

Harrison, J. A., Matson, P. A., and Fendorf, S. E.: Effects of a diel oxygen cycle on nitrogen transformations and greenhouse gas emissions in a eutrophied subtropical stream, Aquat. Sci. 67, 308–315, https://doi.org/10.1007/s00027-005-0776-3, 2005.

Hoving, I. E., van den Akker, J. J. H., Massop, H. T. L., Holshof, G. J., and van Houwelingen, K.: Precisiewatermanagement op veenweidegrond met pompgestuurde onderwaterdrains, Wageningen Livestock Research report No. 1123, Wageningen Livestock Research, Wageningen, https://doi.org/10.18174/461252, 2018.

Huttunen, J. T., Alkm, J., Liikanen, A., Juutinen, S., Larmola, T., Hammar, T., Silvoa, J., and Martikainen, P. J.: Fluxes of methane, carbon dioxide and nitrous oxide in boreal lakes and potential anthropogenic effects on the aquatic greenhouse gas emissions, Chemosphere, 52, 609–621, https://doi.org/10.1016/S0045-6535(03)00243-1, 2003.

IPCC: Fifth assessment report, available at: https://archive.ipcc.ch/pdf/assessment-report/ar5/syr/SYR_AR5_FINAL_full_wcover.pdf (last access: 24 February 2020), 2014.

IPCC: Refinement to the 2006 IPCC Guidelines for National Greenhouse Gas Inventories, in: chap. 7: Wetlands, available at: https://www.ipcc-nggip.iges.or.jp/public/2019rf/index.html (last access: 24 February 2020), 2019.

Jurasinski, G., Günther, A., Huth, V., Couwenberg, J., and Glatzel, S.: 5.1 Greenhouse gas emissions, in: chap. 5 Ecosystem services provided by paludiculture, Paludiculture – productive use of wet peatlands, Climate protection – biodiversity – regional economic benefits, edited by: Wichtmann, E., Schröder, and Joosten, H., Schweizerbart Science Publishers, Stuttgart, 79–93, 2016.

Koschorreck, M., Downing, A. S., Hejzlar, J., Marcé, R., Laas, A., Arndt, W. G., Keller, P. S., Smolders, A. J. P., van Dijk, G., and Kosten, S.: Hidden treasures: Human-made aquatic ecosystems harbour unexplored opportunities, Ambio, 49, 531–540, https://doi.org/10.1007/s13280-019-01199-6, 2020.

Moore, T. R. and Dalva, M.: The influence of temperature and water table position on carbon dioxide and methane emissions from laboratory columns of peatland soils, J. Soil Sci., 44, 651–664, https://doi.org/10.1111/j.1365-2389.1993.tb02330.x, 1993.

RIVM: Greenhouse gas emissions in the Netherlands 1990–2017, National Inventory Report 2019, available at: https://www.rivm.nl/bibliotheek/rapporten/2019-0020.pdf (last access: 24 February 2020), 2019.

Sanches L. F., Guenet, B., Marinho, C. C., Barros, N., and de Assis Esteves, F.: Global regulation of methane emission from natural lakes, Sci, Rep., 9, 255, https://doi.org/10.1038/s41598-018-36519-5, 2019.

Schrier-Uijl, A. P., Veenendaal, E. M., Leffelaar, P. A., van Huissteden, J. C., and Berendse, F.: Spatial and temporal variation of methane emissions in drained eutrophic peat agro-ecosystems: drainage ditches as emission hotspots, Biogeosciences Discuss., 11, 1237–1261, https://doi.org/10.5194/bgd-5-1237-2008, 2008.

Schrier-Uijl, A. P., Veraart, A. J., Leffelaar, P. A., Berendse, F., and Veenendaal, E. M.: Release of CO_2 and CH_4 from lakes and drainage ditches in temperate wetlands, Biogeochemistry, 102, 265–279, 2011.

Schrier-Uijl, A. P., Kroon, P. S., Hendriks, D. M. D., Hensen, A., Van Huissteden, J., Berendse, F., and Veenendaal, E. M.: Agricultural peatlands: towards a greenhouse gas sink – a synthesis of a Dutch landscape study, Biogeosciences, 11, 4559–4576, https://doi.org/10.5194/bg-11-4559-2014, 2014.

Snip L., and F. Oesterholt: Berekening CO_2-voetafdruk van drinkwaterbedrijven, KWR PCD 11:2018, Januari 2019, available at: http://library.wur.nl/WebQuery/hydrotheek/2250061 (last access: 24 February 2020), 2019.

Trolle, D., Staehr, P. A., Davidson, T. A., Bjerring, R., Lauridsen, T. L., Søndergaard, M., and Jeppesen, E.: Seasonal dynamics of CO_2 flus across the surface of shallow temperate lakes, Ecosystems, 15, 336–347, 2012.

Troost, S., Kuipers, H., and Hoefsloot, N.: Toekomstverkenning bodemdaling AGV, Report HJGK/001/162262, Aveco de Bondt, Amersfoort, 2018.

Van Bergen, T. J. H. M., Barros, N., Mendonca, R., Aben, R. C. H., Althuizen, I. H. J.,Huszar, V., Lamers, L. P. M., Lürling, M., Roland, F., and Kosten, S.: Seasonal and diel variation in greenhouse gas emissions from an urban pond and its major drivers, Limnol. Oceanogr., 64, 2129–2139, https://doi.org/10.1002/lno.11173, 2019.

Van den Born, G. J., Kragt, F., Henkens, D., Rijken, B., van Bemmel, B., and van der Sluis, S.: Dalende bodems, stijgende kosten, Mogelijke maatregelen tegen veenbodemdaling in het landelijk en stedelijk gebied, PBL 1064, available at: https://www.pbl.nl/sites/default/files/cms/publicaties/pbl-2016-dalende-bodems-stijgende-kosten-1064.pdf (last access: 25 February 2020), 2016.

Van der Hoek, J. P.: Towards a climate neutral water cycle, J. Water Clim., 3, 163–170, https://doi.org/10.2166/wcc.2012.015, 2012.

Van der Nat, F.-J. W. A., Middelburg, J. J., van Meteren, D., and Wielemakers, A.:. Diel methane emission patterns from *Scirpus lacustris* and *Phragmites australis*, Biogeochemistry, 41, 1–22, https://doi.org/10.1023/A:1005933100905, 1998.

Van Rotterdam, D., Kros, J., de Pater, J., Vogel, J., and Ros, G. H.: Agrarische fosforbelasting van het oppervlaktewater en het handelingsperspectief binnen het beheergebied van waterschap Amstel, Gooi en Vecht, Rapport 1685.N.16, Nutriënten Management Instituut BV, Wageningen, 2019.

Vermaat, J. E., Hellmann, F., Dias, A. T. C., Hoorens, B., van Logtestijn, R. S. P., and Aerts, R.: Greenhouse gas fluxes from Dutch peatland water bodies: Importance of the surrounding landscape, Wetlands, 31, 493–498, https://doi.org/10.1007/s13157-011-0170-y, 2011.

Wu, S., Li, S., Zou, Z., Hu, T., Hu, Z., Liu, S., and Zou, J.: High methane emissions largely attributed to ebullitive fluxes from a subtropical river draining a rice paddy watershed in China, Environ. Sci. Technol., 53, 3499–3507, https://doi.org/10.1021/acs.est.8b05286, 2019.

Xing, Y., Xie, P., Yang, H., Ni, L., Wang, Y., and Tang, W.: Diel variation of methane fluxes in summer in a eutrophic subtropical lake in China, J. Freshwater Ecol., 19, 639–644, 2004.

Proc. IAHS, 382, 143–147, 2020
https://doi.org/10.5194/piahs-382-143-2020

PDCA method for management of land subsidence

Yoshiyuki Muramoto, Susumu Hayatsu, Michiharu Hiyama, Daisuke Murai, and Shoji Kunisue

Kanto Natural Gas Development Co., Ltd, Mobara city, Chiba prefecture, 297-8550, Mobara, Japan

Correspondence: Yoshiyuki Muramoto (y.muramoto@k-and-o-energy.co.jp)

Published: 22 April 2020

Abstract. In Chiba prefecture in Japan, it has been reported land subsidence for many decades. One of the causes of land subsidence is considered gas production. To reduce and control land subsidence, we applied PDCA method in a certain new development area. As a result, we could maintain successfully the land subsidence less than the target value, 20 mm yr^{-1} at the present moment.

1 Background

The Southern Kanto gas field, the largest field of natural gas dissolved in water in Japan, is located primarily under the Chiba prefecture (Fig. 1). In this field, eight companies produce 460 million $m^3\,yr^{-1}$ of natural gas (Japan Natural Gas Association, 2019). On the other hand, there are some environmental issues such as land subsidence. Generally speaking, land subsidence results from various causes such as natural compaction, tectonic movement and ground water withdrawal for agricultural or industrial use.

The gas production is also considered one of the causes the land subsidence. To produce natural gas dissolved in water, it is necessary to produce formation water too. As a result, the formation pressure is reduced and land surface subsides. There are some causes in land subsidence other than natural gas and formation water production, but as natural gas production company's responsibility, we are making some efforts to reduce the land subsidence.

As a part of our efforts, we have been conducting land subsidence PDCA management in a certain new development area. The land subsidence in this area is thought to be affected by ground water withdrawal for agricultural use and tectonic movement as well as natural gas production. Because the study area is rural, the pump discharge rate is not clear but the ground water is withdrawn for agricultural use to some extent. In addition, Chiba prefecture containing the study area is located near the plate boundary between the Pacific Plate and the Philippine Sea Plate. In this area, the earthquakes often occur.

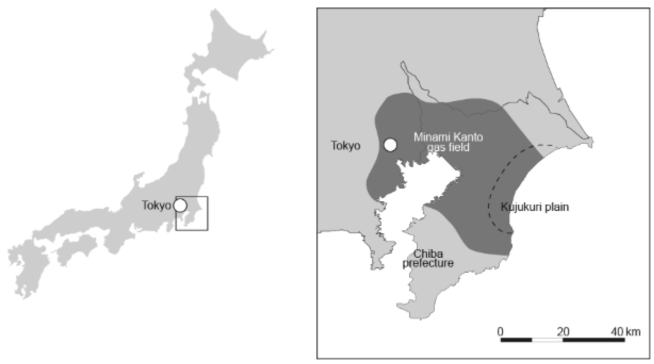

Figure 1. Southern Kanto gas field (Kunisue and Kokubo, 2010). Minami Kanto gas field in this figure means Southern Kanto gas field.

In this paper, we introduce land subsidence PDCA management. The purpose of this management is to control land subsidence less than the target value, 20 mm yr^{-1}.

2 Land subsidence PDCA management method

PDCA consists of four steps (Plan, Do, Check, Act). It is based on the "Shewhart cycle" (Moen and Norman, 2006; Chakraborty, 2016). PDCA is a continuous feedback loop to identify and change process elements to reduce variation (Gupta, 2006). In general, PDCA aims at the control and continuous improvement of processes and products.

As a measure for controlling land subsidence, we apply PDCA method in a certain new development area and repeat it every year (Fig. 2).

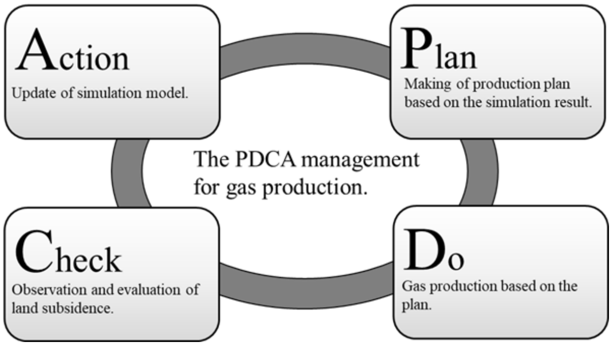

Figure 2. Land subsidence PDCA management method.

2.1 Plan

We make production plan based on the result of geomechanical reservoir simulation. The simulator is called "JARAS/3D" which was developed as a result of joint study between Japan Oil, Gas and Metals National Corporation (formerly Japan National Oil Corporation), and the eight gas production companies in Southern Kanto gas field. This simulator is adjusted for Southern Kanto gas field and it can evaluate the amounts of land subsidence associated with natural gas production.

2.2 Do

We produce natural gas and formation water based on the production plan. However, the land subsidence is occurred by not only the effect of natural gas and formation water production but also natural compaction, tectonic movement, etc. Sometimes unexpected large subsidence is occurred by those effect. Against such situation, we set a criterion of land subsidence for the each well as a precaution. When the land subsidence is larger than this criterion, we stop the natural gas and formation water production from the corresponding well in order to avoid further land subsidence. The measurement method of land subsidence is mentioned in Sect. 2.3.

2.3 Check

We observe the land subsidence and compare it with the criterion every month (Fig. 3). To observe land subsidence, measurement of the relative height from the reference point which is free from the effect of the natural gas and formation water production is necessary. Such point is far from natural gas and formation water production area. Therefore, the levelling requires a huge time to obtain the observation result. On the other hand, GNSS (Global Navigation Satellite System) can obtain it continuously and rapidly. To observe land subsidence at the target points rapidly, we apply the combination of GNSS measurement and levelling.

First, we established GNSS station in the target area, and measure the relative height of the GNSS station from the reference GNSS station which locates out of the effect of natural gas and formation water production. Next, the height of benchmarks around the GNSS station are measured by levelling. Finally, the height of target benchmarks are obtained by combining the GNSS measurement and levelling result (Fig. 4).

To get the baseline data, the GNSS measurement has been conducted before the natural gas and formation water production start.

Furthermore, we compared the land subsidence results with those by the local government.

2.4 Act

We observe not only the land subsidence but also the water level which reflect the formation pressure. We update the simulation model based on these observation data every year if necessary. Commonly permeability and firmness are modified to reproduce the water level and land subsidence respectively. Then we use the updated simulation model on the Plan in the next PDCA.

3 Results

We applied PDCA method in a certain new development area to reduce and control land subsidence. Based on a result of land subsidence, we changed the production plan if necessary. When the land subsidence became larger than the criterion, we stopped the production. After that, when it became smaller than the criterion, we restarted the production.

As a result of the PDCA management, we could maintain successfully the land subsidence less than the target value, $20\,\mathrm{mm\,yr^{-1}}$ at the present moment. In addition, the observation results conducted by the local government shows less than $20\,\mathrm{mm\,yr^{-1}}$ (Fig. 5).

We could obtain the land subsidence observation results close to Government's result in 2015 and 2016. However, the Government's result was small in 2017. In 2018, the Government's result has not disclosed yet.

Comparing the land subsidence result before and after the start of natural gas and formation water production, it became smaller. The land subsidence in benchmark 1 (BM1) was $-13.4\,\mathrm{mm\,yr^{-1}}$ in 2013 before the natural gas and formation water production, but it was -11.6 and $-10.3\,\mathrm{mm\,yr^{-1}}$ in 2015 and 2016 after the natural gas and formation water production. Similarly, Benchmark 2 (BM2) was $-15.2\,\mathrm{mm\,yr^{-1}}$ in 2013, while $-12.3\,\mathrm{mm\,yr^{-1}}$ in 2015 and $-10.2\,\mathrm{mm\,yr^{-1}}$ in 2016. Benchmark 3 (BM3) was $-14.4\,\mathrm{mm\,yr^{-1}}$ in 2013, while $-12.1\,\mathrm{mm\,yr^{-1}}$ in 2015 and $-8.2\,\mathrm{mm\,yr^{-1}}$ in 2016 (Table 1). The reason is not clear but it could be the effect of factors other than natural gas and formation water production.

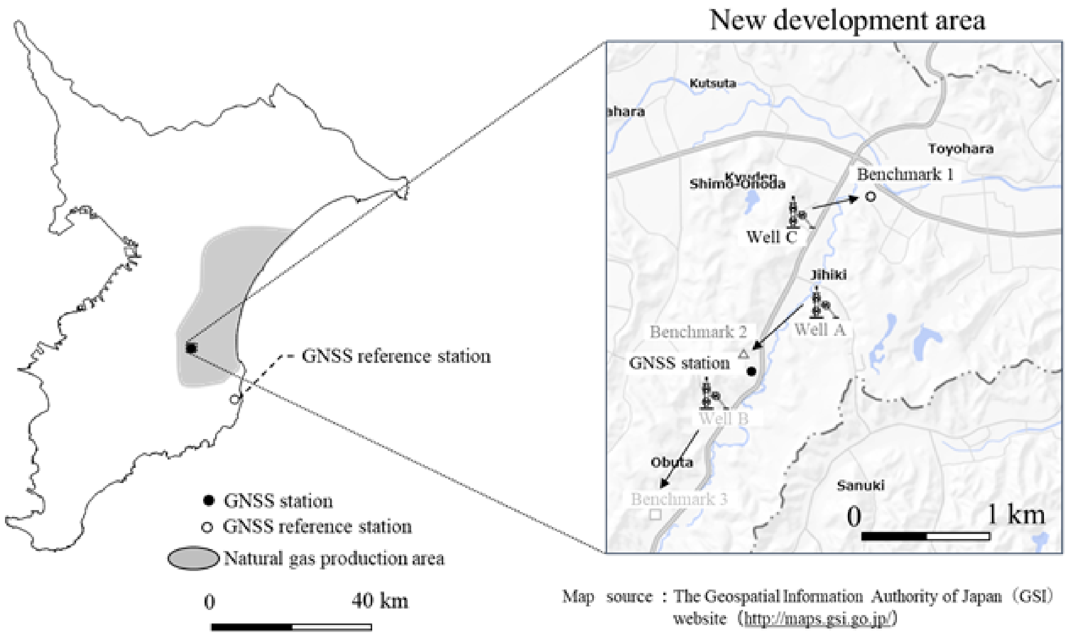

Figure 3. New development area.

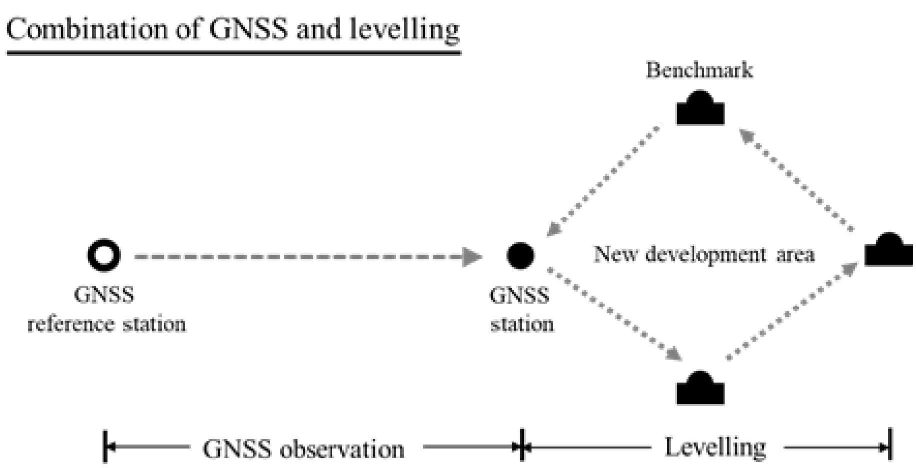

Figure 4. Land subsidence observation method.

4 Conclusions

The results of our work show us possibility to control land subsidence. By repeating this method every year, we will improve the management method. On the other hand, they also show us some issues as mentioned in Sect. 3. To improve this method, we will study on these problems in the future.

Data availability. For more information about the used data, please contact the corresponding author Yoshiyuki Muramoto (y.muramoto@k-and-o-energy.co.jp).

Author contributions. YM, SH, DM and SK conceived the idea of the method. YM,SH,MH collected the data. YM, SH, DM and SK analysed the data. YM wrote the manuscript.

Competing interests. The authors declare that they have no conflict of interest.

Special issue statement. This article is part of the special issue "TISOLS: the Tenth International Symposium On Land Subsidence – living with subsidence". It is a result of the Tenth International Symposium on Land Subsidence, Delft, the Netherlands, 17–21 May 2021.

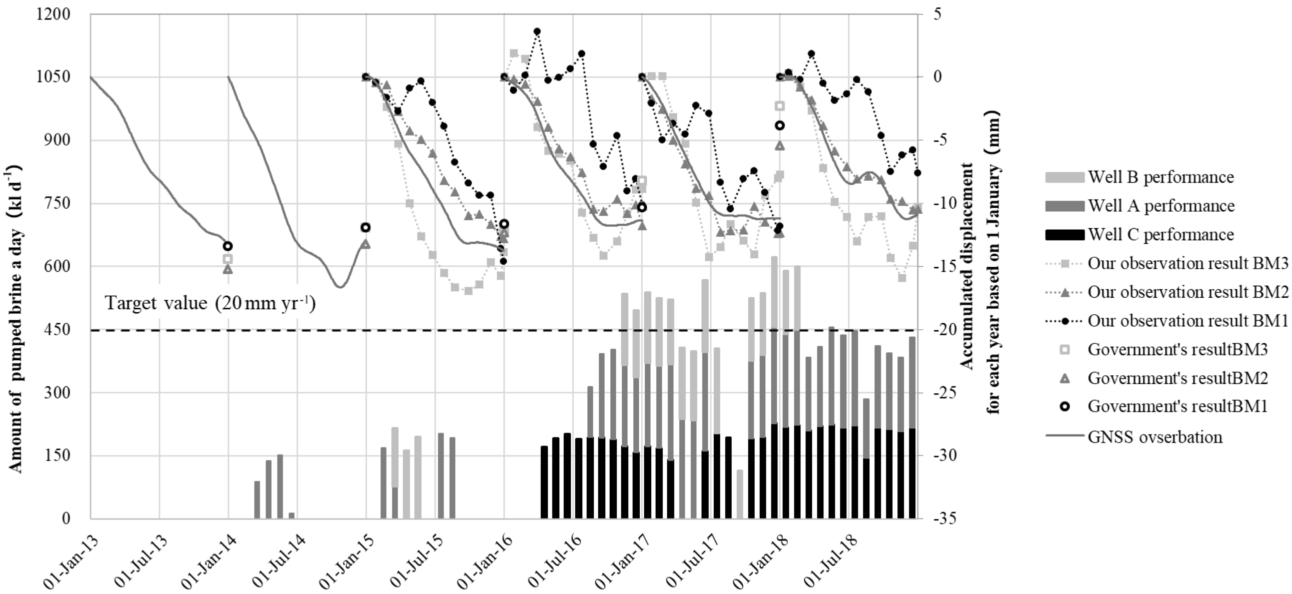

Figure 5. Production and land subsidence results.

Table 1. Land subsidence results in each benchmark (mm yr^{-1}).

Benchmark	Executor	Before production	After production			
		2013	2015	2016	2017	2018
Benchmark 1	Company	No DATA	−14.6	−10.1	−11.8	−7.6
	Local government	−13.4	−11.6	−10.3	−3.8	No DATA
Benchmark 2	Company	No DATA	−12.8	−11.8	−12.3	−10.4
	Local government	−15.2	−12.3	−10.2	−5.4	No DATA
Benchmark 3	Company	No DATA	−13.9	−8.8	−7.7	−10.3
	Local government	−14.4	−12.1	−8.2	−2.3	No DATA

References

Chakraborty, A.: Imprtance of PDCA Cycle for SMEs, SSRG-IJME, 3, 30–34, 2016.

Gupta, P.: Beyond PDCA A New Process Management Model, Qual. Prog., 39, 45–52, 2006.

Japan Natural Gas Association: available at: http://www.tengas.gr.jp/keiyo_outline.html, last access: 5 August 2019.

Kunisue, S. and Kokubo, T.: In situ formation compaction monitoring in deep reservoirs by using optical fibres, Eighth International Symposium On Land Subsidence, Juriquilla, Queretaro, México, 17–22 October, Vol. 339, 368–370, 2010.

Moen, P. and Norman, C.: Evolution of the PDCA Cycle, 2006.

InSAR Detection of Localized Subsidence Induced by Sinkhole Activity in Suburban West-Central Florida

T. Oliver-Cabrera[1], S. Wdowinski[1], S. Kruse[2], T. Robinson[2]

1Department of Earth and Environment, Florida International University, Miami, FL, 33199, USA
2 School of Geosciences, University of South Florida, Tampa, FL, 33620, USA

Correspondence to: Talib Oliver-Cabrera (toliverc@fiu.edu)

Abstract

Sinkhole activity in west-central Florida is a major hazard for people and property. Increasing frequency of sinkhole collapse is often related to an accelerated use of groundwater and land resources. In this work, we use radar interferometry acquired over a selected region in Hernando County in west-central Florida to observe small localized deformation possibly caused by sinkhole activity. The data used for the study consist of acquisitions from one TerraSAR-X frame covering a time span of approximately 1.7 years with spatial resolution of 0.25 by 0.60 m. We applied the Persistent Scatterer Interferometry (PSI) technique using the Stanford Method for Persistent Scatterers (StaMPS). Results reveal several areas of localized subsidence at rates ranging from -3.7 to -4.9 mm/yr. Ground truthing and background verification of the subsiding locations confirmed the relationship of the subsidence with sinkhole presence.

Introduction

Sinkholes form when rocks or sediments move into a void created by rock dissolution (Dobecki et al., 2006). They can induce subsidence in the form of gradual surface drop with no apparent rupture, which may later collapse due to a break of rock and soil (Ford et al., 2007). In Florida, sinkhole activity occurs frequently due cap rock subsidence or collapse into existing cavities within the shallow carbonate bedrock, which were formed during the Holocene and Pleistocene. Accelerated use of groundwater and land resources has promoted an increase in the rate of sinkhole formation (Tihansky, 1999; Veni et al., 2014). These circumstances have made sinkhole collapse one of the leading natural disasters in Florida, with almost 25,000 insurance claims between the years 2006-2010 (Florida Office of insurance regulation, 2010). Sinkholes are present through much of Florida. However, reported sinkhole incidences as subsidence and collapse occur mainly in the west-central region of the state (Florida Geological Survey, 2015) (Figure 1). This sinkhole-active corridor extends over a large area (hundreds of km2) covering three of the most densely populated cities in Florida: Orlando, Tampa and St. Petersburg, which is located west of Tampa (Figure 1).

Detecting a sinkhole before collapse is a difficult task, as sinkholes often display unnoticeable surface changes. Geophysical techniques such as ground penetrating radar (GPR), electrical resistivity tomography (ERT), and shallow seismic surveys (refraction tomography, reflection, surface wave inversion) are commonly used to image with high detail sinkhole characteristics beneath the surface (Dobecki et al., 2006; Theron et al., 2018). However, these techniques require a priori information of sinkhole location and are limited to small study areas (up to hundreds of m2). Geological and geophysical information is often used for sinkhole hazard and risk assessments, based on modelling and probabilistic approaches (Frumkin et al., 2011; Galve, Remondo et al., 2011; Kim et al., 2014; Theron et al., 2018). Calculated hazard and risk maps rely on sinkhole information that is often incomplete or not available. Small sinkhole size and sparse distribution makes detection and monitoring a challenging task. In places such as Florida, monitoring techniques are needed that could cover large areas to complement and support ground-based surveys.

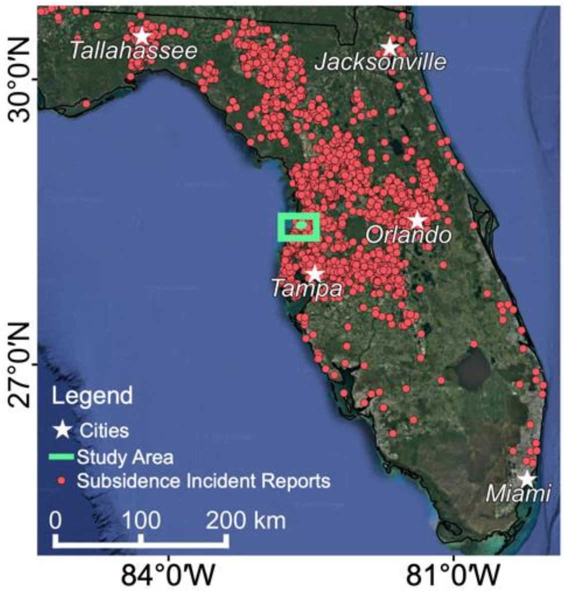

Figure 1 Location map of sinkhole and subsidence reports in Florida (red circles) collected by the Florida Geological Survey (Florida Geological Survey, 2015). White stars show the location of the largest cities in the state. Green frame shows the location of the Timber Pines study area. Map data: Google, Maxar Technologies.

Interferometric Synthetic Aperture Radar (InSAR) technique is a remote sensing technique that can detect surface movements with high detail, while covering vast areas (Massonnet et al., 1998; Bürgmann et al., 2000; Rosen et al., 2000). The technique has been successfully applied to observe sinkhole activity in arid places such as west Texas and the Dead Sea shores (Nof et al., 2013; Atzori et al., 2015; Baer et al., 2018; Kim et al., 2018), in urban settings like Heerlen in Netherlands, Gauteng province in South Africa and Quebec City in Canada (Chang et al., 2014; Theron et al., 2017a; Martel et al., 2018) and in vegetated regions like Bayou Corne, Louisiana and Tampa, Florida (Jones et al., 2013; Oliver-Cabrera et al., 2019). The above InSAR implementation examples were conducted in areas where interferometric coherence is maintained over long periods of time, through stable radar scattering from bare surfaces, rocks, and man-made structures. In cases where land-cover changes occur rapidly and frequently, as in highly vegetated regions such as Louisiana or Florida, effective InSAR tends to be limited to areas with buildings (e.g. Oliver-Cabrera et al., 2019). An alternative to maintain high coherence in densely vegetated regions are radar systems with a very short revisit time, like the Uninhabited Aerial Vehicle SAR (UAVSAR) (Jones et al., 2013).

This study expands upon our previous study of InSAR-based detection of sinkhole activity in west-central Florida (Oliver-Cabrera et al., 2019), which demonstrated the capability of InSAR for detecting sinkhole related deformation in the challenging scattering environment of west-central Florida. In the current study we focus on a smaller area, the region of the Timber Pines housing development in west-central Florida, and analyze the effectivity of the InSAR results, which are verified using both ground based observations and official reports of sinkhole induced damage.

Study area

The study area covers the region of Timber Pines in Hernando County, roughly 60 km north of Tampa in west-central Florida. Timber Pines is a private community that hosts 3,452 homes, characterized by sparse residential and commercial buildings. This study site was selected because numerous homes have reported sinkhole activity. Also, the county provides openly available lists of reported sinkholes, allowing us to verify the deformation sources of our InSAR analysis.

Data

Our data consists of TerraSAR-X (TSX) (3.1cm wavelength) Staring SpotLight (ST) SAR imagery. TSX ST mode has a pixel resolution of 0.25 m in azimuth and 0.60 m range. A total of 45 acquisitions were obtained to cover a time span of 1.7 years between 2015-2017 with a repeated pass of 11 and 22 days. Variation in the repeated pass acquisition frequency its due to budget constraints. Sinkhole activity verification was done through the sinkhole reports provided by Hernando County through their website (www.hernandocounty.us).

Methods

Our InSAR processing and analysis follows the proposed methodology of Oliver-Cabrera et al. (2019). SAR data processing to obtain InSAR time series is followed by a spatial clustering analysis. First, a stack of single master interferometric pairs is generated using the Doris (v4.02) software package to generate interferograms. Doris was developed by the Delft Institute of Earth Observation and Space Systems (DEOS) Delft University of Technology (Kampes et al., 2003). The selected master is a SAR acquisition with low noise levels and centered, as much as possible, in the middle of the time vector. No resampling (multi-looking) was applied to the interferometric products. The stack of single master interferograms was used as an input for the second processing stage, time series analysis using the Persistent Scatterer Interferometry method (PSI) (Ferretti et al., 2001). This technique focuses on the use of high backscatter signature sources (e.g. buildings), minimizing the use of pixels with low or variable backscatter (e.g. vegetation). Thus, only the Persistent Scatterers (PS) are kept. We implement the Stanford Method for PS (StaMPS) (Hooper et al., 2004) in order to estimate the displacement time series of individual points.

A PS distribution analysis post-processing is performed to find the possible sinkhole-related signals. We isolate the scatterers that display deformation trends from the stable ones, by separating the scatterers with deformation trends beyond 3 standard deviations (3σ), leaving just the peak moving scatterers. The applied threshold of 3σ was selected from a range of thresholds between 1 to 3σ as it was found most suitable to isolate the moving scatterers. To find the sinkhole-related signals we search for groups of subsiding scatterers that are concentrated spatially. A Density-Based Spatial Clustering Analysis (DBSCAN) algorithm (Ester et al., 1996) is implemented to find groups of moving scatterers based on their spatial distribution. The criteria used in the DBSCAN algorithm is a distance of 6 m, double of the average sinkhole radius reported in the Florida subsidence reports (Florida Geological Survey, 2015) and a minimum of five PS points per group.

Results

InSAR time series results are shown as a map of surface velocities (Figure 2). The velocity map indicates stability in most of the study area (green color in Figure 2). Results also display points of high positive and negative velocities, which likely represent noise due to the short duration of the acquisition span (1.7 years). Small scattered areas of localized deformation can be found throughout the study area (e.g. red circles in Figure 2). A total of 85 clusters of subsidence were obtained from the spatial clustering analysis. Results show that the majority of the clusters are located over houses. A few of the clusters are located over roads, including one with 46 PSs (Site a). From all the clusters with more than 15 PSs, just one appeared to be part of a noisy area, considered as non-reliable. Three clusters with a higher density of subsiding scatterers were selected for a detailed inspection (Sites a, b and c in Figure 3). Site a is located in the middle of a road, approximately 30m long. Site b and c are located in two houses of roughly 20 x 20 m of size. Detailed inspection of the data shows a peak downwards movement starting on the first quarter of 2016 and reaching the lowest point around August 2016. The county database does not show a sinkhole report for this area, however, there are several nearby sinkhole activity reports. Also, Oliver-Cabrera et al.(2019) found that GPR surveys show irregular strata along the road near the signal and from neighboring homes, which suggest prior and perhaps ongoing subsidence at this site. Time series observations of Site b show a downwards step-like movement in the second half of 2015. County reports confirmed sinkhole activity at this location, however no specifics regarding dates of events or collapses were found. Observations from Site c also show a step-like movement, but in this case towards the end of the first half of 2016. County documents for this site also reported sinkhole activity. A sharp peak up and down in 2016 suggest that an abrupt change happened to the building, perhaps related to repair works to the property, although no documentation was found to confirm this.

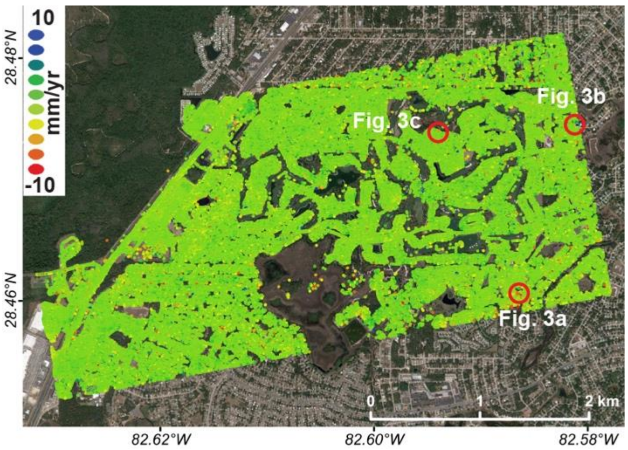

Figure 2 Velocity map of the Timber Pines study area determined from TSX ST data covering a time span of 1.7 years. Red circles show the location of the clusters with highest density of subsiding scatterers. Map data: Google, Maxar Technologies.

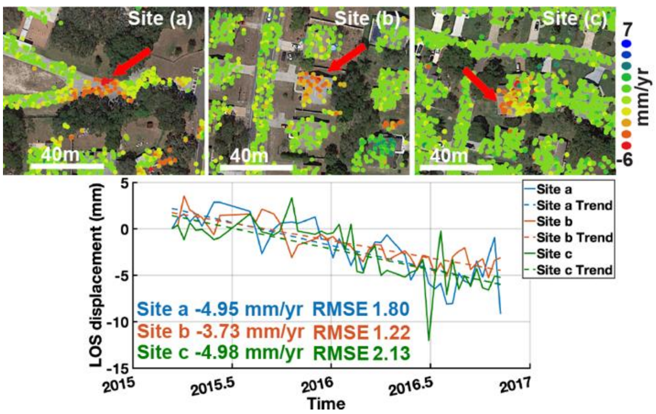

Figure 3 Zoom-in to the clusters with highest density of subsiding scatterers, sites a, b and c. The red arrow shows the scatterers shown in the time series plot. Detected pixel movement time series shows subsiding trends of -4.95, -3.73 and – 4.98 mm/yr, respectively. Map data: Google, Maxar Technologies.

Overall, results show that the technique effectively detects localized deformation and that the calculated clusters coincide with reported sinkhole locations. InSAR derived deformation for this area is limited mainly to constructed areas. Sources of displacement can be related to activity that is not associated with sinkholes, so field and background verification surveys are essential to properly define the observed deformation sources. InSAR alone is not sufficient for determining sinkhole presence. However, InSAR yields highly valuable information of location, size and magnitude of displacement from suspicious locations and provides valuable warning information. Compared to other studies, deformation observed in this work is constrained to very small areas, which together with the densely vegetated ground cover of suburban Florida makes the use of high-resolution data a key component of the analysis. The work by Oliver-Cabrera et al., 2019 explains the level of impact that high-resolution data has on areas like Timber Pines. An image with spatial resolution of 2.5 x 22 m (e.g. Sentinel-1) is able to detect 152 PS per km2 while and image with resolution of 0.25 x 0.6 m (e.g. TSX ST) can detect 69733 PS per km2.

Conclusions

High-resolution InSAR time series analysis combined with a clustering algorithm appears to be a promising tool for detecting sinkhole activity. The use of high-resolution InSAR allows us to observe small subsidence signals over the size of a small house or less. Due to the short duration of the InSAR time series (1.7 year), the InSAR detected velocity maps tend to be noisy. However, the clustering algorithm allowed us to eliminate much of the noise in the results by identifying subsiding clusters, which are characteristics of subsiding buildings. The time series analysis of the TSX ST over Timber Pines reveals localized deformation at several sites. Velocity trends of three selected sites that were observed in detail, yield subsidence rates ranging between -3.7 to -4.9 mm/yr. A cross checking with Hernando County sinkhole reports confirmed sinkhole presence in the vicinity of these three sites. Our results suggest that high-resolution InSAR subsidence detection combined with clustering analysis can serve as a useful tool for detecting sinkhole activity in challenging scattering environments, as in west-central Florida.

Acknowledgements

This research was supported by NSF grants EAR-1620617 and EAR-1713420. Authors would like to thank the German Aerospace Center (DLR) for the access to TerraSAR-X imagery through the GEO3330 project. First author would like to acknowledge Conacyt and Fulbright for supporting this research.

References

Atzori, S., Antonioli, A., Salvi, S. and Baer, G., InSAR-Based Modeling and Analysis of Sinkholes Along the Dead Sea Coastline. *Geophysical Research Letters*, *42*(20), 8383–8390, 2015.

Baer, G., Magen, Y., Nof, R. N., Raz, E., Lyakhovsky, V. and Shalev, E., InSAR Measurements and Viscoelastic Modeling of Sinkhole Precursory Subsidence: Implications for Sinkhole Formation, Early Warning, and Sediment Properties. *Journal of Geophysical Research: Earth Surface*, *123(4)*, 678–693, 2018.

Chang, L. and Hanssen, R. F., Detection of Cavity Migration and Sinkhole Risk Using Radar Interferometric Time Series. *Remote Sensing of Environment*, *147*, 56–64, 2014.

Dobecki, T. L. and Upchurch, S. B., Geophysical Applications to Detect Sinkholes and Ground Subsidence. *The Leading Edge*, *25*(3), 336, 2006.

Ester, M., Kriegel, H.-P., Sander, J., and Xu, X., A density-based algorithm for discovering clusters in large spatial databases with noise. *KDD*, *96*(34), 226–231, 1996.

Ferretti, A., Prati, C. and Rocca, F., Permanent Scatterers in SAR Interferometry. *IEEE Transactions on Geoscience and Remote Sensing*, *39*(1), 8–20, 2001.

Florida Geological Survey, *Florida Subsidence Incidents Reports*, 2015.

Ford, D. and Williams, P., *Karst Hydrogeology and Geomorphology*. Chichester: John Wiley & Sons, 2007.

Frumkin, A., Ezersky, M., Al-Zoubi, A., Akkawi, E. and Abueladas, A. R., The Dead Sea sinkhole hazard: Geophysical assessment of salt dissolution and collapse. *Geomorphology*, *134*(1–2), 102–117, 2011.

Galve, J. P., Remondo, J. and Gutiérrez, F., Improving sinkhole hazard models incorporating magnitude-frequency relationships and nearest neighbor analysis. *Geomorphology*, *134*(1–2), 157–170, 2011.

Hooper, A., Zebker, H., Segall, P. and Kampes, B., A New Method for Measuring Deformation on Volcanoes and other Natural Terrains Using InSAR Persistent Scatterers. *Geophysical Research Letters*, *31*(23), 1–5, 2004.

Jones, C. E. and Blom, R. G., Bayou Corne, Louisiana, Sinkhole: Precursory Deformation Measured by Radar Interferometry. *Geology*, *42*, 111–114, 2013.

Kampes, B. M., Hanssen, R. F. and Perski, Z., Radar Interferometry with Public Domain Tools. In *Proceedings of FRINGE* (Vol. 3, pp. 59–68), 2013.

Kim, J.-W. and Lu, Z., Association between localized geohazards in West Texas and human activities, recognized by Sentinel-1A/B satellite radar imagery. *Scientific Reports*, *8*(1), 4727, 2018.

Kim, Y. and Nam, B. H., A Comparative Study of Karst Sinkhole Hazard Mapping Using Frequency Ratio and Artificial Neural Network for East Central Florida, 105–114, 2014.

Martel, R., Castellazzi, P., Gloaguen, E., Trépanier, L. and Garfias, J., ERT, GPR, InSAR, and tracer tests to characterize karst aquifer systems under urban areas: The case of Quebec City. *Geomorphology*, *310*, 45–56, 2018.

Nof, R. N., Baer, G., Ziv, A., Raz, E., Atzori, S. and Salvi, S., Sinkhole Precursors Along the Dead Sea, Israel, Revealed by SAR Interferometry. *Geology*, *41*(9), 1019–1022, 2013.

Oliver-Cabrera, T., Wdowinski S., Kruse S. and Robinson T., Detection of Sinkhole Activity in West-Central Florida Using InSAR Time Series Observations. *Geomorphology Submitted*, 2019.

Theron, A. and Engelbrecht, J., The Role of Earth Observation, with a Focus on SAR Interferometry, for Sinkhole Hazard Assessment. *Remote Sensing*, *10*(10), 2018.

Theron, A., Engelbrecht, J., Kemp, J., Kleynhans, W. and Turnbull, T., Detection of Sinkhole Precursors Through SAR Interferometry: Radar and Geological Considerations. *IEEE Geoscience and Remote Sensing Letters*, *14*(6), 871–875, 2017.

Tihansky, A. B., Sinkholes, West-Central Florida. *Land Subsidence in the United States: US Geological Survey Circular*, *1182*, 121-140, 1999.

Veni, G., Brashear, C. C. and Glasbrenner, D., Building Codes to Minimize Cover Collapses in Sinkhole-Prone Areas, *14th Sinkhole Conference*, 471–476, 2014.

Proc. IAHS, 382, 669–675, 2020
https://doi.org/10.5194/piahs-382-669-2020

A social costs and benefits analysis of peat soil-subsidence towards 2100 in 4 scenarios

Tim A. H. M. Pelsma[1], **Anne Marieke Motelica-Wagenaar**[1], **and Simon Troost**[2]

[1]Waternet, P.O. Box 94370, 1090 GJ, Amsterdam, the Netherlands
[2]'t Salland, Luttenberg, the Netherlands

Correspondence: Tim A. H. M. Pelsma (tim.pelsma@waternet.nl)

Published: 22 April 2020

Abstract. Waternet is the executive agency of the regional water authority Amstel, Gooi and Vecht. Water authority Amstel, Gooi and Vecht manages the water levels (ditches) for 19 400 ha of peat meadows around the Netherlands capital Amsterdam. At present the ditches levels at about 40–60 cm beneath the peat meadow surface, resulting in a groundwater level between from 30 until 80 cm below peat surface and a subsidence of about 9 mm each year. A study was carried out on peat soil subsidence in the Amstel, Gooi and Vecht water authority water management area towards 2100: for short term effects (until 2027), midterm effects (until 2050) and longer term effects (until 2100). This study explores 4 scenarios: (1) present policy (maintain ditch waterlevel at maximum 60 cm below surface); (2) active rewetting, groundwater level at surface; (3) passive rewetting, subsidence is not compensated by lowering of water levels; (4) subsurface irrigation by submerged drains (infiltration in summer, drainage in winter). The scenarios are compared on farming, houses, public infrastructure, greenhouse gases and water management.

At present, the total net benefit for farmers are EUR 7 million per year for the whole area, while the costs for the water authority are EUR 37 million per year for managing ditches, dikes and pumps. Costs for greenhouse gases are EUR 18 million (at a price of EUR 40 per ton CO_2-eq). Active rewetting would reduce soil subsidence maximally from 2 to 0.5 m towards 2100 but reduces the benefits for farming, whilst the costs for water management stay alike. The costs for greenhouse gases however drops with EUR 3 million per year immediately because CO_2-eq emissions drops. Best (financial) results (with respect to all stakeholders) on the long term are booked by passive rewetting with lower costs for water management, houses, public works and greenhouse gases. This scenario will eventually take away the farming possibilities, but not before 2050 and could be too slow to contribute strongly to Paris agreement goals. Best result with respect to climate for short and long term is active rewetting, which will drop the greenhouse gas emissions strongly (equivalent of EUR 2.3 million per year), reduce soil subsidence, but makes farming harder (drop from 7.1 up to EUR 2.5 million per year benefit) and brings no direct reduction of costs for the water authority. Best result on short term for farmers is submerged infiltration drains. However, the effect of this scenario on GHG emission is limited in this study.

1 Introduction

Water authority Amstel, Gooi and Vecht (AGV, operated by Waternet; see AGV, 2019 for policy on soil subsidence) is responsible for water levels and water quality in the peat-meadow area around the capital Amsterdam (see Fig. 1 for distribution of the peat soils). The drainage ditches in the peat levels in the area between 30 and 60 cm (by policy of the authority) below the peat surface, thus draining the toplayer of the peatsoil. This management causes the soil subsidence by 9 mm each year (van den Born et al., 2016) as a side effect of making the soils suitable for agricultural use. The latter works well, the soils are very productive grasslands, cattle (milk) farming on peat soil is profitable. Before the year 1200, the peatbogs elevated above the rivers and lakes, but after eight hundreds of years of soil subsidence, this has turned around. The peatsoils dropped several meters and are now low lands: polders. Polders with typically an elevation around or even well below (-3 m) sea-level. In the peat-meadow area of AGV the yearly costs for one hectare of water maintenance (dikes and assets) are around EUR 1539 (this study), whilst the (net) profits of a farmer are lower (around 200–EUR 1000 per hectare per year, van den Born et al., 2016). The landuse (grassland farming with drainage ditches) is not without consequences. Besides subsidence and direct cost like pumping stations and dikes, or foundations of houses, the emitted (large) amounts of CO_2, CH_4 and N_2O from the peat has be taken in to account too. Subsidence and oxidation of the peat also causes the cover layer (on sand or clay) of polders to disappear, making them more vulnerable to seepage from higher water levels around, leakage in fact. This seepage water could be salt or brackish, thus causing troubles in nature, agriculture and the preparation for drinking water. The higher parts in the area (often peat wetlands or peaty nature reserves) are drained by the surrounding lower polders. A very important aspect of peat drainage (and peat soil subsidence) is the release of nutrients from the peat itself by oxygen and other (oxidizing) substances (like SO_4 or NO_3) entering the peat. It appears (van Beek et al., 2007) that the decomposition of peat is an important source for the loads of nitrogen and phosphorus to the waterbodies in peat area's and can be seen as a result of land-use, even without taking the fertilizer into account.

By performing a social costs and benefit analysis, the water authority gains more insight in several aspects of the water management in peat areas and takes more responsibility for side effects of drainage of peat. The aim of our authority (with respect to soil subsidence and water related land use) is to contribute to a sustainable development of the peat areas, including its users, over time.

The present policy in peat-meadow "polders" is to "follow" the subsidence with lowering of the ditch waterlevels from time to time, with some exceptions. Basically we expect this present policy to be suitable for the future. The cost/benefit analyses was carried out to reject or prove this hypothesis by comparing present policy with 3 alternatives towards 2027, 2050 and the year 2100.

We further expect that a future cost/benefit exploration will give more insight for policy makers to decide on strategy against (peat)soil subsidence, which typically is a long term process. We think that by calculating the more extreme scenarios of measures taken everywhere (active rewetting, submerged infiltration pipes) against the present policy will make a clear difference on the longer term of 2050 or even the year 2100. Because changes in land use will be required on quite a large scale to really slow down the soil subsidence, it is required to have a few looks from different angles of view toward the future, since changes in land use takes many years or even decades to be implemented.

Which approach in water management of the peat area of AGV is most sustainable for farmers and water authority but also for society (including all economical aspects) as a whole? In each approach: what will be the soil subsidence, farmer profit, emissions of greenhouse gases, costs for houses, costs for infrastructure and costs for water authority towards 2027, 2050 and 2100?

2 Material and Methods

For the water management area of the Water Authority AGV, an analysis is performed to determine the social costs and benefits due to soil subsidence for four scenarios (see Table 1). Three of these scenarios represent comparable policies to the policies analyzed in the study of van den Born et al. (2016). Active rewetting is added as an extra scenario as this is expected to have the highest impact in lowering GHG emissions and soil subsidence:

All scenarios are analysed in year 2016–2017 (as "present")

- 2027 – Shows effects on the short term (within 1 term of policy)
- 2050 – Shows effects on the mid-term (fitting in 1 human generation)
- 2100 – Shows effects on the long term (fitting in 2 human generations and fitting the terms used in climate adaptation)

The analyses were carried out with the model RE:PEAT (Developed at water authority Stichtse Rijnlanden, Houten, Netherlands). RE:PEAT (Waterschap Stichtse Rijnlanden, 2017) is available as a spreadsheet calculation core. Soil subsidence is calculated for those land-areas with a peat soil or a peat soil with a clay cover, using the land subsidence model Phoenix in RE:PEAT, as follows:

$$\begin{aligned}&\text{Soil subsidence rate (m yr)} = 0.02354\\&\cdot [\text{mean lowest groundwaterlevel (m)}] + 0.01834\\&\cdot [\text{thickness clay cover (m)}] + 0.00668\end{aligned}$$

In the study, the AGV water management area is subdivided into urban and rural area. The analysis is performed for each polder subunit. Effects of soil subsidence on economy of urban and rural areas are based on PBL study (van den Born et al., 2016). The analysed features in the analysis are shown in Table 2. Note: The individual results of the polder subunits are not presented in this paper, but are available. We only present the results of the complete AGV peat area.

Taxes (for households, farmers as a cost or for authorities as a profit) were not modelled.

An analyses of Sensitivity to assumptions was carried out for milk price, food price, paludiculture (only added in sensitivity analysis), interest rate, climate scenario.

Other important settings and basic assumptions for the model were:

Table 1. The applicable scenarios in the analysis.

Scenario number	0 (PP)	1 (AR)	2 (PR)	3 (SD)
Title	Present policy	Active rewetting	Passive rewetting	Submerged irrigation drainage
Purpose of scenario	To show the consequences of the present policy of continous ditch level lowering	To minimize the soil-subsidence by strong ditch level rise	To minimize or stop the soil-subsidence on the long term	To slow down the soil-subsidence by applying submerged irrigation drains.
Waterlevel (2016)	Present water levels (between 25 and 60 cm below landsurface)	Waterlevel 10 cm below land surface	Present water levels	Present water levels
Waterlevel alteration after 2016	Adjust the ditch level with the average subsidence of the polder section	Adjust the ditch level with the average subsidence of the polder section	None, unless waterlevel within 10 cm of land surface (in that case as AR)	Adjust the ditch level with the average subsidence of the polder section
Exceptions in waterlevels	Fixed levels in urban areas	No alteration in level in urban areas in comparison with present	Fixed levels in urban areas	Fixed levels in urban areas, but also in area's with seepage

Table 2. Analyzed features.

Stakeholder/theme	Kind of effect
Water authority	Costs sluices/pump. stations & watermanagement Costs sludge removal Costs dikes Shortage of waterstorage
Public works	Roads, sewage system and cables
Households	Costs foundation Costs groundwater damage
Nature & Landscape	Landscape Meadow birds Water quality, nutrients in surface water
Farmes + food/supply chain	Nett added value of Agriculture activity
Environment	Greenhouse gasses

2.1 Soil type, groundwater table and presence of clay on peat

The exact thickness of the peat soil is unknown, it is assumed in the calculations that for all peat soils, soil subsidence continues until 2100. For the soil type and the presence of a clay layer the BOFEK 2012 soil map of The Netherlands was used (Wosten et al., 2013). Very thin clay layers ($<$ 7.5 cm of clay) were ignored, because the field experience of employees of the water authority pointed out that in these areas there was no clay at all (but strongly decomposed peat). See Fig. 2 for the used clay thickness.

2.2 Greenhouse gases

Effects of soil subsidence on greenhouse gas (GHG) emissions are based on the relation between mean groundwater level and GHG emission (Jurasinski et al., 2016). The GHG emission is corrected for clay cover thickness. We assumed EUR 40 per ton carbon dioxide as a price in the model, making the emissions from peat, a cost. Jurasinski's et al. (2016) tool is performed on mean groundwater levels and calculates for CO_2, CH_4 and N_2O. Note that soil subsidence in our approach is based on the mean *lowest* groundwater levels, while

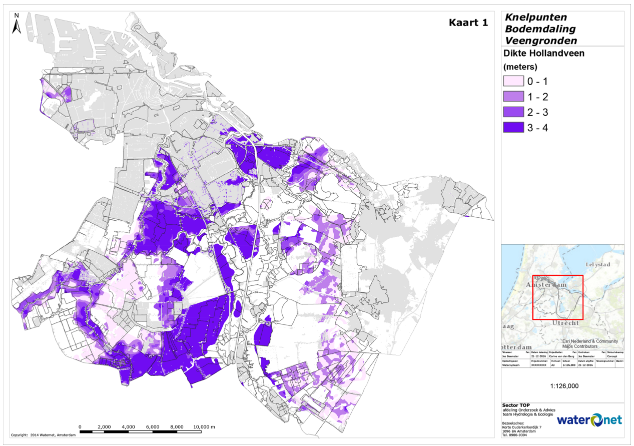

Figure 1. Water authority area Amstel Gooi and Vecht (with Amsterdam middle-north/west of map) and the presence of peat soils. Gray/white is urban area or no peat soils. Dikte Hollandveen = Thickness peatlayer. Map and map-topography is a strongly modified version of dutch GEOTOP map, published by TNO- Geologische Dienst Nederland, 2012.

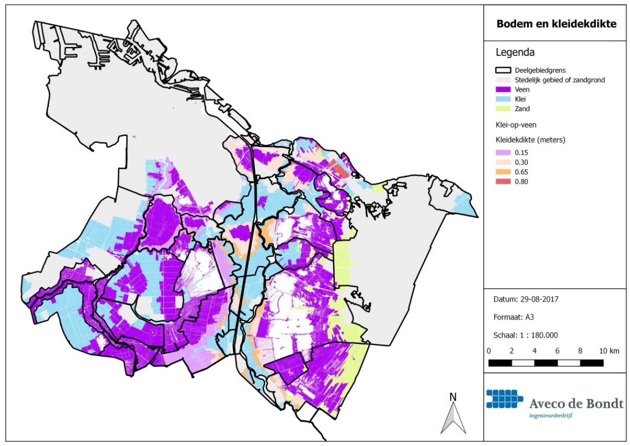

Figure 2. Soil types and thickness of clay layer in the AGV area. Veen = Peat; Klei = clay; Zand = sand; kleidekdikte = thickness of claylayer. Grey = Urban area or sand soil. Map is a modified version of BOFEK2012, de nieuwe bodemfysische schematisatie van Nederland. Published by Alterra 2013.

the emissions of GHG is based upon *mean* groundwater levels.

2.3 Agriculture chain

In most scenarios the meadows become wetter. As a result the grass yield is modelled less and therefore also more costs for cattle-food. In other words: wetter peat means more costs for the farmer. Other figures for agriculture costs and profits (like milk price or costs for new sheds) are not included in this paper, but of course play an important role in the modelled calculations (see also the sensitivity analysis in Results and Discussion).

The effects on the market chain (milk products, food suppliers) is not part of the model. We follow in this the line of van den Born (2016), where is stated that effects in one part of the chain should not be transferred to the next part in a healthy market. The food industry is considered as a healthy market. We also assume in our model that farmers will continue the present use of the farm and the land use will remain.

2.4 Foundations of buildings

The lowest groundwater levels determine the effect on the wooden foundation piles, hence the period that wooden parts are exposed to oxygen and starts weakening. The longer the period of low groundwater levels (related to subsidence) the higher the (long term) costs. Only one repair is taken into account, existing damage is not taken into the model. Older houses brings higher costs. High ground water levels can also bring costs. The model assumes costs when the highest groundwater level is more than 70 cm below surface. Costs for water damage because of more rain, more upward seepage, already fixed water levels and flotation of peat are not modelled.

2.5 Public works (roads, pipes, cables)

Subsidence makes that these assets must be repaired more often, the stronger the subsidence, the higher the costs. Differences in costs were made for sewage systems, dikes, roads and pipes. Peat subsidence has an oxidation and a compression factor in it. Only the oxidation factor is modelled.

2.6 Water authority

Assets (like pumps, pipes and weirs) were written off in 25 years. Polders are subdivided into areas with the same water level. More divisions as a consequence of ongoing subsidence were not taken into the model. In scenario 1 (AR) the initial costs for water-assets were not taken into account.

The sludge layer is modelled as removed once in 10 years in all scenarios, but the production of sludge differs between the scenarios, where strong drainage leads to strong growth of sludge.

Water storage (in the ditches) decreases if the soil subsides, but the levels are not adjusted. In the scenario of active rewetting this is modelled as "no storage" (this means that storage on the fields is not taken into the model). Although most scenarios will require more water (to moisten the peat), this was not taken into the model as cost or a check on availability.

In case of increasing difference in height, exceeding 60 cm, new dikes ware modelled. The more the height of the dike, the higher the costs. Existing dikes are modelled written off in 50 years.

2.7 Submerged irrigation drains

Costs for the irrigation drains were modelled as costs for the farmer as well as the profits of it. Costs for installation is modelled as EUR 2100 per hectare over 20 years life. The irrigation drains (scenario 3) are applied at 4500 ha of the total of 19.400 ha of peat in the AGV area. This is roughly the area where the ditch waterlevels are between 30 and 60 cm lower than the meadow surface level. Only the reach 30–60 cm is regarded as suitable for submerged irrigation drains (Troost et al., 2018). In wetter conditions the drains would "drain" too much, taking nutrient rich water to the ditch whereas in more dry peat (ditch waterlevel lower than 60 cm of land surface) there will be still oxygen entering below the irrigation-drain and also the tubes would have to be dug very deep. Areas with (upward) seepage are regarded as not suitable for this measure and were left out of the model.

2.8 Water quality

Mineralization of peat leads to P and N loads to the ditch.

We assume a P load of 0.00015 g per $m^2\ yr^{-1}$ surface water per 100 cm subsidence (Troost et al., 2018). Abrupt rewetting (scenario 1) is modelled with a big initial P-load towards the ditches.

3 Results and Discussion

As shown in Table 3 the subsidence will be up to 1.5 m by the year 2100 if we don't change policy (but in some polder units just 20 cm). The strongest reduction in subsidence is calculated for scenario 1, active rewetting. This scenario will decrease the subsidence from 1.5 to just 0.5 m by 2100. Passive rewetting decreases the subsidence by half, but will only do so after 2050, since in this approach the subsidence will not drop in the first ten years or so. Submerged drains (over 4500 ha, see Material and Methods) will have immediate effect, but the gain is 50 cm in 2100 compared with present policy (still 1 m subsidence), therefore shows the least reduction of subsidence of the 3 alternatives in 2100. The profit for the farmers (with submerged infiltration) on the other hand (Table 4), keeps in line until 2100, like the present policy, whereas in active or (a little less) in passive rewetting the profits for the farmers will be minimized by 2100.

The costs and profits (Table 4) shows a strong negative effect on farming profit in the scenario of active rewetting (drop from 7.1 to EUR 2.5 million yearly profit) and decrease in costs of houses. In scenario 2 (passive rewetting), the costs for water authority drop (from 37.7 to EUR 29.6 million per year) (Table 4).

The results shows that the costs for water authority, greenhouse gases or public works are larger than the profit of the farmer. The houses (repair costs of foundation) show a large effect of the alternatives active and passive rewetting (cut down from 3.1 to less than EUR 1 million) but almost no effect of the alternative submerged infiltration drains. The latter can be explained by the fact that the infiltration drains will only be applied in the fields and not near the houses. But the alternatives active and passive rewetting (of the polder as a whole) will influence the foundation of the houses too. Note that (by court decision) the owners of the houses in The Netherlands will have to pay the repairs of foundation themselves.

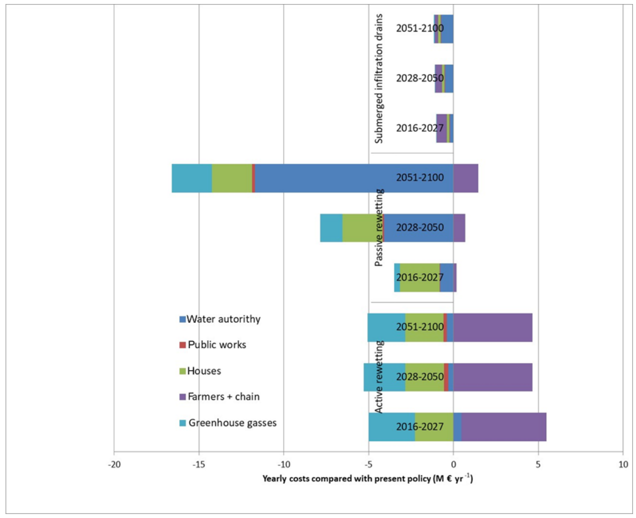

Figure 3. Average differences in yearly costs (EUR million per year) in each period in each of the 3 scenarios, compared with present policy.

Moreover, the costs for greenhouse gases remain high in 2100, even if active rewetting is applied. In tons CO_2-eq the emission at present (2016) is 469 kton (or 0.469 Mton) for the AGV area and will drop to 393 kton in 2100 in case of active rewetting. There is no satisfactory explanation for this result, but is well in line with the predicted subsidence in Table 3. But a likely cause is the fact that RE:PEAT uses the average groundwater levels to predict GHG emission, instead of the (perhaps more predictive with respect to GHG emissions and subsidence) mean lowest ground waterlevel.

Figure 3 shows the effects of the scenarios over the periods 2016–2027; 2027–2050 and 2050–2100 separately. This figure also zooms in on the differences in the 3 scenarios and shows a few new things:

- Scenario 3 (submerged infiltration drainage) shows little effect on costs and benefits compared to present policy.
- Passive rewetting (scenario 2) shows little effect in the first decades compared to present policy, but a strong effect towards 2100.
- Active rewetting (scenario 1) shows immediate effect compared to present policy, but no further progress as time passes. This scenario also shows that the loss in profit of the farmers is bigger than the reduction of the costs for the rest of society, in the first 10 years.

Table 3. Soil subsidence in the 4 analyzed scenarios.

		Soil Subsidence in timeframe 2016–2100			
		Scenario 0 (PP)	Scenario 1 (AR)	Scenario 2 (PR)	Scenario 3 (Submerg. Infilt.)
Soil Subsidence (meters)	Min	0.20	0.10	0.15	0.15
	Max	1.50	0.50	0.75	1.00
Reason for slowing down the subsidence →			High groundwater-levels	High groundwater-levels, but after some time	High groundwater-levels in summer-time.

Table 4. Main results in EUR million per year for the period 2016–2100. The table shows yearly costs, but yearly profits if the figures are negative.

	present policy	active rewetting	passive rewetting	infiltration/ drains
water autority	37.773	37.505	29.592	37.182
public works	22.143	21.965	22.005	22.109
houses	3.177	0.911	0.825	3.037
farmers + chain	−7.123	−2.478	−6.037	−7.423
Greenhouse gasses	18.053	15.731	16.237	18.007

Public works (roads, sewage, cables) show only small differences between different scenarios and appear relatively insensitive to the scenarios and time. Or one might say that public works remain a strong source of costs in peat areas.

3.1 Sensitivity to assumptions

The analyses showed strong sensitivity for the following parameters:

Milk price and *food price* in profits for the farmers. The *interest*, a change of 1 % in interest results in a change of 15 % in costs. The *climate scenario*: If a less strong climate scenario was used, the subsidence by 2100 would be 10 cm less. This especially has an effect on the costs of infrastructure (dikes, roads, pipes).

The sensitivity analysis was not carried out for method of calculation of GHG emission and the used soil map. GHG emission could also be calculated based on mean lowest groundwater level instead of mean groundwater level.

3.2 Discussion

The analysis was carried out to obtain a first impression and was not meant to be a very precise scientific study. It does however give some clues to fields of interest in which more elaboration is desired: a reliable groundwater model, groundwater measurements and the same holds for the emission of greenhouse gases. Also more elaboration is desired for the effects (and water consumption) of submerged infiltration drains and (the appliance of) paludiculture in case of strong rewetting.

As GHG emissions are predicted based on mean groundwater level in peat areas and submerged infiltration drains have little effect on mean groundwater levels, the effect on lowering GHG emissions will probably be underestimated.

The analysis shows that the costs for greenhouse gases plays a role, but at EUR 40 per ton cannot cover the extra costs as shown in Fig. 3, except from scenario 1 (immediate active rewetting). To cover the peat area related costs for the water authority in the period 2050–2100, would require a CO_2 price of EUR 63 per ton CO_2-eq. At present this would require a CO_2 price of EUR 50 per ton CO_2-eq.

The approach of a social costs and benefits analyses cannot show all aspects, but gives some interesting insights. Of course, there is more than money: farming is rooted in the culture and the peat meadow landscape is unique. But one could wonder if things are sustainable in the end as it is now. This study also shows that changes in land use, will not immediately stop the emissions of greenhouse gases and as well that it is not easy to take good measures against soil subsidence without making real choices in land use.

We suggest to use the model RE:PEAT in the discussions in the local areas of interest, if possible as an interactive "serious game". Local stakeholders (farmers, house owners, regional government, water authority) will have to be involved to produce tailor-made measurements against soil subsidence.

4 Conclusions

Based on this cost-benefit study in RE:PEAT, a change of the current water management policy is necessary to reduce societal costs due to soil subsidence. For all alternative scenarios (active rewetting, passive rewetting and submerged infiltration drains), soil subsidence will decrease compared to the standard water management policy and the societal costs will drop towards 2100.

On short term (before 2027), active rewetting has highest impact on reducing soil subsidence and GHG emission.

However, this would imply lower income for farmers and higher costs for water authorities on the short term. In this study, the farmer profits may be underestimated as paludiculture was not included as a business model. On short term (before 2027), submerged infiltration drains will reduce soil subsidence, while farmers will have higher income and water authorities lower costs. However, the effect of submerged infiltration drains on GHG emission is much lower than in case of active rewetting.

On long term (2100), passive rewetting will lead to the highest cost reduction for water authorities, and comparable GHG reduction and comparable cost reduction for houses as active rewetting. This would cause lower income for farmers (but not as low as in case of active rewetting).

The model is sensitive to the assumptions used, especially for farming prices. More insights are needed to improve the models in RE:PEAT, especially regarding the calculation of GHG emissions. The model should be calibrated by measurements of GHG emissions and groundwater levels.

The Paris Climate agreement (and the GHG emissions from peat) has raised the urgency to reduce the GHG emission from peat areas. Reduction of GHG emissions is a supplemental policy-goal in peat meadow areas to the subsidence itself.

Data availability. The data used for the model re:peat is inside the publication Troost et al. (2018). Furthermore data of groundwatertables were derived from within company models.

Author contributions. TP took the lead to write this paper. AMMW supported in writing the paper. ST did all of the analyses and primary reports on the work with the tool Re:Peat.

Competing interests. The authors declare that they have no conflict of interest.

Special issue statement. This article is part of the special issue "TISOLS: the Tenth International Symposium On Land Subsidence – living with subsidence". It is a result of the Tenth International Symposium on Land Subsidence, Delft, the Netherlands, 17–21 May 2021.

Acknowledgements. We would like to acknowledge Corine van den Berg for her lead in the process and Johan Ellen for his contribution in the analysis. Huub Kuipers also worked on the analysis in RE:PEAT and Niels Hoefsloot supported on the cost-benefit aspects of the study.

References

AGV: Waterbetrokken, Bestuursakkoord Waterschap Amstel, Gooi en Vecht 2019–2023, available at: (last access: 2 March 2020), 2019.

Jurasinski, G., Günther, A., Huth, V., Couwenberg, J., and Glatzel, S.: 5.1 Greenhouse gas emissions, in: Chap. 5 Ecosystem services provided by paludiculture, Paludiculture – productive use of wet 35 peatlands, Climate protection – biodiversity – regional economic benefits, edited by: Wichtmann, E., Schröder, and Joosten, H., Schweizerbart Science Publishers, Stuttgart, 79–93, 2016.

Troost, S., Kuipers, H., and Hoefsloot, N.: Toekomstverkenning bodemdaling AGV, Maatschappelijke kosten en baten analyse, Aveco De Bondt, in opdracht van Waternet, Internal publication, 2018.

Waterschap Stichtse Rijnlanden: Re:peat a model for soil subsidence in peat meadow area, available at: https://www.hdsr.nl/beleid-plannen/veenweide/onderzoeken/re-peat/ (last access: 2 March 2020), 2017.

Wosten, J. H. M., de Vries, F., Hoogland, T., Massop, H. T. L., Veldhuizen, A. A., Vroon, H. R. J., Wesseling, J. G., Heijkers, J., and Bolman, A.: BOFEK2012, de nieuwe bodemfysische schematisatie van Nederland, Wageningen, Alterra (Alterra-rapport 2387) – 46, available at: https://research.wur.nl/en/publications/bofek2012-de-nieuwe-bodemfysische-schematisatie-van-nederland (last access: 2 March 2020), 2013.

van Beek, C. L., Droogers, P., van Hardeveld, H. A., van den Eertwegh, G. A. P. H., Velthog, G. L., and Oenema, O.: Water Air Soil Pollut, Leaching of Solutes from an Intensively Managed Peat Soil to Surface Water, 182, 291, https://doi.org/10.1007/s11270-007-9339-7, 2007.

van den Born, G. J., Kragt, F., Henkens, D., Rijken, B., van Bemmel, B., and van der Sluis, S.: Dalende bodems, stijgende kosten: mogelijke maatregelen tegen veenbodemdaling in het landelijk en stedelijk gebied: beleidsstudie, (PBL-publicatie; No. 1064), Den Haag: Planbureau voor de Leefomgeving, available at: (last access: 2 March 2020), 2016.

Mapping and characterizing land deformation over the Gulf Coast using multi-temporal InSAR

Feifei Qu[1], Zhong Lu[1], Jinwoo Kim[1], Michael J. Turco[2]

1 Roy M. Huffington Department of Earth Sciences, Southern Methodist University, Dallas, Texas, USA, 75025;
2 Harris-Galveston Subsidence District, Friendswood, Texas, USA, 77546.
Contact: zhonglu@smu.edu

Abstract

Land subsidence has occurred in the Gulf Coast (GC) of the U.S. as a consequence of complex geological conditions and high-intensity resource exploitation, causing extensive damage to buildings and other infrastructures. Using1650 images from 33 ALOS-1 paths during 2007-2011 based on multi-temporal interferometric synthetic aperture (InSAR) techniques, we have constructed, for the first time, a deformation map over 500,000 km2 of the 1900-km-long GC, with an RMSE of <10 mm/yr. Numerous land deformation zones have been discovered, including at least 30 subsidence patterns and 14 uplift features. Most of the identified ground instabilities are newly discovered as a result of this study. The land deformation along GC is caused by both regional geological conditions and human activities that have influenced natural surroundings and consequentially exacerbated ground instability. Depressurization of petroleum reservoirs and aquifer compaction related to groundwater withdrawal are the principal impactors on observed subsidence. Other processes, including wastewater injection, sulfur/salt mining, dewatering, oxidation, and construction work, also contributed to the ground instability. Our large-scale deformation mapping will help the scientific community and relevant agencies better understand land deformation rates and extents, identify the processes responsible for the coastal deformation, and provide a critical dataset for hazard prediction and mitigation in the GC.

Introduction

Subsidence is a nationwide problem: ~44,000 km2 in 45 states of the U.S. have been permanently subsided (Galloway 2008). The GC has been exposed to land deformation due to its complicated geological constitution and high intensity of land use. The goal of this study is to provide a complete map of land deformation rates and extents over 500,000 km2 of the 1900-km-long GC and identify the processes responsible for the coastal deformation using InSAR imagery and auxiliary data source. By employing the multi-temporal InSAR (MTI) techniques (Hooper 2008) and L-band SAR images from ALOS-1 (2007-2011), this work provides, for the first time, a comprehensive analysis of spatial distribution and characteristics of land deformation at a finer spatial resolution over a large span of the GC. This paper summarizes the discovered instability zones and major deformation features (Qu et al. 2023).

Methods, datasets, and processing

About 1650 SAR images from 33 ascending L-band ALOS PALSAR tracks have been utilized in this study to illustrate the spatial distributions of land deformation over the whole GC. The overlap area of about 10 km between neighboring ALOS tracks was used for validating and mosaicking. Ionospheric anomalies were present in some interferograms where the split-spectrum method was applied to mitigate the phase error. The 33 data stacks were then processed using the StaMPS MTI method (both PS and SBAS, respectively) (Hooper 2008). A deramp processing was also applied to interferograms to eliminate the residual orbital error and long-wavelength atmospheric error. Finally, remaining tropospheric artifacts were further estimated and mitigated through temporal high-pass filtering and spatial low-pass filtering. Innocuous turbulent tropospheric delays might still reside in some interferograms due to the limited number of ALOS-1 images in each track. Please refer to Qu et al. (2023) for detailed processing procedures.

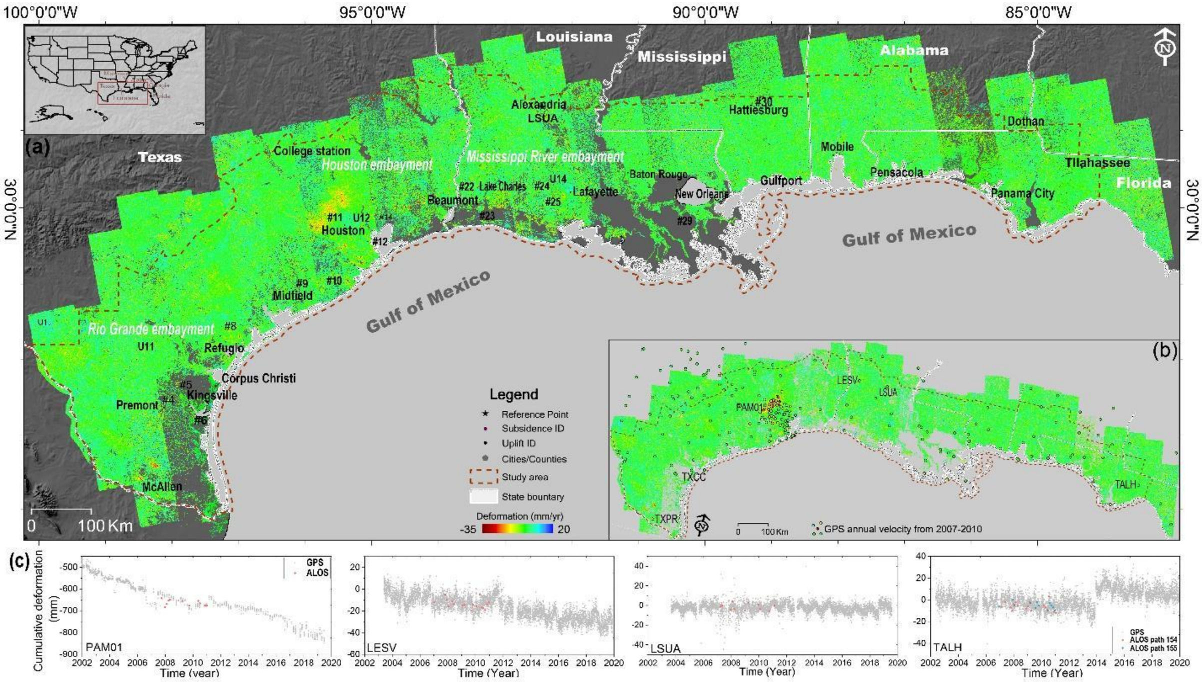

Figure 1 A seamless deformation map over 500,000 km2 areas of GC: (a) Average vertical deformation map over GC by mosaicking InSAR products from 33 ALOS-1 tracks; (b) Comparison of the average vertical deformation rate between InSAR and GPS measurements during 2007-2011 at stations established after 2009 (Blewitt 2018); (c) Comparison between InSAR-derived time series deformation and GPS observations at 4 stations, whose locations were marked on (b); The "#1 - #30" label the measured subsidence zones and "U1-U14" indicate the identified uplift features. The U.S. map is an inset on the upper-left, where the red solid rectangle shows the approximate extent of (a).

A total of 33 average line-of-sight (LOS) deformation velocities between 2007 and 2011 were generated utilizing the MTI method. The deformations were transferred into the vertical direction according to the incidence angles to minimize the effects of imaging geometry. Overall, there is a generally good agreement for both the patterns and rates of deformation between adjacent tracks before mosaicking. To generate a seamless velocity map of GC all stacks were referenced to LASU Continuously Operating Reference Station (CORS) (black star, Fig.1a), situating at Rapides County, LA, where there was a wealth of high coherence points around and almost no deformation was observed at this station since Aug 31, 2003 (Blewitt et al. 2018). The average standard deviation of the 32 differential maps over the overlapped regions of neighboring tracks is ~9 mm/yr. Finally, a seamless deformation map over about 500,000km2 areas of GC was produced for the first time by mosaicking 33 ALOS tracks (Fig.1).

Results

The GC is generally stable, but numerous land deformation zones have been realized, including at least 30 subsidence patterns and 14 uplift features (Fig.1). InSAR-derived average deformation observations were compared with velocity measurements from 190 GPS stations coastal-wide (Blewitt et al. 2018). Time-series deformation plots at 4 GPS stations, whose positions can be found in Fig.1b, are also shown in Fig.1c. There is a universal agreement between the daily/monthly GPS solutions and the InSAR time-series measurements (Fig.1c), with an average RMSE (root mean square error) of approximately 10 mm/yr for the difference between vertical deformation measurements from InSAR and GPS.

We observed broad-scale subsidence caused by groundwater pumping near major metropolitan areas, such as Houston and New Orleans (Fig. 1). We have found some of the published subsidence zones have ceased to be detectable from 2007 to 2011 while continuing deformation has been observed at the Greater Houston and New Orleans regions at reduced rates. Our InSAR-derived deformation map has also allowed us to discover one new subsidence feature caused by groundwater withdrawal at Beaumont, TX.

More than 20 subsidence cones with a velocity larger than 10 mm/yr have been detected through our MTI analysis over the GC, including particularly striking ground settlement patterns over Hidalgo County, TX, and Corpus Christi, TX (Fig. 2a). The subsidence patterns, with spatial scales ranging from 1 to 10 km in diameter, were likely caused by hydrocarbon extraction.

Subsidence of ~60 mm/yr has also been recognized at The Five Islands of Louisiana. The high spatial correlation between subsidence and salt mining systems as well as the absence of oil/gas exploration activities indicate that the conventional room-and-pillar salt mining method depending on heavy machinery in the underground could be responsible for the observed subsidence at Avery Island (Fig. 2b), Weeks Island, and Cote Blanche Island.

Our study revealed a high subsidence rate localized to construction-related areas on the south bank of the Mississippi River, mainly Jefferson Parish, providing insight into shallow sediment compaction as a causal factor of subsidence (Fig. 2c). The occurrence of shallow sediment compaction due to construction loading could last longer than a decade following the construction over the New Orleans area.

Finally, we identified significant uplift signals with amplitudes ranging from 3~10 cm/yr mainly over Duval County of South TX (Fig. 2d). At least 11 cones of uplift that are roughly circular and typically span ~2 km in diameter have been discovered, almost all of which had never been noticed and reported before this study. Our InSAR observations indicate a localized uplift feature occurs over the storage facilities, which fluctuates over time, responding to the seasonal nature of gas injection operations in summer. We attribute the recognized localized uplift signal over the North Dayton salt dome gas storage facility to the circulated operations of injection/withdrawal into/from the salt cavern.

Conclusion

This paper presents the land deformation of the GC during 2007-2011 and unveils the related geohazards by using satellite radar image processing techniques. We have constructed, for the first time, a deformation map for 500,000 km2 over the Gulf Coast, spanning ~1900 km from east to west. The accuracy of the InSAR observations of deformation is 10 mm/yr based on comparison with GPS measurements. Ground deformation over the GC is not solely attributed to a single cause, but a combination of several different factors that involve large volumes of extraction of underground reservoirs (water, hydrocarbons, sulfur, and salt) and wastewater injection, as well as processes of sediment compaction, tectonics, and gravity-driven process. Our results enhance the understanding of the state of land deformation and causal mechanisms in the GC and are critically important for hazard prediction and mitigation in the region.

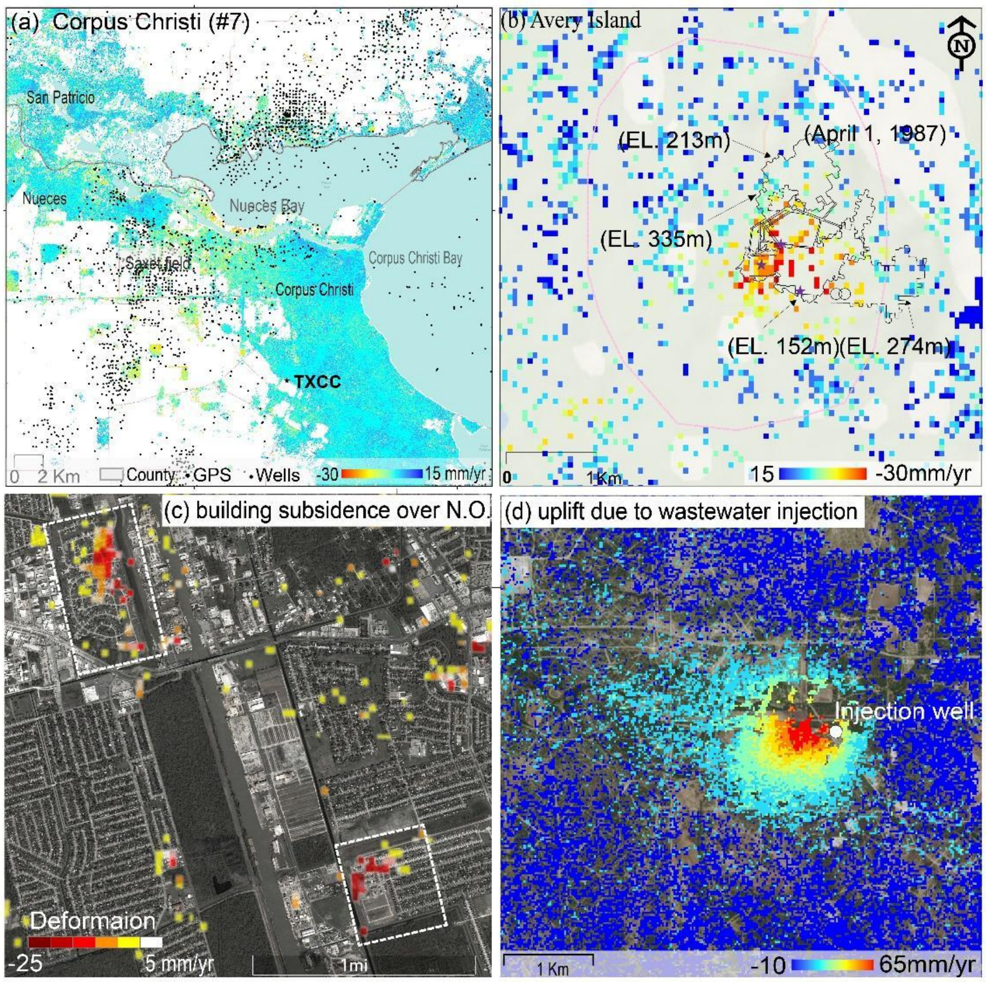

Figure 2 Highlights of deformation features observed along the GC. (a) Land subsidence caused by hydrocarbon extraction at Corpus Christi, Texas. (b) Ground subsidence due to underground mining at Avery Island, Louisiana. (c) Building subsidence due to sediment compaction at Jefferson Parish, Louisiana. (d) Ground uplift due to wastewater disposal over Duval County, Texas.

References

Blewitt, G., Hammond, W.C., Kreemer. C. (2018). Harnessing the GPS Data Explosion for Interdisciplinary Science. Earth & Space Science News, 99.

Hooper, A. (2008). A multi-temporal InSAR method incorporating both persistent scatterer and small baseline approaches. Geophysical Research Letters, 35, L16302.

Qu, F., Lu, Z., Kim, J.W., Turco, M.J. (2023). Mapping and characterizing land deformation during 2007-2011 over the Gulf Coast by L-band InSAR: Remote Sensing of Environment, 284, 113342, https://doi.org/10.1016/j.rse.2022.113342.

Exploring drivers of spatio-temporal variation of subsidence in the San Joaquin Valley, California, USA

Ryan Smith

Colorado State University
Contact: ryan.g.smith@colostate.edu

Abstract

The San Joaquin Valley, California, USA, has experienced massive amounts of land subsidence dating from the 1920s to present day (2022). The regions experiencing the most subsidence have shifted from the mid-1900s to present day, but the drivers for this shifting spatio-temporal pattern have not been explored. In this study, we model deformation in two areas: the Los Banos/Kettleman City region, which experienced up to 8.9 m of subsidence from 1926 to 1972, and the Tulare/Pixley region, which has been experiencing over 20 cm/yr of subsidence in some regions since 2007. We implement a novel technique to reduce noise in estimates of change in groundwater level, or head, aggregated over large regions and long (80 year) time periods by solving systems of linear equations composed of measured head change over multiple overlapping periods. We find that the distinct stress histories of the two regions drives their response to historic and current declines in head. The Los Banos/Kettleman City aquifer has only recently experienced heads at or below historically low heads that were experienced in the 1960s, while the Tulare/Pixley aquifer has been at historically low heads since the mid-2000s. We find that although the Los Banos/Kettleman City region has experienced relatively low subsidence rates over the past two decades, it is likely to begin experiencing dramatic subsidence now that heads are once again at historically low levels.

Introduction

The San Joaquin Valley comprises the southern portion of the Central Valley, California, which is home to 6.5 million people, a $50 billion agricultural industry (California Department of Food and Agriculture, 2021). The Los Banos/Kettleman City region (region a in Figure 1) has experienced up to 8.9 m of historical subsidence due to groundwater extraction, with a regionally averaged subsidence rate from 1926 to 1969 of 7.9 cm/yr (Poland, 1975), but has experienced little long-term subsidence in the recent droughts of the 2000s (Chaussard and Farr, 2019). In contrast, the Tulare/Pixley region (region b in Figure 1) experienced much lower historical subsidence, with a regionally averaged subsidence rate of 4.7 cm/year from 1926 to 1970, but subsidence has increased substantially with greater than 20 cm/year of sustained subsidence from 2007 to present that has been characterized as primarily inelastic (Smith et al., 2017; Chaussard and Farr, 2019; Lees et al., 2022). One challenge in evaluating mechanisms driving these changes is that the key temporal input, groundwater levels, have been sparsely monitored with a changing network of wells. In this paper, we present a new approach to model subsidence in both regions with sparsely sampled head measurements. We show that the lower subsidence rates experienced in the Los Banos/Kettleman City region in the 2000s is driven primarily by the high pre-consolidation stress in the region, but that recent droughts threaten to make this region once again a subsidence hot-spot.

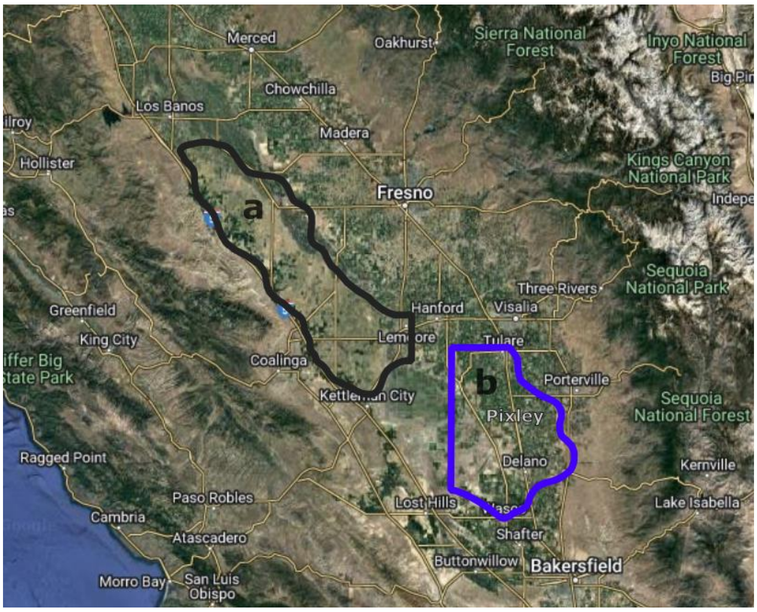

*Figure 1 Regions of subsidence modeled in this study. Region **a** has a high historic subsidence and is near Los Banos and Kettleman City, and region **b** has high recent subsidence and is near Tulare and Pixley.*

Methods

In order to understand the mechanisms driving spatiotemporal changes in deformation in the San Joaquin Valley, a model was developed that simulates deformation as a function of head changes within the aquifer. The method to determine head change within the aquifer is described in Section 2.1. The head in the aquifer is then used to simulate the distribution of head within fine-grained units, which is then used to estimate deformation. This process is described in Section 2.2. The model was calibrated using deformation estimates from both InSAR (Tre Altamira, 2022) and historical leveling surveys (Poland, 1975). This is done over two distinct regions: the area with highest historical subsidence, denoted as the Los Banos/Kettleman City area (Figure 1, region a) and the area with highest recent subsidence, denoted as the Tulare/Pixley area (Figure 1, region b). The time period of the model is from 1940 to 2022

Estimating changes in head

Typically, regional changes in head are best estimated by measuring head changes at an individual well and averaging these head changes over multiple wells (i.e. Butler et al., 2016). This approach reduces error that can occur by comparing heads over time at different wells, which are likely tapping different portions of the aquifer system, and are subject to errors due to the natural spatial variability in head. However, this method is challenging to implement in the San Joaquin Valley over long time periods because the wells that have been monitored over the past 80 years have changed significantly.

InSAR data processing techniques implement a method called Small Baseline Subset (SBAS, Berardino et al., 2002) that creates a system of equations from multiple overlapping interferograms containing information of change in surface elevation over different combinations of single measurements. This approach reduces noise by using redundant measurements. In this study, we implement a similar approach, using measurements of change in head for every 1, 2, 5, 10, 15 and 20 years at each well where data over these time spans is available. Each of these periods with head-change data is treated like an interferogram. These datasets are averaged over all wells containing the time spans, producing a system of equations that is used to solve for the average annual change in head, X:

$$TX = Y, \quad (1)$$

where T is an m x n matrix representing time in years between each estimate of head change, with m rows for each period of change in head measurements and n columns for each year of the period of record containing a value of 0 or 1. X is an m x 1 matrix with m rows representing the change in head for each year, and Y is an m x 1 matrix with m rows representing the average change in head over each period of change in head measurements. The change in head during each year, X, is solved for by inverting the matrix in Equation 1. A visual representation of T, X and Y is given for the Tulare/Pixley region in Figure 2a, b and c respectively. Figure 2d shows the head relative to 1940 given by integrating X over time.

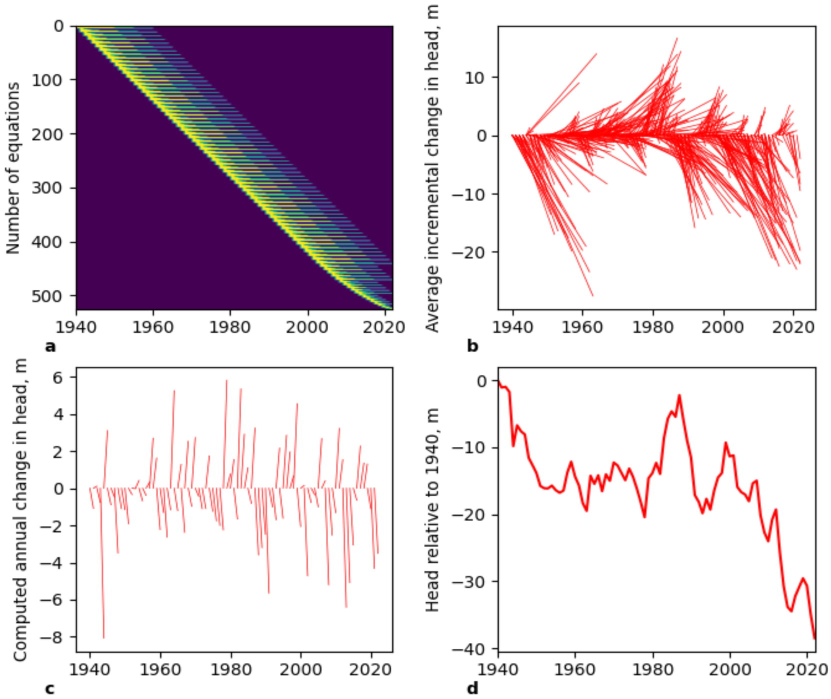

Figure 2 Example of our approach for estimating head in the Tulare/Pixley region. ***a)*** *A visual representation of the matrix T from Equation 1. Yellow pixels represent a value of 1, and the blue pixels represent a value of 0.* ***b)*** *Average head changes measured at wells in the valley in increments of 1, 2, 5, 10, 15 and 20 years. This is a visual representation of matrix Y from Equation 1.* ***c)*** *Average yearly change in head, solved for by invertong Equation 1. This is a visual representation of matrix X.* ***d)*** *Integrated change in head to produce head relative to 1940 levels.*

Modeling deformation as a function of changes in head

Deformation in compressible fine-grained units is modeled as a function of change in head using the following equation:

$$d = \Delta h S_{sk} b_0, \qquad (2)$$

where d is the deformation, Δh is the change in head, S_{sk} is the skeletal specific storage, and b_0 is the original thickness of the compacting layer. There are two possible values for S_{sk}, one that represents elastic deformation (S_{ske}), which occurs when the head is above the previously lowest experienced head (preconsolidation head), and one that represents inelastic deformation (S_{skv}) when the head is below the preconsolidation head. S_{skv} is roughly 100 times larger than S_{ske} (i.e. Sneed, 2001).

Since head measurements are made primarily in coarse-grained units and are not representative of head within fine-grained units, the following equation is used to estimate the vertical and temporal distribution of head within fine-grained units:

$$\frac{\partial}{\partial z}\left(K_v \frac{\partial h}{\partial z}\right) = S_s \frac{\partial h}{\partial t}, \qquad (3)$$

Where z is the vertical position along the fine-grained layer, K_v is the vertical hydraulic conductivity, h is head, S_s is the specific storage (approximated here as the skeletal specific storage), and t is time. These equations are used together to model deformation as a function of change in head. The parameters K_v, S_{skv}, S_{ske}, b_0, as well as a seasonal head fluctuation added to the annual head time series, are estimated in a grid search with roughly 30,000 simulations. This is done in the two areas shown in Figure 1, referred to as Los Banos/Kettleman City (a) and Tulare/Pixley (b). The reader is referred to Smith and Li (2019) for more details on the modeling approach.

Results and discussion

Figure 3 shows the results of our deformation model. The Los Banos/Kettleman City aquifer is shown in Figure 3a and b, and the Tulare/Pixley region is shown in Figure 3c and d. It is clearly visible in Figure 3 that the Tulare/Pixley region has been experiencing historically low groundwater levels since the early 2000s, resulting in accelerated inelastic deformation relative to historic levels. The Los Banos/Kettleman City aquifer, by contrast, is near its historically lowest groundwater level but has not exceeded it in recent years. These variations in preconsolidation head explain most of the variation in subsidence in these areas. However, continued pumping in the Los Banos/Kettleman City region could result in significant drawdown below the preconsolidation head, causing significant subsidence in that region to resume. In both regions, there is strong evidence for delayed subsidence, supporting previous work by Lees et al. (2022).

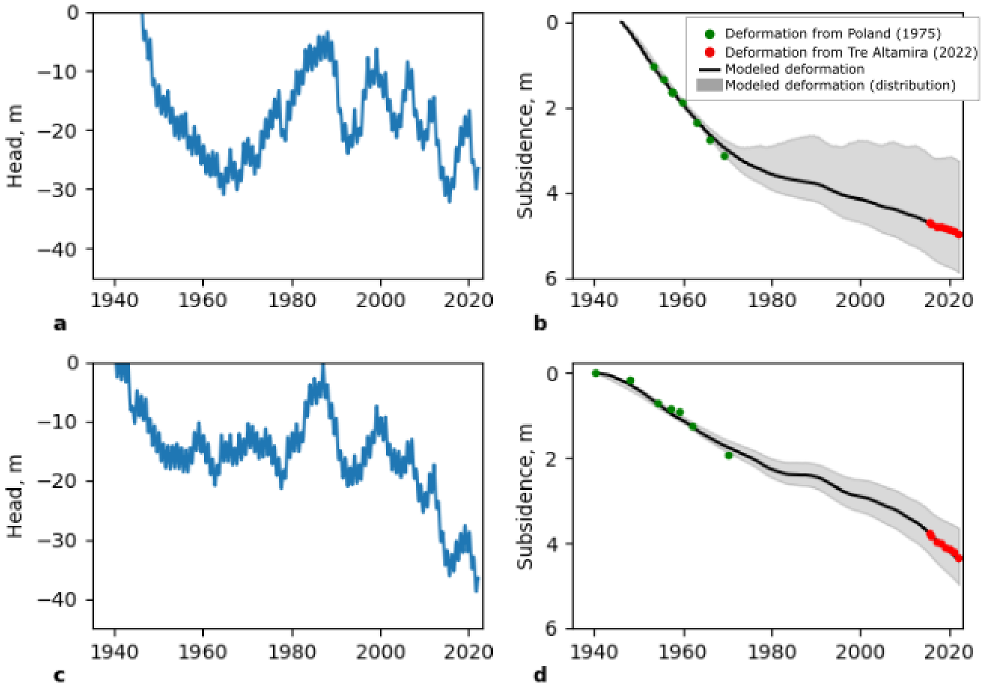

Figure 3 ***a)*** *and* ***b)*** *head and deformation, respectively, relative to 1940 in the Los Banos/Kettleman City region;* ***c)*** *and* ***d)*** *head and deformation, respectively, relative to 1940 in the Tulare/Pixley region.*

Conclusion

In this study, a new approach is presented that makes use of sparsely sampled well data to produce a long-term time series of changes in groundwater levels. This dataset is then used to model deformation in two key regions of the San Joaquin Valley: the Los Banos/Kettleman City region, which experienced massive historic subsidence, and the Tulare/Pixley region, which is currently experiencing over 20 cm/year of subsidence. Our models indicate that the primary driver for the spatiotemporal change in deformation patterns is the preconsolidation head, which was much lower in the Los Banos/Kettleman City region. However, recent droughts have caused stress levels in this region to approach the preconsolidation stress, risking renewed subsidence in that region to accompany ongoing subsidence in the Tulare/Pixley region.

References

Berardino, P., Fornaro, G., Lanari, R., & Sansosti, E. (2002). A new algorithm for surface deformation monitoring based on small baseline differential SAR interferograms. *IEEE Transactions on geoscience and remote sensing, 40*(11), 2375-2383.

Butler, J.J., Whitermore, D.O., Wilson, B.B., and Bohling, G.C., (2016). A new approach for assessing the future of aquifers supporting irrigated agriculture. *Geophysical Research Letters*. http://dx.doi.org/10.1002/2016GL067879.

California Department of Food and Agriculture, California Agricultural Statistics Review 2020-2021, 2021: https://www.cdfa.ca.gov/Statistics/PDFs/2021_Ag_Stats_Review.pdf/.

Chaussard, E., & Farr, T. G. (2019). A new method for isolating elastic from inelastic deformation in aquifer systems: Application to the San Joaquin Valley, CA. *Geophysical Research Letters*, 46, 10800–10809. https://doi.org/10.1029/2019GL084418

Lees, M., Knight, R., & Smith, R. (2022). Development and application of a 1D compaction model to understand 65 years of subsidence in the San Joaquin Valley. *Water Resources Research, 58*, e2021WR031390. https://doi.org/10.1029/2021WR031390

Poland, J. F., Lofgren, B. E., Ireland, R. L., & Pugh, R. G. (1975). *Land Subsidence, in the San Joaquin Valley, California, as of 1972: A History of Land Subsidence Caused by Water-level Decline in the San Joaquin Valley, from the 1920's to 1972* (Vol. 437). US Government Printing Office.

Smith, R. G., Knight, R., Chen, J., Reeves, J. A., Zebker, H. A., Farr, T., and Liu, Z. (2017), Estimating the permanent loss of groundwater storage in the southern San Joaquin Valley, California, *Water Resour. Res*., 53, 2133– 2148, doi:10.1002/2016WR019861.

Smith, R.G., Li, J. (2021). Modeling elastic and inelastic pumping-induced deformation with incomplete water level records in Parowan Valley, Utah. *Journal of Hydrology*. https://doi.org/10.1016/j.jhydrol.2021.126654.

Sneed, M. (2001), Hydraulic and mechanical properties affecting ground-water flow and aquifer-system compaction, San Joaquin Valley, California, *U.S. Geol. Surv. Open File Rep*., 01–35, pp. 5–17.

Tre Altamira, InSAR Land Surveying and Mapping Services to DWR Supporting SGMA – October 2021 Update, 2022: https://data.cnra.ca.gov/dataset/tre-altamira-insar-subsidence/resource/50cfe183-de14-4d7c-adfe-26bf43b80421

Proc. IAHS, 382, 809–813, 2020
https://doi.org/10.5194/piahs-382-809-2020

Open Access PIAHS

Mitigating Land Subsidence in the Coachella Valley, California, USA: An Emerging Success Story

Michelle Sneed and Justin T. Brandt

California Water Science Centre, U.S. Geological Survey, Sacramento, California, 95819, USA

Correspondence: Michelle Sneed (micsneed@usgs.gov)

Published: 22 April 2020

Abstract. Groundwater has been a major source of agricultural, municipal, and domestic water supply since the early 1920s in the Coachella Valley, California, USA. Land subsidence, resulting from aquifer-system compaction and groundwater-level declines, has been a concern of the Coachella Valley Water District (CVWD) since the mid-1990s. As a result, the CVWD has implemented several projects to address groundwater overdraft that fall under three categories – groundwater substitution, conservation, and managed aquifer-recharge (MAR). The implementation of three projects in particular – replacing groundwater extraction with surface water from the Colorado River and recycled water (Mid-Valley Pipeline project), reducing water usage by tiered-rate costs, and increasing groundwater recharge at the Thomas E. Levy Groundwater Replenishment Facility – are potentially linked to markedly improved groundwater levels and subsidence conditions, including in some of the historically most overdrafted areas in the southern Coachella Valley. Groundwater-level and subsidence monitoring have tracked the effect these projects have had on the aquifer system. Prior to about 2010, water levels persistently declined, and some had reached historically low levels by 2010. Since about 2010, however, groundwater levels have stabilized or partially recovered, and subsidence has stopped or slowed substantially almost everywhere it previously had been observed; uplift was observed in some areas. Furthermore, results of Interferometric Synthetic Aperture Radar analyses for 1995–2017 indicate that as much as about 0.6 m of subsidence occurred; nearly all of which occurred prior to 2010. Continued monitoring of water levels and subsidence is necessary to inform the CVWD about future mitigation measures. The water management strategies implemented by the CVWD can inform managers of other overdrafted and subsidence-prone basins as they seek solutions to reduce overdraft and subsidence.

1 Introduction and Background

Groundwater has been a major source of agricultural, municipal and domestic water supply in the Coachella Valley, California, USA, since the early 1920s (Fig. 1). By about 2010, water levels in many wells in the Coachella Valley had declined by as much as 30 m and water levels in some wells were at their lowest recorded values (Fig. 1a). Declining water levels can contribute to, or induce, land subsidence in alluvial aquifer systems with compressible fine-grained deposits such as that of the Coachella Valley. Results of Global Positioning System and spirit-leveling surveys were used to determine that as much as 0.15 m of subsidence occurred in the southern parts of the Coachella Valley during 1930–1996 (Ikehara et al., 1997). Interferometric Synthetic Aperture Radar (InSAR) analyses were used to determine that as much as 0.6 m of subsidence occurred during 1995–2010 along the southwestern margins of Coachella Valley in the urban areas of Palm Desert, Indian Wells and La Quinta (Sneed et al., 2014; Fig. 1b). Land subsidence has caused earth fissures and has damaged buildings, roads and water conveyance canals near La Quinta (Clay Stevens, TerraPacific Consultants, Inc., written communication, 2006). Subsidence-induced sags along the Coachella branch of the All-American Canal (Coachella Canal) adversely affected flow, caused loss of freeboard, and caused the water surface to overtop the concrete liner in some areas, which prompted the CVWD to realign a portion of the canal in 2014. Since about 2010, the combination of several water management projects implemented by the CVWD have markedly improved groundwater levels in some of the historically most overdrafted areas of the valley. The projects fall under three categories – conservation, managed aquifer-recharge (MAR), and groundwater substitution (using Colorado River and recycled water). The groundwater substitution is used for agriculture, golf-course irrigation, and other non-potable water uses through the Coachella Canal and the Mid-Valley Pipeline (MVP) project (Coachella Valley Water District, 2012; Fig. 1a). Monitoring has tracked the effect that MAR and the reduction in pumpage resulting from these projects have had on groundwater levels (Fig. 1a, b). The marked improvement in groundwater levels that began around 2010 was timely. In 2014, the California legislature passed the Sustainable Groundwater Management Act (SGMA), which stipulates sustainable management of groundwater resources by avoiding certain "undesirable results," including groundwater-level declines and land subsidence. CVWD's groundwater management plans received state approval and meet the requirements of the SGMA (California Department of Water Resources, https://water.ca.gov/Programs/Groundwater20Management/SGMA-Groundwater-Management/Alternatives, last access: 21 August 2019).

2 Geographic and Hydrogeologic Setting

The Coachella Valley is a $1000\,\mathrm{km}^2$ northwest-trending valley in arid southeastern California (Fig. 1); the valley receives only about 75 mm of precipitation annually (California Department of Water Resources, 1964). The northern part of the valley is largely rural but includes the city of Palm Springs. The southern part of the valley has larger urban centers including the cities of Palm Desert, Indian Wells, La Quinta, and Indio, which are interspersed with about 120 golf courses, as well as smaller urban centers such as Coachella and Mecca, where agricultural land use is more prevalent.

The 600 m thick aquifer system in the Coachella Valley comprises a complex unconsolidated to partly consolidated assemblage of gravel, sand, silt and clay of alluvial and lacustrine origins (California Department of Water Resources, 1979). In the southern Coachella Valley, the aquifer system consists of a semiperched aquifer zone, an upper aquifer, a confining layer (lacustrine deposits), and a lower aquifer. The lower aquifer is the most productive source of groundwater in the southern Coachella Valley. In the northern Coachella Valley, the confining layer is absent such that the aquifer system is not subdivided. Sediments tend to be finer grained (contain more silt and clay) in the southern part of the valley compared to the northern part because of the greater distance from the sediment source areas in the north and because of lacustrine deposition in the ancient Lake Cahuilla (California Department of Water Resources, 1964, 1979). Furthermore, lithologic analyses indicated that fine-grained compressible sediments were preferentially deposited in the southwestern margin of the valley, resulting in interbedded aquitards with variable thicknesses (Sneed et al., 2014).

The general direction of groundwater flow is southeastward toward the Salton Sea. Northwest trending faults generally are parallel to the flow direction but affect the movement of groundwater in some parts of the valley (California Department of Water Resources, 1964). InSAR analysis indicated that the northern and eastern extents of subsidence in Palm Desert, Indian Wells, and La Quinta terminate abruptly, and are coincident with an inferred fault (Jennings, 1977; Sneed et al., 2014; Fig. 1). Abrupt areal changes in subsidence can be the result of faults separating compressible from less-compressible deposits or acting as barriers to groundwater flow (Galloway et al., 1999). Hydrostratigraphic analyses led Sneed et al. (2014) to conclude that differences in the sediment compressibilities across the inferred fault are probable.

3 Groundwater Levels and Land Subsidence

Groundwater pumping between the early 1920s and the late 1940s resulted in seasonal groundwater-level fluctuations superimposed on declines of as much as 15 m. In 1949, the importation of Colorado River water through the Coachella Canal to the southern Coachella Valley began. The importation of surface water resulted in decreased groundwater pumping during the 1950s through the 1970s, and groundwater levels in some wells consequently recovered by as much as 15 m. Starting in the late 1970s, however, the demand for water increased to the point that groundwater levels again declined in response to increased pumping. By about 2010, water levels in many wells in the southern Coachella Valley had declined by as much as 30 m, with some reaching historically low levels (Fig. 1a, b).

Land subsidence in the southern part of the Coachella Valley has been monitored since 1995 using InSAR methods. As much as 0.6 m of subsidence had occurred by 2010, with the local maxima in the urbanized areas along the southwestern margin of the valley (Sneed et al., 2014; Fig. 1b). Analysis indicated subsidence rates as high as about $50\,\mathrm{mm\,yr^{-1}}$ in some areas over the 15 year period – including during periods of seasonal water-level recovery. Subsidence occurring during periods of water-level recovery indicates that residual compaction of thick clay aquitards occurred and could be a substantial component of total compaction in these areas (Sneed et al., 2014). Land subsidence in the northern part of the valley prior to 2010 had not been monitored as closely as in the southern part, but InSAR analyses indicated land-surface stability during 2003–2005 (Martin et al., 2011).

Since about 2010, groundwater and land subsidence conditions – including in some of the historically most overdrafted areas in the southern part of the valley – have markedly improved. Groundwater-level recovery during 2010–2017 coincided with substantially reduced subsidence rates or up-

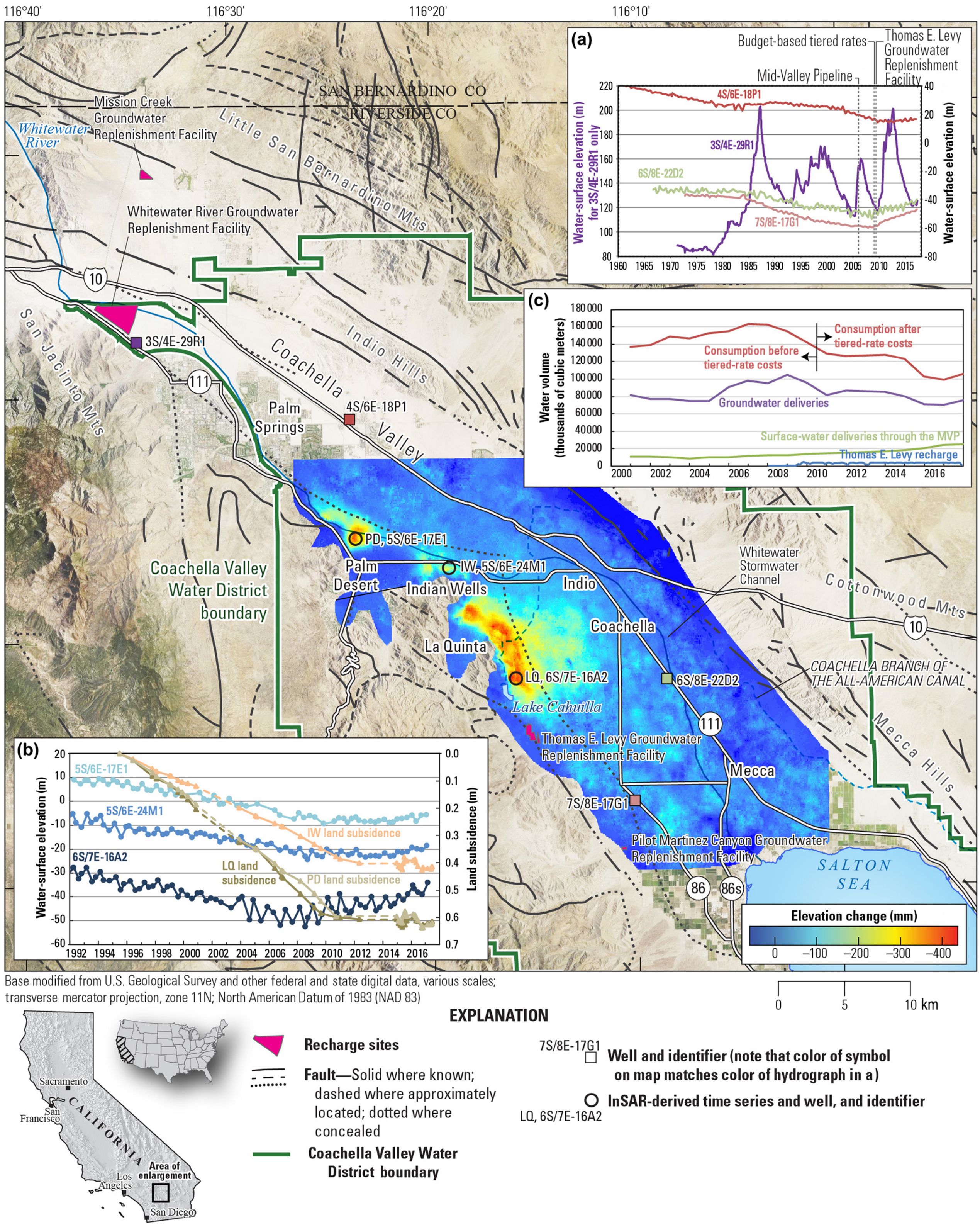

Figure 1. The Coachella Valley, California, USA with an interferogram showing land-surface deformation for 1995–2017 (excludes 8 November 2000–30 November 2003 and 19 September 2010–28 December 2014); **(a)** Groundwater levels in selected wells and mitigation strategies, 1960–2017; **(b)** InSAR-derived deformation at selected locations (dashed where estimated), and groundwater levels in selected wells, 1992–2017; **(c)** Water volumes for groundwater deliveries, surface-water deliveries through the Mid-Valley Pipeline, recharge at the Thomas E. Levy Groundwater Replenishment Facility, and consumption according to the implementation of tiered-rate costs, 2000–2017.

lift compared to subsidence rates during 1995–2010, when groundwater levels declined (Fig. 1b). Subsidence rates during 2010–2017 were generally less than half the rates computed for 1995–2010, and in most cases the rates were reduced by 75 %. Furthermore, the subsidence rates generally slowed throughout 2010–2017. The northern part of the valley uplifted by as much as 60 mm during 2014–2017.

The trend reversal in the southern part of the valley provides new insights into aquifer-system mechanics. While many areas had stopped subsiding or had uplifted during 2010–2017 during water-level recovery, the few areas that did subside during water-level recovery indicate a mixed aquifer-system response. It is likely that the coarser-grained aquifers and thin, quickly equilibrating aquitards expanded elastically, while the thicker, slowly draining aquitards compacted (residual compaction). This mixed, mechanical response of the aquifer system indicates that the stresses causing compaction of the thicker aquitards are not represented by the measured stresses (water levels in aquifers). Because of the impedance of groundwater flow in the aquitards, changes in hydraulic head in the aquifers may not have yet occurred throughout a significant part of the thicker aquitards. If this is the case, subsidence rates are expected to slow asymptotically if groundwater levels continue to recover or stabilize.

4 Mitigation of Groundwater Overdraft and Land Subsidence

The stabilization and recovery of groundwater levels, and the reduced rates or cessation of subsidence, correspond to the timing of various conservation, MAR, and groundwater substitution projects implemented by the CVWD to increase recharge or reduce reliance on groundwater (Fig. 1c). Projects have been implemented by the CVWD since 1973 throughout the valley to address overdraft, but the implementation of three projects in particular are potentially linked to markedly improved groundwater levels since about 2010 in some of the historically most overdrafted areas of the valley. These projects are groundwater substitution through the MVP project since 2006, budget-based tiered-rate costs since 2009, and MAR at the Thomas E. Levy Groundwater Replenishment Facility since 2009. Additionally, drought-induced conservation requirements mandated by the State of California beginning in 2014 likely contributed to the improved conditions.

The multi-pronged water-resource management approach includes agricultural and urban (recreational, residential, and commercial) water users. In the mostly rural northern parts of the Valley, the fluctuations in groundwater levels are partly driven by recharge operations at the Whitewater and Mission Creek Groundwater Replenishment Facilities, which began in 1973 and 2002, respectively (Fig. 1, for example, well 3S/4E-29R1 in Fig. 1a; Coachella Valley Water District, 2012). These groundwater replenishment facilities are in the northwest part of the valley, such that the recharged water flows southeasterly towards agricultural and urban centers. Further south, near Palm Desert, Indian Wells, and La Quinta, where the highest subsidence rates were measured between 1995 and 2010, groundwater-level responses to those recharge operations diminish and seasonal and longer-term trends in groundwater-levels and land-surface deformation become more prevalent (Fig. 1a, b). This largely urbanized area is where many of the conservation projects were expected to be more commonly adopted. The conservation projects include turf conversion to less water-intensive landscape (including golf courses), residential and large landscape smart water controllers, and smart water nozzles, among other conservation projects. The implementation of budget-based tiered-rate costs in 2009 most closely coincides with the reversal of long-term groundwater-level declines in the area (Fig. 1a, b). In addition, more than a dozen new connections from golf courses, resorts, and other businesses to the MVP project since 2006 have contributed to reduced groundwater use (Fig. 1c).

In the largely rural and agricultural areas south of La Quinta, the effects of recharge operations at the Thomas E. Levy Groundwater Replenishment Facility, which began in 2009, are superimposed on the seasonal and longer-term trends in both groundwater levels and land-surface deformation (Fig. 1a–c). These recharge operations coincide with the abrupt reversal of long-term groundwater-level declines in the area. Additionally, the flood-to-drip agricultural rebate conservation project implemented by CVWD starting in 2016 was expected to be more commonly adopted in this area but has since been discontinued.

5 Summary

Groundwater has been a major source of agricultural, municipal and domestic water supply in the Coachella Valley, resulting in water-level declines of as much as 30 m by about 2010, when many reached historically low levels (Sneed et al., 2014). These declines resulted in as much as 0.15 m of subsidence by 1996 in the southern part of the valley, and as much as 0.6 m of subsidence between 1995 and 2010 along the southwestern margin of the valley, where differential subsidence has damaged buildings, roads, water conveyance canals, and other infrastructure. Starting in about 2010, the combination of several projects implemented by the CVWD to increase recharge or reduce reliance on groundwater coincided with wide-spread stabilization and recovery of groundwater levels and a substantial slowing or cessation of subsidence in some of the historically most overdrafted areas. Phase 1 of the Palm Desert Groundwater Replenishment Facility, which consists of recharge ponds adjacent the Whitewater Stormwater Channel in Palm Desert, began recharge operations in January 2019, with the management goal of mitigating the continued, albeit slowed, groundwater-level declines and associated subsidence in the Palm Desert and Indian Wells areas. Phase II of the Palm Desert Groundwater Replenishment Facility involves construction of additional recharge ponds in the Whitewater Stormwater Channel in Palm Desert. As the CVWD continues to implement such projects, future monitoring could track the resulting effects on the aquifer system and help inform future mitigation measures, as the CVWD has done using the results of previous studies. The water management strategies implemented by the CVWD can inform managers of other overdrafted and subsidence-prone basins as they seek solutions to comply with the SGMA.

Data availability. The InSAR data presented in this report are available at https://www.sciencebase.gov/catalog/item/5cfea3cfe4b0156ea564502c (last access: 10 March 2020, Sneed, 2020). The water-surface elevation and water volume data were provided by the Coachella Valley Water District.

Author contributions. MS designed and directed the study. JB processed the data. MS and JB analyzed the data and wrote the paper.

Competing interests. The authors declare that they have no conflict of interest.

Special issue statement. This article is part of the special issue “TISOLS: the Tenth International Symposium On Land Subsidence – living with subsidence”. It is a result of the Tenth International Symposium on Land Subsidence, Delft, the Netherlands, 17–21 May 2021.

References

California Department of Water Resources: Coachella Valley investigation: California Department of Water Resources, Bulletin 108, 145 pp., 1964.

California Department of Water Resources: Coachella Valley area well standards investigation: Los Angeles, California Department of Water Resources, Southern District, 40 pp., 1979.

Coachella Valley Water District: Coachella Valley Water Management Plan 2010 Update, available at: http://www.cvwd.org/DocumentCenter/View/1321/Coachella-Valley-Water-Management-Plan-Final-Report-PDF?bidId (last access: 21 August 2019), Final Report, 286 pp., 2012.

Galloway, D. L., Jones, D. R., and Ingebritsen, S. E: Land subsidence in the United States, U.S. Geological Survey Circular 1182, 175 pp., 1999.

Ikehara, M. E., Predmore, S. K., and Swope, D. J.: Geodetic network to evaluate historical elevation changes and to monitor land subsidence in Lower Coachella Valley, California, 1996, U.S. Geological Survey Water-Resources Investigations Report 97-4237, scale 1 : 63 000, 1 sheet (folded in envelope), 1997.

Jennings, C. W.: Geologic Map of California, California Division of Mines and Geology, Geologic Data Map No. 2, scale 1 : 750 000, 1977.

Martin, P. (Ed.): with contributions by Brandt, J., Catchings, R. D., Christensen, A. H., Flint, A. L., Gandhok, G., Goldman, M. R., Halford, K. J., Langenheim, V. E., Martin, P., Rymer, M. J., Schroeder, R. A., Smith, G. A., and Sneed, M.: The source, discharge, and chemical characteristics of water from Agua Caliente Spring, Palm Springs, California: U.S. Geological Survey Scientific Investigations Report 2011–5156, 106 pp., 2011.

Sneed, M.: Global Positioning System Survey data for 2015, and Interferometric Synthetic Aperture Radar Data for 1995–2017, Coachella Valley, Riverside County, California: U.S. Geological Survey data release, available at: https://www.sciencebase.gov/catalog/item/5cfea3cfe4b0156ea564502c, last access: 10 March 2020.

Sneed, M., Brandt, J. T., and Solt, M.: Land subsidence, groundwater levels, and geology in the Coachella Valley, California, 1993–2010, U.S. Geological Survey Scientific Investigations Report 2014–5075, https://doi.org/10.3133/sir20145075, 62 pp., 2014.

Proc. IAHS, 382, 173–177, 2020
https://doi.org/10.5194/piahs-382-173-2020

Open Access PIAHS

Tenth International Symposium on Land Subsidence (TISOLS)

A multiscale approach for detection and mapping differential subsidence using multi-platform InSAR products

Dario E. Solano-Rojas[1], **Shimon Wdowinski**[2], **Enrique Cabral-Cano**[3], **Batuhan Osmanoglu**[4], **Emre Havazli**[5], and **Jesus Pacheco-Martínez**[6]

[1]Universidad Nacional Autónoma de México, Facultad de Ingeniería, Mexico City, 04510, Mexico
[2]Florida International University, Earth & Environment, Miami, FL 33199, USA
[3]Universidad Nacional Autónoma de México, Instituto de Geofísica, Mexico City, 04150, Mexico
[4]NASA Goddard Space Flight Center, Greenbelt, MD 20771, USA
[5]University of Miami, Marine Geology and Geophysics, 4600 Rickenbacker Causeway, Miami, FL 33149, USA
[6]Universidad Autónoma de Aguascalientes, Aguascalientes, 20130, Mexico

Correspondence: Darío E. Solano-Rojas (dario.e.solano@gmail.com)

Published: 22 April 2020

Abstract. Detecting and mapping subsidence is currently supported by interferometric synthetic aperture radar (InSAR) products. However, several factors, such as band-dependent processing, noise presence, and strong subsidence limit the use of InSAR for assessing differential subsidence, which can lead to ground instability and damage to infrastructure. In this work, we propose an approach for measuring and mapping differential subsidence using InSAR products. We consider synthetic aperture radar (SAR) data availability, data coverage over time and space, and the region's subsidence rates to evaluate the need of post-processing, and only then we interpret the results. We illustrate our approach with two case-examples in Central Mexico, where we process SAR data from the Japanese ALOS (L-band), the German TerraSAR-X (X-band), the Italian COSMO-SkyMed (X-band) and the European Sentinel-1 (C-band) satellites. We find good agreement between our results on differential subsidence and field data of existing faulting and find potential to map yet-to-develop faults.

1 Introduction

Several locations around the world experience land subsidence due to groundwater extraction (e.g. Gambolati and Teatini, 2015; Semple et al., 2017). Central Mexico alone, has more than twenty urban areas reported as subsiding (Brunori et al., 2015; Cabral-Cano et al., 2008; Chaussard et al., 2017; Pacheco-Martínez et al., 2015). More importantly, spatial variation of subsidence in several of such locations has led to differential subsidence and, consequently, to ground faulting and infrastructure damage (Avila-Olivera and Garduño-Monroy, 2008; Pacheco-Martínez et al., 2013).

City-scale subsidence patterns and rates have been characterized since the 1940's using multiple geodetic techniques. In recent decades, InSAR measurements have allowed the mapping of large subsiding areas at the scale of entire cities and with frequent observations (e.g. Amelung et al., 1999; Hoffmann et al., 2001). However, several factors limit the application and interpretation of InSAR results for differential subsidence mapping, such as data availability, processing particularities, data integration, and signal interpretation in the presence of strong subsidence.

In this work, we illustrate an approach focused specifically on detecting and mapping differential subsidence based on SAR data from different platforms, elevation data and basic field information. We illustrate our approach with two case studies in Central Mexico, which have different subsidence characteristics and different data availability. The ultimate goal of our approach is to share the expertise we have acquired after studying several cases of differential subsidence for expanding its application to other areas with data availability constrains.

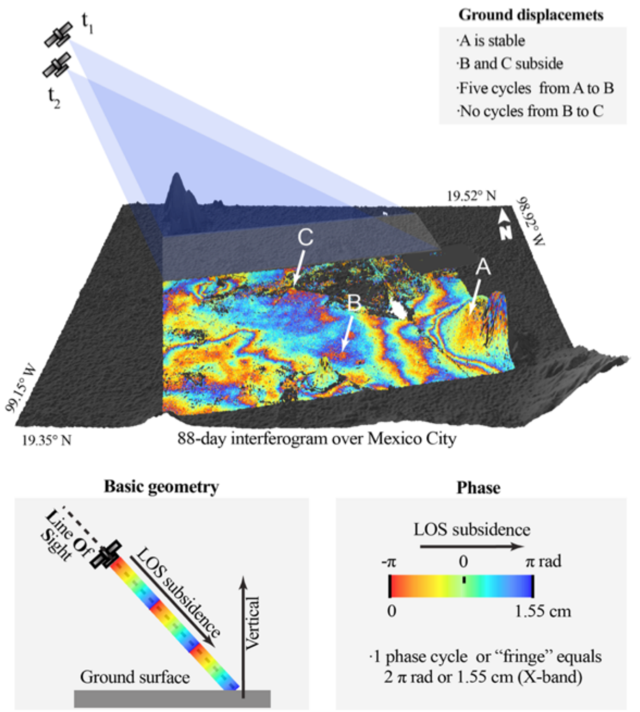

Figure 1. Schematic illustration describing the concept of repeat-pass InSAR. The interferogram was calculated from a COSMO-SkyMed SAR pair acquired on 3 April and 30 June 2012 over Mexico City. Point A is a stable area known as Chimalhuache hill. Point B is located close to Peñón de los Baños. Point C is located over Benito Juárez International Airport. Shaded relief from SRTM data.

2 Materials and Methods

We propose using SAR data, a digital elevation model (DEM) from the Shuttle Radar Topography Mission (SRTM) mission, and surface field data when available.

We rely on four SAR datasets, of which two cover Aguascalientes and two Mexico City. The two datasets covering Aguascalientes consist on 34 ALOS PALSAR scenes acquired form August 2007 to March 2011 and six TerraSAR-X acquired from December 2009 and September 2012. The two datasets covering Mexico City consist of 144 Sentinel-1 scenes acquired from 2014 to 2017 and 21 COSMO-SkyMED scenes acquired from December 2011 to June 2012. We process the SAR using InSAR techniques, which relies on the existence of at least two satellite acquisitions to perform pixel-wise phase differences to generate a map of interferometric phase differences, so-called interferogram (Fig. 1).

We perform single-interferogram processing using the Delft object-oriented radar interferometric software (Doris) (Kampes et al., 2004) and time series processing using either the Stanford Method for Persistent Scatterers (StaMPS) (Hooper et al., 2007) or the Miami InSAR time-series software in Python (MintPy) (Yunjun et al., 2019). Additionally, we perform post-processing of the InSAR velocity maps results using subsidence gradient (Cabral-Cano et al., 2008) or band pass filtering (Solano-Rojas, 2018).

3 Case studies

3.1 Aguascalientes

The valley of Aguascalientes experiences subsidence rates of up to 100 [$\mathrm{mm\,yr^{-1}}$] due to overexploitation of its aquifer system (Chaussard et al., 2014). The city is located within a tectonic graben (Fig. 2a). The topographic slopes map of the area shows flat topography in the middle of the graben, which forms the valley (Fig. 2b). Mapped surface faults in the region show that the graben-delimiting faults are orientation roughly NE–SW, in agreement with the topographic slopes. The InSAR velocity map from ALOS data (Fig. 2c) shows a clear subsidence pattern within the graben, in agreement with previous observations (Pacheco-Martínez et al., 2015). However, the graben limits do not exactly coincide with the transition between subsiding and stable areas (see northern portion of the eastern main fault). There seems to be, instead, a better agreement between the topographic slope map and the faults location.

High-resolution single interferograms produced with pairs of TerraSAR-X (TSX) images (Fig. 2d–g) reveal a-few-fringes patterns in the easternmost portion of the study area, as opposed to the many-fringes pattern observed in the centre of the interferograms. Evidently, interferograms comprising a longer time span shows a more complex interferometric pattern, due to the accumulation of subsidence (compare Fig. 2d vs Fig. 2f, for instance). The discontinuities in the phase coincide well with the presence of the field-surveyed surface faulting. As a matter of fact, the interferometric pattern shows additional phase discontinuities that may correspond to not-yet mapped or not-yet-developed surface faults. We interpret that these phase discontinuities.

3.2 Mexico City

Mexico City is one of the largest and most populated urban areas in the world. The city was built on a highly compressible lacustrine sediment sequence, which has been subjected to fast land subsidence with rates exceeding 350 $\mathrm{mm\,yr^{-1}}$, in response to aggressive groundwater extraction,

Our Sentinel-1 InSAR velocity map from 2014 to 2017 (Fig. 3a) shows that Sierra de Santa Catarina is stable, while its surroundings subside rapidly ($\sim -400\,\mathrm{mm\,yr^{-1}}$). We calculate a gradient velocity map, which shows the highest values around Sierra de Santa Catarina (Fig. 3b). Additionally, we calculate a velocity map from the COSMO-SkyMed constellation data and obtain the boundaries of sharp transition between highly-subsiding and highly-uplifting (Fig. 3c). The areas of pronounced differential displacements agree well with the location of pre-existing, subsidence-related faults

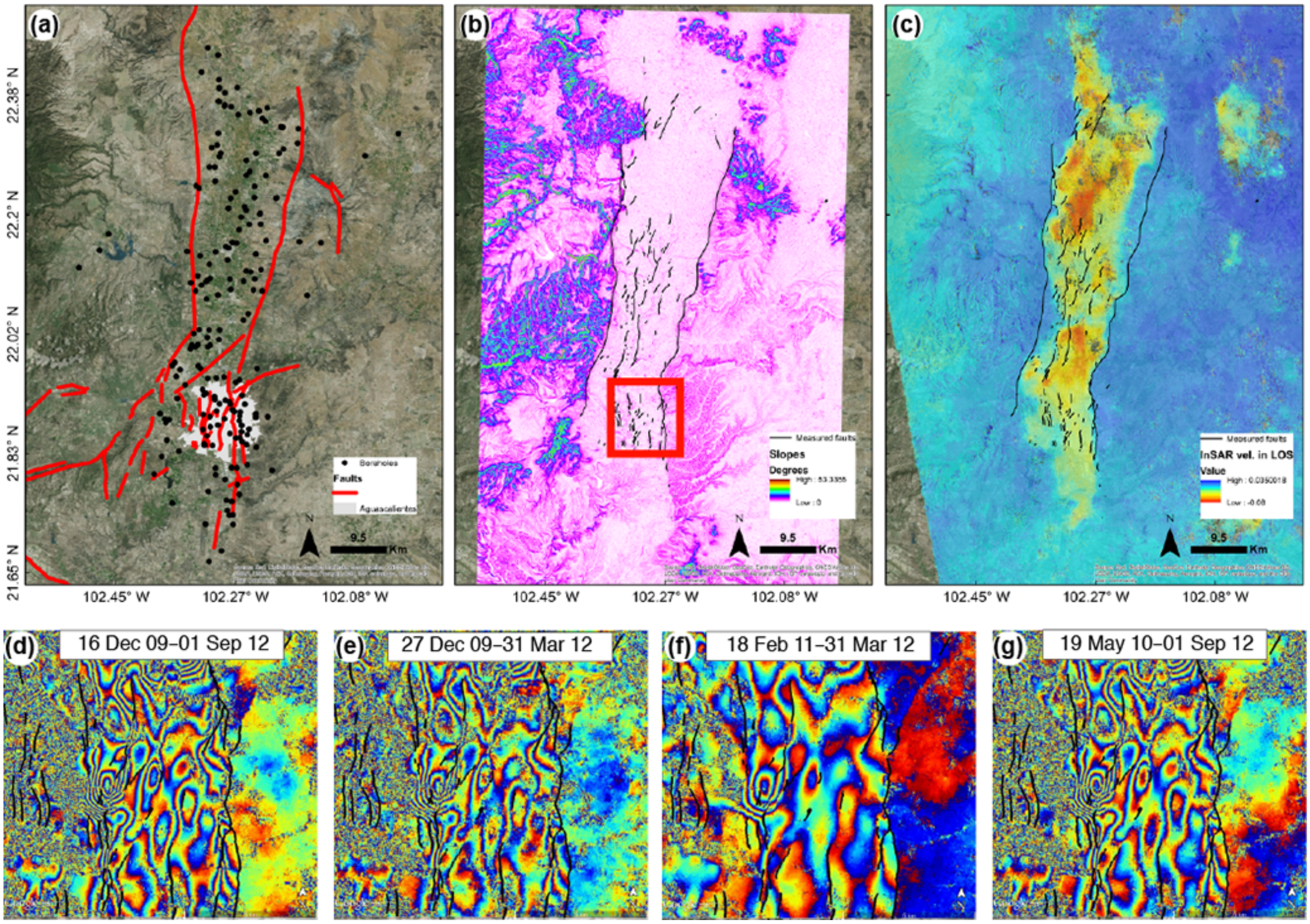

Figure 2. Case example of differential subsidence analysis over Aguascalientes Valley. **(a)** Satellite image (source: © Esri, Digital Globe, GeoEye, Earthstar Geographics, CNES Airbus, USDA, USGS, ADX, Getmapping, Aerogrid, IGN, swisstopo, and the GIS community) overlaid by locations of groundwater-extraction wells in the area. Red lines represent faults mapped in the city. **(b)** Slopes map from SRTM topographic data. Red square shows the limits of **(d)**–**(g)**. **(c)** Velocity map from 34 ALOS PALSAR scenes acquired form August 2007 to March 2011. **(d)**–**(g)** High resolution interferograms of Aguascalientes' urban area from TerraSAR-X data. Each fringe corresponds to 1.55 cm of subsidence.

identified during 10 years of field surveys (CENAPRED, 2017).

4 Conclusions

The proposed approach shows the capability of multiplatform, multiresolution InSAR for detecting and mapping differential subsidence and surface faulting. The strategic advantage of this approach is its reliance on mostly available products (i.e. SAR data, SRTM DEM, basic field surveys). Medium-resolution results from ALOS and Sentinel-1 satellites depict well the larger-scale subsidence patterns. Detailed faulting cartography in the urban area coincide with phase discontinuities in this interferograms produced with higher-resolution data from TerraSAr-X, with potential for mapping of not-reported faults and improved understanding of the subsurface.

Additionally, post-processing techniques from both low resolution (such as subsidence gradient) and high resolution (such as band-pass filtering) datasets provide a tool for improving the understanding of differential subsidence, as shown in the Mexico City study case. Differential subsidence shows to be particularly large in areas of sharp geotechnical transitions denoted by topographic slope changes.

Data availability. The SAR data that support the findings of this study are available from e-GEOS (http://www.e-geos.it) (Italian Space Agency, 2020), the German Space Agency (DLR: http://www.dlr.de) (German Aeroespace Center, 2020), the European Space Agency (ESA: https://www.esa.int) (European Space Agency, 2020) and the Japan Aerospace Exploration Agency (JAXA: http://www.global.jaxa.jp) but restrictions apply to the availability of these data, which were used under license for the current study (Japan Aerospace Exploration Agency, 2020). The to-

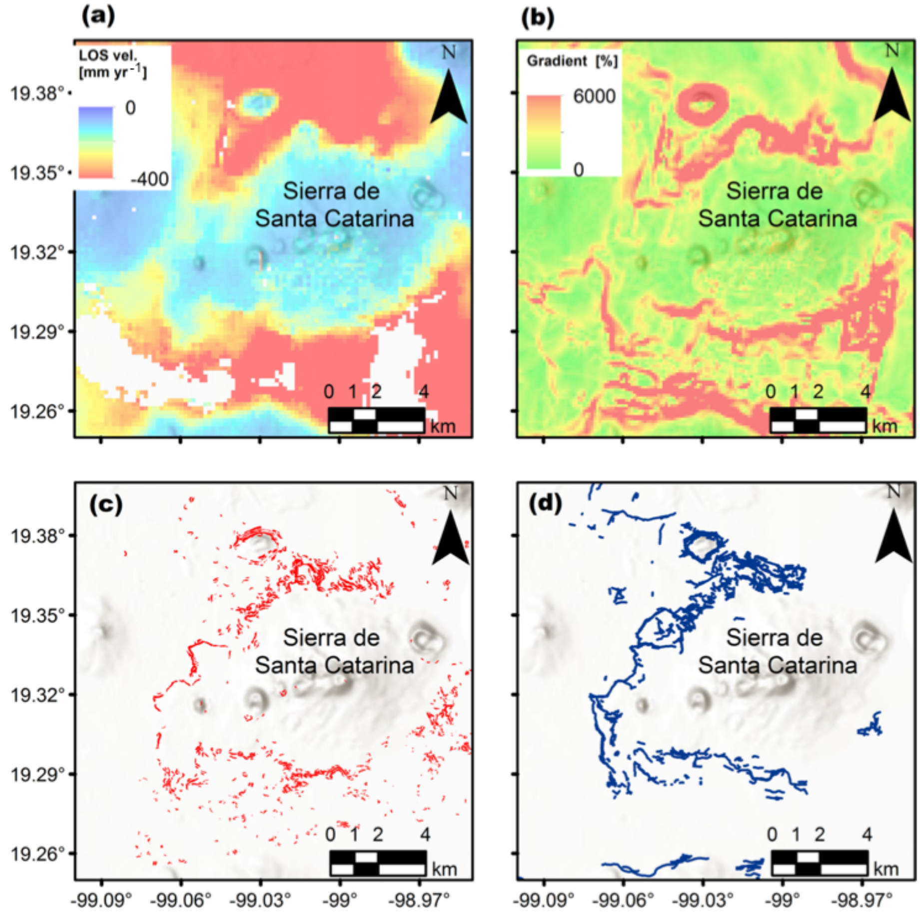

Figure 3. Case example of differential subsidence analysis over South Mexico City. **(a)** Velocity map from 144 Sentinel-1satellites acquired from 2014 to 2017. **(b)** Horizontal gradient calculated from **(a)**. **(c)** Areas of differential subsidence calculated from high-resolution COSMO-SkyMED data. **(d)** 10-year worth of subsidence-related shallow faults mapped by the city's government (CENAPRED, 2017). Shaded relief from SRTM data.

pographic data used for shaded relief maps and topographic correction of InSAR results are available in the USGS repository (https://earthexplorer.usgs.gov/) (Farr et al., 2007). The InSAR results are available from the corresponding author upon reasonable request.

Author contributions. DS and SW conceptualized the research and developed the methodology, DS processed the X-band and ALOS data and EH processed the Sentinel data. DS conducted the investigation under the supervision of SW. JP provided all the field data over Aguascalientes. The SAR data was obtained by EC and BO. DS and SW wrote the manuscript and all authors revised it.

Competing interests. The authors declare that they have no conflict of interest.

Special issue statement. This article is part of the special issue "TISOLS: the Tenth International Symposium On Land Subsidence – living with subsidence". It is a result of the Tenth International Symposium on Land Subsidence, Delft, the Netherlands, 17–21 May 2021.

Acknowledgements. Dario E. Solano-Rojas acknowledges funding from CONACyT and Fulbright-García Robles for his doctoral studies. Shimon Wdowisnki acknowledges funding from NASA project NNX12AQ08G and Enrique piahs-382-173-2020-f01.pngCabral-Cano acknowledges support from UNAM-PAPIIT projects IN104213, IN109315-3 and IV100215 and CONACyT projects 256012, and 253760 and supplemental support from UNAM-Instituto de Geofísica.

Financial support. This research has been supported by the NASA (grant no. NNX12AQ08G), the UNAM-PAPIIT (grant nos. IN104213, IN109315-3, and IV100215), and the CONACyT (grant nos. 256012 and 253760).

References

Amelung, F., Galloway, D. L., Bell, J. W., Zebker, H. A., and Laczniak, R. J.: Sensing the ups and downs of Las Vegas: InSAR reveals structural control of land subsidence and aquifer-system deformation, Geology, 27, 483–486, 1999.

Avila-Olivera, J. A. and Garduño-Monroy, V. H.: A GPR study of subsidence-creep-fault processes in Morelia, Michoacán, Mexico, Eng. Geol., 100, 69–81, https://doi.org/10.1016/j.enggeo.2008.03.003, 2008.

Brunori, C. A., Bignami, C., Albano, M., Zucca, F., Samsonov, S., Groppelli, G., Norini, G., Saroli, M. and Stramondo, S.: Land subsidence, ground fissures and buried faults: InSAR monitoring of Ciudad Guzmán (Jalisco, Mexico), Remote Sens., 7, 8610–8630, https://doi.org/10.3390/rs70708610, 2015.

Cabral-Cano, E., Dixon, T. H., Miralles-Wilhelm, F., Díaz-Molina, O., Sánchez-Zamora, O., and Carande, R. E.: Space geodetic imaging of rapid ground subsidence in Mexico City, Bull. Geol. Soc. Am., 120, 1556–1566, https://doi.org/10.1130/B26001.1, 2008.

Centro Nacional de Prevención de Desastres (CENAPRED): Fracturas en la Ciudad de Mexico, Atlas Nac. Riesgos, available at: http://www.atlasnacionalderiesgos.gob.mx/archivo/visor-capas.html (last access: 20 August 2005), 2017.

Chaussard, E., Wdowinski, S., Cabral-Cano, E., and Amelung, F.: Land subsidence in central Mexico detected by ALOS InSAR time-series, Remote Sens. Environ., 140, 94–106, https://doi.org/10.1016/j.rse.2013.08.038, 2014.

Chaussard, E., Milillo, P., Bürgmann, R., Perissin, D., Fielding, E. J., and Baker, B.: Remote Sensing of Ground Deformation for Monitoring Groundwater Management Practices: Application to the Santa Clara Valley During the 2012–2015 California Drought, J. Geophys. Res.-Sol. Ea., 122, 8566–8582, https://doi.org/10.1002/2017JB014676, 2017.

European Space Agency: Sentinel-1 data archieve, available at: https://scihub.copernicus.eu/dhus/#/home (last access: 20 August 2002), 2020.

Farr, T. G., Rosen, P. A., Caro, E., Crippen, R., Duren, R., Hensley, S., Kobrick, M., Paller, M., Rodriguez, E., Roth, L., Seal, D., Shaffer, S., Shimada, J., Umland, J., Werner, M., Oskin, M., Burbank, D., and Alsdorf, D. E.: The shuttle radar topography mission, Rev. Geophys., 45, 1–43, https://doi.org/10.1029/2005RG000183, 2007.

Gambolati, G. and Teatini, P.: Geomechanics of subsurface water withdrawal and injection, Water Resour. Res., 51, 3922–3955, https://doi.org/10.1002/2014WR016841, 2015.

German Aeroespace Center: TerraSAR-X data archieve, available at: https://terrasar-x-archive.terrasar.com/ (last access: 20 April 2002), 2020.

Hoffmann, J., Zebker, H. A., Galloway, D. L., and Amelung, F.: Seasonal subsidence and rebound in Las Vegas Valley, Nevada, observed by synthetic aperture radar interferometry, Water Resour. Res., 37, 1551–1566, https://doi.org/10.1029/2000WR900404, 2001.

Hooper, A., Segall, P., and Zebker, H.: Persistent scatterer interferometric synthetic aperture radar for crustal deformation analysis, with application to Volcan Alcedo, Galapagos, J. Geophys. Res.-Sol. Ea., 112, 1–21, https://doi.org/10.1029/2006JB004763, 2007.

Italian Space Agency: COSMO-SkyMed data archieve, available at: http://catalog.e-geos.it/ (last access: 20 March 2009), 2020.

Japan Aerospace Exploration Agency: ALOS PALSAR data archieve (through Vertex), 2020.

Kampes, B. M., Hanssen, R. F., and Perski, Z.: Radar interferometry with public domain tools, Eur. Sp. Agency, Special Publ. ESA SP, 550, 59–68, 2004.

Pacheco-Martínez, J., Cabral-Cano, E., Wdowinski, S., Hernández-Marín, M., Ortiz-Lozano, J. Á., and Zermeño-de-León, M. E.: Application of InSAR and Gravimetry for Land Subsidence Hazard Zoning in Aguascalientes, Mexico, Remote Sens., 7, 17035–17050, https://doi.org/10.3390/rs71215868, 2015.

Semple, A. G., Pritchard, M. E., and Lohman, R. B.: An incomplete inventory of suspected human-induced surface deformation in North America detected by satellite interferometric synthetic-aperture radar, Remote Sens., 9, 1–26, https://doi.org/10.3390/rs9121296, 2017.

Solano-Rojas, D.: Geological Hazard Assessments for Mexico City and its Surroundings Based on Synthetic Aperture Radar Interferometry (InSAR) Observations, University of Miami, available at: https://scholarlyrepository.miami.edu/oa_dissertations/2157 (last access: 22 March 2020), 2018.

Yunjun, Z., Fattahi, H., and Amelung, F.: Small baseline InSAR time series analysis: unwrapping error correction and noise reduction, 133, 104331, https://doi.org/10.1016/j.cageo.2019.104331, 2019.

Synthesis of coastal subsidence measurements in the Ganges-Brahmaputra Delta, Bangladesh

Michael S. Steckler[1], Carol A. Wilson[2], Md. Hasnat Jaman[3], Steven L. Goodbred[4], Bar Oryan[5], Céline Grall[1], Scott DeWolf[7], Scott L. Nooner[8], S. Humayun Akhter[9]

1 Lamont -Doherty Earth Observatory of Columbia University, Palisades, NY, United States
2 Department of Geology and Geophysics, Louisiana State University, Baton Rouge, LA, United States
3Department of Geology and Mining, University of Barishal, Barishal, Bangladesh
4 Department of Earth and Environmental Sciences, Vanderbilt University, Nashville, TN, United States
5 Laboratoire de Géologie, Ecole Normale Supérieure, Paris, France.
6 LIENSs, La Rochelle University, La Rochelle, France
7 Department of Environmental Engineering and Earth Sciences, Clemson University, Clemson, SC, United States
8 Department of Earth and Ocean Sciences, University of North Carolina Wilmington, Wilmington, NC, United States
9 Vice Chancellor, Bangladesh Open University, Gazipur, Bangladesh
Contact: steckler@ldeo.columbia.edu

Introduction

Coastal regions worldwide face an ever-increasing sustainability issue as millions continue to migrate to these vulnerable regions susceptible to rising seas, increasing storms, and decimation of ecologically fragile areas. Deltas, the low-lying land at rivers mouths, are particularly sensitive to the delicate balance between sea level rise, land subsidence and sedimentation (e.g., Giosan et al., 2014). Bangladesh and the Ganges-Brahmaputra Delta (GBD) have been highlighted as a region at risk from sea level rise, but reliable estimates of land subsidence have been limited. While early studies in the GBD suggested high rates of relative sea level rise, recent papers estimate more modest rates. However, these estimates represent an aggregate of multiple, spatiotemporally variable processes that are not often separated into their relevant components. Furthermore, values for subsidence are typically taken as mean rates of vertical change and applied across entire delta systems, even where significant variations are well recognized (Passalacqua et al., 2021). Our objective is to better quantify the magnitude and spatial variability of subsidence in the GBD, to better evaluate the processes controlling it and the pattern of relative sea level rise in this vulnerable region.

Methods

To better understand subsidence, we use multiple measurements at different timescales and vertical sensitivity across the coastal zone of SW Bangladesh. At the longest timescales, Grall et al. (2018) used hand-drilled tube wells and a very high resolution seismic line to determine the Holocene-average subsidence rate. Several studies have used 300-600 year old Mosques, Hindu Temples and salt-making kilns to estimate centennial scale subsidence rates (Sarker et al., 2012; Hanebuth et al., 2013, 2021; Chamberlain et al., 2020; Steckler et al., 2022). Becker et al. (2020) analyzed tide and river gauges for decadal scale subsidence rates. We have rehabilitated older GNSS and installed new ones co-located with Rod Surface Elevation Tables-Marker Horizons (RSET-MH) to quantify the balance of subsidence and sedimentation in the coastal zone. The continuous GNSS installed in 2003 and 2012 were mounted on reinforced concrete building roofs. We also utilized a compaction meter array consisting of a set of 6 wells with depths from 20-300 m outfitted with optical fiber strainmeters (referred to as KHLC – the Khulna compaction meter; Steckler et al., 2022; DeWolf et al., in prep.).

Finally, in early 2020 we performed a campaign GNSS survey of 48 concrete Survey of Bangladesh (SoB) geodetic monuments in SW Bangladesh that were installed in 2002. Although only measured at the start and end of the period, the time span between the two measurements is ~18 years enabling us to estimate subsidence over this timespan. Sites were generally occupied for ~24 hrs, although some were established for up to 4 days.

Results

On longer timescales, Grall et al. (2018) find that Holocene averaged subsidence rates increase from the Hinge Zone of the early Cretaceous passive margin seaward (0 – 4.5 mm/yr). The rates from the 300-600 year old archeological sites are 1 – 4 mm/yr, similar to the estimated Holocene rates (Fig. 1; Sarker et al., 2012; Hanebuth et al., 2013, 2021; Chamberlain et al., 2020; Steckler et al., 2022).

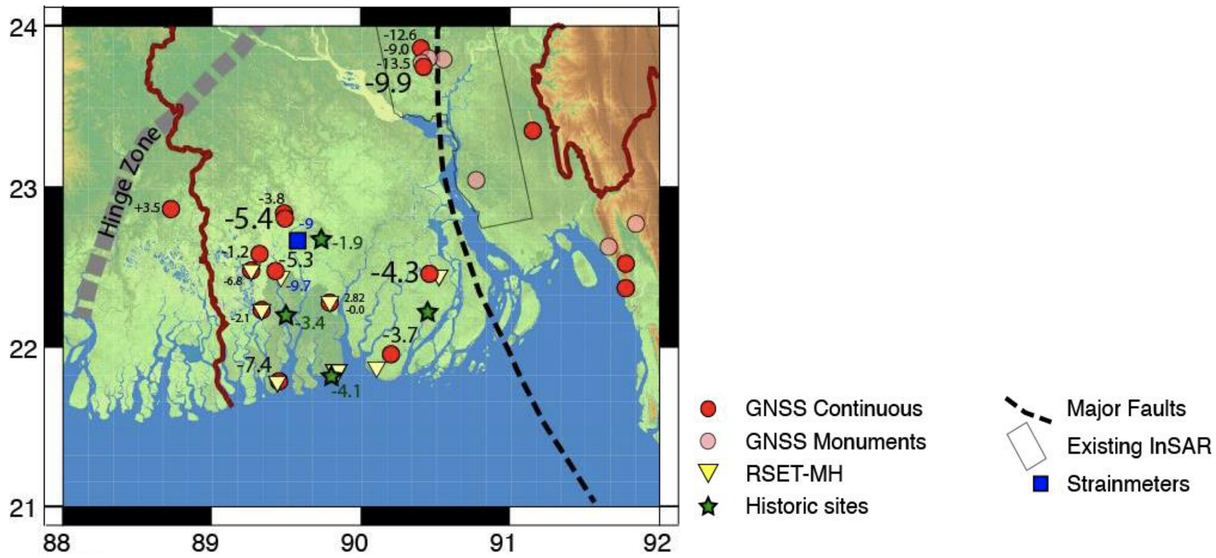

Figure 1 Subsidence rates in coastal GBD west of the deformation front (dashed line). Text size is proportional to the √(time series length) to represent the reliability of the values, except for historic sites. Historic sites values are similar to Holocene average rates in Grall et al. (2018) as are the rates at the easternmost GNSS sites. GNSS farther west rates are slightly higher, especially in the muddy Sundarbans Mangrove Forest. Rapid subsidence is seen in Dhaka, to the north due to groundwater withdrawal.

Decadal measurements from continuous GNSS stations and the tide gauges yield slightly higher subsidence rates of 3-7 mm/y (Fig. 1; Becker et al., 2020; Steckler et al., 2022). We note that while the tide gauges and GNSS rates are similar, the pattern of subsidence differs slightly. The more recent RSET-MH and vertical strainmeters (KHLC) show much higher rates of 9-10 mm/yr (Fig. 1; Bomer et al., 2019; Steckler et al., 2022). These instruments, in sites of active sedimentation, include a new spatial component: shallow subsidence that is not recorded by the deeply rooted river gauges and GNSS. However, it should be noted that continuous GNSS do include deep subsidence, which is not included by the RSET-MH or KHLC. These results combined indicate that there is a considerable amount of ongoing shallow sediment compaction.

Figure 2 shows newly obtained subsidence rates from the campaign GNSS sites. About half the sites yielded very high subsidence rates. We strongly suspect that the monuments at these sites are unstable and have undergone local (shallow) subsidence. To examine the possibility that the very high rates of subsidence recorded are due to monument instability, we reoccupied 4 sites near Barisal in October 2022 during a lull in COVID. Two sites with lower rates yielded linear trends for the three measurements. In contrast, the remaining two sites with higher subsidence rates yielded non-linear subsidence. Thus, we exclude stations with these high rates from further analysis. The remaining sites show an increase in subsidence from the NW to the SE, consistent with estimates of average Holocene subsidence (Grall et al., 2018). However, rates from the campaign stations are still much higher than those from continuous GPS sites. We believe that the continuous building GPS omits very shallow compaction-related subsidence. The remaining 22 sites show an increase in subsidence from the NW to the SE (Fig. 2) consistent the pattern of Holocene subsidence (Grall et al., 2018). However, the rates increase from near zero in the NW to ~14-15 mm/y. The sites in the northwest that show little to no subsidence are where the Holocene sediments are sandy based on tube well drillings, while the remaining coastal sites are dominantly muddy (Fig. 2, bottom right). We note rates from the campaign GNSS are still much higher than those from continuous GNSS sites. We believe that the continuous GNSS buildings omit very shallow compaction-related subsidence.

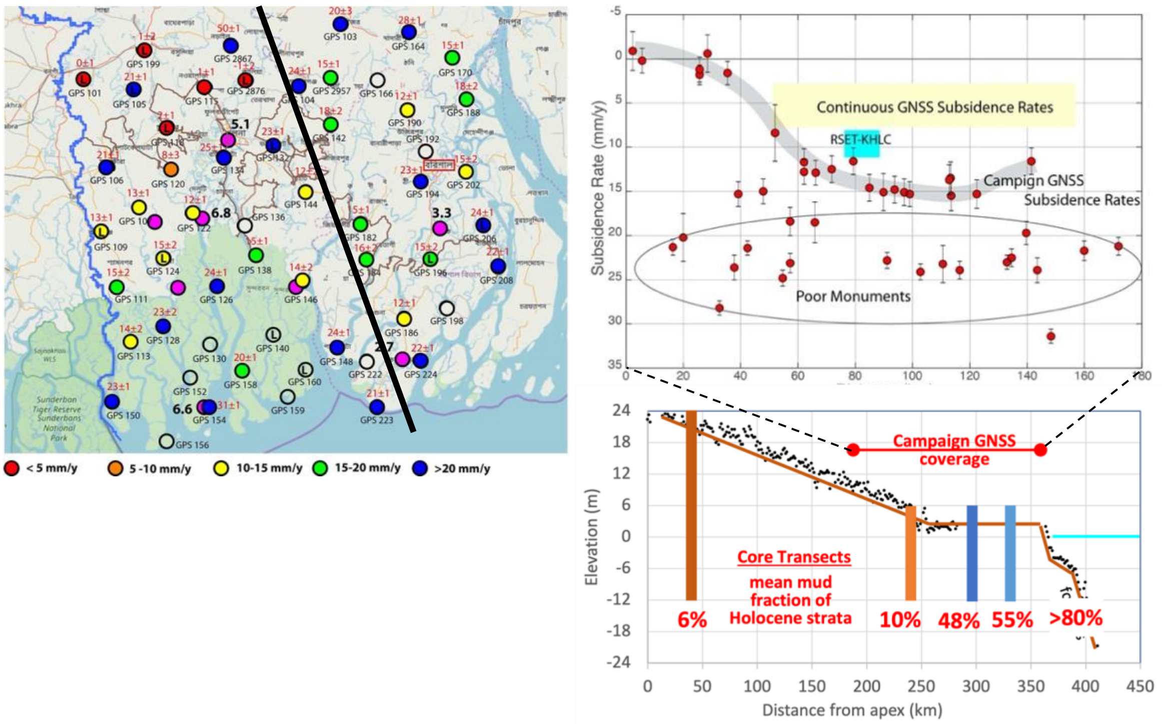

Figure 2 (Left) Position of the 55 geodetic monuments installed by the SoB in SW Bangladesh. We successfully remeasured 47 sites with campaign GNSS. Color-coded dots display the site names and average subsidence rates over ~18 years from 2002 to 2020. An 'L' indicates where leveling was used to link the GNSS to the monument because of poor sky view. Magenta dots are the positions of our continuous GNSS sites with their subsidence rates in bold black (Right) Transect of subsidence rates measured by campaign GNSS along the profile. The gray band shows the average subsidence rates from reliable measurements. We interpret the highest rates as unreliable due to settling or instability of the monuments, confirmed by selected reoccupation of 4 monuments in October 2020. (Lower Right) Plot showing the elevation and lithology change along the profile.

Conclusion

Steckler et al. (2022) found subsidence measurements using different methodologies exhibit variations that show systematic patterns spatially—both in the horizontal and with depth—and temporally (Fig. 3). Overall, subsidence rates are inversely time-dependent, with younger deposits consolidating at greater rates commensurate with their age (i.e., Sadler effect). GNSS subsidence rates near the Lower Meghna River are within about a millimeter/year of the Holocene rates. However, farther west, continuous GNSS subsidence rates are consistently a few mm/y higher than the longer-term rates (for example, the Sundarbans at 7.4 mm/y). We ascribe this difference to greater sediment compaction in the muddier sediments. Very high rates of subsidence are located north of the coastal zone near Dhaka (Fig. 1) due to groundwater extraction. Devices measuring shallow subsidence, the

RSET-MH and KHLC strainmeter, show higher rates of 9-10 mm/y (Fig. 1). These instruments, located in sites of active sedimentation, include shallow subsidence not recorded by either the river gauges or continuous GNSS. These GNSS sites are installed on reinforced concrete buildings which have foundations or footings below ground level. Continuous GNSS do include deep subsidence that occurs below the base of the RSET or strainmeters. The total subsidence at a site with active sedimentation may be equal to the values obtained by the campaign GNSS and may therefore reach values of 14-15 mm/y. Parsing the subsidence rates by depth, we estimate that the deep subsidence from below the Holocene strata is 2-3 mm/y and likely due to isostatic loading (Fig. 3). There is little contribution from sediment compaction at great depths due to the deep incision of the river valleys during the last ice age. Deeper sediments will not start to compact again until the weight of the sediments above them exceed the maximum reached before the incision. At intermediate depths (Fig. 3), perhaps corresponding to the Holocene, we estimate only 1-4 mm/y.

There appears to be a lithologic control north to south (Fig. 2), and in the coastal zone east to west (Fig. 1), whereby sandier sediments impart lower compaction and subsidence in the GBD. Continuous GNSS subsidence rates are consistently a few mm/y higher towards the SW, farther from the sandy main mouth of the Ganges River. Similarly, there is minimal subsidence of the 5 campaign sites to the NW (red circles; Fig. 2). At these sites, Holocene sediments are only ~10% mud, much lower than farther south where they are 48-80% mud.

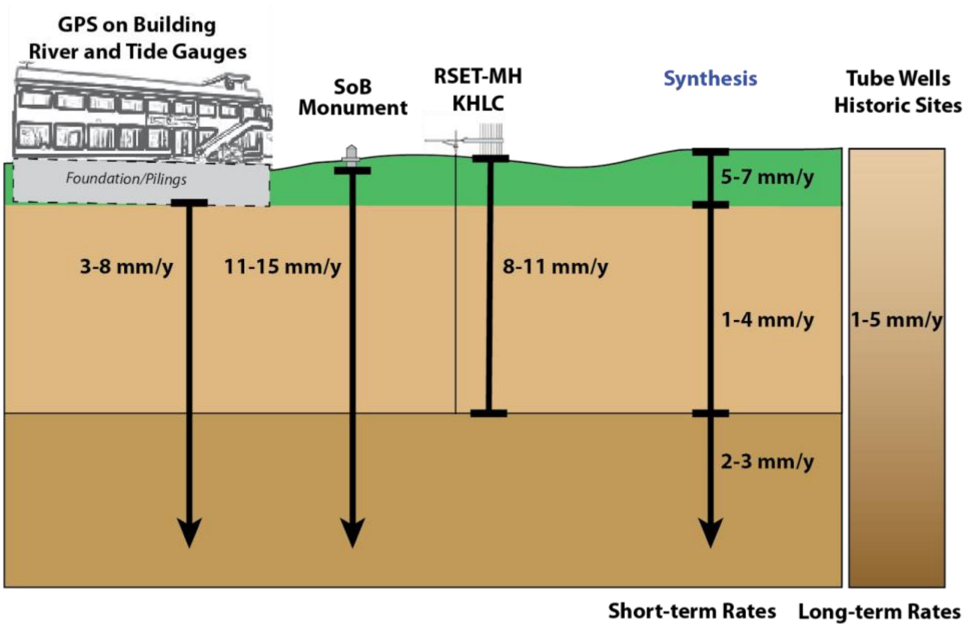

Figure 3 Cartoon presenting a synthesis of subsidence versus depth based on combining measurements from multiple instruments, each of which measure compaction or subsidence over a different depth range. GNSS on building and tide gauges measure subsidence below the building or gauge foundations and miss shallow compaction. The RSET-MH and KHLC measure compaction above the base of their instruments. The campaign GNSS on SoB monuments measures both shallow and deep subsidence. Combining the results, the synthesis column shows a preliminary estimate of subsidence in each depth range. The long-term rates correspond to the sum of the two deeper brown layers.

References

Bahr, D.B., Hutton, E.W.H., Syvitski, J.P.M., Pratson, L.F., (2001). Exponential approximations to compacted sediment porosity profiles. Computers & Geosciences 27, 691–700.

Becker, M., F. Papa, M. Karpytchev, C. Delebecque, Y. Krien, J.U. Khan, V. Ballu, F. Durand, G. Le Cozannet, A.K.M.S. Islam, S. Calmant, C.K. Shum (2020). Water level changes, subsidence, and sea level rise in the Ganges–Brahmaputra–Meghna delta, Proceedings of the National Academy of Sciences, 117 (4) 1867-1876; doi:10.1073/pnas.1912921117.

Bomer, E.J., C.A. Wilson and D.K. Datta, (2019). An Integrated Approach for Constraining Depositional Zones in a Tide-Influenced River: Insights from the Gorai River, Southwest Bangladesh, Water 11, 2047; doi:10.3390/w11102047

Chamberlain, E.L., S.L. Goodbred, R. Hale, M.S. Steckler, J. Wallinga, C. Wilson (2020). Integrating geochronologic and instrumental approaches across the Bengal Basin, Earth Surface Processes and Landforms, 45, 56-74., https://doi.org/10.1002/esp.4687.

Giosan, L, J. Syvitski, S. Constantinescu and J. Day (2014). Protect the world's deltas. Nature 516, 31–33.

Grall, C., M.S. Steckler, J.L. Pickering, S. Goodbred, R. Sincavage, C. Paola, S.H Akhter, V. Spiess (2018). A base-level stratigraphic approach to determining Holocene subsidence of the Ganges–Meghna–Brahmaputra Delta plain. Earth and Planetary Science Letters, Earth and Planetary Science Letters 499, 23–36, 10.1016/j.epsl.2018.07.008.

Hanebuth, T.J.J., Kudrass, H.R., Linstaedter, J., Islam, B., Zander, A.M., (2013). Rapid coastal subsidence in the central Ganges–Brahmaputra Delta (Bangladesh) since the 17th century deduced from submerged salt-producing kilns. Geology 41 (9), 987–990. http://dx.doi.org/10.1130/G34646.1.

Hanebuth, T.J.J., Kudrass, H.R., Zander, A.M., Akhter, H.S., Neumann-Denzau, G., Zahid, A., (2021). Stepwise, earthquake-driven coastal subsidence in the Ganges–Brahmaputra Delta (Sundarbans) since the eighth century deduced from submerged in situ kiln and mangrove remnants. Nat. Hazards.

Passalacqua, P., Goodbred, S., Giosan, L., Overeem, I., (2021). Stable ≠ Sustainable: Delta dynamics versus the human need for stability, Earth's Future. 10.1029/2021EF002121

Sarker, M.H., Choudhury, G.A., Akter, J., Hore, S.K., (2012). Bengal Delta Not Sinking at a Very High Rate. Daily Star (23rd December 2012).

Steckler, M.S., B. Oryan, C.A. Wilson, C. Grall, S.L. Nooner, D.R. Mondal, S.H. Akhter, S. DeWolf, S.L. Goodbred, Synthesis of the Distribution of Subsidence of the Lower Ganges-Brahmaputra Delta, Bangladesh, Earth-Science Reviews, 224, 103887, doi:10.1016/j.earscirev.2021.103887.

Proc. IAHS, 382, 815–819, 2020
https://doi.org/10.5194/piahs-382-815-2020

Dutch national scientific research program on land subsidence: Living on soft soils – subsidence and society

Esther Stouthamer[1], Gilles Erkens[7,1], Kim Cohen[1], Dries Hegger[2], Peter Driessen[2], Hans Peter Weikard[6], Mariet Hefting[4], Ramon Hanssen[5], Peter Fokker[8], Jan van den Akker[9], Frank Groothuijse[3], and Marleen van Rijswick[3]

[1]Department of Physical Geography, Utrecht University, Princetonlaan 8A, 3584 CB Utrecht, the Netherlands
[2]Copernicus Institute of Sustainable Development, Utrecht University, Princetonlaan 8A, 3584 CB Utrecht, the Netherlands
[3]Utrecht University, Centre for Water, Oceans and Sustainability Law, Newtonlaan 201, 3584 BH Utrecht, the Netherlands
[4]Department of Environmental Biology, Utrecht University, Padualaan 8, 3584 CH Utrecht, the Netherlands
[5]Faculty of Civil Engineering, Delft University of Technology, 2628 CD Delft, the Netherlands
[6]Department of Social Sciences, Wageningen University, Hollandseweg 1, 6706 KN Wageningen, the Netherlands
[7]Deltares Research Institute, Daltonlaan 600, 3584 BK Utrecht, the Netherlands
[8]TNO-Geological Survey of The Netherlands, Princetonlaan 6, 3584 CB Utrecht, the Netherlands
[9]Wageningen Environmental Research, Droevendaalsesteeg 3, 6708 PB Wageningen, the Netherlands

Correspondence: Esther Stouthamer (e.stouthamer@uu.nl)

Published: 22 April 2020

Abstract. In the Netherlands land subsidence is a continuously ongoing process. Consequently, an increasing number of people and economic assets are exposed to subsidence, damage costs are soaring, and flood risk and greenhouse gas emissions are increasing. In some areas tipping points have already been reached, where current land-use can no longer be maintained without considerable costs, underlining the urgency to take action.

Together with a consortium consisting of universities, research institutes, governmental agencies, public and private partners we have developed a national, multidisciplinary research programme aiming to develop an integrative approach to achieve feasible, legitimate and sustainable solutions for managing the negative societal effects of land subsidence, connecting fundamental research on subsidence processes to socio-economic impact of subsidence and to governance and legal framework design.

The program is designed to co-create insights that help to effectively mitigate and adapt to subsidence within the Netherlands by making major improvements in measuring and modeling the processes and consequences of subsidence, identifying, developing and critically evaluating control measures and designing governance and legal approaches that facilitate their implementation. Hereto we will develop (a) new satellite-based technology to measure, attribute and monitor subsidence, (b) solid understanding of the interacting multiple processes contributing to total subsidence, (c) sophisticated physical and economic numerical models to predict human-induced subsidence rates and impacts, and (d) implementation strategies that go beyond technical measures, to strengthen governance and financing capacities as well as legal frameworks. This fully integrated approach deals with all impacts of land subsidence on society and the economy.

1 Land subsidence in the Netherlands

In the Netherlands land subsidence is a continuously ongoing process due to (1) drainage of peatlands and areas reclaimed from the sea, (2) expansion of built-up areas and the infrastructural network on soft soil, (3) salt mining and gas extraction (Fig. 1). These human-induced drivers result in relatively high rates of subsidence ($\sim$ 0.5–10 cm yr^{-1}. An increasing number of people and economic assets are exposed to subsidence and damage costs are soaring, accumulating to over EUR 5 billion for infrastructure alone till 2050 (Van den Born et al., 2016). Moreover it gives rise to serious safety issues due to increased flood risks and in case of subsidence as a result of peat oxidation – causes considerable greenhouse gas (GHG)emissions which will further contribute to climate change. Because the shallow subsurface of $\sim$ 50 % of the Netherlands and $\sim$ 80 % of the low lying western and northern part contains organic material (peat and organic clay) (Koster et al., 2018), subsidence rates will increase further due to climate change (> oxidation and GHG emission). In some areas (e.g. parts of polder Groot-Mijdrecht, Zuidplaspolder) tipping points have already been reached, where current land use can no longer be maintained without considerable costs, underlining the urgency to take action.

During the last decades a range of mitigation and adaptation measures have been developed, however these are mostly ad-hoc applied local measures in response to incidents. This is caused by the fact that there is still little understanding of the exact rates and processes causing subsidence. That makes that timeliness of implementing measures and their effectiveness are hard to assess by land owners and responsible authorities, stalling implementation of measures at the large scale on which the problem is occurring. The implementation of measures for mitigating or adapting to land subsidence poses governance, economic and legal challenges. Mitigating measures may to some extent enable the continuation and reconciliation of certain land-use functions such as agriculture and nature conservation, but this is not without limits. At some point political choices might need to be made that deviate drastically from existing and historical policies and impact numerous interests and stakeholders.

Subsidence and GHG emissions *can* be mitigated by smart and efficient management strategies regarding e.g. spatial planning, extraction of hydrocarbons and groundwater, groundwater tables, and land use. However, this requires thorough knowledge on the (interacting) processes causing subsidence, its impacts and possible integrated solutions.

2 National scientific research program

The threat of land subsidence, the knowledge hiatus on process-interplays causing it, and lacking mid- to long-term coping strategies, ask for an integrated research program that addresses the issue of land subsidence in a holistic way, whereby insights about physical-chemical-biological system functioning, development, evaluation and implementation of measures as well as an assessment of their governance and legal implications co-evolve.

Therefore, together with a consortium consisting of 3 universities (Utrecht University, Delft University of Technology, Wageningen University), research institutes (Deltares, TNO-Geological Survey of The Netherlands, Wageningen Environmental Research), governmental agencies, public and private partners we have developed a national, multidisciplinary research programme (runtime: 2020–2024) *aiming* to develop an integrative approach to achieve feasible, legitimate and sustainable solutions for managing the negative societal effects of land subsidence, connecting fundamental research on subsidence processes to socio-economic impact of subsidence and to governance and legal framework design. The program is to contribute significantly to the ability to mitigate and adapt to subsidence in populated, governed deltas in the short and in the long term and via management of subsidence, lower GHG emissions and decrease risks and looming damage for low-lying delta plains under climate change.

2.1 Program objectives

The underlying scientific challenges and objectives of this program are to:

1. tailor latest satellite-based radar technology to measure and monitor ground movement at high spatio-temporal resolutions, integrate this with inverse-modelling techniques to disentangle total shallow and deep subsidence, anthropogenic and natural contributions, and offer conscious choices when recombining the geophysically separated components in subsidence projections (spatial forecasts);

2. understand and quantify all mechanisms causing subsidence and associated GHG emission currently at play in the Netherlands, with attention to interrelationships and process-separation uncertainties, offering models of the processes affecting the aerated topsoil and actively consolidating subsoil, which are calibrated at experiment plot scale and recalibrated to coarser cell-scales of the spatial forecasts;

3. develop a set of reliable, alternative-scenario-sensitive spatial forecasts for actual and projected subsidence rates, including modules that convert subsidence rates (mm yr^{-1}) to costs (EUR yr^{-1}) and use these as operational tools to develop strategies to convey results of cost-benefit analyses to decision makers. The step to costs (pricing) requires to develop algorithms to (i) account for risk of structure-failure under differentiated subsidence, (ii) assessing impacts on agriculture and, (iii) integration of costs and benefits per potential mea-

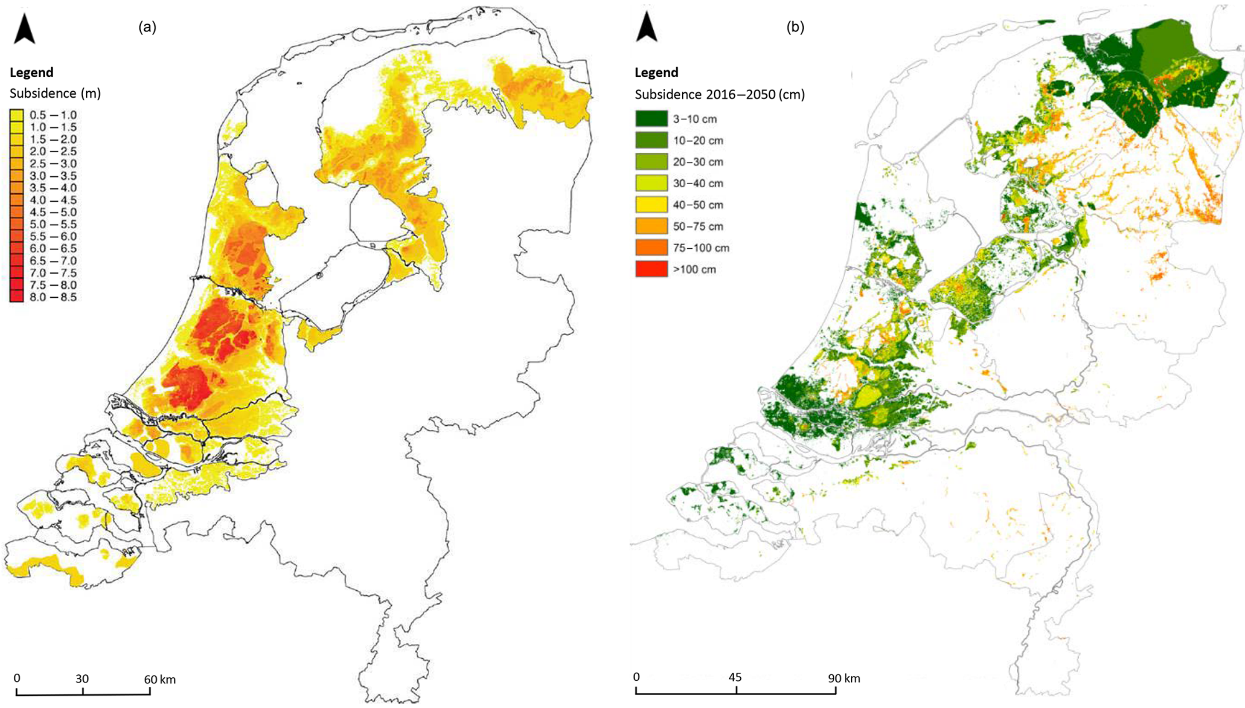

Figure 1. **(a)** Land subsidence over the last 1000 years in the coastal peat lands of the Netherlands due to drainage, loading and peat mining (Erkens et al., 2016). **(b)** Prediction of the amount of land subsidence for the coming decades, showing land subsidence of soft soils, salt mining and gas extraction (Erkens et al., 2017).

sure (implementation costs, damage, social/health risks, GHG emissions);

4. develop effective and legitimate subsidence mitigation strategies, making use of the findings on drivers of subsidence and its socio-economic impact, supported by governance approaches and the necessary financial and legal frameworks to enable successful selection and implementation of these future-proof, context-sensitive management strategies for intensively used agro-urban delta plains.

2.2 Program set-up

The program consists of four scientific work packages and a fifth one on knowledge utilization. To enable direct use of results in policy making, the program covers the 6M approach in dealing with subsidence (Erkens and Stouthamer, 2020): subsidence measuring and analysis of mechanisms, quantifying impacts, deliberating measures and evaluating performance (Figs. 2–3). Each work package delivers knowledge of direct use to activities of the linked step in the policy cycle.

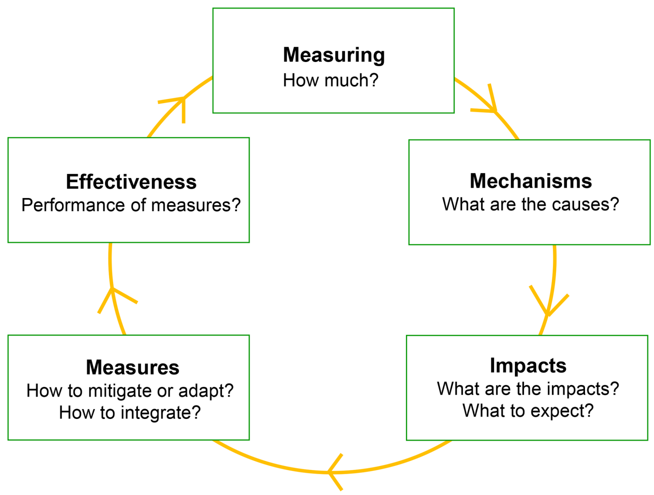

Figure 2. The program framework and approach link up with the policy cycle to ensure uptake of the research results in policy and to facilitate implementation of effective measures (after: Erkens and Stouthamer, 2020).

2.2.1 Work packages

WP1 – Measuring and monitoring of subsidence rates at local and regional scales: will utilize InSAR satellite-based radar technology at high spatio-temporal resolutions and integrate this with geophysical modelling techniques, to disentangle total ground movement into shallow and deep and anthropogenic and natural contributions, including sea-level rise related subsidence

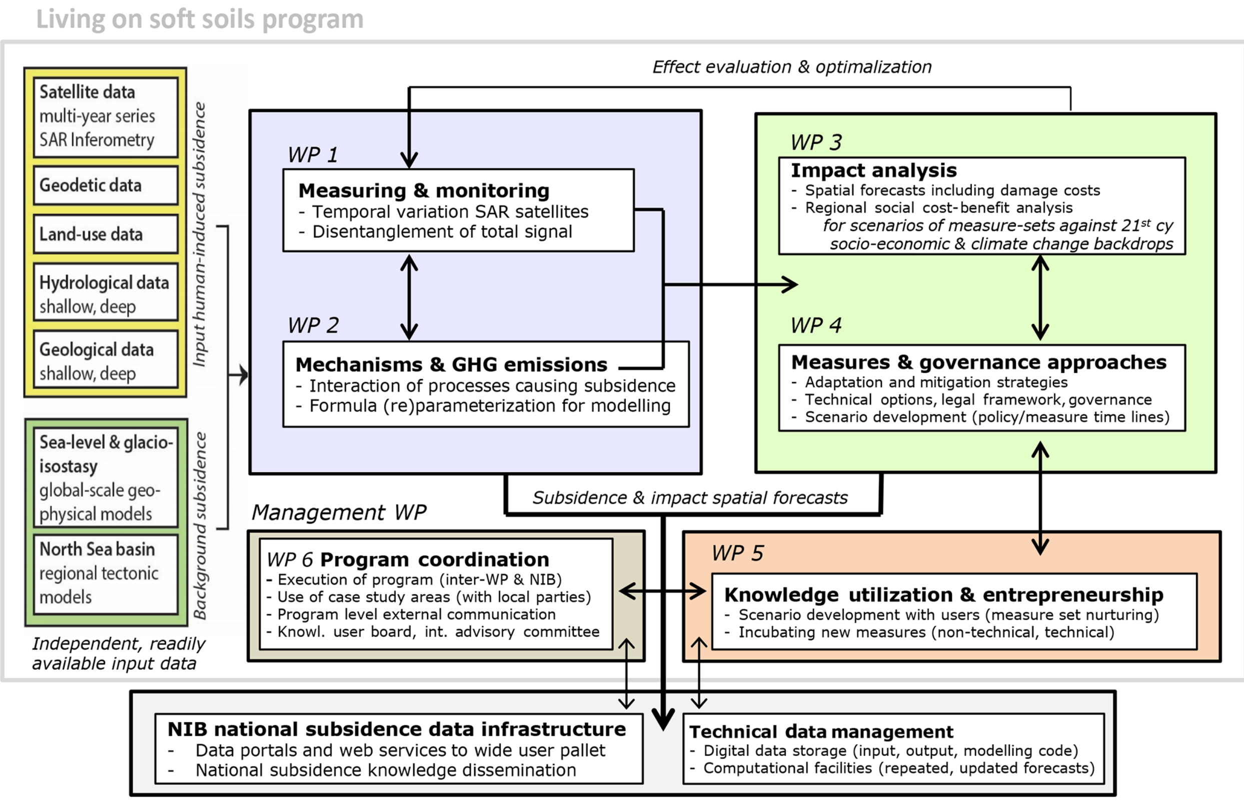

Figure 3. Program structure. We will follow an iterative approach whereby insights from the different work packages feed into one another and enrich the knowledge needs addressed by other WPs.

components. InSAR techniques will be developed to monitor soft soil subsidence in agricultural and urban areas, with disentangled signals of groundwater, salt and hydrocarbon extractions (inverse modelling) and glacio- and hydro-isostasy (GIA modelling, gravimetry, background regional relative sea-level rise).

WP2 – Mechanisms and GHG emissions: aims to unravel, better understand and quantify the interacting subsidence processes such as peat oxidation with associated GHG emissions, compaction, shrinkage, creep, and examine the environmental impact of subsidence mitigation measures. It includes parameterization and calibration of process models used to analyze and forecast subsidence.

WP3 – Impact analysis: focusses on predictive modelling by integration of process models in one numerical framework to predict subsidence under different management scenarios, and the development of new methods to estimate subsidence-related damage to infrastructure, buildings and agriculture, besides GHG emissions, as input for an socio-economic cost-benefit analysis (SCBA, converting mm yr^{-1} to EUR yr^{-1}). This work package has a focus on numerical model development and (big) data analyses and includes geomodelling, material science research and economic modeling.

WP4 – Measures and governance approaches: aims to (i) identify suitable mitigation, adaptation and compensation measures, (ii) develop economic and financial tools aiming at supporting parties to carry the costs of damage and/or implementation of measures, (iii) provide recommendations for strengthening governance capacities for dealing with existing and new challenges (e.g. drought, salinization due to sea-level rise) in water management and spatial planning, (iv) develop equitable and legitimate legal frameworks to effectively implement new strategies of dealing with subsidence.

WP5 – Knowledge utilization and entrepreneurship: will translate the scientific results to practice in close cooperation with knowledge-users and entrepreneurs; design and development of innovative mitigation and management strategies under different scenarios of socio-economic and climatic circumstances.

Knowledge utilization is an integral part of this research program. Knowledge-users are part of the consortium and stakeholders in case study areas will be actively involved.

2.2.2 Expected deliverables

As results, the program is expected to deliver:

1. Technology for satellite-based subsidence monitoring, interpretation and use in forecasting (WP1);

2. Improved empirical understanding and knowledge integration on individual processes and their interactions and feedbacks driving soft soil subsidence, including upscaled calibration allowing to implement it in spatial models (WP2), and operationalize it for damage quantifications and cost-benefit analysis (WP3);

3. Open-source spatial subsidence models and forecast maps (scenarios), that will support decision-making and policy-design (WP3–4), developed aligned with existing (TNO-GSN) and newly launched (NIB) national data infrastructure, to feed, host and reiterate such modelling.

4. Technical and economic measures to mitigate and adapt to subsidence.

5. Governance and legal strategies that facilitate the implementation of proposed measures: policy and decision support tools to manage subsidence.

Data availability. No data sets were used in this article.

Author contributions. ES wrote the paper. GE commented on an earlier draft of this paper. This paper is based on the research proposal “Living on Soft Soils: Subsidence and Society” (NWO-NWA) that was initiated and coordinated by ES. All authors of this paper contributed to the design and writing of the research proposal.

Competing interests. The authors declare that Gilles Erkens is member of the editorial board of this special issue but has not reviewed this paper, nor has he influenced the publication decision process.

Special issue statement. This article is part of the special issue “TISOLS: the Tenth International Symposium On Land Subsidence – living with subsidence”. It is a result of the Tenth International Symposium on Land Subsidence, Delft, the Netherlands, 17–21 May 2021.

Financial support. The Dutch National Scientific Research Program on Land Subsidence: Living on Soft Soils – Subsidence and Society will be primarily funded by the Dutch scientific organization (NWO-NWA, grant: NWA.1160.18.259), and will be co-funded and supported by 17 consortium partners (see above).

References

Erkens, G. and Stouthamer, E.: The 6M approach to land subsidence, Proc. IAHS, this volume, 2020.

Erkens, G., Van der Meulen, M. J., and Middelkoop, H.: Double trouble: Subsidence and CO_2 respiration due to 1,000 years of Dutch coastal peatland cultivation, Hydrogeol. J., 24, 551–568, 2016.

Erkens, G., Stafleu, J., and Van den Akker, J. J. H.: Bodemdalingvoorspellingskaarten van Nederland, versie 2017, Deltares rapport klimaateffectatlas, 2017.

Koster, K., Stafleu, J., Cohen, K. M., Stouthamer, E., Busschers, F. S., and Middelkoop, H.: 3D distribution of organic matter in coastal-deltaic peat: implications for subsidence and CO_2 emissions by human induced peat oxidation, Anthropocene 22, 1–9, https://doi.org/10.1016/j.ancene.2018.03.001, 2018.

Van den Born, G. J., Kragt, F., Henkens, D., Rijken, B., Van Bemmel, B., and Van der Sluis, S.: Dalende bodems, Stijgende kosten, Report Planning Agency for the Environment (PBL), report nr. 1064, 93 pp., 2016.

How to reach societal impact with land subsidence research

Bernardien Tiehatten[1,2], Esther Stouthamer[1], Gilles Erkens[1,3]

1 Faculty of Geosciences, Utrecht University, 3584 BK, Utrecht, the Netherlands
2 Ambient Advies, Lange Hagelstraat 30, 3531 BK, Utrecht, the Netherlands
3 Deltares Research Institute, Daltonlaan 600, 3584 BK, Utrecht, the Netherlands
Correspondence: Bernardien Tiehatten (b.tiehatten@ambient.nl)

Introduction

Many low-lying river deltas, home to over 500 million people, host vast areas of intensely used land surface that are subsiding due to natural causes and human-induced activities. The physical consequences of subsidence are manifold: relative shallowing of groundwater tables, salinization of ground and surface water, emission of greenhouse gasses (GHG), damage to buildings and infrastructure, and increased flood risk, flood water depth and flood duration. For delta societies this leads to serious economic loss through reduced agricultural yields, arable land loss, rising costs of maintenance and repair of lost assets, and forced sectoral divestments. For the Netherlands, economic damage of progressive subsidence could add up to 22 billion Euros by 2050 with continuing current policy (Van den Born et al. 2016).

An urgent need exists to strengthen the capacity to develop (innovative) management strategies mitigating subsidence on both local and regional spatial scales and on the short- to long-term. This requires fundamental knowledge on causes, mechanisms and rates of land subsidence, scenario forecasts and action perspectives that can be applied by policy makers and other stakeholders to take well-informed and fair decisions (Erkens et al., 2015; Erkens & Stouthamer, 2020, Stouthamer et al., 2020).

The research programme Living on Soft Soils – subsidence and society (LOSS) is an integrated research programme that addresses the issue of land subsidence in a holistic way, whereby insights about physical-chemical-biological system functioning, development, evaluation, and implementation of measures as well as an assessment of their governance and legal implications co-evolve (Stouthamer et al., 2020). The overall aim of this programme is to develop an integrative approach to achieve feasible, legitimate, and sustainable solutions for managing the negative societal effects of land subsidence. LOSS connects fundamental research on subsidence processes to socio-economic impact of subsidence and to governance and legal framework design.

With the LOSS programme and other research programmes, The Netherlands invests heavily in scientific and applied scientific research on land subsidence. The challenge is to implement the resulting (fundamental) knowledge in practice and to reach societal impact. But how can scientific programmes go about this challenge and what is needed to be successful in this regard? In this extended abstract we describe how, in the case of the Living on Soft Soils (LOSS) programme, this challenge is addressed and what we have learned in the past three years.

Theory of Change and the Impact pathway

LOSS is a programme within the Dutch national science agenda (NWA) which is coordinated by the Dutch Research Council (NWO). NWA is organized around societal focus areas and strives to ensure that (scientific) knowledge developed in the funded programmes is used to tackle social challenges. To reach 'knowledge utilisation' and 'societal impact' (Barnett & Gregorowski, 2013; NWO, 2022) there is a new standard for programme set-ups. In this set-up, programmes must define their intended societal impact, and their plan to achieve this, in the proposal. This standard is now increasingly followed by other international programmes, and it is expected that it will become more common practice in Dutch and international research funding (Barnett & Gregorowski, 2013; NWO, 2022; van Droogе et al. (2022)).

NWA developed guidelines to incorporate societal impact and knowledge utilisation in the proposal and throughout the research; the Theory of Change. The Theory of Change provides guidelines for proposals on describing how and when research and stakeholders are expected to bring about a desired change in a specific context (Barnett & Gregorowski, 2013; NWO, 2022). The theory consists of a problem analysis and an impact pathway design (Fig. 1).

The first step is to analyse and describe the problem and underlying causes. This step contributes to creating a joint vision and thus a joint interest in the research. Because there are (or can be) different views, backgrounds, and experiences, this is best done with all stakeholders involved. Being aware of (sometimes implicit) assumptions of different stakeholders is important in this process. These assumptions should be made explicit so that all stakeholders know assumptions made by their colleagues or other stakeholders. By identifying the problem, the causes and assumptions of knowledge needs will become clear. These knowledge needs are then translated into desired research output for the overall programme and the individual researchers.

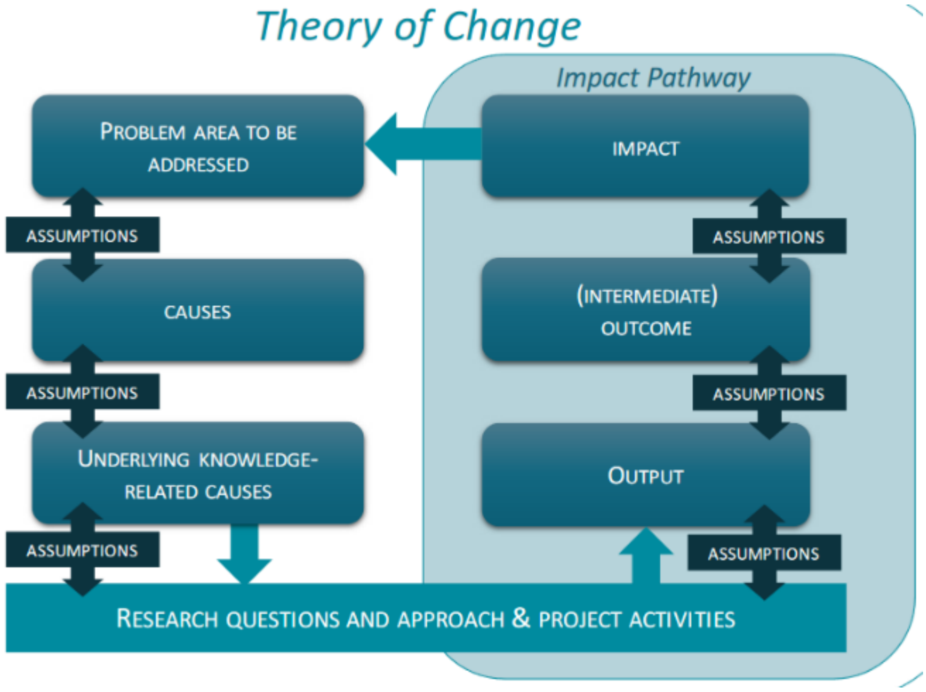

Figure 1 Theory of Change (NWO, 2022). The method aims to reach societal impact and offers tools to (research) programmes for a structured approach dealing with the challenge of facilitating and stimulating the use of scientific results in practice. It starts with a problem definition resulting into research outputs. The impact pathway defines the steps to optimise the changes of societal impact.

Impact pathway

By drafting an Impact Pathway scheme, the steps and efforts of stakeholders needed to reach the desired societal change, are determined. The Impact pathway reasons back from the desired impact and defines which research outcomes are needed for the desired impact and which research outputs are needed for the research outcome (see Fig. 1).

In the Impact Pathway scheme, impact is defined as changes that are in part or entirely the consequence of knowledge and expertise generated by research. These changes can be behavioural, cultural, economic, industrial, ecological, or social. Who needs to do what differently if the desired impact were to be achieved, is indicated in de outcome. The outcomes are generated by stakeholders and (partly) in collaboration with the programme. Outcomes require the research outputs as input (Fig. 2). Research outputs are directly generated by a research programme and may consist of scientific papers, new articles, or numerical models.

Figure 2 Impact pathway; from research outputs via research outcomes to impact (source: NWO). To reach impact, stakeholders need to change behaviour. By determining outcomes, it becomes clear who needs to do what differently. Outputs then are generated to support those different stakeholders (the who) to be able to change behaviour (the what) - stakeholders use the results of the programme.

Stakeholders' role to reach societal impact: lessons learned from the LOSS programme

The desired societal impact of the LOSS programme is 'contributing to knowledge-based, well-informed decision making on land subsidence' and outcomes and outputs are set to contribute to this desired impact (see Fig.2). LOSS aims to optimise the flow from output to outcome. One strategy to do so was working with stakeholders to peel back integral societal issues into research questions and via outputs and outcomes back to societal answers. To stimulate and facilitate working together, LOSS aims to create an open environment and the right preconditions. In the next paragraphs we describe how LOSS has been doing this and what we have learned writing the proposal and during the course of the research.

Five stakeholder groups

Stakeholders were actively involved in the development of the proposal to tailor the structure of the programme to optimise (intended) research output and the coordination between output and outcome. The problem definition and shared sense of urgency did not need much attention. Attention for the (consequences of) land subsidence was already established and there was a joint vision that research into physical-chemical-biological system functioning, development, evaluation, and implementation of measures as well as an assessment of their governance and legal implications were needed.

However, it became clear in this early stage that although the overall vision and interests were aligning, stakeholders had different interests, needs, expertise and roles regarding knowledge development and dissemination. As a result, the LOSS programme distinguished five 'stakeholder groups': universities, knowledge institutes, consultancies, governments, and society.

Stakeholders focus on output or outcome

Some stakeholders have a focus on research output, where others are more focussed in research outcome or even on impact. Fig. 3 shows that all stakeholders are essential in the impact pathway, but that they have their own role in reaching societal impact. The differences in interests, needs, expertise and roles regarding knowledge development and dissemination are essential, since the different roles in the pathway ask for these differences. A lesson learned from setting up the LOSS programme is that an early engagement of stakeholders groups specifically for research output, outcome, and impact, improves the research uptake during and after the programme execution.

Universities and (applied) research institutes are output-focussed and develop knowledge and techniques and apply this knowledge (through models) mostly on national or international scale. In this, universities are mostly concerned with fundamental understanding, while (applied) research institutes mainly translate this into possible consequences. For example: calculation rules are typically developed by (applied) research institutes, while the process understanding of these rules mostly comes from universities.

Both universities and institutes are essential to translating societal issues into societal questions and research questions since comprehension or recognition of the problem is needed to define research questions. Universities and (applied) research institutes develop new knowledge, but generally have only limited capacity for the full dissemination of knowledge.

Consultancies and governments are more outcome focussed. They use and disseminate the knowledge to understand and untangle (provincial or municipality scaled) problems, providing them with a knowledge base for policy development. For example, civil servants that advise policy makers or politicians, need fundamental knowledge when they are faced with problems such as land subsidence to understand the problem at hand. This fundamental knowledge about mechanisms or impact of land subsidence most likely comes in the form of calculation rules, scientific explanations in (scientific) papers and numerical models. The civil servant receiving this information therefore needs to have a scientific background in the relevant field to be able to use this information. This is rarely the case. Consultancies have more possibilities to specialize and consequently do have the knowledge needed. The lesson learned in LOSS: If a research programme aims to generate long-lasting societal impact, it is essential to include partners such as consultancy bureaus, that translating fundamental knowledge into studies used in policy design and implementation.

LOSS stakeholder involvement

LOSS has been organising stakeholders-researchers meetings at least twice a year, one-on-one meetings and site visits where stakeholders and researchers are stimulated to show, share, and discuss needs and expectations. The goal is to enable stakeholders to follow and monitor research output and talk about their wishes and needs regarding the research output, allowing for intermediate adjustments in the research. It also aims to optimise co-creation and collaboration between all stakeholders and in extension optimise the chances of knowledge utilisation. This approach also contributed with incorporating stakeholders needs into the programmes proposal. For example, the ministries need for a detailed land subsidence model to formulate realistic objectives (rail)ways.

Additionally, researchers help governments to disentangle the complex societal problems into comprehensible (research) questions.

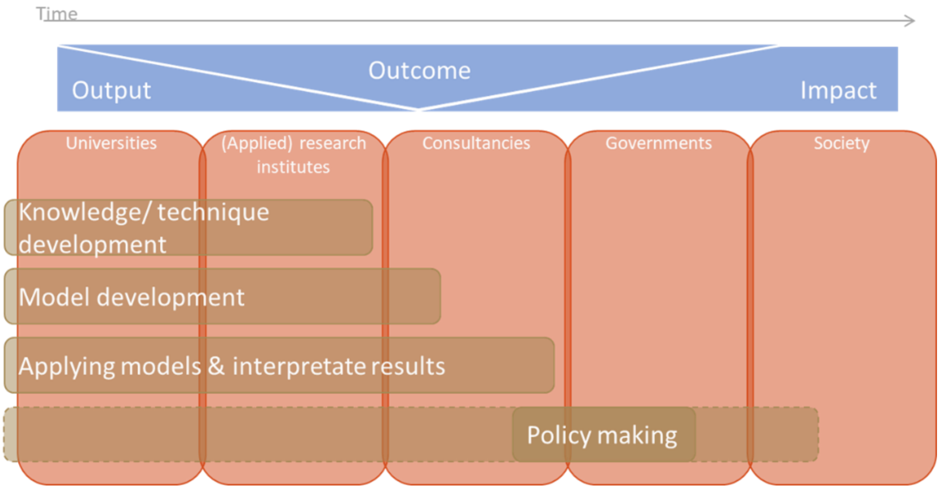

Figure 3 Stakeholder groups (pink) and roles (brown bars) in realizing the impact pathway (blue bar). Every stakeholder group is essential in the pathway from output to impact and have a specific role. For example: To give good advice to the government about possible and effective measures, consultancies need state of the art models and knowledge. Consultancies need universities and (applied) research institutes to do (fundamental) research and develop knowledge that can help them improve their models. Universities and (applied) research institutes need consultancies to bring knowledge into practice. In the end, society benefits when governments use up to date knowledge to make their policies effective and efficient.

Concluding remarks

How can scientific programmes go about the challenge of (applied) research utilisation in practice and, by extension, reach societal impact? Specifically for the LOSS research programme we conclude three key factors for success:

- A joint problem statement and articulation resulting in a research proposal including an impact pathway; The Theory of Change and Impact Pathway scheme give a valuable framework to structure research programmes in such a way that the chances of contributing to societal impact are optimised.

- Assigning roles to stakeholders, based on interests, needs, expertise regarding knowledge development and dissemination; For each element in the Impact Pathway scheme, output, outcome, and impact, different stakeholders group are relevant, they should be identified and included.

- Follow the Impact Pathway scheme as a guideline throughout the project, and update and adjust when needed. During the LOSS programme it became clearer that the role of consultancies in the knowledge chain is essential, since they are the link between (applied) research institutes and policy makers and are crucial for the pivot point 'outcomes'. We think that societal impact cannot be achieved if this group is not included. Simultaneously LOSS experienced that involving consultancies in research programmes is a challenge and needs more attention.

This approach is likely to be also successful outside the Dutch context and culture. Most international research programmes are rooted in societal issues and aim to reach societal impact. Also, the different stakeholder groups and their role in knowledge development, dissemination and implementation are not typically Dutch. Because the emphasis of the method lies societal impact through co-creation and durable engagement of stakeholders, the Theory of Change, Impact Pathway scheme and three key factors for success would also be relevant elsewhere.

Acknowledgement

The research presented here is part of the NWA project Living on Soft Soils: Subsidence and Society (grantnr.: NWA.1160.18.259).

References

Barnett, C., & Gregorowski, R. (2013). Learning about theories of change for the monitoring and evaluation of research uptake. https://www.ids.ac.uk/publications/learning-about-theories-of-change-for-the-monitoring-and-evaluation-of-research-uptake/

van Drooge, L., Spaapen, J. Evaluation and monitoring of transdisciplinary collaborations. J Technol Transf 47, 747–761 (2022). https://doi.org/10.1007/s10961-017-9607-7

Erkens, G., Bucx, T., Dam, R., de Lange, G., and Lambert, J. (2015). Sinking coastal cities, Proc. IAHS, 372, 189–198, https://doi.org/10.5194/piahs-372-189-2015

Erkens, G., & Stouthamer, E. (2020). The 6M approach to land subsidence. Proceedings of the International Association of Hydrological Sciences, 382, 733-740.

NWO (2022). Impact Plan Approach. Retrieved from https://www.nwo.nl/en/impact-plan-approach

Stouthamer, E., Erkens, G., Cohen, K.M., Hegger, D.L.T., Driessen, P.P.J., Weikard, Hans-Peter, Hefting, M., Hanssen, R.F., Fokker, P.A., van den Akker, J., Groothuijse, F.A.G. & van Rijswick, H.F.M.W. (2020). Dutch National Scientific Research Program on Land Subsidence - Living on Soft Soils - Subsidence and Society. Proc. IAHS, 382, 815–819, https://doi.org/10.5194/piahs-382-815-2020

Proc. IAHS, 382, 361–365, 2020
https://doi.org/10.5194/piahs-382-361-2020

Land subsidence due to groundwater extraction and tectonic activity in Pingtung Plain, Taiwan

Duc-Huy Tran and Shih-Jung Wang

Graduate Institute of Applied Geology, National Central University, Taoyuan City, 32001, Taiwan

Correspondence: Shih-Jung Wang (sjwang@ncu.edu.tw)

Published: 22 April 2020

Abstract. Pingtung coastal plain, located at the active convergent boundary between Philippine Sea Plate and Eurasian Plate, is one of the most active areas regarding tectonic deformation in Taiwan. Groundwater over-pumping for aquaculture along the coast area of Pingtung plain induced a serious land subsidence problem for decades. How much land subsidence contributed by tectonic activity and groundwater pumping is a crucial issue for tectonic study and groundwater management in this area. This study collected the data in different fields and proposed a conceptual model to calculate the quantities of land subsidence caused by natural (tectonic) and human (pumping) factors. The data from the Global Positioning System (GPS) are used to illustrate the total subsidence concerning vertical displacement. A system called the multi-level compaction monitoring well (MCMW) is able to measure the vertical compaction in different depths from the earth surface to the depth of 200 m. Two GPS stations, named CLON and FALI, close to two MCMWs, named Jiadong and Fangliao, are adopted for analysis The data during 2007 and 2016 taken from MCMWs and groundwater observation wells indicate that the compaction in the shallow depth should be mainly caused by groundwater over-pumping due to their high correlation coefficients (from 0.58–0.95). The difference of the vertical deformation between GPS and MCMW indicates that there is deformation beyond the depth within 200 m. From the data and literature, the further vertical deformation should be due to tectonic activity associated with tectonic escape and extrusion of the Taiwan orogen with average vertical deformation from − 3.0 to −4.4 mm. Therefore, the quantities of land subsidence contributed by local groundwater over-pumping and regional tectonic activities are successfully separated. The method and concept proposed in this study can be used in land subsidence quantification due to both tectonic activity and groundwater over-pumping.

1 Introduction

In southwest Taiwan, the Eurasian Plate is subducting with south-east direction beneath the Philippine Sea Plate at the Manila trench (Wu, 1978). In the previous studies with the moving speed of the Philippine Sea Plate of about $8.2\,\mathrm{cm\,yr^{-1}}$, the force from the Philippine Sea Plate was much greater than that of the Eurasian plate, which collided with the east of Taiwan orogeny to create a series of thrust faults (Yu, 1997). Pingtung plain is located in South-western Taiwan, where the land use is mainly for agricultural and aquaculture. The unconsolidated sediments of the Pingtung plain form a basin and lie on the wedge-top depozone which form the main aquifer (Chiang et al., 2004). Covey (1986) and Chiang et al. (2004), they pointed out Pingtung plain is located in major piggyback basin of the wedge-top depozone where is lied on the foreland basin. Moreover, Pliocene-Quaternary sedimentary from offshore to onshore have been deposited on the wedge-top depozone.

Taiwan is ranked 56th in the world regarding population with 667 person $\mathrm{km^{-2}}$ (United Nations World Prospects Report, 2017). With an economic development, the demand for water resources in Taiwan is increasing; however, the current water supply in Taiwan is insufficient compared with population density. Since the amount of surface water is inadequate to supply whole public water, groundwater exploitation becomes a must and causes land subsidence in the coastal plain, which leads to serious land subsidence (Chang et al., 2004; Hung et al., 2010; Wang, 2015).

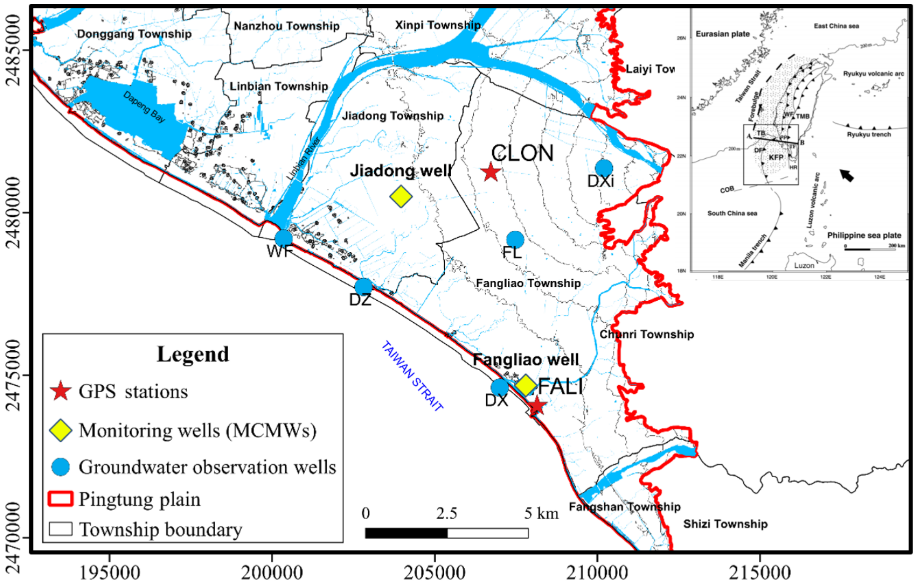

Figure 1. The distribution of monitoring system in the study area (Modified from Chiang et al., 2004).

The purpose of this research is to summarize information from the aforementioned research papers to propose a conceptual model to estimate how much land subsidence is due to the tectonic activities and non-tectonic activities. In this study, the data from global positioning system (GPS) is used to measure the vertical land deformation and a nearby system called the multi-level compaction monitoring well (MCMW) measures the compaction within 200 m. These two survey data conducted from 2007 to 2016. Moreover, the correlation between the data of compaction monitoring wells, groundwater monitoring wells, and rainfall quantity are compared to realize the seasonal influence. After the data analysis, then knowing the area where the land surface changes occur and strongly affected by the change in the groundwater level, the elemental frequency analysis is proposed. This approach provides additional ideas on geological surveys as well as estimation of subsidence caused by plate tectonics in different sensitive tectonic regions in the world.

2 Monitoring system

Nowadays, the methodology for measuring land subsidence has been upgraded for years, and there are new studies to find out the past and present geological issues. In Taiwan, there are four techniques commonly used to observe land subsidence such as leveling, GPS, MCMW, and differential interferometric synthetic aperture radar (DInSAR). These techniques support each other in spatial and temporal domains. Three of them are used to measure the total subsidence consists of leveling, continuous GPS, and DInSAR. The one left measure compaction in different layers are MCMWs. Following Hung et al. (2010), the advantage of GPS is the daily sampling which provides sufficient data as well as high mobility and a quick survey. The next one is the MCMWs are used to measure the compaction of aquifer systems by anchoring several magnetic rings to aquifer systems at different depths with the advantage is its high accuracy of (about 1–5 mm). The final technique, DInSAR is used to measure landscape changes by using many images at different times to create the interferogram images. The advantage is a spatial resolution, but there are various errors, especially for the atmospheric error which reduces the accuracy up to 2 cm. Therefore, using survey data from continuous GPS and MCMW is proposed which are the powerful technique in this research. The distribution of monitoring system used in this study is shown in Fig. 1.

From the 10-year continuous leveling data, it has been shown that changing land surfaces at CLON station and Jiadong well is similar, so the CLON station is closest to Jiadong well. Besides that, there is a total of five wells for monitoring groundwater levels which were chosen in the study area. We divided into two areas of subsidence measuring in Jiadong township and Fangliao township, so the division of groundwater monitoring wells in two areas is also carried out for easy analysis. In Jiadong township area (Fig. 2), they include three groundwater observation wells named Wenfeng (WF), Dazhuang (DZ), Daxiang (DXi). In the Fangliao township area, the remaining two wells are named Fangliao (FL), and DeXing (DX). The groundwater observation wells have from the first aquifer to third aquifer and its distribution from the depth of 25 to 200 m. In this study, the GPS and groundwater level data are based on the daily solution. However, the MCMW result is based on a monthly solution.

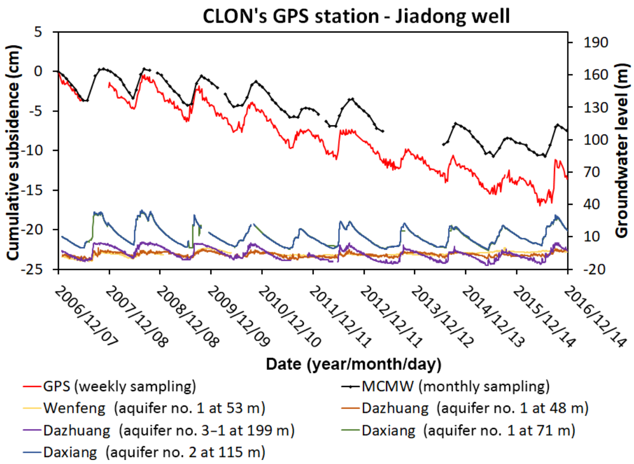

Figure 2. Cumulative subsidence of GPS data, MCMW data are in the left y-axis, and groundwater level variation, represented in right y-axis.

3 Methodology

A new idea with a simple equation to estimate subsidence in depths of below 200 m. We rather suspect that the deep subsidence part is caused by natural impact. There are two main factors of the natural impact such as natural compaction and plate tectonics. Following the rock cycle, there are three main types of rocks: sedimentary, metamorphic, and igneous. Under the influence of nature, each type of rock when altered or destroyed will create loose materials or unconsolidated soil. That material would be sedimented respect to the time-consuming transitions through geologic time is called natural compaction. Tectonic subsidence commonly occurs at a subduction zone, especially in Pingtung plain that is very active so it can easily lead to land subsidence. In the conceptual model, we separated into two main causes likely human and natural impact. Where a GPS station and MCMW device were established to measure the total subsidence and the changing of stratigraphic column within 200 m. Thus, the equation to estimate land subsidence due to tectonic activities is proposed:

$$\begin{aligned}&\text{Tectonic subsidence} = \text{Total subsidence}\\&-\text{Subsidence due to groundwater extraction}\\&-\text{Natural compaction}\end{aligned}\tag{1}$$

However, in the Geologist point of view, with the basic concept in geology when the physical and chemical weathering process forms the loose or weathering materials that have to change a type to another concerning geology time. From the unconsolidated soil to consolidated soil mechanism is a time-consuming process. Thus, we use the data set for 10 years then the factor of natural compaction will not affect much. Besides, as mentioned in the previous section and the limit of the thickness of the alluvial deposit which is approximately smaller than 250 m (Jiang, 2018), we assume that the subsidence at the depth of more than 200 m equal to 0 caused by natural compaction. In addition, from the correlation coefficient matrix among each component that we know the relationship between groundwater and compaction in Multi-level compaction monitoring well (MCMW) is a positive relation. Whereas, the negative relation was shown in Table 1 between estimating tectonic and groundwater. Thus, the groundwater pumping in the depth greater than 200 m is impossible. Then, Eq. (1) will become:

$$\begin{aligned}&\text{Tectonic subsidence} = \text{Total subsidence}\\&-\text{Subsidence due to groundwater extraction}\end{aligned}\tag{2}$$

4 Results and discussion

4.1 Data analysis

Figure 2 shows a variation of the time series under the seasonal effect. The most subsidence often falls during the dry season, so that the annual compactions in the dry season which calculated from the data of MCMW at both areas that range from −64.4 and −40.1 mm. In this study, we used the Pearson's r correlation coefficient in order to analyse the correlation among data collected from subsidence observing wells and data from groundwater observation wells. In addition, since the same survey method was conducted in two different areas, it is significant to shed light on the correlation between them. To understand physical properties inside, we need to optimize the current data, hence analyzing the correlation of values is also necessary. Since calculation results were seasonally changed, especially subsidence data from both GPS stations and MCMW observing wells were deformed, there was a tendency of subsidence for a long time. Therefore, we utilized different methods and detrending method with the resampling data to analyse.

The correlation coefficients among the data from MCMWs and groundwater monitoring wells are high with the values from 0.58 to 0.95, as listed in Table 1. That illustrated that MCMW can measure the land subsidence due to groundwater pumping from the Earth's surface to a depth of 200 m. As mentioned previously, GPS station is established at the ground surface to measure the total subsidence that means that GPS system observes the whole vertical deformation including a movement of tectonic activity.

4.2 Tectonic subsidence estimation

The measurement period of MCMW device is one-month interval, while that of GPS system is daily interval. However, GPS system is very susceptible to atmospheric, so we used resampling and average method to analyze the data to avoid the errors. Therefore, subsidence data from GPS are

Table 1. Correlation coefficient matrix between subsidence and groundwater level.

r value	FALI GPS	Fangliao MCMW	Fangliao Tectonic	DZ1	DZ2	WF	DXi1	DXi2	FL1	FL2	DX1	DX2	DX3
CLON GPS	0.89	0.87	0.46	0.71	0.86	0.47	0.76	0.74	0.86	0.86	0.10	0.68	0.69
Jiadong MCMW	0.66	0.86	−0.02	0.82	0.92	0.58	0.78	0.77	0.90	0.90	0.04	0.73	0.71
Jiadong Tectonic	0.56	−0.18	0.66	−0.03	0.09	−0.08	0.15	0.16	0.12	0.13	0.13	0.07	0.11
DZ1	0.56	0.84	−0.19	1.00	0.86	0.62	0.66	0.65	0.76	0.76	0.19	0.71	0.73
DZ2	0.61	0.91	−0.27	0.86	1.00	0.58	0.93	0.92	0.98	0.97	0.30	0.86	0.87
WF	0.47	0.58	−0.06	0.62	0.58	1.00	0.49	0.49	0.49	0.50	0.04	0.38	0.47
DXi1	0.55	0.83	−0.25	0.66	0.93	0.49	1.00	1.00	0.95	0.96	0.39	0.84	0.87
DXi2	0.54	0.83	−0.25	0.65	0.92	0.49	1.00	1.00	0.95	0.95	0.40	0.84	0.87
FL1	0.62	0.91	−0.34	0.76	0.98	0.49	0.95	0.95	1.00	1.00	0.27	0.86	0.89
FL2	0.62	0.91	−0.28	0.76	0.97	0.50	0.96	0.95	1.00	1.00	0.24	0.86	0.89
DX1	0.01	0.18	−0.15	0.19	0.30	0.04	0.39	0.40	0.27	0.24	1.00	0.33	0.30
DX2	0.60	0.90	−0.26	0.71	0.86	0.38	0.84	0.84	0.86	0.86	0.33	1.00	0.91
DX3	0.68	0.95	−0.18	0.73	0.87	0.47	0.87	0.87	0.89	0.89	0.30	0.91	1.00

Note: DZ1, DZ2, WF, DXi1, DXi2, FL1, FL2, DX1, DX2, DX3 are the abbreviated name of groundwater observation wells.

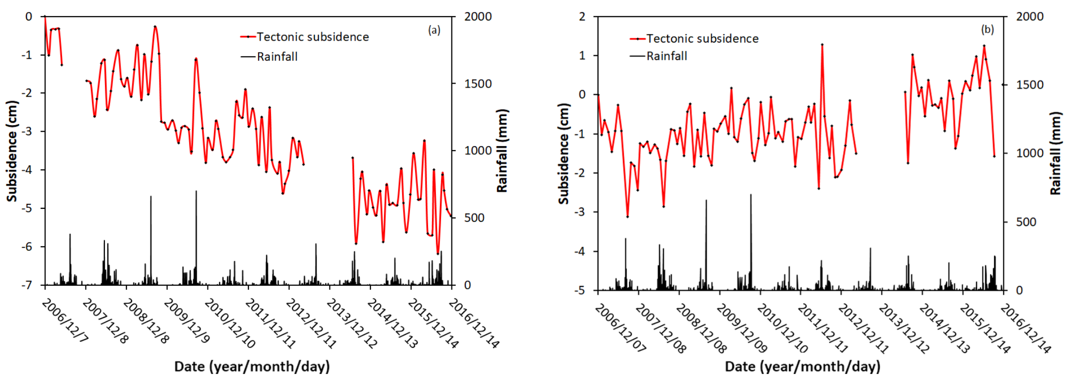

Figure 3. Monthly tectonic subsidence in **(a)** Jiadong area and **(b)** Fangliao area.

processed by using the weekly mean value cooperated with the resampling point. The calculation concept is that based on the date when MCMW data are collected, resample the point of GPS at the same date and averaged the seven values from before three days to after three days. This method is called the mid-point weekly sampling in this study.

After the pre-processes, Eq. (2) is adopted to calculate the tectonic subsidence, the results are shown in Fig. 3. The average deformation in Jiadong area and Fangliao area are −4.4 and −3.0 mm, respectively. The Pingtung area and the south-eastern region of Taiwan in general must have a big creative stress from Philippine Sea Plate. With respect of time, Pingtung plain reaches the critical state, then lead to finding a way to release this stress. Tectonic escape accompanied with the transtensional deformation is occurred in the south-west direction (azimuth 243.9–245.7°) because of the free boundary at Taiwan strait. From these estimation results, the tectonic subsidence of coastal zone of Pingtung plain quite consistent with previous research which indicated the transtensional deformation associated with the tectonic extrusion (Hu et al., 2006).

5 Conclusions

MCMW is a system to monitor land subsidence due to groundwater over-pumping. The data collected from the groundwater monitoring wells and MCMW in Pingtung plain have the correlation coefficients varied from 0.58–0.95, which express that the subsidence within 200 m is highly correlative to groundwater level variations and could be due to groundwater over pumping. Under the assumption of small influence of natural compaction, the vertical deformation induced by tectonic activity can be obtained using total subsidence minus subsidence within 200 m. Then, both the vertical deformation contributed by natural factor of tectonic activity and human factor of groundwater over pumping can be estimated. For nature factor, the tectonic activity causes an average vertical deformation of −4.4 and −3.0 mm in Jiadong and Fangliao areas, respectively. There are 70 %

and 82 % of total subsidence are contributed by human factor. Comparing with the literature, the regional subsidence is caused by the transtensional deformation associated with the tectonic extrusion, then occurring tectonic escape in the south-west direction with azimuth 243.9–245.7°.

Data availability. The GPS data used in this study was obtained from the website of Academia Sinica, Taiwan, through http://gps.earth.sinica.edu.tw/ (IESAS, 2007–2016). The groundwater level data can be obtained from the website of Water Resources Agency, Taiwan, through https://gweb.wra.gov.tw/wrhygis/ (Water Resources Agency, 2007–2016). However, the data of multi-level compaction monitoring well are not opened for public use at this moment, the raw data is belonged to Water Resources Agency, Taiwan.

Author contributions. The reference review, data analyses, figure and table preparations, and manuscript writing are done by DHT. SJW is the advisor, who provides the idea, data, comments, and suggestions for this research and revises the manuscript.

Competing interests. The authors declare that they have no conflict of interest.

Special issue statement. This article is part of the special issue “TISOLS: the Tenth International Symposium On Land Subsidence – living with subsidence”. It is a result of the Tenth International Symposium on Land Subsidence, Delft, the Netherlands, 17–21 May 2021.

Acknowledgements. The authors would like to thank Professor Jyr-Ching Hu in National Taiwan University, Wei-Chia Hung in Green Environmental Engineering Consultant Co. LTD, and an anonymous reviewer for providing the valuable comments and suggestions to improve this research. The data provided by Academia Sinica, Taiwan, and Water Resources Agency, Taiwan, are much appreciated.

Financial support. This research has been supported by the Ministry of Science and Technology, Taiwan (grant no. MOST 106-2116-M-008-023-MY3).

References

Chang, C. P., Chang, T. Y., Wang, C. T., Kuo, C. H., and Chen, K. S.: Land-surface deformation corresponding to seasonal groundwater fluctuation, determining by SAR interferometry in the SW Taiwan, Math. Comput. Simulat., 67, 351–359, 2004.

Chiang, C. S., Yu, H. S., and Chou, Y. W.: Characteristics of the wedge-top depozone of the southern Taiwan foreland basin system, Basin Res., 16, 65–78, 2004.

Covey, M.: The evolution of foreland basins to steady state: evidence from the western Taiwan foreland basin, Spec. Publ. Int. Ass. Sediment, 8, 77–90, 1986.

Hu, J. C., Chu, H. T., Hou, C. S., Lai, T. H., Chen, R. F., and Nien, P. F.: The contribution to tectonic subsidence by groundwater abstraction in the Pingtung area, southwestern Taiwan as determined by GPS measurements, Quat. Int., 147, 62–69, 2006.

Hung, W. C., Hwang, C., Chang, C. P., Yen, J. Y., Liu, C. H., and Yang, W. H.: Monitoring severe aquifer-system compaction and land subsidence in Taiwan using multiple sensors: Yunlin, the southern Choushui River Alluvial Fan, Environ. Earth Sci., 59, 1535–1548, 2010.

Institute of Earth Sciences, Academia Sinica (IESAS): Establishing an Automated GPS Processing and Analysis System to Provide an On-line Service for the Earth Sciences Research, available at: http://gps.earth.sinica.edu.tw/, 2007–2016.

Jiang, J. Y.: Shallow S-wave Velocity Structure of Pingtung Plain by Microtremor HVSR Simulation, M.S. Thesis, National Central University, 2018.

United Nations: World Population Prospects 2017 – Data Booklet (ST/ESA/SER.A/401), Department of Economic and Social Affairs, Population Division, 2017.

Wang, S. J.: Dimensional Upgrade Approach for Spatial-Temporal Fusion of Trend Series in Subsidence Evaluation, Entropy, 17, 3035–3052, 2015.

Water Resources Agency, Ministry of Economic Affairs, Taiwan: Hydrological year book of Taiwan, Republic of China, Part III – Groundwater, 2007–2016.

Wu, F. T.: Recent tectonics of Taiwan, J. Phys. Earth, 26, S265–S299, 1978.

Yu, S. B., Chen, H. Y., and Kuo, L. C.: Velocity field of GPS stations in the Taiwan area, Tectonophysics, 274, 41–59, 1997.

Groundwater Regulation and the Development of Alternative Source Waters to Prevent Subsidence, Houston Region, Texas, USA

Michael J. Turco[1], Ashley Greuter[1], Alia Vinson[2], Joseph A. Turco[4], Alan Petrov[1], Mark Evans[3]

1 Harris-Galveston Subsidence District, Friendswood, Texas, USA
2 Allen Boone Humphries & Robinson LLP, Houston, Texas, USA
3 North Harris County Regional Water Authority, Houston, Texas, USA
4 Northeastern University, Boston, MA, USA
Correspondence to: Michael J. Turco (mturco@subsidence.org)

Abstract

Since the development of the coastal areas near present-day Houston, Texas, USA, subsidence has been a significant public policy concern. Subsidence in this area is caused by the extraction of groundwater from the Coastal Lowlands aquifer system, locally referred to as the Gulf Coast Aquifer. Concerns associated with subsidence in the Houston area include coastal inundation from storm surge, inland flooding, and critical infrastructure damage. The Houston area receives about 126 cm of precipitation each year, making flooding a critical issue in the region. The Houston area is the 4th largest city in the United States with a population of about 6.89 million (2017) and has a total water demand of about 4 Mm3 per day (2017). In the 1950s the City of Houston began the development of several reservoirs to provide water for the rapidly growing city. In 1975, following decades of subsidence totaling over 3 m, the Harris-Galveston Subsidence District (District) began regulating the use of groundwater and shifting the primary water supply for the region from groundwater to treated surface water to cease on-going and prevent future subsidence. Leveraging the alternative resources developed by the City of Houston in the 1950s, the District's regulatory framework focuses on spatial prioritization and the systematic conversion to alternative source waters. The District's regulatory plan includes three planning areas. Currently, the regional water authorities and the City of Houston are developing nearly five billion dollars ($US) in infrastructure to produce and deliver an additional 1.2 Mm3 per day of treated surface water to Houston and the surrounding communities. Resource development, public engagement, and political foresight have resulted in a reasonable approach to shift source waters and implement a plan to dramatically reduce and stop subsidence in the region. Figure 2 presents subsidence rates (2017) by regulatory area. Results show that the implementation of the regulatory program has substantially slowed subsidence in Areas 1 and 2, where full conversion has taken place. Planning the future water needs of the Houston area resulted in a robust and effective collaboration between the regulated community and the District. Analysis of historical source water use, aquifer response, and subsidence in the Houston area shows that the reasonable management of groundwater use in the Houston region is vital for the long-term prevention of subsidence and increases the resilience of the entire region.

Introduction

The Houston Region has relied on groundwater as a primary source of water since the early 1900s. During and following the economic boom of the 1940s, rapid population expansion and increased water demand resulted in potentiometric water-level declines in the Chicot and Evangeline aquifer of 76- and 91-meters respectively from 1943-1977 (Gabrysch, 1982).

The reliance on groundwater and subsequent subsidence that was caused by its regional development resulted in the creation of the Harris-Galveston Subsidence District in 1975 and the Fort Bend Subsidence District in 1989.

The Harris-Galveston Subsidence District's mission is to regulate the use of groundwater in the Houston Region (Harris and Galveston counties) to cease ongoing and prevent future subsidence that can lead to infrastructure damage and contribute to flooding.

The Harris-Galveston Subsidence District ("District") regulates groundwater use by subdividing Harris and Galveston county into three regulatory areas: Area 1 includes the Houston Ship Channel, Industrial Corridor, and coastal areas; Area 2 is primarily an urban intermediate area that includes the Texas Medical Center; and Area 3 includes the remaining areas of the District in northern and western Harris County. In 2021, Area 3 used nearly 6.4 x 105 m3 of groundwater each day, nearly five times the other two areas combined (Greuter, 2022). Overall, the total water demand in the District in 2021, including all sources of water, was about 3.73 x 106 m3 per day (Greuter, 2022).

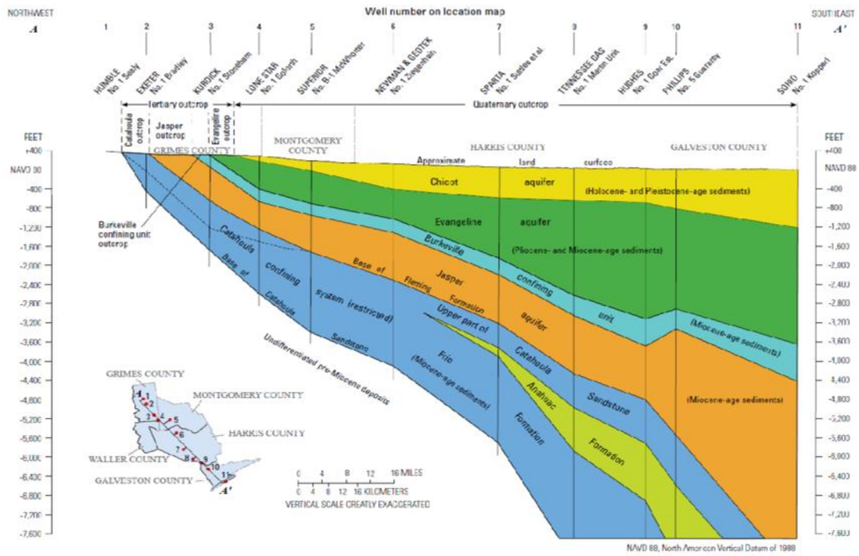

Figure 1 Hydrogeologic cross-section of the Gulf Coast aquifer system in the Houston Region, Texas, USA (modified from Kasmarek, 2014)

Groundwater

Groundwater is derived from the Coastal Lowland Aquifer, locally referred to as the Gulf Coast Aquifer System, and includes three primary water bearing units, the Chicot, Evangeline, and Jasper aquifers (Figure 1). The aquifers are comprised of inter-bedded lenticular lenses of sand, silt, and clay which are not regionally extensive and have a highly variable thickness (Chowdhury and Turco, 2006) in the Houston Area.

The Evangeline aquifer is the most widely utilized aquifer in the Houston area accounting for more than half of all the groundwater used. The Chicot aquifer is used appreciably in the areas closer to the coast, although it can be used for domestic supply north of the District. The Jasper aquifer is used primarily in the northern areas of the District where the unit is closer to the surface and better quality.

Compaction and subsidence

Subsidence has been occurring in the Houston Region since the early 1900s. Located along the Gulf of Mexico, the topography of the region is a flat coastal plain with little relief that generally slopes about 0.2 meters/kilometer.

The first documented case study in the Houston Region linking shallow fluid withdrawal and land surface subsidence occurred at the Goose Creek Oilfield near Baytown, TX (Pratt and Johnson, 1926). Oil and water production at this site occurred at depths up to about 1,500 meters in as old as Miocene-age sediments. This area experienced nearly a meter of subsidence over about a three-year period, and dramatic surficial fissures.

As the Houston area developed, experiencing dramatic growth in the 1940s during Word War II and sustaining the regional growth through the present, groundwater resources were the primary source water for the region and subsidence in the region reached magnitudes of concern.

Historically, subsidence has occurred over a broad region that encompasses most of the City of Houston with specific areas of increased magnitude. The Houston ship channel, a large industrial and commerce area in Houston that is part of the second largest port (by tonnage) in the United States, is located near the center of an area where over 3 meters of subsidence as occurred since 1906.

Regulatory controls in Harris, Galveston and Fort Bend County are implemented based on a specific portion of an entities total water demand sourced from groundwater, with the remaining portion sourced from an alternative source that does not contribute to subsidence (treated surface water, reclaimed water, etc.) In 2019, regulatory requirements in Areas 1 and 2 allow groundwater to be utilized for 10% and 20% respectively of the water users total water demand. In Area 3, water users without a groundwater reduction plan are regulated to the same requirements as Area 2. However, if a water user has an approved groundwater reduction plan, then groundwater may provide up to 70% of their total water demand, with future reductions in the allowed percentage of groundwater to 40% and 20% in 2025 and 2035, respectively in Harris and Galveston counties. This regulatory approach has been greatly successful in reducing subsidence rates while accounting for the time needed to develop infrastructure to treat and convey water throughout the Houston region (Figure 2 and 3).

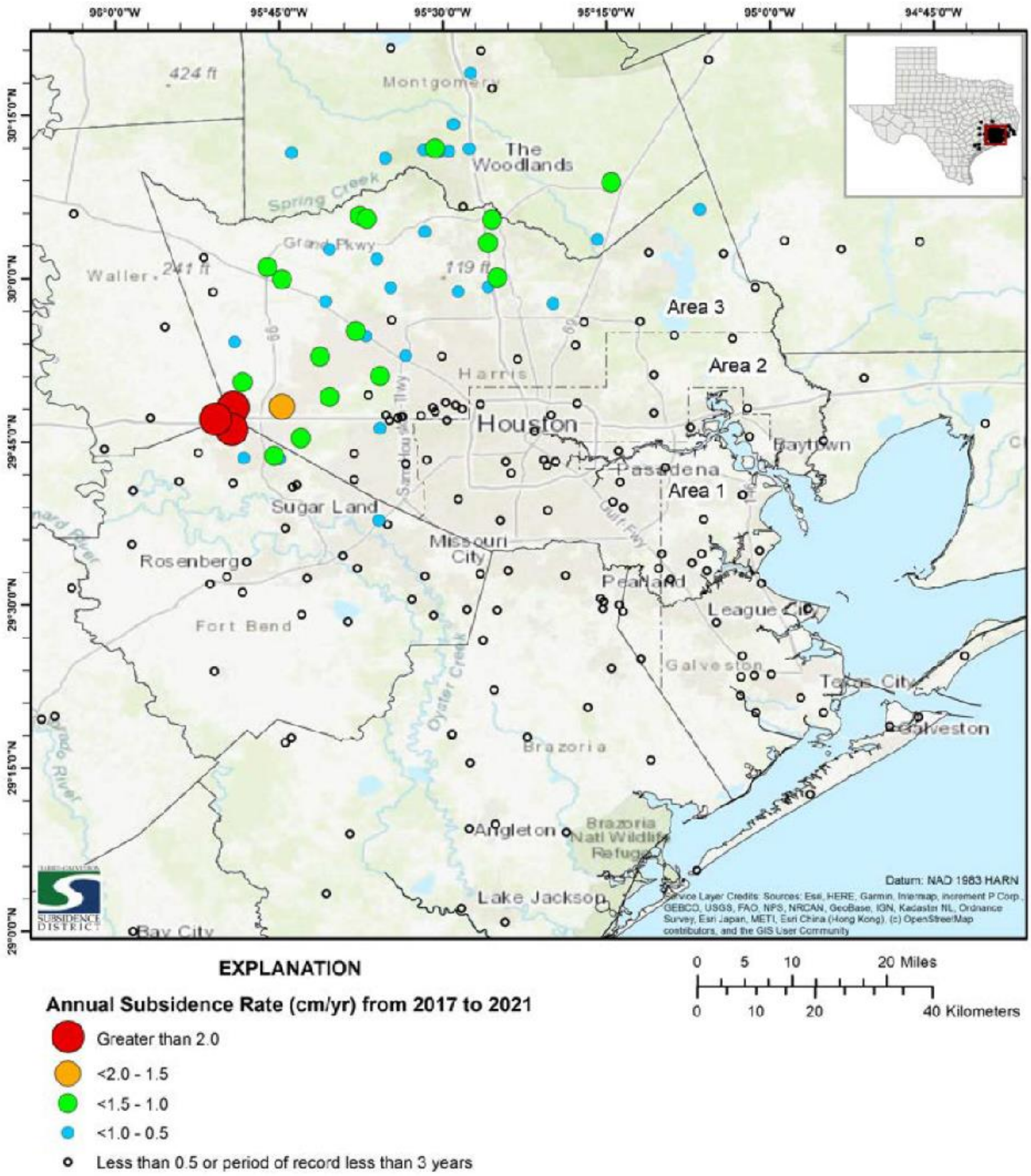

Figure 2 Annual rate of ellipsoid height estimated from available GPS data measured monitoring location withon the Houston Region, 2017-2021 (Greuter, 2022).

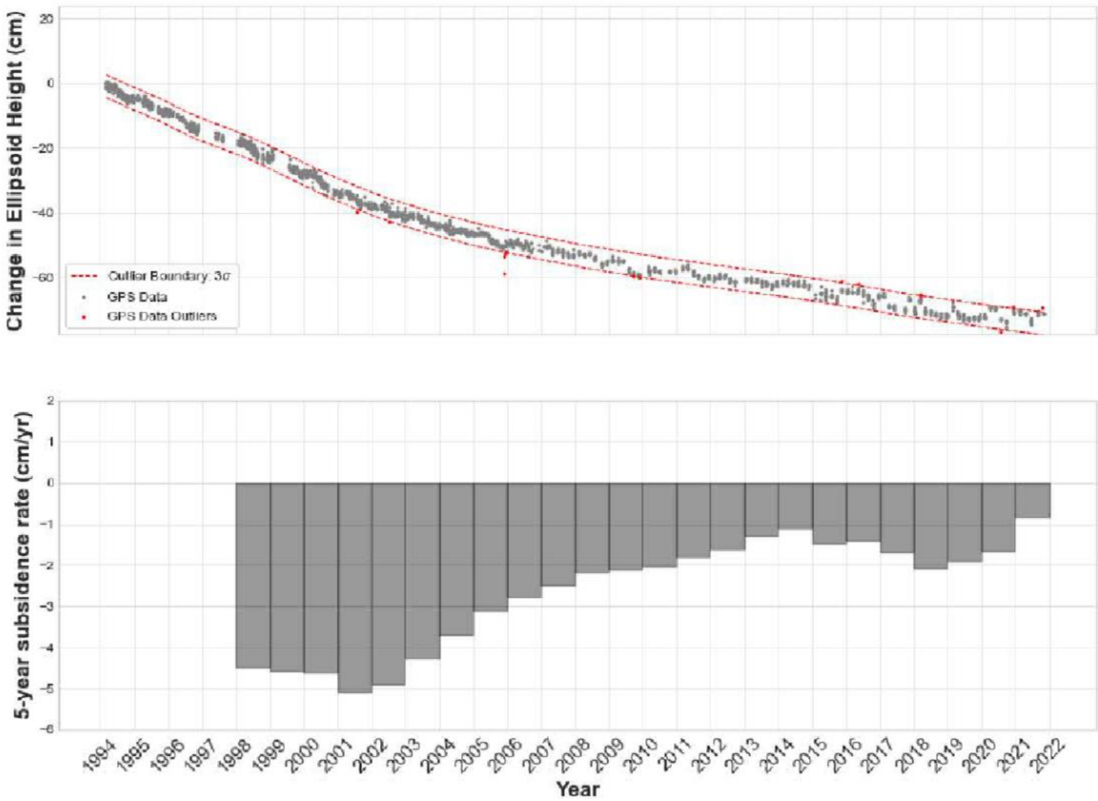

Figure 3 Measured and estimated annual rate of change in ellipsoid height at Harris-Galveston Subsidence District monitoring site P001 located near Jersey Village, TX, 1994-2021 (Greuter, 2022).

Alternative water supplies

In the 1950s the City of Houston began the development of several reservoirs to provide water for the rapidly growing region within the San Jacinto and Trinity River Basins. Other entities in the region have also developed surface water supply from the Trinity, San Jacinto, and Brazos Rivers. The treatment plants served by these surface water sources are operated by the City of Houston, City of Sugar Land, City of Richmond, the Gulf Coast Water Authority, the Brazosport Water Authority, and others.

To meet the Harris-Galveston and Fort Bend Subsidence Districts' regulatory requirements to convert from groundwater to surface water, the City of Houston and four regional water authorities—Central Harris County Regional Water Authority, North Fort Bend Water Authority, North Harris County Regional Water Authority, and West Harris County Regional Water Authority (collectively, the "Water Authorities") are working together to plan, design, construct, and finance several major infrastructure projects. These projects are regional in scale and are interrelated. All the projects must be constructed on the same timeline to ensure that surface water will be available to northern and western Harris County and northeast Fort Bend County to comply with the Subsidence District's regulatory conversion schedule.

The first project is called the Luce Bayou Interbasin Transfer Project ("Luce Bayou"). Luce Bayou is currently under construction and will pump untreated surface water from the Trinity River through a series of canals and water pipelines to Lake Houston (northeast of the City of Houston). Luce Bayou is being constructed by the Coastal Water Authority, but the project is being funded by the entities that will be purchasing the transferred water, which includes the City of Houston and the Water Authorities.

The second project is called the Northeast Water Purification Plant ("NEWPP") Expansion Project. The NEWPP expansion is a design-build project under construction on the banks of Lake Houston. The project will expand the existing plant's capacity from 3.03 x 105 m3 per day up to 1.51 x 106 m3 per day, in order to treat the raw surface water conveyed by Luce Bayou into Lake Houston (Figure 4). The City of Houston is the owner of this project, but the Water Authorities have purchased 84% of the capacity of the NEWPP and are each paying their respective shares of the costs.

The third project is a transmission line called the Northeast Transmission Line ("NETL"), which will convey treated water from the NEWPP into central and northern Harris County. The NETL is expected to be primarily a 2.74-meter diameter steel water line that is approximately 43.5 kilometers in length. The City of Houston is the owner of this project, but the North Harris County Regional Water Authority and the Central Harris County Regional Water Authority have purchased capacity in the line and are each paying their respective shares of the costs (the West Harris County Regional Water Authority and the North Fort Bend Water Authority are also participating in the initial segment of the NETL).

The fourth project is a transmission line (and two pump stations) called the Surface Water Supply Project ("SWSP"), which will convey treated water from the NEWPP into western Harris County and north-eastern Fort Bend County. The SWSP is expected to be primarily a 2.4-meter diameter steel water line that is approximately 64 kilometers in length. The West Harris County Regional Water Authority is the owner of this project, but the North Fort Bend Water Authority has purchased capacity in the line and is paying its share of the costs.

In addition to the four projects described above, the City of Houston and the Water Authorities are each designing and constructing their own distribution systems to convey the treated surface water to their customers.

Both the NETL and the SWSP are massive transmission lines running through densely populated and congested areas. The transmission lines must be installed in narrow easement corridors, which adds to the complexity and ultimately the cost of the projects. Currently (2019), both the NETL and the SWSP are under design and are expected to commence construction soon.

Due to the technical and financial challenges associated with these projects, it is critical for the City of Houston and the Water Authorities to have regulatory certainty from the Harris-Galveston and Fort Bend Subsidence Districts. The transmission and treatment capacity have been sized to meet the current District's conversion requirements in 2025, 2027, and 2035.

These interrelated regional projects are planned to be completed by 2025, when the next conversion requirement of the Harris-Galveston Subsidence District go into effect. While these projects are time consuming and costly (the costs are likely to total close to $5 Billion (USD)), the City of Houston, Coastal Water Authority, and the Regional Water Authorities have been able to work together to create economies of scale and maximize efficiencies. This regional effort could serve as a model for other locations seeking to address large scale water supply needs.

Figure 4 (main) Photo of construction of dual 2.74-meter raw water lines from Lake Houston to the Northeast Water Purification Plant (courtesy Steve Berckenhoff); (inset) Subsidence District officials near raw water pipeline (courtesy Harris-Galveston Subsidence District).

Conclusions

The Gulf Coast Aquifer System in the State of Texas, USA has been a primary source of water for the Houston region since development began early in the 1900’s Since that time extensive data collection and research has been conducted to better understand the impact of anthropogenic stress on the aquifer’s water levels, compaction, and subsidence. The State of Texas created a unique regulatory agency to address the issue by regulating the amount of ground water use in Harris, Galveston, and Fort Bend counties. Since the creation of the Subsidence Districts, areas nearest the coast have been converted to alternative source waters and subsidence rates of declined significantly.

Currently, in more inland areas of the District’s, extensive water infrastructure development is ongoing. These efforts require the coordination of multiple regional water authorities and the City of Houston to ensure the compliance with planned future conversion requirements to further reduce the amount of groundwater use. This effort is planned to be completed before the next regulatory conversion deadline in 2025. This regional effort that includes coordination and collaboration amongst the regulated community as well as the coordination between the regulator and regulated community serves as a good model for similar infrastructure development.

References

Chowdury, A.H., and Turco, M.J.: Geology of the Gulf Coast aquifer, Texas, chap. 2 of Mace, R.E., Davidson, S.C., Angle, E.S., and Mullican, W.F., eds., Aquifers of the Gulf Coast of Texas: Texas Water Development Board Report 365, p. 23–50, 2006.

Gabrysch, R.K.: Ground-Water Withdrawals and Land-Surface Subsidence in the Houston-Galveston Region, Texas, 1906-80, U.S. Geological Survey, Open-File Report 82-571, 68 p., 1982.

Greuter, A.: Determination of Groundwater Withdrawal and Subsidence in Harris and Galveston Counties – 2021, Harris-Galveston Subsidence District, Report 2022-01, 356 p., 2022.

Kasmarek, M.C., and Johnson, M.R.: Groundwater withdrawals 1976, 1990, and 2000–10 and land-surface-elevation changes 2000–10 in Harris, Galveston, Fort Bend, Montgomery, and Brazoria Counties, Texas: U.S. Geological Survey Scientific Investigations Report 2013–5034, 17 p., 2013.

Pratt, W.E., and Johnson, D.W.: Local Subsidence of the Goose Creek Oil Field: Journal of Geology, Vol. 34, No.7, Part 1., 1926.

Disentangling shallow and deep sources of subsidence on a regional scale in the Netherlands

M.A.M. Verberne[1,2], K. Koster[3], T. Candela[2] and P.A. Fokker[2]

1 Utrecht University, Geosciences, Utrecht, The Netherlands
2 Department Applied Geosciences, TNO – Geological Survey of the Netherlands, Utrecht, the Netherlands
3 Department Geomodelling, TNO – Geological Survey of the Netherlands, Utrecht, the Netherlands
Contact: manon.verberne@tno.nl
Session: Coastal Areas, Mining and Resource Extraction

Introduction

Subsidence is often the sum of contributions at multiple depths (Candela and Koster, 2022; Shirzaei et al., 2021). Near surface causes of subsidence can be related to construction of infrastructure and buildings, land use and phreatic water level management, and the withdrawal of groundwater at various depths (Koster et al., 2018). Deep subsurface causes are related to the extraction of hydrocarbons (Chaussard et al., 2013), salts (Mancini et al., 2009), and geothermal production (Massonnet et al., 2009). Most studies are only focusing on potential subsidence processes at single depth levels, although subsidence processes at different depths have been observed in several areas (Candela and Koster, 2022 Shirzaei et al., 2021). Neglecting the contribution of various subsidence processes that influence the total signal of subsidence, potentially leads to erroneous interpretations of the physical process driving the subsidence (Schroot et al., 2005).

We have combined the exhaustive datasets of the shallow subsurface of the Netherlands (TNO-GSN, 2022), that previously has been implemented in a regional lithological and groundwater model, with reservoir data to model gas extraction related subsidence to arrive at a regional multi-depth subsidence model. We introduce a workflow to regionally forecast subsidence originating from causes at multiple depths in the Netherlands, with the use of a forward model optimized in a data assimilation approach. This workflow is subsequently tested with realistic complex synthetic data. We test how well subsidence can be estimated, given the a-priori expected contribution and noise levels.

Materials and methods

Figure 1 shows the overview of the proposed workflow. The first step is to combine subsidence from deep and shallow causes, to arrive at subsidence predictions. These subsidence predictions are benchmarked with measured subsidence, or, in this paper, with synthetic data. A new subsidence prediction is formed with refined parameters. The refinement of the subsidence predictions is done in multiple subsequent steps, gaining confidence with each step. The used data, the forward models and data assimilation approach are further explained in the sections below.

(Synthetic) data sets

To arrive at a realistic synthetic model of subsidence, we used actual subsurface models for lithology and groundwater. For the deep processes a pressure depletion model is used over a period of 5 years inspired by data from a small gas field in the north of the Netherlands. The modelled subsidence region is 20 by 20 kilometers.

GeoTOP is a 3-D geological subsurface model with a x,y,z resolution of 100 x 100 x 0.5 meters. The model schematizes the voxels with 100 realizations of the lithology (grainsize composition), following the statistical probability of the interpolation. GeoTOP was constructed based on digital borehole logs, cone penetrations tests and digitized geological maps, available in the database of the Geological Survey of the Netherlands (Stafleu et al., 2011; TNO-GSN, 2022). For this study we have used the upper 5 meters of the GeoTOP model. For the lithology one of the 100 realizations is taken. Figure 2A shows the lithological map of the area at a depth of 5 meters with respect to NAP (NAP is the Dutch ordnance datum approximating mean sea level).

We used the groundwater model Groundwatertools, with the same spatial extent and resolution as the GeoTOP model. The groundwater model is the result of interpolation of data available at the online portal of TNO-GSN, 2022. The model includes a monthly estimate of the phreatic surface level (Dabekaussen et al., 2020; Zaadnoordijk et al., 2018). For this study we have taken the average slope (m/month) and phreatic surface height from the monthly data over a modelled period of 20 years at a random point in time. Figure 2B shows the average height of the phreatic surface at t=0 with respect to NAP.

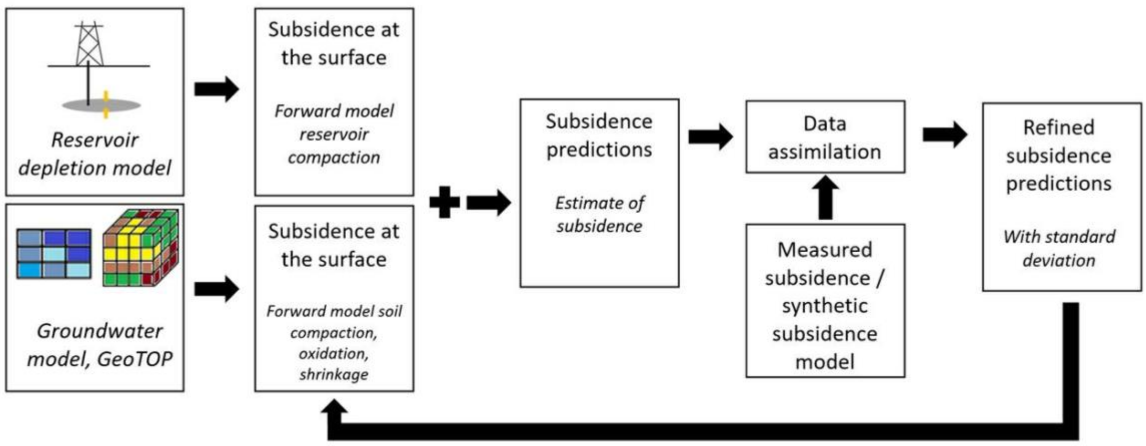

Figure 1 Overview of workflow. Shallow and deep causes of subsidence are combined into one subsidence prediction. This prediction is checked against the observational data to refine the subsidence predictions by optimization of the parameters. This process is repeated multiple times. Image adapted after Candela et al., 2020.

For the pressure field related to reservoir depletion in the deep subsurface, a 2-D grid was constructed. The data contains a yearly value of pressure over the 2-D reservoir grid, a value for the average reservoir depth, and a value for the grid block volume. Figure 2C shows the total pressure depletion over the study time, for the extent of the gas field, with coordinates in the same synthetic system as the GeoTOP and groundwater model. As realistic for reservoirs, there are multiple centers of increased pressure depletion, which results in two subsidence bowls (see Fig 2C).

Forward model

A forward model is a schematized representation of the physics driving the subsidence processes. The subsidence is calculated as the combined effect of the deep and shallow causes. The models are kept simple to compare the influence of each process and not dive in the details the modelling. The pressure depletion is defined as the drop in pressure between two consecutive timesteps. To calculate reservoir compaction from pressure depletion we used a linear elastic compaction model (Candela et al., 2022). Cm,, the compaction coefficient of the reservoir is the single value to optimize in this study. To calculate surface movement from reservoir compaction, an influence function (Green's function) was used (see Geertsma, 1973).

Shallow causes of subsidence are compression, oxidation and shrinkage of peat and clay beds. Compression models often follow a logarithmic equation (e.g. Den Haan, 1996) while oxidation (and sometimes shrinkage) follows an exponential decay function (Van den Akker, 2008; Fokker et al., 2019). We have chosen to only account for an exponential decay function to calculate the subsidence, with variable parameters for peat and clay. This is justified by the length of the study: for a 5 year period logarithmic equation for compression can be estimated with a linear function. Hence equation 1 is assumed to account for subsidence of compression, oxidation and shrinkage.

The equation calculates the subsidence for the part of the layer that is susceptible to subsidence. The effects of swelling are ignored. For a completely dry layer we can determine the fraction of a layer susceptible to subsidence hst=ht- R*h0 where R is the residual height, the fraction of the layer that is left after the full process of subsidence and h0 the original layer thickness. The groundwater variation in time is taken into account by calculating the fraction of the layer above the phreatic surface for each timestep, assuming no subsidence takes place below the phreatic surface. Over time the subsidence for a single layer can be calculated as:

$$\Delta h = (1 - e^{-V \Delta t})(h(t) - h_{wet} - R\,[h_0 - h_{wet}]) \qquad (1)$$

In which V is the rate of subsidence and h_{wet} the height of the phreatic surface within the layer.

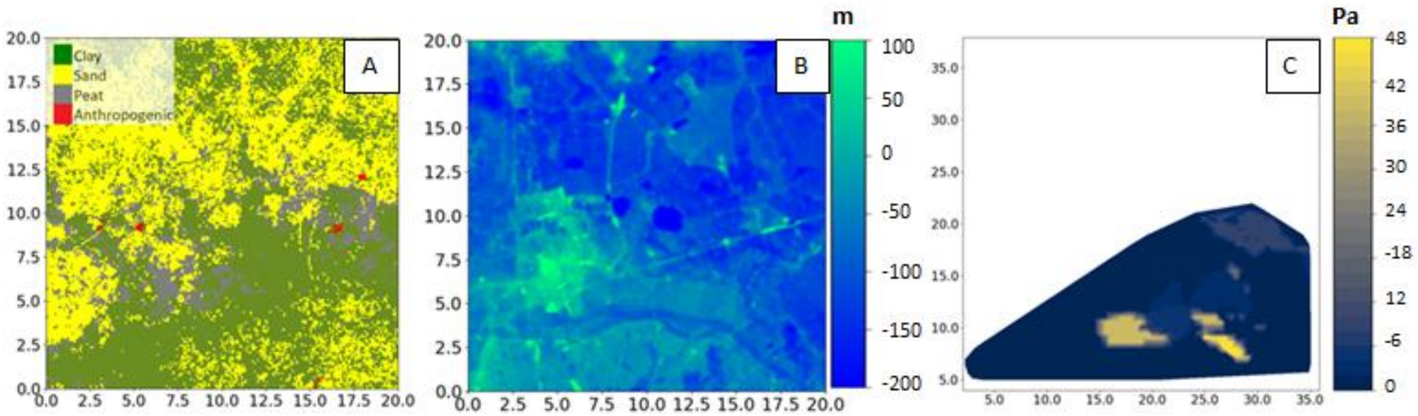

Figure 2 This image shows A) the lithological model of the synthetic area at a depth of 5 meters below NAP in 4 different lithologies, B) the phreatic surface height at t=0 of the synthetic study with respect to NAP and C) the pressure depletion of our 2D upscales gas reservoir over a period of 5 years.

ES-MDA

For the parameter estimation method we used an algorithm often used in parameter estimation studies related to subsidence (e.g. Fokker et al., 2019; Gazzola et al., 2021). ES-MDA stand for Ensemble Smoothing with Multiple Data Assimilation (Emerick and Reynolds, 2016). An ensemble is a collections of members, resulting from a Monte Carlo analysis. Members represent single realizations of the subsidence with specific values for different parameters. A forward model calculates subsidence according to the set of parameters in each member. Subsequently the ES-MDA algorithm minimizes the mismatch between the estimated subsidence and the measured subsidence, by taking multiple steps in which the parameters are modified to reduce mismatch and increase the certainty in the parameter values and standard deviation. For the description of the model see Emerick and Reynolds, 2016 and Fokker et al., 2019.

Experimental set-up

The synthetic subsidence data was created by the sum of the contribution of each subsidence process for 100x100 meter grid cells in the study area for a period of 5 years with monthly timesteps.. From the dataset 1500 random x,y locations were taken. Normally distributed noise was added to the data and functions as input for the covariance of the data. Noise levels and the compaction coefficient are varied. The quality of the estimate is quantified by the absolute error (AE) and absolute ensemble spread (AES) (see Baù et al, 2015).

Results

Figure 3 shows the parameter fit of four different models (A, B, C and D). The variance in fit is related to different noise levels, compaction coefficients and prior ensemble spread, from which the values are given for each model in the figure. Hence, the effects of prior parameter estimates, relative noise and signal contribution are tested. The estimated subsidence rate for peat and clay and the compaction coefficient of the gas reservoir for the prior estimate and each step in the assimilation are plotted on the y axis versus the ensemble member on the x axis. The black line denotes the actual value for that parameter.

Discussion and conclusion

We have introduced a workflow to disentangle the multiple-depth causes of the subsidence signal and identified potential assessment risk for when this method is applied to real data. By comparing four different model outcomes of a realistic synthetic data, we can draw conclusions on what factors should be considered when applying the methodology to real data.

With model A and B of Figure 3 we have compared the influence of noise of the synthetic data to the subsidence fit. The lower the noise level, the lower the spread in our ensemble estimates (AES) and the lower the absolute error (AE) of the estimates. The AE and AES are scaled to the noise level given to the data. With model B and C we have compared the effect of relative influence of the different subsidence processes. In model C, we have chosen a value for Cm as such that the magnitude of subsidence of gas is in the same order as the magnitude of subsidence due to the shallow processes (peat and clay). From this comparison follows that if both multi-depth processes are in the same order, correctly estimating the contributions of the different processes becomes harder. The AES is larger for model C compared to model B, pointing towards a higher uncertainty in the subsidence estimate. From the comparison of model B with model D follows that the initial spread of our parameters has influence on the final estimate of subsidence. The prior spread of the estimate of Cm does not include the true value. As a result, the final Cm is overestimated, although the ensemble spread is reduced with each assimilation step. The estimates of peat and clay in model D are a bit below the true value, to compensate for the over estimation of Cm, resulting in a comparable AE and AES for model B and D.

We show in our analysis that a combination of noise level, relative importance of multi-depth subsidence processes and the chosen prior spread in the ensemble parameters all influence the ability to estimate subsidence correctly. With synthetic data we have the advantage of the known true values of the parameters, whilst with real data this information is unknown. Hence, it if of imminent importance that the effects of each of the factors is understood correctly. When the methodology is applied to a real multi-source subsidence case study, a range of scenarios with varying ratios of the different influence factors should be tested. This means that parameter estimates outside the original distribution window should lead to critically review the prior values, and when different sources of subsidence contribute to the total subsidence, their potential relative contribution should be reviewed. Additionally, with a low ensemble spread, the noise level of the subsidence measurements should be checked.

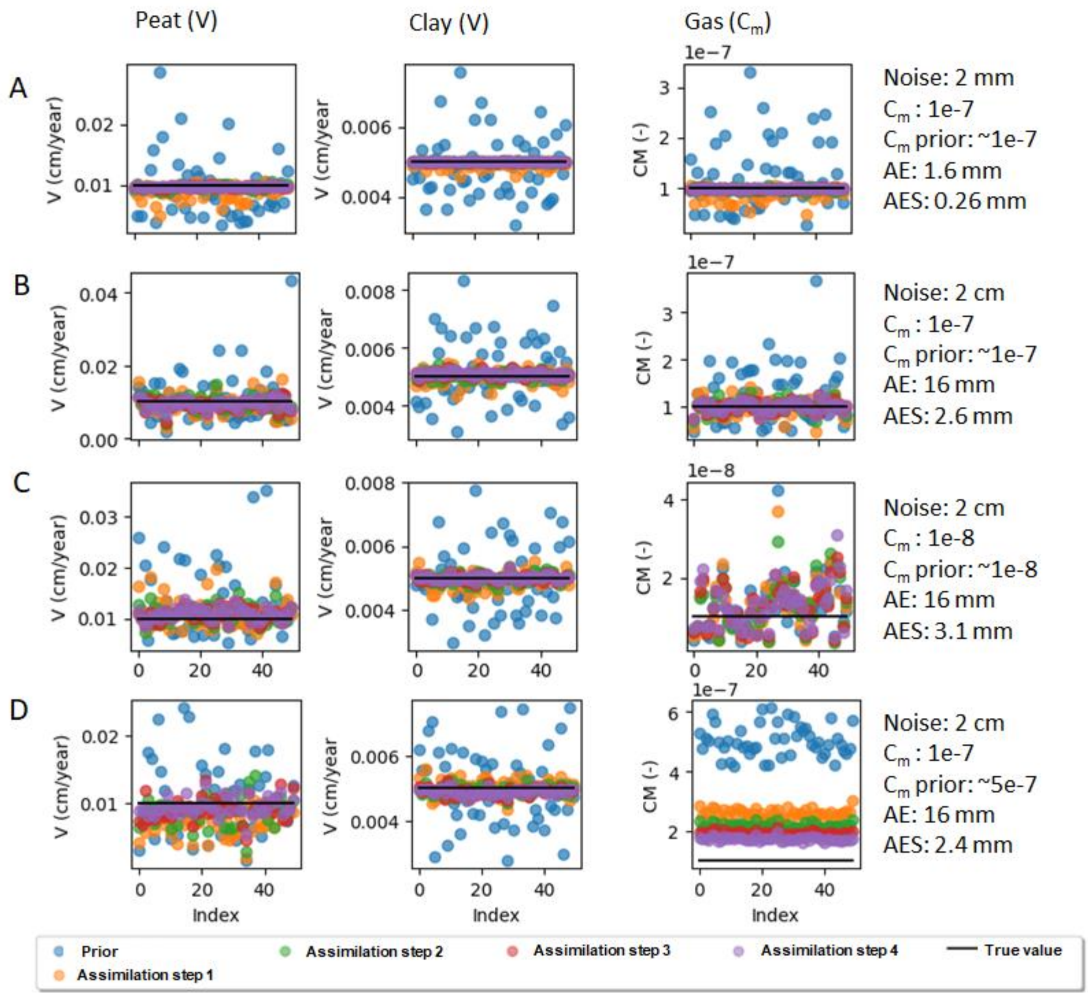

Figure 3 Results of the parameter estimation of 3 different models for 4 assimjlation steps with 50 ensemble members. The estimated parameters for peat and clay (subsidence rate) and gas related subsidence (compaction coefficient) are shown for each assimilation step. Black is the actual parameter value. For each model the noise level, the prior and post estimate chi-square error and the true compaction coefficient are indicated.

Acknowledgements

The research presented in this paper is part of the project Living on soft soils: subsidence and society (grantnr.: NWA.1160.18.259). This project is funded through the Dutch Research Council (NWO-NWA-ORC).

References

Baù, D., Ferronato, M., Gambolati, G., Teatini, P., and Alzraiee, A. (2015). Ensemble Smoothing of Land Subsidence Measurements for Reservoir Geomechanical Characterization. Int. J. Numer. Anal. Meth. Geomech. 39 (2), 207–228

Candela, T., Koster, K., Stafleu, J., Visser, W. and Fokker, P. (2020) Towards regionally forecasting shallow subsidence in the Netherlands. *Proc. IAHS*, 382, 427-431

Candela, T. and Koster, K. (2022). The many faces of anthropogenic subsidence. *Science, 376*(6600), 1381-1382.

Chaussard, E., Amelung, F., Abidin, H., & Hong, S. H. (2013). Sinking cities in Indonesia: ALOS PALSAR detects rapid subsidence due to groundwater and gas extraction. *Remote sensing of environment*, 128, 150-161.

Dabekaussen, W., Lourens, A. and Zaadnoordijk, W.J. (2020), Simulation of groundwater heads for the Think or Sink project. TNO report, Unpublished. pp. 12

Den Haan, E. (January 1996). A compression model for non-brittle soft clays and peat. Géotechnique, 46(1), 1–16.

Fokker, P. A., Gunnink, J. L., Koster, K., & de Lange, G. (2019). Disentangling and parameterizing shallow sources of subsidence: Application to a reclaimed coastal area, Flevoland, the Netherlands. *Journal of Geophysical Research: Earth Surface, 124*(5), 1099-1117.

Gazzola, L., Ferronato, M., Frigo, M., Janna, C., Teatini, P., Zoccarato, C., ... & Mantica, S. (2021). A novel methodological approach for land subsidence prediction through data assimilation techniques. *Computational Geosciences, 25*(5), 1731-1750.

Geertsma, J. (1973). Land subsidence above compacting oil and gas reservoirs. *Journal of petroleum technology, 25*(06), 734-744.

Mancini, F., Stecchi, F., Zanni, M., & Gabbianelli, G. (2009). Monitoring ground subsidence induced by salt mining in the city of

Tuzla (Bosnia and Herzegovina). *Environmental Geology, 58*(2), 381-389.

Massonnet, D., Holzer, T., & Vadon, H. (1997). Land subsidence caused by the East Mesa geothermal field, California, Observed using SAR interferometry. *Geophysical research letters, 24*(8), 901-904.

Schroot BM, Fokker PA, Lutgert JE, Van der Meer BGH, Orlic B, Scheffers BC, Barends FBJ (2005) Subsidence induced by gas production: an integrated approach. In: Proc SISOLS'05, special volume, geodelft, Millpress Rotterdam, pp 121–135

Shirzaei, M., Freymueller, J., Törnqvist, T. E., Galloway, D. L., Dura, T., & Minderhoud, P. S. (2021). Measuring, modelling and projecting coastal land subsidence. *Nature Reviews Earth & Environment, 2*(1), 40-58.

Stafleu, J., Maljers, D., Gunnink, J. L., Menkovic, A., & Busschers, F. S. (2011). 3D modelling of the shallow subsurface of Zeeland, the Netherlands. *Netherlands Journal of Geosciences, 90*(4), 293-310.
TNO-GSN (2022) DINOloket, https://www.dinoloket.nl/

Van den Akker, J.J.H., Kuikman, P.J., De Vries, F., …, Kwakernaak, C., 2008. Emission of CO2 from agricultural peat soils in the Netherlands and ways to limit this emission. In: Farrell, C., Feehan, J. (Eds.), Proc. of the 13th Int. Peat Congr., , pp. 1–6.

Zaadnoordijk, Willem J., et al. "Automated time series Modeling for piezometers in the National Database of The Netherlands." Groundwater 57.6 (2019): 834-843.

An economic optimal control model of land subsidence (extended abstract)

Dewy Verhoeven[1], Suphi Sen[1], Hans-Peter Weikard[1]

1 Environmental Economics and Natural Resources Group, Wageningen University, Wageningen, The Netherlands
Contact: dewy.verhoeven@wur.nl

Background

Land subsidence is a common problem in delta regions due to soft soils and it is accelerated by human-induced processes such as intensive agriculture and urbanization (Koster and van Ommelen, 2015; Van den Born, 2016). Deltaic subsidence threatens the liveability of roughly half a billion people worldwide (Syvitski, 2009).

In this paper, we investigate how land subsidence can best be mitigated and managed. To keep subsiding land in deltas dry enough for human activity, groundwater levels are artificially lowered, in turn speeding up subsidence, depleting the fertile upper soil layer. The societal costs of subsidence are potentially very large, as it may damage the built environment and infrastructure, and increase flood risks, CO2-emissions and water management costs (Pelsma 2020; Van den Born, 2016). Maintaining higher water levels would slow down subsidence but also reduce land productivity. Thus, policy makers are faced with an intertemporal trade-off between the longer-term damage costs of land subsidence and short-term costs of mitigating subsidence through maintaining higher water levels. This paper is the first that develops a geophysical, economic model that integrates the dynamics of land subsidence and groundwater management with economic effects to derive socially optimal paths for water level control, through the application of optimal control theory. We focus on a paradigm example of subsidence management in agricultural areas inspired by the dynamics of peat soils in the Netherlands that are mainly used as grasslands. The objective of our model is to find the optimal path of the groundwater level over time that maximises the total discounted production value of the land minus the cost of water management over time. The model design allows for convenient additions (e.g. the nexus of subsidence and CO2 emissions) and modifications to be applicable to other settings (e.g. urban areas) in the future.

Our paper contributes to informed policy design and decision making by providing an economic analysis of land subsidence as a natural resource management problem. Earlier economic studies of subsidence assessed the societal damage costs of subsidence (Wade, 2018; Willemsen, 2020) or evaluated the costs and benefits of predetermined changes to water drainage regimes (van Hardeveld, 2017) or other sub-optimal policy scenarios (Kok, 2020; Pelsma, 2020) that reduce subsidence. In contrast, this study develops a bio-economic model that is able to derive long-term economically optimal groundwater management pathways in subsiding areas.

Our paper extends the literature that applies optimal control theory on water management and land issues, which has mostly focused on optimal groundwater extraction as a resource for agriculture and other uses (Gisser, 1980; Reinelt, 2020) with only limited attention to subsidence as either a constraint (Larson, 2001) or an extra cost factor (Chu, 2007). In contrast, our study treats the fertile soil itself as the scarce resource and models the unique trade-offs in groundwater management that apply to subsiding deltaic agricultural systems.

Model and method

Our model is set in the context of the drained peat grasslands of the Netherlands. We devise a schematic deterministic model for a single agricultural plot of land in which the groundwater level of that plot can be fully controlled by water pumping and other water management practices. We do not yet consider the external damage costs from subsidence.

We define S_t as the height at time t of the upper soil layer (consisting of peat and clay) above the sand or rock on which it lies. Let S_0 be the initial level of the soil surface. Land subsidence in our setting is defined as the vertical shrinkage of this upper soil layer such that S_t is declining over time. The decision maker can control the groundwater depth of the plot through the use of pumps, ditches, embankments and other water infrastructure. The control variable in our model is therefore the groundwater level g, measured as water height within the upper soil layer above the sand or rock. The difference between the soil thickness and the groundwater level is the groundwater depth, which we call the root zone $R_t = S_t - g_t$[1]. The speed of subsidence depends on the size of the root zone, such that $\dot{S} = \dot{S}(S, g)$. In the initial situation, groundwater levels are already artificially lowered below the natural water table to keep land sufficiently dry for cultivation. Figure 1 shows a schematic vertical cross section for a typical plot in our model, with the state and control variables depicted.

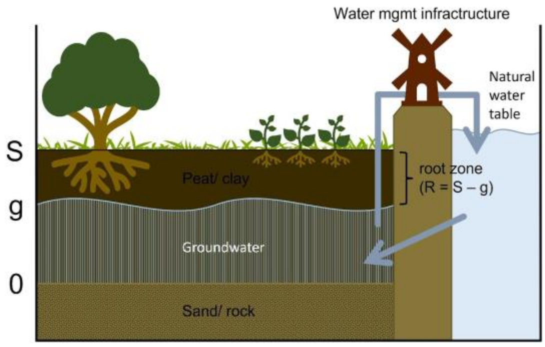

Figure 1 Schematic vertical cross section of a plot of peat land depicting the soil height S, groundwater level g and root zone R = S – g.

The farmer's net revenues from agriculture yt depends on the depth of the root zone, so $y = y(S, g)$, such that revenues are reduced when the plot is too wet (small root zone), but also when it is too dry (very large root zone). The costs of water management ct consist of the pumping effort and the investment in and management of the water infrastructure to reach a certain groundwater depth, which both increase by the depth of the groundwater level relative to the natural water table, such that $c = c(g)$ with $\frac{\partial g}{\partial c} < 0$.

The decision maker's objective is to find the optimal path for the artificial groundwater level over time that will maximise the production value of the land (agricultural net revenues) minus the cost of water management:

---

[1] In the remainder we drop time subscripts for ease of notation.

$$V^* = maxV\,[S, g, t] \;=\; \int_0^{\infty}\big(y(S,g) - c(g)\big)e^{-\delta t}dt \qquad (1)$$

Subject to:

$$\dot{S} = \dot{S}(S, g) \qquad (2)$$

with $S(0) = S_0 > 0$ given.

We rely on insights from soil and agronomic sciences to define the functional specification of our model, which we use to obtain analytical results to derive rules that describe the optimal behaviour of our control and state variable. Next, we use a number of data sets and existing model applications of subsidence studies in Dutch drained peat grasslands to assign values to the parameters in our model. Particularly, we use the ’Waterwijzer Landbouw’ tool and WOFOST models for the relation between agricultural yields and groundwater levels, cost estimates from Van den Born et al. (2016) and the empirical subsidence relation for Dutch peat areas of Van den Akker et al. (2008). Our approach is similar to the work of van Hardeveld et al. (2017; 2018) regarding the integration of these geophysical and economic dynamics of subsidence for Dutch peat areas. The key difference is that in van Hardeveld et al.’s approach groundwater management strategies are externally determined as input for their Re:Peat model to run simulations of different policy options, while our work applies an optimization framework that endogenously determines the optimal policy path for groundwater management over time given the contextual parameter values. We provide sensitivity analyses with respect to water management costs, agricultural prices and the discount rate.

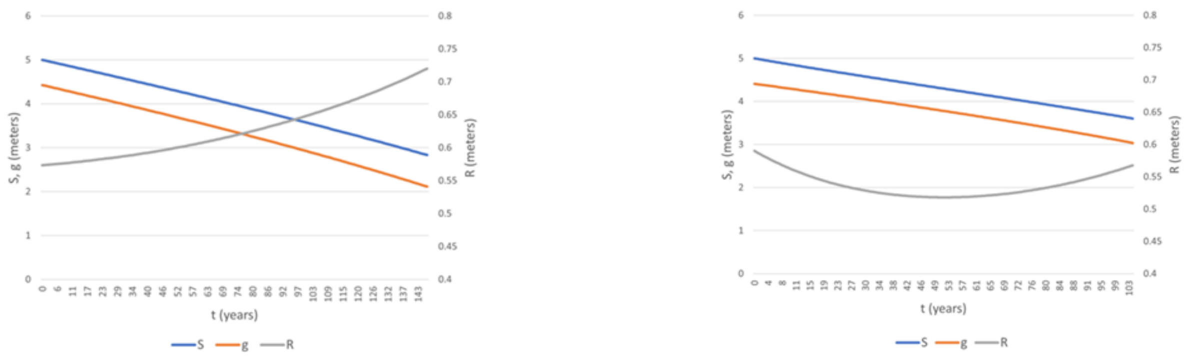

(a) linear marginal costs in depth

(b) quadratic marginal costs in depth

Figure 2 Model simulation of optimal groundwater and subsidence paths for a typical 1 ha grassland plot with a peat soil layer of 5m.

Results and discussion

Our analytical analysis shows that when water management costs are linearly increasing in depth, the optimal groundwater lowering is slower than when we would maximise agricultural yields. Consequently the optimal root zone is smaller and full subsidence of the peat soil is stretched out over a longer period. The optimal path reflects the fact that larger harvests in the near future come at the cost of reduced harvests later on. When marginal costs are increasing in depth, the optimal rate of groundwater lowering additionally slows down, reducing the root zone and therefore the rate of subsidence over time and we never fully deplete the peat soil.

Figure 2 shows the optimal paths for the groundwater and soil levels when these two variants of our model are simulated with the data described above and are applied to a typical 1 ha grassland plot with a pure peat layer of 5 meters. This simulation example reflects the same patterns and additionally shows that when costs are quadratic in depth, we should stop groundwater lowering after about 1.5 meters of subsidence as costs become too high. Sensitivity analysis shows that with lower discount rates and/or higher marginal pumping costs, groundwater tables are lowered less quickly and eventually kept at higher levels, resulting in a lower subsidence rate and less depletion of the soil.

What lacks in this model, but will be included in a future version of this paper, are the social damage costs of subsidence, particularly Greenhouse Gas (GHG) emissions. These are an important rationale for reducing subsidence in agricultural lands. This will allow us to calculate the welfare loss as a result of deviating from the optimal policy path for different policy scenarios typically considered in subsidence management. We also plan to adapt the model specification in the future so that it can be applied in an urban context. In addition, we propose a stochastic adaptation of the model that removes the assumption of full control of the groundwater level. In reality, there are external factors such as precipitation variability that lead to stochastic fluctuations in groundwater levels that affect subsidence.

Conclusion

Our results show that both the pure time preference trade-off between short-term and long-term production losses as well as water management costs can be rationales for slowing down land subsidence over time, even when we disregard the social damage costs of subsidence normally considered the main reason for subsidence mitigation. This analysis, together with the extensions proposed here, provide valuable input for decision-makers in the design of more efficient long-term policies for groundwater and subsidence management in the Netherlands.

Acknowledgement

The research presented in this paper is part of the project Living on soft soils: subsidence and society (grantnr.: NWA.1160.18.259). This project is funded by the Dutch Research Council (NWO-NWAORC), Utrecht University, Wageningen University, Delft University of Technology, Ministry of Infrastructure and Water Management, Ministry of the Interior and Kingdom Relations, Deltares, Wageningen Environmental Research, TNO-Geological Survey of The Netherlands, STOWA, Water Authority: Hoogheemraadschap de Stichtse Rijnlanden, Water Authority: Drents Overijsselse Delta, Province of Utrecht, Province of Zuid-Holland, Municipality of Gouda, Platform Soft Soil, Sweco, Tauw BV, NAM.

References

Chu, H.-j., Hsiao, C.-t., and Chang, L.-C. (2007). Optimizing Groundwater Supply with Land Subsidence Limit. In *World Environmental and Water Resources Congress 2007*, pages 1–16, Reston, VA. American Society of Civil Engineers.

Gisser, M. and Sanchez, D. A. (1980). Competition Versus Optimal Control in Groundwater Pumping. *Water Resources Research*, 16(4):638–642.

Kok, S. and Hommes-Slag, S. (2020). Cost-benefit analysis of urban subsidence mitigation strategies in Gouda, the Netherlands. PIAHS, 382:761–766.

Koster, H. R. and van Ommeren, J. (2015). A shaky business: Natural gas extraction, earthquakes and house prices. European Economic Review, 80:120–139.

Larson, K., Basagaoglu, H., and Marino, M. (2001). Prediction of optimal safe ground water yield and land subsidence in the Los Banos-Kettleman City area , California, using a calibrated numerical simulation model. Journal of Hydrology, 242:79–102.

Pelsma, T. A. H. M., Motelica-Wagenaar, A. M., and Troost, S. (2020). A social costs and benefits analysis of peat soil-subsidence towards 2100 in 4 scenarios. *PIAHS*, 382:669–675.

Reinelt, P. (2020). Spatial-dynamic seawater intrusion and pumping cost externalities in a confined aquifer. *Resource and Energy Economics*, 59:101117.

Syvitski, J. P. M., Kettner, A. J., Overeem, I., Hutton, E. W. H., Hannon, M. T., Brakenridge, G. R., Day, J., V¨or¨osmarty, C., Saito, Y., Giosan, L., and Others (2009). Sinking deltas due to human activities. *Nature Geoscience*, 2(10):681–686.

Van den Akker, J., Kuikman, P., De Vries, F., Hoving, I., Pleijter, M., Hendriks, R., Wolleswinkel, R., Simoes, R., and Kwakernaak, C. (2008). Emission of co2 from agricultural peat soils in the Netherlands and ways to limit this emission. In *Proc. 13th Intl. Peat Congress After Wise Use–The Future of Peatlands, Tullamore, Ireland, 8–13 june 2008*, volume 1, pages 645–648.

Van den Born, G., Kragt, F., Henkens, D., Rijken, B., Van Bemmel, B., and Van der Sluis, S.

(2016). Dalende bodems, stijgende kosten. Technical report, Planbureau voor de Leefomgeving, Den Haag.

van Hardeveld, H. A., Driessen, P. P. J., Schot, P. P., and Wassen, M. J. (2018). Land Use Policy Supporting collaborative policy processes with a multi-criteria discussion of costs and benefits : The case of soil subsidence in Dutch peatlands. *Land Use Polic*y, 77:425–436.

van Hardeveld, H. A., Driessen, P., Schot, P., and Wassen, M. (2017). An integrated modelling framework to assess long-term impacts of water management strategies steering soil subsidence in peatlands. *Environmental Impact Assessment Review*, 66:66–77.

Wade, C. M., Cobourn, K. M., Amacher, G. S., and Hester, E. T. (2018). Policy Targeting to Reduce Economic Damages From Land Subsidence. *Water Resources Research, 54*(7):4401–4416.

Willemsen, W., Kok, S., and Kuik, O. (2020). The effect of land subsidence on real estate values. *PIAHS*, 382:703–707.

Ground Subsidence socioeconomic vulnerability in Salamanca, Celaya and Irapuato, Central Mexico

K.M. Villarnobo-Gonzalez[1], E. Cabral-Cano [2*], E.A. Fernández-Torres[3].

1 Facultad de Ciencias, Universidad Nacional Autónoma de México.
2 Departamento de Geomagnetismo y Exploración, Instituto de Geofísica, Universidad Nacional Autónoma de México.
3 Posgrado en Ciencias de la Tierra, Instituto de Geofísica, Universidad Nacional Autónoma de México.

Corresponding author: ecabral@igeofisica.unam.mx

Abstract

We use a 2014-2020 ground subsidence velocity field obtained with InSAR techniques and data from Sentinel-1 and the Mexican 2020 census to estimate the shallow faulting risk associated with ground subsidence and the estimation of its socioeconomic vulnerability in Salamanca, Celaya and Irapuato, Central Mexico. The fastest recorded subsidence velocities (-7.0 cm/year) and the largest subsidence-affected urban area (84.62% of its area exposed) are localized in Celaya. The highest socioeconomically vulnerable to subsidence municipality is Salamanca, (92.65% of the population has very high and high socioeconomic vulnerability), followed by Celaya (77.09%) and Irapuato with (43% of their population). The municipality with the largest area affected by low socioeconomic risk to ground subsidence is Irapuato (67.7 km2), followed by Celaya (58.4 km2) and Salamanca (38 km2).

Background

Land subsidence and associated shallow faulting is developed along clearly defined swaths in urban zones where shallow faulting damages critical underground urban infrastructure and larger civil structures and housing are affected by differential settlement and angular distortion as a result of ground deformation. Guanajuato is the heart of the industrial corridor in central Mexico, where industrial and agricultural development and population growth has resulted in excessive groundwater extraction, inducing land subsidence. Synthetic Aperture Radar (InSAR) interferometry was used to characterize the land subsidence process in the Celaya, Irapuato, and Salamanca, municipalities and determined the socioeconomic vulnerability and exposure to this process.

Methods

InSAR time series are based on a sequence of interferograms covering the cities of Irapuato, Salamanca, and Celaya. We used Sentinel 1A and B data between April 3, 2014, and December 31, 2020. We selected Orbit 114 covering the cities of Irapuato and Salamanca, and Orbit 41 to cover the city of Celaya. The unwrapped interferograms and time series analysis was processed with the ISCE, SNAPHU and the MintPy packages at UNAM's Miztli (Figure 1).

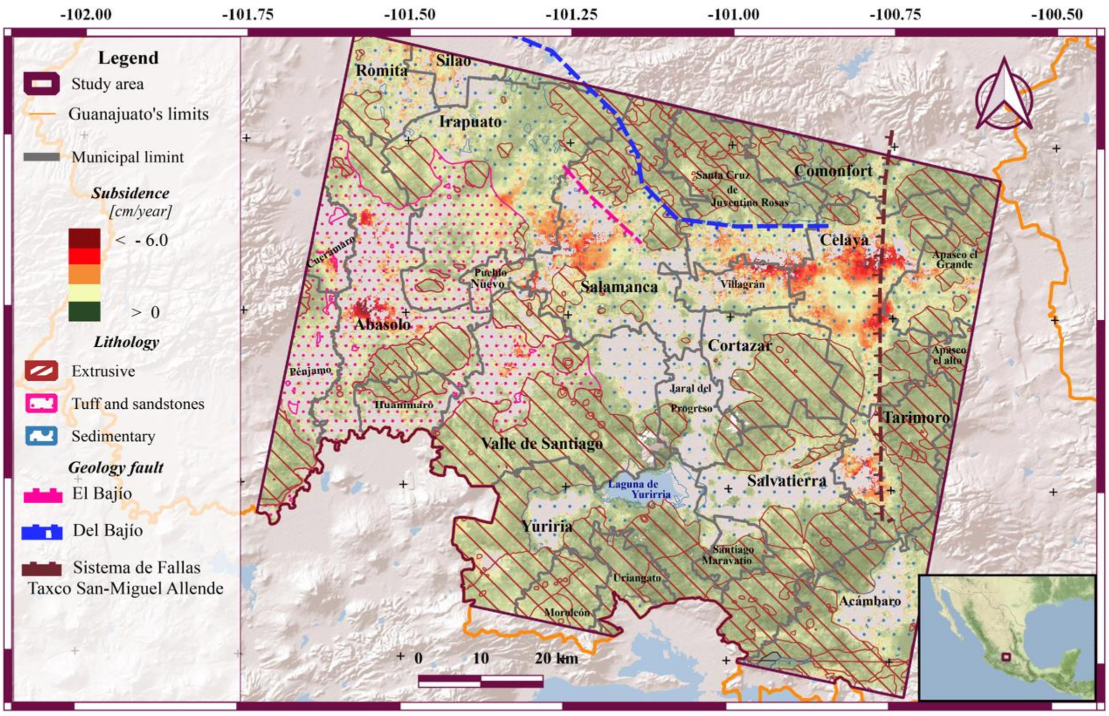

Figure 1 Subsidence velocity map with coherence mask of 0.75. Del Bajío Fault trace and Sistema de Fallas Taxco-San Miguel Allende is taken from Alaniz Álvarez et al. (2005), El Bajío Fault trace is taken from Nieto Samaniego et al. (2012). The base relief map is taken from ESRI (2016).

To determine the socioeconomically vulnerability to subsidence, we used a methodology developed by Novelo-Casanova et al. (2021). This approach is based in the analytical hierarchical process proposed by (Saaty, 1987) and considers 13 parameters that encompass economic factors of the population such as access to basic services, access to health services, population density per dwelling, population with some type of disability and education level, which were considered as social and economic circumstances of the population which may lead a community to have different resiliency to the ground subsidence process and its associated effects. We used the Mexican 2020 population and housing Census (INEGI, 2020,) and the 2020 Guanajuato Geostatistical framework (INEGI, 2020), normalized and then weighted each parameter. This data was then joined with the subsidence velocity map and divided into 5 categories: Very high, High, Moderate, Low and Very Low. The socioeconomic risk is then calculated by multiplying the vulnerability and the subsidence hazard (Figure 2).

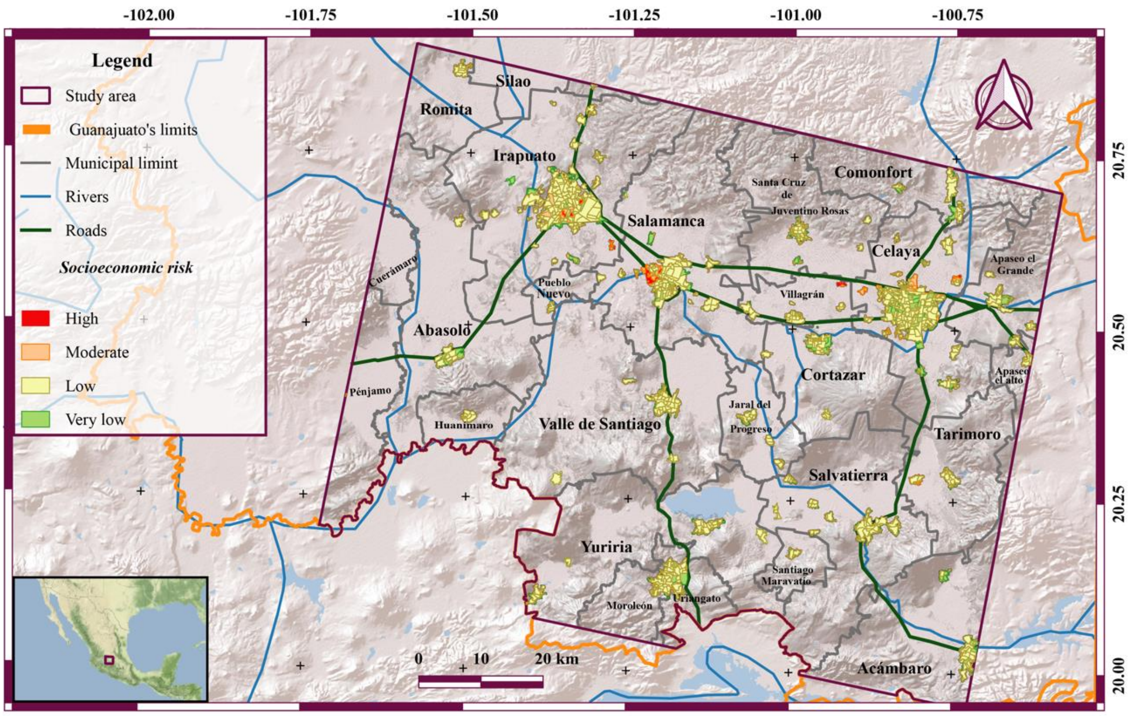

Figure 2 Map of ground subsidence socioeconomic risk.

Results

Our analysis shows that 6.4 km^2 is affected by land subsidence within the municipality of Celaya, 6.6 km^2 within the municipality of Irapuato and 5.7 km^2 within the municipality of Salamanca. The municipality with the highest exposure to subsidence, is Celaya with 84.62% of its urban area exposed, followed by Salamanca with 58.16% and finally Irapuato with 56.5%.

The maximum observed subsidence velocities for Irapuato, Salamanca and Celaya are -4.6 cm/year, -5.8 cm/year and -7.0 cm/year respectively (Figure 1). In Celaya, 71.18% of its population is affected within the low hazard category, which is in the northern sector of the municipality and 15.29% of its population isn't affected by land subsidence, while 13.44% of people is moderately affected; but only 0.09% of people live within the high hazard region. In Irapuato 47.43% of its inhabitants live in the low hazard region, 41.74% live in the non-subsiding region subsidence and 10.74% of its population is located within the moderate subsidence region; while 48% of Salamanca's population live in a non-subsiding region, 29% in the low hazard region, and finally 23% live within the moderate hazard region.

Socioeconomically Vulnerability.

49.26% of the Irapuato's population is moderately vulnerable to land subsidence, 36.5% is under high vulnerability, 6.62% very high vulnerability, 7.2% low vulnerability and 0.40% very high vulnerability. 58.28% of the Celaya population has moderate vulnerable to land subsidence, 18.89% of the population is highly vulnerable, 17.06% has very low vulnerability and 5.74% has low vulnerability. 2.7% of Salamanca's population is very low socioeconomically vulnerable to land subsidence, 4.7%, low socioeconomically vulnerable, 66.8% present moderate socioeconomically vulnerability and 25.9% are highly socioeconomically vulnerable.

Socioeconomically Risk for Subsidence.

Salamanca's population presents 11% of high risk, 16.5% of moderate risk, 48.8% of low risk and 23.3% of very low risk respectively. The distribution of the percentage of affected areas according to the socioeconomic risk associated with subsidence, where 5.4% presents high risk. 6.4% presents moderate risk, 78.7% presents low risk and 9.3% of the area presents very low risk.

The 47% of Celaya's population present very low socioeconomically risk, 38% present low socioeconomically risk, 12% present moderate socioeconomically risk 3% present high socioeconomically risk

The 23.1% of the population has low risk, 48% low risk, 2.54% moderate risk, and 7.2% high risk. 9.9% of the population has very low risk, 82.1% of the area has low risk, 6.1% of the area has moderate risk, and finally 1.8% are under high risk.

Conclusions

56.5% of Salamanca's population (505,779 inhabitants), 47.43% of Irapuato's population (205,588 inhabitants) and 84.71% of Celaya's population (450,118 inhabitants) live within areas exposed to subsidence.

The most socioeconomically vulnerable municipality is Salamanca, where 11.8% of the population is under moderate and high socioeconomic vulnerability to land subsidence, followed by Celaya with 7.2% and Irapuato with 9.7% of its population. Conversely, the municipality with the largest area affected by a low socioeconomic risk is Irapuato (67.7 km^2), followed by Celaya (58.4 km^2) and Salamanca (38.0 km^2).

References

Alaníz-Álvarez, S. A., Nieto-Samaniego, A. F., Orozco-Esquivel, Ma. T., Vassallo, L. F., & Xu, S. (2002). El sistema de fallas Taxco-San Miguel de Allende: Implicaciones en la deformación post-eocénica del centro de México. Boletín de la Sociedad Geológica Mexicana, 55(1), 12–29.

ESRI. (2016). ESRI Shaded Relief. https://qms.nextgis.com/geoservices/473/

INEGI (2020). Marco Geoestadístico. Instituto Nacional de Estadística y Geografía. INEGI. https://www.inegi.org.mx/temas/mg/#Descargas

INEGI (2020). Censo de Población y Vivienda 2020. https://www.inegi.org.mx/programas/ccpv/2020/#Datos_abiertos.

Nieto Samaniego, Á. F., Ojeda García, Á. C., Alaniz Álvarez, S. A., & Xu, S. (2012). Geología de la región de Salamanca, Guanajuato, México. Boletín de la Sociedad Geológica Mexicana, 64(3), 411–425.

Novelo-Casanova, D. A., Suárez, G., Cabral-Cano, E., Fernández-Torres, E. A., Fuentes-Mariles, O. A., Havazli, E., Jaimes, M. Á., López-Espinoza, E. D., Martin-Del Pozzo, A. L., Morales-Barrera, W. V., Morales-Rodríguez, H. L., Nieto-Torres, A., Rodríguez-Elizarrarás, S. R., Solano-Rojas, D., & Velasco-Herrera, V. M. (2021). The Risk Atlas of Mexico City, Mexico: A tool for decision-making and disaster prevention. Natural Hazards, 1–27. https://doi.org/10.1007/s11069-021-05059-z.

Saaty, T. L. (1987). The Analytical Hierarchy Process. *McGraw-Hill International. l.*

Proc. IAHS, 382, 63–70, 2020
https://doi.org/10.5194/piahs-382-63-2020

Regulating Subsidence and its uncertainty in the Dutch Wadden Sea

Johannes A. de Waal and Mathijs W. Schouten

State Supervision of Mines, The Hague, 2290 AA, the Netherlands

Correspondence: Johannes A. de Waal (j.a.dewaal@sodm.nl)

Published: 22 April 2020

Abstract. At the start of gas production its effects on land subsidence are not certain. There are uncertainties in mechanisms, models and parameters. Examples are non-linear deformation of reservoir rock, fault transmissibility, behaviour of overlaying salt and aquifer activity. Looking back at historical cases in the Netherlands, a factor two or three difference between initial prediction and final outcome is quite common. As the Dutch regulator, SSM is tasked with assuring proper management by operators of the risks associated with land subsidence from natural gas production in The Netherlands. Large initial uncertainties can only be tolerated if operators can demonstrate that timely actions can still be taken when predefined subsidence limits are at risk of being exceeded now or in the future. The applied regulatory approach is illustrated by the case history of gas production induced subsidence in the Dutch Wadden Sea area. This environmentally highly sensitive UNESCO World Heritage Site is a natural gas province. Extensive legal, technical and organisational frameworks are in place to prevent damage to its natural values. Initial uncertainties in the predicted subsidence (rate) were later exacerbated by the detection of strong non-linear effects in the observed subsidence behaviour, leading to new concerns. It was realised that – depending on the underlying physical cause(s) – there will be a different impact on future subsidence. To assure proper management of the additional uncertainty by the operator, several improvements in the regulatory approach have been implemented. Possible underlying mechanisms had to be studied in depth and improved data analysis techniques were requested to narrow down uncertainties as time progresses. The approach involves intensified field monitoring, scenario's covering the full range of uncertainties and a particle filter approach to handle uncertainties in predictions and measurements. Spatial-temporal double differences, production data and the full covariance matrix are used to confront scenario predictions against measurements and to assess their relative probability. The regulator is actively involved in assuring this integrated control loop of predictions, monitoring, updating, mitigation measures and the closing of knowledge gaps. The regulator involvement is supported in the Mining law and by appropriate conditions in the production plan assent. With the approach it can be confidently assured that subsidence (rate) will remain within the allowed range.

1 Introduction

The Dutch regulator State Supervision of Mines (SSM) is, amongst other things, tasked with the supervision of the risk associated with land subsidence due to natural gas production. With half the country near sea level and some of the production activities near the unique natural areas of the Wadden Sea tidal flats, land subsidence from gas production is not an issue that is taken lightly in the Netherlands. Experience over the last 50 years demonstrates that accurate prediction of induced land subsidence at the early stages of a gas production project is difficult. A 100 %–200 % deviation in outcome compared to what was considered the most likely scenario at the start of production is not unusual (de Waal et al., 2012, 2015b). From the perspective of the regulator, initial predictions with such large uncertainties can only be accepted if the operator can demonstrate – at any moment during the production period – that timely actions can still be taken when predefined subsidence limits are at risk of being exceeded now or in the future. A scenario-based approach with uncertainties reducing as time progresses and a contin-

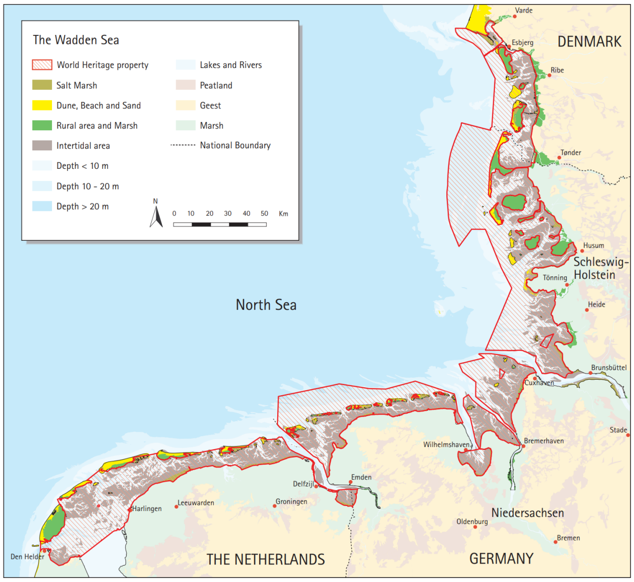

Figure 1. The Dutch Wadden Sea is part of a semi-contiguous UNESCO world heritage site that spans the coastline of The Netherlands, Germany and Denmark. (© UNESCO; source: http://whc.unesco.org, last access: 28 March 2020).

ued demonstration that control can be retained if reality starts to deviate outside the expected range are crucial elements of the regulatory approach. To achieve this SSM has stimulated the development and application of advanced monitoring and data analysis tools by operators as integral part of the regulatory framework (de Waal et al., 2012, 2015b). The need and realisation of these further advances in the regulatory approach are illustrated in this paper by the case history of gas production induced subsidence in the environmentally sensitive Wadden Sea area in the Netherlands.

2 The Wadden Sea case history

The Wadden Sea (Fig. 1) is a large temperate coastal wetland system behind a chain of coastal barrier islands. It is one of the world's most important wetlands and it is on the UNESCO world heritage list, based on its rich diversity, unique morphodynamical features and its wildlife values. It is one of the Netherlands most notable nature conservation areas protected under the European Birds and Habitats Directives. Gas production from fields underneath the Wadden Sea is nevertheless permitted, but only under very strict conditions.

3 Existing regulatory framework

The key question underpinning the applied approach for the Wadden Sea has always been: how much subsidence is acceptable and at which rate? And from the regulator perspective: how can it be reliably assured that (future) subsidence will stay within these limits? To address the issue the concept of "effective subsidence capacity" was developed (van Herk et al., 2010). It is the maximum human-induced subsidence that the affected area can robustly sustain. To determine this "effective subsidence capacity", the maximum volumetric rate of relative sea level rise that can be accommodated in the long term, without damaging the natural values of the Wadden Sea area, was established first. The volume of sediment that can be transported and deposited by nature into the tidal basin where the subsidence occurs ultimately determines the "limit of acceptable average subsidence rate". The capability of the tidal basins to "capture" sediment is the overall rate-determining step (Fig. 2). Effective subsidence capacity is then the maximum average subsidence rate available for human activities. It is obtained by subtracting the subsidence volume rate "consumed" by natural relative subsidence in the area (sea-level rise plus natural shallow compaction) from the total long-term acceptable subsidence volume rate limit.

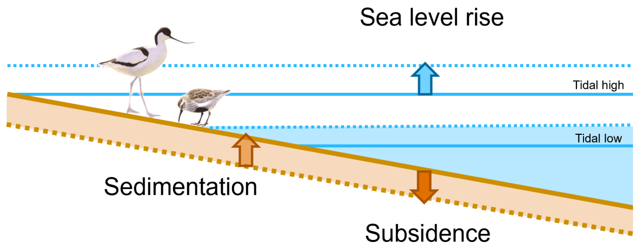

Figure 2. When subsidence and sea level rise are balanced by (extra) sedimentation, the intertidal flats are maintained, and the natural values are likely preserved.

In the operational procedure for mining companies, six-years-average expectation values of subsidence rates are used to calculate the maximum allowable production rates. This is done under the provision that production will be reduced or halted if the expected or actual subsidence rate (natural + man induced) cannot be guaranteed not to exceed the limit of the acceptable subsidence rate now or in the future. The approach is known as the "Hand on the Tap" method. Monitoring and management schemes ensure that predicted and actual subsidence rates stay within the limit of acceptable subsidence rate and that no damage is caused to the protected nature. For further details see (van Herk et al., 2010) and (de Waal et al., 2012).

4 Challenges from observed subsidence delay

Initial uncertainties in the predicted subsidence (rate) of the Ameland field underneath the Wadden Sea were exacerbated by the observation of strongly non-linear (delayed) subsidence during later stages of the production period, see e.g. (Houtenbos, 2015). These were not accounted for in the original subsidence scenarios. Initially the operator assumed that the unexpected behaviour resulted from bi-linear elastic be-

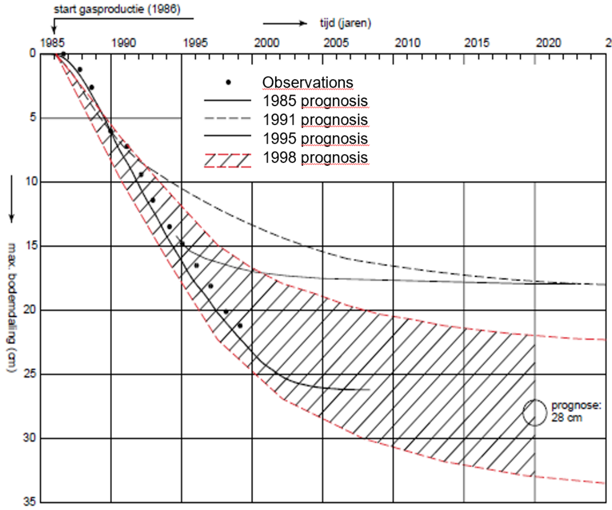

Figure 3. Prognosis for the deepest point on the Wadden Isle of Ameland over time. The current (2019) prognosis for the eventual subsidence is some 40 cm. During the first decades of production, subsidence prognoses were strongly adjusted after each observation survey (© NAM; source: NAM, 1998; Eysink, 1995).

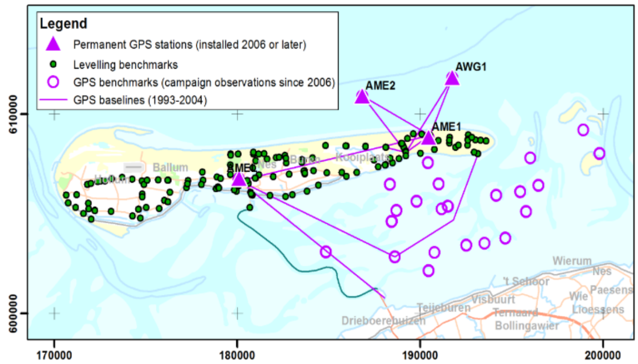

Figure 4. The area around Ameland is measured using a variety of techniques, with different spatial and temporal coverage density (© NAM; source: NAM, 2017).

haviour of the reservoir rock. Later, a continued more or less constant subsidence rate at much reduced reservoir depletion rates was observed, and it became clear that this is too limited an approach (NAM, 2015).

It was realised that – depending on the underlying (combination of) physical cause(s) – the impact on future subsidence could be very different. In addition, it had become clear that the observed steepness of the edges of the subsidence bowl was much larger than predicted and that the apparent reservoir poromechanical compressibilities required to match the geodetic data substantially differed from laboratory compaction data (NAM, 2017). To assure proper management of the uncertainty, several improvements were requested by the regulator to be developed and implemented by the operator:

- Identification and in-depth study of possible mechanisms that could be the cause of the observed subsidence behaviour;
- Improved data assimilation techniques to test if field data can be used to assess which of the above mechanisms play(s) a role in the field;
- Testing of the newly developed approach against the 30-year-plus production/subsidence history of the Ameland gas field located underneath the Wadden Sea.

The project was coined LTS (Long Term Subsidence). The first phase (LTS-I) focussed on identifying possible and credible physical causes for the observed delayed subsidence. The second phase (LTS-II) focussed on applying this knowledge against an actual Wadden Sea field case (Ameland). A sophisticated data assimilation technique was developed and used to test if – using field and surveyance data – it can be determined which of the remaining post-LTS-I mechanisms factually plays a role in the observed delay in the subsidence above the fields underneath the Wadden Sea. Apart from addressing the three main objectives listed above, the LTS studies generated a number of valuable spin-offs:

- Software to manage large volumes of geodetic data;
- A procedure to combine GPS and benchmark data;
- Improved, more formal and objective methods to identify and manage outliers in the geodetic observations;
- An objective method to take noise in the geodetic data from shallow movements into account;
- The use of spatio-temporal double-differences and the full covariance matrix to confront subsidence predictions against geodetic survey data, eliminating the need for (assumed) stable reference points;
- A solution to prevent ensemble collapse from occurring while testing scenario's against field data using an ensemble-based data assimilation technique;
- An improved workflow to derive in-situ compaction from time-lapse GR-logs of signals from radioactive bullets shot into the formation.

5 LTS study organisation

The study had to be carried out to the satisfaction of the Inspector General of Mines (the head of the State Supervision of Mines of the Netherlands). Its execution was an official condition for the approval of a number of Wadden Sea Field Development Plan updates. The aim of the study was to improve knowledge of the physical background of the measured time-dependent effects in the subsidence behaviour and its possible influence on expected subsidence in the long term. The study was to lead to a better understanding of the physical processes that explain the subsidence that had already occurred, with the aim of improving the forecasting of future subsidence. The study had to be based on generally accepted rules of physics, objective measurement data and proven scientific methods. The LTS study was carried out on the basis of a proposal by the operator: "Proposed Research Program for Higher Order Subsidence Modelling of The Netherlands Gas fields" (NAM, 2015). The proposal included an overview of the historical development of existing practices, their identified deficiencies and a proposed research program and deliverables for the LTS study. The document resulted from framing and brainstorm sessions within the operator organisation and with experts from SSM and the TNO AGE group (that exclusively advises SSM and the Ministry of Economic Affairs and Climate). Given the importance of the study, it was decided to establish an independent LTS Steering Committee (the SC LTS). The LTS study was carried out by the operator and external parties (public universities and research laboratories) with oversight provided by the SC LTS and SSM. The Wadden Sea Academy – established in 2008 with the task of providing a scientific basis for the management of the natural and social values of the Wadden Sea Region – was asked to create, facilitate and chair the SC LTS. The committee consisted of six internationally renowned experts in the fields of Geodesy, Experimental Rock Mechanics, Theoretical Rock Mechanics and Mining induced Subsidence. The SC LTS members were proposed partly by the operator and partly by the Wadden Sea Society (an independent NGO). They were subsequently also accepted by the Wadden Academy. Chairman and Technical Secretary for the committee were provided by the Wadden Academy. Representatives from SSM and TNO-AGE participated in the SC LTS as observers. The members met on a bi-annual basis between April 2013 and June 2015 to discuss progress and to provide guidance to the first phase of the LTS study. Between meetings, separate discipline meetings took place as well as telephone discussions and emails. Regular meetings were organised by the Wadden Academy to inform stakeholders from nature conservation and public organisations about the project progress and to address their questions and suggestions. For further details see (Wadden Academy, 2015).

At the end of the project a fully independent review was carried out at the request of SSM by an internationally renowned expert not involved in the LTS study (Teatini, 2017).

6 LTS Phase I

During the first phase of the study (LTS-I) the emphasis was on the identification and study of potential mechanisms that could explain the observed non-linear subsidence behaviour. The following six credible explanations were initially identified:

1. The non-linearity is not real but an artefact from noise and uncertainties in the data;
2. Salt flow in thick layers of rock salt overlaying the gas reservoir causes the observed delays;
3. Slow (delayed) depletion in underlaying and adjacent aquifers not captured in the modelling;
4. Non-equilibrium pressure diffusion within the reservoir during the initial production period;
5. Intrinsic non-linear and/or non-elastic in-situ reservoir rock compaction against pressure drop;
6. Collapse of high porosity reservoir rock intervals after reaching a large depletion of the initially strongly overpressured gas in the reservoir.

The hypotheses were addressed in a number of separate discipline studies. In addition, several other possible influences on the surface subsidence were studied. These included different influence functions relating reservoir compaction to surface subsidence, effects of upscaling and the effects of a strongly heterogeneous and spatially variable overburden. The results of all studies carried out have been published in technical reports and scientific publications (NAM, 2015, 2017) and references therein. The outcomes are briefly summarised below and in Fig. 5.

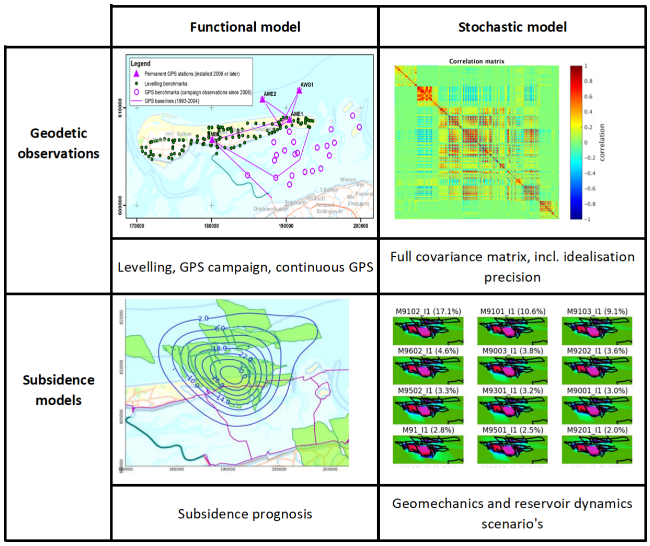

Figure 5. Four quadrant summary of the LTS elements. Both models and measurements are assigned a functional and a stochastic description. The LTS study aims at confronting these. Images from © NAM; source: NAM (2017).

6.1 Noise and uncertainties

The studies carried out concluded that the observed non-linear subsidence behaviour is real and not an artefact of noise and/or uncertainties in the geodetic and other data. The hypothesis was therefore discarded. The studies did show that subsidence modelling precision can be improved significantly by taking correlation structures in the geodetic data into account. Improved methods were developed for objective outlier identification and handling, data reduction techniques for large geodetic data sets and for the processing and use of GPS data (Samiei-Esfahany and Bähr, 2015), (Williams, 2015). The work was supported by the development of a Bayesian framework to test and validate the quality of subsidence predictions against field measurements (Park and Bierman, 2015).

6.2 Salt flow

Extensive 1D and 3D modelling studies were carried out at the University of Utrecht to assess the potential effect of salt flow in the thick halite layers above the gas reservoirs in the Wadden Sea (Marketos et al., 2015). Results demonstrate that – on its own – such salt flow cannot explain the observed subsidence behaviour and in particular not its temporal behaviour. Also, an observed translation of the subsidence bowl over time is likely the result of changes in the reservoir depletion pattern over time and not a result of salt flow. Nevertheless, the studies demonstrate that salt flow can have an effect on the shape of the subsidence bowl and on the time evolution of subsidence, all very much depending on the values of the in-situ salt material properties. Note that salt flow can influence the shape of the subsidence bowl but not its volume.

6.3 Delayed aquifer depletion

Aquifer pressure depletion and its uncertainty range play a key role in the subsidence in the Wadden Sea. Important uncertainties are how well the aquifers are connected to the gas bearing intervals, the permeability in the aquifers and whether or not residual gas (significantly slowing down depletion rates) is present. Existing reservoir engineering models to calculate the effect of aquifer depletion were improved taking new production and well data into account. Results suggest that aquifer depletion is probably slower than originally assumed. Use of the reservoir engineering models under different parameter assumptions allows the calculation of alternative scenarios that can be tested against field production and subsidence data.

6.4 Anomalous pressure diffusion within the reservoir

The mechanism is based on the assumption that low permeability areas within the reservoir and possibly even at the microscopic pore level could result in a long-term (tens of years) non-equilibrium gas pressure distribution within the reervoir rock that would strengthen its effective macroscopic compressibility (Mossop, 2012, 2015). Although not proven impossible, the mechanism seems unlikely and could not be made more plausible on the basis of the study. The hypothesis was discarded.

6.5 Non-linear and/or non-elastic reservoir rock

Extensive long term (up to 12 weeks) laboratory compaction experiments under simulated in-situ conditions were carried out on Rotliegend reservoir rock samples: the gas-bearing rock in the Wadden Sea gas fields (Hol et al., 2015). The rock was sampled specifically for this study from the Wadden Sea Nes field. Results demonstrate that the compaction of the samples becomes increasingly inelastic (up to 80 %) at higher porosities and that the inelastic component remains considerable (some 50 %) at 20 % porosity (representative for the average in-situ reservoir rock). The laboratory derived inelasticity/creep turned out independent of temperature or the type of pore fluid over the ranges applied during the laboratory experiments. Overall, the compaction numbers measured during the laboratory measurements are comparable to those derived from field data. To capture the observed inelastic creep behaviour a rate-type constitutive model (Pruiksma et al., 2015) was used in the subsequent (LTS2) subsidence modelling to describe the constitutive behaviour of the Rotliegend reservoir rock. Note that the degree of non-linear reservoir rock compaction (with pressure drop) in first order does not influence the shape of the subsidence model while it has a large effect on the volume of the subsidence bowl at a given level of pressure depletion.

6.6 Pore collapse at high pressure depletion

The observed increase of subsidence rate would be due to "pore collapse" of weaker (high porosity) intervals in the reservoir at large amounts of pressure depletion during the later stages of production. Such behaviour has been observed during oil and gas production from chalk fields (Smits et al., 1988), and in the laboratory for high porosity samples from highly over-pressured sandstone gas fields (Schutjens and de Ruig, 1997). At high enough effective stresses the phenomenon is observed for all porous rock but usually only at stress levels far above the range that can occur in de Wadden Sea gas fields. The option could be excluded by long term laboratory experiments on high porosity Rotliegend reservoir samples at effective stresses significantly exceeding those that can occur in-situ. The hypothesis was discarded (Hol et al., 2015).

7 LTS Phase II

During the second phase of the LTS study the emphasis was on testing the relevance of the credible explanations that survived LTS-I in the real world and in particular for the observed subsidence delays in the Wadden Sea. A probabilistic Bayesian framework Ensemble based Subsidence Interpretation and Prediction tool (ESIP), was developed by TNO (Candela et al., 2017) to objectively confront a large set of different scenarios against geodetic observations by calculating the match of the model with the data expressed by a $\chi 2$ value. Next to delivering a probabilistic confrontation workflow, the tool also provides an objective statistical description of the outcome, i.e. an expectation case based on the weighted average and a 95 % confidence interval of the posterior model ensemble. TU Delft developed advanced geodetic processing software providing an interface between the geodetic data and the confrontation workflow (van Leijen et al., 2017).

The operator subsequently tested a somewhat modified version of the ESIP tool on the Ameland field underneath the Wadden Sea (NAM, 2017) as recommended by the SC LTS and as requested by SSM. The Ameland case was selected as the first test case given the long (30 year plus) production history and the large set of reservoir, production and geodetic survey data available for the field.

7.1 Scenarios tested

Some 58 history-matched pressure depletion scenarios were tested. Each meets the (gas and water) production data and the pressure data over the full Ameland field history while covering a wide range of different aquifer depletion distributions, with and without the presence of residual gas in the aquifers. For each of these pressure scenarios, parameter values of a generic RTICM subsidence model (Pruiksma et al., 2015) and (van Thienen-Visser et al., 2015) and a (moving) rigid basement influence function (Geertsma, 1966; van Opstal, 1973; Thienen-Visser and Fokker, 2017) were varied in a Monte Carlo simulation. The RTICM model was adapted to be able to handle the large amount of initial gas overpressure in the Ameland field. A time dependent shape factor was added to the influence function with a value dependent on the viscous behaviour of the salt layer above the reservoir. Each set of parameters drawn from the prior distributions during the Monte Carlo simulations results in a subsidence model member with the total set of members defining the ensemble. When confronted against the geodetic data (the full covariant matrix of the spatio-temporal double differences), the resulting fit of each member defines its probability and thereby its weight. The theory used to calculate the test metric accounts for the uncertainties in both the geodetic data and the geomechanical model and is based on a further development of (Nepveu et al., 2010). Modifications were successfully made to the applied goodness-of-fit metric to avoid ensemble collapse problems (Snyder et al., 2008) typical for particle filtering methods involving a large number of independent variables (9 independent parameters in the present study).

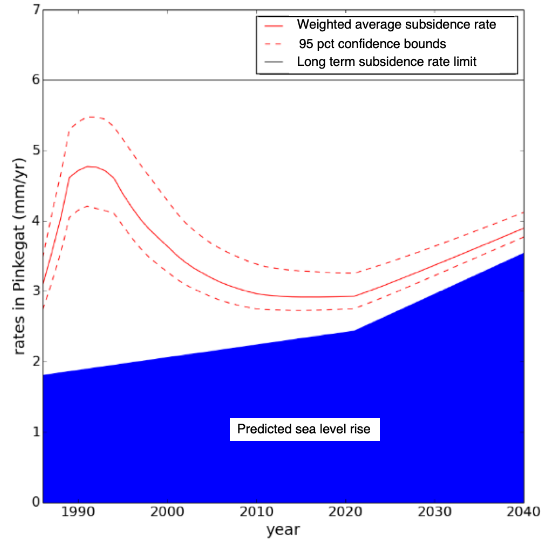

Figure 6. Posterior scenarios within the 95 % confidence band stay below the long-term average subsidence rate limit (© NAM; source: NAM, 2017, Fig. 62).

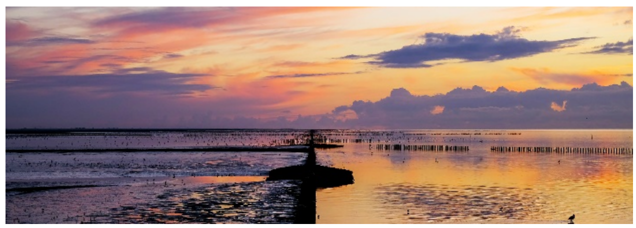

Figure 7. The Wadden sea tidal flats just after sunset.

It is important to not only use the quality of fit of predictions against double difference geodetic data as some simple features of the misfit can then easily be missed. E.g. a relatively small lateral shift of the calculated subsidence bowl relative to its measured position will result in none of the subsidence members achieving a good fit against the double difference geodetic data and ESIP's discriminating capability will be lost. To identify and avoid such issues, visualisation and visual inspection of the predicted and measured subsidence (contours) remains important.

8 Results

Using the ESIP, some 20 000 subsidence members, covering the large range of possible parameter values were tested against the geodetic data for each of the 58 pressure scenarios resulting in a total of more than one million members.

The following results were obtained:

1. Likely reservoir and aquifer depletion scenarios and parameter values for the subsidence model, salt flow and the influence function can be identified for Ameland;

2. Posterior parameter uncertainties are much reduced relative to the prior distributions as more geodetic data becomes available over time. In particular early measurement campaigns already significantly narrow the uncertainty for Ameland;

3. Posterior RTICM parameters derived are consistent with those derived from laboratory measurements (de Waal et al., 2015a);

4. The effect of lateral aquifers seems limited;

5. Salt flow alone cannot explain the observed time dependent (delayed) subsidence;

6. Extrapolations show that the likely scenarios within a 95 % confidence band will stay within the defined subsidence capacity including the longer term "acceptable average subsidence rate" limit (Fig. 6);

7. Emergency stop scenarios demonstrate the feasibility of the "Hand on the Tap" approach with its effectiveness obviously decreasing towards the end of field life.

Data availability. This paper discusses the regulatory approach developed to assure that gas production induced subsidence (rate) in the Dutch Wadden Sea area stays within pre-defined limits, despite large uncertainties in its prediction. The paper adds overview and synthesis from the perspective of the regulator to the results of studies carried out by or for the operator at the request of the regulator. No data other than that resulting from these studies is used. Data availability is via reference to the publications on these studies.

Author contributions. Both authors participated as observers on behalf of State Supervision of Mines on the LTS Steering Committee. They provided regulatory perspective during the LTS studies carried out by the operator and external parties (public universities and research laboratories). Both authors were involved in reviewing the results of the LTS studies as they progressed and in assessing their consequences. The first author wrote the original draft with data visualisation contributions, critical review, comments and revisions provided by the second author.

Competing interests. The authors declare that they have no conflict of interest. Their employer SSM is an independent regulator concerned with the safety of people and the protection of the environment during energy extration and the exploitation of the subsurface, now and in the future.

Special issue statement. This article is part of the special issue "TISOLS: the Tenth International Symposium On Land Subsidence – living with subsidence". It is a result of the Tenth International Symposium on Land Subsidence, Delft, the Netherlands, 17–21 May 2021.

Acknowledgements. We thank the management of State Supervision of Mines for their permission to publish this paper. We also thank staff at TNO and NAM for stimulating discussions and support, although they may not agree with all the interpretations and conclusions of this paper.

References

Candela, T. G. G., Fokker, P. A., and Hegen, D.: Ensemble-based subsidence interpretation and prediction ESIP: Technical Reference Manuel, TNO report R11278, January 2017, available at: https://nam-feitenencijfers.data-app.nl/download/rapport/630f8041-25d9-48cd-9329-1ef0d29fc708?open=true (last access: 22 December 2019), 2017.

de Waal, J. A., Roest, J. P. A., Fokker, P. A., Kroon, I. C., Breunese, J. N., Muntendam-Bos, A. G., Oost, A. P., and van Wirdum, G.: The effective subsidence capacity concept: How to assure that subsidence in the Wadden Sea remains within defined limits?, Neth. J. Geosci., 91, 385–399, 2012.

de Waal, J. A., van Thienen-Visser, K., and Pruiksma, J. P.: Rate type isotach compaction of consolidated sandstone, in: Proceedings 49th US Rock mechanics/Geomechanics symposium (ARMA), San Francisco, 28 June–1 July, Volume: ARMA 15-436, 2015a.

de Waal, J. A., Muntendam-Bos, A. G., and Roest, J. P. A.: Production induced subsidence and seismicity in the Groningen gas field – can it be managed?, Proc. IAHS, 372, 129–139, https://doi.org/10.5194/piahs-372-129-2015, 2015b.

Eysink, W. D., Dijkema, K. S., Smit, C. J., and van Dobben, H. J.: Monitoring the effects of subsidence of the coastal island Ameland in the Wadden Sea, in: Proceedings 5th International Symposium on Land Subsidence, The Hague, 16–20 October 1995, Balkema, Rotterdam, 259–267, 1995.

Geertsma, J.: Problems of Rock Mechanics in Petroleum Production Engineering, in: Proceedings 1st Congress of the International Society of Rock Mechanics, 25 September 1966, Lisbon, I, 585–594, 1966.

Hol, S., van der Linden, A. J., Zuiderwijk P. M. M., and Marcelis, F. H. M.: Geomechanical experiments on Ten Boer rock samples from well Moddergat-3, Shell Report SR.15.11616, 2015.

Houtenbos, A. P. E. M.: Bodemdaling Waddenzee 1997–2011, 38 pp., available at: http://www.waddenzee.nl/fileadmin/content/Bodemdaling/2007/AML07.pdf (last access: 22 December 2019), 2015.

Marketos, G., Broerse, D. B. T., Spiers, C. J., and Govers, R.: Long-term subsidence study of the Ameland gas field: time-dependence induced by rock salt flow, Report RUU, 1874/328461, 2015.

Mossop, A.: An explanation for anomalous time dependent subsidence, in: Proceedings. 46th US Rock Mechanics/Geomechanics Symposium, 24–27 June 2012, Chicago, Illinois, USA, 12–518, 2012.

Mossop, A.: Derivation of a Scale Dependent Pressure Diffusion Equation, NAM Report EP201506209300, 2015.

NAM: Bodemdalingsprognose van Ameland – status rapport 1998, NAM Report nr. 1998.09.000394, 1998.

NAM: Wadden Sea Long term Subsidence Studies – Overview report, Report: EP201506209625, June 2015, available at: http://feitenencijfers.namplatform.nl/download/rapport/2ca6c8d8-c0d4-4c10-8460-672f93b4cdaa?open=true (last access: 22 December 2019), 2015.

NAM: Ensemble Based Subsidence application to the Ameland gas field – long term subsidence study part two (LTS II), Doc. nr. EP201710200509, available at: https://nam-feitenencijfers.data-app.nl/download/rapport/2a2da56c-faee-4453-a8a7-c64c43b418a6?open=true (last access: 22 December 2019), 2017.

Nepveu, M., Kroon, I. C., and Fokker, P. A.: Hoisting a red flag: An early warning system for exceeding subsidence limits, Math. Geosci., 42, 187–198, 2010.

Park, T. and Bierman, S.: A Bayesian framework for validating and comparing models for prediction of surface displacements due to reservoir compaction, Shell report SR13. 11680, 2015.

Pruiksma, J. P., Breunese, J. N., Thienen-Visser, K., and de Waal, J. A.: Isotach formulation of the rate type compaction model for sandstone, I. J. Rock Mech. Min. Sci., 78, 127–132, https://doi.org/10.1016/j.ijrmms.2015.06.002, 2015.

Samiei-Esfahany, S. and Bähr, H.: Research and Development Project for Geodetic Deformation Monitoring – Contribution to the research project: "Long-term study on anomalous time-dependent subsidence in the Wadden Sea Region", NAM report EP201505216980, 2015.

Schutjens, M. T. M. and de Ruig, H.: The influence of stress path on compressibility and permeability of an overpressurised reservoir sandstone: Some experimental data, Phys. Chem. Earth, 22, 97–103 1997.

Smits, R. M. M., de Waal J. A., and Kooten, J. F. C.: Prediction of abrupt reservoir compaction and surface subsidence due to pore collapse in carbonates, SPE Formation Evaluation, 3, June 1988.

Snyder, C., Bengtsson, T., Bickel, P., and Anderson, J.: Obstacles to high-dimensional particle filtering, Mon. Weather Rev., 136, 4629–4640, 2008.

Teatini, P.: The nog term subsidence study of the Wadden Sea Region – review LTS2 final report – Comessa N3E 11/16, April 2017.

Thienen-Visser, K. and Fokker, P. A.: The future of subsidence modelling: compaction and subsidence due to gas depletion of the Groningen gas field in the Netherlands, Neth. J. Geosci., 96, 105–116, 2017.

van Herk, J., Roest, J. P. A., Kroon, I., Breunese, J. N., and de Waal, J. A.: How much subsidence is allowed: The introduction of the effective subsidence capacity concept in The Netherlands, Proc. IAHS, 339, 420–425, 2010.

van Leijen, F., Esfahany, S. S., van der Marel, H., and Hanssen, R.: A standardized approach for the integration of geodetic data for deformation analysis, in: 2017 IEEE International Geoscience and Remote Sensing Symposium: International Cooperation for Global Awareness, IGARSS 2017 – Proceedings. Vol. 2017-July Institute of Electrical and Electronics Engineers Inc., 8127112, 957–960 2017.

van Opstal, G. H. C.: The effect of base-rock rigidity on subsidence due to reservoir compaction, in: Proc. 3rd Congress of the Int. Soc. of Rock Mech., Denver, II, Part B, 1102–1111, 1974.

van Thienen-Visser, K., Pruiksma, J. P., and Breunese, J. N.: Compaction and subsidence of the Groningen gas field in the Netherlands, Proc. IAHS, 372, 367–373, https://doi.org/10.5194/piahs-372-367-2015, 2015.

Wadden Academy: Appraisal of the long-term subsidence study of the Wadden Sea region, Technical Report, 14 pp., June 2015, available at: https://www.waddenacademie.nl/fileadmin/inhoud/pdf/03-Thema_s/Geowetenschap/Bodemdaling/Appraisal-LTS-studydef30062015.pdf (last access: 22 December 2019), 2015.

Williams, S.: Description of GPS uncertainties within the Long-Term Study on Anomalous Time-Dependent Subsidence, Nat. Oceanographic Centre, Liverpool, 2015.

A Brief Introduction to Land Subsidence Monitoring in Houston, Texas, USA

G. Wang[1], A. Greuter[2], M. J. Turco[3]

1 Professor, Dept. of Earth and Atmospheric Sciences, Univ. of Houston, Houston, TX 77204 (corresponding author). ORCID: https://orcid.org/0000-0003-3731-3839. Email: gwang@uh.edu
2 Director of Research and Water Conservation, Harris-Galveston Subsidence District, Friendswood, TX 77546. Email: agreuter@subsidence.org
3 General Manager, Harris-Galveston Subsidence District, Friendswood, TX 77546. Email: mturco@subsidence.org

Abstract
This paper has summarized the techniques and methods used for subsidence monitoring in the greater Houston, Texas, region from the 1900s to the 2010s. The primary methods include spirit leveling, extensometer, tide gauge, Global Positioning System (GPS), Interferometric Synthetic Aperture Radar (InSAR), and Light Detection and Ranging (LiDAR). The subsidence monitoring experience learned in the Houston region is expected to be transferable to other areas suffering from land subsidence.

Introduction
For over 100 years, the greater Houston region has been adversely impacted by land subsidence associated with excessive underground-fluid (primarily groundwater) withdrawals. The Houston region, as the term is here used, comprises an area of approximately 22,500 km^2 (150 km by 150 km) and encompasses nine counties in the Texas Gulf Coast plain with a population of over seven million people at the 2020 census estimates (Fig. 1), covering the regulatory areas of the Harris-Galveston Subsidence District (HGSD), Fort Bend Subsidence District (FBSD), Lone Star Groundwater Conservation District (LSGCD), and Brazoria County Groundwater Conservation District (BCGCD). The earliest subsidence was observed in the Goose Creek oil field in the early 1920s, about 40 km east of downtown. From the 1940s through the 1970s, rapid subsidence at several centimeters per year occurred in southeast Houston, including downtown Houston and areas along the Houston Ship Channel and Galveston Bay. In the 1990s, subsidence rates began to increase further inland as the rapid population growth continued in the region. Subsidence caused frequent damage to infrastructure (such as buildings, roadways, bridges, underground utility lines, and levees) and contributed to flooding, ultimately adding financial burdens on local residents and business owners. In order to tackle the problem of subsidence, the U.S. Geological Survey (USGS), National Geodetic Survey (NGS), HGSD, and many other local entities have been conducting subsidence monitoring since the 1900s. This article aims to summarize the tools and methods used for subsidence monitoring in Houston.

Land Surface Elevation Monitoring
Elevation or elevation-change measurements are fundamental to tracking land subsidence over time. Prior to the 1990s, subsidence within the Houston region was primarily measured using spirit-leveling surveys and extensometers. Global Positioning System (GPS) has gradually replaced the conventional leveling surveying and has become the primary tool for subsidence monitoring since the 1990s. Interferometric Synthetic Aperture Radar (InSAR) and Light Detection and Ranging (LiDAR) techniques have been applied to subsidence studies in the Houston region since the 2000s, which provide spatially dense measurements.

Spirit Leveling

NGS and its predecessor agency, United States Coast and Geodetic Survey, had established extensive networks of first- and second-order level lines covering most of the Houston region since the 1900s. The first spirit leveling survey was the first-order level line from Smithville to Galveston, which was run in 1905 and 1906. Since the first leveling survey, this first-order line was resurveyed several times in the following decades, and more first-order and second-order survey lines were added and repeatedly surveyed from the 1940s to 1970s. The subsidence results derived from these leveling surveys were published in USGS reports.

Extensometer

USGS has been operating 13 deep borehole extensometers at 11 sites in Houston since the 1970s and the early 1980s. Several piezometers were installed at each extensometer site for simultaneously monitoring groundwater levels at different depths. A new borehole extensometer was established in Katy, Fort Bend County, in 2017. As of the 2020s, there are 14 borehole extensometers at 12 sites within the Houston region (Fig. 1). Extensometers measure the compaction within the sediments from the land surface to the bottom of the extensometer borehole. USGS publishes the extensometer data to the public annually. These extensometers face the problem of aging equipment after being continuously operated for about half a century. HGSD and the University of Houston (UH) are working together to install permanent GPS stations at extensometer sites to preserve the continuity of subsidence monitoring. As of 2022, seven of these 12 extensometer sites have co-located GPS stations.

Tide Gauge

Tide gauges or stream gages had been used for land subsidence monitoring along the Houston Ship Channel and Galveston Bay areas during the 1960s and 1970s. As of 2022, the Center for Operational Oceanographic Products and Services (CO-OPS) at National Oceanic and Atmospheric Administration (NOAA) operates about 30 tide gauges within the Galveston Bay area (Fig. 1). Most of these stations were installed in the 2010s. The one-century tide gauge data (1904-2021) at the Galveston Pier 21 have been frequently used to delineate natural subsidence in the coastal area. All tide gauge data are available at NOAA (https://tidesandcurrents.noaa.gov).

GPS

Houston is one of the earliest urban areas that employed GPS for land subsidence monitoring. Campaign GPS surveys were employed in subsidence monitoring at benchmarks in Houston in the late 1980s, before the complement of the GPS satellite constellation in 1993. HGSD started to install GPS stations in the early 1990s. The early permanent GPS stations, known as Port-A-Measure (PAM), were designed for periodic surveys rather than continuous surveys, to overcome the high costs of GPS equipment at that time. As of 2021, the PAM network has expanded to over 110 permanent stations. UH has been building a permanent GPS network for urban geological hazards monitoring since 2013 (Wang et al., 2015). As of 2021, the UH GPS network comprises 70 permanent stations. The Texas Department of Transportation (TxDOT), SmartNet, the City of Houston, and several other agencies operate approximately 50 continuous GPS stations in the Houston region. Altogether, there are approximately 230 active permanent GPS stations in the Houston region as of 2021, which is called HoustonNet. Ongoing patterns of subsidence in the Houston region are carefully monitored by HGSD and UH using GPS data from the HoustonNet. The detailed methods for HoustonNet data processing are presented in a recent publication (Wang et al., 2022).

InSAR

InSAR has become a powerful tool for remotely mapping land-surface deformation (e.g., landslide, subsidence, faulting) over time and space. In contrast to benchmark and GPS measurements, the InSAR techniques have the ability to map ground deformation over large areas with a high spatial resolution at a low cost. Numerous researchers from USGS, HGSD, and universities have used InSAR for delineating subsidence in the Houston region since the early 2000s.

Airborne LiDAR

LiDAR mapping has become a powerful tool for obtaining bare-earth digital elevation models (DEMs) for monitoring landslides, volcanos, shoreline erosion, and land subsidence. In October 2001, the Tropical Storm Allison Recovery Project (TSARP) collected airborne LiDAR data over the entire Harris County. The USGS used the 2001 LiDAR data to produce the land subsidence map between the 1915-17 to 2001 in the Harris County (Kasmarek et al., 2009). The map was constructed using geographic information system (GIS) techniques that subtracted 1915–17 land-surface (topographic map) elevations from the 2001 LiDAR-derived DEM. This map provided the high-resolution (5 m by 5 m) subsidence estimates over the entire Harris County for the first time. Multiple airborne LiDAR datasets have been collected since the 2000s within the greater Houston region.

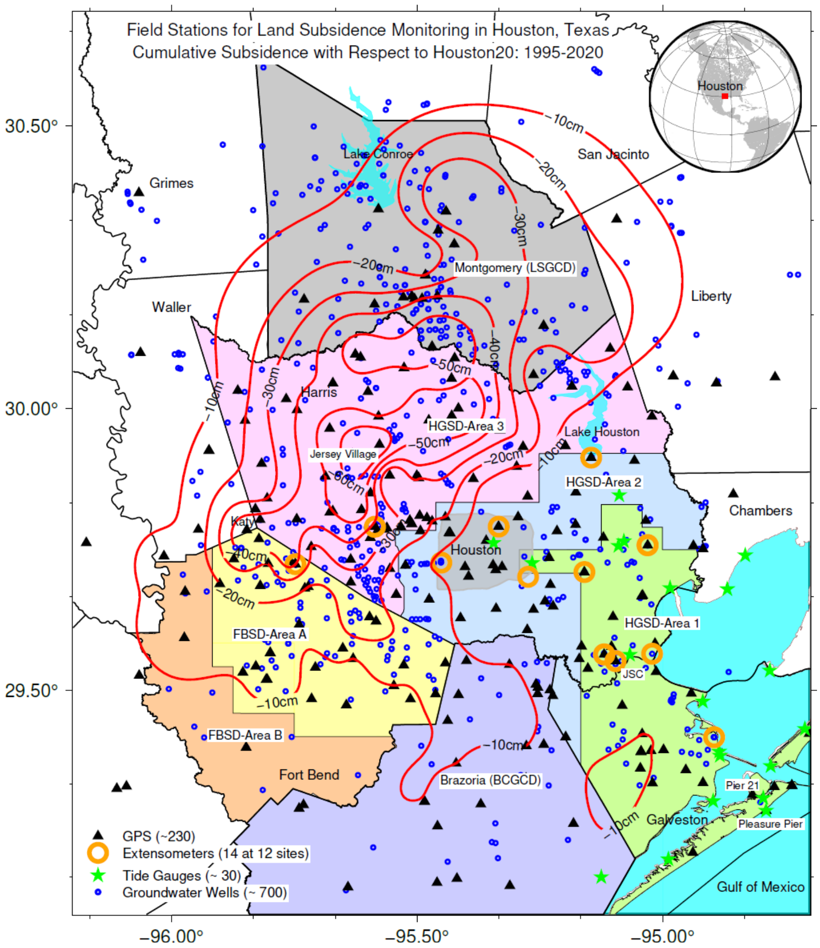

Figure 1 Map showing the current field stations (GPS, Extensometers, Tide Gauges, Groundwater Wells) in the Houston region for land subsidence monitoring. The contour lines depict cumulative land subsidence during the GPS age from 1995 to 2020. The cumulative subsidence measures are estimated according to the observations at approximately 200 permanent GPS sites and 12 extensometer sites. Most GPS stations started after 2000. For those sites that do not have GPS data in the early years or recent years (decommissioned), the subsidence spanning the gap is projected according to its adjacent 3-year-average subsidence rate. The vertical displacements are aligned to the Stable Houston Reference Frame

(Houston20) (Agudelo et al., 2020). A contour map depicting the cumulative subsidence from 1906 to 2000 was presented in Gabrysch and Neighbors (2005), and a contour map depicting the cumulative subsidence from 1978 to 2020 was presented in Greuter et al. (2021).

Groundwater-Level Monitoring

The City of Houston was founded in 1837, and groundwater was the primary source of water resources in its early history. The first well for groundwater pumping was drilled in 1886 to a depth of 43 m in the downtown area. The groundwater was reported as free-flowing. In general, the groundwater levels in the Chicot and Evangeline aquifers were higher than the land surface in the Houston region before the early 1910s. Industrial pumping began after the opening of the Houston Ship Channel in 1915. The USGS began to monitor groundwater levels in the Houston region in the early 1910s. As of the 2020s, USGS routinely measures groundwater levels in over 700 wells in the Houston region for subsidence study and groundwater resource management. The locations of these active wells are plotted in Fig. 1. USGS began to publish an annual report documenting the short-term and long-term groundwater level changes in the Houston region in 1977.

Summary

The rapidly growing population in the Houston region means that groundwater resources must be carefully managed, and subsidence must be vigilantly monitored. High costs for leveling surveys and building extensometers have prohibited frequent releveling and adding more extensometers. GPS techniques have become the primary monitoring tools in the Houston region since the 1990s. Since the late 2010s, HGSD and FBSD have been working towards integrating remote sensing technologies (InSAR, LiDAR) into their routine subsidence monitoring. HGSD and FBSD have developed sophisticated protocols and methods for subsidence monitoring and mitigation. The subsidence monitoring experience learned in Houston is expected to be transferable to other regions suffering from land subsidence.

References

Agudelo, G., Wang, G., Liu, Y., Bao, Y., & Turco, M. J. (2020). GPS geodetic infrastructure for subsidence and fault monitoring in Houston, Texas, USA. *Proc. Int. Assoc. Hydrol. Sci.* 382(4), 11–18. https://doi.org/10.5194/piahs-382-11-2020

Gabrysch, R. K., & Neighbors, R. J. (2005). Measuring a century of subsidence in the Houston-Galveston region, Texas, USA. 7th International Symposium on Land Subsidence, 379–387, Shanghai, P.R. China, October 23–28, 2005.

Greuter, A., Turco, M. J., Petersen, C. M., & Wang, G. (2021). Impacts of groundwater withdrawal regulation on subsidence in Harris and Galveston counties, Texas, 1978-2020. *GeoGulf Trans*. 71, 109–118.

Kasmarek, M. C., Gabrysch, R. K., & Johnson, M. R. (2009). Estimated land-surface subsidence in Harris County, Texas, 1915–17 to 2001, U.S. Geological Survey Scientific Investigations Map 3097, 2 sheets. https://doi.org/10.3133/sim3097

Wang, G., Greuter, A., Petersen, C. M., & Turco, M. J. (2022). Houston GNSS network for subsidence and faulting monitoring: data analysis methods and products, *J. Surv. Eng.* 148(4), 04022008. https:/doi.org/10.1061/(ASCE)SU.1943-5428.0000399

Wang, G., Welch, J., Kearns, T. J., Yang, L., & Serna, J. (2015). Introduction to GPS geodetic infrastructure for land subsidence monitoring in Houston, Texas, USA. *Proc. Int. Assoc. Hydrol. Sci.* 372: 297-303. https://doi.org/10.5194/piahs-372-297-2015

Method of determining early warning water level for controlling regional urban land subsidence

Jianxiu Wang[1], Yuxin Su[1], Tuanzhi Zhao[2], Yansheng Hou[2], Feng Gao[2]

1Tongji University, Shanghai, China
2Ningbo Natural Resources Ecological Restoration and Marine Management Service Center, Ningbo, China

Keywords: land subsidence, early warning groundwater level, pumping, recharge, urban plan

wang_jianxiu@163.com

Abstract

Urban land subsidence is mostly caused by excessive groundwater exploitation, dewatering, and soil disturbance caused by engineering construction. The control of groundwater level in urban areas is helpful to slow down the surface subsidence. However, the superposition effect of engineering construction on the consolidation of shallow soil caused by the drainage of shallow groundwater and the settlement of buildings after construction are mixed and become more obvious. How to warn in early stage and control land subsidence is very important. With Ningbo City as background, the methods to determine early warning groundwater based on geological zones and land subsidence control zones were discussed. The correlation between groundwater level, land subsidence and engineering construction was analyzed, and the evolution of groundwater seepage field was correlated with the future urban planning and construction of Ningbo, together with the control zoning of land subsidence, so as to determine the early warning water level.

Introduction

Urban construction, urban operation, urban emergency water supply and pipe network leakage cause abnormal groundwater level, and abnormal groundwater level may cause land subsidence, ground collapse and other disasters. Due to the interaction between groundwater and land subsidence through fluid-structure coupling, using groundwater level to warn urban land subsidence is an urgent problem to ensure the safety of Ningbo city. Based on the evolution chain of urban operation safety-groundwater level-land subsidence. Combined with the construction of groundwater water-land subsidence observation network, taking urban elevation safety as control target, the early warning safe water level is proposed.

Tosi et al. (2009) revealed the mechanism of shallow soil settlement caused by urban building load based on GPS and InSAR data. Gayarre et al. (2020) used the method of dialectical logic reasoning to discuss the interaction between urban land subsidence and buildings. Truong-Hong et al. (2013) used ground 3D laser scanning technology to study the influence of building detail load changes on settlement, and demonstrated that different building structures would lead to different deformation results. In order to analyze the coupling relationship between groundwater and land subsidence, Zhang et al. (2022) used GRACE-FO data and GLDAS data to inversely show the time series of groundwater changes in the Beijing-Tianjin-Hebei region from 2016 to 2019. Then, MCTSB-InSAR technology was used to invert the settlement change time series of the same period in this area. The variation sequence and trend line of ground water and land subsidence were obtained by experiments, and the inelastic storage coefficient was introduced to analyze the change rule of the influence of ground water on land subsidence. Tian et al. (2022) took the plain area of Chaobai River Basin as an example, comprehensively used synthetic aperture radar interferometry technology, stratification standard and groundwater stratification monitoring technology to conduct three-dimensional monitoring of regional land subsidence and groundwater, and proved the response characteristics of "land subsidence" to the rising process of groundwater level. On the basis of fully discussing the role and characteristics of engineering factors in regional land subsidence in Ningbo Plain, Zhang et al. (2013) established a fully coupled dynamic land subsidence equation under the dual action of groundwater extraction and regional building load with the variation of parameters with stress and strain based on the finite difference method. The comparative study of measured data and simulation results showed that the model had a good fitting relationship, and predicted the development trend of land subsidence from 2012 to 2015. After ignoring the group well effect, Wu et al. (2016) introduced such as drainage with effective stress principle of unsaturated soil, at the same time, considering the seepage force produced by dewatering eventually caused adding the difference variation sequence stress component exists in the horizontal direction, layered summation method was used to calculate the drawdown funnel curve and drainage soil and saturated soil vertical settlement and superposition after smoking precipitation well weeks after final total subsidence on the surface of the earth.

In this paper, Ningbo city center was selected as the demonstration area. The early warning water level was proposed for different land subsidence control zones. The research results have certain reference significance for Ningbo city planning.

Methods

Groundwater warning and zoning control model for urban safety

Utilization of underground water level running safety-chain of ground settlement evolution, combining with the construction of underground water level, land subsidence observation network, with the medium of underground water level, from the engineering measure to partition a given security water level warning value, city scale early warning model results can access Ningbo related geological environment monitoring application, further perfecting the urban groundwater monitoring and early warning technology system.

Analysis of urban land subsidence regionalization and prevention and control index

To collect land subsidence zoning and land subsidence prevention and control planning in Zhejiang Province and Ningbo City, The characteristics of human engineering activities and geological environment are analyzed for each zoning management area. Besides, the land subsidence control indexes are extracted for each land subsidence zone.

Spatio-temporal analysis of urban land subsidence and groundwater level monitoring network

To collect and quantitatively analyze the spatio-temporal coverage of the land subsidence monitoring network and groundwater level monitoring network in Ningbo City, conduct interpolation analysis on the relationship between land subsidence and groundwater level under the accuracy of the existing network. Based on the integration degree of existing land subsidence monitoring points and groundwater level monitoring points, the possible error of interpolation analysis and the elimination method are studied.

Analytical methods for controlling water level in monitoring Wells

In the process of urban construction in recent years, foundation pit dewatering in the development of underground space has the greatest impact on land subsidence. Foundation pit dewatering causes the variation of water level of aquifer with submersible and confined water. The mining data of monitoring wells are systematically sorted out. Based on the data of existing ground subsidence monitoring points and groundwater level monitoring points, the corresponding relationship between groundwater level and land subsidence at each monitoring well is established by least square fitting, and the land subsidence value at each monitoring well is studied. Then, the typical deep well is related to the representative geological unit, and the control water level of the monitoring well is determined by using the quantitative relationship between land subsidence and groundwater level according to the defined index of land subsidence zoning.

Results

The above methods include several parts. However, the key element of the method is the determination of early warning water level through the threshold of land subsidence. The key result of the method is to obtain the relationship between groundwater level and land subsidence, and obtain the early warning ground water level by input the threshold of land subsidence through the trend relationship between groundwater level drawdown and land subsidence.

Urban land subsidence regionalization and prevention and control indicators

Based on the existing basic data collection and field investigation of land subsidence in Ningbo, this paper further summarized the characteristics of land subsidence, compiled the prone degree map of land subsidence and the risk zoning map of land subsidence, and strengthened the risk control of urban geological safety.

Spatio-temporal analysis results of urban land subsidence and groundwater level monitoring network

By inputting the data of land subsidence monitoring points from 2015 to 2020 into Surfer, the land subsidence rate contour map of Ningbo City from 2015 to 2020 can be obtained according to its built-in Kriging interpolation method. Then interpolated by residuals command in Surfer, the land subsidence value at each water level monitoring well can be calculated.

Monitoring well control water level analysis results

As shown in Figure 1 and Figure 2, according to the water level data recorded from 1980 to 2022 in the data collection table of groundwater level monitoring wells, the variation of water level of each monitoring well in the phreatic aquifer, confined aquifer Ⅰ and confined aquifer Ⅱ can be obtained by entering Origin software, and the dynamic evolution law of water level can be obtained. According to the completed time history curve of groundwater level, the trend line was added to filter, and the variation trend of water level in each monitoring well was analyzed and the water level was controlled. According to the chart of water level variation, firstly, the abnormal water level over the years can be analyzed and obtained, which provided a more complete basis for determining the variation of monitoring well location data caused by foundation pit dewatering. Secondly, the trend line of water level of monitoring well can be obtained by fitting water level data, and the trend of water level change can be obtained. Third, according to the historical data combined with the land subsidence value and the general situation of typical geological zones, the monitoring well water level warning index can be given.

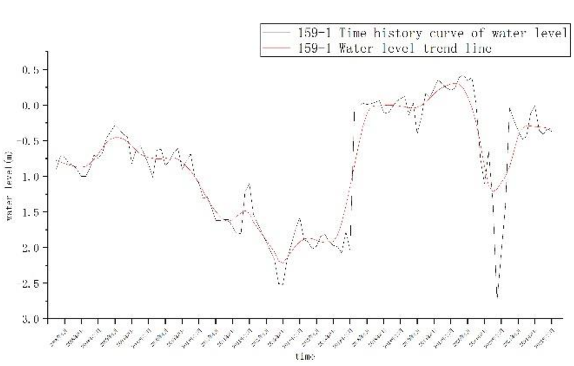

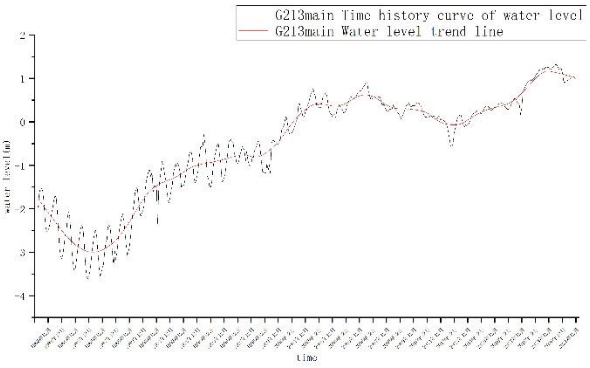

Figure 1 Time history curve and trend line of water level in 159-1 Figure 2 Time history curve and trend line of water level in G213 main

The mining data of deep wells were systematically sorted out. Based on the data of existing land subsidence monitoring points and groundwater level monitoring points, the corresponding relationship between groundwater level and land subsidence at each monitoring well was established by least square fitting, and the land subsidence value at each monitoring well was studied. Then, the typical deep well was related to the representative geological unit, and the control water level of the monitoring well was determined by using the quantitative relationship between land subsidence and groundwater level according to the defined index of land subsidence zoning.

Taking well Measure 13-I as an example, the output value was the water level variation, and the input value was land subsidence. The quantitative relationship between the two was obtained. According to (Equation 1), the control water level of the well can be determined (Fig. 3).

$$y = -9.08022 \times 10^{-4} e^{\frac{x+8.40138}{0.96633}} + 0.14091 \quad (1)$$

Taking well G216 vice as an example, the output value was the water level variation, and the input value was land subsidence. The control water level of the well can be determined (Fig.4).

$$y = 0.0011 e^{\frac{-x}{4.91407}} + 0.03682 \quad (2)$$

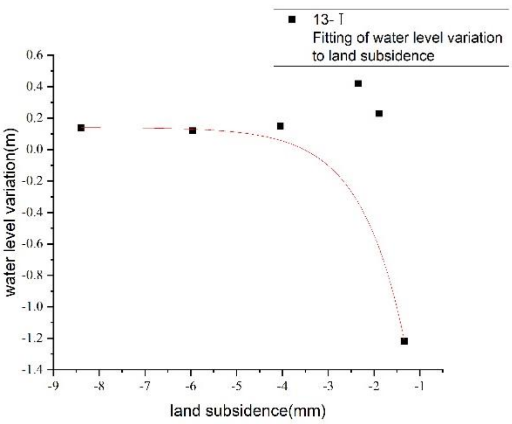

Figure 3 Fitting of 13-I

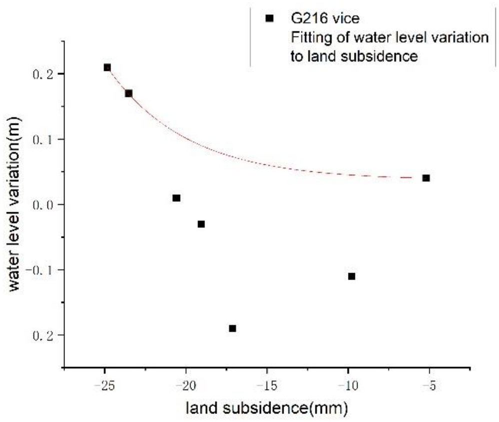

Figure 4 Fitting of G216 vice

Conclusions

The establishment of the groundwater level early warning index needed the municipal data of Ningbo city. After collecting the data, the evolution chain of urban operation safety, groundwater level and land subsidence was established. By establishing urban land subsidence zoning and prevention and control indicators, the land subsidence control indicators of different geological areas were given. The land subsidence value at the water level monitoring well was obtained based on the spatio-temporal interpolation analysis of urban land subsidence and groundwater level monitoring network. Then the trend line was added to the time history curve of the groundwater level which has been made to filter, and the fluctuation range and trend of the monitoring well water level were obtained. The groundwater level and land subsidence were fitted to establish the quantitative relationship between the groundwater level and land subsidence at each monitoring well. The land subsidence control index in different geological areas was taken as the input value, and the early warning value of groundwater level was obtained from the output.

References

Tosi L, Teatini P, Carbognin L, Brancolini G. Using high resolution data to reveal depth-dependent mechanisms that drive land subsidence: the Venice coast, Italy[J]. *Tectonophysics*, 2009, 474(1/2): 271-284.

Gayarre F L, Álvarez-Fernández M I, González-Nicieza C, Álvarez-Vigil A E, García G H. Forensic analysis of buildings affected by mining subsidence[J]. *Engineering Failure Analysis*, 2010, 17(1): 270-285.

Truong-Hong L, Laefer D F. Impact of modeling architectural detailing for predicting unreinforced masonry response to subsidence[J]. *Automation in Construction*, 2013, 30: 191-204.

Zhang Yupeng, Zhang Yonghong, Liu Qinghao. Coupling analysis of land subsidence and groundwater in Beijing-Tianjin-Hebei Region using GRACE data [J]. *Bulletin of Surveying and Mapping*,2022(05):89-94+125.

Tian Miaozhuang, Zhao Long, Cui WenJun, Guo Gaoxuan, Liu He, Sun Aihua, Wang Xinhui, Chen Hang, Wu Pan. Control and influence of groundwater level rise on land subsidence under the background of South-to-North Water Diversion: A case study of Chaobai River groundwater system in Beijing [J/OL].*Geology in China*:1-17[2022-10-13].

Zhang Honghuai, Zheng Juanxin, Tang Zhonghua, Hou Yansheng. Full coupling numerical simulation of land subsidence in Ningbo Plain [J]. *Hydrogeology & Engineering Geology*,2013,40(04):77-82+87.

Wu Yiqian, Zhu Yanpeng. An improved algorithm for ground subsidence induced by foundation pit dewatering in diving area [J]. *Journal of Zhejiang University(Engineering Science)*,2016,50(11):2188-2197.

Data Availability induced Geological Model Uncertainty in Groundwater Flow and Land Subsidence Simulations

Shih-Jung Wang[1]*, Quoc Cuong Nguyen[1,2], Yu-Chen Lu[3], Yonatan Garkebo Doyoro[4,5,6], Duc-Huy Tran[1]

1 Graduate Institute of Applied Geology, National Central University, Taoyuan, Taiwan, R.O.C.
2 DRAGON - Mekong Institute, Can Tho University, Vietnam
3 Institute of Materials Science & Engineering, National Central University, Taoyuan, Taiwan, R.O.C.
4 Earth System Science, Taiwan International Graduate Program (TIGP), Academia Sinica, Taipei, Taiwan, R.O.C.
5 Department of Earth Science, National Central University, Taoyuan, Taiwan, R.O.C.
6 Department of Applied Geology, School of Natural Sciences, Adama Science and Technology University, Adama, Ethiopia

sjwang1230@gmail.com

Abstract

The study adopted a synthetic geological model (SGM) based on the geological characteristics in Taiwan as the baseline. Considering various data availability based on multiple borehole numbers, the incorporation of geological knowledge, and combining geophysical data, several simulated geological models were obtained and used in groundwater flow and land subsidence simulations. The results show that 17 boreholes at a 300 m × 300 m site with incorporating geological knowledge provides good assessment of land subsidence. The model using geophysical data with correction from 13 boreholes provided good results. This study demonstrates that additional data can decrease the uncertainty in geological and numerical models. The results can be used by engineers to construct a suitable geological model for engineering projects based on the precision requirements and budget. This study was part of the content published in Bulletin of Engineering Geology and the Environment (Wang et al., 2022).

Keywords: Geological model uncertainty; Data availability; Geological knowledge; Borehole number; Geophysical data assimilation; Land subsidence.

Background

Uncertainty in hydrogeological modeling has received attention for decades (Lelliott et al. 2009; Benedek and Molnár 2013; Mahmoudpour et al. 2016; Juang et al. 2019; Tran et al. 2022) and it becomes an important topic for hydrogeological simulations (Marinoni 2003; Shi et al. 2008; Guillaume et al. 2012). Previous studies have shown that the sources of uncertainty in groundwater hydrology simulations come from numerical model settings, data input, and the geological model (Refsgaard et al. 2006; Hassan et al. 2008). Numerous studies have analyzed uncertainty in land subsidence and groundwater flow modeling (e.g., Ferronato et al. 2006, Wang et al. 2015). However, relatively few have considered the uncertainty in geological models (e.g., Tran et al. 2022). The present study thus focuses on evaluating geological model uncertainty based on the availability of input data during the construction of a geological model for groundwater flow and land subsidence modeling. Geological models with (1) various numbers of boreholes (to evaluate the influence of borehole density on the simulated geological model), (2) with and without the incorporation of geological knowledge (to evaluate the suitability of incorporating geological knowledge into a geological model), and (3) with and without geophysical data assimilation (to evaluate the effectiveness of combining different and complementary data types to minimize geological model uncertainty) were assessed. The results of this study can be used to reduce the uncertainty of geological models with various data availability. They can also minimize risk when modelers and stakeholders make decisions. This study was part of the content published in Bulletin of Engineering Geology and the Environment (Wang et al. 2022).

Methodology

This study investigates the effect of the uncertainty in geological models with various data availability on groundwater flow and land subsidence. The baseline is a synthetic geological model (SGM) developed in this study. MODFLOW and Aquifer-System Compaction (SUB) packages in groundwater modeling system (GMS) are adopted to simulate groundwater flow and land subsidence, sequentially. The numerical results from each geological model were compared with those of SGM. To evaluate the effect of the number of boreholes, data from 1 to 17 boreholes were taken from SGM to reconstruct a geological model (i.e., simulated geological model). More borehole numbers are not feasible in reality thus it is not considered here. The horizon ID method was used in the geological model simulation with correction based on geological knowledge. To evaluate the effect of geological knowledge, the horizon ID method was used in the geological model simulation without correction based on geological knowledge. To evaluate the effect of geophysical data assimilation, electrical resistivity tomography (ERT) was used in SGM to assess the clay thickness. The original estimated clay thickness and that corrected based on data from 9, 13, and 17 boreholes with the cokriging method were input into the SUB package in MODFLOW, respectively, to estimate the influence on land subsidence simulations.

Results and discussions

Geological model

The developed SGM with a multilayer system was built in the GMS, as shown in Fig. 1. The model consisted of nine layers but the silt layer at the top layer of the model was not used in the numerical simulation because it was too thin and discontinuous, making the grid setting difficult. Clay material in the model was considered the target of compressive medium, which typically results in high land subsidence.

Simulated geological models were constructed based on various data availability. Five step of borehole numbers (1, 5, 9, 13, and 17) are adopted to simulate the geological models. Data from 1 or 5 boreholes were insufficient for capturing the distribution of clay. Data from 9, 13 and 17 boreholes were more sufficient for constructing an approximate clay distribution. The distribution of clay thickness became closer to that of SGM with increasing borehole number. Geological knowledge was considered in the horizon ID method for various borehole numbers. The simulated geological models are more close to the SGM than those without the incorporation of geological knowledge. Geophysical data (ERT) and various borehole numbers are assimilated. The simulated geological models are much close to the SGM than those only using various boreholes or ERT data.

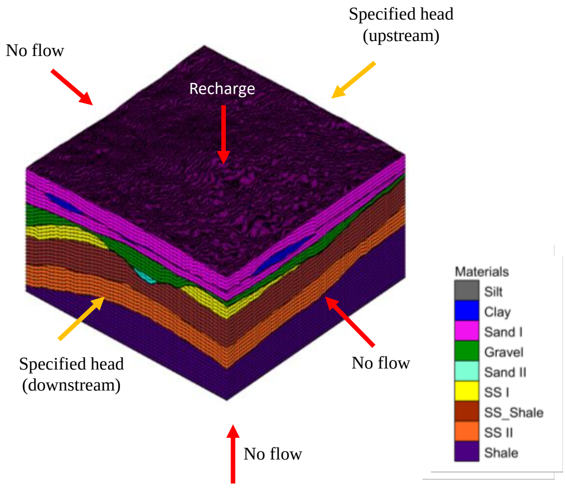

Figure 1 Synthetic geological model and boundary conditions. The two specified heads represent the upstream (north) and downstream (south), respectively. To control the groundwater flow from the upstream to the downstream, the east and west boundaries of the model were set as no-flow boundaries. Because of the low permeability bedrock, the bottom boundary of the model was set as a no-flow boundary. The top boundary was set to a constant recharge. SS = sand stone. (Wang et al. 2022)

Model comparisons

Since land subsidence assessment in this study is focused on clay material, the comparison on the distribution of clay thickness between the simulated geological model and SGM was conducted first. A comparison of clay thickness accuracy between the simulated geological models based on data from various numbers of boreholes and SGM is shown in Fig. 2. There is no correlation (R^2 = 0) between the model based on data from one borehole and SGM. The R^2 values increase with increasing number of boreholes (R^2 = 0.733 for 17 boreholes). RMSE decreases from 2.252 m for one borehole to 0.770 m for 17 boreholes. The quantification results show that increasing the number of boreholes in the study area for the geological model construction can decrease uncertainty. The trend is nonlinear and affected by the location of selected boreholes and the distribution of clay. Although increasing the borehole number to check if the results are convergent in this kind of synthetic model is possible, it is not feasible in reality thus more borehole numbers are not considered here.

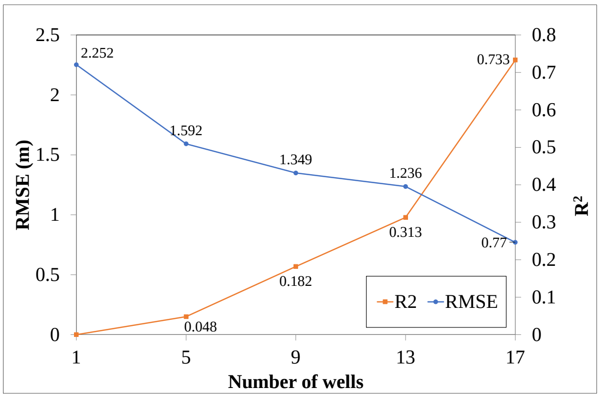

Figure 2 Comparison of clay thickness accuracy between SGM and simulated geological models based on data from various numbers of boreholes. Blue and orange lines indicate RMSE and R^2, respectively. RMSE decreases from 2.252 to 0.770 m and R^2 value increases from 0 to 0.733 when the borehole number increases from 1 to 17. (Wang et al. 2022)

Groundwater flow and land subsidence are simulated based on the simulated geological models and then the results are compared to those of SGM using an error assessment. Figure 3 shows a comparison of the numerical results of land subsidence between the simulated geological model based on data from various data availability and SGM. For the model based on data from 17 boreholes without the incorporation of geological knowledge, the R^2 value slightly increases to 0.316 and RMSE decreases to 7 mm. The results show that the accuracy of this method is very low. The use of data from 17 boreholes and the incorporation of geological knowledge improve the results. The results demonstrate that geological knowledge is necessary for simulating a geological model and land subsidence based on borehole data; its incorporation dramatically increases the accuracy of numerical results and reduces model uncertainty.

The results obtained from the model that used only ERT data show an improvement compared to those for data from boreholes without the incorporation of geological knowledge. The R^2 value is 0.640 and RMSE is 7 mm (Fig. 3). These values are worse than those for the model based on data from 17 boreholes with the incorporation of geological knowledge. Using only ERT data for land subsidence simulation embeds high uncertainty. The results of the simulated geological model that used ERT data with corrected data from 13 and 17 boreholes show a remarkable improvement in the land subsidence simulation. Specifically, the R^2 values are 0.812 and 0.894 and the RMSE values are 3 and 3 mm, respectively (Fig. 3). The results also show higher accuracy than that obtained using 17 boreholes with the incorporation of geological knowledge. The R^2 value increases from 0.787 to 0.894 and RMSE decreases from 4 to 3 mm. The results demonstrate that using data from a limited number of boreholes or only ERT data cannot provide reliable numerical results of land subsidence. A combination of borehole data and ERT data effectively reduces the required well number and uncertainty of geological models and increases numerical model accuracy.

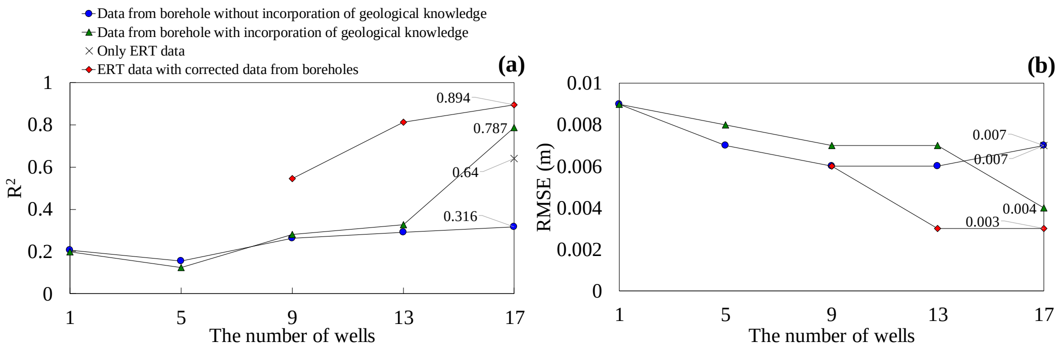

Figure 3 (a) R^2 and (b) RMSE values of comparison in land subsidence assessment between numerical results obtained from SGM and simulated geological models based on data from boreholes without incorporation of geological knowledge, data from boreholes with incorporation of geological knowledge, only ERT data, and ERT data with corrected data from boreholes. (Wang et al. 2022)

Conclusions

This study performed numerical simulations of groundwater flow and land subsidence for SGM as the baseline. Geological models with various data availability were built. The results from these models were compared with those of SGM to assess the geological model uncertainty. The quantification results show that the clay thickness, groundwater level, and land subsidence results for the model based on borehole data approach those of SGM with increasing borehole number. The model based on data from 17 boreholes that incorporates geological knowledge provided acceptable groundwater flow and land subsidence results for a 300 m × 300 m site. Applying the horizon ID method without the incorporation of geological knowledge yielded assessment results that were far from those of SGM. To increase accuracy and decrease the uncertainty of the geological model, borehole data can be combined with ERT data via the cokriging interpolation method. This combination decreases the required borehole number and yields a dramatic improvement compared with the results obtained using only ERT data or borehole data. The study results can be used by engineers or researchers to determine a suitable strategy for engineering geology projects based on the precision requirements and budget.

References

Benedek K, Molnár P (2013) Combining structural and hydrogeological data: Conceptualization of a fracture system. *Engineering Geology* 163:1-10.

Ferronato M, Gambolati G, Teatini P, Bau D (2006) Stochastic poromechanical modeling of anthropogenic land subsidence. *International Journal of Solids and Structures* 43(11-12): 3324-3336.

Guillaume JH, Qureshi ME, Jakeman AJ (2012) A structured analysis of uncertainty surrounding modeled impacts of groundwater-extraction rules. *Hydrogeology journal* 205:915-932.

Hassan AE, Bekhit HM, Chapman JB (2008) Uncertainty assessment of a stochastic groundwater flow model using GLUE analysis. *Journal of Hydrology* 3621-2:89-109.

Juang CH, Zhang J, Shen M, Hu J (2019) Probabilistic methods for unified treatment of geotechnical and geological uncertainties in a geotechnical analysis. *Engineering Geology* 249:148-161

Lelliott M, Cave M, Wealthall G (2009) A structured approach to the measurement of uncertainty in 3D geological models*. Quarterly Journal of Engineering Geology Hydrogeology* 421:95-105.10.1144/1470-9236/07-081

Mahmoudpour M, Khamehchiyan M, Nikudel MR, Ghassemi MR (2016) Numerical simulation and prediction of regional land subsidence caused by groundwater exploitation in the southwest plain of Tehran, Iran. *Engineering Geology* 201:6-28.

Marinoni O (2003) Improving geological models using a combined ordinary–indicator kriging approach. *Engineering Geology* 691-2:37-45 .

Refsgaard JC, Van der Sluijs JP, Brown J, Van der Keur P (2006) A framework for dealing with uncertainty due to model structure error*. Advances in Water Resources* 2911:1586-1597.

Shi X, Wu J, Ye S, Zhang Y, Xue Y, Wei Z, Li Q, Yu J (2008) Regional land subsidence simulation in Su-xi-Chang area and Shanghai City, China. *Engineering Geology* 1001-2:27-42.

Tran D-H, Wang S-J, Nguyen QC (2022) Uncertainty of Heterogeneous Hydrogeological Models in Groundwater Flow and Land Subsidence Simulations – A Case Study in Huwei Town, Taiwan. *Engineering Geology* 298:106543.

Wang S-J, Lee C-H, Hsu K-C (2015) A technique for quantifying groundwater pumping and land subsidence using a nonlinear stochastic poroelastic model*. Environmental Earth Sciences* 7312: 8111-8124.

Wang S-J, Nguyen QC, Lu Y-C, Doyoro YG, Tran D-H (2022) Evaluation of Geological Model Uncertainty Caused by Data Sufficiency Using Groundwater Flow and Land Subsidence Modeling as Example. *Bulletin of Engineering Geology and the Environment* 81(331).

Land subsidence contribution to coastal flooding hazard in southeast Florida – An update

S. Wdowinski[1], T. Oliver-Cabrera[1], S. Fiaschi[2]

1 Institute of Environment, Department of Earth and Environment, Florida International University, Miami, FL, 33199, USA
2 TRE ALTAMIRA s.r.l., 475 W Georgia St, Suite 410, Vancouver, BC

Session: Measuring & Monitoring

swdowins@fiu.edu

Abstract

The current study updates the results of our TISOL 2020 paper describing geodetic measurement efforts in southeast Florida to monitor local subsidence and evaluates its contribution to coastal flooding hazards. Over the past three years, we established a Global Navigation Satellite System (GNSS) monitoring network in Miami-Dade County, acquired and processed the GNSS data, and continued Interferometric Synthetic Aperture Radar (InSAR) monitoring using Sentinel-1 observations. The GNSS observations spanning over a period of 2.35 years revealed that all four stations have subsided at rates of 1.7-5.8 mm/yr. InSAR time series analysis of the Sentinel-1 data acquired during 2016-2021 indicates a shift in subsidence pattern with respect to the 1993-1999 ERS-1/2 results. The Sentinel-1 results show mostly localized subsidence associated with recent large building constructions, whereas the ERS-1/2 results show mainly pockets of subsidence in the western section of the city, where the city was built over reclaimed wetlands. The one exception in the ERS-1/2 results was localized subsidence in the eastern part of the city of a 12-story condominium building, the Champlain Tower South in Surfside, which collapsed in 2021 and attracted worldwide attention.

Background

Florida coastal communities are periodically subjected to flooding events, which are induced by heavy rain, high tide, and storm surge. Over the past decades, several coastal communities have experienced a significant increase in flooding frequency, causing significant disturbance to property, commerce, and overall quality of life (Wdowinski et al., 2016). In the current study, we measure land subsidence along the urban section of the Miami-Dade coastline using precise geodetic observations. These measurements are used to evaluate the contribution of land subsidence to the increased coastal flooding hazards along the coast of Mami-Dade County.

Methods

The project aims at monitoring land subsidence along the urban section of the Miami-Dade coastline using two advanced geodetic measurement techniques, GNSS and InSAR. Precise GNSS measurements require the installation of continuous GNSS units in subsiding coastal areas and monitoring the movements over a period of at least 3-4 years. InSAR uses space-borne radar observations acquired over a period of 5+ years to detect small movements of the Earth's surface. In this project, we installed four GNSS units along the urban section of the Miami-Dade shoreline and processed InSAR data acquired by the Sentinel-1 satellite constellation. By using both measuring techniques, we obtain detailed temporal information on subsidence processes in the four GNSS station locations and high spatial coverage of land subsidence along most of the urban sections of the Miami-Dade County coastline.

Results

Data processing of our four GNSS stations was conducted by the Nevada Geodesy Lab (NGL - http://geodesy.unr.edu/) and presented in the International Terrestrial Reference Frame 2014 (ITRF14). Here we focus on the vertical (Up) component, in which negative values represent subsidence. A visual presentation of the four stations' vertical movements during the 2.35 years (February 2020 – June 2022) measurement period is presented in Figure 1. The time series show three main features, long-term trend, seasonal component, and high-frequency variability (noise). The rates of subsidence were estimated using the MIDAS algorithm (Blewitt et al., 2018). The calculated subsidence rates show that all stations are subjected to subsidence at rates of 1.7-5.8 mm/yr.

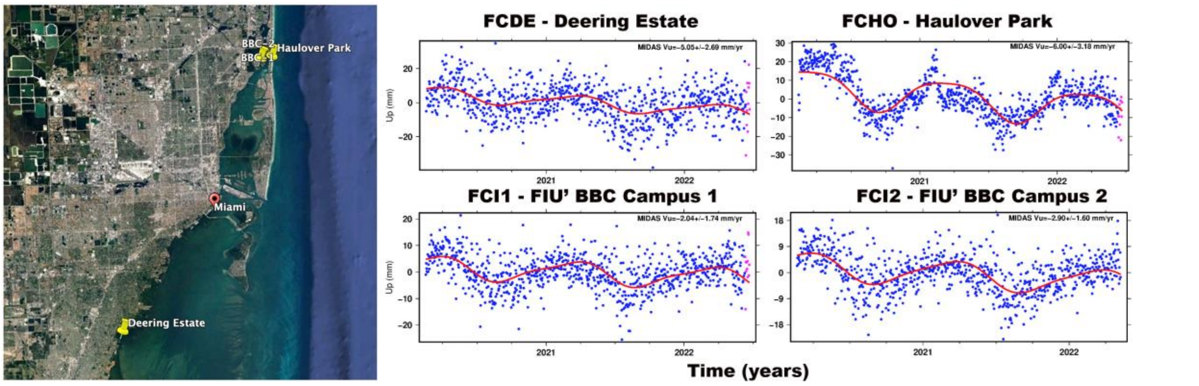

Figure 1 (Left) Location of the four GNSS sites constructed along the coast of the urban section of Miami-Dade County. (Left) Subsidence time series of all four GNSS stations.

InSAR time series processing of the Sentinel-1 data (2016-2021) indicated that mostly localized subsidence was associated with recent large building constructions. This subsidence pattern differs from measurements obtained by ERS-1/2 data (1993-1999) indicating that subsidence occurred mainly in pockets in the western section of the city, where the city was built over reclaimed wetlands. The one exception in the ERS-1/2 results was localized subsidence in the eastern part of the city of a 12-story condominium building, the Champlain Tower South, which collapsed in 2021 and attracted worldwide attention.

Acknowledgements

The authors thank UNAVCO and particularly John Galetzka for constructing the GNSS stations. This study was supported by the Florida Office of Insurance Regulations, and the National Aeronautics and Space Administration (NASA) grant # 80NSSC22K0462.

References

Blewitt, G., Kreemer, C., Hammond, W. C., & Gazeaux, J. (2016). MIDAS robust trend estimator for accurate GPS station velocities without step detection. *Journal of Geophysical Research: Solid Earth*, *121*(3), 2054-2068.

Fiaschi, S. and S. Wdowinski, (2020). Local land subsidence in Miami Beach (FL) and Norfolk (VA) and its contribution to flooding hazard in coastal communities along the US Atlantic coast. *Ocean & Coastal Management*, *187*, 105078.

Wdowinski, S., R. Bray, B. P. Kirtman, and Z. Wu (2016), Increasing flooding hazard in coastal communities due to rising sea level: Case study of Miami Beach, Florida, Ocean & Coastal Management, Volume 126, Pages 1-8, ISSN 0964-5691, http://dx.doi.org/10.1016/j.ocecoaman.2016.03.002.

Wdowinski, S., Oliver-Cabrera, T., and Fiaschi, S. (2020): Land subsidence contribution to coastal flooding hazard in southeast Florida, Proc. IAHS, 382, 207–211, https://doi.org/10.5194/piahs-382-207-2020.

Reconstructing Holocene regional subsidence in the Netherlands, utilizing interpolated coastal plain water table rise

K. de Wit[1], R. S. W. van de Wal[1,2], K. M. Cohen[1]

1 Department of Physical Geography, Utrecht University, The Netherlands
2 Institute for Marine and Atmospheric research Utrecht, Utrecht University, The Netherlands

Keywords: Subsidence, glacio-isostatic adjustment (GIA), relative sea-level rise (RSLR), basal peat data

k.dewit@uu.nl

Abstract

Land subsidence is of major concern to coastal plains and deltas, especially when both shallow soft soil subsidence (alteration of Holocene strata) and deeper natural subsidence (including tectonic tectono-sedimentary basin loading and sinking and glacio-isostatic adjustment (GIA)) occur simultaneously, as is the case in the Netherlands. Separation of deeper subsidence components, such as GIA vs. basin tectonics in the total subsidence signal can be difficult, since they often act on similar spatial scales and similar rates. The aim of this study is to improve the estimation and separation of the spatio-temporal GIA component within the total subsidence signal across the Netherlands using a data based approach. Our main observational data for this is a database of all relevant geological paleo-water level index points (e.g. basal peats) in the Dutch coastal plain. Interpolation of this data in a spatio-temporal grid, calculates continuous coastal plain water table maps per time slice and relative groundwater level (GWL) rise curves for any location in the Dutch coastal plain. The spatial parameters in the interpolation formulae and derivates of the interpolation outputs are used to identify and analyse subsidence-induced regional patterns in the relative sea-level rise controlled subareas. Further processing of the results and comparison with alternative interpolation runs (e.g. input undone from components attributable to basin-tectonics), complement the analysis. The ability to produce data-driven, spatially causal break downs of continuous deeper subsidence across the full coastal plain, with the spatial and Holocene-temporal variance quantified as well, is the main result of the current research.

Introduction

Land subsidence is a major societal problem affecting deltas and coastal plains all over the world (Syvitski et al., 2009; Brown & Nicholls, 2015; Minderhoud et al., 2020). Currently, relative sea-level rise (RSLR) is increasing in many coastal areas due to the combined effects of accelerating sea-level rise and exacerbated land subsidence (Oppenheimer et al, 2019). In the Netherlands, both shallow soft soil subsidence and deeper subsidence components are in play, the latter including glacio-isostatic adjustment (GIA) and tectono-sedimentary basin loading and sinking (e.g. Kooi et al., 1998; Fokker et al., 2018). It is difficult to directly measure the current rate-contributions of individual deeper subsidence components, because they are due to slower operating, long term processes, with rates an order of magnitude smaller than that of shallow subsidence (e.g. peat and clay compaction and peat oxidation) (Van de Plassche, 1982; Koster et al., 2018). Additionally, GIA and tectonic subsidence rates appear to be of the same order of magnitude and regional scale in the western and northern Netherlands, but with different orientations.

Figure 1 (panels a and b) illustrates the subsidence bullseyes that are generally regarded to differ between the basin and GIA components. The magnitudes and exact locations of the basin and GIA bullseyes are not precisely known, and so far have mostly been studied separately, because different methods are used to reconstruct them. Basin sinking under depocenter loading, for example, has been reconstructed with a tectono-sedimentary back-stripping analysis that uses the thickness of the Quaternary and Neogene sequence below the North Sea floor to determine vertical land motion as averaged over the last 2.6 Myr (Kooi et al., 1998; Cohen et al., 2022). The GIA contribution since the last glacial maximum (LGM) in the North Sea area is often assessed using numerically coarse output from large-scale geophysical models. This has used Holocene geological observational sea level index point data (so-called SLIPs) to verify the outcomes of these models at selected sites (e.g. Vink et al., 2007). However, multiple combinations of GIA input result in fairly equal data fits and notable differences in predicted current rates (e.g. reviews in Vermeersen et al., 2018). In other words, the rates and locations of the respective bullseyes and the relative importance of basin and GIA components, and how this spatially varies in the coastal plain and over time are not well known.

The aim of this study is to use a data-based approach to reconstruct the contribution of GIA and basin tectonics to regional subsidence in the Netherlands during the Holocene using coastal plain water level indicators. We perform an analysis of paleo-sea-level and other coastal plain paleo-water level geological data, by means of a spatial-temporal interpolation method that reconstructs Holocene RSLR in four dimensions (X-, Y-, Z- and Time). We use the parameterization of the interpolation trend to identify regional trends in RSLR, and we use kriging of the residuals to resolve sub-regional patterns in the RSLR.

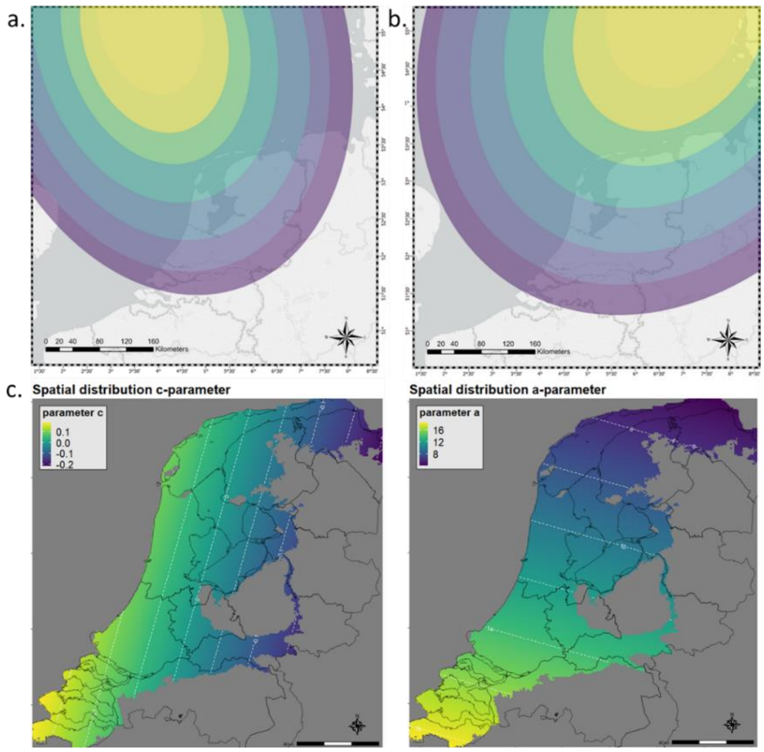

Figure 1 Upper panels: Simplified visualization indicating the expected general orientations of subsidence components attributable to a.) the tectono-sedimentary subsidence of the North Sea basin and b.) glacio-isostatic adjustment in the periphery of the former Scandinavian ice mass. Lower panels the c.) example of the spatial distribution of the c-parameter and a-parameter specified in the interpolation formulae.

Methods

We apply a 3D KT-kriging interpolation method to our dataset (Kriging residuals after applying a Trend function (Eq.1)), performed over the X,Y and T domain. The interpolation predicts GW-table elevations (Z) for given locations of X and Y (study area in Fig. 2; currently at 1x1 km resolution) and for a discrete moment in time, T (from 10 ka to 1 ka, with timesteps of 200 years; Cohen, 2005; Koster et al., 2017). The trend function step of the KT-kriging procedure predicts Z in a normalized form (Z_n) as shown in Eq. 1. Zn is the position between a lower (Z_n=0) and an upper (Z_n=1) bounding envelope surface that were independently reconstructed for both 10 ka and 1 ka (Cohen, 2005). The parameters $c_{(x,y)}$ and $a_{(x,y)}$ in the trend function (Eq. 1) are spatially dependent and optimized by non-linear least squares regression analysis on the observations (the GWL data, 576 observations of X,Y,T and Z (Figure 2), taken from many sea-level and inland water table reconstruction studies, notably: Jelgersma, 1961; Van de Plassche, 1982; Kiden, 1995; Cohen, 2005; Koster et al., 2017; Meijles et al., 2018; Hijma & Cohen, 2019). The inputs $q_{(x,y)}$ and $p_{(t)}$ are prescribed: they are the normalized thickness of the Holocene wedge and the moment in time normalized between 10 ka ($p_{(t)}$ = 0) and 1 ka ($p_{(t)}$ = 1).

$$Z_n = \left(1 - c_{(x,y)}\right)\left(1 - e^{-a_{(x,y)}q_{(x,y)}p_{(t)}{}^{b}}\right) + \left(c_{(x,y)} * p_{(t)}\right) \; (Equation\ 1)$$

After the trend function step (estimation of parameters $a_{(x,y)}$, b, and $c_{(x,y)}$), Z_n results are transformed back to absolute GW-table elevations (Z). At all observation locations residuals (observed – trend) are calculated as input for the kriging step of the KT-kriging procedure. The latter uses ordinary block kriging interpolation (blocks of 1x1 km and 200 years). The combined interpolation output (trend + kriging) thus contains an observations-derived (i) spatially continuous parameterization of trend function parameters and 3D-gridded output (Z_{trend}), and (ii) subregional correction for subregional GWL variation not captured by the overall fitted trend ($Z_{kriging}$). This output is produced independently of GIA modelling which enables cross-comparison.

The KT-kriging method includes spatial variance (interpolation uncertainty, accuracy) outputs. From the trend step, the total standard deviation of the interpolation GWL fields is c. 1.1 m (= trend fitting performance). Close to datapoints, the kriging step lowers this to a block-averaged nugget value of c. 0.2 m (= limitation of basal peat as geological water table reconstruction). The spatial parameters $c_{(x,y)}$ and $a_{(x,y)}$ trend-fitted solutions are used to identify and analyze subsidence-induced regional patterns (Figure 1). Doing this for interpolation runs on different subsets (north-northwest-west-southwest; seaward-inland), helps to understand method input sensitivity, as well as the spatial differences in timing and tempo of relative GWL rise throughout the coastal plain.

Parameter $c_{(x,y)}$ in equation 1 determines the contributions of the non-linear ('sigmoid') and linear term describing Z_n, while parameter $a_{(x,y)}$ (and b) influence the sigmoid shape of the normalized GWL rise curve (more sigmoid when a is high). In a run as in Figure 1c, this means that in inland areas where parameter $a_{(x,y)}$ is low, the relative GWL rises slower and linear, and in seaward areas where it is high it is more sigmoid. Taking in the pattern of $c_{(x,y)}$ as well, this allows to split the trend-function predicted total GWL rise in a Holocene-constant 'linear' part and Holocene-variable 'non-linear' part (decelerating from onset Middle Holocene, 9-8 ka onwards).

Post-processed derivatives of the interpolation outputs are further used to identify and analyse subsidence-induced regional patterns. This processing includes 4D filtering the results to constrain analysis to areas where local GWL variability is mainly mean sea-level rise attributable (not too far inland, not too early in the Holocene when areas were not yet lagoonal-inundated). This feeds an analysis of regional variation and allows to attribute variations in thickness of the Holocene sedimentary wedge to intrinsic topographic (e.g. valleys visible in depth to Top Pleistocene, Figure 2) and differential subsidence causes (Figure 1), besides contrasting the temporal variation in GWL rise between areas.

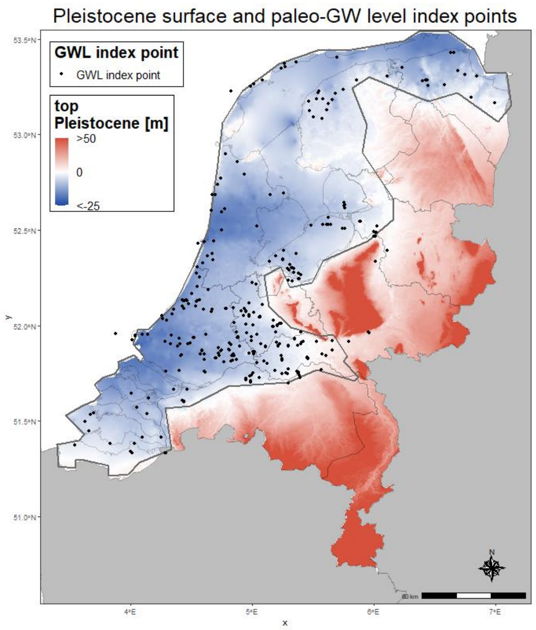

Figure 2 Distribution of geological observations on Holocene GWL index points locations used for this study. The study area is marked with a grey polygon. Depth to base coastal plain is indicated in blue (top Pleistocene, 0 = 0 m NAP ≈ present MSL).

Holocene coastal plain water table rise results

The 4D interpolation output has a flexible hypercube structure, easing the visualization of the data in different forms, such as predicted GWL maps shown (Figure 3 shows four slices, the hypercube stores output every 200 yr). Figure 3 shows that at 8 ka BP the GWL was still very low throughout the coastal plain, with most of the GWL close to the topographic surface of the time (compare patterns in Top Pleistocene in Fig. 2) that features several valleys inherited from the Last Glacial. Note that in the inland direction, the water table rises modestly to grade with Pleistocene surface and feeding river valleys. From 8 ka onwards the GWL starts to rise and topographic gradients in the west and north flatten as the coastal plain establishes over the buried valleys. At 6 ka BP the GWL has risen some 10 meters, subtly more in the North than in the Southwest. Surfaces of that age are encountered c. 2 m lower in the north compared to the southwest. At 4 ka BP, subtle regional differences in GWL are apparent (South to North: meter scale regional variations between Rhine delta, central lagoon and Wadden Sea fringe). The panel for 2 ka BP shows the flattest coastal plain water table reconstruction, just above but close in elevation to that of 4 ka.

The interpolation approach works well for simulating Holocene GWL fields, especially in the previous studied areas at the west coast of the Netherlands. However, work is still ongoing on optimizing the parameterization of the trend function especially in the northern part of the Netherlands, where the GWL index point density is lower (Figure 2). Further development of output visualization (masking, uncertainty) is also foreseen.

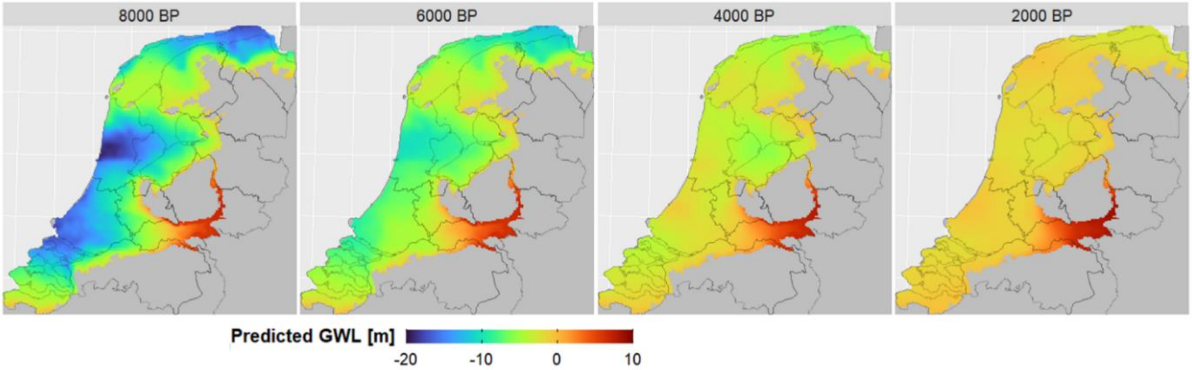

Figure 3 Holocene relative groundwater levels for selected moments as predicted by our 3D KT block kriging procedure.

Preliminary subsidence analysis and discussion

Figure 3 shows that 8 ka, 6 ka and 4 ka 'Middle Holocene' coastal water tables in the Netherlands are geologically encountered deeper in the North than in the South. This implies a different pacing of relative GWL rise in the north, and a greater contribution of subsidence in the relative rise signal in these regions. Presuming that the non-subsidence part of GWL rise in these areas was similar (at least near the modern coast, driven by post-glacial sea level rise), and noting that the basal peat input data is essentially unaffected by shallow soft soil subsidence, Figure 3 and the output of the interpolation in general thus hold a quantification of large scale differential subsidence due to deeper processes, i.e. GIA and basin subsidence (Fig. 1ab). Of these, tectonic subsidence is assumed to be nearly constant during the Holocene, with differences in subsidence rates up to 0.2 m/kyr in the Netherlands, subsidence increasing in a north-west direction (Kooi et al., 1998; Cohen et al., 2022). In contrast, GIA subsidence is expected to decrease from 'Middle' (8-4 ka) to 'Late' Holocene (last 4 ka) times (Vink et al., 2007; Steffen & Wu, 2011). The parameter fitting, the differential subsidence results in Fig. 3, and independent observations (e.g. GPS, tide gauges and InSAR data – beyond the scope of this abstract) suggest that this is quantifiable from the interpolation output.

Stronger GIA-lowering of the north and northeast relative to the southwest can explain part of the differential subsidence observed for the Middle Holocene. In the Late Holocene and modern situation, preliminary interpolation results and comparison with values in literature indicates that 'constant' basin subsidence is of similar magnitude as the decreased GIA signal, at least in the northwest. Also, in the Late Holocene (last 4 ka) the differential subsidence due to deeper subsidence processes is less pronounced and overprinted by other signals, such as soft soil subsidence or seepage. As the parameter fitting steps of our method are sensitive to observational data distribution, it is still difficult to fully determine the relative contributions of GIA and tectonic subsidence to the relative greater subsidence in the North, and quantify the uncertainty. In future work we will run interpolation experiments with GWL index point depths that are corrected for independently estimated basin subsidence rates (source material cited earlier), to isolate the GIA component. Furthermore, a closer cross-comparison between the data-based interpolation outcome and the physics-based GIA models will help further disentangle the GIA and tectonic subsidence signals within the Netherlands.

Conclusion

This study presents a 3D Holocene relative GWL interpolation for the Netherlands, that incorporates regional trends in relative GWL rise, and the output embeds spatio-temporally variant signals of regional scale differential subsidence processes attributable to GIA (Scandinavia peripheral) and basin subsidence (North Sea Basin). The data-driven methodology for analysing background differential subsidence across the Netherlands, runs independently from physical GIA modelling, allowing for a cross-comparison with such results in the near future.

The current results are nationwide, spatially-continuous coastal plain water table reconstructions through Holocene time. Differential subsidence is particularly visible in the Middle Holocene (8-4 ka) and more subtle in the Late Holocene (last 4 ka). The north of the Netherlands subsided faster than the southwest of the Netherlands, notably in the Middle Holocene when the GIA signal was strong. The north continues to sink relatively faster in the Late Holocene, but the contribution of GIA versus basin subsidence appears to have become of equal size, especially in the northwest of the country. Further work to disentangle the GIA and tectonic subsidence signals within the Netherlands and quantify uncertainty in their attribution are ongoing.

Author contributions

KW, KMC and RSW designed the research. All authors contributed to the writing of the article.

Competing interests

The authors declare that they have no conflict of interest.

Financial report

The research presented in this paper is part of the project Living on soft soils: subsidence and society (grantnr.: NWA.1160.18.259): PhD project WP1.3 - 2020-2024. This project is funded by the Dutch Research Council (NWO-NWA-ORC), Utrecht University, Wageningen University, Delft University of Technology, Ministry of Infrastructure & Water Management, Ministry of the Interior & Kingdom Relations, Deltares, Wageningen Environmental Research, TNO-Geological Survey of The Netherlands, STOWA, Water Authority: Hoogheemraadschap de Stichtse Rijnlanden, Water Authority: Drents Overijsselse Delta, Province of Utrecht, Province of Zuid-Holland, Municipality of Gouda, Platform Soft Soil, Sweco, Tauw BV, NAM.

References

Brown, S., & Nicholls, R. (2015). Subsidence and human influences in mega deltas: the case of the Ganges–Brahmaputra–Meghna. *Science of the Total Environment, 527*, 362-374.

Cohen, K. M. (2005). 3D geostatistical interpolation and geological interpretation of paleo–groundwater rise in the Holocene Coastal Prism in the Netherlands.

Cohen, K. M., Cartelle, V., Barnett, R., Busschers, F. S., & Barlow, N. L. (2022). Last Interglacial sea-level data points from Northwest Europe. *Earth System Science Data*, *14*(6), 2895-2937.

Hijma, M. P., & Cohen, K. M. (2019). Holocene sea-level database for the Rhine-Meuse Delta, The Netherlands: implications for the pre-8.2 ka sea-level jump. QSR.

Jelgersma, S. (1961). Holocene sea-level changes in the Netherlands. *Ph. D. dissertation, Leiden Univ.*

Kiden, P. (1995). Holocene relative sea-level change and crustal movement in the southwestern Netherlands. *Marine Geology*, *124*(1-4), 21-41.

Kooi, H., Johnston, P., Lambeck, K., Smither, C., & Molendijk, R. (1998). Geological causes of recent (~ 100 yr) vertical land movement in the Netherlands. *Tectonophysics*, *299*(4), 297-316.

Koster, K., Stafleu, J., & Cohen, K. M. (2017, Dec). Generic 3D interpolation of Holocene base-level rise and provision of accommodation space, developed for the Netherlands coastal plain and infilled palaeovalleys. *Basin Research, 29*(6), 775-797.

Koster, K., Cohen, K. M., Stafleu, J., and Stouthamer, E.: Using ^{14}C-dated peat beds for reconstructing subsidence by compression in the Holland coastal plain of the Netherlands, J. Coastal Res., 34, 1035–1045, 2018.

Meijles, E. W., Kiden, P., Streurman, H.-J., van der Plicht, J., Vos, P. C., Gehrels, W. R., & Kopp, R. E. (2018). Holocene relative mean sea-level changes in the Wadden Sea area, northern Netherlands. *Journal of Quaternary Science, 33*(8), 905-923.

Minderhoud, P., Middelkoop, H., Erkens, G., & Stouthamer, E. (2020). Groundwater extraction may drown mega-delta: projections of extraction-induced subsidence and elevation of the Mekong delta for the 21st century. *Environmental Research Communications, 2*(1), 011005.

Oppenheimer, M., B.C. Glavovic, J. Hinkel, R. van de Wal, A.K. Magnan, A. Abd-Elgawad, R. Cai, M. Cifuentes-Jara, R.M. DeConto, T. Ghosh, J. Hay, F. Isla, B. Marzeion, B. Meyssignac and Z. Sebesvari (2019). Sea Level Rise and Implications for Low-Lying Islands, Coasts and Communities. IPCC Special Report on the Ocean and Cryosphere in a Changing Climate. Intergovernmental Panel on Climate Change.

Van de Plassche, O. (1982). Sea-level change and water-level movements in the Netherlands during the Holocene. *Ph. D. dissertation, Vrije Universiteit Amsterdam*.

Steffen, H., & Wu, P. (2011). Glacial isostatic adjustment in Fennoscandia—a review of data and modeling. *Journal of geodynamics, 52*(3-4), 169-204.

Syvitski, J. P., Kettner, A. J., Overeem, I., Hutton, E. W., Hannon, M. T., Brakenridge, G. R., Day, J., Vörösmarty, C., Saito, Y., & Giosan, L. (2009). Sinking deltas due to human activities. *Nature Geoscience, 2*(10), 681-686.

Vink, A., Steffen, H., Reinhardt, L., & Kaufmann, G. (2007). Holocene relative sea-level change, isostatic subsidence and the radial viscosity structure of the mantle of northwest Europe (Belgium, the Netherlands, Germany, southern North Sea). *Quaternary Science Reviews, 26*(25-28), 3249-3275.

Vermeersen, B. L., Slangen, A. B., Gerkema, T., Baart, F., Cohen, K. M., Dangendorf, S., ... & Van Der Wegen, M. (2018). Sea-level change in the Dutch Wadden Sea. *Netherlands Journal of Geosciences*, *97*(3), 79-127.

Proc. IAHS, 382, 219–224, 2020
https://doi.org/10.5194/piahs-382-219-2020

Study on the influence of supertall building load on adjacent tunnel subsidence

Yan Xu[1,2,3], **Xuexin Yan**[1,2,3], **and Tianliang Yang**[1,2,3]

[1]Key Laboratory of Land Subsidence Monitoring and Prevention, Ministry of Nature and Resource of China, Shanghai, 200072, China
[2]Shanghai Institute of Geological Survey, Shanghai, 200072, China
[3]Shanghai Engineering Research Center of Land Subsidence, Shanghai, 200072, China

Correspondence: Yan Xu (xuyan@sigs.com.cn)

Published: 22 April 2020

Abstract. With the rapid growth of economy in coastal megacities, the construction of supertall buildings with deep pile foundations adjacent to tunnels in soft soil is inevitable. The additional subsidence of tunnel and long-term subsidence of soft soil was appeared caused by the supertall building load transferred through pile foundation. In this paper, a typical case in Shanghai where deep piles of supertall building group adjacent to a metro tunnel was selected, and the long-term monitoring data of tunnel deformation was collected and analysed. The layered subsidence of surrounding soft soil was analysed by using the monitoring data of extensometers in a land subsidence monitoring station near the study area. The results of data analysis showed that the construction of supertall building had a significant impact on the adjacent tunnel subsidence. Moreover, with the increase of the load transferred from building structure to pile foundation, the adjacent tunnel appeared sustained uneven subsidence. And the subsidence of tunnel in the study area mainly depended on the deformation of underlying soil.

1 Introduction

With the rapid growth of economy in coastal megacities (e.g. Shanghai and Tokyo), the construction of supertall buildings with deep piles adjacent to metro tunnels in the soft soil is inevitable. British engineers were aware of the interaction between new pile and an existing tunnel as early as the 1950s (Measor and New, 1951). Underground subway operators have developed restrictive guidelines for the construction and loading of piles in the vicinity of tunnels based on this experience (Schroeder et al., 2004). Mohammad et al. (2013) presented a neural network combined with a finite element method to analyse the interaction between the building and adjacent metro tunnel. The friction resistance generated by supertall building pile will cause the change of foundation stress field through the stress transfer of soil mass, thus additional subsidence of these tunnels and long-term subsidence of soft soil will develop as a consequence, which will impact the tunnel stability and thus the Metro operation (Weng et al., 2016). The safety of megacities is threated by all these unpredictable problems.

In this paper, a typical case in Shanghai where deep piles of supertall building group adjacent to a metro tunnel (see Fig. 1) and the long-term monitoring data of tunnel deformation is presented. In order to accurately analyse the influence of supertall building loads, three measured data datums of the tunnel elevation were adopted respectively: the elevation when the subsidence monitoring on metro tunnel began in 1999, the elevation when the foundation pit base of Building A was completed in 2009, and the elevation at the position near the Park where was away from the building load. These results provide an example and can be used as a test case and example for similar engineering problems faced by other coastal megacities throughout the world.

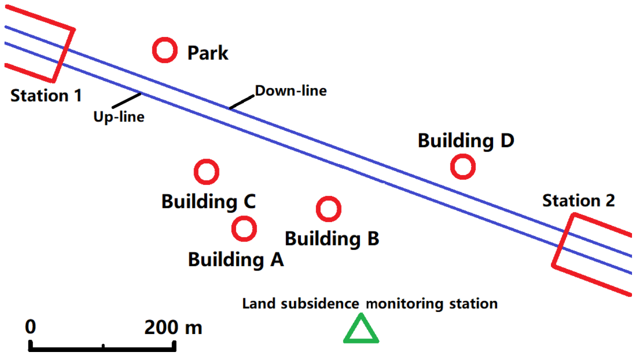

Figure 1. Plan view of the case study area.

2 Description of project

The construction of pile foundation for Building A started in November 2008, and the foundation pit base completed in March 2010, the main structure completed in August 2013, and the civil engineering work basically completed by the end of 2014. Building A started operation in mid-2015.

The soil composition underneath Building A within the depth of 150 m is mainly composed of saturated clay, silt and sand. The soil layers and test pile profile are shown in Fig. 2. The foundation pit of the main building was excavated at a depth of 31 m. The top of the engineering pile is located in the sandy and silty soil layer, while the pile end in the silty sand layer, and the effective pile length was all located in the sandy soil layer. The water level is generally 1.0–1.7 m below the ground surface, while 12.3–14.2 m for the water head of silty confined aquifer.

The study area was selected around the metro tunnels (up-line and down-line) adjacent to Buildings A–C (see Fig. 1 for details). The construction of Building C was started in May 1994 and structure completed in August 1997, while the construction of Building B began in November 2005 and structure completed in September 2007. The heights of Building A–C are more than 400 m above the ground surface. The large-diameter (1000 mm) and ultra-long (88 m) cast-in-situ piles were constructed as the foundation of Building A, which were different from the steel pipe piles used in Building B and C (Jiang and Chao, 2012).

3 Analysis of tunnel subsidence

3.1 Subsidence analysis since 1999

In the study area, the subsidence monitoring on the metro tunnel began in November 1999, and this levelling results was used as the baseline for subsequent levelling analysis. Figure 3 illustrates the adjacent tunnel subsidence during the construction and operation of Building A.

It can be seen from Fig. 3 that the up-line tunnel represented a gradual trend of rebound in general, and the deformation pattern was consistent at different positions. The cumulative subsidence of tunnel is the largest at the position of Park, and the minimum at the position of Building A, and the cumulative subsidence is relatively similar at other positions. On the whole, after the completion of civil engineering work of Building A, the overall rebound rate of the tunnel tended to decrease.

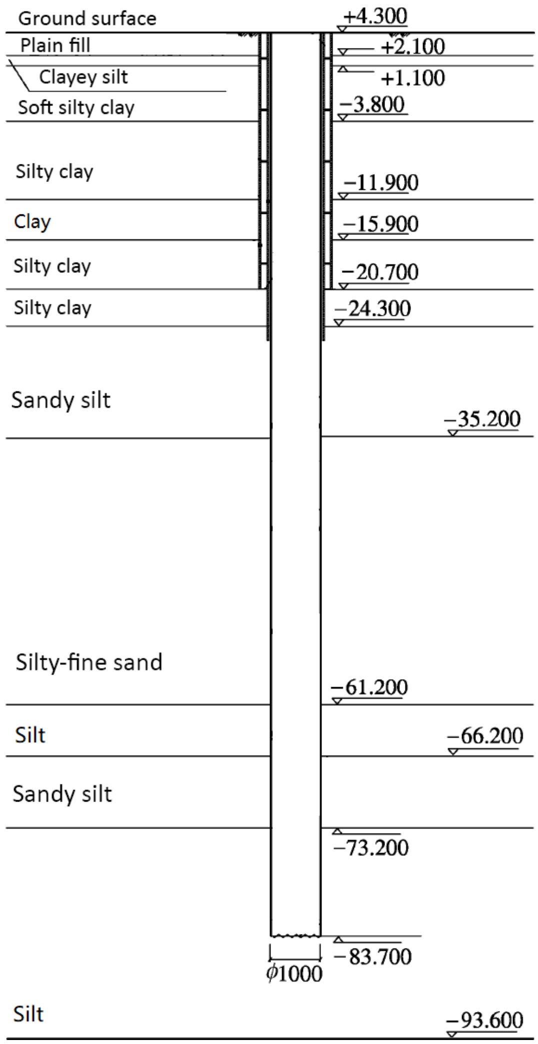

Figure 2. Soil and pile profile at the study site (modified from Wang et al., 2011).

In order to clearly illustrate the differential subsidence of the station-to-station tunnel, the cumulative subsidence of the interval section was drawn with the starting point of Station 1 and the end point of Station 2 (Fig. 4). It can be seen from Fig. 4a, the levelling data of up-line tunnel, that the cumulated subsidence near Station 1 is relatively large, and there was a subsidence peak between Building B and C, indicating that pile foundation group of supertall buildings had some influence on the subsidence of adjacent tunnel. Figure 4b shows that the location of subsidence peak of the down-line

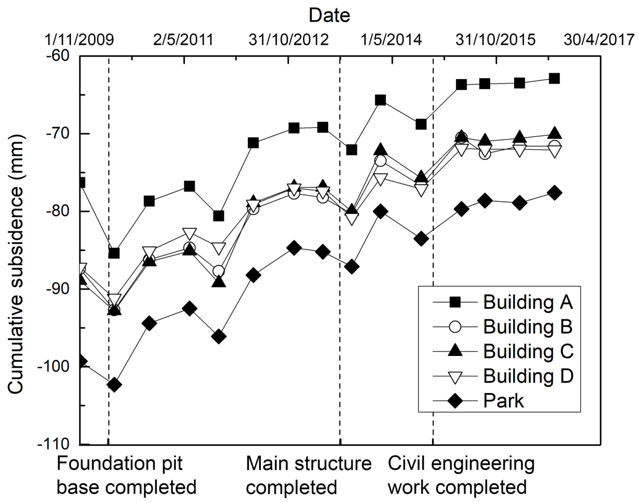

Figure 3. Tunnel subsidence at different position since 1999 during the construction and operation of Building A.

tunnel, which is relatively away from Building A, shifted eastward, and it might be related to the stress redistribution of the tunnel structure caused by the transfer of additional stress from the load of this supertall building.

3.2 Subsidence analysis since 2009

The structures of Building B and C were completed in August 1997 and September 2007 respectively. The influence of their construction and operation on adjacent tunnel cannot be ignored. In order to eliminate as far as possible, the influence of engineering activities in the study area before the load of Building A, the levelling data in November 2009, when the foundation pit base of Building A was completed, is considered as the baseline in the following analysis.

It can be seen from Fig. 5a that the cumulative subsidence (rebound) of the up-line tunnel was the largest (minimum) at the position of Building A, while the cumulative subsidence (rebound) was the minimum (largest) at the position of Park. Figure 5a shows opposite pattern of that in Fig. 3, which suggested that the construction of Building A had a significant impact on the deformation of adjacent tunnel. Figure 5b presents the deformation pattern of the down-line tunnel, and it was not typical compared with that of the up-line. The down-line tunnel is on the opposite side away from Building A, and the load of pile foundation may have been attenuated in the stress transfer process, which to some extent was benefited from the interaction between tunnel structure and surrounding soil layer.

According to the cumulative subsidence of the station-to-station tunnel in Fig. 6, the subsidence peak near Building A was obviously appeared, and was closer to Building A than that in Fig. 4. Figures 5 and 6 also show that tunnels in the study area were in a constant rebound trend due to the influence of the change of surrounding geological environment.

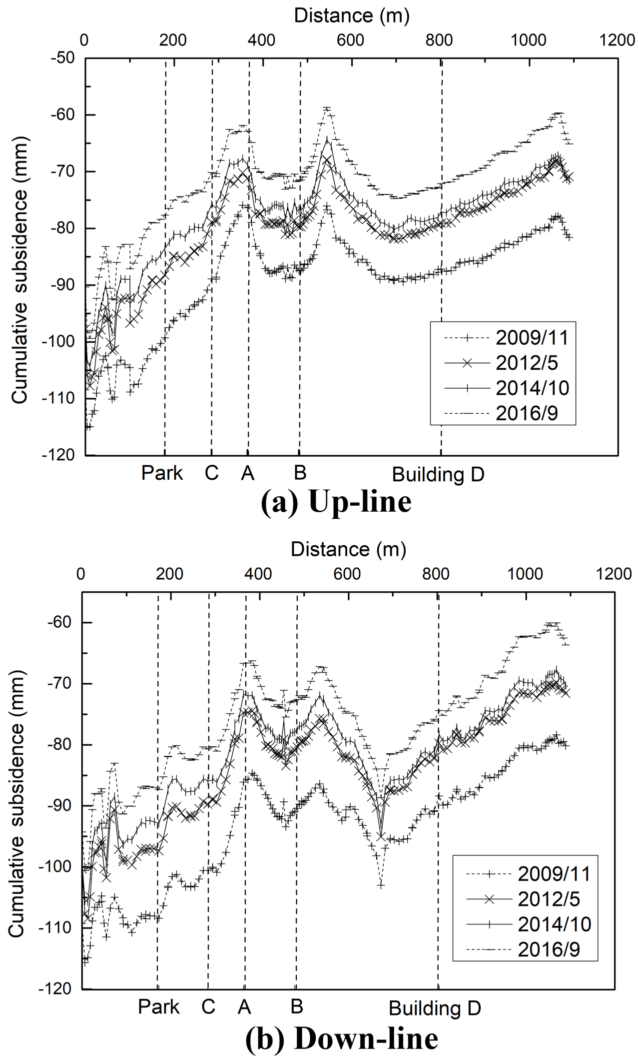

Figure 4. Subsidence of the station-to-station tunnel section since 1999.

Meanwhile, it can be seen that at the position of Park, the tunnel appeared peak of rebound.

3.3 Uneven subsidence analysis

The structures in each position of the station-to-station tunnel are associated with each other, so that the tunnel deformation at a certain position will cause the follow-up deformation of surrounding tunnel structures. In order to eliminate the impact of the overall rebound of the station-to-station tunnel, the point at the position of Park was adopted to be the reference, where was most significantly affected by the surrounding geological environment because it was relatively far away from the supertall buildings, to analyse the relative subsidence of tunnel in study area (Figs. 5 and 6).

Taking the tunnel elevation at the position of Park as the reference point, the relative deformation at different posi-

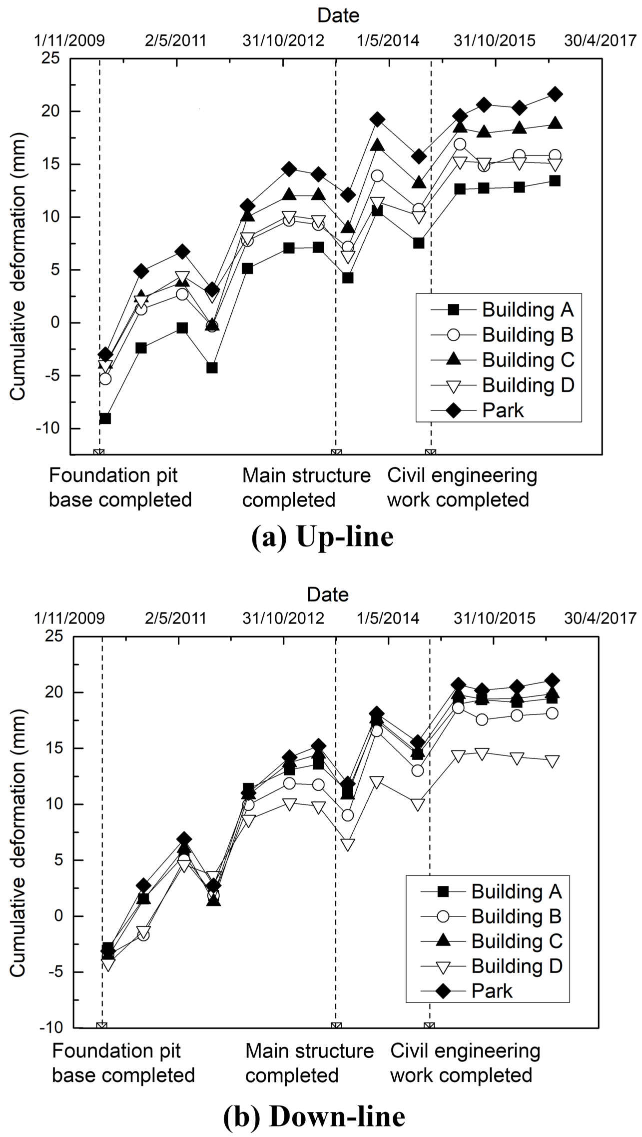

Figure 5. Tunnel deformation at different position since 2009 during the construction and operation of Building A.

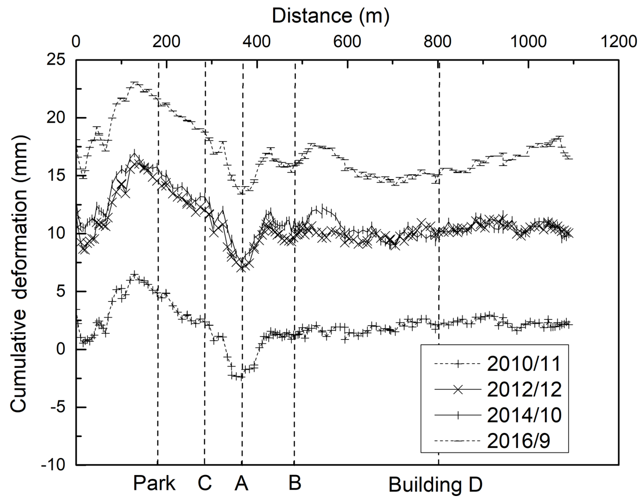

Figure 6. Deformation of the up-line station-to-station tunnel section since 2009.

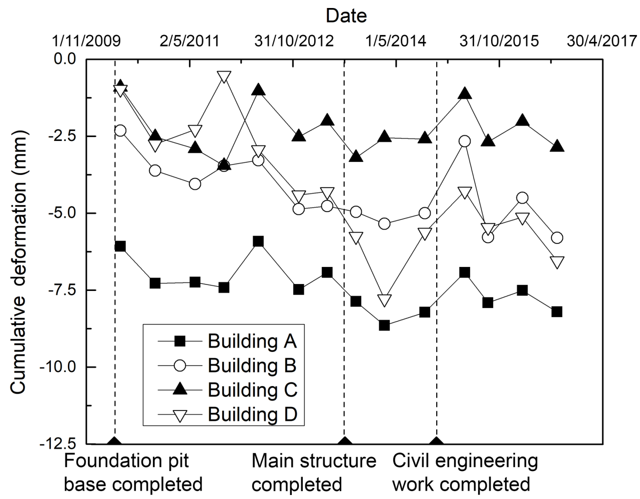

Figure 7. Relative up-line tunnel deformation at different position since 2009.

tions was drawn based on the adopted initial value in November 2009 (Fig. 7). It can be seen from Fig. 7 that the whole up-line tunnel was basically in a state of relative subsidence, and the accumulated subsidence was the largest near Building A, the pattern of which was consistent with the analysis in Sect. 3.2. Figure 7 also shows that during the Building construction period from May 2012 to March 2014, with the increase of load transferred from the structure to the pile foundation, the tunnel structure adjacent to Building A appeared continuous relative subsidence.

The uneven subsidence peak of the tunnel at the position of Building A was showed more clearly in Fig. 8a, and the relative subsidence rate tended to decrease. The down-line subsidence curve in Fig. 8b illustrates that the tunnel on the side away from the supertall buildings would also be affected by the load transfer of pile foundation, but the effect was obviously weakened, which demands for further research.

4 Analysis of soil layer deformation

A land subsidence monitoring station (LSMS) is located within 300 m from Building A and the tunnels (see Fig. 1), in which a group of extensometers were installed. The extensometers were often used to monitor soil deformation (Yang et al., 2015). According to the monitoring data, the layered deformation of soil in this area after November 2009 is illustrated in Fig. 9.

Figure 9 shows that the main deformation of the soil in this region occurred in the shallow layer (1.2–15.5 m), where the tunnels in the study area were located. Figure 9 also il-

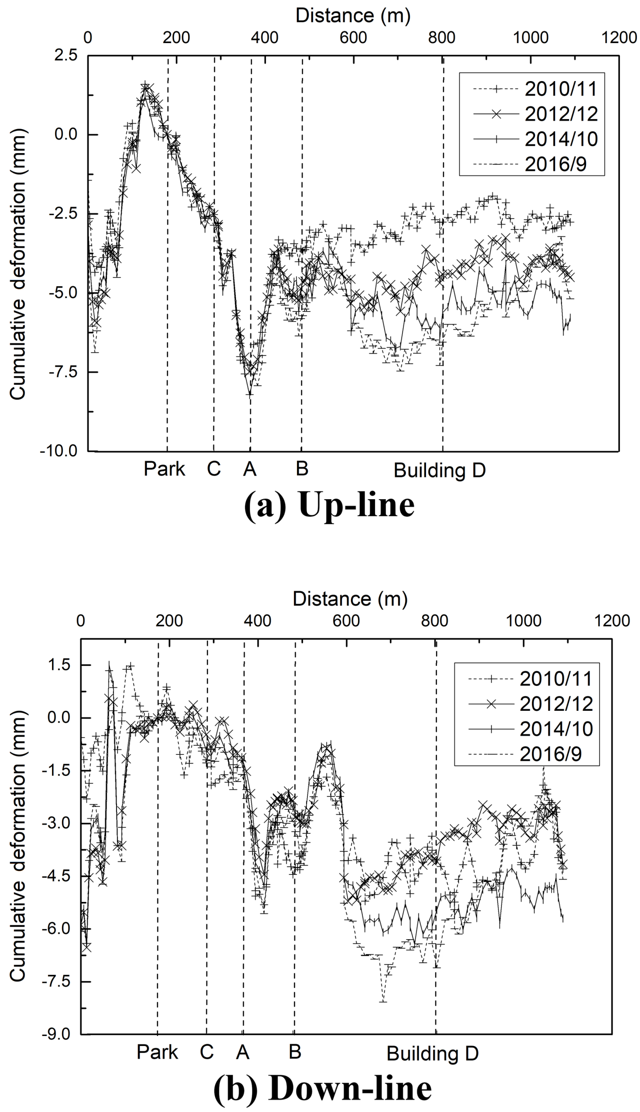

Figure 8. Relative deformation of the station-to-station tunnel section since 2009.

lustrates that, before the structure completion of Building A, the land subsidence rate was basically lower than the deformation rate of shallow soil layer. After the structure completion of Building A, the land subsidence rate gradually exceeded the deformation rate of shallow soil layer, which indicated that the load of the supertall building was gradually transferred to the deeper soil layer through pile foundation, resulting in the compression of the deeper soil layers. Comparing with Fig. 6, it can be seen that the subsidence of metro tunnel mainly depended on the deformation of soil layer beneath the tunnel structure. Therefore, to study on the impact of pile foundation load on adjacent tunnels, the stress transfer pattern and deformation of deep soil layers under supertall building load should be focused on.

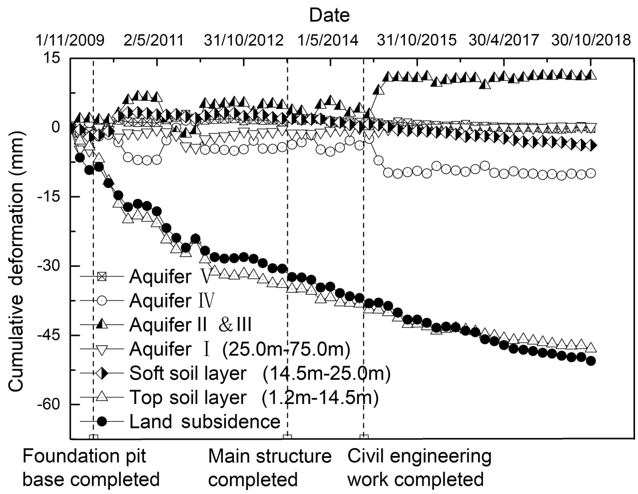

Figure 9. Layered deformation of soil in study area since 2009.

5 Conclusions

In this study, the field monitoring data analyses were performed to evaluate the influence of supertall building load on adjacent tunnel subsidence. Based on the results, the following conclusions can be drawn:

1. the construction of Building A had a significant impact on the adjacent tunnel subsidence;
2. with the increase of the load transferred from building structure to pile foundation, the tunnel adjacent to Building A appeared sustained uneven subsidence;
3. the subsidence of tunnel in the study area mainly depended on the deformation of underlying soil, and the stress transfer pattern was the key to evaluate the influence of high-rise building load on adjacent tunnel.

Data availability. All data generated or used during the study appear in the submitted article.

Author contributions. YX did the formal analysis and wrote the paper. XY and TY were responsible for the conceptualization and supervision of the project.

Competing interests. The authors declare that they have no conflict of interest.

Special issue statement. This article is part of the special issue "TISOLS: the Tenth International Symposium On Land Subsidence – living with subsidence". It is a result of the Tenth International Symposium on Land Subsidence, Delft, the Netherlands, 17–21 May 2021.

Acknowledgements. This is a contribution of the IGCP-663 project "Impact, Mechanism, Monitoring of Land Subsidence in Coastal cities" of the IUGS and UNESCO.

Financial support. This research has been supported by the International Geoscience Programme (grant no. IGCP 663) and the Shanghai Science and Technology Commission (grant no. 18DZ1201100).

References

Jiang, W. H. and Chao, S.: Variable rigidity design in the pile foundation of Shanghai Tower, Build. Struct., 42, 131–134, 2012.

Measor, E. O. and New, D. H.: The design and construction of the Royal Festival Hall, South Bank, J. Inst. Civ. Eng., 36, 241–318, 1951.

Mohammad, A., Shahram, P., and Ali, K.: Assessment of optimum settlement of structure adjacent urban tunnel by using neural network methods, Tunnel. Undergr. Space Technol., 37, 1–9, 2013.

Schroeder, F. C., Potts, D. M., and Addenbrooke, T. I.: The influence of pile group loading on existing tunnels, Geotechnique, 54, 351–362, 2004.

Wang, W. D., Li, Y. H., and Wu, J. B.: Field loading tests on large-diameter and super-long bored piles of Shanghai Center Tower, Chin. J. Geotech. Eng., 33, 1817–1826, 2011.

Weng, X. L., Sun, T., and Feng, Y.: Influence of loading pile foundation on existing neighboring subway tunnel, J. Harb. Inst. Technol., 48, 138–142, https://doi.org/10.11918/j.issn.0367-6234.2016.03.023, 2016.

Yang, T. L., Yan, X. X., Wang, H. M., Huang, X. L., and Zhan, G. H.: Comprehensive experimental study on prevention of land subsidence caused by dewatering in deep foundation pit with hanging waterproof curtain, Proc. IAHS, 372, 1–5, https://doi.org/10.5194/piahs-372-1-2015, 2015.

Rapid Land Subsidence in Tianjin, China Derived from GPS and InSAR Data (2010-2022)

R. Zhao[1], G. Wang[2], X. Yu[2], X. Sun[3], Y. Bao[4], G. Xiao[5], W. Gan[6], S. Shen[7]

1 School of Geology and Geomatics, Tianjin Chengjian University, Tianjin 300384, China
2 Department of Earth and Atmospheric Sciences, University of Houston, Houston 77204, USA
3 School of Civil Engineering, Tianjin Chengjian University, Tianjin 300384, China
4 Key Laboratory of Urban Security and Disaster Engineering of Ministry of Education, Beijing University of Technology, Beijing 100124, China
5 Key Laboratory for Digital Land and Resources of Jiangxi Province, East China University of Technology, Nanchang 330013, China
6 State Key Laboratory of Earthquake Dynamics, Institute of Geology, China Earthquake Administration, Beijing 100029, China.
7 Key Laboratory of Intelligent Manufacturing Technology of Ministry of Education, Shantou University, Shantou, Guangdong 515063, China

Correspondence to: Guoquan Wang (gwang@uh.edu)

Abstract

This is an update of the study that we submitted to the TISOLS 2020: Rapid Land Subsidence in Tianjin, China Derived from Continuous GPS Observations (2010–2019) (https://piahs.copernicus.org/articles/382/241/2020/) (Zhao et al. 2020). Recently, we reprocessed the GPS observations (2010-2021) at five continuous GPS stations (JIXN, YJBD, TJBH, HECX, TJWQ) in Tianjin. The new data indicate that the overall subsidence has slowed down since around 2019, and a slight land rebound has been observed in the Wuqing District (Fig. 1). Our recent subsidence studies using InSAR (Sentinel-1A/B, 2014-2021) also indicate that the subsidence rates across the entire previously subsiding areas in Tianjin have reduced remarkably since 2019 (Yu et al. 2023). Further investigations suggest that the reduction of subsidence rates is resulted by the South–to-North Water Diversion Project (SNWDP), which has brought over 7 billion m^3 of water from the Yangtze River system to Tianjin from 2015 to 2021. The South-to-North Water Diversion Project was designed to channel water from the Yangtze River in southern China to the more arid and industrialized north, comprising three canal systems: the Eastern Route, the Central Route, and the Western Route. The Western Route is still at the planning phase as of 2022. The Central Route and the Eastern Route began to bring water to Tianjin in 2014 (December) and 2021, respectively. The Yangtze water diverted to Tianjin was about 1.1 billion m^3 in 2021, accounting for about 35% of the annual total water use (~3.2 billion m^3). Groundwater was about 25% of the total water use in Tianjin for the public, industrial, and agriculture before 2015, and has been reduced to 0.8% of the total water use in 2021 (Tianjin Water Resources Bulletin).

The ongoing subsidence in Tianjin is primarily caused by the groundwater withdrawals from the deep aquifers, approximately 150 m to 400 m below the land surface. The amount of the deep-groundwater withdrawal was 0.23 billion m^3 in 2014 and had been reduced to 0.06 billion m^3 in 2021. Currently (as of 2021), there are still about 0.25 billion m^3 groundwater withdrawals in the shallow aquifers (within 150 m) (Tianjin Water Resources Bulletin). However, the withdrawals in the shallow aquifers are balanced by natural and human recharge, thus, do not considerably contribute to ongoing land

subsidence. Groundwater-levels in deep aquifers have elevated across the Tianjin area since around 2017. In turn, the rates of land subsidence have reduced gradually, and a slight land rebound (a few millimeters per year) has been observed in several areas since 2019. We will present detailed information about the change in subsidence rates before and after the available of the Yangtze water in Tianjin.

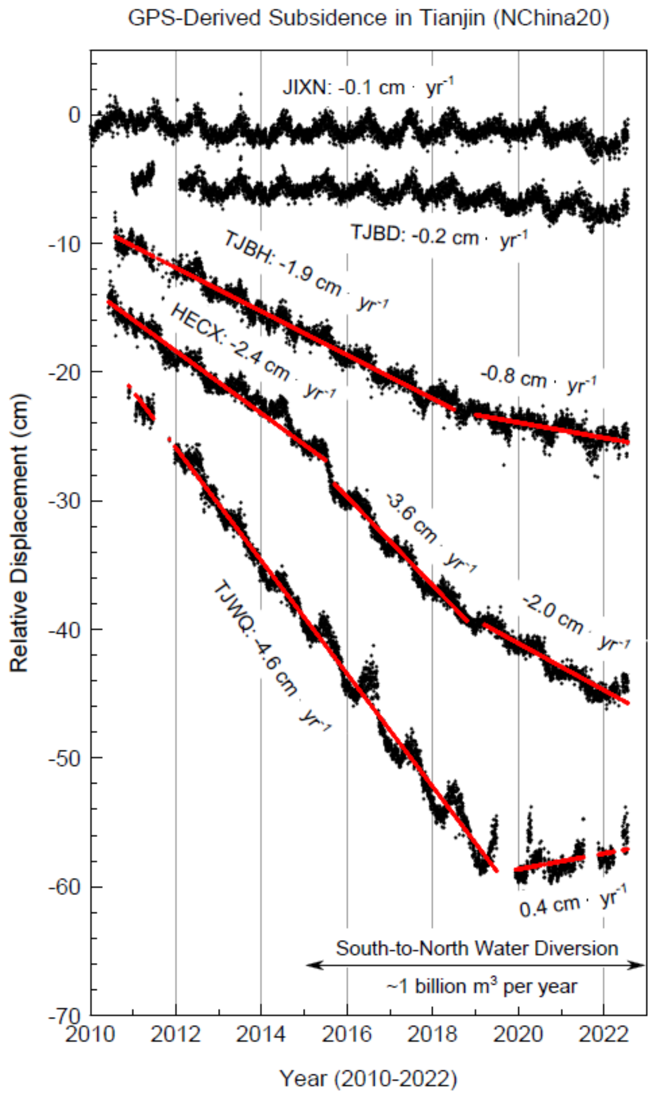

Figure 1 GPS-derived subsidence time series recorded at four GPS stations (JIXN, TJBD, TJBH, TJWQ) within and one (HECX) adjacent to the municipality of Tianjin. The subsidence time series are aligned to the stable North China Reference Frame 2020 (NChina20) (Bao et al. 2021).

References

Bao, Y., Wang, G., Yu, X., Xiao, G., Zhao, R., and Gan, W.: Establishment and applications of Stable North China Reference Frame: NChina20. Earthquake Research in China, 36(4): 788-805, 2020.

Yu, X., Wang, G., Hu, X., Liu, Y., and Bao, Y.: Land Subsidence in Tianjin, China: Before and after the South-to-North Water Diversion. Remote Sensing, 15(6): 1647, 2023. https://doi.org/10.3390/rs15061647

Zhao, R., Wang, G., Yu, X., Sun, X., Bao, Y., Xiao, G., Gan, W., and Shen, S.: Rapid Land Subsidence in Tianjin, China Derived from Continuous GPS Observations (2010–2019), Proc. IAHS, 382, 241–247, https://doi.org/10.5194/piahs-382-241-2020, 2020.

Tianjin Water Resources Bulletin: http://swj.tj.gov.cn/zwgk_17147/xzfxxgk/fdzdgknr1/tjxx/